NATIONAL ADVISORY COMMITTEE FOR AERONAUTICS

NACA CONFERENCE ON AERODYNAMIC PROBLEMS OF TRANSONIC AIRPLANE DESIGN

A COMPILATION OF THE PAPERS PRESENTED

Langley Aeronautical Laboratory
Langley Air Force Base, Virginia

September 27-29, 1949

NACA

REPRODUCED BY
NATIONAL TECHNICAL
INFORMATION SERVICE
U.S. DEPARTMENT OF COMMERCE
SPRINGFIELD, VA. 22161

N65-86451 N65-86488
(ACCESSION NUMBER) (THRU)
(PAGES) (CODE)
(NASA CR OR TMX OR AD NUMBER) (CATEGORY)
FACILITY FORM 602

NACA CONFERENCE ON AERODYNAMIC PROBLEMS OF TRANSONIC AIRPLANE DESIGN

A Compilation of the Papers Presented

Langley Aeronautical Laboratory
Langley Air Force Base, Va.

September 27-29, 1949

TABLE OF CONTENTS

	Page
INTRODUCTION	vii
LIST OF CONFEREES	ix
TECHNICAL PAPERS PRESENTED	
INTRODUCTION	1
Introductory Remarks on Transonic Testing Techniques . . . by Floyd L. Thompson	3
AIRFOILS AND WINGS	13
The Effects of Systematic Variation of Several Shape Parameters on the Characteristics of Airfoil Sections at High-Subsonic Mach Numbers . . . by Donald J. Graham	15
Preliminary Investigation of Airfoil Characteristics near M = 1 . . . by Bernard N. Daley and Louis W. Habel	41
The Lift, Drag, and Pitching-Moment Characteristics of Wings and Wing-Body Combinations in the Transonic Speed Range . . . by Edward C. Polhamus	57
Wing Characteristics near and at Maximum Lift for Transonic Speeds . . . by Thomas R. Turner	75
AEROELASTICITY AND FLUTTER	81
Status of the High-Speed Flutter Problem . . . by I. E. Garrick and D. J. Martin	83
The Rolling Power of Two Wing-Aileron Configurations as Affected by Flexibility . . . by Warren A. Tucker and Paul E. Purser	97
The Effect of Aeroelasticity on the Static Longitudinal Stability of an Example Swept-Wing Bomber . . . by Richard B. Skoog	107
Wing Selection as Influenced by the Effect of Wing Bending on Aerodynamic-Center Shift . . . by Charles W. Mathews	129

Preceding page blank

Page

Loss of Longitudinal Damping in Pitch Due to Flexibility of Wings in Bending . . . by Reginald R. Lundstrom . . . 135

BODIES AND WING–BODY INTERFERENCE 143

Drag Characteristics at Zero Lift of Bodies at Transonic Speeds . . . by Ellis R. Katz and Clarence W. Matthews . 145

The Flow over Moderately Swept Wings at High-Subsonic Speeds Including the Effects of Nacelle Interference . . by George G. Edwards and Lee E. Boddy 159

Effect on Force Coefficients of Bodies of Revolution Attached to Straight and Swept Wings . . . by H. Normal Silvers 177

Assessment of the Drag Problem . . . by Richard I. Sears . 185

AIRSPEED MEASUREMENT 195

Design and Calibration of Airspeed Installations . . . by William Gracey 197

STABILITY AND CONTROL 205

Stability, Control, and Drag Characteristics of a Canard Airplane Configuration at Transonic Speeds . . . by Christopher C. Kraft, Jr., and Harold L. Crane . . . 207

Some Effects of Sweepback and Airfoil Thickness on Longitudinal Stability and Control Characteristics at Transonic Speeds . . . by Charles J. Donlan and Arvo A. Luoma 219

A Comparison of the Longitudinal Stability and Control Characteristics of Three Airplane Configurations . . . by Clarence L. Gillis 231

Downwash and Wake Characteristics at Transonic Speeds . . . by Joseph Weil and Ralph P. Bielat 245

Page

Effect of Stall-Control Devices on the Low-Speed Characteristics of Swept Wings . . . by G. Chester Furlong and William B. Kemp, Jr. 261
Part I.- Fixed Sweep . . . by G. Chester Furlong 261
Part II.- Variable Sweep . . . by William B. Kemp, Jr. . 270

Effect of Twist and Camber on the Low-Speed Characteristics of a Swept Wing . . . by Lynn W. Hunton 283

Preliminary Investigations of the Effect of Plan Form, Sweep, and Section on the Damping-in-Roll Characteristics of Wings through the Transonic Speed Region . . . by David G. Stone and John W. McKee 297

Control-Surface Characteristics at Transonic Speeds . . . by John G. Lowry and Carl A. Sandahl 309

Dynamic Lateral Stability of Transonic Airplanes . . . by William M. Kauffman and Charles H. Zimmerman 325

INLETS, DIFFUSERS, AND JETS 351

Summary of Information on Air Inlets. Nose and Wing-Root Inlets . . . by Mark R. Nichols 353

Summary of Information on Air Inlets. NACA Submerged Inlets . . . by Emmet A. Mossman 367

Diffusers for High-Speed Aircraft . . . by Kennedy F. Rubert 381

Analysis of the Stability Characteristics of Twin-Intake Air-Induction Systems . . . by Norman J. Martin 393

Jet Exhaust Characteristics . . . by Morris D. Rousso . . . 403

PROPELLERS FOR AIRCRAFT 421

Blade-Section Characteristics from Pressure Distributions on the Sections of Operating Propellers . . . by Julian D. Maynard 423

An Experimental Investigation of Single-Rotation Propeller Characteristics at High-Subsonic Mach Numbers . . . by Richard T. Whitcomb, James B. Delano, and Melvin M. Carmel 437

INTRODUCTION

This document contains reproductions of technical papers on some of the recent research results from the NACA Laboratories on aerodynamic problems pertinent to the design of transonic airplanes. These papers were presented at the NACA conference held at the Langley Aeronautical Laboratory September 27, 28, and 29, 1949. The purpose of this conference was to convey to those involved in the study of the aerodynamic problems of transonic aircraft these recent research results and to provide those attending an opportunity for discussion of the results.

The papers in this document are in the same form in which they were presented at the conference so that distribution of them might be prompt. The original presentation and this record are considered as complementary to, rather than as substitutes for, the Committee's system of complete and formal reports.

A list of the conferees is included.

Page

Summary of Results of United Aircraft Wind-Tunnel Tests of a Supersonic Propeller . . . by Thomas B. Rhines 447

Investigation of a Dual Propeller at High Subsonic Mach Numbers . . . by Robert J. Platt, Jr., and Jean Gilman, Jr. 451

Vibration of Aircraft Propellers . . . by Mason F. Miller and W. H. Gray 457

Prediction of First-Order Vibratory Stresses for a Propeller Operating in the Flow Field of a Wing-Nacelle-Fuselage Combination . . . by Vernon L. Rogallo 467

The Propeller Flutter Problem for High-Speed Airplanes . . by John E. Baker and Arthur A. Regier 475

Trends in the Design and Performance of High-Speed Propellers . . . by Eugene C. Draley, Blake W. Corson, Jr., and John L. Crigler 483

LIST OF CONFEREES

The following were registered at the NACA Conference on Aerodynamic Problems of Transonic Airplane Design, Langley Aeronautical Laboratory, Langley Air Force Base, Virginia, September 27-29, 1949:

Abzug, Malcolm	Sperry Gyroscope Co., Inc., Great Neck, Long Island, N. Y.
Allen, H. J.	NACA - Ames Laboratory
Ames, M. B., Jr.	NACA Headquarters
Anderson, H. L.	USAF Air Materiel Command, Wright-Patterson Air Force Base
Anderson, R. A.	NACA Headquarters
Arnold, Alison	Bell Aircraft Corp., Buffalo, N. Y.
Arnoldi, Walter E.	United Aircraft Corp., Hamilton Standard Prop. Div., E. Hartford, Conn.
Baals, Donald D.	NACA - Langley Laboratory
Babberger, Carl	Hughes Aircraft Co., Culver City, Calif.
Bailey, F. J.	NACA - Langley Laboratory
Baker, John E.	NACA - Langley Laboratory
Baker, Paul S.	Chance Vought Aircraft, Dallas, Texas
Bashark, N.	USAF Air Materiel Command, Wright-Patterson Air Force Base
Becker, J. V.	NACA - Langley Laboratory
Beeler, De E.	NACA High-Speed Flight Research Station, Muroc, Calif.
Bielat, Ralph P.	NACA - Langley Laboratory
Blom, T.	USAF Air Materiel Command, Wright-Patterson Air Force Base
Boddy, Lee E.	NACA - Ames Laboratory
Bonney, E. A.	Johns Hopkins Univ., Applied Physics Lab., Silver Spring, Md.
Borst, H. V.	Curtiss-Wright Corp., Prop. Div., Caldwell, N. J.
Boshar, John	Dept. of Commerce, CAA, Washington, D. C.
Bowe, D. D.	General Motors Corp., Aeroproducts Div., Dayton, Ohio
Bowman, R. G.	Republic Aviation Corp., Farmingdale, Long Island, N. Y.

Preceding page blank

Boykin, J. A., Jr.	USAF Air Materiel Command, Wright-Patterson Air Force Base
Breuhaus, W. O.	Cornell Aeronautical Lab., Buffalo, N. Y.
Brewer, G. W.	NACA - Langley Laboratory
Brewer, J. D.	NACA Headquarters
Brom, J. R.	University of Chicago
Burgess, John A.	Research and Development Board, Washington, D. C.
Butterworth, Wesley T.	Curtiss-Wright Corp., Airplane Div., Columbus, Ohio
Campbell, J. P.	NACA - Langley Laboratory
Carman, L. R.	NACA High-Speed Flight Research Station, Muroc, Calif.
Carmel, Melvin M.	NACA - Langley Laboratory
Carner, H. A.	NACA High-Speed Flight Research Station, Muroc, Calif.
Carran, John A.	Dept. of Commerce, CAA, Washington, D. C.
Celniker, Leo	Fairchild Engine and Airplane Corp., NEPA Div., Oak Ridge, Tenn.
Champine, R. A.	NACA High-Speed Flight Research Station, Muroc, Calif.
Charters, A. C.	Ballistic Research Laboratories, Aberdeen, Md.
Clark, E. C.	Glenn L. Martin Co., Baltimore, Md.
Clark, L. P.	Naval Air Materiel Center, Philadelphia, Pa.
Clayton, Harry H.	Muroc Air Force Base, Muroc, Calif.
Cohn, Benedict	Boeing Airplane Co., Seattle, Washington
Colman, Phillip A.	Lockheed Aircraft Corp., Burbank, Calif.
Conrad, D. S.	United Aircraft Corp., Pratt & Whitney Aircraft Div., E. Hartford, Conn.
Corson, Blake W., Jr.	NACA - Langley Laboratory
Crane, Harold L.	NACA - Langley Laboratory
Crane, R. M.	NACA - Ames Laboratory
Crigler, John L.	NACA - Langley Laboratory
Crowley, J. W.	NACA Headquarters
Daley, Bernard N.	NACA - Langley Laboratory
Davis, Frank W.	Consolidated-Vultee Aircraft Corp., San Diego, Calif.
Dearborn, Clinton H.	NACA - Langley Laboratory
Delano, James B.	NACA - Langley Laboratory
Dernbach, A. F.	USAF Air Materiel Command, Wright-Patterson Air Force Base

Desmond, G. L.	Navy Department, Bur. Aero., Washington, D. C.
Dickey, D. A.	USAF Air Materiel Command, Wright-Patterson Air Force Base
Diehl, Capt. W. S.	Navy Department, Bur. Aero., Washington, D. C.
Dietz, Robert O.	NACA - Headquarters
DiFranco, Dante	Bell Aircraft Corp., Buffalo, N.Y.
Donely, Philip	NACA - Langley Laboratory
Donlan, Charles J.	NACA - Langley Laboratory
Draley, Eugene C.	NACA - Langley Laboratory
Drake, H. M.	NACA High-Speed Flight Research Station, Muroc, Calif.
Dryden, H. L.	NACA Headquarters
Eastman, Donald R.	Research and Development Board, Washington, D. C.
Edwards, George G.	NACA - Ames Laboratory
Egbert, D. T.	Navy Department, Bur. Aero., Washington, D. C.
Ellis, J. W.	RAND Corporation, Santa Monica, Calif.
Ellis, M. C., Jr.	NACA - Langley Laboratory
Emmons, Paul C.	Bell Aircraft Corp., Buffalo, N. Y.
Enos, L. H.	Curtiss-Wright Corp., Prop. Div., Caldwell, N. J.
Evans, George D.	Sperry Gyroscope Co., Great Neck, Long Island, N. Y.
Fedziuk, H. A.	NACA - Langley Laboratory
Feldmann, F. K.	North American Aviation, Inc., Aerophysics Lab., Los Angeles, Calif.
Ferri, Antonio	NACA - Langley Laboratory
Flader, Fredric	Fredic Flader, Inc., N. Tonawanda, N. Y.
Flax, A.	Cornell Aeronautical Lab., Buffalo, N. Y.
Fleming, Frank N.	Douglas Aircraft Co., Inc., Santa Monica, Calif.
Fleming, William A.	NACA - Lewis Laboratory
Floyd, J. F. R.	Johns Hopkins Univ., Applied Physics Lab., Silver Spring, Md.
Forry, J. E.	Navy Department, Bur. Aero., Washington, D. C.
Furlong, G. Chester	NACA - Langley Laboratory
Garrick, I. E.	NACA - Langley Laboratory
Genta, Cmdr. J. L.	Naval Air Test Center, Patuxent River, Md.
George, J.	Navy Department, Bur. Aero., Washington, D. C.
Gillis, Clarence L.	NACA - Langley Laboratory

Gilman Jean, Jr.	NACA - Langley Laboratory
Gilruth, R. R.	NACA - Langley Laboratory
Glodeck, Edward	Research and Development Board, Washington, D. C.
Goda, Herbert L.	Research and Development Board, Washington, D. C.
Goett, H. J.	NACA - Ames Laboratory
Goode, J. E.	Consolidated-Vultee Aircraft Corp., Ft. Worth, Texas
Goodell, Maj. Howard C.	AMCEFO, Langley Air Force Base, Va.
Gough, M. N.	NACA - Langley Laboratory
Gracey, William	NACA - Langley Laboratory
Grady, W.	USAF Air Materiel Command, Wright-Patterson Air Force Base
Graff, G. S.	McDonnell Aircraft Corp., St. Louis, Mo.
Graham, Donald J.	NACA - Ames Laboratory
Gray, W. H.	NACA - Langley Laboratory
Gustafson, Robert	Grumman Aircraft Engineering Corp. Bethpage, Long Island, N. Y.
Gutheim, Robert	Navy Department, Bur. Ord., Washington, D. C.
Habel, Louis W.	NACA - Langley Laboratory
Hall, C. L.	USAF Air Materiel Command, Wright-Patterson Air Force Base
Hanes, Col. H. A.	Office of Deputy Chief of Staff, Materiel, Washington, D. C.
Harris, T. A.	NACA - Langley Laboratory
Harshe, Marshall L.	Fairchild Engine and Airplane Corp., NEPA Div., Oak Ridge, Tenn.
Hartman, Edwin P.	NACA Western Coordinator
Hazen, Ronald M.	General Motors Corp., Allison Div., Indianapolis, Ind.
Heald, E. R.	Douglas Aircraft Company, Inc., El Segundo, Calif.
Hill, P. R.	NACA - Langley Laboratory
Hoadley, Henry H.	United Aircraft Corp., E. Hartford, Conn.
Hoekstra, Harold D.	Dept. of Commerce, CAA, Washington, D. C.
Holtoner, Col. J. S.	Office of Deputy Chief of Staff, Materiel, Washington, D. C.
Hood, M. J.	NACA - Ames Laboratory
Hoover, H. H.	NACA - Langley Laboratory
Hunton, Lynn W.	NACA - Ames Laboratory
Hutton, Richard	Grumman Aircraft Engineering Corp., Bethpage, Long Island, N. Y.
Jacobson, D. H.	General Motors Corp., Aeroproducts Div., Dayton, Ohio

Jones, Robert T.	NACA - Ames Laboratory
Kamm, Robert W.	Research and Development Board, Washington, D. C.
Kaplan, C.	NACA - Langley Laboratory
Kartveli, A.	Republic Aviation Corp., Farmingdale, Long Island, N. Y.
Kasley, J. H.	Curtiss-Wright Corp., Prop. Div., Caldwell, N. J.
Katz, Ellis R.	NACA - Langley Laboratory
Katzoff, S.	NACA - Langley Laboratory
Kauffman, William M.	NACA - Ames Laboratory
Kayten, Gerald G.	Navy Department, Bur. Aero. Washington, D. C.
Kemp, William B., Jr.	NACA - Langley Laboratory
Kiefer, Eugene P.	Washington AMC Engineering Field Office, Washington, D. C.
Kirkwood, T. F.	RAND Corporation, Santa Monica, Calif.
Klepinger, R. H.	USAF Air Materiel Command, Wright-Patterson Air Force Base
Kluge, R. W.	Cornell Aeronautical Lab., Buffalo, N. Y.
Knight, E. J.	Northrop Aircraft, Inc., Hawthorne, Calif.
Kraft, Christopher C., Jr.	NACA - Langley Laboratory
Kuethe, A. M.	USAF Air Materiel Command, Wright-Patterson Air Force Base
Lancaster, O. E.	Navy Department, Bur. Aero., Washington, D. C.
Lee, John G.	United Aircraft Corp., E. Hartford, Conn.
Lewis, D. S.	McDonnell Aircraft Corp., St. Louis, Mo.
Lewis, R. B.	Wright Aeronautical Corp., Wood-Bridge, N. J.
Loening, Grover	NACA Headquarters
Lombard, Albert E., Jr.	Chief of Staff, U. S. Air Force, Washington, D. C.
Louden, F. A.	Navy Department, Bur. Aero. Washington, D. C.
Lowry, John G.	NACA - Langley Laboratory
Lundstrom, Reginald R.	NACA - Langley Laboratory
Lundquist, E. E.	NACA - Langley Laboratory
Luoma, Arvo	NACA - Langley Laboratory
Luskin, Harold	Douglas Aircraft Company, Inc., Santa Monica, Calif.

McAvoy, W. H.	NACA - Ames Laboratory
McKay, Capt. A. L.	AMCEFO, Langley Air Force Base, Va.
McKee, John W.	NACA - Langley Laboratory
Maggin, B.	NACA Headquarters
Martin, D. J.	NACA - Langley Laboratory
Martin, Norman J.	NACA - Ames Laboratory
Mathews, Charles W.	NACA - Langley Laboratory
Mattson, A. T.	NACA - Langley Laboratory
Matthews, Clarence W.	NACA - Langley Laboratory
Maxam, Frederick A.	Curtiss-Wright Corp., Airplane Div., Columbus, Ohio
Maynard, Julian D.	NACA - Langley Laboratory
Mezger, B. J.	Wright Aeronautical Corp., Wood-Bridge, N. J.
Miller, Mason F.	NACA - Langley Laboratory
Mokrzycki, Andrew	Ryan Aeronautical Co., San Diego, Calif.
Morse, John C.	Dept. of Commerce, CAA, Washington, D. C.
Morton, E. E.	Fairchild Aircraft Div., Hagerstown, Md.
Moskovitz, A. I.	Navy Dept., Bur. Ord., Washington, D. C.
Mossman, Emmet A.	NACA - Ames Laboratory
Munk, M. M.	Naval Ordnance Lab., White Oak, Md.
Murrow, R. B.	RAND Corporation, Santa Monica, Calif.
Myers, Dale D.	North American Aviation, Inc., Aerophysics Lab., Los Angeles, Calif.
Nagamatsu, Henry	California Institute of Technology, Pasadena, Calif.
Nelson, A. M.	USAF Air Materiel Command, Wright-Patterson Air Force Base
Nelson, Maj. Conrad	Sandia Base, Albuquerque, N. M.
Nichols, Mark R.	NACA - Langley Laboratory
Norris, R. Hosmer	General Electric Co., Project HERMES, Schenectady, N. Y.
O'Donnell, W. J.	Republic Aviation Corp., Farmingdale, Long Island, N. Y.
Outman, V.	McDonnell Aircraft Corp., St. Louis, Mo.
Owen, J. C.	Bendix Aviation Corp., Eclipse-Pioneer Div., Teterboro, N. J.
Palmer, Carl B.	NACA - Headquarters
Pappas, C. E.	Republic Aviation Corp., Farmingdale, Long Island, N. Y.
Parkinson, J. B.	NACA - Langley Laboratory

Parsons, J. F.	NACA - Ames Laboratory
Pass, Herbert R.	U. S. Naval Air Missile Test Center, Pt. Mugu, Calif.
Passman, Richard	Bell Aircraft Corp., Buffalo, N. Y.
Patton, R. J.	Consolidated-Vultee Aircraft Corp., Ft. Worth, Texas
Pearson, E. O., Jr.	NACA Headquarters
Pearson, H. A.	NACA - Langley Laboratory
Pfenninger, W.	Northrop Aircraft, Inc., Hawthorne, Calif.
Phillips, W. H.	NACA - Langley Laboratory
Platt, Robert J., Jr.	NACA - Langley Laboratory
Polhamus, Edward C.	NACA - Langley Laboratory
Pooler, L. G.	Navy Dept., Bur. Ord., Washington, D. C.
Poor, C. L., 3d	Ballistic Research Laboratories, Aberdeen, Md.
Prachar, Otokar P.	General Motors Corp., Allison Div., Indianapolis, Ind.
Puckett, A. E.	Hughes Aircraft Company, Culver City, Calif.
Purser, Paul E.	NACA - Langley Laboratory
Rafferty, C. A.	Bendix Aviation Corp., Eclipse-Pioneer Div., Teterboro, N. J.
Redding, A. H.	Westinghouse Electric Corp., Philadelphia, Pa.
Regier, Arthur A.	NACA - Langley Laboratory
Reid, H. J. E.	NACA - Langley Laboratory
Rhines, Thomas B.	United Aircraft Corp., Hamilton Standard Propellers Div., E. Hartford, Conn.
Rhode, R. V.	NACA - Langley Laboratory
Ridley, Maj. J. L.	Muroc Air Force Base, Muroc, Calif.
Robinson, R. G.	NACA Headquarters
Roche, J. A.	AMCEFO, Langley Air Force Base, Va.
Rogallo, F. M.	NACA - Langley Laboratory
Rogallo, Vernon L.	NACA - Ames Laboratory
Rogin, L.	Naval Air Materiel Center, Philadelphia, Pa.
Root, L. E.	RAND Corporation, Santa Monica, Calif.
Rosen, George	United Aircraft Corp., Hamilton Standard Propellers Div., E. Hartford, Conn.
Roth, Capt. Russell M.	Muroc Air Force Base, Muroc, Calif.
Rousso, Morris D.	NACA - Lewis Laboratory
Rubert, Kennedy F.	NACA - Langley Laboratory

Sandahl, Carl A.	NACA - Langley Laboratory
Schairer, George S.	Boeing Airplane Company, Seattle, Washington
Schneiter, L. E.	NACA Headquarters
Schoolfield, William C.	Chance Vought Aircraft, Dallas, Texas
Schueller, Carl F.	NACA - Lewis Laboratory
Schuldenfrei, Marvin	Navy Department, Bur. Aero. Washington, D. C.
Schumacher, Floyd E.	USAF Air Materiel Command, Wright-Patterson Air Force Base
Schwarzbach, J. M.	Naval Air Test Center, Patuxent River, Md.
Sea, A. L.	USAF Air Materiel Command, Wright-Patterson Air Force Base
Sears, Richard I.	NACA - Langley Laboratory
Seckel, Edward	Cornell Aeronautical Laboratory, Buffalo, New York
Seidman, O.	Navy Department, Bur. Aero., Washington, D. C.
Sheeren, M. L.	NACA High-Speed Flight Research Station, Muroc, Calif.
Sherby, Cmdr. S. S.	Navy Department, Bur. Aero., Washington, D. C.
Shortal, J. A.	NACA - Langley Laboratory
Shue, G. L.	Naval Ordnance Lab., White Oak, Md.
Silvers, H. Norman	NACA - Langley Laboratory
Silverstein, A.	NACA - Lewis Laboratory
Sjoberg, S. A.	NACA - Langley Laboratory
Skoog, Richard B.	NACA - Ames Laboratory
Smith, C. Branson	United Aircraft Corp., E. Hartford, Conn.
Smith, J. E.	Cooperative Wind Tunnel, Pasadena, Calif.
Soule, H. A.	NACA - Langley Laboratory
Springer, Burdell L.	Dept. of Commerce, CAA, Washington, D. C.
Stack, John	NACA - Langley Laboratory
Sternfield, L.	NACA - Langley Laboratory
Stevenson, David B.	Dept. of Commerce, CAA, Washington, D. C.
Stillman, William P.	University of Chicago, Ordnance Research 1,
Stirling, Cmdr. C. W.	David Taylor Model Basin, Navy Dept., Washington, D. C.
Stoeckly, E. E.	General Electric, Aircraft Gas Turbine Engineering Div., West Lynn, Mass.

Stoller, M. J.	NACA - Langley Laboratory
Stone, David G.	NACA - Langley Laboratory
Storms, Harrison A.	North American Aviation, Inc., Los Angeles, Calif.
Stulen, F. B.	Curtiss-Wright Corp., Prop. Div., Caldwell, N. J.
Sturdevant, C. V.	RAND Corporation, Santa Monica, Calif.
Swanson, Robert S.	U. S. Naval Air Missile Test Center, Pt. Mugu, Calif.
Tauson, Peter	Fredric Flader, Inc., N. Tonawanda, N. Y.
Thieblot, A. J.	Fairchild Aircraft, Hagerstown, Md.
Thompson, Floyd L.	NACA - Langley Laboratory
Toll, T. A.	NACA - Langley Laboratory
Trimble, G. S., Jr.	Glenn L. Martin Co., Baltimore, Md.
Tucker, Warren A.	NACA - Langley Laboratory
Turner, Thomas R.	NACA - Langley Laboratory
Twomey, Irving	United Aircraft Corp., E. Hartford, Conn.
Underwood, William J.	NACA Liaison Officer at AMC, Wright-Patterson Air Force Base
Van Every, K. E.	Douglas Aircraft Co., Inc., El Segundo, Calif.
Von Doenhoff, A. E.	NACA - Langley Laboratory
Wade, William E., Jr.	Grumman Aircraft Engineering Corp., Bethpage, Long Island, N. Y.
Walker, J. A.	NACA - Lewis Laboratory
Wasserman, L. S.	USAF Air Materiel Command, Wright-Patterson Air Force Base
Weil, Joseph	NACA - Langley Laboratory
Wein, K.	USAF Air Materiel Command, Wright-Patterson Air Force Base,
Weller, Royal	U. S. Naval Air Missile Test Center, Pt. Mugu, Calif.
Welling, Omer	Dept. of Commerce, CAA, Washington, D. C.
Wetmore, J. W.	NACA - Langley Laboratory
Whitcomb, David W.	Cornell Aeronautical Laboratory, Buffalo, New York
Whitcomb, Richard T.	NACA - Langley Laboratory
Williams, W. C.	NACA High-Speed Flight Research Station, Muroc, Calif.
Wilson, H. A.	NACA - Langley Laboratory
Wood, C.	NACA Headquarters
Zimmerman, Charles H.	NACA - Langley Laboratory

INTRODUCTION

Preceding page blank

INTRODUCTORY REMARKS ON TRANSONIC TESTING TECHNIQUES

By Floyd L. Thompson

Langley Aeronautical Laboratory

N65-86452

During the past several years it has been necessary for aeronautical research workers to exert a good portion of their effort in developing the means for conducting research in the high-speed range. The transonic range particularly has presented a very acute problem because of the choking phenomena in wind tunnels at speeds close to the speed of sound. At the same time, the multiplicity of design problems for aircraft introduced by the peculiar flow problems of the transonic speed range has given rise to an enormous demand for detail design data. Substantial progress has been made, however, in developing the required research techniques and in supplying the demand for aerodynamic data required for design purposes.

In meeting this demand, it has been necessary to resort to new techniques possessing such novel features that the results obtained have had to be viewed with caution. Furthermore, the kinds of measurements possible with these various techniques are so varied that the correlation of results obtained by different techniques generally becomes an indirect process that can only be accomplished in conjunction with the application of estimates of the extent to which the results of measurements by any given technique are modified by differences that are inherent in the techniques. Thus, in the establishment of the validity and applicability of data obtained by any given technique, direct comparisons between data from different sources are a supplement to but not a substitute for the detailed knowledge required of the characteristics of each technique and fundamental aerodynamic flow phenomena.

The purpose of these "Introductory Remarks" is to review briefly the characteristics of the numerous techniques that have been employed in obtaining the data which form the basis for the papers to be presented in this conference. In addition, I shall discuss in somewhat greater detail our opinion regarding the validity and applicability of data obtained from one of these techniques, the wing-flow and bump technique, because, although it has proven to be a very fruitful source of detailed aerodynamic data, it possesses some rather obvious faults that have continually given rise to a healthy skepticism and caution in its use.

First, the various techniques used will be briefly reviewed. At the bottom of figure 1 is shown the speed range for the conventional closed-throat wind tunnel in two versions: the subsonic one, which is capable of producing reliable data at Mach numbers up to about 0.8 or slightly above; and the supersonic one, which operates satisfactorily at Mach numbers above 1.3. The improved closed-throat tunnel has been

obtained by large increases in power and fundamental modifications to the throat, model support system, and balances. The subsonic range in this case has been extended to a Mach number M of about 0.95 and the range for the supersonic version starts at a Mach number of about 1.2. The types of measurement possible can be assumed to be the same as for the conventional tunnel but the operation of a tunnel so close to the speed of sound requires that the air-stream disturbance produced by the model be of much smaller relative magnitude than that which can be tolerated at lower speeds. Hence, the permissible model size is greatly reduced and, with particular reference to the subsonic case, it will be impossible to operate the tunnel or to obtain reliable measurements at large angles of attack except at reduced tunnel speeds or with a very small model. It is worthy of note that the Langley 8-foot high-speed tunnel has been equipped for the past $1\frac{1}{2}$ years with a throat of temporary construction that permits testing in the subsonic range indicated and, in addition, at $M = 1.2$ in the supersonic range.

The falling-body technique is capable of providing data continuously from the upper subsonic range through the speed of sound up to about $M = 1.3$. It has the advantages of large scale and an unrestricted flow field. This technique has been used primarily for measurements of drag at zero lift on fundamental body shapes and wing-body combinations. It has been possible with this technique to measure simultaneously the drag of the wings and body separately on various wing-body combinations so as to provide very useful information on the mechanism of wing and body interference. Other applications of this technique have yielded valuable information on the distribution of pressures over a body in the transonic range and on the stability and control characteristics of certain airplane configurations. In general, this technique is unsuited to extensive detailed investigations and is useful primarily as a supplement to other methods which are better suited to extensive systematic studies but which require verification by a method having the advantages of large Reynolds number and an unrestricted flow field. The fact that these models in general are accelerating during the period of measurement seems to be without significance as regards the validity of the data obtained. According to theory, appreciable effects would be expected at very large accelerations.

The wing-flow and wind-tunnel bump techniques are classed together because of their very close similarity. They have provided the means for obtaining extensive detailed aerodynamic data on numerous models over about the same range of Mach numbers as the falling-body technique. Let us skip this item for a moment, however, and return to it for a more detailed discussion later.

The use of rocket-powered models launched from the ground has proven to be another versatile and very productive means of acquiring aerodynamic data. The useful range for this technique starts in the upper subsonic range and extends far into the supersonic range beyond the value of $M = 1.6$, which is merely taken as the maximum value of interest in the present discussion. This technique has the same advantages as the falling-body technique; that is, a large Reynolds number and an unrestricted flow field. In this case, the models generally are decelerating during the period of data recording but here again the rate of change of velocity appears to be low enough to be without significant effects. The kinds of measurements for which the rocket technique has been used most extensively and which are pertinent to this conference can be broadly characterized as: (a) measurements of drag at zero lift of bodies, wings, and wing-body combinations; (b) studies of control effectiveness as affected by various factors; (c) studies of stability parameters particularly as regards complete configurations; and (d) studies of aeroelastic phenomena. In studies of wing drag, a fundamental point that must be kept in mind with particular reference to the problem of correlation with other data is that wing drag has usually been obtained as the difference between the drag of a wing-body combination and the drag of a similar body without wings installed. Thus, such favorable or unfavorable wing-body interference as may exist will appear in the wing drag deduced by this means.

The transonic tunnel referred to in figure 1 is the unconventional apparatus described by Mr. John Stack at the NACA Biennial Inspection in May 1949 at this laboratory in which the model under test is mounted on the rim of a rotating disk. By this means the model is made to rotate rapidly in an annular passage through which the air is moving at a relatively slow speed in a direction parallel to the axis of the disk. The speed of rotation is such as to give the model the velocity range shown on the chart, extending from the subsonic range into the lower supersonic range. The axial movement of the air is adjusted so as to regulate the angle of attack of the model under test and to insure sufficient pitch to the helical path of the model so that is is not affected by an interference flow generated by itself. This technique is used for fundamental two-dimensional studies of airfoils by means of pressure distribution. By means of rather elaborate precautions to eliminate the effects of the boundary layers in the annular passage, an effective two-dimensional flow condition has been achieved so that for the limited type of measurement possible with this apparatus there appears to be no reason to suspect the validity of the results obtained.

There are many pitfalls for the experimentalist in any technique, but it appears appropriate to review certain peculiarities of the wing-flow and bump technique in some detail. In figure 2 is shown a wing-body combination installed in this particular case on a wind-tunnel bump.

The semispan is about 5 inches but smaller models are sometimes used. There are certain inherent features of this installation that should be noted. The model inherently is a semispan one requiring that the surface on which it is mounted act as a reflection plane. The perfection with which this is achieved depends on the details of the juncture of the model with the surface of the bump. Some clearance is necessary but a perceptible gap may permit enough air flow so that, for example, the aerodynamic forces may be affected to such an extent as to reduce the slope of the lift curve and increase the drag due to lift by appreciable amounts. Another point to observe is that the model fuselage is curved to conform to the curved surface of the bump. Furthermore, the fuselage model must of necessity lie in the boundary layer over the bump. This boundary layer is only a fraction of an inch thick but the model is small, and even that may be sufficient to affect the flow over the model fuselage appreciably. It is probable that the effect on the wing–body combination or on the wing alone without fuselage is of little consequence, but one would view with caution data that might be deduced for the fuselage alone.

Another point to observe concerns the velocity gradients in the field of flow over the model. In the spanwise direction the gradient is generally of the order of 0.007 to 0.01 M per inch or a total of 3 to 5 percent for a 5-inch span. In the chordwise direction the gradients, particularly at the highest Mach numbers, are fairly large and amount to as much as 2 percent for a typical case. Some effects of such variations in velocity would be expected but any quantitative evaluation of such effects have eluded us. The least that one would expect is that, for those forces that vary abruptly at a critical Mach number, the abruptness would be somewhat reduced. It is probable that such generally is the case, but even in that respect direct valid comparisons that do not involve good possibilities of other important effects are difficult to find. Wing-flow and bump models are necessarily small and, like small models anywhere, the effects of very small defects in coutour, particularly at the leading edge, can easily nullify the validity of what might seem to be a perfectly valid comparison.

Evidence of the nature of the discrepancies that are sometimes observed from the results of tests with different techniques is shown in figure 3. The techniques used involved: (a) a sting-supported full-span model in the Langley high-speed 7- by 10-foot tunnel, (b) a semispan model attached to the wall of the same tunnel, and (c) a wing-flow model. The figure shows the effectiveness of the flap in producing pitching moment (C_{m_δ}) at various Mach numbers for the airplane configuration illustrated. The discrepancies noted for the critical range near Mach number 1.0 are about as large as are likely to be encountered. It may be noted in this case that the semispan model referred to is one-half of the same model that was used on the sting

support. The wing-flow model is somewhat smaller than the 5-inch-semispan model shown in figure 2. The chief point to be made is that it is in this critical range where forces change abruptly at a critical Mach number that discrepancies are likely to be greatest.

In figure 4 is shown a comparison of the elevator angle required to trim an airplane configuration as deduced from wing-flow results for three different lift coefficients, 0, 0.1, and 0.2. The zero case required some extrapolation of data. It will be observed that the elevator angle required to trim according to these results is changed enormously by variations in the lift coefficient. Also shown are points obtained from flight tests for the full-size airplane. At the top of the figure is shown a variation in lift coefficient from 0.1 to 0 experienced by the airplane in passing through the range of Mach numbers shown. This figure illustrates some of the difficulties involved in correlating data from one source with those from another. In this particular case the elevator angle required is so critically dependent on the lift coefficient that it is difficult to determine whether the correlation is good or not. To one person the correlation may appear good, but to another poor.

Certain general statements regarding our opinion of the validity of results obtained from the bump and wing-flow technique are as follows:

(1) Rounding off of relatively sharp breaks that occur with changes in Mach number can be expected since there is a variation of Mach number along the span of the model.

(2) Comparisons of drag coefficients obtained by the various facilities indicate that although the absolute values of drag coefficient obtained from bump and wing flow are qualitative in nature, the variation with Mach number shows reasonable agreement except for abrupt changes. Drag due to lift shows reasonable correlation and, in general, is of the right order of magnitude.

(3) In general, the variation of lift-curve slope and its absolute magnitude are found to be in good agreement regardless of the testing facility used.

(4) The pitching moments obtained on wing-fuselage combinations and wing alone show reasonable agreement except for abrupt changes and for configurations that are particularly susceptible to Reynolds number effects.

(5) The control effectiveness obtained by bump and wing-flow techniques show reasonable agreement with rocket-powered models and flight both as to absolute magnitude and variation of effectiveness with Mach number. Certain discrepancies do occur, however, where there are

rapid changes with Mach number where the control is adversely affected by separation and for controls that are critical to Reynolds number changes.

(6) Only a limited amount of pressure-distribution data is available. One comparison of bump and semispan wall tests of the same model indicate excellent agreement except for a small Mach number range where the upper-surface shock is extremely critical to local Mach number. No direct comparisons are available for bodies, but trends shown by wing flow and free fall on two different configurations look reasonable.

Further detailed comparisons of results obtained by various techniques might have been incorporated in this discussion, but it did not appear appropriate to make the subject of correlation as an isolated subject a major item on the program. Rather, numerous detailed comparisons of results from different sources have been incorporated at appropriate points in the many papers to be presented subsequently.

[redacted]

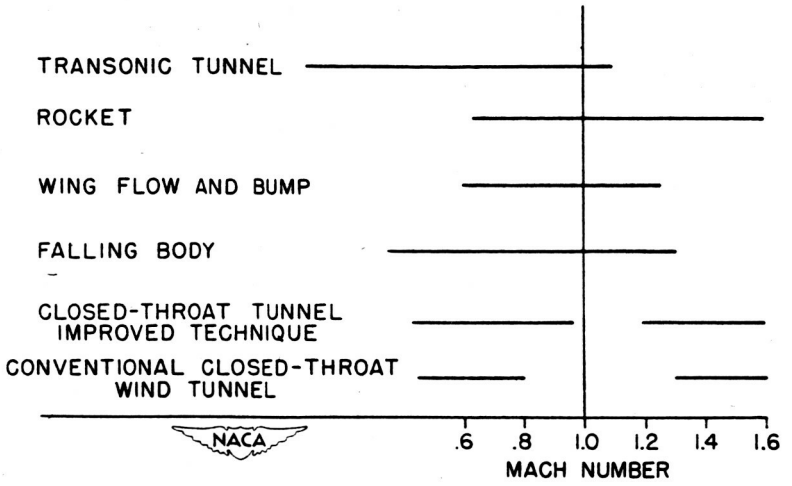


Figure 1.- Speed ranges covered by various transonic research techniques.

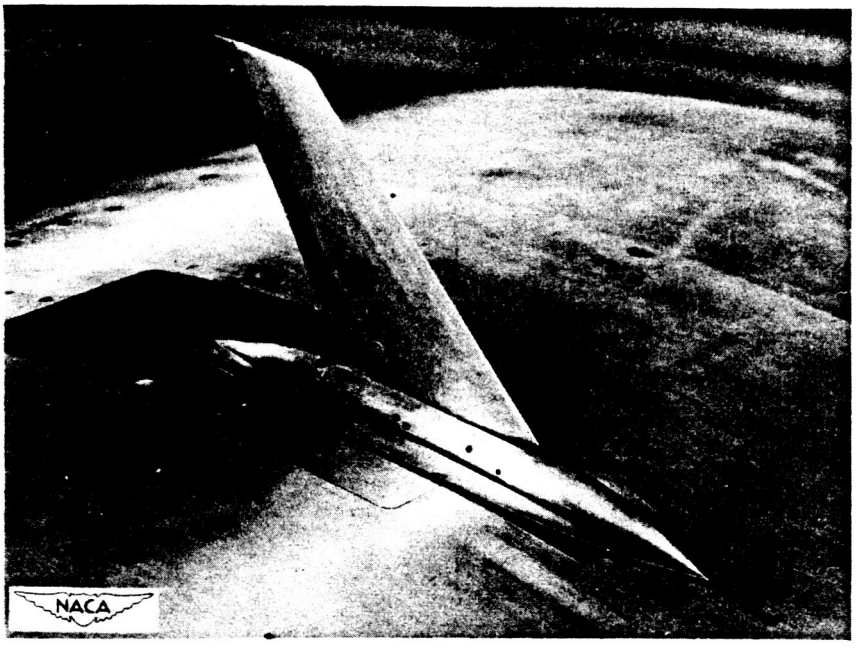


Figure 2.- Semispan model mounted on wind-tunnel bump.

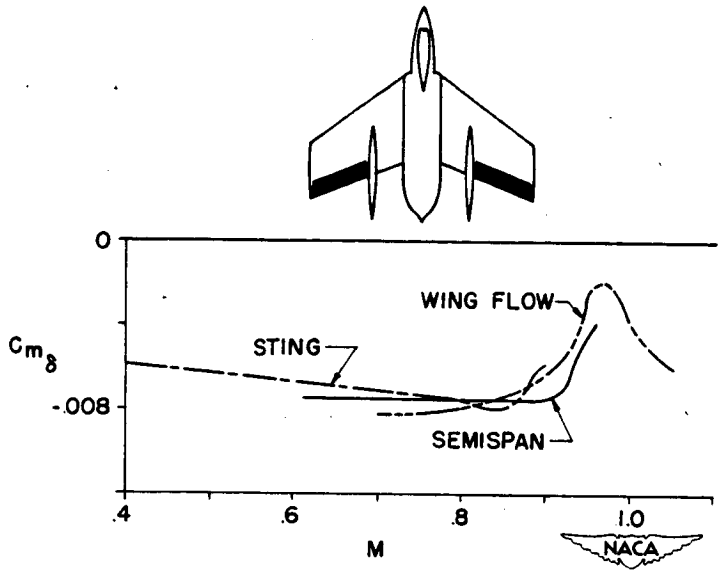


Figure 3.- Variation of C_{m_δ} with Mach number as obtained by three techniques.

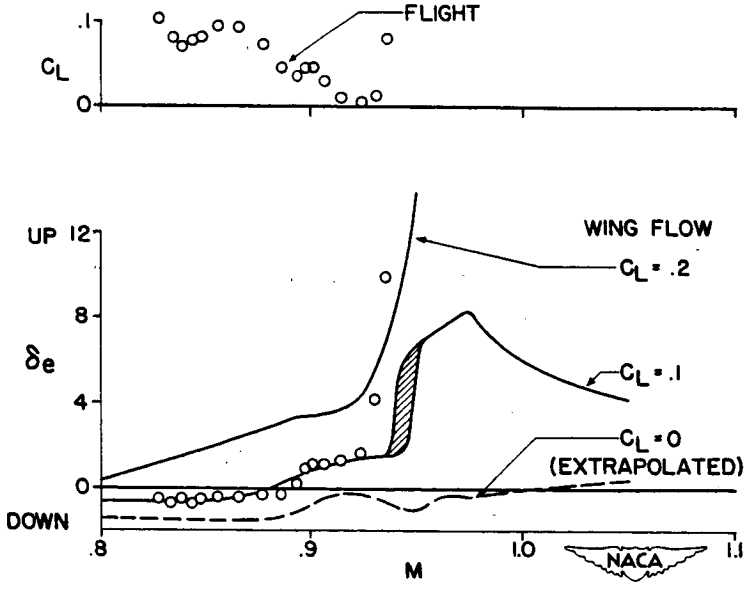


Figure 4.- Effect of lift coefficient on variation of elevator deflection with Mach number.

Preceding page blank

AIRFOILS AND WINGS

Preceding page blank

N65-86453

THE EFFECTS OF SYSTEMATIC VARIATION OF SEVERAL SHAPE PARAMETERS ON THE CHARACTERISTICS OF AIRFOIL SECTIONS AT HIGH-SUBSONIC MACH NUMBERS

By Donald J. Graham

Ames Aeronautical Laboratory

INTRODUCTION

The need for additional information on the characteristics of thin airfoil sections at high subsonic Mach numbers is apparent to all those actively engaged in the design of airplane lifting surfaces for transonic Mach number applications. In the summer of 1948, a systematic program of wind-tunnel investigations to provide some of the desired information was formulated jointly by the NACA and the aircraft industry through their representatives on the NACA Special Subcommittee on Research Problems of Transonic Aircraft Design. The principal objective of this program was the assessment of the effects on the characteristics of thin airfoil sections of systematic variations of trailing-edge angle, leading-edge radius, camber, thickness distribution, and thickness-chord ratio at Mach numbers approaching unity. The purpose of this paper is to summarize briefly the results of the experimental investigations.

Most of the data have been obtained from tests of 6-inch-chord airfoils in the Ames 1- by $3\frac{1}{2}$-foot high-speed tunnel at Mach numbers from 0.3 to a maximum of 0.92 and at Reynolds numbers which varied correspondingly from approximately 1 to 2×10^6.

TRAILING-EDGE ANGLE

There has been much speculation concerning the influence of the trailing-edge angle on the characteristics of airfoil sections at high subsonic Mach numbers, but to date there has been little real information of a systematic nature on the subject. The stimulus for interest in this geometric parameter consists chiefly in reports of poor lift-curve slopes and control-surface-effectiveness characteristics associated with trailing-edge angles greater than 18° (references 1 to 4). In an effort to isolate the effect of this variable and to provide a basis for a more detailed study of the problem, a preliminary

experimental investigation was undertaken in the Ames 1- by $3\frac{1}{2}$-foot high-speed wind tunnel.

The aerodynamic characteristics of a 10-percent-chord-thick airfoil section, both alone and with a 25-percent-chord plain flap, were determined for trailing-edge angles of 6°, 12°, and approximately 18°. The characteristics for the profile without a flap are reported in reference 5. The airfoil thickness distribution was chosen as that of the modified NACA four-digit series. (See reference 6.) This thickness distribution is expressed by a fourth-power equation which permits the trailing-edge portion of the profile to be varied without essentially changing the shape forward of the maximum thickness position. The trailing-edge shapes investigated are illustrated in figure 1.

The only appreciable effects of the trailing-edge-angle variation on the characteristics of the airfoil without a flap were observed in the lift-curve slope, maximum lift-coefficient variation with Mach number, and the drag-divergence Mach number at low lift coefficients. In figure 2, the lift-curve slope $dc_l/d\alpha$ at 0° angle of attack is shown as a function of Mach number M for the three trailing-edge angles. The differences are small and of no particular importance in that the variation with Mach number was not significantly changed. This result is nothing like that of Göthert in reference 1, where a pronounced effect of trailing-edge angle was observed on the lift-curve slope of a 15-percent-chord-thick airfoil section. This would seem to indicate a lessening influence of trailing-edge angle with decreasing thickness-chord ratio.

In figure 3, an improvement in the maximum section lift coefficient $c_{l_{max}}$ at Mach numbers above about 0.7 is seen to accompany a reduction in the trailing-edge angle. Reduction of the trailing-edge angle adversely affected the drag-divergence Mach number M_d of the airfoil section at lift coefficients near zero as is evidenced in figure 4. The difference at zero lift coefficient over the range of angles investigated amounted to approximately 0.04 Mach number. At lift coefficients above 0.2, the difference disappeared.

The effects of changes in trailing-edge angle on the variation with Mach number of the lift effectiveness of a plain flap are shown in figure 5. In this figure, the rate of change of section lift coefficient with flap deflection $dc_l/d\delta$ for deflections from -2° to 6° is shown as a function of Mach number for the three trailing-edge angles and for angles of attack of 0°, 4°, and 6°. In the zero-lift case, an abrupt loss of effectiveness beginning at a Mach number in the vicinity of 0.8 is evident for all trailing-edge angles. The interesting feature of these results is the very small benefit derived from

reduction of the trailing-edge angle even to a value as low as 6°. The only favorable effect of the decrease in trailing-edge angle was the elimination of the reversal of effectiveness indicated for the 18° angle. This result is not too surprising because, from visual observations of the flow field at zero angle of attack and small flap angles, the flap lay entirely within the region of separated flow aft of the compression shock on the airfoil and therefore could develop virtually no lifting pressures.

At the higher angles of attack, reduction of the trailing-edge angle did effect an improvement in the variation of the flap effectiveness with Mach number. It is probable that, had the investigation been extended to encompass larger flap deflections, the beneficial effects of trailing-edge-angle reduction would have been noted even for the lower angles of attack.

From the results of this and free-flight investigations (references 7 and 8), it is fairly obvious that the trailing-edge angle alone is not the governing airfoil-shape parameter in the variation of control-surface effectiveness with Mach number. Satisfactory effectiveness cannot be assured at all lift coefficients merely by holding the trailing-edge angle to a value less than, say, 10° or 12°, which has been tacitly accepted in some quarters as an upper limit for satisfactory characteristics.

LEADING-EDGE RADIUS

An analysis of the characteristics at high Mach numbers of a large number of airfoil sections has indicated the shape of the forward portion of an airfoil to be an important parameter governing these characteristics. To a first order this shape is expressed by the leading-edge radius. In the course of a preliminary investigation (reference 5) of the influence of this parameter, the characteristics of a 10-percent-chord-thick airfoil of the modified NACA four-digit series have been determined for leading-edge radii of 1.10, 0.70, and 0.27 percent of the airfoil chord. The nose shapes investigated are illustrated in figure 6. The leading-edge-radius variation was accomplished without altering the profile aft of the maximum thickness position.

The effect of the variation in leading-edge radius on the lift-curve slope of the airfoil section is shown in figure 7 to be unimportant. Figure 8 demonstrates a small favorable effect of reduction in leading-edge radius on the maximum section lift coefficient at Mach numbers above 0.65. The results shown in figure 9 indicate that Mach numbers of drag divergence were decreased somewhat at low lift

coefficients with decreasing radius. The effects on all these characteristics were considerably smaller than those noted previously for the variation in trailing-edge angle. The pitching-moment characteristics were not significantly affected by the changes in leading-edge radius.

The effects of similar variations of leading-edge radius on 4- and 6-percent-chord-thick sections were not sufficiently important to warrant discussion.

CAMBER

The effects of large camber variation on the characteristics of a 10-percent-chord-thick airfoil section at high Mach numbers have recently been determined from tests of an NACA 64A-series profile cambered for design lift coefficients ranging from 0 to 0.9. In figure 10, the lift-divergence Mach number M_l is plotted as a function of lift coefficient for the various design lift coefficients c_{l_i}. It is obvious that, for applications calling for operating lift coefficients up to 0.5, the symmetrical section would be the most desirable. For lift coefficients greater than 1.0, the sections cambered for design lift coefficients of 0.6 and 0.9 would afford the best characteristics. Similarly, in figure 11, the value of camber in providing a larger range of lift coefficient for favorable drag-divergence characteristics is indicated.

The variation of maximum lift coefficient with Mach number for the various amounts of camber is illustrated in figure 12. At Mach numbers below about 0.6, by virtue of the relatively low test Reynolds numbers, the results cannot be used with assurance in the prediction of large-scale characteristics. Ample evidence exists (reference 9), however, to indicate that at the higher Mach numbers, the influence of Reynolds number on the maximum lift coefficient is small. It is interesting to note that the beneficial effect of camber on the maximum lift coefficient persists throughout the Mach number range of the investigation.

In figures 13 and 14, respectively, are shown the variations with Mach number of the angle of attack for lift coefficients of 0 and 0.9 for the various amounts of camber. The familiar adverse effects of camber on the longitudinal trim characteristics of straight-wing airplanes employing such wing sections are evident here. The variations of angle of attack for intermediate lift coefficients lie within those shown on these two figures. The variation of lift-curve slope with Mach number at the design lift coefficient is shown in figure 15 for each of the cambered sections. It is this unfavorable effect of camber on the lift-curve slope coupled with the previously indicated adverse

lift characteristics for airplane trim (figs. 13 and 14) which makes the cambered sections inferior to the symmetrical profiles for high-speed straight-wing airplanes.

In the case of swept wings, however, the position of camber should be reappraised. The theoretical foundations upon which two-dimensional airfoil data may safely be applied to the design of swept wings are yet to be laid; but sufficient evidence has been obtained to indicate the usefulness of section characteristics in such cases if the stream velocity be considered resolved into components normal and parallel to what might be termed the lifting axes of the wing and the section be considered as that normal to such axes. The lift characteristics of thin symmetrical sections handicap the performance of swept-wing airplanes in both the landing and high-altitude, high-speed flight conditions. Utilization of large amounts of camber in the sections comprising such wings therefore becomes desirable. Furthermore, for swept wings, it is possible that, if the high positive camber desirable for landing and high-speed high-altitude performance is suitably distributed along the span of the wing, the trim changes promoted by the camber will give to an airplane in an overspeed condition a nosing-up tendency in place of the diving tendency noted for the straight-wing airplane. That is, for highly cambered wing tip sections, the lift carried at the tips will be lost (as the lift-divergence Mach numbers of these sections are exceeded) before that of the lower cambered inboard sections and, by virtue of the large longitudinal moment arm of the tip region, a nosing-up moment will be experienced by the airplane. If the nose-up is not too rapid, this characteristic might even be considered a favorable one for a bomber-type airplane.

THICKNESS DISTRIBUTION

Some of the principal questions that have been raised concerning the effects of thickness distribution on section characteristics of thin airfoils are: (a) what is the effect of removing the cusp from the trailing edge of a low-drag airfoil, (b) how do the characteristics of the NACA four-digit-series (conventional) airfoils compare with those of the NACA six-series (low drag) family, and (c) how does changing the position of maximum thickness affect the properties of conventional airfoils? In order to answer these questions, section data were procured for four 10-percent-thick airfoils considered sufficiently representative to permit generalization of the results. The airfoils chosen were the NACA 64-010, 64A010, 0010, and 0010-64. The characteristics of the first two airfoils are reported in reference 10, and those of the latter two in reference 11.

Curves summarizing the lift characteristics are presented in figures 16 to 18. Figure 16 illustrates the variation of lift-curve slope with Mach number. It is immediately apparent that this parameter is unaffected by the presence or absence of a cusped after-profile by a change in the position of maximum thickness from 30 to 40 percent of the chord for the conventional sections, or even by the differences in profile between low-drag and conventional sections. Similar observation can be made with respect to the Mach number of lift divergence (fig. 17). The maximum lift coefficients, however, shown in figure 18, are considerably greater at Mach numbers above 0.7 for the low-drag than for the conventional sections.

The Mach number for drag divergence (fig. 19) has been selected to illustrate the effects of removing the cusp from the low-drag airfoil, of a change in thickness distribution from that of a low-drag to that of a conventional section, and of shifting the maximum thickness position of a conventional section rearward. Although it is apparent that the absence of the cusp has no important effect on the Mach number for drag divergence for 10-percent-thick low-drag airfoils, one may conclude that the uncambered low-drag airfoils are superior in this respect to conventional sections at lift coefficients above 0.4; and also that, for conventional airfoil sections at low lift coefficients, a considerable gain may accrue from shifting the maximum-thickness location rearward.

THICKNESS-CHORD RATIO

Ample evidence has been obtained (references 12 and 13) to indicate the favorable effect of reduction in thickness-chord ratio t/c upon the characteristics of airfoil sections at high Mach numbers. No information has been available, however, on the effects of a systematic reduction of thickness-chord ratio down to 4 percent for a single thickness form. The results of a recently completed investigation of the characteristics of four symmetrical NACA four-digit-series airfoil sections ranging in thickness from 10 to 4 percent of the chord therefore become of interest. The thickness distribution investigated was that of the NACA 00XX-64 family of profiles.

From the variation of lift-curve slope with Mach number shown in figure 20 for the various thickness-chord ratios, significant effects are apparent only at the higher Mach numbers and are what should be expected in that each successive reduction of thickness delays the Mach number at which the lift-curve slope breaks. The trend and magnitude of the differences are somewhat more clearly illustrated in figure 21 which is a plot of the Mach number of lift divergence as a

function of thickness-chord ratio for three lift coefficients. In this figure, it is seen that the increase of lift-divergence Mach number amounts to approximately 0.1 for a reduction in thickness from 10 to 4 percent of the airfoil chord and that this improvement is realized at lift coefficients at least as large as 0.6.

Reduction of maximum thickness below 10 percent of the chord also has beneficial effects on the maximum lift coefficient attainable at the higher subsonic Mach numbers. (See fig. 22.) The reduction in thickness is observed to result in marked improvement at Mach numbers above 0.75. The values obtained at Mach numbers below about 0.6 may possibly suffer from the effects of low scale.

The effect on airfoil drag characteristics of reducing the maximum thickness to values as low as 4 percent of the chord is illustrated by the variation of the Mach number for drag divergence with thickness-chord ratio for two different values of the lift coefficient. (See fig. 23.) For the sacrifice in thickness-chord ratio from 10 to 4 percent the gain in drag-divergence Mach number is relatively small. This result, however, is essentially that which would be predicted from consideration of the critical Mach number variation.

It may be stated, therefore, that, within the range of subsonic Mach numbers investigated, the effects on lift characteristics of reducing the maximum thickness-chord ratio are both large and beneficial. The corresponding effects on drag, although appreciable, may not be sufficiently great in themselves to justify the structural complexity required in the utilization of thickness-chord ratios as low as 4 percent for transonic aircraft.

SUMMARY AND CONCLUSIONS

In summary, the attempt has been made to give a general view of the effects of a systematic variation of five major geometric variables on the more important characteristics of thin airfoil sections at high subsonic Mach numbers. The principal conclusion drawn is that, save for the effect of trailing-edge angle on control-surface effectiveness, camber and maximum thickness are the only shape parameters which decisively influence the characteristics of airfoil sections of 10 percent and less thickness-chord ratio at these Mach numbers. Stated in another manner, given a profile of particular camber and a low thickness-chord ratio, the choice of values for the other shape parameters is of little consequence as far as the high-speed characteristics of the airfoil sections are concerned.



It follows from this reasoning that, in the choice of thickness distribution for an airfoil of 10 percent or less thickness-chord ratio, considerable freedom may be exercised to obtain a desirable characteristic at low speeds without compromising the characteristics at high speeds. The import of this conclusion is illustrated by the example to follow of what was accomplished in this respect in one instance having important significance in the design of swept wings.

It has been found very difficult to provide highly swept wings with adequate maximum lift at low speeds. Camber has been employed to overcome this difficulty but the airfoil sections used have been those thought favorable to the promotion of good performance at high speeds. The sections have accordingly been of the NACA 6-series type with maximum-lift characteristics at low speeds known to be poorer than those of the NACA four-digit series which are characterized by more bulbous nose shapes. It was therefore reasoned that, if it were possible to employ the desired camber on a section of the latter type without seriously penalizing the high-speed characteristics, the low-speed difficulties of the swept wing would be materially lessened.

The work of Nitzberg, Crandall, and Polentz in reference 14, indicated that an NACA 0010 profile cambered for a design lift coefficient of 0.3 with an NACA $a = 1.0$ mean line had characteristics at high speeds which were at least as good in several respects as those of an NACA 64A-series profile of comparable thickness considered to be an optimum section for high Mach number applications. A test to establish the relative merit of the two sections with respect to maximum-lift characteristics at low speeds was therefore made in the Ames 7- by 10-foot tunnel at a Reynolds number of approximately 5×10^6. The results of this test, along with a further evaluation of the characteristics at higher Mach numbers, are presented in figures 24 to 28.

In figure 24, the ratio of maximum section lift coefficient for the NACA four-digit series airfoil to that of the NACA 64A310 section is plotted as a function of Mach number. A gain of approximately 15 percent in the value of the maximum lift coefficient at low speeds would apparently be derived from the use of the NACA four-digit series thickness distribution over that of the NACA 6-series. As would be expected, this gain was not obtained without some sacrifice at higher Mach numbers, but, for the application in mind, it substantially outweighs the loss. The effects on the characteristics of lift-curve slope (fig. 25), angle of attack for the design lift coefficient (fig. 26), and lift-divergence Mach number (fig. 27) at high Mach numbers are of even less importance. In the case of drag-divergence Mach number (fig. 28), the NACA four-digit series section is somewhat inferior to the NACA 6-series section at lift coefficients above 0.4. In the design of swept wings, however, it may often be preferable to accept this penalty in return for improved lift at low speeds.



The significance of the foregoing result can perhaps not be over-emphasized, for it indicates the existence of a field of investigation that may yield answers to some of the vexatious problems of transonic airplane design.

[redacted]

REFERENCES

1. Göthert, B.: German High Speed Wind-Tunnel Results Collected by Dr. B. Gothert, with Comments by W. A. Mair. TN Aero 1684, British R.A.E., August 1945.

2. Stevenson, David B., and Byrne, Robert W.: High-Speed Wind-Tunnel Tests of an NACA 16-009 Airfoil Having a 32.9-Percent-Chord Flap with an Overhang 20.7 Percent of the Flap Chord. NACA TN 1406, 1947.

3. Stevenson, David B., and Adler, Alfred A.: High-Speed Wind-Tunnel Tests of an NACA 0009-64 Airfoil Having a 33.4-Percent-Chord Flap with an Overhang 20.1 Percent of the Flap Chord. NACA TN 1417, 1947.

4. Lindsey, W. F.: Effect of Compressibility on the Pressures and Forces Acting on a Modified NACA 65,3-019 Airfoil Having a 0.20-Chord Flap. NACA ACR L5G31a, 1946.

5. Summers, James L., and Graham, Donald J.: Effects of Systematic Changes of Trailing-Edge Angle and Leading-Edge Radius on the Variation with Mach Number of the Aerodynamic Characteristics of a 10-Percent-Chord-Thick NACA Airfoil Section. NACA RM A9G18, 1949. (Prospective NACA paper.)

6. Stack, John, and Von Doenhoff, Albert E.: Tests of 16 Related Airfoils at High Speeds. NACA Rep. 492, 1934.

7. Sandahl, Carl A.: Free-Flight Investigation at Transonic and Supersonic Speeds of the Rolling Effectiveness of Several Aileron Configurations on a Tapered Wing Having 42.7° Sweepback. NACA RM L8K23, 1949.

8. Sandahl, Carl A., Bland, William M., Jr., and Strass, H. Kurt: Effects of Some Airfoil-Section Variations on Wing-Aileron Rolling Effectiveness and Drag as Determined in Free Flight at Transonic and Supersonic Speeds. NACA RM L9D12, 1949.

9. Spreiter, John R., and Steffen, Paul J.: Effect of Mach and Reynolds Numbers on Maximum Lift Coefficient. NACA TN 1044, 1946.

10. Hemenover, Albert D.: Tests of the NACA 64-010 and 64A010 Airfoil Sections at High Subsonic Mach Numbers. NACA RM A9E31, 1949.

[redacted]

11. Polentz, Perry P.: Comparison of the Aerodynamic Characteristics of the NACA 0010 and 0010-64 Airfoil Sections at High Subsonic Mach Numbers. NACA RM A9G19, 1949.

12. Van Dyke, Milton D., and Wibbert, Gordon A.: High-Speed Aerodynamic Characteristics of 12 Thin NACA 6-Series Airfoils. NACA MR A5F27, Army Air Forces, 1945.

13. Ferri, Antonio: Completed Tabulation in the United States of Tests of 24 Airfoils at High Mach Numbers (Derived from Interrupted Work at Guidonia, Italy, in the 1.31- by 1.74-Foot High-Speed Tunnel). NACA ACR L5E21, 1945.

14. Nitzberg, Gerald E., Crandall, Stuart M., and Polentz, Perry P.: A Preliminary Investigation of the Usefulness of Camber in Obtaining Favorable Airfoil-Section Drag Characteristics at Supercritical Speeds. NACA RM A9G20, 1949. (Prospective NACA paper.)

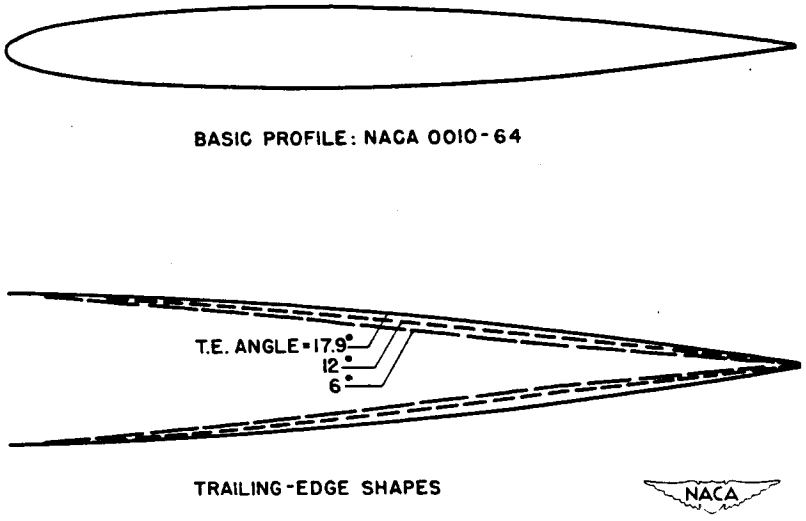


Figure 1.– Basic profile and trailing–edge shapes investigated.

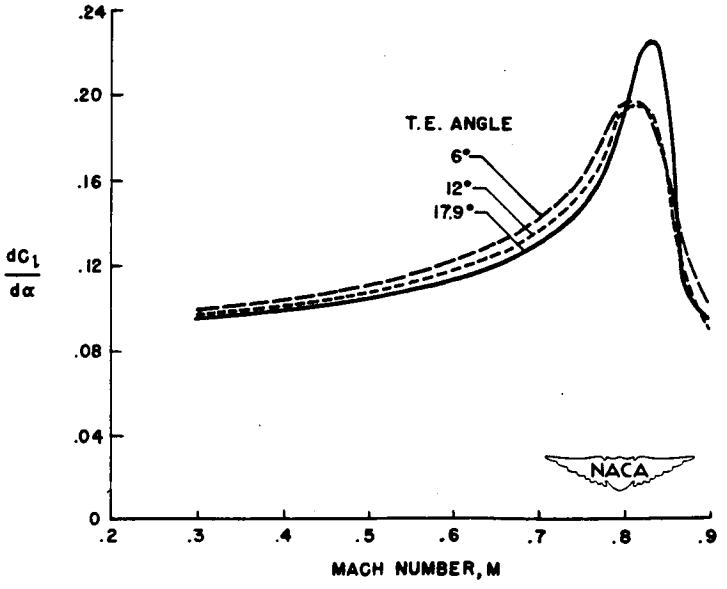


Figure 2.– Effect of trailing–edge angle on the variation of lift–curve slope with Mach number.

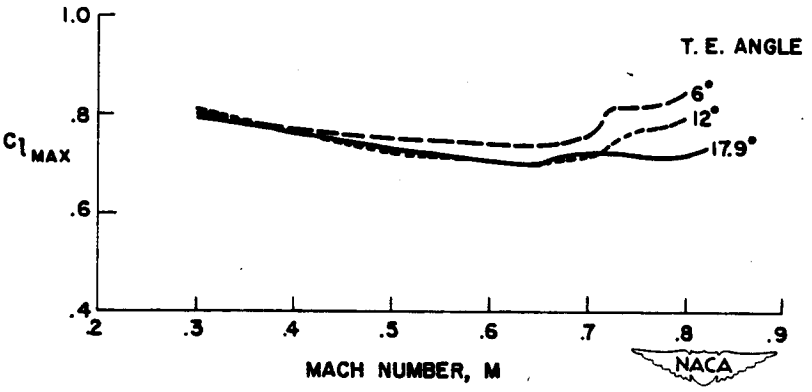


Figure 3.– Effect of trailing–edge angle on the variation of maximum lift coefficient with Mach number.

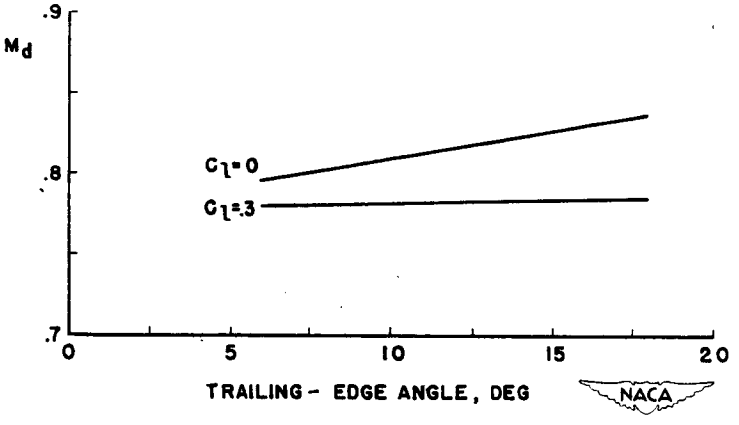


Figure 4.– Effect of trailing–edge angle on drag–divergence Mach number.

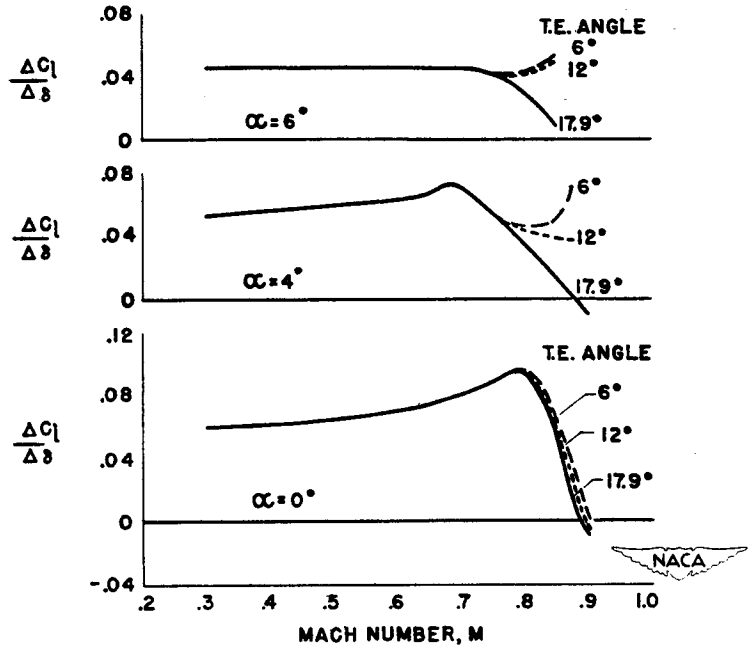


Figure 5.– Effect of trailing-edge angle on the variation of flap effectiveness with Mach number.

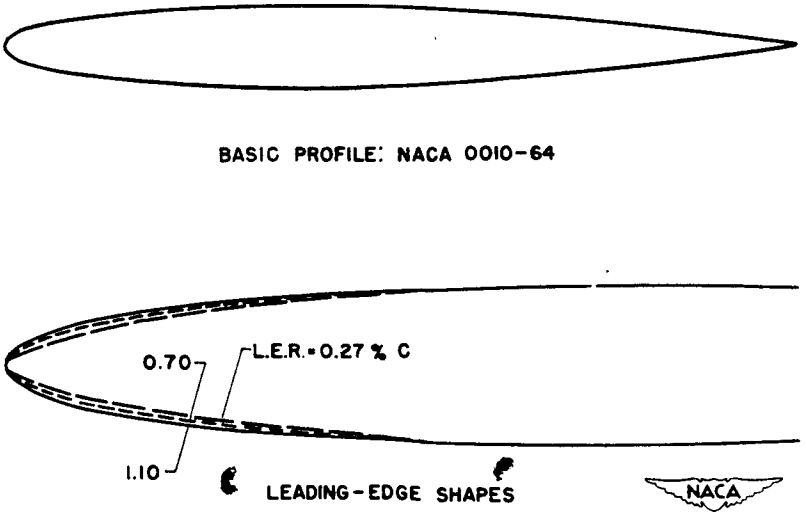


Figure 6.– Basic profile and nose shapes investigated.

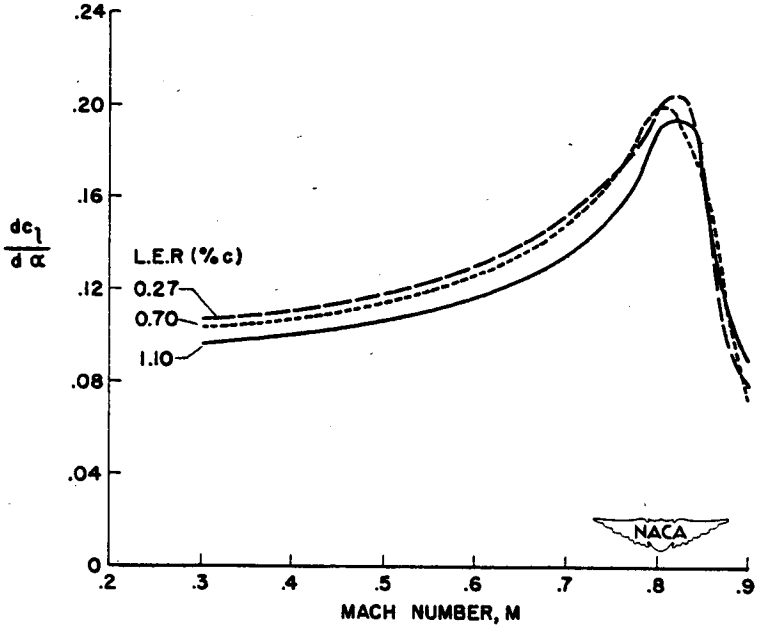


Figure 7.– Effect of leading–edge radius on the variation of lift–curve slope with Mach number.

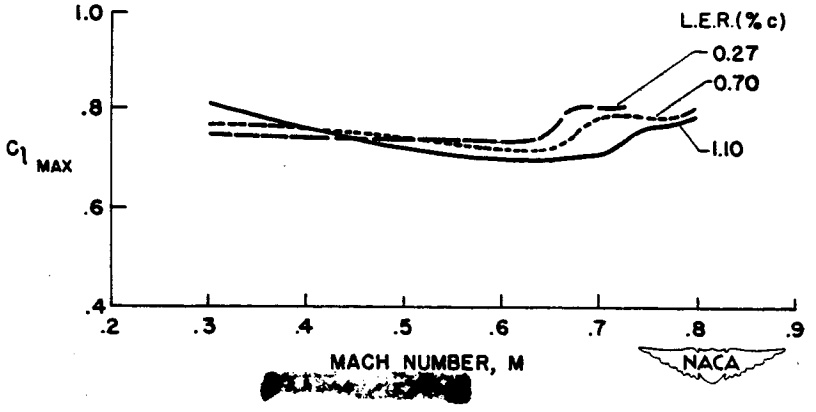


Figure 8.– Effect of leading–edge radius on the variation of maximum lift coefficient with Mach number.

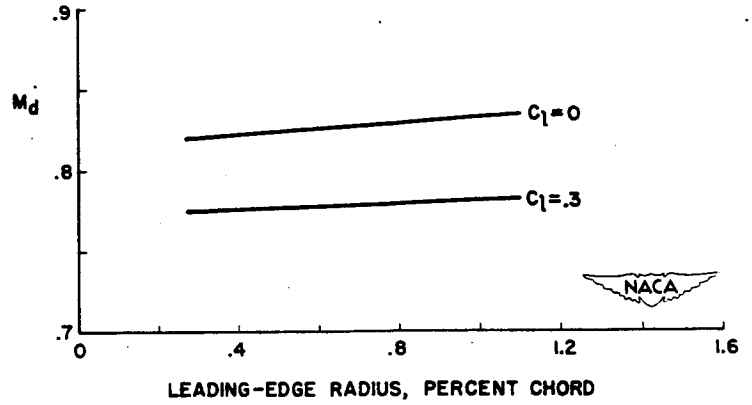


Figure 9.– Effect of leading–edge radius on drag–divergence Mach number.

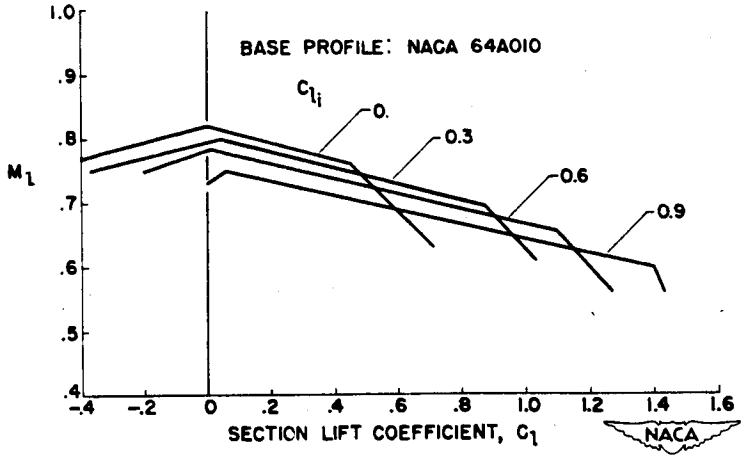


Figure 10.– Effect of camber on the variation of lift–divergence Mach number with lift coefficient.

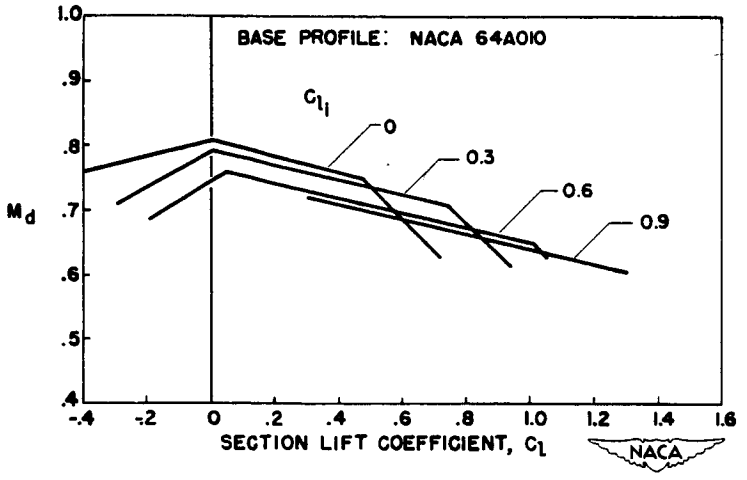


Figure 11.– Effect of camber on the variation of drag-divergence Mach number with lift coefficient.

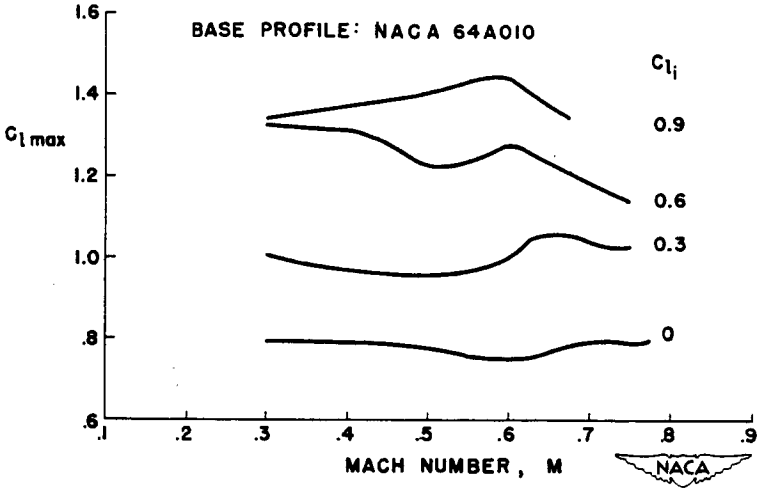


Figure 12.– Effect of camber on the variation of maximum lift coefficient with Mach number.

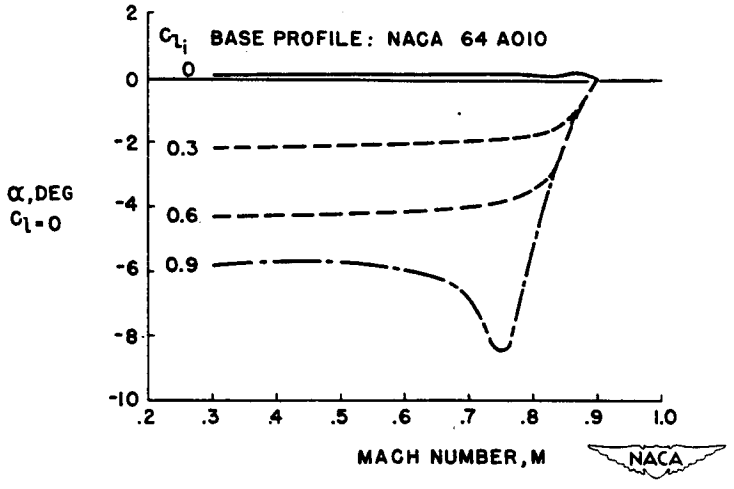


Figure 13.– Effect of camber on the variation with Mach number of the angle of attack for zero lift.

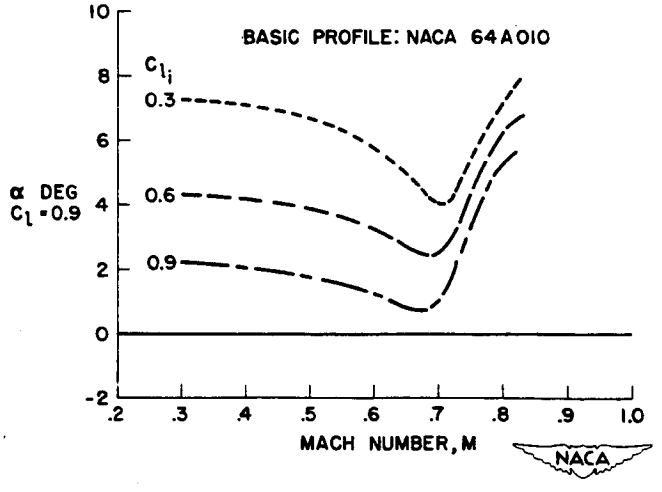


Figure 14.– Effect of camber on the variation with Mach number of the angle of attack for 0.9 lift coefficient.

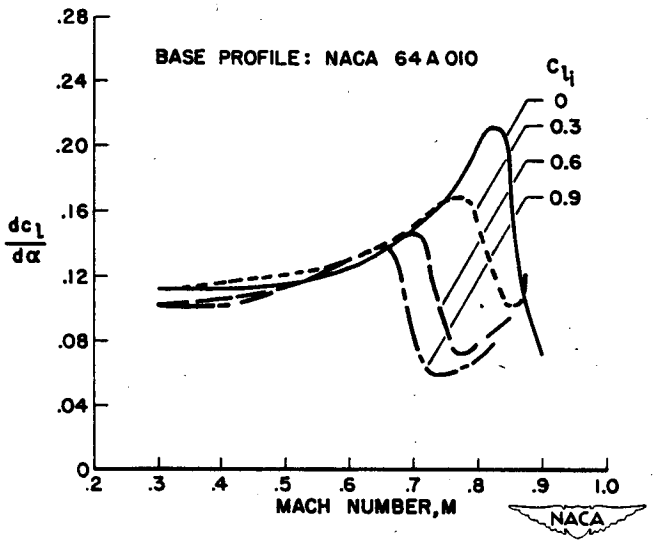


Figure 15.– Effect of camber on the variation with Mach number of the lift–curve slope at the design lift coefficient.

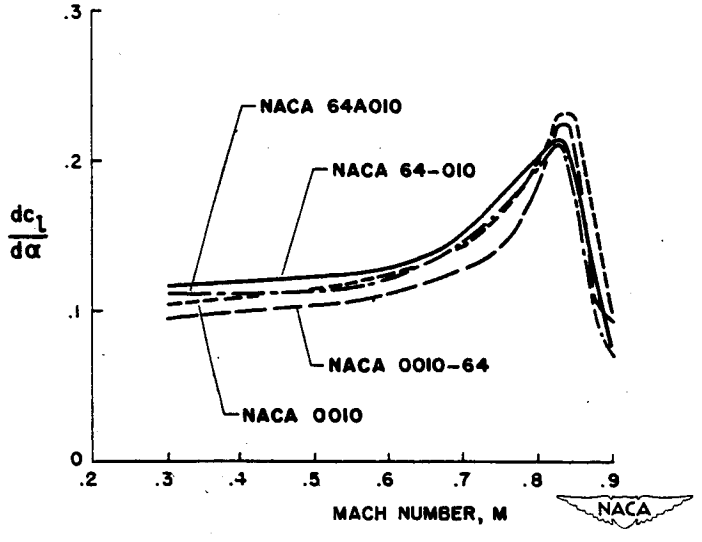


Figure 16.– Effect of thickness distribution on the variation of lift–curve slope with Mach number.

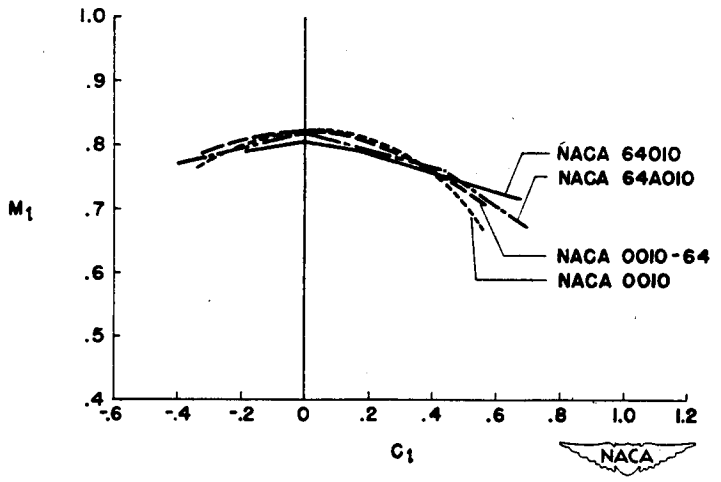


Figure 17.– Effect of thickness distribution on the variation of lift-divergence Mach number with lift coefficient.

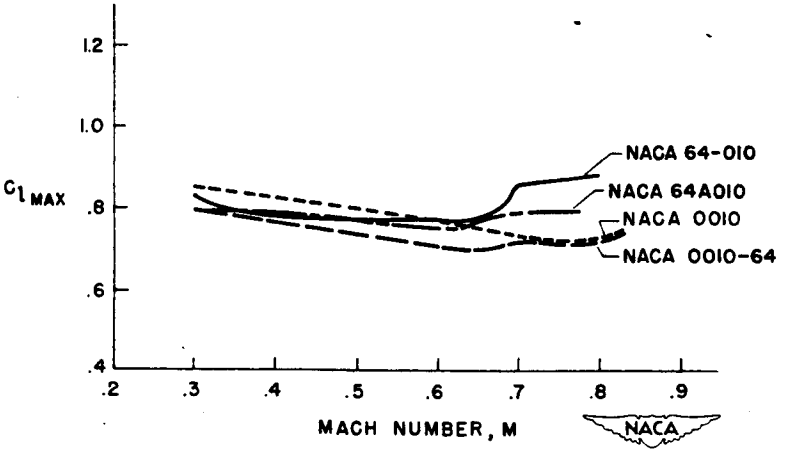


Figure 18.– Effect of thickness distribution on the variation of maximum lift coefficient with Mach number.

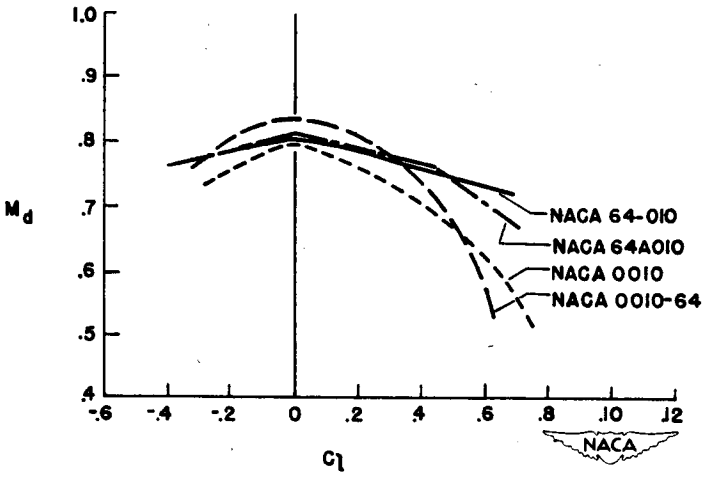


Figure 19.– Effect of thickness distribution on the varitation of drag-divergence Mach number with lift coefficient.

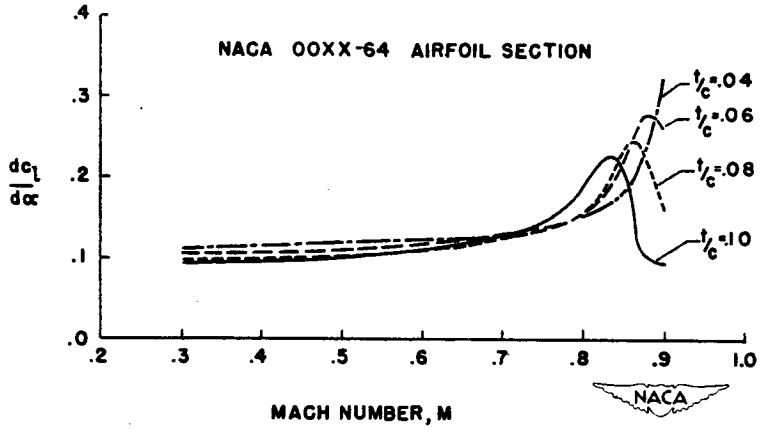


Figure 20.– Effect of thickness–chord ratio on the variation of lift-curve slope with Mach number.

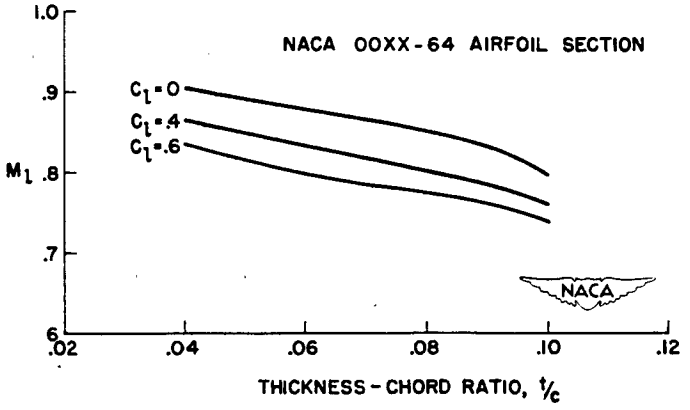


Figure 21.– Effect of thickness–chord ratio on lift–divergence Mach number.

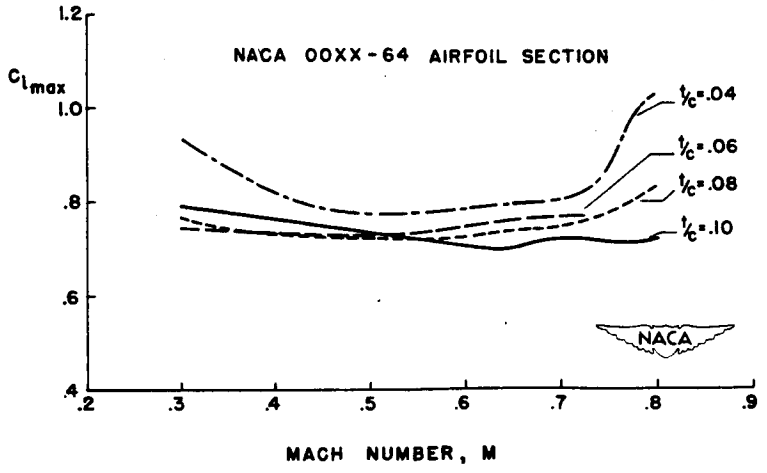


Figure 22.– Effect of thickness–chord ratio on the variation of maximum lift coefficient with Mach number.

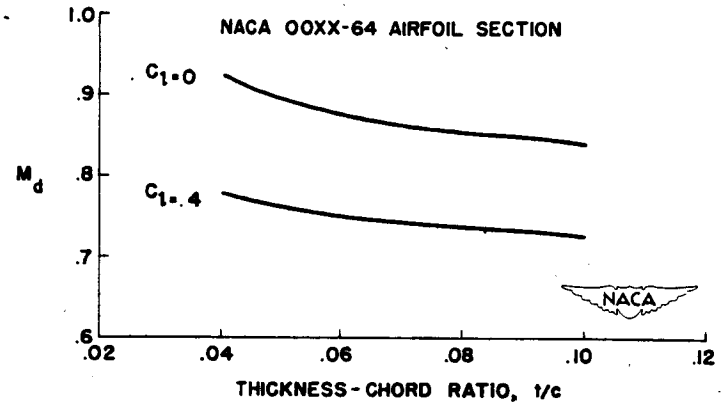


Figure 23.— Effect of thickness—chord ratio on drag-divergence Mach number.

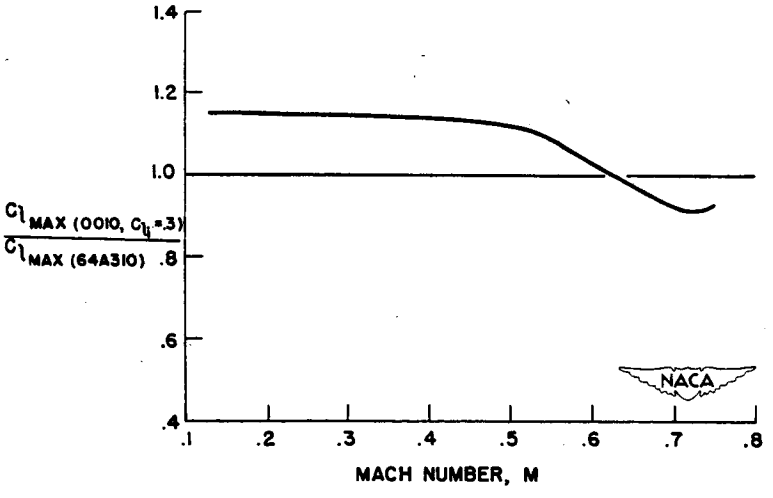


Figure 24.— Comparison of the variation of maximum lift coefficient with Mach number for two equally cambered NACA airfoils differing only in thickness distribution.

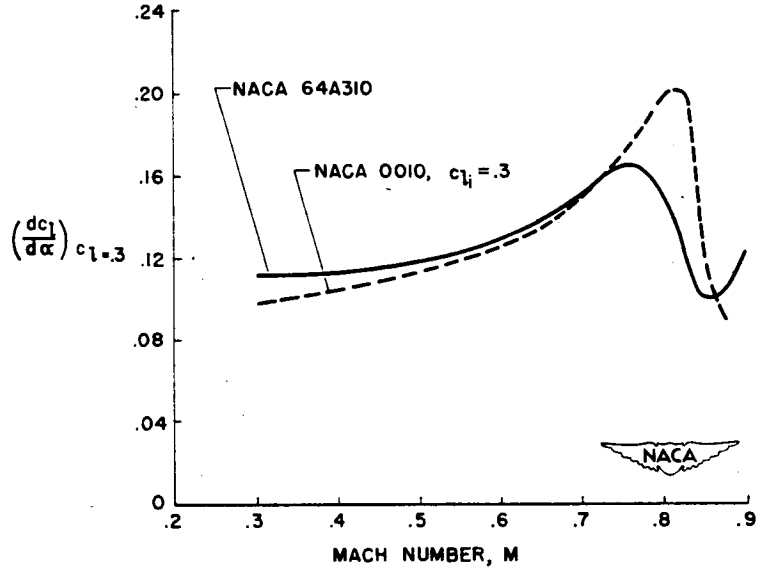


Figure 25.– The variation of lift–curve slope with Mach number for two equally cambered NACA airfoils differing only in thickness distribution.

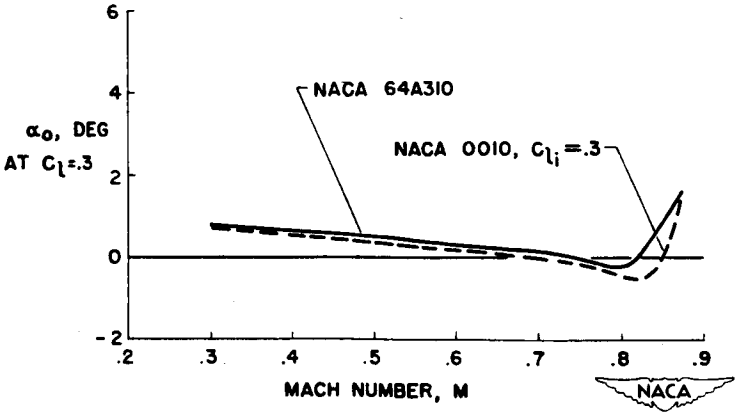


Figure 26.– The variation with Mach number of the angle of attack for the design lift coefficient for two equally cambered NACA airfoils differing only in thickness distribution.

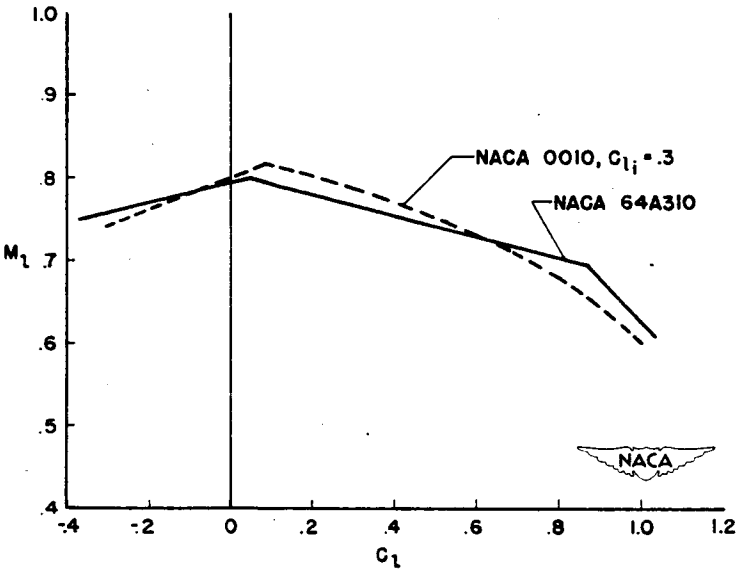


Figure 27.– The variation of lift–divergence Mach number with lift coefficient for two equally cambered NACA airfoils differing only in thickness distribution.

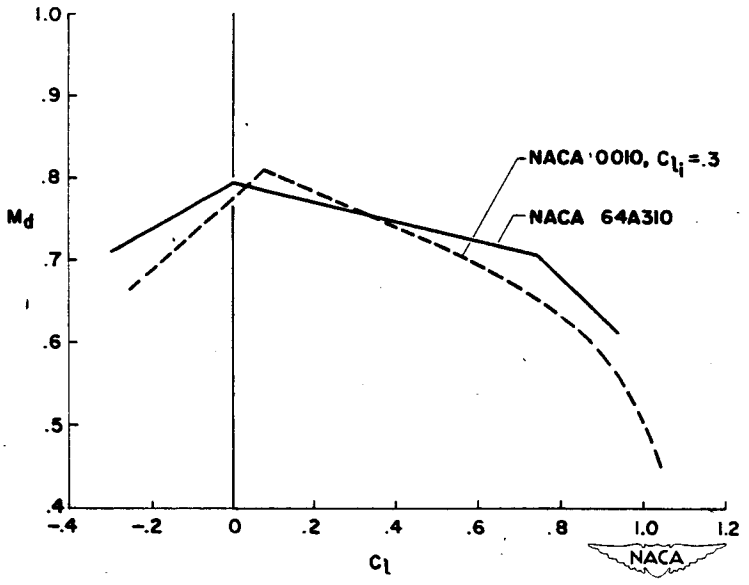


Figure 28.– The variation of drag–divergence Mach number with lift coefficient for two equally cambered NACA airfoils differing only in thickness distribution.

Preceding page blank

N65-86454

PRELIMINARY INVESTIGATION OF AIRFOIL CHARACTERISTICS NEAR M = 1

By Bernard N. Daley and Louis W. Habel

Langley Aeronautical Laboratory

The present paper presents preliminary data from two facilities which have been developed by the NACA to obtain two-dimensional aerodynamic characteristics at Mach numbers near and through unity. One of these facilities is the Langley annular transonic tunnel which is shown schematically in figure 1. Briefly, this tunnel, which was described more thoroughly by Mr. Floyd L. Thompson, consists essentially of a rotor which whirls a model in an annular passage. A relatively low-speed axial flow is induced in the annular passage to control the angle of attack of the model and to prevent the model from operating in its own wake. This tunnel was described in reference 1, but for the tests reported herein the length of the annular passage upstream of the model has been reduced in order to improve the spanwise or radial velocity distributions. Since there are no boundaries to restrain the flow above and below the model, the choking phenomenon is avoided and continuous testing through sonic velocity is possible.

The second research facility developed by the NACA to provide two-dimensional aerodynamic data near a Mach number of 1.0 is the Langley 4- by 19-inch tunnel, shown schematically in figure 2. Air from the atmosphere flows through the entrance nozzle blocks into the test section and flows out through the exit cone. In order to stabilize the flow and to control the speed of the tunnel, an adjustable choking device was installed in the exit cone. The tunnel Mach number can thereby be fixed at any desired value in the range from 0.3 to about 1.0 at Reynolds numbers up to about 1.6 million. Two parallel plates or side walls form fixed boundaries to the flow in the plane of the figure. The test section of the tunnel is sealed from the atmosphere but the flow over the top and bottom of the test section is not restrained by fixed boundaries. An external air passage (not shown) connects the upper with the lower chamber. For two-dimensional models this results in an essentially open-throat tunnel which is not subject to the usual choking limitations of a closed-throat tunnel. Test data are obtained by surface pressure distribution measurements and by wake surveys. Schlieren photographs of the flow are also obtained.

The low-speed jet-boundary correction for a two-dimensional open-throat tunnel (reference 2) has been applied to the lift coefficient or to the angle of attack. The same correction was used at all Mach numbers. Corresponding corrections for drag and moment coefficients are very small and were not applied. No corrections for the effects of Mach number have

[redacted]

been applied because the value of the correction is only 1 percent at Mach numbers of about 0.7 and then becomes indeterminate near a Mach number of 1.0. It is realized that a more detailed study of jet-boundary interference is needed and this work is in progress.

Because of the unconventional design of these facilities, an attempt has been made to establish the validity of the test results by comparing data from one with those of the other and, where possible, with data obtained from theory and from tests in free air.

Figure 3 presents a comparison of a pressure distribution for the NACA 65-110 airfoil obtained in the Langley annular transonic tunnel with one obtained from unpublished flight tests of an unswept full-scale wing having an aspect ratio of about 6. The flight data were measured near the midsemispan station where fuselage interference effects should be small. The comparison is made at a Mach number of 0.79 and a lift coefficient of 0.38. (The term lift coefficient as used herein is more accurately the normal-force coefficient.) The Langley annular transonic tunnel indicates somewhat more positive pressures over the whole surface. However, the important features of the flow, such as shock position and load distribution, are the same for the two test techniques.

In figure 4 is shown a comparison at fixed lift coefficients of the pressure distributions for the NACA 66-006 airfoil obtained in the two research facilities. For the lifting condition, data obtained in the Langley 4- by 19-inch tunnel are at 3° angle of attack and those in the Langley annular transonic tunnel are at 4° angle of attack. The lift-curve slopes obtained from Langley 4- by 19-inch tunnel data agree reasonably well with those obtained from other sources in the Mach number range where comparisons can be made; whereas the slopes from the Langley annular transonic tunnel appear to be too low. In figures 4(a) and 4(b) are shown data at a Mach number of 0.74 for lift coefficients of zero and 0.47. The agreement between the pressure distributions from the two facilities is seen to be excellent when compared on the basis of equal lift coefficients. At a Mach number of 1.00 the shapes of the curves and the loadings experienced in both tests are similar (figs. 4(c) and 4(d)). The difference lies in the general level of the data, the Langley annular transonic tunnel data again being more positive. The general nature of the flow is also indicated by this figure. At $M = 0.74$ the flow is subsonic throughout for both lifting conditions, except for the region ahead of the shock wave on the upper surface when the model is at an angle of attack. The critical pressure coefficient is indicated by the tick. At Mach number 1.00 the pressure distributions at both lifting conditions are fairly smooth and flat, with supersonic velocities over most of the airfoil surface; these distributions indicate that the shock waves on both surfaces have progressed to the trailing edge.

[redacted]

Dr. Guderley has computed the pressure distribution at a Mach number of 1.00 over a profile having a cusped leading edge (reference 3). Recently, in conjunction with Dr. Yoshihara (reference 4), he has extended his original results to apply to a symmetrical double wedge. These are the only theoretical pressure distributions available at a Mach number of 1.0. Figure 5 presents a comparison of their theoretical pressure distribution for a 10-percent-thick wedge and the experimental pressure distributions from the Langley annular transonic tunnel and the Langley 4- by 19-inch tunnel. The angle of attack is 0° and the Mach number is 1.00. The only appreciable differences occur over the forward part of the model, where the general level of the data from the Langley 4- by 19-inch tunnel is somewhat higher than that from the Langley annular transonic tunnel or from the theory. The agreement over the rear half of the model can be slightly improved by applying a correction for the calculated effect of the boundary layer.

These comparisons were all concerned with the pressure distributions at specific Mach numbers. In figure 6 are shown the variations with Mach number of the lift and moment coefficients for the NACA 66-006 airfoil, obtained from both the Langley 4- by 19-inch tunnel and the Langley annular transonic tunnel. The comparison is made at the same angles of attack which were previously shown to give equal lifts. It can be seen that the variations with Mach number are in excellent agreement. At a Mach number of 0.70 the lift coefficient begins to increase with Mach number as a result of the growth of the supersonic flow region beginning near the leading edge on the upper surface of the model. After a peak value is reached at a Mach number of about 0.85, the lift coefficient falls rapidly as the Mach number is increased to 0.95 primarily as a result of the attainment and growth of a supersonic region over the lower surface. At a Mach number of 0.95 the shock waves from both surfaces are almost at the trailing edge, and further increases in Mach number to 1.0 have only a small effect on the lift coefficient. The lift coefficient developed at a Mach number of 1.0 was about the same as that obtained at a Mach number of 0.60 to 0.65. The moment coefficient remained at about zero until a Mach number of 0.80 was reached; then it decreased suddenly and generally remained at this low value throughout the higher speed range.

Figure 7 presents the variation with Mach number of the pressure drag coefficient for the 10-percent-thick wedge at 0° angle of attack. The diamond at a Mach number of 1.0 identifies the theoretical pressure drag computed by Guderley and Yoshihara (reference 4). The plus symbols represent pressure-drag data from the Langley 4- by 19-inch tunnel, and the three circular symbols in the high Mach number range represent the pressure drag obtained from the Langley annular transonic tunnel. The agreement of these experimental values between themselves and with the theory is in general satisfactory.

[redacted]

Figure 8 presents the variation with Mach number of the total drag coefficient of the 4-inch-chord NACA 64A012 airfoil from tests in the Langley 4- by 19-inch tunnel and the drag coefficient obtained by the freely falling body technique for an 8-inch-chord NACA 65_1-012 wing having an aspect ratio of 7.6 (reference 5). At the lower Mach numbers, both sets of the data were taken at nearly the same Reynolds number. The drag indicated by the tunnel tests of a two-dimensional model is slightly higher than that found on the finite span model, as expected. The general agreement of the data is again satisfactory.

In order to illustrate the flow at near-sonic velocities, schlieren photographs obtained in the Langley 4- by 19-inch tunnel are shown in figure 9 for an NACA 64A009 profile at an angle of attack of 3°. The object which appears to protrude from the airfoil surface is outside the tunnel and has no significance to the flow. At a Mach number of 0.91 a normal shock with a forked foot is located at the 70-percent-chord station on the upper surface. The separation which occurs just upstream of the shock leads to a turbulent wake which is much thicker than the model. A shock wave has just formed on the lower surface. As the Mach number is increased to 0.97, the shock waves and separation points move progressively rearward. In figure 10 it is shown that further increases in Mach number to about 1.03 cause a continued rearward progression of the shock waves to the trailing edge of the airfoil. The oblique foot of the upper surface shock tends to disappear and the wake width and pulsations diminish.

Tests of a preliminary nature have recently been completed in the Langley 4- by 19-inch tunnel on several 64A-series airfoils, varying in thickness from 4 to 12 percent. In figure 11(a) are presented the variations with Mach number of the lift-curve slope $dc_l/d\alpha$ of these airfoils. The values of the lift-curve slope for the 4- and 6-percent-thick models at a given Mach number were constant over a lift-coefficient range from 0 to about 0.35. For the 9-percent-thick model and, especially, the 12-percent-thick model, the lift-curve slope changed rapidly with lift coefficient in the upper Mach number range. For these thicknesses two values of lift-curve slope are presented, the generally higher curve applying at lift coefficients of about 0.2 and the lower curve applying at a lift coefficient of 0. At low Mach numbers the thicker airfoils have the higher lift-curve slopes, about 0.13. After an initial increase in this value with Mach number, the lift-curve slope of each of the airfoils decreases very rapidly, the break occurring at Mach number 0.75 for the 12-percent-thick model and progressively increasing to Mach number 0.95 for the 4-percent-thick model. After this decrease, the lift-curve slopes for the 9- and 12-percent-thick airfoils increase with Mach number. At Mach numbers near unity the lift-curve slopes of all of the airfoils tend to converge at a value only slightly below the low-speed value.

[redacted]

The similarity law for transonic flow (reference 6 and 7) can be put into a form which states that the lift-curve slope of a basic airfoil section should vary inversely with the 1/3 power of the airfoil thickness ratio at $M = 1.0$. The similarity law applies at other near-sonic Mach numbers, provided the similarity parameter $\frac{1 - M}{(0.01t)^{2/3}}$ is held constant. In figure 11(b) are presented the experimental and theoretical variations of lift-curve slope with airfoil thickness for several values of the similarity parameter. For values of this parameter of 0.06, 0.20, 0.40, and 0.60, the Mach numbers are around 0.98, 0.96, 0.93, and 0.89, respectively. The experimental data for lifting conditions are presented as individual symbols. The curves present the theoretical extrapolation to higher values of airfoil thickness, starting at the experimental value for the 4-percent-thick airfoil or for the lowest thickness for which data are presented. The comparison of experiment with theory is reasonably good for the low thickness ratios, but at the larger thicknesses the correlation becomes poor. In general, best agreement with the theory would be expected for the thinner sections and for Mach numbers close to unity, that is, for small values of the similarity parameter.

Corresponding variations of the stability derivative $dc_{m_{c/4}}/dc_l$ with Mach number are presented in figure 12(a). At Mach numbers up to about 0.8 a small positive value is generally indicated. At somewhat higher Mach numbers the stability derivative is erratic in its variation with Mach number. The values for the thicker airfoils vary most with Mach number. The data for the 12- and 9-percent-thick airfoils are again shown as two curves, the upper curves in this case corresponding to $c_l = 0$ and the lower curves to $c_l = 0.2$. At Mach numbers near 1.0, the values of $dc_{m_{c/4}}/dc_l$ for all of the airfoils fall in a range from 0 to -0.15.

The similarity law states that airfoil lift and moment coefficients vary in the same manner with airfoil thickness, for fixed values of the similarity parameter. Therefore, no change in stability derivative $dc_{m_{c/4}}/dc_l$ with thickness should occur. Figure 12(b) presents the theoretical and experimental variation of stability derivative with airfoil thickness for several values of the similarity parameter. Experimental data are shown by the symbols, which are defined on the right. The theoretical extrapolations, the dashed lines, start at the experimental data for the 12-percent-thick model. Good correlation was obtained for similarity parameters of 0.20 and 0.60, but the correlation was poor for other values of the parameter. The erratic nature of the correlation is not understood.

The zero-lift drag coefficients of these same airfoils are compared in figure 13. At subcritical Mach numbers the drag coefficients of all airfoils have about the same value. The Mach number of the drag rise increases from about 0.80 for the 12-percent-thick model to about 0.90 for the 4-percent-thick model. At a Mach number near 1.0 the drag coefficient of the 12-percent-thick model is about five times as great as that of the 4-percent-thick model. The transonic similarity law indicates that the drag coefficient should vary as the 5/3 power of the thickness ratio for constant values of the parameter $\frac{1 - M}{(0.01t)^{2/3}}$. In figure 13(b) are compared the experimental and theoretical variations of drag coefficient with airfoil thickness. The theoretical estimations, the dashed lines, start at the experimental data for the 12-percent-thick model. The correlation of theory and experiment at other thicknesses is in general excellent.

In figure 14 is presented the variations of drag coefficient with Mach number for the various airfoils at 3° angle of attack. At this angle of attack the 9-percent-thick airfoil has the lowest drag coefficient at all except the lowest Mach numbers. The 4- and 6-percent-thick models probably have poor flow characteristics near the leading edge which cause their relatively high drag coefficients at this angle of attack. The data of figure 14(b) compare the theoretical and experimental variations of drag coefficient with airfoil thickness. This chart was constructed in a manner similar to the previous figure, except that the angle of attack of the experimental points had to vary with airfoil thickness to satisfy the requirements of the similarity law at finite lift coefficients. The agreement of experiment and theory is not so good for this lifting condition as it was at zero angle of attack.

Considerable effort has been directed at devising methods whereby the pressure distribution over an airfoil could be estimated in the transonic region. The recent theoretical work of Guderley (references 3 and 4) provides accurate zero-lift pressure distributions for two specific profile families, but comparably accurate solutions for the general case have not yet been found. In the absence of precise methods, various semiempirical schemes have been advanced to provide rough indications of airfoil characteristics in the sonic region. One of the assumptions which is often involved in these methods is that the expansion in the local supersonic region of the airfoil follows the Prandtl-Meyer theory for pure supersonic flow. The two-dimensional data now available afford a means of checking the accuracy of these approximate methods. Figure 15(a) shows that if the Prandtl-Meyer theory is applied, beginning at the sonic point, the resulting pressures are more negative than actually measured on an NACA 16-308 airfoil. If applied at the 50-percent-chord station, however, better agreement results. Mr. J. P. Mayer of the Langley

Aeronautical Laboratory has recently evolved a simple semiempirical method which includes the assumption of Prandtl-Meyer flow from estimated sonic points (reference 8). As illustrated in figure 15(b) the predicted pressure distribution is considerably in error. However, in the few cases for which comparisons have been made (reference 8), the integrated lift and drag coefficients are generally in approximate agreement with experimental results.

In conclusion, it may be stated that satisfactory correlation of the data from the various experimental techniques and theory in the region of sonic velocity was obtained at zero lift. The agreement of pressure distributions obtained from the two new facilities and flight tests was reasonably good when compared on the basis of equal lift coefficients. The experimental decrease in lift-curve slope with increasing thickness in the sonic region was in approximate agreement with the transonic similarity law for the thinner sections. The increase in drag coefficient with thickness in this speed range was also predicted with reasonable accuracy by the similarity law, especially for the nonlifting conditions.

REFERENCES

1. Habel, Louis W.: The Langley Annular Transonic Tunnel and Preliminary Tests of an NACA 66-006 Airfoil. NACA RM L8A23, 1948.

2. Glauert, H.: Wind Tunnel Interference on Wings, Bodies and Airscrews. R. & M. No. 1566, British A.R.C., 1933.

3. Guderley, G.: Singularities at the Sonic Velocity. Tech. Rep. No. F-TR-1171-ND, Air Materiel Command (Wright Field), Nov. 1947. (Preprint.)

4. Guderley, G., and Yoshihara, Hideo: The Flow over a Wedge Profile at Mach Number 1. (Proposed Tech. Rep., Air Materiel Command (Wright Field).)

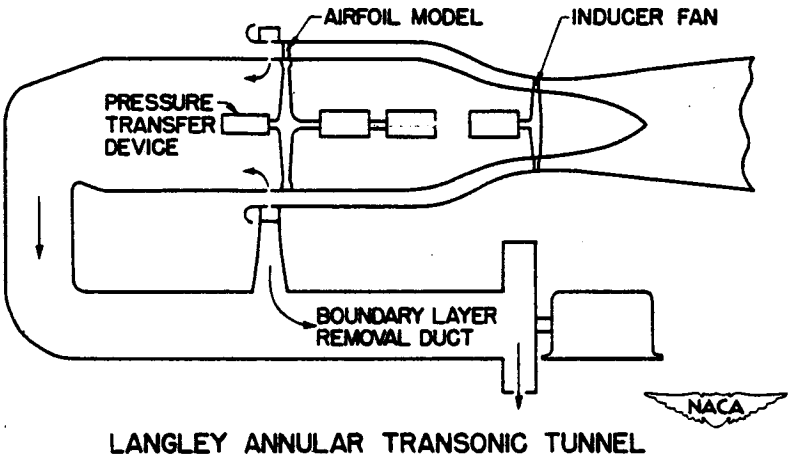
5. Thompson, Jim Rogers, and Mathews, Charles W.: Measurements of the Effects of Thickness Ratio and Aspect Ratio on the Drag of Rectangular-Plan-Form Airfoils at Transonic Speeds. NACA RM L7E08, 1947.

6. Von Kármán, Theodore: The Similarity Law of Transonic Flow. Jour. Math. and Phys., vol. XXVI, no. 3, Oct. 1947, pp. 182-190.

7. Kaplan, Carl: On Similarity Rules for Transonic Flows. NACA Rep. 894, 1948.

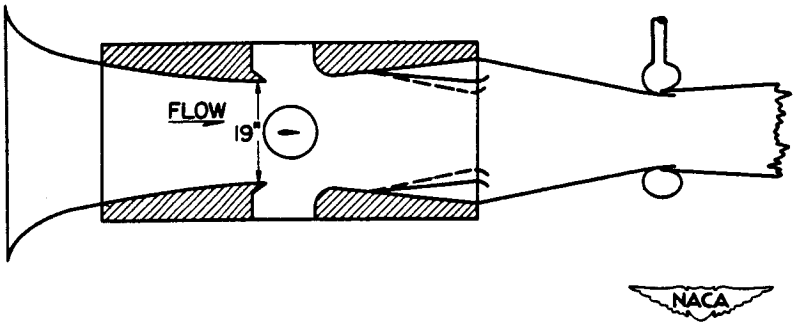
8. Mayer, John P.: Estimation of Lift and Drag of Airfoils at Near Sonic Speeds and in the Presence of Detached Shock Waves. NACA RM L8L07, 1949.

[redacted]



LANGLEY ANNULAR TRANSONIC TUNNEL

Figure 1.– Schematic view of the Langley annular transonic tunnel.



LANGLEY 4-X 19-INCH TUNNEL

Figure 2.– Schematic view of the Langley 4– by 19–inch tunnel.

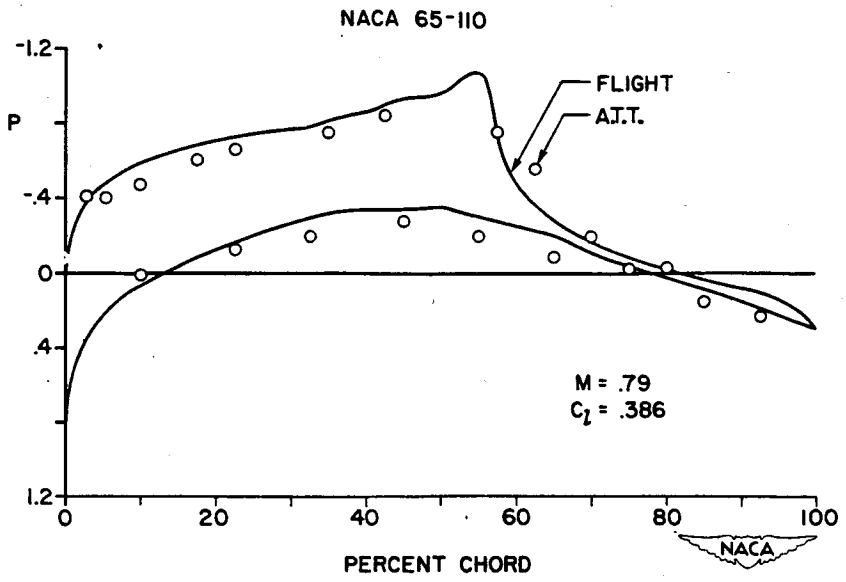


Figure 3.— A comparison of the pressure distribution obtained from full-scale flight tests of a straight wing with that obtained in the Langley annular transonic tunnel

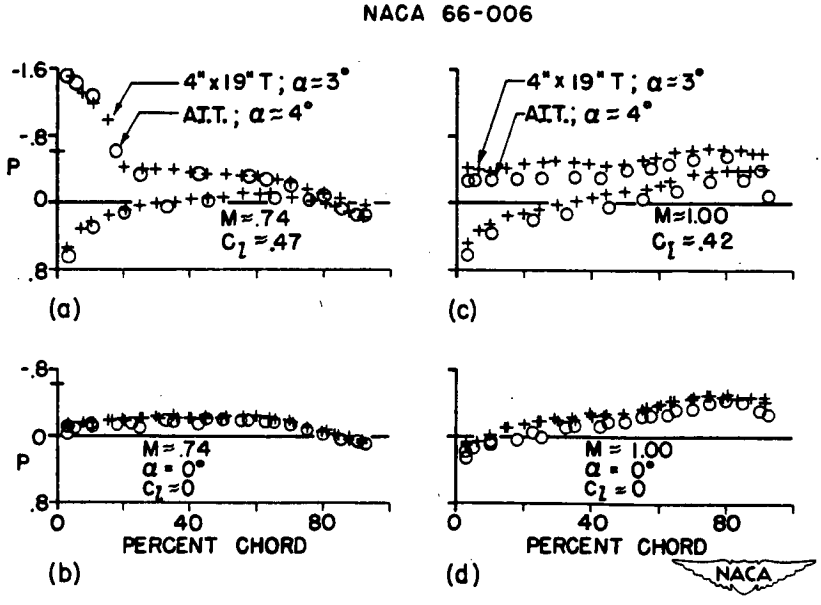


Figure 4.— A comparison of pressure distributions obtained in the Langley annular transonic tunnel with those obtained in the Langley 4— by 19-inch tunnel.

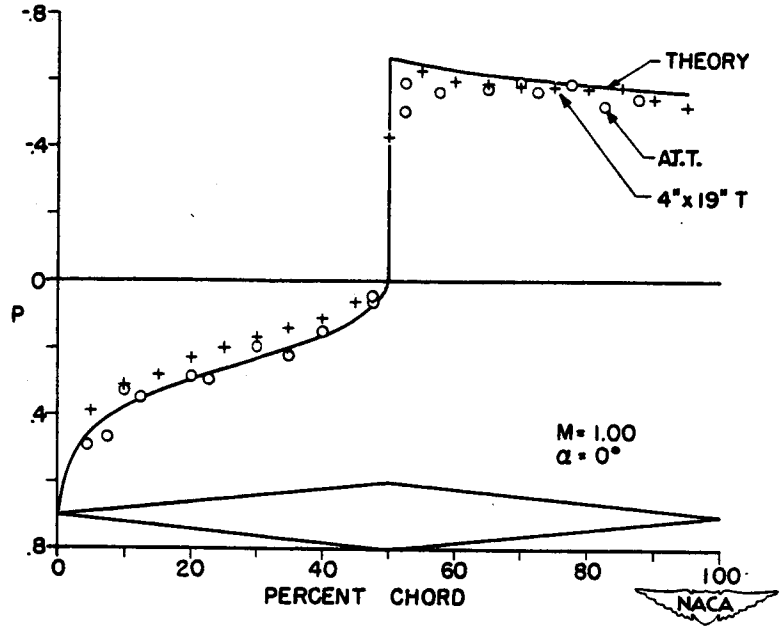


Figure 5.— A comparison of theoretical and experimental pressure distributions over a wedge airfoil at a Mach number of one.

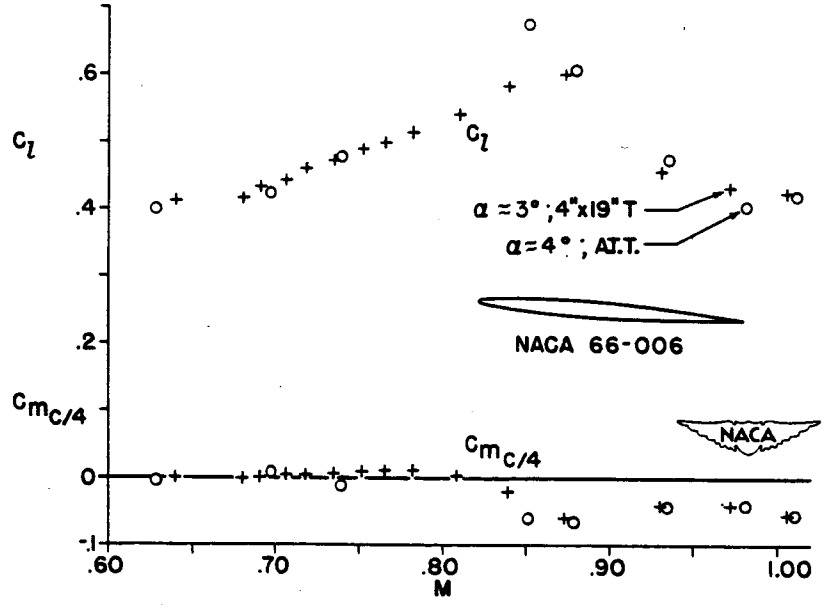


Figure 6.— Variation with Mach number of the lift and moment coefficient obtained in the Langley annular transonic tunnel and the Langley [illegible] by 19-[illegible] tunnel.

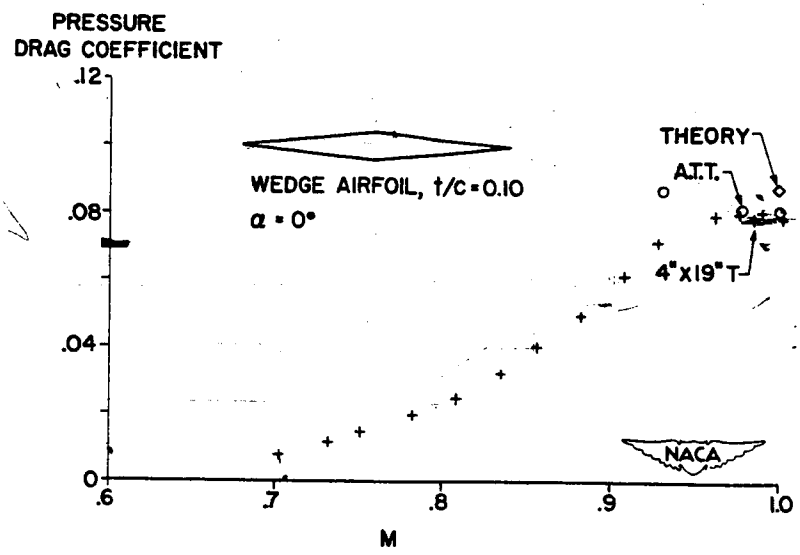


Figure 7.– The pressure drag coefficient of the wedge airfoil, as obtained from theory and experiment.

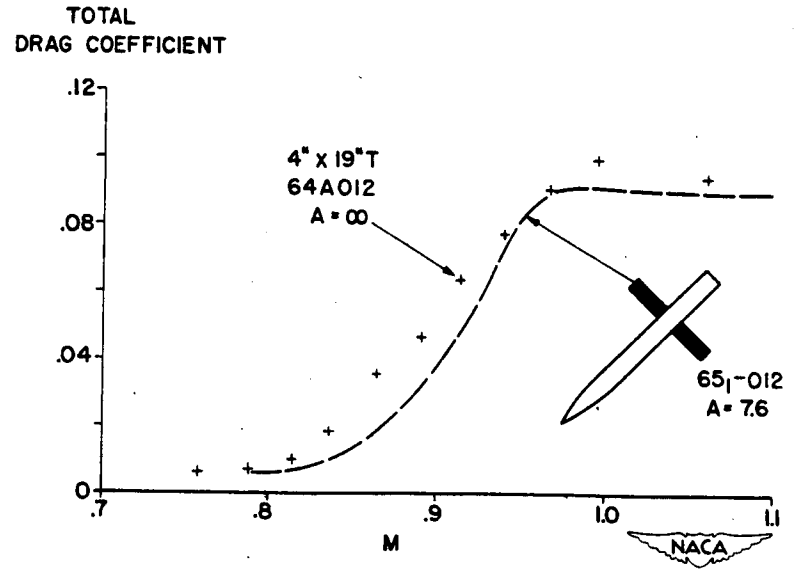


Figure 8.– Variation with Mach number of the drag coefficient obtained from two-dimensional tunnel tests and from measurements by the freely falling body technique.



M=.91 M=.97

Figure 9.— Schlieren photographs of the flow over the NACA 64A009 profile at 3° angle of attack.



M=.99 M=1.03

Figure 10.— Schlieren photographs of the flow over the NACA 64A009 profile at 3° angle of attack.

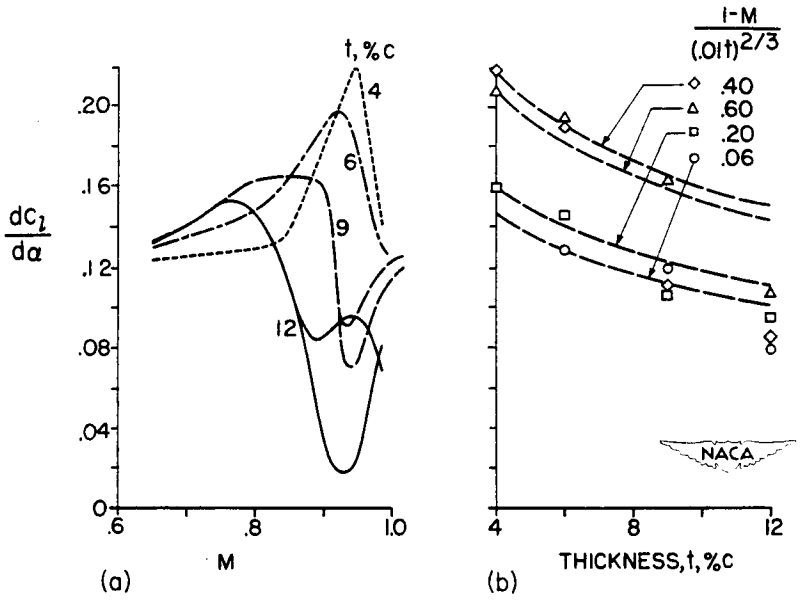


Figure 11.— Variation with Mach number of the lift-curve slope of several NACA 64A-series airfoils.

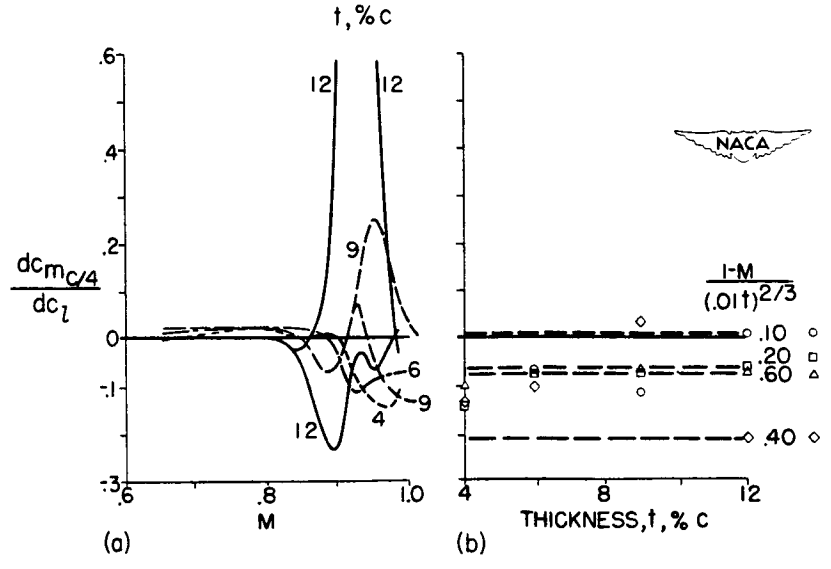


Figure 12.— Variation of the stability derivative with Mach number and airfoil thickness for several NACA 64A-series airfoils.

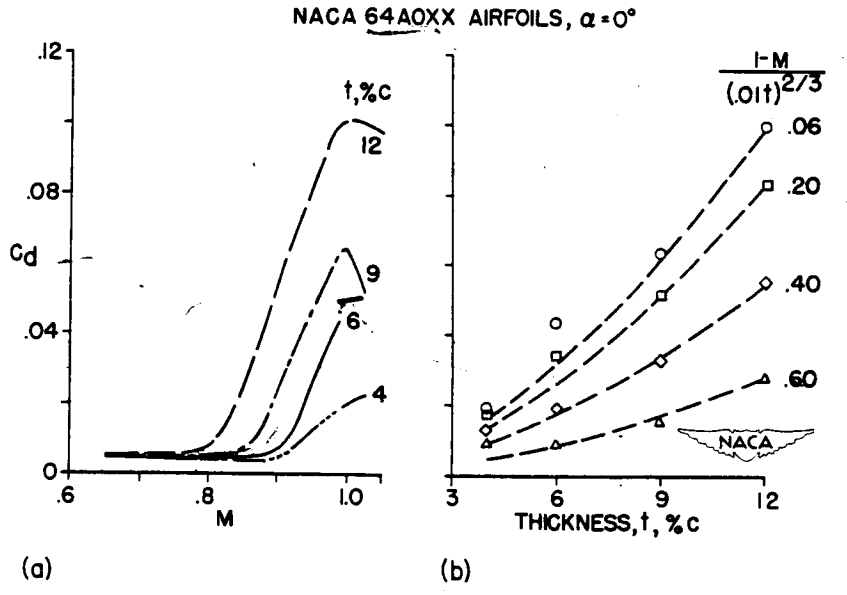


Figure 13.— Variation of the drag coefficient at zero lift with Mach number and airfoil thickness for several NACA 64A-series airfoils.

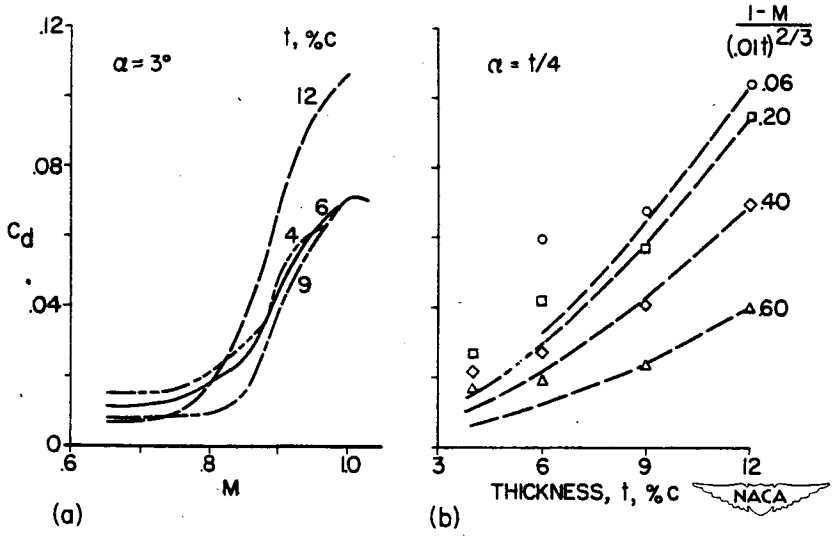


Figure 14.— Variation of the drag coefficient at positive lift coefficient with Mach number and airfoil thickness for several NACA 64A-series airfoils.

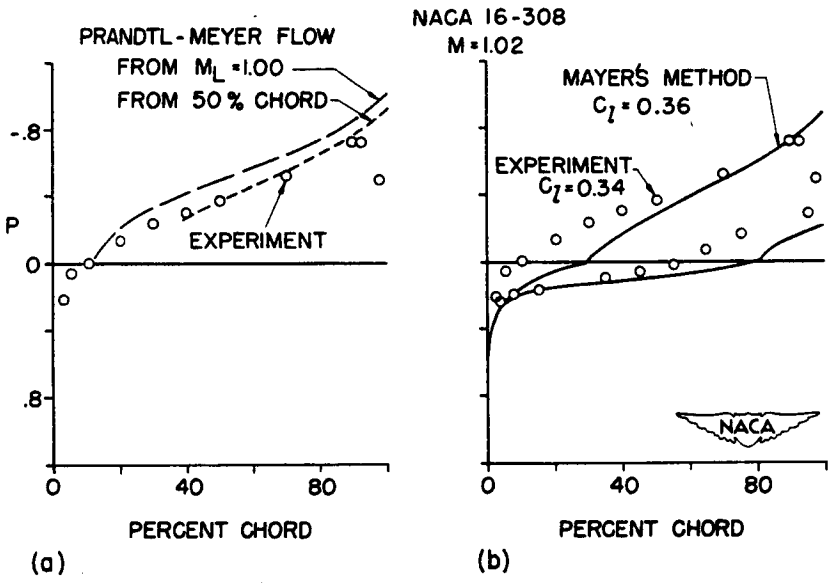


Figure 15.– Estimations of airfoil pressure distributions.

CONFIDENTIAL

THE LIFT, DRAG, AND PITCHING-MOMENT CHARACTERISTICS OF WINGS AND WING-BODY COMBINATIONS IN THE TRANSONIC SPEED RANGE

By Edward C. Polhamus

Langley Aeronautical Laboratory

INTRODUCTION

The effects of plan form and profile on the lift, drag, pitching-moment, and downwash and wake characteristics of wings and wing-body combinations have recently been obtained from systematic transonic investigations.

Because of the limited time available, a discussion of all the results obtained to date cannot be presented. Instead, some of the more interesting results, both published and unpublished, pertaining to the lift, drag, and pitching-moment characteristics at transonic speeds will be discussed in the present paper. Other characteristics and applications of data to design problems will be presented in later papers.

The principal sources of the information that will be presented are the high-speed tunnels, covering the lower end of the transonic range up to Mach numbers of 0.9 to 0.95, the transonic-bump and wing-flow techniques and the rocket-propelled and free-fall methods all of which cover the entire transonic range.

LIFT CHARACTERISTICS

The effect of sweepback on the variation of the lift-curve slope with Mach number from the results of transonic-bump tests of a systematic series of wings (references 1 to 4) is illustrated in figure 1. The wings were of aspect ratio 4, taper ratio 0.6, and had NACA 65A006 airfoil sections placed parallel to the plane of symmetry. Also presented are the subsonic theoretical values obtained by applying the three-dimensional Prandtl-Glauert transformation to the Weissenger modified lifting-line theory for swept wings (reference 5). The results in the subsonic range are in very good agreement with the theory and indicate that sweep decreases both the lift-curve slope and its variation with Mach number. Increasing

the sweep also increases the Mach number at which the lift force break occurs and eliminates the rather irregular variation of the lift-curve slope with Mach number beyond the force break that occurs for the unswept wing. In the supersonic range the lift-curve slope decreases with Mach number and the transonic-bump results appear to fair into the unpublished results obtained at a Mach number of 1.37 in the Langley 6-inch supersonic tunnel.

The variation of the lift-curve slope with Mach number for an aspect ratio 4 delta wing (reference 6) is also presented. This wing has a leading-edge sweep of 45° and the quarter-chord line has approximately 37° of sweep with an NACA 65A006 airfoil section placed parallel to the plane of symmetry. The results indicate that the delta wing has a slightly lower lift-curve slope throughout the Mach number range and a slightly higher force-break Mach number than does the 35° swept wing. To avoid confusion between the rather large number of curves the theoretical curve for the delta wing is not shown, however, it is in good agreement with the test results.

The effect of aspect ratio on the variation of the lift-curve slope with Mach number is shown in figure 2. The two solid curves were obtained from the results of transonic bump tests of two unswept wings of 4-percent thickness (references 7 and 8) and the two dashed curves from tests in the Langley 8-foot high-speed tunnel of two unswept wings of 10-percent thickness (reference 9). The high-speed-tunnel results were obtained by subtracting the fuselage-alone results from the wing-fuselage results and therefore include the wing-fuselage interference. The results indicate that a decrease in aspect ratio from 4 to 2 is accompanied by a decrease in lift-curve slope and a decrease in the variation with Mach number. For both thickness ratios, decreasing the aspect ratio from 4 to 2 increased the Mach number for force break by about 0.05. Decreasing the aspect ratio also decreased the abruptness of the force break. The variation of the lift-curve slope with Mach number for the 4-percent-thick aspect-ratio-2 wing is so slight that the incorporation of sweep would not be expected to appreciably improve the lift characteristics. The difference between the lift-curve slope of the 4- and 10-percent-thick wings below the force-break Mach number is probably due to the wing-fuselage interference that is included in the data for the 10-percent-thick wing.

Figure 3 illustrates the effect of thickness ratio on the variation of the lift-curve slope with Mach number. All the data presented were obtained from transonic-bump tests (references 1, 7, 10, and 11) except those for the 10-percent-thick unswept wing which were obtained from results from the Langley 8-foot high-speed tunnel (reference 9). Decreasing the thickness ratio increases the Mach number for force break and decreases the abruptness of the force

break for both the swept and unswept wing. Thinning the wing tended to eliminate the "bucket" type of variation with Mach number above the force break that occurs for thick wings. Thickness had little effect at low subsonic Mach numbers or at supersonic Mach numbers above about 1.1.

In order to summarize the effect of aspect ratio and thickness ratio on the variation of the lift-curve slope with Mach number above the force break for unswept wings figure 4 has been prepared. In addition to the data already presented some additional data from high-speed tunnel tests are summarized (references 12, 13 and unpublished data). The loss of lift that occurs in the "bucket" type variation of lift-curve slope with Mach number is plotted against the thickness ratio for several aspect ratios. The results indicate that either a decrease in aspect ratio or thickness ratio results in a decrease in the loss in lift in the "bucket." Although it is not illustrated, sweeping the wing also decreases the loss of lift in the "bucket" as was illustrated by figure 1.

DRAG CHARACTERISTICS

Drag at zero lift.- The effect of thickness ratio and sweepback on the drag at zero lift is illustrated in figure 5. The data were obtained from unpublished rocket tests of untapered wings of aspect ratio 3.7. The top portion of the figure shows the effect of decreasing the thickness ratio from 9 percent to 6 percent on the drag of the 45° sweptback wing. The results indicate that decreasing the thickness ratio increased the Mach number for the drag rise and decreased the drag above the rise by approximately 50 percent. The bottom portion of the figure shows the effect of decreasing the thickness from 9 to 6 and 3 percent on the drag of the unswept wing. Decreasing the thickness ratio increased the drag-rise Mach number and had a very pronounced effect in decreasing the rate of drag rise. In the supersonic range a decrease in thickness from 9 percent to 3 percent caused a decrease in drag of about 70 percent. The drag near a Mach number of 1.0 was calculated for the 6- and 3-percent-thick unswept wings by using the experimental drag of the 9-percent-thick unswept wing and the transonic similarity rule (reference 14). The agreement for the 6-percent-thick wing is good but the theory underestimates the drag of the 3-percent-thick wing. The fact that the similarity rule underestimates the drag for thin wings has also been observed in two-dimensional investigations. Also shown in figure 5 is the effect of sweeping the wing back 45° for thickness ratios of both 9 and 6 percent. The results indicate that sweep increases the drag-rise Mach number and decreases the rate of rise. Above the drag rise, 45° sweep d[redacted] drag by about 60 percent.

These wings have also been tested with different airfoil section profiles and the results are summarized in figure 6. All the sections were 9 percent thick and included low-drag, circular-arc and double-wedge profiles. The effect of profile on the drag at zero lift of the unswept wing is shown in the bottom portion of the figure. The results indicate that profile has a rather large effect on the unswept wing and to a Mach number of about 1.1 the double wedge had the highest drag while above a Mach number of about 1.2 it had the lowest drag. The top portion of the figure illustrates the effect of profile on the sweptback wing and the results indicate that the effect of profile is less for this wing. However, it is interesting to note that for the sweptback wing the effect of profile is the reverse of that for the unswept wing with the low-drag section having the highest drag in the lower Mach number range and the lower drag in the higher Mach number range.

The effect of taper ratio is illustrated by figure 7. Three different taper ratios were tested by the rocket technique on a wing of aspect ratio 4 with the 50-percent-chord line swept back 50° and with a 6-percent-thick double-wedge airfoil section. The drag coefficient at zero lift is plotted against Mach number for the three taper ratios and the results indicate that tapering the wing increases the drag up to a Mach number of about 1.3. At a Mach number of 1.0 the fully tapered wing had about twice the drag of the wing with a taper ratio of 0.67. However, above a Mach number of about 1.3 the fully tapered wing had the lowest drag. Although increasing the taper increases the drag in the transonic range, the reduction in thickness ratio made possible by the increase in taper can be beneficial. This effect is illustrated in figure 8. The top portion of the figure presents the results obtained from two free-fall models of aspect ratio 4 with the 50-percent-chord lines swept back 45° (reference 15 and unpublished data). Both wings have approximately the same strength, one being untapered with a thickness ratio of 7.1 percent while the other had a taper ratio of 0.2 and a thickness ratio of 2.2 percent. The drag of the wings was measured by means of strain-gage balances mounted inside the fuselage and the results indicate that above a Mach number of about 1.0 the drag of the thin tapered wing is less than that of the thick untapered wing, being about 50 percent less at a Mach number of about 1.15. Actually, to have the same strength, the tapered wing should have had a thickness ratio of about 3.0 percent and the drag of the thin tapered wing would then be approximately 35 percent less than the thick untapered wing at a Mach number of 1.15. However, when the drag of the wing-fuselage combination was measured, it was found that the thin tapered wing was better only above a Mach number of about 1.1 and that the improvement was very slight, as illustrated

in the bottom portion of the figure. Below a Mach number of about 1.1 the thick untapered wing had the lower drag and it was found that this is due to the fact that the thick wing had a favorable effect on the fuselage drag while the thin wing had no effect on the fuselage drag. An airplane configuration, however, would probably have the wing mounted in a more forward position and the results show that moving the thick untapered wing forward caused a large increase in total drag which was found to be due to an unfavorable effect of the wing on the drag of the fuselage. Since the thin tapered wing had no effect on the fuselage drag when in the rearward position it should have very little, if any, effect in the forward position. Therefore, it appears that for a configuration with the wing at or ahead of the maximum-diameter position of the fuselage the drag will be less for the tapered wing if the reduction in thickness is utilized. Another point in favor of the tapered wing is that less exposed area can probably be used because of the larger carry-over of lift across the fuselage associated with the larger root chord.

Drag due to lift.- In figure 9 the effect of aspect ratio on the drag due to lift of an unswept wing with an NACA 65A004 airfoil section at a Mach number of 1.0 as obtained from transonic-bump tests (references 7 and 8) is presented. The wings were of aspect ratio 2 and 4 and the results indicate, as do subsonic theory and experimental results, that the drag due to lift of the wing with aspect ratio 2 is greater than that of the wing with aspect ratio 4. However, when the drag was compared with the theory for full leading-edge suction $\left(C_L^2/\pi A\right)$, it was found that the experimental drag was about twice that given by the theory. With no leading-edge suction the resultant force will be normal to the chord line rather than the relative wind and the induced drag will be given by $C_L \tan \alpha$ and the wing with the lower lift-curve slope will have the higher drag. The experimental drag was almost as high as that given by the zero-leading-edge suction theory, and it therefore appears that these thin wings with relative sharp leading edges are developing very little leading-edge suction.

The effect of sweepback on the drag due to lift at a Mach number of 1.02 for wings of aspect ratio 4 and taper ratio 0.6 with NACA 65A006 airfoil sections tested on the transonic bump (reference 16) is illustrated in figure 10. The results indicate that increasing the sweepback increases the drag due to lift, the 60° wing having about twice the drag of the unswept wing; although the theory for full leading-edge suction indicates little effect of sweep. This increase in drag with increasing sweep is due to the large loss of leading-edge suction that was discussed previously. The lift-curve slope of the 60° swept wing is about one-half that for the unswept wing at a Mach number of 1.02 and with zero leading-edge

suction the resultant force at a given lift coefficient would be tilted rearward at an angle that is about twice that of the unswept wing. Inasmuch as sweep causes large increases in the drag due to lift, it appears that airplane configurations that are required to operate at moderate or high lift coefficients might be more efficient if unswept thin wings are employed. However, there is evidence that the drag due to lift of swept wings can be improved somewhat by the use of camber and twist (reference 17).

A comparison of the drag due to lift at a Mach number of 1.0 for an aspect-ratio-4 delta wing (reference 6) with the drag for two swept wings of aspect ratio 4 and taper ratio 0.6 (references 2 and 3) is presented in figure 11. All three wings had NACA 65A006 airfoil sections placed parallel to the plane of symmetry. The drag due to lift of the delta wing is approximately 30 percent greater than that for the 35° swept wing which had approximately the same sweep of the quarter-chord line as the delta wing. The drag of the delta wing is also slightly higher than that of the 45° swept wing.

The effect of a fuselage on the drag due to lift is illustrated by figure 12. In this figure the drag due to lift is plotted against lift coefficient for the wing alone and the wing-fuselage combination at two different Mach numbers for both an unswept and a swept wing (references 1 and 3). The results indicate that the fuselage decreases the drag due to lift. This effect also is probably due to the loss in leading-edge suction on these thin wings. The fuselage increases the lift-curve slope and, therefore, at a given lift coefficient the angle of attack is less for the wing-fuselage combination and a reduction in drag is realized.

PITCHING-MOMENT CHARACTERISTICS

Figure 13 illustrates the large changes in the variation of the pitching-moment characteristics with Mach number associated with combined changes in plan form and thickness ratio. The data were obtained from the results of wing-flow tests (reference 18) on two wing-fuselage combinations representing the unswept and swept versions of a specific airplane configuration. The data are presented in the form of pitching-moment coefficient plotted against lift coefficient for several Mach numbers. The unswept, aspect-ratio-5, 12-percent-thick wing had a large forward shift of the aerodynamic center between Mach numbers of 0.7 and 0.9 followed by a large rearward shift as the Mach number was increased to 1.05. The pitching-moment curve at a Mach number of 0.9 was very nonlinear. However, when a low-aspect-ratio sweptback wing with a thickness ratio of 10 percent

was incorporated the pitching-moment curves were very linear and there was a gradual rearward movement of the aerodynamic center with increasing Mach number. For these thick wings the improvement in the pitching-moment characteristics is probably due primarily to sweep and aspect ratio.

In order to illustrate the effect of aspect ratio alone on the pitching-moment characteristics, figure 14 has been prepared. The two wings, one of aspect ratio 4.2 and the other of aspect ratio 2, had NACA 65-110 airfoil sections and were unswept. The data were obtained from tests in the Langley 8-foot high-speed tunnel (reference 9) and include the wing-fuselage interference. The wing of aspect ratio 4.2 had a large forward movement of the aerodynamic center as the Mach number was increased from 0.7 to 0.9 while the wing of aspect ratio 2 had only a slight forward movement with increasing Mach number.

The effect of thickness ratio on the pitching-moment characteristics of a 45° swept wing of aspect ratio 6 in combination with a fuselage is presented in figure 15 for several Mach numbers from results obtained by the transonic-bump technique (references 10 and 11). The results for the 9-percent-thick wing are presented in the left-hand half of the figure while the results for the 6-percent-thick wing are presented on the right-hand half of the figure. The 9-percent-thick wing had a large forward shift of the aerodynamic center in the low lift range as the Mach number was increased from 0.93 to 1.0. At a Mach number of 1.15 the aerodynamic center in the low lift range returned to the position it occupied at a Mach number of 0.93. However, the variation of the aerodynamic center with Mach number for the 6-percent-thick wing is much more gradual. For both wings an increase in Mach number had the effect of decreasing the unstable variation of the pitching moments at the higher lift coefficients.

Figure 16 shows the effect of sweep on the pitching-moment characteristics at several Mach numbers for 6-percent-thick wings of aspect ratio 4 in combination with a fuselage as obtained by transonic-bump tests (references 1 and 3). Also presented is a comparison at a Mach number of 0.88 of the bump data with unpublished data obtained from Langley high-speed 7- by 10-foot tunnel and the agreement is fairly good. The results indicated that there were no abrupt changes in the pitching-moment characteristics for either of these thin wings. For the unswept wing the aerodynamic center moved gradually rearward as the Mach number was increased. The swept wing had an even more gradual movement of the aerodynamic center with Mach number in the low lift range but had a larger variation in the higher lift range.

CONCLUSIONS

In conclusion some of the more important results discussed can be summarized as follows:

Thickness ratio appears to be the most important factor as far as the lift characteristics are concerned, and for a thin low-aspect-ratio wing little benefit could be expected from sweep.

Both increases in sweep and decreases in thickness ratio have large beneficial effects on the drag at zero lift; however, an increase in sweep is accompanied by a large increase in the drag due to lift. Decreasing the taper ratio increased the drag at zero lift, but from structural considerations a thinner section can probably be used with a tapered wing and an improvement in the drag might then be obtained.

Decreasing the thickness ratio had a large beneficial effect on the pitching-moment characteristics and an increase in sweep and a decrease in aspect ratio had a beneficial effect on thick wings. For thin wings, however, no abrupt changes in the pitching-moment characteristics with Mach number occurred for either the swept or unswept wing.

REFERENCES

1. Goodson, Kenneth W., and Morrison, William D., Jr.: Aerodynamic Characteristics of a Wing with Unswept Quarter-Chord Line, Aspect Ratio 4, Taper Ratio 0.6, and NACA 65A006 Airfoil Section. Transonic-Bump Method. NACA RM L9H22, 1949.

2. Sleeman, William C., Jr., and Becht, Robert E.: Aerodynamic Characteristics of a Wing with Quarter-Chord Line Swept Back 35°, Aspect Ratio 4, Taper Ratio 0.6, and NACA 65A006 Airfoil Section. Transonic-Bump Method. NACA RM L9B25, 1949.

3. Weil, Joseph, and Goodson, Kenneth W.: Aerodynamic Characteristics of a Wing with Quarter-Chord Line Swept Back 45°, Aspect Ratio 4, Taper Ratio 0.6, and NACA 65A006 Airfoil Section. Transonic-Bump Method. NACA RM L9A21, 1949.

4. King, Thomas J., Jr., and Myers, Boyd C., II: Aerodynamic Characteristics of a Wing with Quarter-Chord Line Swept Back 60°, Aspect Ratio 4, Taper Ratio 0.6, and NACA 65A006 Airfoil Section. Transonic-Bump Method. NACA RM L9G27, 1949.

5. DeYoung, John: Theoretical Additional Span Loading Characteristics of Wings with Arbitrary Sweep, Aspect Ratio, and Taper Ratio. NACA TN 1491, 1947.

6. Sleeman, William C., Jr., and Becht, Robert E.: Aerodynamic Characteristics of a Delta Wing with Leading Edge Swept Back 45°, Aspect Ratio 4, and NACA 65A006 Airfoil Section. Transonic-Bump Method. NACA RM L9G22a, 1949.

7. Myers, Boyd C., II, and Wiggins, James W.: Aerodynamic Characteristics of a Wing with Unswept Quarter-Chord Line, Aspect Ratio 4, Taper Ratio 0.6, and NACA 65A004 Airfoil Section. Transonic-Bump Method. (Prospective NACA paper)

8. Polhamus, Edward C., and Campbell, George S.: Aerodynamic Characteristics of a Wing with Unswept Quarter-Chord Line, Aspect Ratio 2, Taper Ratio 0.78, and NACA 65A004 Airfoil Section. Transonic-Bump Method. (Prospective NACA paper)

9. Wright, John B., and Luoma, Arvo A.: Longitudinal Stability and Control Characteristics at High Subsonic Speeds of 2 Models of a Transonic Research Airplane with Wings and Horizontal Tails of Aspect Ratios 4.2 and 2. (Prospective NACA paper)

10. Goodson, Kenneth W., and Few, Albert G., Jr.: Aerodynamic Characteristics of a Wing with Quarter-Chord Line Swept Back 45°, Aspect Ratio 6, Taper Ratio 0.6, and NACA 65A006 Airfoil Section. Transonic-Bump Method. NACA RM L9I08, 1949. (Prospective NACA paper)

11. Spreemann, Kenneth P., Morrison, William D., Jr., and Pasteur, Thomas B., Jr.: Aerodynamic Characteristics of a Wing with Quarter-Chord Line Swept Back 45°, Aspect Ratio 6, Taper Ratio 0.6, and NACA 65A009 Airfoil Section. Transonic-Bump Method. (Prospective NACA paper)

12. Hamilton, William T., and Nelson, Warren H.: High-Speed Characteristics of a Model NACA 65_1-210(a = 1) Wing with 2° Washout and an Aspect Ratio of 9. NACA MR A5F06, Army Air Forces, 1945.

13. Hamilton, William T., and Nelson, Warren H.: High-Speed Characteristics of a Model NACA 65_1-212 Wing of Aspect Ratio 9. NACA MR A5E07, Army Air Forces, 1945.

14. Kaplan, Carl: On Similarity Rules for Transonic Flows. NACA Rep. 894, 1948.

15. Mathews, Charles W., and Thompson, Jim Rogers: Comparison of the Transonic Drag Characteristics of Two Wing-Body Combinations Differing Only in the Location of the 45° Sweptback Wing. NACA RM L7I01, 1947.

16. Turner, Thomas R.: Effects of Sweep on the Maximum Lift Characteristics of a Wing of Aspect Ratio 4 at Transonic Speeds. (Prospective NACA paper)

17. Jones, J. Lloyd, and Demele, Fred A.: Aerodynamic Study of a Wing-Fuselage Combination Employing a Wing Swept Back 63°.- Characteristics throughout the Subsonic Speed Range with the Wing Cambered and Twisted for a Uniform Load at a Lift Coefficient of 0.25. NACA RM A9D25, 1949.

18. Silsby, Norman S., and Kennedy, Robert M.: Longitudinal Characteristics of a Semispan Model of the Grumman Airplane Design 83 Having a Sweptback Wing and of the Model with a Straight Wing, as Determined from Wing-Flow Tests at Transonic Speeds - TED No. NACA DE337. NACA RM SL9A19, Bur. Aero., 1949. (Prospective NACA paper)

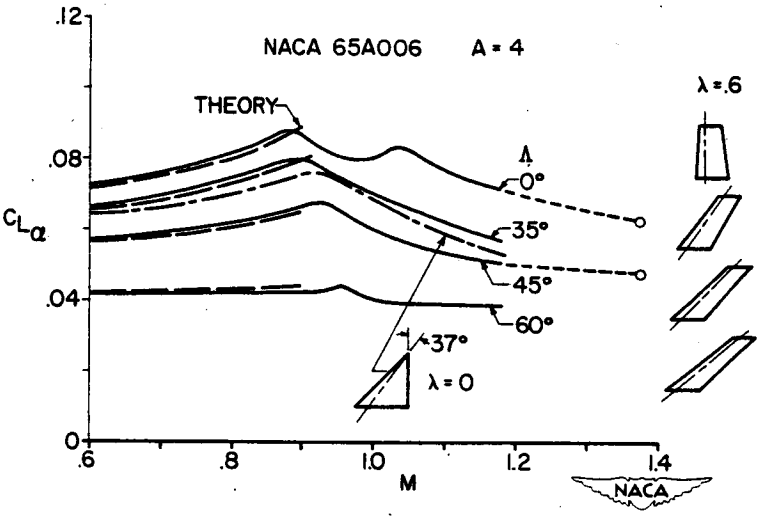


Figure 1.— Effect of sweepback on the variation of the lift-curve slope with Mach number.

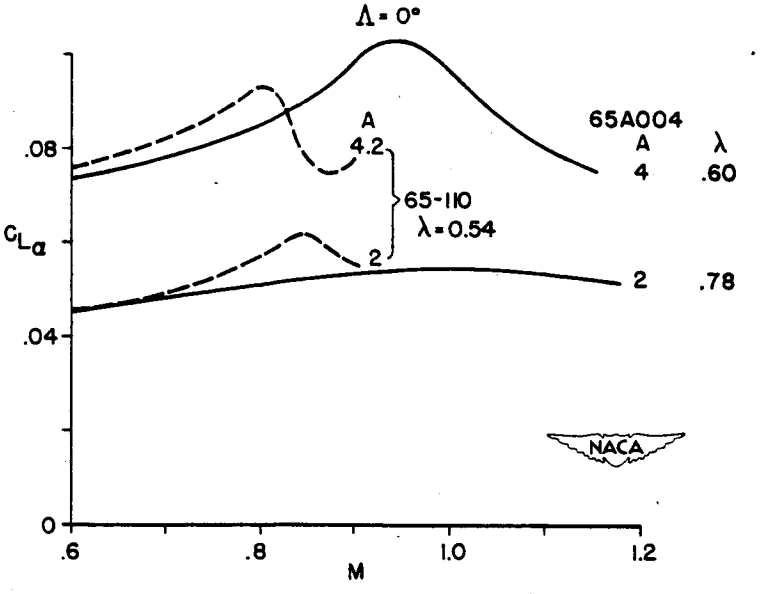


Figure 2.— Effect of aspect ratio on the variation of the lift-curve slope with Mach number.

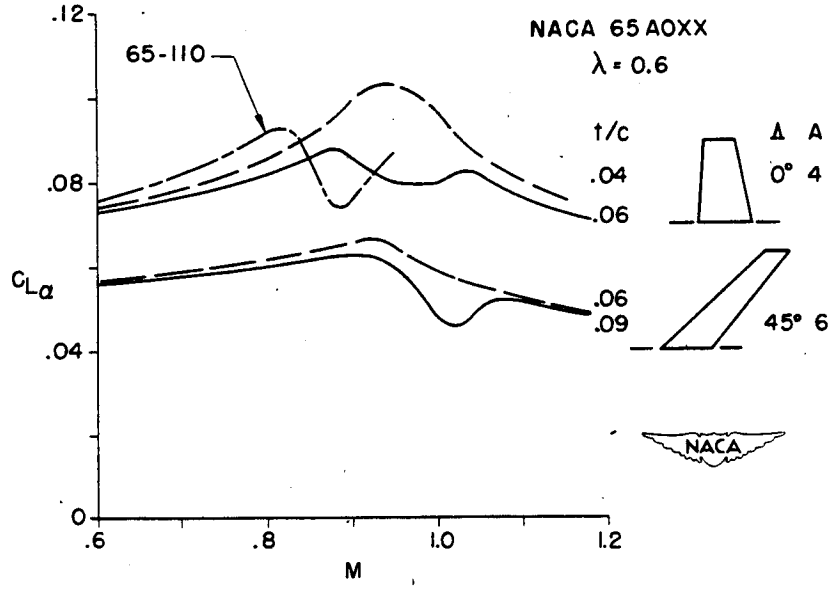


Figure 3.- Effect of thickness ratio on the variation of the lift-curve slope with Mach number.

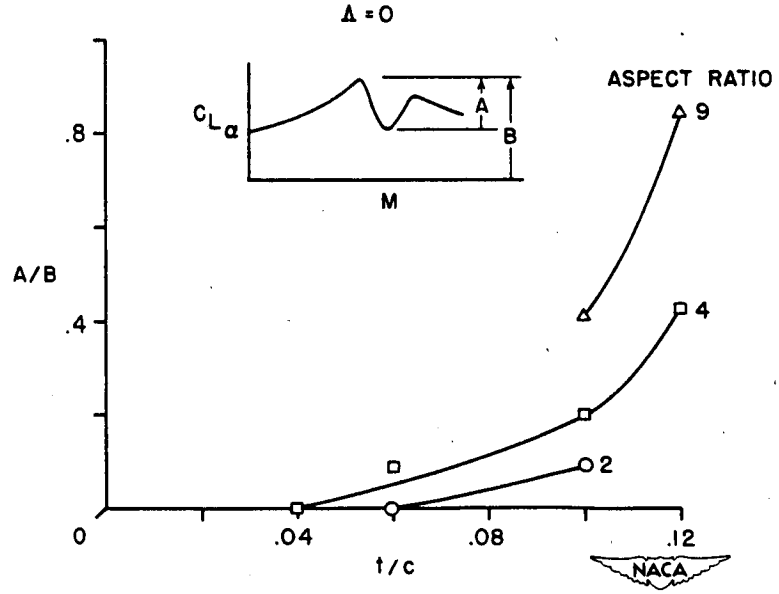


Figure 4.- Effect of thickness ratio and aspect ratio on the magnitude of the lift force break.

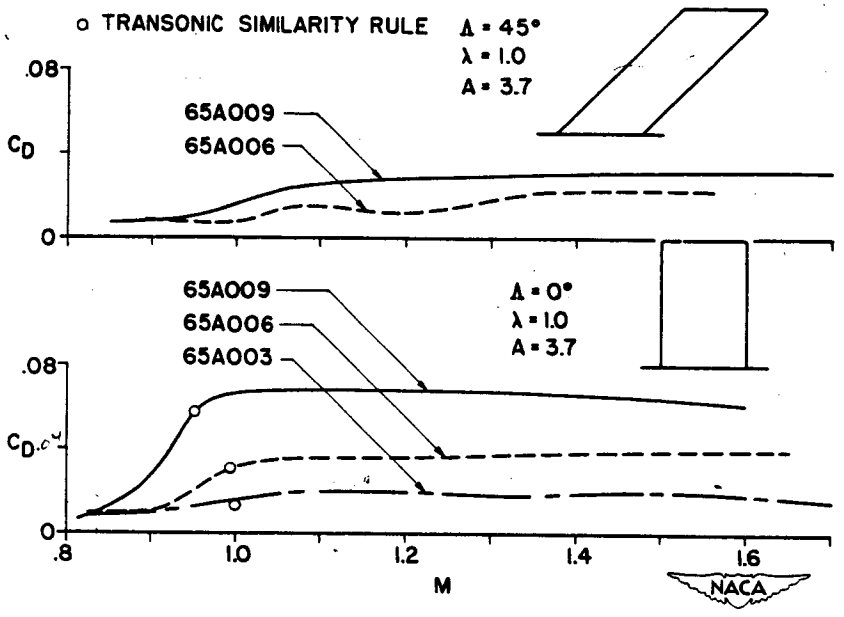


Figure 5.– Effect of thickness ratio and sweep on the drag at zero lift.

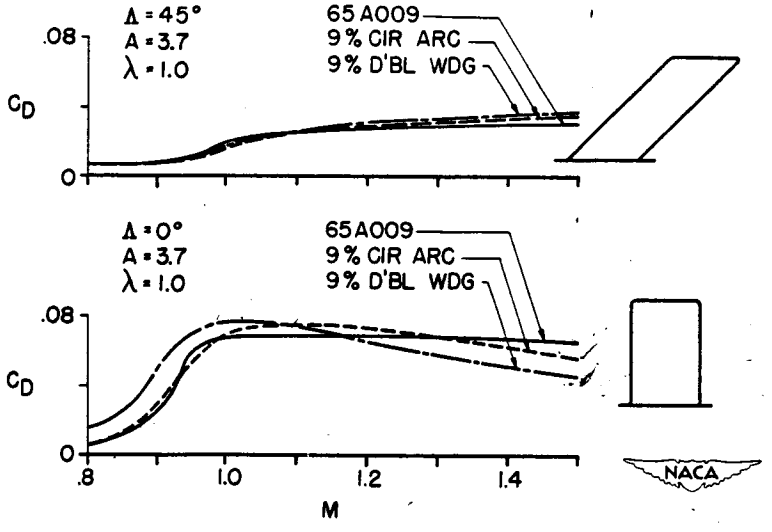


Figure 6.– Effect of profile on the drag at zero lift.

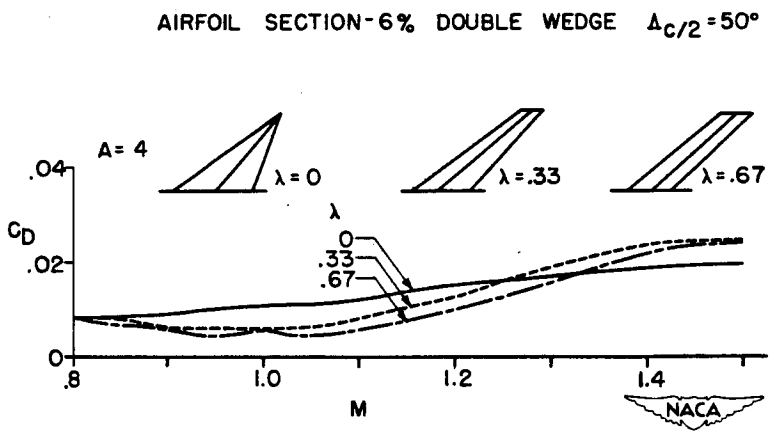


Figure 7.- Effect of taper ratio on the drag at zero lift.

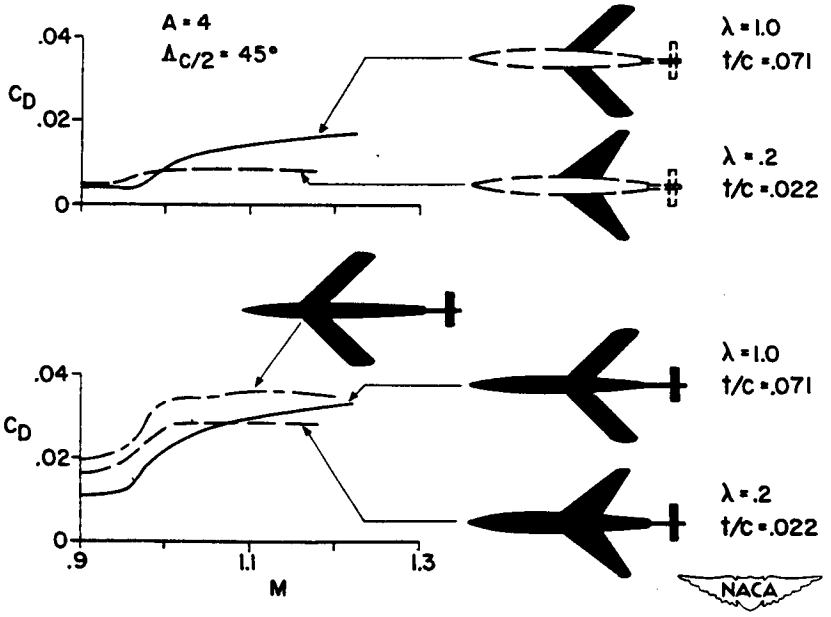


Figure 8.- Effect of thickness ratio and taper on the drag at zero lift.

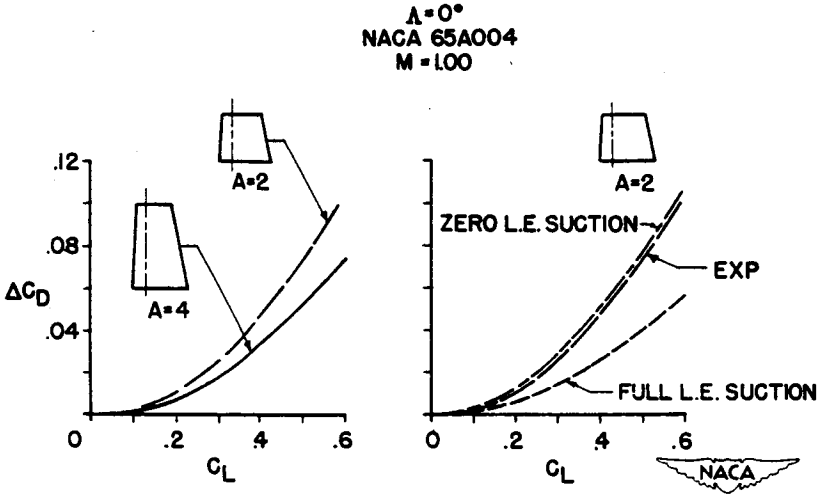


Figure 9.– Effect of aspect ratio on the drag due to lift.

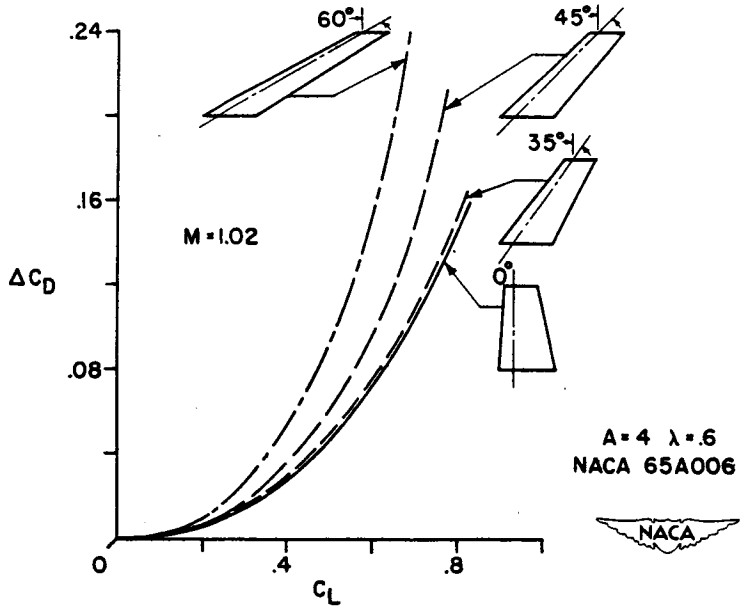


Figure 10.– Effect of sweep on the drag due to lift.

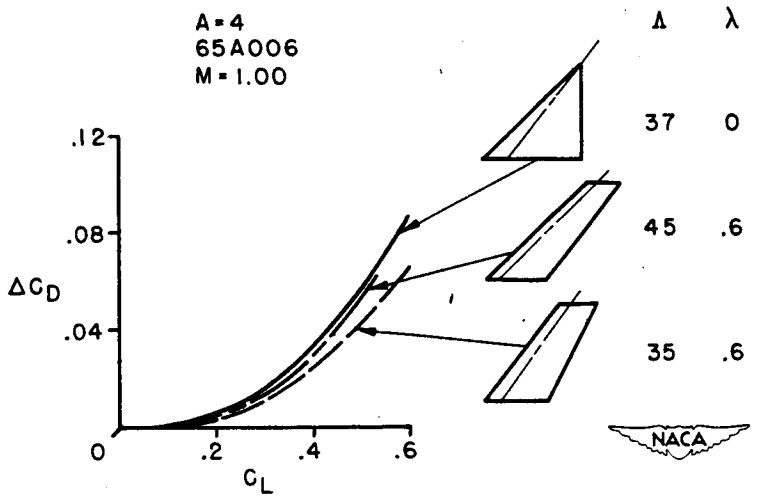


Figure 11.– Comparison of the drag due to lift of a delta wing with that for two swept wings.

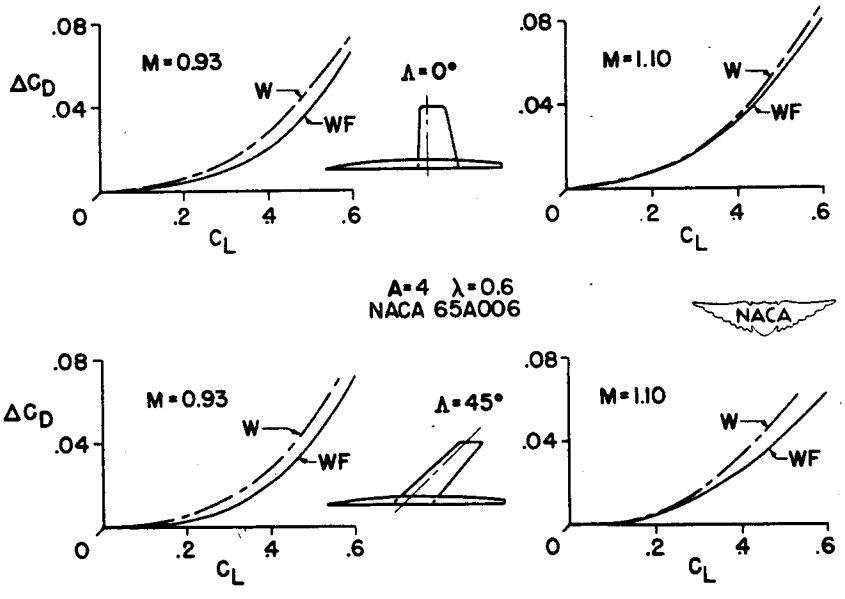


Figure 12.– Effect of the fuselage on the drag due to lift.

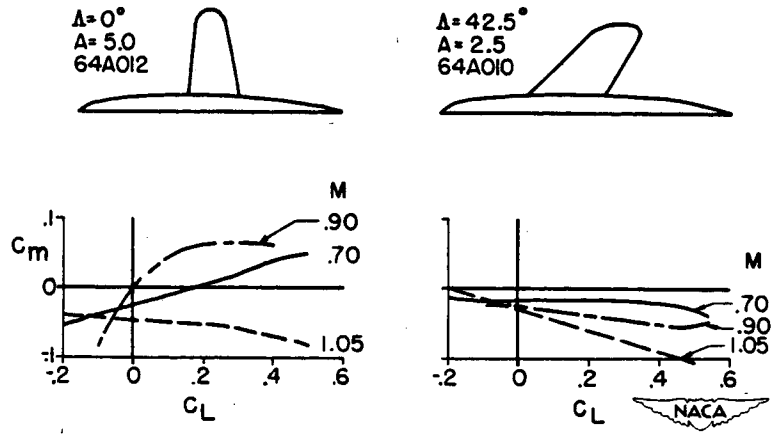


Figure 13.— Effect of combined changes in plan form and thickness ratio on the pitching-moment characteristics.

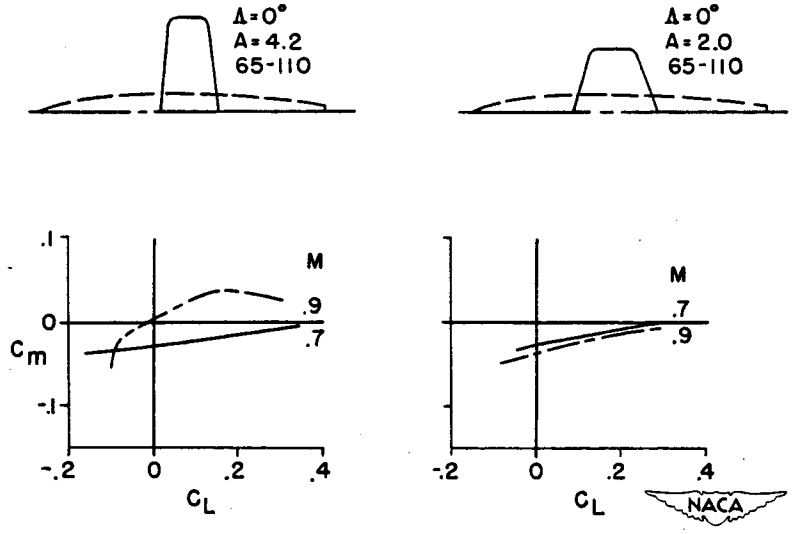


Figure 14.— Effect of aspect ratio on the pitching-moment characteristics.

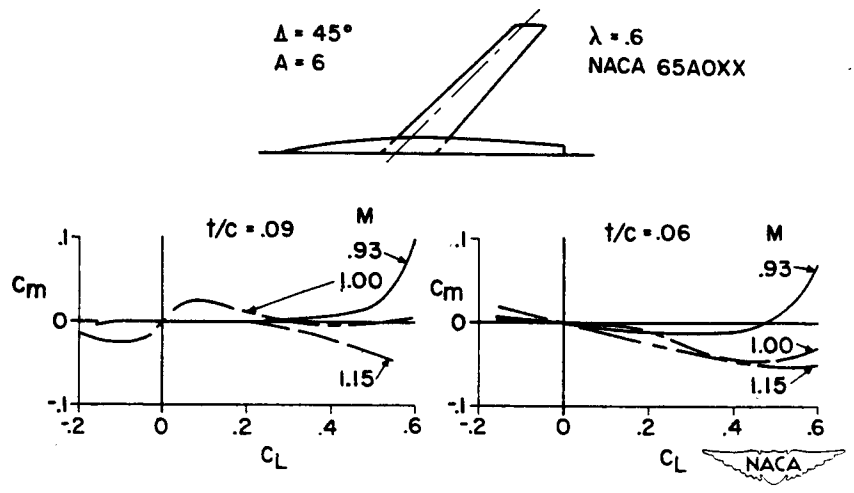


Figure 15.– Effect of thickness ratio on the pitching-moment characteristics.

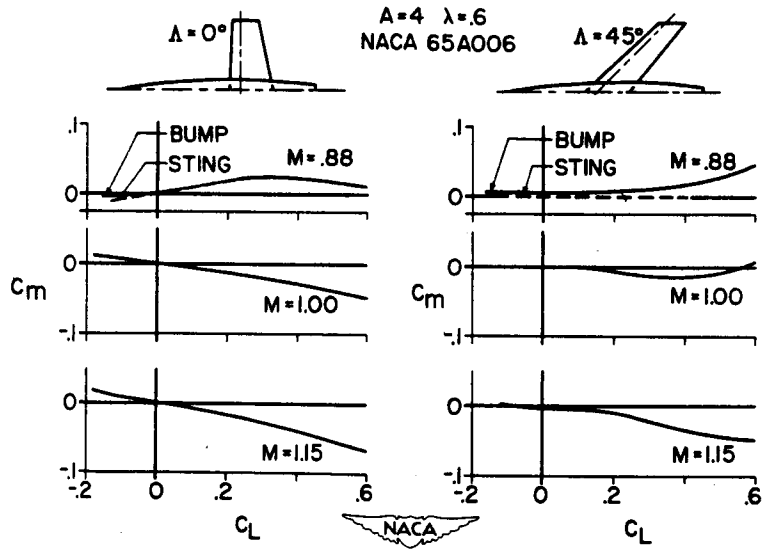


Figure 16.– Effect of sweep on the pitching-moment characteristics.

N65-86455

WING CHARACTERISTICS NEAR AND AT MAXIMUM LIFT FOR TRANSONIC SPEEDS

By Thomas R. Turner

Langley Aeronautical Laboratory

A knowledge of the effects of Mach number on wing aerodynamic characteristics near maximum lift is becoming of great importance as the speeds and altitudes flown by modern aircraft continue to increase. High-speed, high-altitude aircraft fly at rather high lift coefficients and may reach or exceed the angle of attack for the maximum lift of the aircraft in maneuvers. It is the purpose of this paper to present briefly the limited amount of available data obtained at transonic speeds at and near maximum lift. Most of the data presented are at low Reynolds numbers and were obtained by means of the transonic bump.

Figure 1 presents maximum-lift-coefficient data obtained by several testing methods for several wings having slightly different geometric characteristics (references 1, 2, and 3). Two different size models with NACA 64_1-112 sections normal to the 27-percent-chord line and with the 27-percent-chord line swept back 40° were investigated with the regular reflection-plane setup in the Langley high-speed 7- by 10-foot tunnel in order to determine the Reynolds number effects at high subsonic Mach numbers (reference 1). The Reynolds numbers of the two models were in a ratio of about 6 to 1, as indicated in the figure. This Reynolds number difference makes an appreciable difference in the maximum lift coefficient at the lower Mach numbers, the model with the lower Reynolds number giving the lower $C_{L_{max}}$. However, the Reynolds number effect decreased as the Mach number was increased, indicating that at transonic Mach numbers Reynolds number effects on $C_{L_{max}}$ are small. Although the geometry of the models is different, the maximum-lift-coefficient curves for the wings tested on the transonic bump (reference 2) and the wing tested by the NACA wing-flow method (reference 3) show the same trends with Mach numbers. Also the reflection-plane data showed the same trends that the bump and wing-flow data did, in that all showed a sharp rise in the maximum-lift-coefficient curve beginning at a Mach number of approximately 0.85. Perhaps it should be mentioned that the maximum lift for the wing-flow model having NACA 65-009 sections with the quarter-chord line swept back 35° was unsteady around a Mach number of 1.1 and that the curve presented is the average of the variations. It is not known whether similar fluctuations in the maximum lift coefficients occurred during the transonic-bump tests because of the high damping in the measuring instruments.

Figure 2 presents the variation of the maximum lift coefficient $\left(C_{L_{max}}\right)$ with Mach number for a series of wings having NACA 65A006 sections parallel to the free-stream direction, aspect ratio 4, taper ratio 0.6, and with the quarter-chord line swept back 0°, 35°, 45°, and 60° (reference 2). The data above a Mach number of 0.60 were obtained on the transonic bump at a Reynolds number of approximately 450,000; the points at 0.10 Mach number were obtained in the Langley two-dimensional low-turbulence pressure tunnel at a Reynolds number of 3,000,000 (reference 4). The maximum lift coefficients at $M = 0.1$ show a systematic and reasonable relation to the high Mach number data. The maximum lift coefficient increased with increased sweep below a Mach number of about 0.80 and decreased with increased sweep above a Mach number of about 0.95 but appeared to be practically independent of angle of sweep around a Mach number of 0.90. It should also be noted that the variation of the maximum lift coefficient with Mach number through the transonic range decreased with increased sweep angle. The maximum lift coefficient at high transonic Mach numbers was almost twice the low Mach number value for the wing with zero sweep. Although only the maximum-lift-coefficient data are presented here, the lift, drag, and pitching-moment coefficients were obtained for all the wings of this series over an angle-of-attack range from -2° to as high as 50° at each Mach number.

Figure 3 shows the variation of lift coefficient with angle of attack for the 0°, 45°, and 60° swept wings of the series presented in figure 2 at three representative Mach numbers and at Reynolds numbers of approximately 450,000. As can be seen from this figure, the lift-curve slope decreased with increased sweep angle at each Mach number. As was also shown in figure 2, at a Mach number of 0.61 the maximum lift coefficient increased as the sweep angle was increased, but at a Mach number of 1.12 the maximum lift coefficient decreased with increase in sweep angle. However, at a Mach number of 0.92 the maximum lift coefficient was practically independent of sweep angle. The extremely high angles of attack at which maximum lift occurred, 40° or 50° in some cases, should be noted. In most cases the loss in lift after the angle of attack for maximum lift had been reached was very gradual.

Figure 4 presents the drag characteristics at high angles of attack for the same three wing configurations and at the same three representative Mach numbers as presented in figure 3. The data are presented as lift-drag (L/D) ratios plotted against angle of attack. Above approximately 10° angle of attack, changes in either sweep angle or Mach number had very little effect on the lift-drag ratio. The lift-drag ratio for all sweeps and Mach numbers investigated was approximately 1 at 45° angle of attack. The resultant force for this series of wings, above an angle of attack of approximately 10°, is normal to the chord plane for all practical purposes.

[redacted]

Figure 5 presents the curves of pitching-moment coefficient against angle of attack for the same three wings and three Mach numbers for which data were presented in figures 3 and 4 - that is, wings having NACA 65A006 sections parallel to free stream, aspect ratio 4, taper ratio 0.6, and with the quarter-chord line swept back 0°, 45°, and 60° - at Mach numbers of 0.61, 0.92, and 1.12. The moments presented are about the quarter-chord point of the wing mean aerodynamic chord. As can be seen from this figure, above approximately 10° angle of attack, the pitching-moment coefficients became more negative as the Mach number was increased and became more positive as the angle of sweep was increased.

If results such as those shown for the very low Reynolds number (450,000) persist at flight Reynolds numbers, it appears that severe stability problems may be encountered at large angles of attack.

In summary, the variation of the maximum lift coefficient with Mach number in the transonic range decreased with increased sweep; maximum lift coefficients increased with increased sweep at the lower Mach numbers but decreased with increased sweep at the higher Mach numbers. At high angles of attack the pitching-moment coefficients became more positive as the sweep increased and more negative as the Mach number increased, and the curves of lift-drag ratios indicate that the resultant forces were normal to the chord plane.

REFERENCES

1. Turner, Thomas R.: Maximum Lift Investigation of a 42° Sweptback Wing at Mach Numbers from 0.05 to 1.20. (Prospective NACA paper)

2. Turner, Thomas R.: Effects of Sweep on the Maximum Lift Characteristics of an Aspect Ratio 4 Wing at Transonic Speeds. (Prospective NACA paper)

3. Johnson, Harold I.: Measurements of Aerodynamic Characteristics of a 35° Sweptback NACA 65-009 Airfoil Model with $\frac{1}{4}$-Chord Plain Flap by the NACA Wing-Flow Method. NACA RM L7F13, 1947.

4. Cahill, Jones F., and Gottlieb, Stanley M.: Low-Speed Aerodynamic Characteristics of a Series of Swept Wings Having NACA 65A006 Airfoil Sections. NACA RM L9J20, 1949. (Prospective NACA paper)

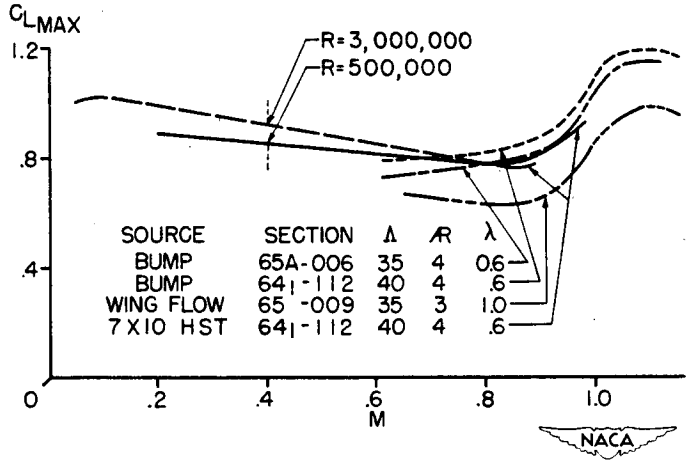


Figure 1.- Variation of maximum lift coefficients with Mach number obtained from several test techniques.

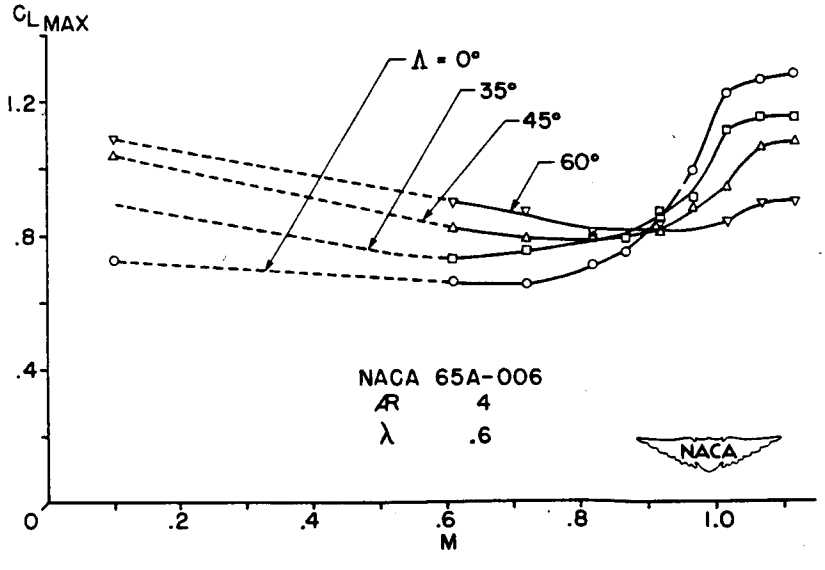


Figure 2.- Effect of sweep on the maximum lift coefficient.

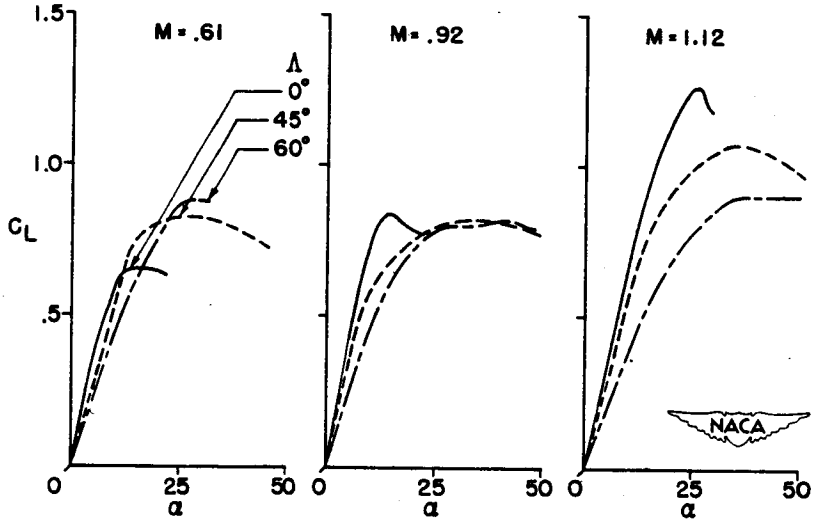


Figure 3.- Typical variations of lift coefficient with angle of attack for a 6-percent-thick, aspect-ratio-4 wing.

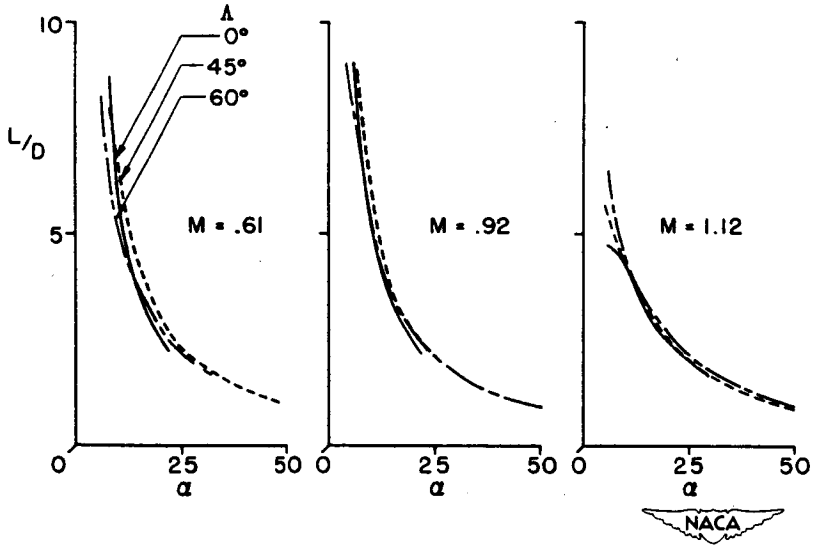


Figure 4.- Typical lift-drag ratios for a 6-percent-thick, aspect-ratio-4 wing.

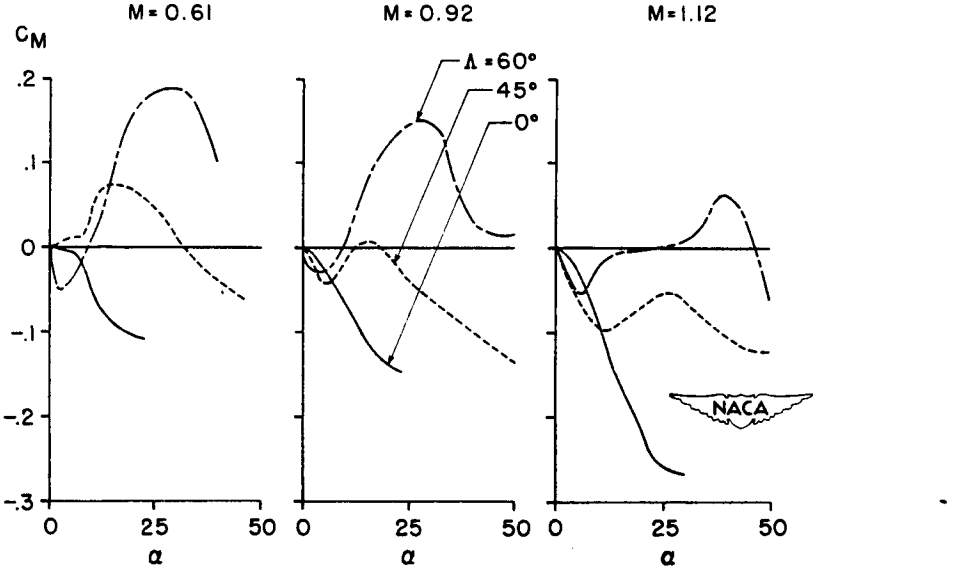


Figure 5.- Typical pitching-moment variations with angle of attack for a 6-percent-thick, aspect-ratio-4 wing.

AEROELASTICITY AND FLUTTER

Preceding page blank

N65-86456

STATUS OF THE HIGH-SPEED FLUTTER PROBLEM

By I. E. Garrick and D. J. Martin

Langley Aeronautical Laboratory

The purpose of this paper is to present a summary of some recent investigations of high-speed flutter. It may be recalled that a brief review was given at the NACA Conference on Aerodynamic Problems of Transonic Airplane Design, November 1947, in a paper entitled "Some High-Speed Flutter Studies" by I. E. Garrick. The study of the flutter phenomenon with its numerous parameters and variables has been continued both theoretically and experimentally. Theoretically, solutions are sought for various partial differential equations governing the structural and aerodynamic phases of the problem for a variety of boundary conditions and plan forms. Experimentally, data are sought by a variety of methods, utilizing subsonic and supersonic wind-tunnel research, rocket and dropped-body techniques, modern vibration equipment, electronic methods, and techniques of telemetering.

Flutter is a particularly dynamic phase of the aeroelastic field and may in a certain sense contain many of the other aeroelastic problems such as divergence or loss of control due to elastic deformation. It is concerned with the interaction of the aerodynamic and the elastic and inertia forces of the structure. Flutter itself is a self-excited, undamped oscillation that takes place when the aerodynamic and structural forces interact in a manner to feed energy from the air stream into the structure; however, the approach to flutter is also significant. Flutter may involve one or more modes of vibration, may imply either high or low frequencies of the structure, established or broken-down flow, and may also be concerned with the stability modes.

An investigation into flutter, for convenience, may be concerned primarily with a study of aerodynamic effects or structural effects. There are two basic methods of experimentally studying these effects. Briefly, the first consists of an integrated program where the interest is in integrated results and over-all trends. The second method consists of a longer-range program interested in the derivative components, where the attempt is made to isolate and study the individual parameters.

As an example of the integrated method, one may mention the experiments on complete structures of various configurations intended to investigate the effects of such parameters as plan form, sweepback, concentrated masses, and other structural variations. The results, however, usually contain effects of variations in the aerodynamic

parameters involving in some measure such considerations as Mach number, Reynolds number, airfoil shape, aspect ratio, and of course, frequency.

As an example of a study of the derivative components one may mention the direct measurements of the oscillating air forces by pressure-distribution methods. This problem is being worked on at this Laboratory, at Ames, and in England. A study of components requires difficult and highly specialized techniques; hence, this work is long-range in nature.

Figure 1 is representative of some of the integrated studies obtained by various combined research techniques in which there are utilized subsonic and supersonic wind tunnels, rockets, and dropped bodies. (See references 1 to 7.) The figure is a composite chart of wing bending–torsion flutter and shows some trends throughout an important Mach number range for a group of similar wings. The abscissa is the Mach number, the ordinate is the experimentally measured flutter speed divided by a reference speed $V_{Ref.}$, which is the flutter speed calculated by use of the simple theory for incompressible, two-dimensional flow. The data points are for some flutter experiments on a series of wings whose center-of-gravity locations are close to the 45-percent chordwise position, a thickness ratio of 9 percent, and an aspect ratio of approximately 6. The solid curve is drawn through the data points for the straight unswept wings. The dashed curve is for the 60° sweptback wings. The lower portion of the curves up to a Mach number of about 0.9 has been studied mainly with the use of subsonic wind tunnels and with rocket vehicles. The upper portion has been studied by the use of dropped-body techniques and in the small supersonic flutter tunnel at Langley Laboratory. It may be recalled that the theoretical calculations for the transonic range are at present necessarily an arbitrary extrapolation of the high subsonic and the low subsonic values. Experimental results like those shown in figure 1 are of interest for they furnish a comparison between the simple calculations based on low-speed flow and experiment for a wide range of Mach numbers.

Some observations of interest can be made from a figure of this type. Notice, first, that both the abscissa and the ordinate are nondimensional quantities and that each contains the flight velocity in the numerator. The slope of a straight line radiating from the origin would then be $a/V_{Ref.}$, a being the velocity of sound. Thus, a straight line is obtained for each assumed value of $V_{Ref.}$ (for simplicity of discussion the velocity of sound a may be temporarily considered to be constant). Greater values of $V_{Ref.}$ are represented

by lines of smaller slope. The intersection of one of these lines with the representative curve determines the Mach number at which flutter may occur for the assumed value of $V_{Ref.}$. A number of these lines are shown in figure 2. It will be recalled that $V_{Ref.}$ is the flutter speed calculated from the simple theory for two-dimensional, incompressible flow and is a function of a number of parameters; however, for this discussion, only the torsional stiffness and the air density are considered. For a given air density or altitude, these straight lines may be regarded as representing wings of different torsional stiffness, stiffer wings being indicated by lines of smaller slopes. Alternatively, for a given wing, these lines may be considered as air-density or altitude lines (including, if desired, appropriate changes in the velocity of sound); higher altitudes are also shown by lines of smaller slopes.

Consideration of the straight lines as representing constant values of torsional stiffness indicates that the line which is tangent to the representative curve determines the critical value of stiffness required to avoid flutter at the chosen altitude since no intersection can occur for stiffer wings. On the other hand, if the stiffness is held constant and the lines are regarded as altitude lines, the altitude line which is tangent to the representative curve is the altitude above which flutter may not be encountered for the chosen stiffness.

Notice that for straight unswept wings, the point of tangency occurs at a Mach number of approximately 0.9; however, for the 60° sweptback wings, such a point of tangency would occur at a higher Mach number, if the representative curve for sweptback wings turns up in a manner similar to the curve for unswept wings. Some other work on the flutter of swept wings is reported in reference 8. A large expenditure of additional research effort is still needed for these high-speed studies.

Before leaving this subject, it is interesting and may be informative to mention some of the features of various experimental techniques and the way in which the representative curve is approached. In flutter research using rocket vehicles at sea level, the air density decreases usually only slightly as the rocket climbs and gains speed. If the straight lines in figure 2 are again regarded as representing altitude lines, we may trace the path of such a rocket. The rocket starts at the altitude line which represents sea level. As the rocket gains speed and climbs, the path slowly shifts to a higher altitude line. In the freely-falling-body technique, the air density increases as the body falls. The path begins along the line representing the altitude at which the body is dropped. The body may reach a very high speed before falling to the altitude line which may intersect the representative curve (fig. 2, the dashed curves). This type of research is convenient for exploring the upper portions of the representative

curve. A study of this type of chart may be of special interest with reference to operational plans of flight involving involving wide ranges of altitude and Mach number.

The upper portion of the representative curve may also be studied in a supersonic wind tunnel, for example, by a technique of restraining the model while the tunnel accelerates to supersonic speeds, or by a technique of withholding the model from the air stream during the starting and stopping transient tunnel conditions. The latter method has been used in obtaining some of the results to be discussed. The supersonic flutter tunnel employed is of the intermittant type operating from atmospheric stagnation pressure to a vacuum chamber. The model is withheld from the starting and stopping transient conditions by mounting the model on a sliding base which is controlled by a large hydraulic cylinder. After the tunnel has reached steady supersonic conditions, the model is inserted into the tunnel. If flutter is encountered before the model is fully into the flow, the model is quickly withdrawn and a change is made such as a shift in the center of gravity, length, or weight position. This process is repeated until the model flutters when it is all the way into the tunnel, thus, yielding the flutter point.

The results of a series of supersonic flutter experiments have been reported in reference 9 and are presented in figure 3. The experimentally measured flutter coefficients $V/b\omega_\alpha$ are plotted against the coefficients predicted by the simple theory for two-dimensional supersonic flow as given in reference 10. The symbols in the ordinate are V the velocity, b the semichord, and ω_α the circular torsional frequency. The experiments were on various wings of thick and thin sections, of blunt and sharp leading edges, of double-wedge and of circular-arc sections. The small figures are exaggerated sketches of the airfoil sections corresponding to the data points. The figure shows some scatter in the data but in view of the wide variety of the conditions included in the experiments, the comparison is gratifying. The results indicate no systematic variation in flutter speed that might be directly attributed to airfoil shape although it is appropriate to mention that shape did sharply affect the divergence speed. In spite of the three-dimensional nature of the tests and the wide assortment of shapes, the tests provide a noteworthy comparison for theory. The comparison indicates that the theory may serve as a useful guide. Some additional supersonic flutter experiments have recently been reported in reference 11.

It is of interest to mention that a recent contribution on the effect of aspect ratio has been made to the theory of the torsional oscillations of rectangular wings at supersonic speeds, reference 12.

For many years, it has been suspected without experimental substantiation, that the type of free-body modes which are used in discussions of airplane stability may also enter significantly into flutter, interacting with modes involving structural deformations. The stability modes usually imply low frequencies, the structural modes imply high frequencies. In some of our experiments on flutter with the aid of rocket vehicles, we have occasioned some failures which seemed to involve a significant amount of the structural mode, wing bending, and the free-body or stability mode, missile pitching. In these cases the wings were located rearward of the center of gravity of the missile. Theoretical analysis of some of these failures has confirmed our views of the possible interaction of these two modes, wing bending, and missile pitching.

In figure 4 are given some flutter curves that were calculated by using only these two modes for a wing-body configuration that would include one of these rocket failures. The abscissa is a nondimensional moment-of-inertia factor for the wing-rocket combination, where I is the moment of inertia in pitch of the entire missile about its center of gravity, $2l$ is the span of the missile, and $\pi\rho b^4$ is a measure of the moment of inertia of the air surrounding the wing. The ordinates of this figure are the flutter frequency ratio ω/ω_h on the left, where ω_h is the first natural bending frequency and on the right are shown the flutter speed coefficients $V/b\omega_h$. The data points are for flutter speed coefficient and the flutter frequency ratio for the start of the oscillation which resulted in one of the rocket failures. In this case, the flutter frequency was approximately one-fourth the first natural wing bending frequency.

It may be said in this case that the uncontrollable instability of flutter is approaching, relatively speaking, the normally controllable oscillations of the entire aircraft. The effect of the introduction of a stability mode should be considered for unconventional body-wing arrangements or configurations, such as tailless designs, sweptback wings, and certain missile arrangements.

All this has a direct bearing on the important question of endowing more meaning to design criteria as related to flutter. Consider, for example, the effect on the type of flutter as the wings are displaced forward toward the center of gravity from the rearward position for a missile similar to the one previously mentioned. For a forward location, one may be concerned primarily with ordinary wing bending-torsion flutter and for a rearward position with the wing-bending missile-pitching type of flutter, for example, as presented in figure 4. Clearly there must be a transition of some kind as the wings are moved forward. In the forward position, as is well known, a criterion based on the

torsional stiffness may be used, in the rearward position, however, a different criterion based on bending stiffness is required, while intermediate wing positions may involve both conceptions. These conditions have not been fully explored.

Calculations have recently been made in England based on similar considerations for the case of symmetrical modes of a sweptback wing in reference 13 and also for the antisymmetrical modes in reference 14. One result of such work has been the broadening of the conception of criteria to include the shape of the nodal lines of various natural modes. The general conclusions drawn from the calculations were that, for certain specific shapes of the nodal lines, a critical interaction with body freedom or stability modes could be expected. This work is a worthwhile attempt to retain the elements of simplicity inherent in the concept of criteria, yet to broaden the basis. Further confirmation and development of these ideas are desirable.

The concept of a criterion may be based upon experience or calculation; however, a knowledge of the actual or calculated margins of safety is extremely important. A combined analytical and experimental investigation of wings carrying concentrated masses furnished some useful information on this subject of margins of safety. (See references 15, 16, and 17.) A comparison was made for two methods of analysis, one a differential-equation treatment of the wing as a continuous structure, a method which is ordinarily too tedious and difficult in actual practice, and the other, a method of employing a few selected modes or degrees of freedom, a method commonly used in industry. Figure 5 shows some of the experimental data together with the calculations. The experiments were upon a wing carrying a large concentrated weight whose center of gravity was located ahead of the elastic axis of the wing. The flutter speed ratio is plotted here as the weight is moved to various spanwise positions. The circles represent the experimental points, the solid curves are the flutter speeds calculated by the Rayleigh type analysis using two, three, and four chosen modes, the dashed curve is the flutter speed calculated by the differential-equation method. It is remarked that the divergence speed of the wing V_D was such that flutter data could not be obtained over the entire range of spanwise positions.

The differential-equation procedure reproduces well even the peculiar trends of the experimental data but the chosen mode procedure is satisfactory only if a sufficient number of modes are included in the analysis. This work furnishes a means of appraisal of the accuracy of this common procedure. It is interesting to note that the computed results using a few modes were unconservative, that is, above the experiment and approached the data as more modes were used. For an analysis of data in which experiments were made on the same wing with the center of gravity of the mass located behind the elastic axis, the calculated results were cons[redacted]verged upon the experimental

data from below as more modes were included. For the case where the concentrated weight was located on the elastic axis, two modes gave reasonable agreement, the addition of more modes produced little improvement.

These results indicate that the designer must be cautious for cases of large mass coupling, as the use of too few modes in the analysis may give results that are conservative if the masses are located rearward, or unconservative if located forward of the elastic axis. This study shows that the margins of safety inherent in the criterion are related to the method of calculation. The additional effects of body freedom need to be considered here, too.

It may be recalled that the Langley 4.5-foot flutter research tunnel is a variable-density, variable Mach number tunnel. The density of the testing medium may be varied through a ratio of 30 to 1 and the Mach number can be changed at the same density by using different media having different velocities of sound. It may be of interest to present a series of data from this tunnel (reference 18) that may have a direct bearing on the question of criteria as modified by compressibility effects. In figure 6 are shown the results of fluttering a single model (wing 1) over a wide range of densities and Mach numbers. The plot of velocity is made against the wing density parameter $1/\sqrt{\kappa}$, which may also be looked upon as altitude, increasing altitude toward the right. Curve A is for data taken in air, curve B is for a gas which has a velocity of sound approximately one-half that of air. Points on the two curves at the same value of $1/\sqrt{\kappa}$ differ essentially in Mach number. The numbers on the curves are values of the Mach number.

There exists a considerable amount of work on the effect of Mach number on flutter and the theory is in general extremely complicated. A simple fourth-foot-type correction similar to the Prandtl-Glauert correction for steady flow was suggested some years ago. In an attempt to correlate the data, the factor $(1 - M^2)^{1/4}$ was applied to both sets of data. The lower part of the figure shows the same data after the correction is made. The Mach number effect is apparently extracted and the data form a single curve that is approximately a straight line for the range of variables investigated. This rather simple result was also borne out by all the experimental results on another model (wing 2) shown in figure 7. This investigation leads to the hope that the more complicated analyses may be circumvented at times and that simple corrections may suffice for certain ranges of parameters. Further experiments are required to determine the ranges in which such simple corrections are valid.

The discussion thus far has considered only the classical coupled flutter associated with an [redacted] of flow pattern. As a last

item to be mentioned, reference is made to some types of flutter associated with a single degree of freedom and to an extent with a broken-down flow. Propellers, especially very thin propellers, may encounter the phenomenon of propeller stall flutter which involves predominantly a single degree of freedom. Of particular interest is its merging with classical coupled-flutter conditions. A further discussion of this topic is given in the subsequent paper by John E. Baker and Arthur R. Regier entitled "The Propeller Flutter Problem for High-Speed Airplanes." It is of interest here to mention that a criterion for this type of flutter, based on experimsnt, indicates that the torsional-stiffness criterion of classical flutter may merge into a frequency criterion for the stall conditions.

Another related single-degree type of flutter has been encountered on some ailerons at transonic speeds and has been termed aileron buzz. The marginal character of this type of flutter presents some difficulties. Research on such aileron flutter is continuing at Ames and at Langley. At the Ames Aeronautical Laboratory the emphasis is upon large-scale studies, in particular, upon the measurement of the oscillating pressure distribution over wing and aileron. At Langley Aeronautical Laboratory the phenomenon has recently been duplicated in flight by the wing-flow method. (See reference 19.) It is also being studied in wind tunnels. (See reference 20.) In brief, the results may be summarized as follows: Aileron buzz is limited to a range of Mach numbers near the critical Mach number of the airfoil section; consequently, the phenomenon is strongly affected by the section shape. Damping has a marked influence; however, the damping required to eliminate aileron buzz needs further study. Tests in the Langley 4.5-foot flutter research tunnel indicate that the buzz Mach number is nearly independent of the air density or altitude and thus behaves in a manner similar to that of propellers at the stall; a similar criterion is therefore indicated and the desirability of high natural frequencies is confirmed. Some of the transonic airplanes that have not experienced difficulties have had very high stiffness in the control systems, approaching irreversible control.

In conclusion, it is pointed out that the foregoing discussion and figures have dealt with an outline of some of the principal fields of activity on flutter. It will be noted that the emphasis has been upon the integrated studies of over-all effects. In our further program it is hoped to add to the understanding and control of flutter and to isolate more of the component effects.

REFERENCES

1. Barmby, J. G., and Clevenson, S. A.: Initial Test in the Transonic Range of Four Flutter Airfoils Attached to a Freely Falling Body. NACA RM L7B27, 1947.

2. Angle, Ellwyn E.: Initial Flight Test of the NACA FR-1-A, a Low-Acceleration Rocket-Propelled Vehicle for Transonic Flutter Research. NACA RM L7J08, 1948.

3. Barmby, J. G., and Teitelbaum, J. M.: Initial Flight Tests of the NACA FR-2, a High-Velocity Rocket-Propelled Vehicle for Transonic Flutter Research. NACA RM L7J20, 1948.

4. Clevenson, S. A., and Lauten, William T., Jr.: Flutter Investigation in the Transonic Range of Six Airfoils Attached to Three Freely Falling Bodies. NACA RM L7K17, 1948.

5. Angle, Ellwyn E., Clevenson, Sherman A., and Lundstrom Reginald R.: Flight Test of NACA FR-1-B, a Low-Acceleration Rocket-Propelled Vehicle for Transonic Flutter Research. NACA RM L8C24, 1948.

6. Lundstrom, Reginald R., Lauten, William T., Jr., and Angle, Ellwyn E.: Transonic-Flutter Investigation of Wings Attached to Two Low-Acceleration Rocket-Propelled Vehicles. NACA RM L8I30, 1948.

7. Lauten, William T., Jr., and Barmby, J. G.: Continuation of Wing Flutter Investigation in the Transonic Range and Presentation of a Limited Summary of Flutter Data. NACA RM L9B25b, 1949.

8. Barmby, J. G., Cunningham, H. J., and Garrick, I. E.: Investigation of the Effect of Sweep on the Flutter of Cantilever Wings. NACA RM L8H30, 1948.

9. Tuovila, W. J., Baker, John E., and Regier, Arthur A.: Initial Experiments on Flutter of Unswept Cantilever Wings at Mach Number 1.3. NACA RM L8J11, 1949.

10. Garrick, I. E., and Rubinow, S. I.: Flutter and Oscillating Air-Force Calculations for an Airfoil in a Two-Dimensional Supersonic Flow. NACA Rep. 846, 1946.

11. Flutter Section: Supersonic Flutter Model Tests at Mach No. 1.5. (Air Force Contract No. W33-038ac-15033) Rep. No. H-49-1, Curtiss-Wright Corp., Airplane Div. (Columbus Plant), March 24, 1949.

12. Watkins, Charles E.: The Effect of Aspect Ratio on Undamped Torsional Oscillations of a Thin Rectangular Wing in Supersonic Flow. NACA TN 1895, 1949.

13. Broadbent, E. G.: Flutter Problems of High Speed Aircraft. Rep. No. Structures 37, British R.A.E., April 1949.

14. Houbolt, John C.: Investigation of Antisymmetrical Body Freedom Flutter for Swept Wing Aircraft. Rep. No. Structures 41, British R.A.E., June 1949.

15. Runyan, Harry L., and Sewall, John L.: Experimental Investigation of the Effects of Concentrated Weights on Flutter Characteristics of a Straight Cantilever Wing. NACA TN 1594, 1948.

16. Woolston, Donald S., and Runyan, Harry L.: Appraisal of Method of Flutter Analysis Based on Chosen Modes by Comparison with Experiment for Cases of Large Mass Coupling. NACA TN 1902, 1949.

17. Runyan, Harry L., and Watkins, Charles E.: Flutter of a Uniform Wing with an Arbitrarily Placed Mass According to a Differential-Equation Analysis and a Comparison with Experiment. NACA TN 1848, 1949.

18. Castile, George E., and Herr, Robert W.: Some Effects of Density and Mach Number on the Flutter Speed of Two Uniform Wings. (Prospective NACA paper)

19. Crane, Harold L.: An Investigation of Aileron Oscillations at Transonic Speeds on NACA 23012 and NACA 65-212 Airfoils by the Wing-Flow Method. NACA RM L8K29, 1948.

20. Clevenson, Sherman A.: Some Wind-Tunnel Experiments of Single Degree of Freedom Flutter of Ailerons in the High Subsonic Speed Range. NACA RM L9B08, 1949.

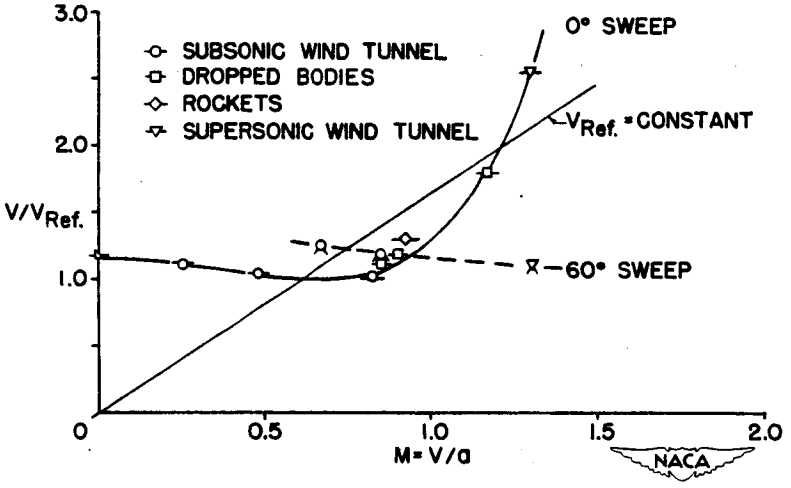


Figure 1.- Composite results for wing bending-torsion flutter.

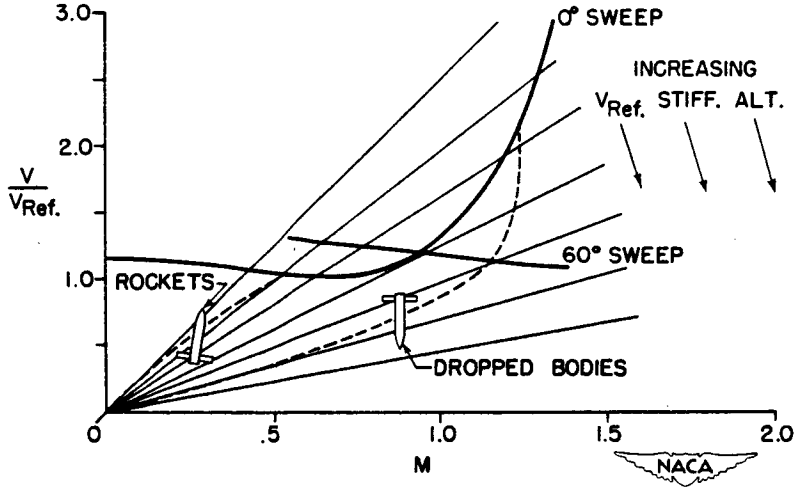


Figure 2.- Illustrating significance of $V_{Ref.}$ lines.

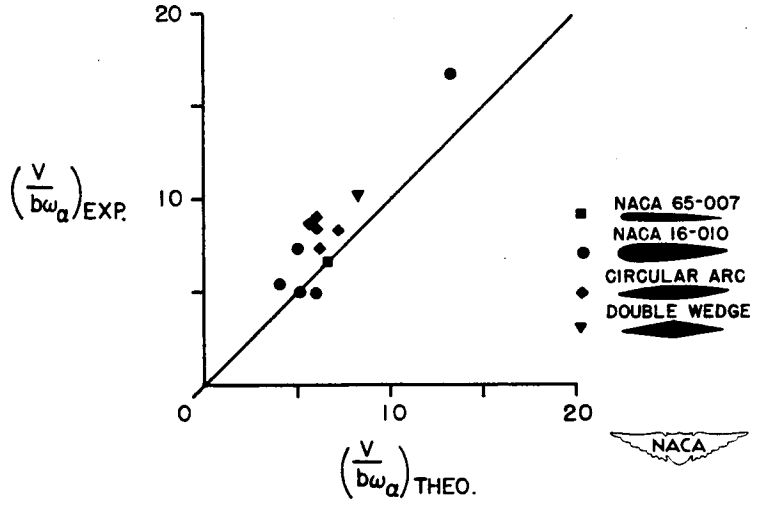


Figure 3.- Flutter of unswept cantilever wings at supersonic speeds. M = 1.3.

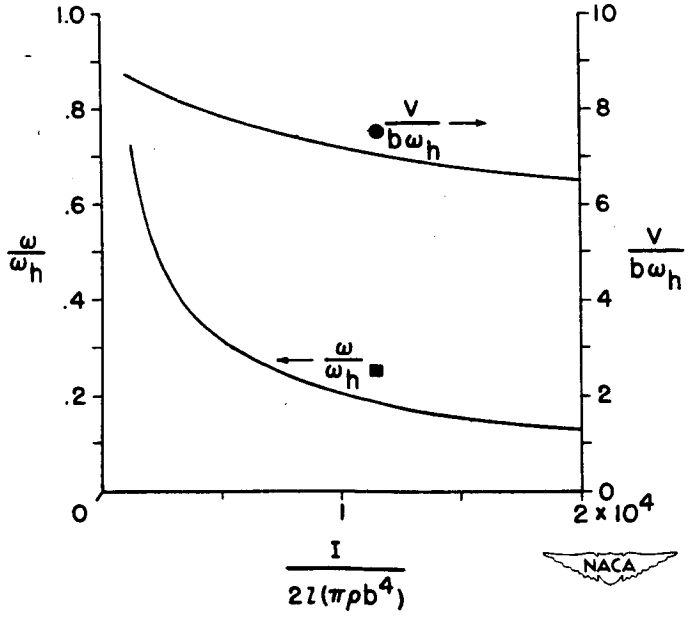


Figure 4.- Missile-pitching and wing-bending flutter.

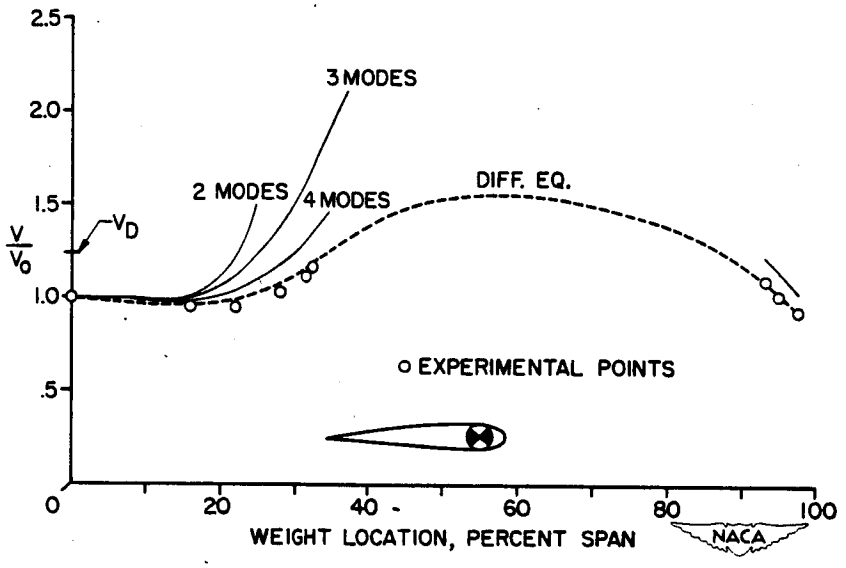


Figure 5.- Comparison and appraisal of various methods of calculation.

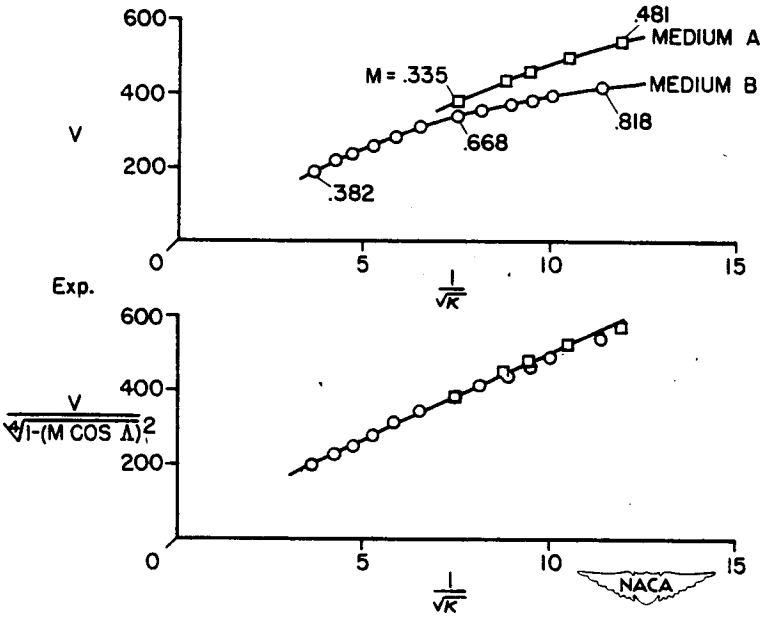


Figure 6.- Density and Mach number effects on flutter, wing 1. $\Lambda = 15^{\circ}$.

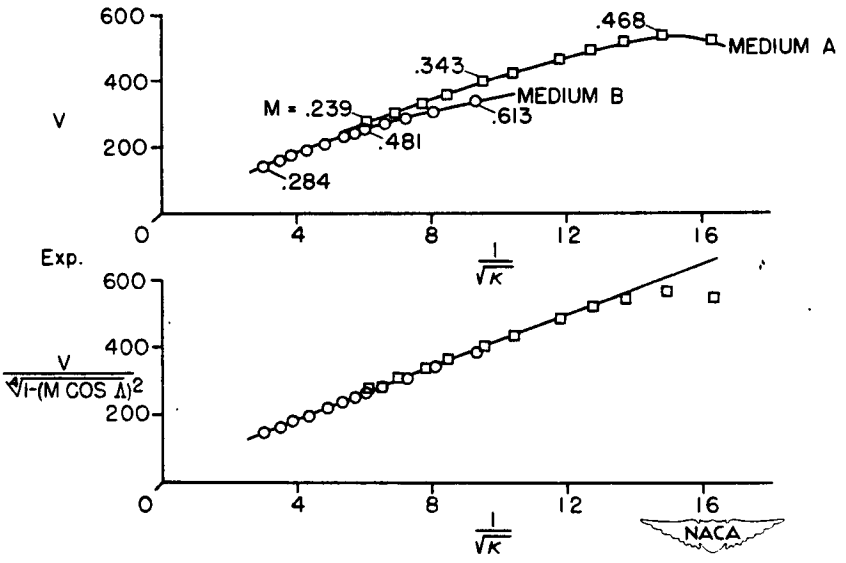


Figure 7.- Density and Mach number effects on flutter, wing 2. $\Lambda = 0^{\circ}$

[redacted]

97 N65-86457

THE ROLLING POWER OF TWO WING–AILERON CONFIGURATIONS AS AFFECTED BY FLEXIBILITY

By Warren A. Tucker and Paul E. Purser

Langley Aeronautical Laboratory

I – PRESENTATION OF DATA AND COMPARISON WITH THEORY

INTRODUCTION

This paper presents the results of a recent investigation, using the free–flight rocket–model technique, to obtain information on the effect of torsional flexibility on the rate of roll of two wing–aileron configurations. These two configurations are given in figure 1 and are identical in aspect ratio, taper ratio, flap chord, and flap span and differ only in the angle of sweepback.

Several models of each configuration were constructed and flown. These models were alike in their external geometry, but by means of metal plates of different sizes and materials set within the wing surface the torsional flexibility of each series of models was made to vary over a wide range. The torsional flexibility of each model was measured by applying a known couple at the wing tip, as shown in figure 1, and measuring the resulting twist along the span. The adequacy of this method as applied to the swept wings can, of course, be questioned. The torsional flexibility is expressed as $\frac{1}{m_{\theta_r}}$, the twist at the flap midspan due to a unit couple at the tip (for all the models, the twist varied linearly with distance along the span). For purposes of comparison with wings of other sizes, $\frac{1}{m_{\theta_r}}$ should be replaced by $\frac{l^3}{m_{\theta_r}}$, where l may be any characteristic dimension of the wing.

RESULTS AND DISCUSSION

The experimental data are shown in figures 2 and 3. The effect of increasing torsional flexibility is quite evident; two of the models were so flexible as to roll against the applied moment. Because of the flight path followed by the models, the static pressure varied with Mach number. (See fig. 4.)

[redacted]

The remainder of this discussion will be devoted to the data for the unswept wings. The swept-wing results will be mentioned again in the second part of the paper.

The data in figure 3 have been cross-plotted and extrapolated a small amount to $\frac{1}{m_{\theta_r}} = 0$ (infinite torsional stiffness) to provide the information given in figure 5. The ordinate represents the ratio of the rate of roll for a wing of given flexibility to the rate of roll for a perfectly rigid wing. The linearity of the curves is in agreement with theoretical considerations. The increase in percent loss in rate of roll as the Mach number increases is largely the result of the decrease in rate of roll of the rigid wing and the change in static pressure with Mach number. It is emphasized that the curves of figure 5 were derived from a particular set of data and are, therefore, applicable only to these data.

Because of the nature of the curves of figure 5, the same information can be given by a single curve plotted against Mach number. This curve is shown in figure 6 together with the corresponding theoretical curves. Also presented in the same figure are the experimental and theoretical values for $\left(\frac{pb}{2V}\right)_R$, the rate of roll for a perfectly rigid wing. The theoretical values for the subsonic range were obtained from reference 1; a lifting-surface-theory correction determined from reference 2 was applied to the values of $\left(\frac{pb}{2V}\right)_R$. The theoretical values for the supersonic range were calculated from reference 3 with the trailing-edge-angle reduction factor of that paper replaced by the corresponding factor of reference 4; this procedure was found to produce more consistent results than did the unmodified use of reference 3. The corresponding theory for the tapered unswept wing is available in reference 5.

The comparison between theory and experiment is rather encouraging, particularly inasmuch as it shows that the theory predicts equally well both the rate of roll for the rigid wing and the loss due to flexibility, so that any experimental checks of calculated values of $\frac{pb}{2V}$ for a given flexible wing will not be regarded as wholly accidental.

The value of $\frac{pb}{2V}$ for any particular wing can be calculated from the relation

$$\frac{pb}{2V} = \left(\frac{pb}{2V}\right)_R \left[1 + \frac{d(p/p_R)}{d\left(1/m_{\theta_r}\right)} \frac{1}{m_{\theta_r}}\right]$$

Calculations from the theory have been made for two of the wings tested and the results are compared in figure 7 with the test values. The agreement is considered to be acceptable for many purposes. The lack

of theoretical information in the transonic range is glaringly evident. A method for estimating the relative loss in this range has been proposed by Mr. Purser of the Langley laboratory. This method, which is no less accurate for swept wings than for unswept wings, is given in the following section.

II – EMPIRICAL METHOD FOR TRANSONIC SPEEDS AND SWEPT WINGS

The material presented in the first part of this paper has shown that the theories for the unswept wing at subsonic and supersonic speeds are reasonably reliable; however, for the unswept wing at transonic speeds and for the swept wing at all speeds, no theories are available.

The experimental data already presented and some additional data have been analyzed in an attempt to develop an empirical procedure for use while more exact methods are being derived for calculating the loss in rolling effectiveness due to wing twist at transonic speeds. The rolling effectiveness for the rigid wing must be obtained by other means. The basis for the analysis is to evaluate from the experimental data the twisting moments that cause the loss in aileron effectiveness. In evaluating these twisting moments the method of Pearson and Aiken (reference 1) was applied in reverse; that is, the values of one minus the ratio of flexible wing rate of roll to rigid wing rate of roll measured from cross plots of the experimental data were substituted in Pearson's equation (equation (A-24) of reference 1) to obtain effective values of $\frac{dc_m/d\delta}{d\alpha/d\delta}$ or $\frac{c_{m_\delta}}{\alpha_\delta}$, which may be regarded as proportional to the twisting moments acting on the wing.

Effective values of $\frac{c_{m_\delta}}{\alpha_\delta}$ evaluated from flights of the series of rocket models having NACA 65A009 airfoils are shown in figure 8. Also shown in figure 8 are values of $\frac{c_{m_\delta}}{\alpha_\delta}$ estimated from references 1 and 6 and theory for 0.20c ailerons with trailing-edge angles of 10°. The effective values of $\frac{c_{m_\delta}}{\alpha_\delta}$ for the unswept wing show fair agreement with the theoretical values. The values for the 45° swept wing are very nearly equal to the values for the unswept wing multiplied by the cosine of the sweep angle for Mach numbers between 0.8 and 1.2. This result, however, is only fortuitous since an inspection of other pitching-moment data shows no such simple relation in the general case. The large increase in $\frac{c_{m_\delta}}{\alpha_\delta}$ for the unswept wing at $M = 0.925$ is a result of the reduced value of α_δ which is indicated by the low value of $\left(\frac{pb}{2V}\right)_R$ in figure 6.

[redacted]

Pitching moments were also evaluated from flights of unswept NACA 65A003 airfoils. The data for the thinner wing of reduced trailing-edge angle showed slightly greater effective pitching moments except in the region between $M = 0.9$ and 1.0. The peak at $M = 0.925$ was reduced markedly; the thinner wing $\frac{c_{m_\delta}}{a_\delta}$ peaked at 2.1 at $M = 0.95$. The agreement of these pitching-moment data with other experimental data (reference 7, for instance) is about as good as the agreement with theory and indicates, therefore, that, in the absence of more exact methods for the transonic range, the method of Pearson and Aiken may be used to compute the effects of flexibility in the following manner:

(a) Experimental or estimated values of $\frac{c_{m_\delta}}{a_\delta}$ for the transonic range are substituted in equation (A-24) of reference 1 in place of $\sqrt{1 - M^2}\,\frac{dc_m/d\delta}{d\alpha/d\delta}$.

(b) The torsional stiffness parameter m_{θ_r} is determined from moments applied and twist angles measured in planes parallel to the plane of symmetry.

Values of $\left(\frac{pb}{2V}\right)_R$ may be obtained from other sources, for example, other papers at this conference.

[redacted]

REFERENCES

1. Pearson, Henry A., and Aiken, William S., Jr.: Charts for the Determination of Wing Torsional Stiffness Required for Specified Rolling Characteristics or Aileron Reversal Speed. NACA Rep. 799, 1944.

2. Swanson, Robert S., and Priddy, E. LaVerne: Lifting-Surface-Theory Values of the Damping in Roll and of the Parameter Used in Estimating Aileron Stick Forces. NACA ARR L5F23, 1945.

3. Tucker, Warren A., and Nelson, Robert L.: The Flexible Rectangular Wing in Roll at Supersonic Flight Speeds. NACA TN 1769, 1948.

4. Tucker, Warren A., and Nelson, Robert L.: Theoretical Characteristics in Supersonic Flow of Constant-Chord Partial-Span Control Surfaces on Rectangular Wings Having Finite Thickness. NACA TN 1708, 1948.

5. Tucker, Warren A., and Nelson, Robert L.: The Effect of Torsional Flexibility on the Rolling Characteristics at Supersonic Speeds of Tapered Unswept Wings. NACA TN 1890, 1949.

6. Langley Research Staff (Compiled by Thomas A. Toll): Summary of Lateral-Control Research. NACA Rep. 868, 1947.

7. Luoma, Arvo A.: An Investigation of a High-Aspect-Ratio Wing Having 0.20-Chord Plain Ailerons in the Langley 8-foot High-Speed Tunr 1. NACA RM L6H28d, 1946.

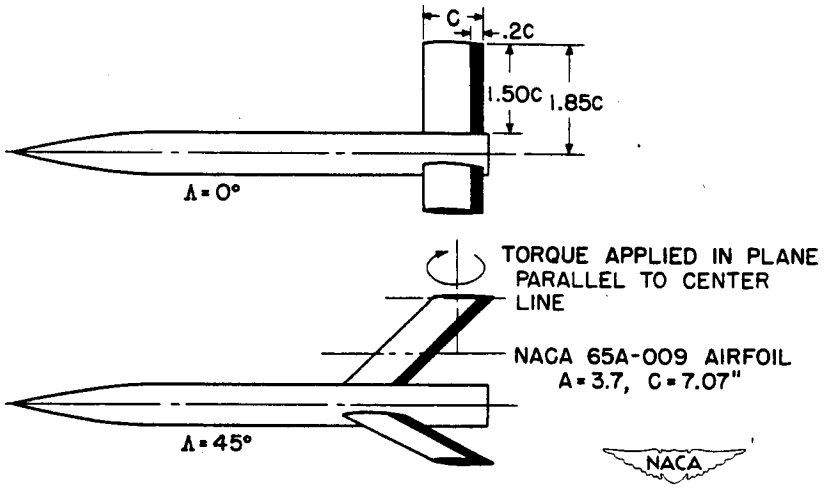


Figure 1.- Rocket models used for wing flexibility investigation.

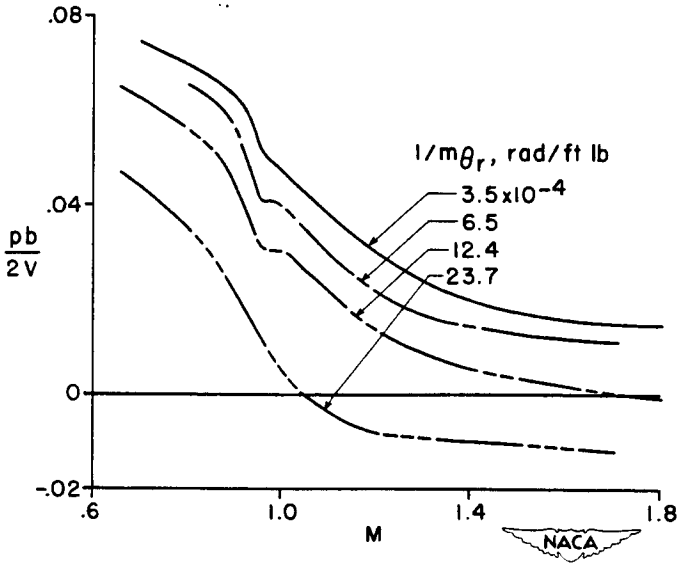


Figure 2.- Experimental results for the swept wings. Control-surface deflection is 10° total; see figure 4 for static pressure.

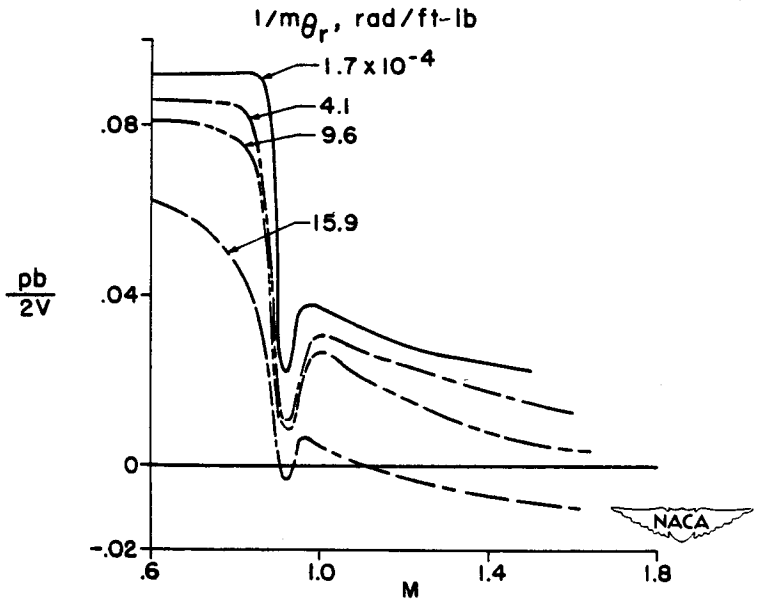


Figure 3.- Experimental results for the unswept wings. Control-surface deflection is 10° total; see figure 4 for static pressure.

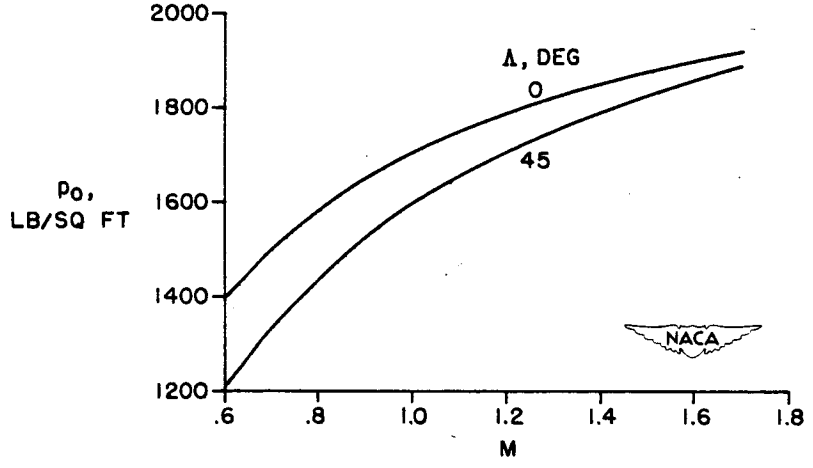


Figure 4.- Static pressure variation for test flights.

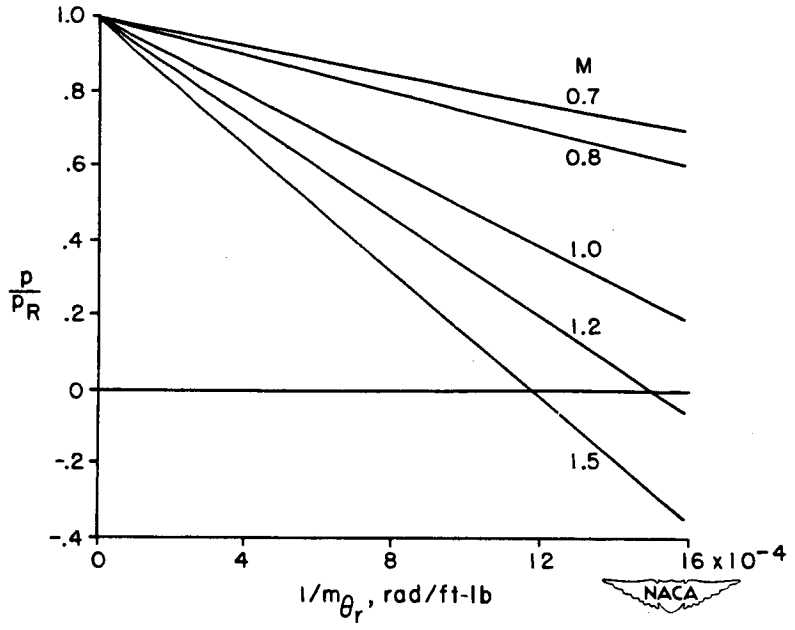


Figure 5.- Effect of torsional flexibility for the data of figure 3; see figure 4 for static pressure.

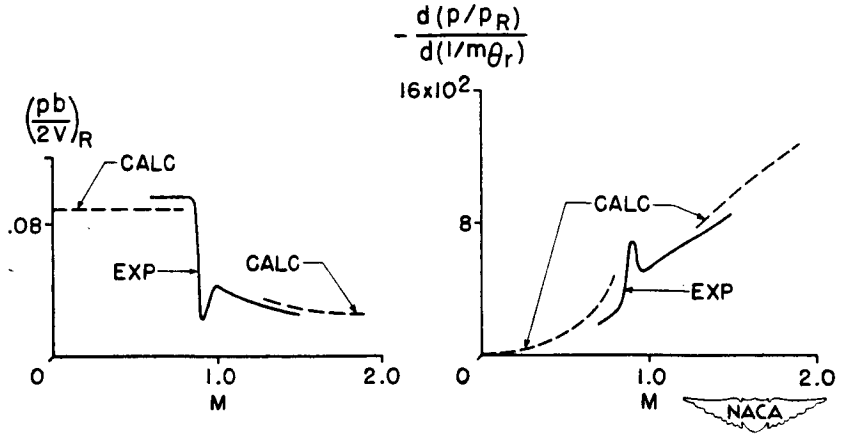


Figure 6.- Comparison between theory and experiment for the unswept wings. Control-surface deflection is 10° total.

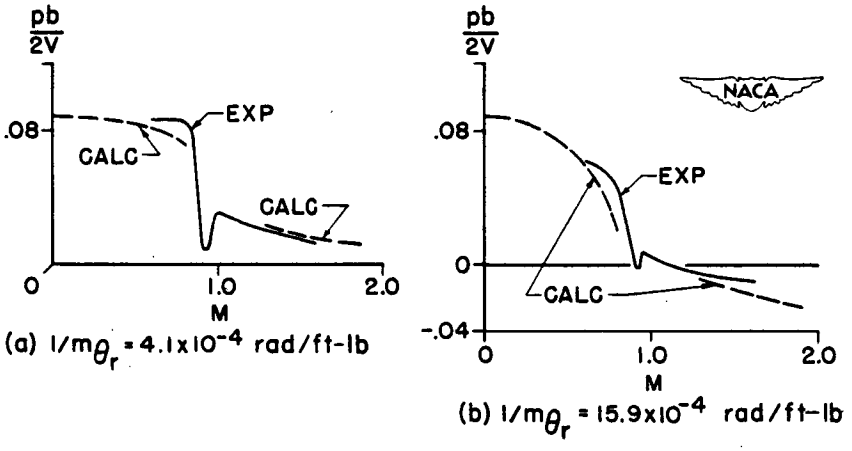


Figure 7.- Comparison between theory and experiment for two specific unswept wings. Control-surface deflection is 10° total.

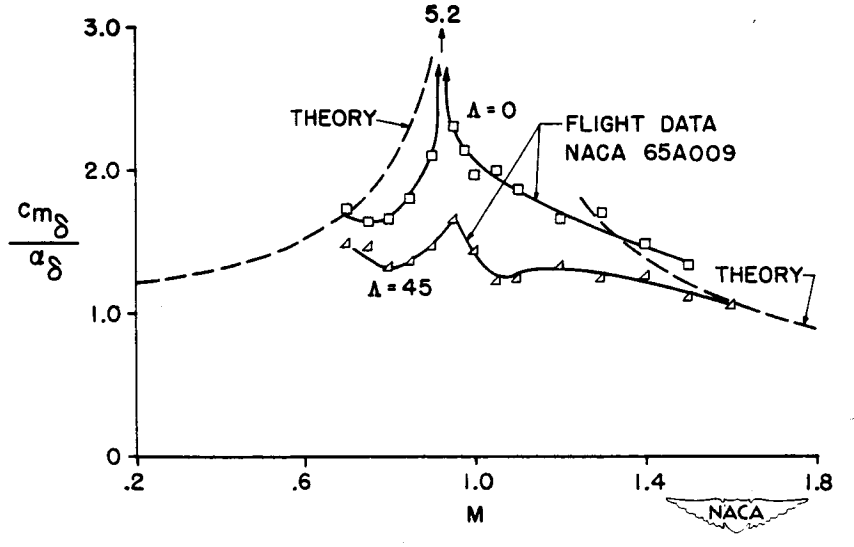


Figure 8.- Pitching moments evaluated from flights of NACA 65A009 airfoils on rocket models.

Preceding page blank

THE EFFECT OF AEROELASTICITY ON THE STATIC LONGITUDINAL STABILITY OF AN EXAMPLE SWEPT-WING BOMBER

By Richard B. Skoog

Ames Aeronautical Laboratory

N65-86458

INTRODUCTION

The effect of structural deflections on the static longitudinal stability of an airplane has become of increased interest with the application of sweptback wings for high-speed flight. It was the purpose of the analysis reported herein to evaluate the magnitudes and trends of the various factors involved in the stability change for a given airplane. The analysis was applied to an example swept-wing bomber which was known to have a relatively flexible structure. Through the cooperation of the Boeing Aircraft Company, it has been possible to use structural and weight data for the B-47 airplane in this analysis and thus assure that a realistic relation exists between the elastic characteristics of the various airframe components. Compressibility considerations were neglected, since a preliminary estimate over the Mach number range for which the Glauert factor applies showed them to be unimportant for the particular configuration being studied.

In order to analyze the problem, it was necessary to use some method for estimating the changes in span load distribution associated with the aforementioned aeroelastic effects. Much previous work has been done (e.g., references 1, 2, and 3) but the methods were not amenable to the type of analysis desired. A more exact treatment of the aerodynamic part of the analysis also was needed than was possible to incorporate in certain of those methods. The method finally developed (reference 4) consists of an iterative approach using aerodynamic loadings from reference 5. Over-all lift-curve slope for the rigid wing was also obtained from that reference. As in previous work on the subject, the method assumes the existence of a straight elastic axis based on no rotation for those chord sections perpendicular to the swept span.

The airplane configuration which was examined is shown in figure 1 with the pertinent geometric parameters indicated. The sweep angles of wing and tail are 35° and 33°, respectively; the wing aspect ratio is 9.43, wing taper ratio 0.42; tail length is 0.95 wing semispan, tail aspect ratio 4.06, tail taper ratio 0.423, and tail volume 0.672. The effect of the engine nacelles on the aerodynamic span load distribution was neglected in the analysis as was the effect of the fuselage. The elastic axis for the wing is located at 38 percent chord and for the tail is located at 50 percent chord.

THE STABILITY EQUATION

The familiar longitudinal-stability equation representing the stability contribution of the wing and tail is as follows:

$$\frac{dC_M}{dC_L} = \frac{x}{c} + \frac{C_{L_{\alpha_t}}}{C_{L_\alpha}}\left(1 - \frac{d\epsilon}{d\alpha} - \frac{di_t}{d\alpha}\right)\bar{V}\frac{q_t}{q}$$

The five factors in the equation which are subject to aeroelastic change are:

(a) Wing-aerodynamic-center position, $\frac{x}{c}$

(b) Wing lift-curve slope, C_{L_α}

(c) Rate of change of downwash at tail, $\frac{d\epsilon}{d\alpha}$

(d) Tail lift-curve slope, $C_{L_{\alpha_t}}$

(e) Fuselage bending term, $\frac{di_t}{d\alpha}$ $\left(\text{for rigid case } \frac{di_t}{d\alpha} = 0\right)$

The other factors in the equation are the tail volume and dynamic-pressure ratio. The first three of the aeroelastic factors are affected solely by wing flexibility, with the last two factors being affected by tail flexibility and fuselage flexibility, respectively. In this analysis the effects of wing flexibility will be discussed first, followed by discussion of effects due to flexibility of the tail and fuselage. In evaluating the wing and tail effects the fuselage is assumed to be rigid; that is, $\frac{di_t}{d\alpha}$ was assumed to be equal to zero. Throughout the analysis the ratio of tail dynamic pressure to free-stream dynamic pressure is assumed to be equal to 1.0.

EFFECTS OF WING FLEXIBILITY

The spanwise distributions of load present on the rigid wing are considered to be the following for this analysis:

(a) Additional type

(b) Basic type

[redacted]

(c) Pitching-moment type

(d) Wing-inertia type

The additional and basic types make up the distribution of aerodynamic loading normal to the plane of the wing with the additional type proportional to lift coefficient and the basic type proportional to the amount of washout or washin. The pitching-moment type is an aerodynamic torsional load which depends on the amount and kind of camber. The wing-inertia type is that due to the dead weight of the wing and is proportional to acceleration normal to the wing. Although all these loadings exert their individual effects on wing deflection, only the deflections due to the additional and inertia loadings have an influence on the wing stability factors, since only these deflections vary with lift coefficient (or with normal acceleration at a constant dynamic pressure). In order to simplify the presentation, the influence of wing inertia will be left until later in the discussion. The only wing deflections considered in the first part of this analysis, therefore, are those of a weightless wing subjected to an additional-type loading. Throughout this presentation the term "weightless wing" will be used to describe a wing having no inertia. Having now established the basis for discussion, the effect on aerodynamic-center position of the interaction between the additional loading and the resulting wing deflections will be considered, to be followed by consideration of the other factors in turn.

Aerodynamic-Center Position

Since all loadings normal to the plane of the wing are assumed to be concentrated along the quarter-chord line, it is fairly evident that the aerodynamic-center position of a weightless wing is the position along the quarter-chord line corresponding to the location of the centroid of the additional span load distribution. The relation between rigid-wing span load distribution and aerodynamic-center position is shown in figure 2 for the wing under consideration. The loading curve presents the additional loading coefficient for the rigid wing plotted against fraction of the semispan as obtained from reference 5. The centroid along the spanwise axis of the area so enclosed is also noted, together with the associated aerodynamic-center position. The loading coefficient is a function of section lift coefficient, local wing chord, average wing chord, and total wing lift coefficient. Since the curve of additional loading coefficient at any other wing lift coefficient is obtained merely by multiplying all the ordinates along the curve by a constant, it is plainly evident that the centroid for the rigid wing (and consequently the aerodynamic-center position for the rigid wing) is not a function of lift coefficient since the shape of the curve remains unchanged at other lift coefficients. The same also can be said for normal acceleration, since at a given dynamic pressure a linear relationship

[redacted]

between lift coefficient and normal acceleration must always exist. If this reasoning is extended to the case of a flexible wing, it can be shown that the aerodynamic-center position for the flexible wing at a given dynamic pressure also is independent of lift coefficient or normal acceleration. The only difference between the rigid and flexible cases is the difference in shape of the load-distribution curve, an example of which is shown in figure 3 for a dynamic pressure of 500 pounds per square foot. The loading curve for the flexible wing includes the calculated effects of both bending and torsional deflections along and about the elastic axis, with the effect of bending predominating, as will be discussed later. The loading coefficient applies to both the rigid and flexible cases since the modifying influence of flexibility is proportional to lift coefficient. As can be seen from the figure the over-all effect of wing flexibility on the additional-type loading is to relieve the tip sections and load up the root sections at a given lift coefficient. As also can be seen from the figure the centroid of the loading for the flexible wing lies inboard of that for the rigid wing, which has the result of a forward shift in the aerodynamic center as shown. The forward movement in aerodynamic-center position with increase in dynamic pressure is shown in figure 4 together with the associated stability change. As can be seen, the aerodynamic center moves forward from the rigid-wing value of 25 percent of the mean aerodynamic chord until at a dynamic pressure of about 650 pounds per square foot the aerodynamic center is at the leading edge of the reference chord. At higher values of dynamic pressure the aerodynamic center moves even farther ahead.

With reference to the stability equation, it will be remembered that the change in stability due to the wing is exactly equal to the change in aerodynamic-center position for the wing. Since the aerodynamic-center position moves forward with increasing dynamic pressure and only with dynamic pressure, as was shown, the resulting loss in stability due to the wing can be plotted as a single curve of stability change against dynamic pressure as shown in the figure. As can be seen from the values of stability change, the effect of aerodynamic-center shift in itself is very large. For example, at a dynamic pressure of 500 pounds per square foot, the neutral point of the wing has shifted forward by 20 percent, which of itself would introduce a serious stability problem.

It is of some interest to know how much of this stability change is due to bending deformations and how much is due to torsional deformations. The relative contribution of the two deflection modes is shown in figure 5 together with the net effect. As can be seen from the figure, the effect of torsional deflections was stabilizing, while the effect of bending deflections was destabilizing. The contribution due to torsion is seen to be about one-fifth of that due to bending. This ratio, of course, depends on the ratio of torsional to

bending rigidities and location of the elastic axis and hence would not necessarily be the same for all airplanes. An equally important factor to consider is the effect of changing the sweep angle. The extremes of zero sweep and 90° sweep best illustrate the point, since for zero sweep only torsion is a factor, while for 90° sweep only bending is a factor. The net effect of the two deflection modes is the same as was shown in figure 4. It should be pointed out here that the effects due to bending and torsion shown in the figure are not for pure bending and pure torsion, since the calculation procedure accounts for the aeroelastic interaction inherent in the physical setup. Because of the small magnitude of the interaction effects for this airplane, however, this distinction is primarily of academic interest only.

Wing Lift-Curve Slope

The effect of wing flexibility on wing lift-curve slope and the associated stability change is next in order of discussion. The reason for a change in lift-curve slope for a sweptback wing is, of course, that at a given angle of attack the wing deflections are normally such as to reduce progressively the local angle of attack along the span for streamwise sections. The effect of angle-of-attack reduction for the tip sections is to cause a reduction in lift over that portion of the wing so that the over-all lift is lowered. The amount of lift which is lost is proportional to the angle of attack of the undeflected wing (over the usual range of angles of attack) so that the net effect of wing flexibility on the lift curve is merely to rotate the entire rigid-wing curve as a unit to a lower value of lift-curve slope. The lift curve for the rigid and flexible wing of this analysis (neglecting the angle for zero lift) is presented in figure 6 for a dynamic pressure of 500 pounds per square foot. Also in the same figure is presented the stability contribution of the tail as represented by the second term of the stability equation previously referred to. In the figure the pitching-moment coefficient is the contribution of the tail to the pitching-moment coefficient for the airplane. In evaluating the stability term for the flexible wing, the only parameter which was changed from that for the rigid airplane is the value of wing lift-curve slope. As can be seen from the stability curves the effect of the reduction in lift-curve slope is to increase the nose-down pitching moment for a given lift coefficient which corresponds to an increase in the stability contribution of the tail. The ratio of flexible to rigid lift-curve slope and the associated increase in tail contribution are presented in figure 7 as a function of dynamic pressure for the weightless wing together with the associated stability change. At a dynamic pressure of 500 pounds per square foot the lift-curve slope is reduced to 64 percent of the rigid-wing value. The associated increase in tail stability contribution amounts to 25 percent, or a rearward neutral-point shift of that amount. At this same dynamic pressure the

stability contribution of the wing aerodynamic center was shown to be a forward neutral-point shift of 20 percent, or almost the same magnitude, so that the two wing factors so far discussed would appear to be largely canceling. Whether canceling of these effects will exist in general for all configurations cannot be determined at this time. Calculations for a fighter configuration of markedly different geometric and structural characteristics, however, resulted in essentially the same relation between these wing factors. An interesting extreme to consider is the case of the flying wing for which the second term of the equation does not exist. In this case no canceling of these effects will be possible so that the net stability change will be due solely to any aerodynamic-center shift.

Since the effect on stability of reduction in wing lift-curve slope is large, it is of interest for this factor as well as for the first factor (namely the aerodynamic-center position) to consider the relative contribution of bending and torsion. These contributions are shown in figure 8, which is merely a repeat of figure 7 with the individual effects of bending and torsion added. As can be seen, the contribution of torsion to the lift-curve slope causes an increase, while the larger effect due to bending causes a decrease which is about ten times greater. The associated stability changes are shown to be a decrease due to torsion and an increase about seven times larger due to bending. The effect of bending is somewhat greater in this case than was the case for aerodynamic center for which a factor of five was shown.

Rate of Change of Downwash at Tail

Having examined two of the wing stability factors in some detail, the remaining factor for the wing (namely, the rate of change of downwash at the tail) can now be considered. The aeroelastic factors which influence the rate of change of downwash at the tail are the redistribution of the additional-type span load distribution and the reduction of lift-curve slope already discussed. To analyze the downwash changes, it was believed sufficient to determine the change in maximum downwash at the tail location (that is, the downwash in the plane of the vortex sheet) on the basis that any effect so determined should be conservative. The variation along the swept-tail span of the rate of change of downwash in the plane of the vortex sheet is presented in figure 9 for several values of dynamic pressure. The method used to estimate maximum downwash (given in reference 6) is based on the semisurface loading theory of reference 5 as applied to any arbitrary continuous span load distribution. The location of the tip of the horizontal tail is indicated in the figure. As can be seen, large changes in downwash are indicated behind the outer sections of the wing and in the plane of symmetry; however, the average downwash over the tail is changed only slightly. The change in average downwash would appear to depend to a minor extent

on the ratio of tail span to wing span. The downwash factor $1 - \frac{d\epsilon}{d\alpha}$ based on the average downwash over the tail is presented in figure 10 as a function of dynamic pressure along with the associated change in stability contribution of the tail. The stability change was determined as before as the change in the second term of the stability equation. As can be seen from the figure the change in downwash factor is very slight, being of the order of 5 percent at the highest dynamic pressure considered. The stability change, as would be expected, is correspondingly small and relatively unimportant compared to the other stability factors so far discussed.

Dead Weight

The aeroelastic effects due to wing flexibility so far discussed have been with regard to a weightless wing. The effect of wing inertia or dead weight on these factors $\left(\text{namely } \frac{x}{c}, C_{L_\alpha}, \text{ and } \frac{d\epsilon}{d\alpha}\right)$ will now be considered. The general effect which can be observed immediately is that inertia is always of a relieving nature in that it tends to reduce the magnitudes of the aerodynamic changes. The relieving nature of the wing dead weight is fairly self-evident, since the physical influence of the weight is to reduce the deflections due to aerodynamic load for the weightless wing in proportion to the load factor normal to the plane of the wing. The extent to which the aerodynamic changes are reduced, however, depends on the spanwise distribution of the wing weight and the wing loading of the airplane. The more of the wing weight which can be concentrated at the wing tips, the greater the relieving effect will be. Also the smaller the wing loading of the airplane becomes, the greater the relieving effect will be, since higher accelerations can be reached for a given lift coefficient and dynamic pressure. The effect of inertia on the location of the aerodynamic center and on the lift-curve slope for the example wing is presented in figure 11 for airplane wing loadings of 70 pounds per square foot and 100 pounds per square foot. The curve for the weightless wing is the same as would be obtained for the inertia case with a wing loading of infinity. The effect of the jet-engine weights on wing inertia is included. The effect on downwash at the tail is not shown, since the downwash changes for the weightless wing were shown to be unimportant. As can be seen from the figure, the effect of wing inertia is only mildly alleviating. Although the relieving effect in this case is shown to be rather small, the effect for other airplanes may not be of similar magnitude, since the inertia effect depends upon the ratio of wing weight to total airplane weight in addition to the spanwise distribution of the weight previously mentioned. Referring once more to the case of a flying wing, it would appear that wing inertia would have a much greater relieving effect in that case, since more of the total airplane weight is in the wings than for conventional airplanes.

[redacted]

EFFECTS OF TAIL FLEXIBILITY

The general stability equation showed the effect of horizontal-tail flexibility to consist merely of the effect on lift-curve slope. The tail also exhibits a forward shift in aerodynamic center in the same way as the wing, but that factor is negligible for the tail since the aerodynamic center of the tail only enters into the value of tail length used in the calculation of tail volume. Therefore, only the change in lift-curve slope, which depends on the interaction between the additional-type load distribution for the tail and the associated tail deflections - as was the case for the wing, needs to be considered. The ratio of flexible to rigid lift-curve slope and the associated decrease in tail stability contribution is shown in figure 12 for the weightless tail. Corresponding curves for the wing also are presented for comparison. The stability change was found in the same way as for the wing by holding all the parameters in the second term of the stability equation constant except for the tail lift-curve slope. The stability change was then found as before by taking the difference between the pitching-moment slope for the rigid tail and the pitching-moment slope for the flexible tail at a given dynamic pressure. As can be seen from the figure, the effect of flexibility on tail lift-curve slope is not so pronounced as that for the wing, and, as a consequence, the effect on stability contribution of the tail is also correspondingly less.

The effect of inertia on the tail lift-curve slope is shown in figure 13 for a wing loading of 70 pounds per square foot and also for a wing loading of infinity. The corresponding curves for the wing are also shown for comparison. As was stated previously, the curves for a wing loading of infinity correspond to those for a weightless wing and tail. As can be seen, the inertia effect on the tail is small compared with that for the wing.

Effect of Fuselage Flexibility

The effect of fuselage flexibility was shown to introduce an additional parameter into the second term of the stability equation which is similar in effect to the downwash factor previously discussed. The relation which defines the aerodynamic part of the fuselage factor is as follows:

$$\frac{di_t}{d\alpha} = \left[C_{L_{\alpha_t}}\left(1 - \frac{d\epsilon}{d\alpha} - \frac{di_t}{d\alpha}\right)q_t\, S_t\right]\left[I_l\right]$$

[redacted]

The factor contains the product of tail load per unit change in angle of attack multiplied by an influence coefficient depending solely on geometric and structural parameters. The aerodynamic tail load is made up of tail lift-curve slope (which is affected by tail flexibility), the rate of change of downwash at the tail (which is affected by wing flexibility), and also the fuselage factor itself. The dependence of the fuselage factor on dynamic pressure is also apparent. The influence coefficient can be expressed as the change in tail incidence per unit tail load. The relation showing the fuselage factor as an explicit function is as follows:

$$\frac{di_t}{d\alpha} = \frac{1 - \frac{d\epsilon}{d\alpha}}{1 + \frac{1}{C_{L_{\alpha_t}} q_t S_t l_t}}$$

The fuselage factor and the associated tail stability change for the example airplane are presented in figure 14 as a function of dynamic pressure. Curves are presented showing the effect of fuselage flexibility alone and also including the combined effects of wing and tail flexibility. For comparison, curves of average downwash and stability change due to downwash change are also presented. At the higher values of dynamic pressure the fuselage factor becomes of the same order of magnitude as the average rate of change of downwash at the tail and therefore is seen to be of considerable importance. The effect of including wing and tail flexibility in the fuselage factor is to lower the factor slightly as shown. By referring to the stability curves, it can be seen that the stability change due to fuselage bending is of much greater importance than that due to downwash change, as would be expected from the comparison shown in the upper part of the figure. It can also be seen that the effect of wing and tail flexibility is to reduce the stability decrease due to fuselage flexibility.

The inertia of fuselage and tail surfaces reduces the fuselage factor by an amount shown by the following relation:

$$\frac{di_t}{d\alpha} = \left[\frac{C_{L_\alpha} q}{\frac{W}{S}}\right]\left[I_1\right]$$

The relation consists essentially of the product of airplane load factor per unit angle of attack multiplied by an influence coefficient which depends on the weight distribution in addition to the geometric and structural parameters already mentioned. The load factor depends upon wing lift-curve slope (which is affected by wing flexibility) and also

upon dynamic pressure and airplane wing loading. The influence coefficient can be expressed as the change in tail incidence per unit load factor The effect of inertia on fuselage factor for the example airplane is shown in figure 15 for a wing loading of 70 pounds per square foot. Curves are presented for the airplane with inertia showing the effect of fuselage flexibility alone and also including the effect of wing flexibility. Corresponding curves for the weightless airplane from figure 14 are also presented for comparison. As can be seen from the figure, the effect of inertia on fuselage factor is very large and consequently of considerable importance. It will be remembered that the effect of inertia on the wing and tail factors was only slight by comparison. It is interesting to note that consideration of inertia and all the flexibilities involved results (for the example airplane) in a fuselage factor equal essentially to zero - even though the aerodynamic contribution is large. In these estimates of inertia effects, the influence on fuselage factor of wing and tail inertia has been neglected, since these effects are of higher order for this airplane.

RECAPITULATION AND SUMMARY

The effects of wing, tail, and fuselage flexibility on the longitudinal stability $\frac{dC_m}{dC_L}$ of the example airplane are summarized in figure 16, which shows the important individual effects which have been discussed. The upper set of curves presents the aerodynamic effects only - that is, for the weightless airplane. The lower set of curves includes the effect of inertia in addition to the aerodynamic effects for an airplane wing loading of 70 pounds per square foot. The curves presented show the stability change for each of the five factors in the stability equation which are subject to aeroelastic change. As was shown early in this analysis, these factors are:

(a) Wing-aerodynamic-center position, $\frac{x}{c}$

(b) Wing lift-curve slope, C_{L_α}

(c) Rate of change of downwash at the tail, $\frac{d\epsilon}{d\alpha}$

(d) Tail lift-curve slope, $C_{L_{\alpha t}}$

(e) Fuselage bending term, $\frac{di_t}{d\alpha}$

As can be seen from the figure, all the effects are destabilizing except the effect of reduction in wing lift-curve slope on the stability

contribution of the tail. The stability changes due to wing aerodynamic-center shift and reduction in wing lift-curve slope are shown to be by far the largest effects of those shown. Both of these results are shown to be true whether inertia effects are included or not. The net results of the combined effects with and without inertia are presented in figure 17, considering aerodynamic factors only and also including inertia effects. Due to the nature of the second term of the stability equation the effects shown in figure 16 are not all additive algebraically; therefore, these final summary curves were obtained by allowing all of the factors in the equation to vary simultaneously. As is evident from the figure, inertia plays a large part (for this airplane) in alleviating the stability decrease due to the interaction between aerodynamic and structural forces. The over-all stability change for the airplane with inertia is shown to be not nearly so excessive as a partial analysis of the problem might indicate. At a dynamic pressure of 500 pounds per square foot, the stability change for the airplane (with inertia considered) is seen to be equivalent to a neutral-point shift of about 6 percent.

Before terminating this discussion it is important to consider what general conclusions can be drawn from the present analysis. Although the over-all aeroelastic effect on stability for the example airplane was found to be small, it cannot be said that like calculations for any airplane will also yield a small effect, since the subject analysis was limited in scope. It can be said, however, that for any swept-wing airplane with a tail the stability change due to forward shift in wing aerodynamic center will be destabilizing, while the change due to reduction in wing lift-curve slope will be stabilizing so that a certain amount of canceling between these major effects will always be present. As was inferred earlier in the discussion, the degree of completeness of the canceling depends directly on the size, plan form, and location of the tail as they affect the tail factors in the second term of the stability equation. In the event that future extension of this analysis to many more configurations shows that the two major wing effects are strongly canceling, in general, it would appear that reduction in the over-all stability change due to all factors to obtain the minimum aeroelastic effect may be accomplished more advantageously by design changes to the horizontal tail than by similar changes to the wing.

REFERENCES

1. Diederich, Franklin W.: Calculation of the Aerodynamic Loading of Flexible Wings of Arbitrary Plan Form and Stiffness. NACA TN 1876, 1949.

2. Pai, S. I., and Sears, W. R.: Some Aeroelastic Properties of Swept Wings. Jour. Aero. Sci., vol. 16, no. 2, Feb. 1949, pp. 105-116.

3. Miles, John W.: A Formulation of the Aeroelastic Problem for a Swept Wing. Jour. Aero. Sci., vol. 16, no. 8, Aug. 1949, pp. 477-490.

4. Skoog, Richard B., and Brown, Harvey H.: The Effect of Aeroelasticity on the Aerodynamic Spanwise Load Distribution of a Flexible Sweptback Wing. (Prospective NACA paper)

5. DeYoung, John, and Harper, Charles W.: Theoretical Symmetric Span Loading at Subsonic Speeds for Wings Having Arbitrary Plan Form. NACA Rep. 921, 1948.

6. DeYoung, John: Theoretical Symmetric Wing Span Loading at Subsonic Speeds for Wings and Flaps of Arbitrary Plan Form. (Prospective NACA paper)

[redacted]

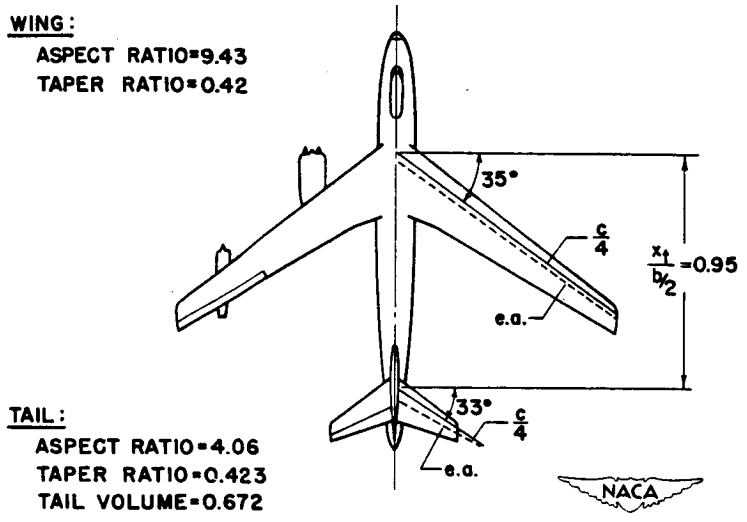


Figure 1.- Geometric characteristics of example airplane.

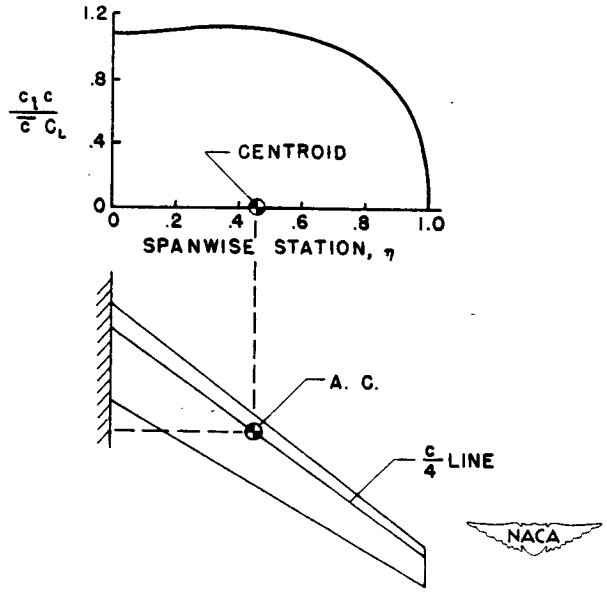


Figure 2.- Relation between centroid of additional span load distribution for rigid wing and aerodynamic-center position.

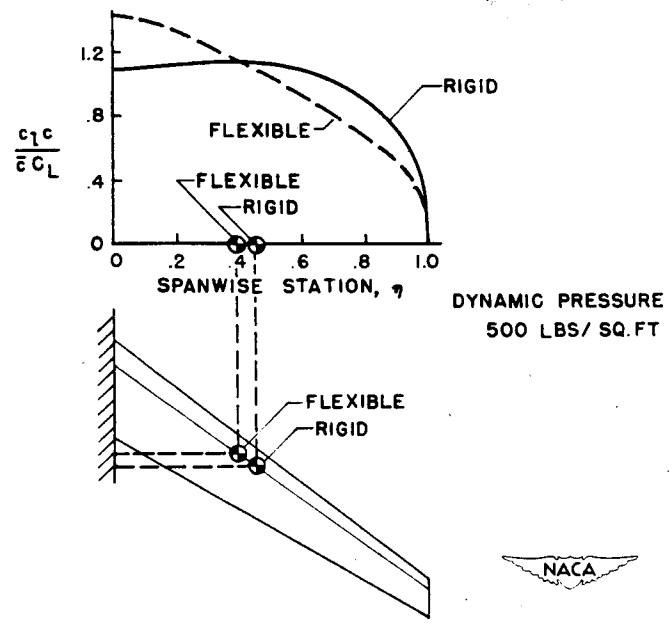


Figure 3.- Aerodynamic-center position for rigid and flexible wing.

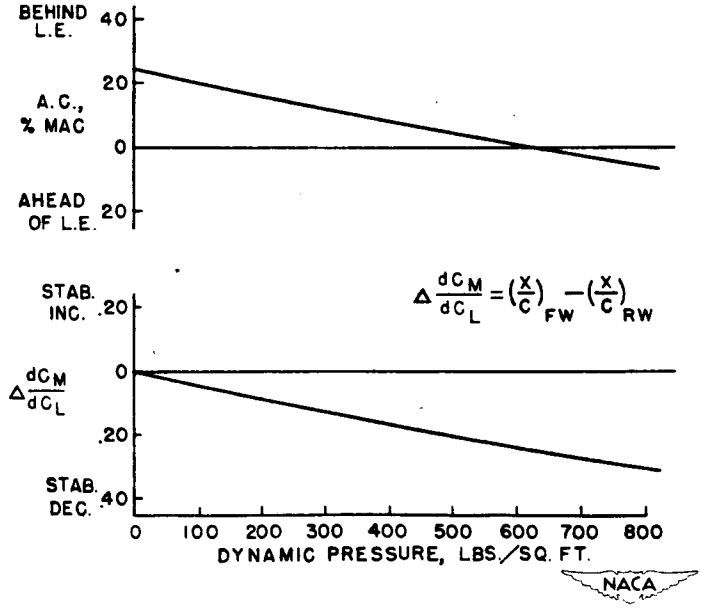


Figure 4.- Wing-aerodynamic-center shift and associated stability change.

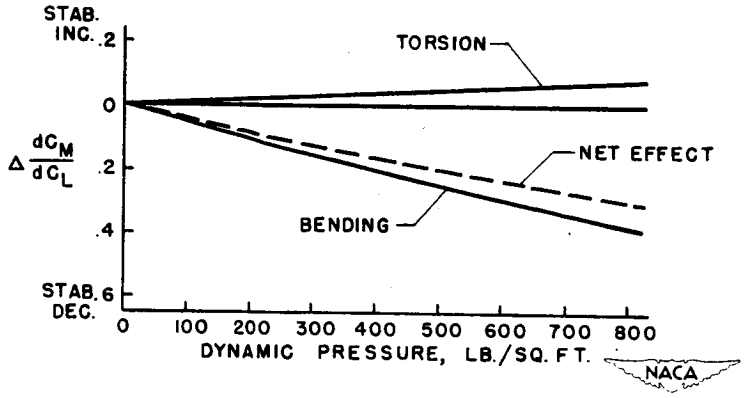


Figure 5.- Relative contribution of wing bending and torsion to the stability change due to wing-aerodynamic-center shift.

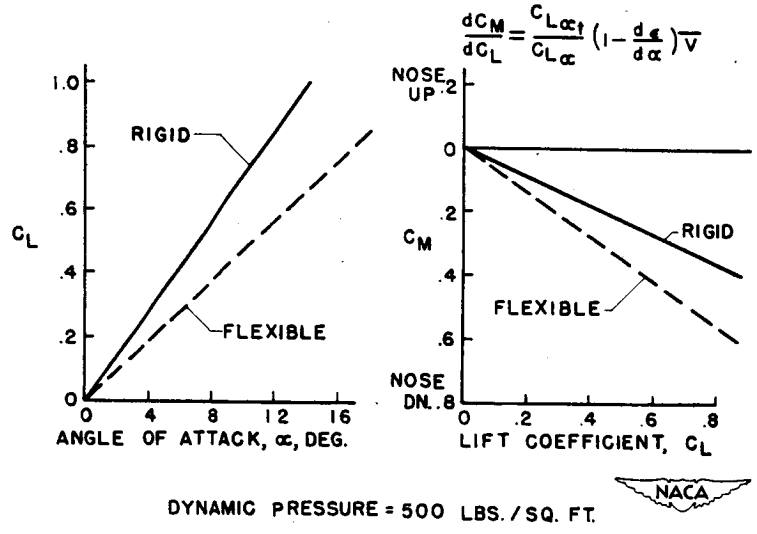


Figure 6.- Wing lift curve and associated tail-stability curve for rigid and flexible wing.

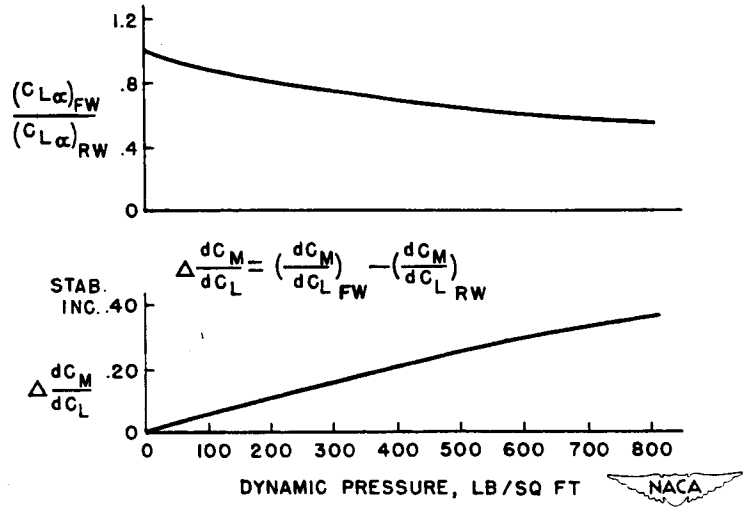


Figure 7.- Wing-lift-curve-slope reduction and associated tail-stability change as a function of dynamic pressure.

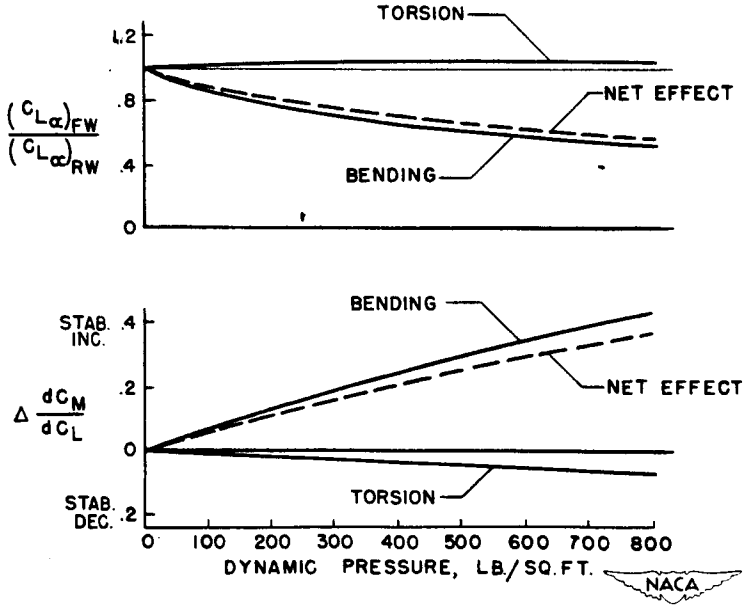


Figure 8.- Relative contribution of wing bending and torsion to the wing lift-curve slope and associated tail-stability change.

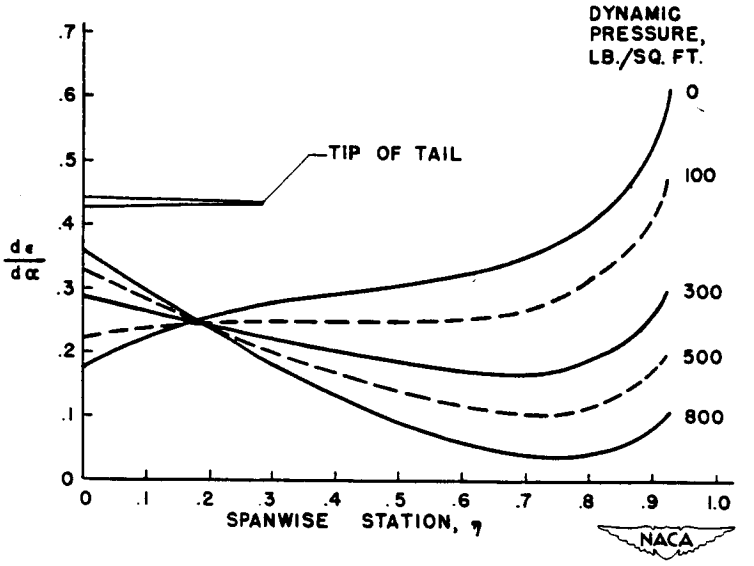


Figure 9.- Variation along the swept-tail span of the rate of change of maximum downwash in the wake for several values of dynamic pressure.

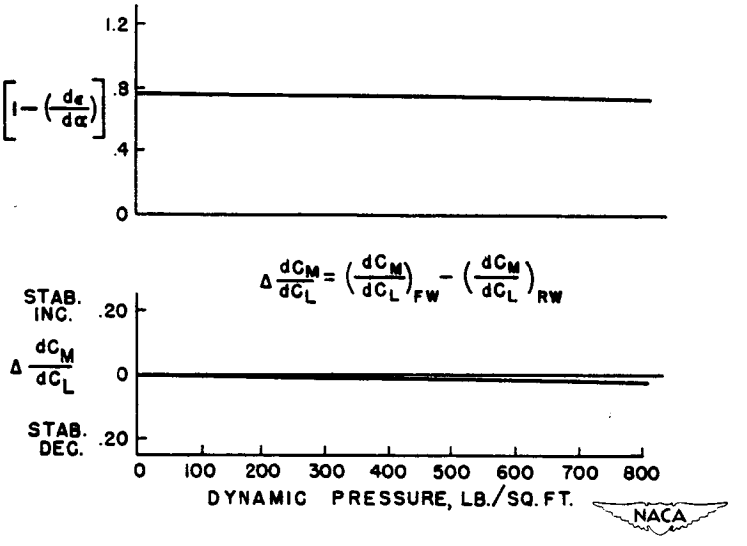


Figure 10.- Downwash factor and the associated tail-stability change as a function of dynamic pressure.

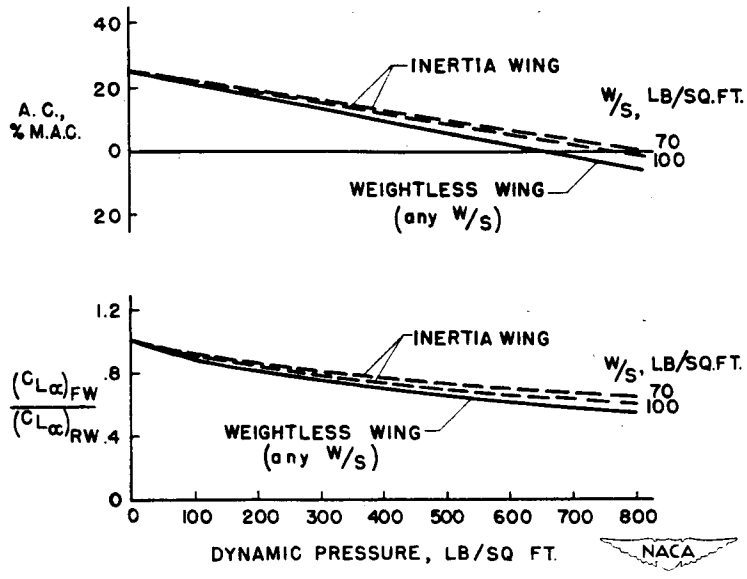


Figure 11.- Effect of inertia on wing-aerodynamic-center position and lift-curve slope for two airplane wing loadings.

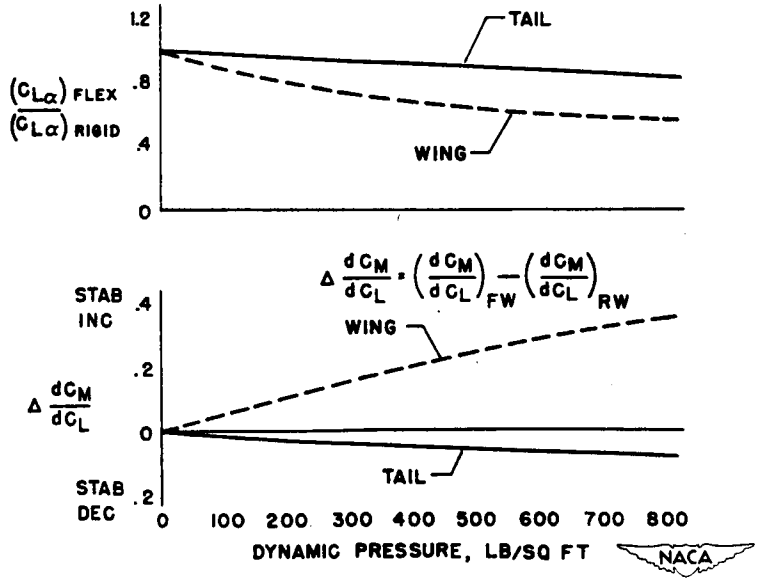


Figure 12.- Tail-lift-curve-slope reduction and associated tail-stability change as a function of dynamic pressure.

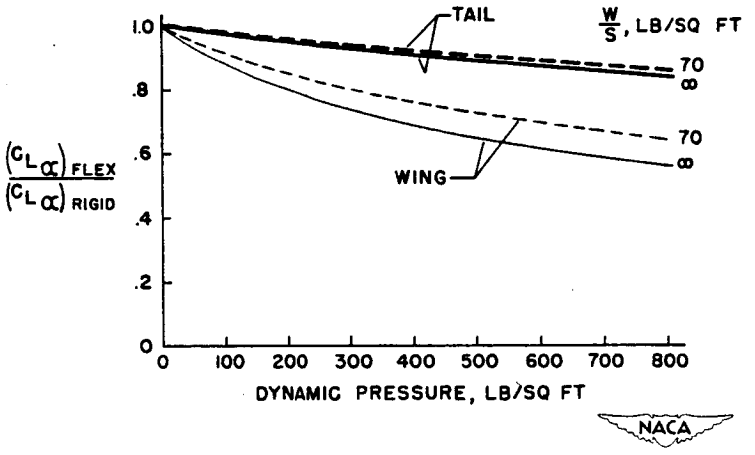


Figure 13.- Effect of inertia on tail lift-curve slope for two airplane wing loadings.

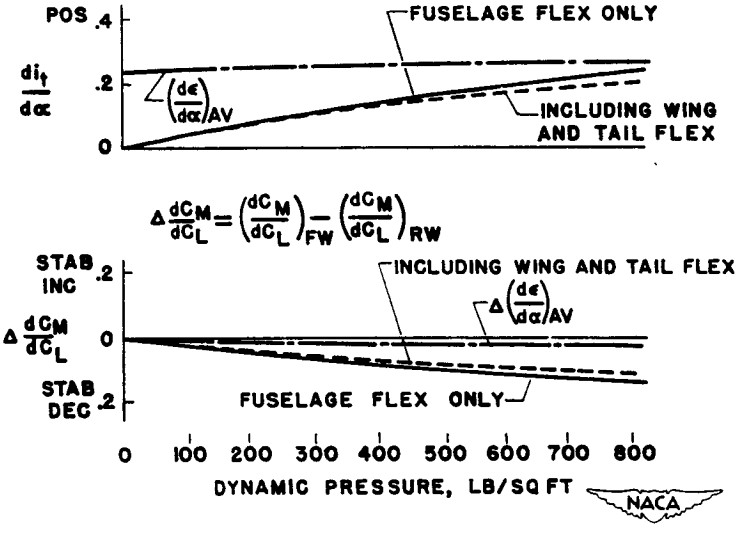


Figure 14.- Fuselage factor and associated tail-stability change as a function of dynamic pressure.

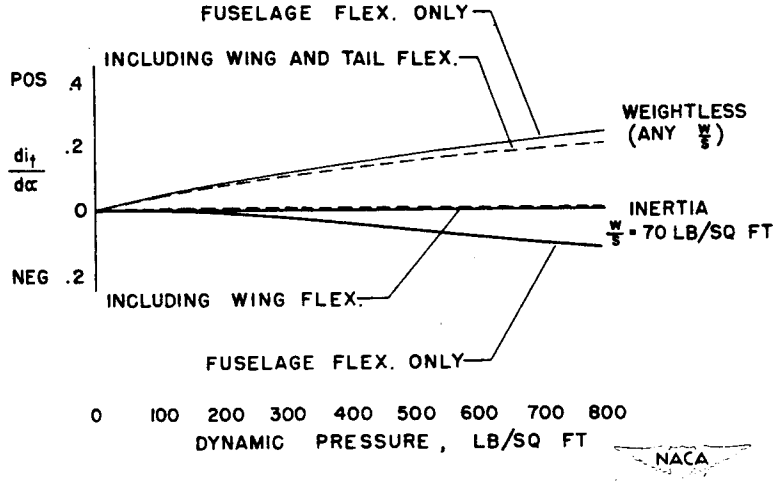


Figure 15.- Effect of inertia on fuselage factor.

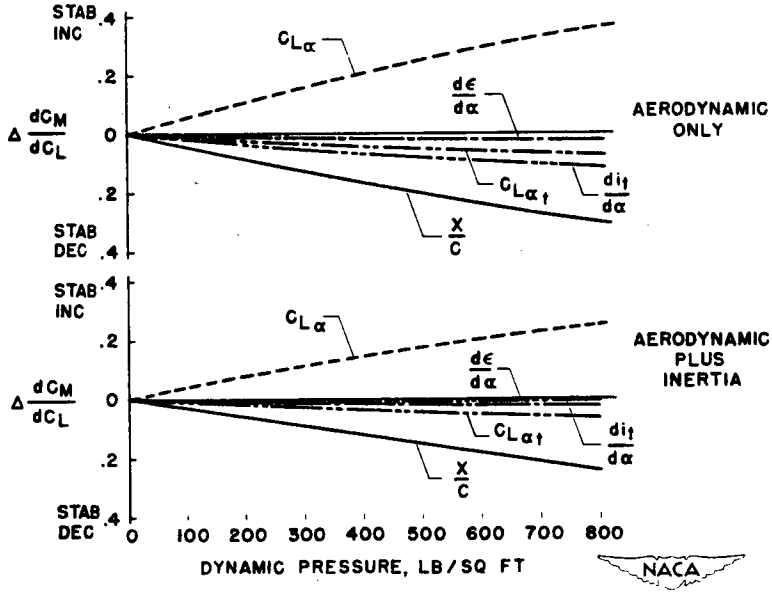


Figure 16.- Summary of the individual aerodynamic and inertia effects on stability.

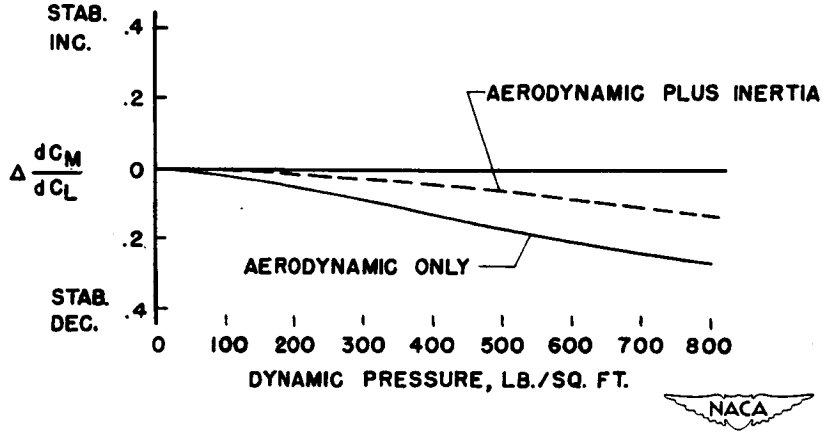


Figure 17.- Summary of all aerodynamic and inertia effects on stability.

Preceding page blank

N65-86459

WING SELECTION AS INFLUENCED BY THE EFFECT OF WING BENDING ON AERODYNAMIC-CENTER SHIFT

By Charles W. Mathews

Langley Aeronautical Laboratory

The use of swept wings has introduced aeroelastic problems not inherent in straight wings. These problems are a consequence of the angle-of-attack changes produced by wing bending. The resulting alterations in load distribution may have a significant effect on the longitudinal stability of a swept-wing airplane. Of current interest is the relation of wing plan form and thickness to the importance of this particular aeroelastic effect. Accordingly, a simplified analysis has been made to determine the effects of variations in wing geometry on one of the several stability parameters affected by this type of aeroelasticity. This parameter is the wing-aerodynamic-center position.

As shown in figure 1, the analysis was applied to shell wing structures in which the chordwise variation in skin thickness is proportional to the local airfoil section thickness and the spanwise variation of skin thickness is such that a constant spanwise stress is produced in the extreme fiber under a uniformly distributed load. A uniform distribution of the aerodynamic load was assumed for purposes of computing the angle-of-attack changes associated with wing bending. This somewhat arbitrary assumption as to the character of the loading is justified in a first-order analysis because these angle-of-attack changes are not greatly affected by fairly large differences between the shape of the assumed loading and the shape of the actual loading. Since the wing-aerodynamic-center shift is dependent solely on these angle-of-attack changes, the assumed approximation of the loading appears adequate. Inertia loads were not considered in the analysis and, therefore, the results apply strictly to airplanes which have a large percentage of their gross weight concentrated near midspan.

In order to compute the angle-of-attack changes that result from the wing bending under load, the swept wings were transformed in the manner indicated in figure 1. This transformation alters the root restraint and assumes that the elastic axis is straight. A limited study, however, indicates that the slopes of the bending curve obtained for the transformed wing closely approximate those for the actual wing, and that neglect of the twist induced by bending near the root of the swept wing does not materially affect the results except for low aspect ratios. Torsional deflections in general were not included in the analysis.

Results of this analysis were obtained in a parametric form which relates the wing-aerodynamic-center shift due to bending to the wing structural weight, structural material, external geometry, and the flight condition under which the wing operates. Results are shown in figure 2 for a specific flight condition, a Mach number of 1 at 40,000 feet altitude. The chart shows the geometric proportions of a series of dural wings all having the same structural weight for a given wing area and all having an aerodynamic-center shift due to bending of 10 percent of the mean aerodynamic chord. The magnitude of the wing structural weight indicated by the value of the parameter $W/S^{3/2}$ in figure 2 is a representative average for modern fighter and bomber airplanes having straight wings. The fact that these wings have the same percent chord shift in aerodynamic center means that the shift in terms of actual distance becomes less as the aspect ratio increases. From some considerations, therefore, it is possible that the same percentage shift does not express an exact equivalence for the wings shown. Another point worth noting is that the aerodynamic-center shift due to bending is nearly proportional to the dynamic pressure and the shift shown here would increase rapidly with either increase in speed or decrease in altitude.

Separate plots are presented (fig. 2) for taper ratios of 0, 0.5, and 1.0, and for each, the angle of sweepback of the quarter-chord line is plotted against aspect ratio for section thickness ratios of 0.05, 0.10, and 0.15 measured in the stream direction. At a given taper ratio and thickness ratio, the combinations of sweep and aspect ratio that satisfy the specified conditions have a nearly linear variation. For a taper ratio of 0.5 and a section thickness ratio of 0.10, the aspect ratio varies from about 6.3 at a sweepback angle of 30° to about 3.2 at a sweepback angle of 60°.

Increase in section thickness ratio to 0.15 enables increases in aspect ratio or sweep, but the magnitudes of these increases are not large in view of the probable large penalty in drag at zero lift resulting from a 50-percent increase in section thickness ratio.

A decrease in taper ratio appears to be a likely means for extending the combinations of sweepback and aspect ratio. This possibility is seen when the results obtained for a decrease in taper ratio from 0.5 to 0 at a thickness of 0.10 are compared with the results previously mentioned for a 50-percent increase in thickness ratio. Note also that at a given sweep and aspect ratio (45° sweep and aspect ratio 5, for example) the section thickness ratio may be at least halved by reduction of taper ratio from 0.5 to 0 without changing the aerodynamic-center shift due to bending or the structural weight.

Obviously larger aspect ratios or sweeps can be used without increase in the aerodynamic-center shift provided the weight penalty of a more rigid structure can be tolerated. In figure 3 the solid curves are the same as those shown in figure 2 for a section thickness ratio of 0.1. The dashed curves are for the same thickness ratio but result from doubling the structural weight of the wing. As may be seen from figure 3 the increases in aspect ratio or sweep afforded by this modification are fairly small even for this large increase in structural weight.

A wing modification not included in this analysis which might be used to alleviate effects of wing bending involves wing torsional deflections. This type of alleviation is possible only if the torsional stiffness or shear-center location can be adjusted so that angle-of-attack changes resulting from torsional deflections are of the same order of magnitude as those resulting from bending. A companion analysis has indicated that, for usual shear-center locations and usual ratios of torsional stiffness to bending moment of inertia, the angle-of-attack changes resulting from torsional deflections are small compared to those resulting from bending for most wing configurations having important bending effects.

The charts presented here are not intended to represent limits on the wing configurations which may be satisfactorily used in a transonic airplane design, but are presented to indicate how various wing geometric parameters influence this aeroelastic effect. Aside from modifications to the wing itself, there are several other possibilities for compensating or reducing the effects of wing bending or longitudinal stability which involve the complete airplane. The previous paper, by Mr. Skoog, has shown that for the XB-47 airplane some reduction in this aeroelastic effect resulted from consideration of inertia loads. An appreciable alleviating effect resulting from the associated loss in wing-lift-curve slope was also indicated by Mr. Skoog's analysis to occur for an airplane having a fairly large tail volume.

In conclusion, it has been shown that for thin swept wings, wing bending may have important effects on longitudinal stability; there are various ways of reducing or compensating for this effect; the choice of method may differ depending on the amount of sweep and aspect ratio desired, and the actual choice will naturally depend on a more complete analysis of each airplane design.

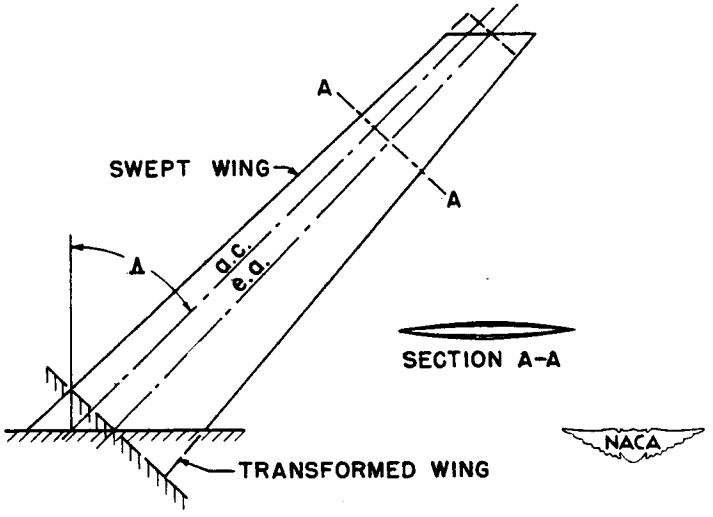


Figure 1.- Details of structural assumptions for typical swept wing.

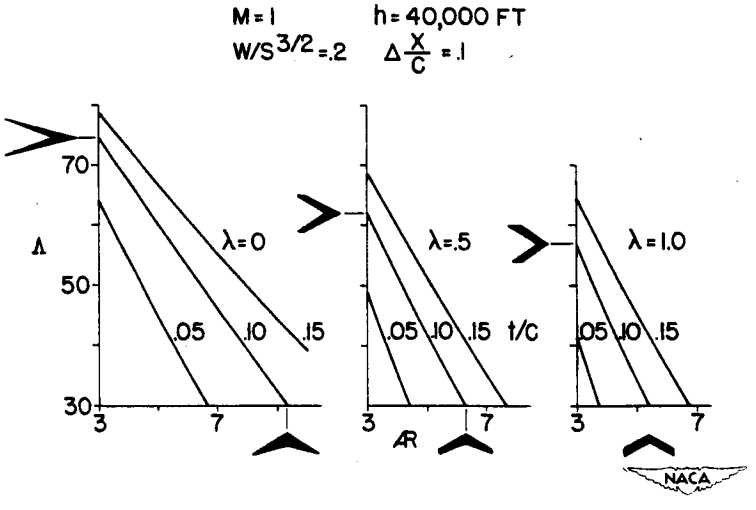


Figure 2.- Effects of variations in wing geometry.

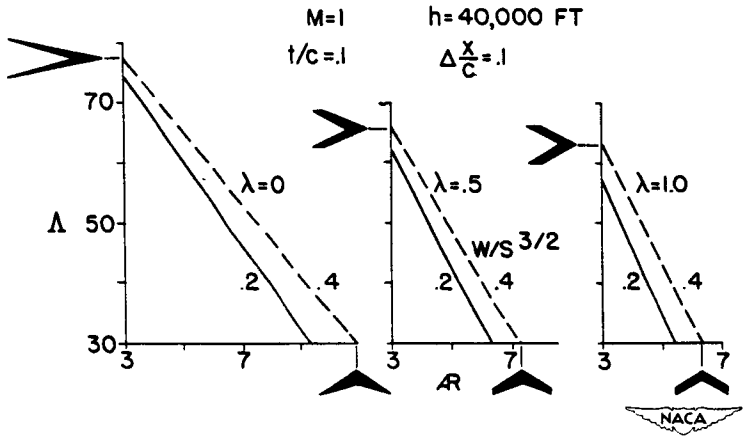


Figure 3.- Effect of variation in wing structural weight.

Preceding page blank

N65-86460

LOSS OF LONGITUDINAL DAMPING IN PITCH DUE TO FLEXIBILITY OF WINGS IN BENDING

By Reginald R. Lundstrom

Langley Aeronautical Laboratory

INTRODUCTION

The three preceding papers discussed the effects of the flexibility of wings on static stability and control effectiveness. This paper is concerned with some of the effects of wing flexibility on aerodynamic damping. During the program to obtain information on wing flutter by means of rocket-powered models, which is being carried out at the Langley Laboratory, a wing failure occurred on two configurations as a result of the whole model's becoming dynamically unstable in pitch. Because the wing was expected to flutter, no instrumentation was present to record the pitching motion of the body but it was noticeable in motion pictures of the flight. A similar model was built and flown with instrumentation to record both wing motion and body motion to determine the cause of this dynamic instability.

SYMBOLS

w_1	vertical velocity due to model translation
w	total average vertical velocity of wing with respect to mean flight path
$b/2$	span of one wing
EI	bending stiffness
θ	pitch angle of model
l	distance from center of gravity of model to center of pressure of wing
α	angle of attack

[redacted]

C_{L_α}	lift-curve slope
S/2	area of one wing
q	dynamic pressure
$\frac{d}{dt}$	derivative with respect to time
W	weight of complete model
c	chord of test wing
A	total aspect ratio

MODEL

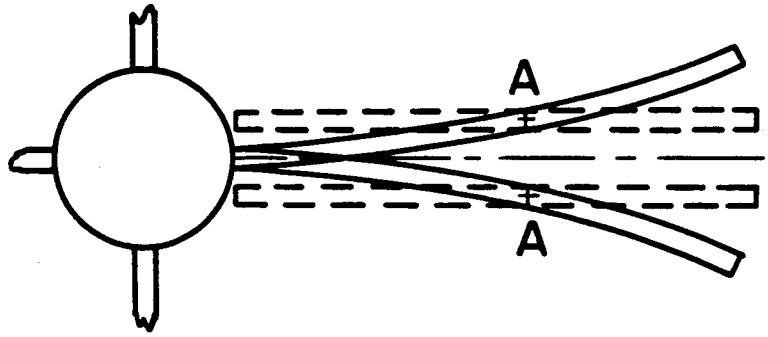
The wings used were 6-percent-thick straight wings of 10-inch chord and total aspect ratio 7 including the body area (fig. 1). The wings had a very high torsional stiffness but were flexible in bending. The model shown in the figure had the test wings as the only horizontal stabilizing surface and static margin about one chord length.

TEST RESULTS AND ANALYSIS

Figure 2 shows part of the flight record. The velocity at 4 seconds is about 450 feet per second; at 5.6 seconds where the oscillation is divergent the velocity is about 650 feet per second. Note that bending of the two wings is in phase, indicating pitch rather than roll, and that the normal acceleration of the model center of gravity, which is a measure of the lift, is also in phase with wing motion. Since the normal acceleration of the model is in phase with wing bending, the model displacement must be approximately 180° out of phase with the wing bending motion. Figure 3 is a view of the rear of the model. As the rear of the body is displaced downward (pitch up), the wing has a positive angle of attack and bends upward because of the lift. These figures show that, as the forward velocity is increased, lift forces increase for a given angle of attack and the deflection of the wing is greater. The damping force on the model is the lift due to the angle of attack caused by the vertical velocity and the forward velocity. At 200 feet per second a small amount of damping is lost at the tip. At 400 feet per second the wing tip has no vertical motion and all damping at the tip is lost. At 600 feet per second the point of no vertical motion moves inboard. Damping is still obtained near the wing root, but the tip now produces a negative damping which cancels it.

[redacted]

At a velocity greater than 600 feet per second the negative damping at the tip exceeds the damping near the root which is the wing–bending body–pitching flutter mentioned in the paper entitled "Status of the High–Speed Flutter Problem" by I. E. Garrick and D. J. Martin. This suggests a gradual loss of damping up to the flutter speed in contrast to other types of flutter which usually occur without much warning. It also suggests that even at speeds far below this flutter speed the damping may be reduced by the flexibility enough to affect the flying qualities. In order to approximate how much damping is lost due to this wing flexibility at velocities well below this flutter speed, it was necessary to assume a lift distribution. A uniformly distributed load was taken; the error probably is not very large because of the high aspect ratio. The motion of the wing in bending is such that there is no deflection at the root and a large deflection at the tip. In order to work with the vertical velocity due to wing bending, the point of average deflection was taken. This point was found by integrating the elastic curve of the wing and dividing by the length. This point (point A) gives the average deflection of the entire span and the resultant motion of the wing is effectively the same as if the entire wing moved, as shown by the dashed lines in the following sketch:



The deflection of this point A for the assumed lift distribution is $\frac{\text{Lift } (b/2)^3}{20\ EI}$. The body has two degrees of freedom, rotation about the center of gravity, and translation of the center of gravity. The vertical velocity of the wing root due to body motion consists of the angular velocity times the distance from the center of gravity to the wing center of pressure $\left(\frac{d\theta}{dt}(l) \approx \frac{d\alpha}{dt}(l)\right)$ and vertical translation of

the entire model which is merely an integration of the normal acceleration of the center of gravity $\left(\int \frac{C_{L_\alpha} Sq\alpha \, dt}{W} = w_1\right)$. If the wing were rigid this vertical velocity of the wing root alone would represent the damping of the motion. The vertical velocity of the wing due to bending, which is the first derivative of the deflection with respect to time, is $\frac{C_{L_\alpha} \frac{S}{2} q (b/2)^3}{20\ EI} \frac{d\alpha}{dt}$. As was seen in figure 3, this bending motion is opposite to the body motion so the vertical velocity due to bending subtracts from the vertical velocity of the wing root and the resultant of the two represents the damping in pitch.

$$w = \frac{d\alpha}{dt}\left(\frac{w_1}{d\alpha/dt} + l - \frac{C_{L_\alpha} Sq(b/2)^3}{20\ EI}\right)$$

The frequency of the motion was taken as the stability natural frequency of the model and the motion as a sine wave. The vertical velocities due to pitch, vertical translation, and bending were computed. The percentage loss in vertical velocity, which is, of course, the percentage loss in damping due to the wing's being flexible, is shown in figure 4 plotted against forward velocity. As may be seen, the calculated values are not conservative near the flutter speed. The greater part of the error is due to the model's oscillating at a frequency greater than the aerodynamic natural frequency as it approaches the flutter speed. As may be seen, even at speeds far below the flutter point, enough damping is lost to affect the flying qualities. Therefore, it will not be sufficient merely to determine the flutter point, but the loss of damping at lower speeds must be determined as well.

Comparison of the flexibility of the wing used in the test with that used in present-day high-speed aircraft shows that it is much less flexible than many wings used. However, the wing loading of the model was very high. Various designs and conditions affect the slope of this curve to some extent. With a flexible wing and rigid tail only the damping of the wing would be affected. A test of another model having rigid tail surfaces and using a similar wing with the center of gravity at the 10 percent chord showed that pitching bending flutter occurred at a 20-percent-higher velocity than in this test. The effect of sweepback is not known but no large effect is expected. The effect of taper should be highly beneficial because of a more favorable lift distribution along the span and a more favorable shape of the elastic curve of the wing. This loss of damping should not be as noticeable at high altitudes since this is a dynamic pressure effect, not a Mach number effect.

It does appear that this loss of damping is of interest on present-day high-speed aircraft and further investigation, both analytical and experimental, should be undertaken.

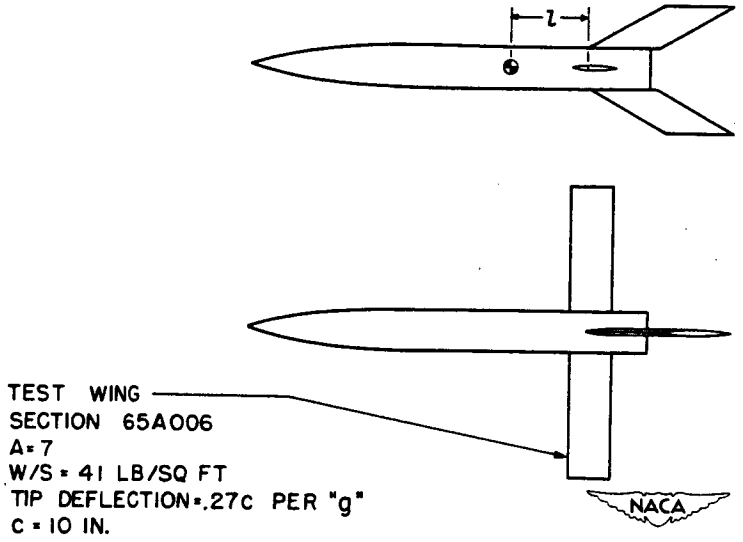


Figure 1.– Model configuration.

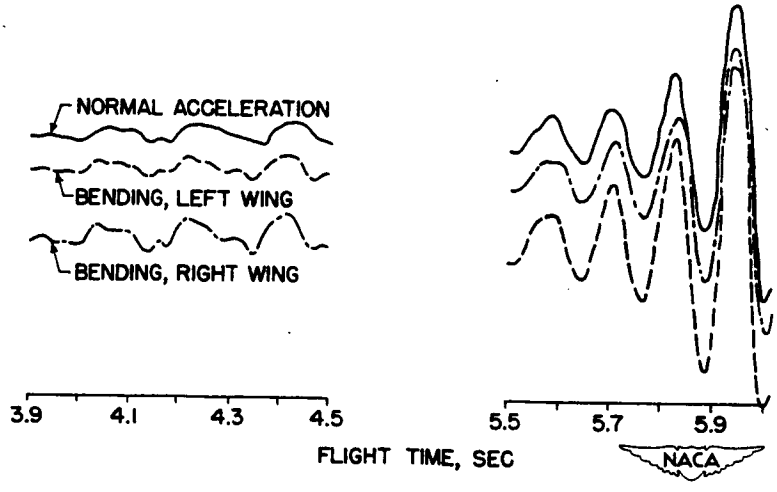


Figure 2.– Portion of flight record.

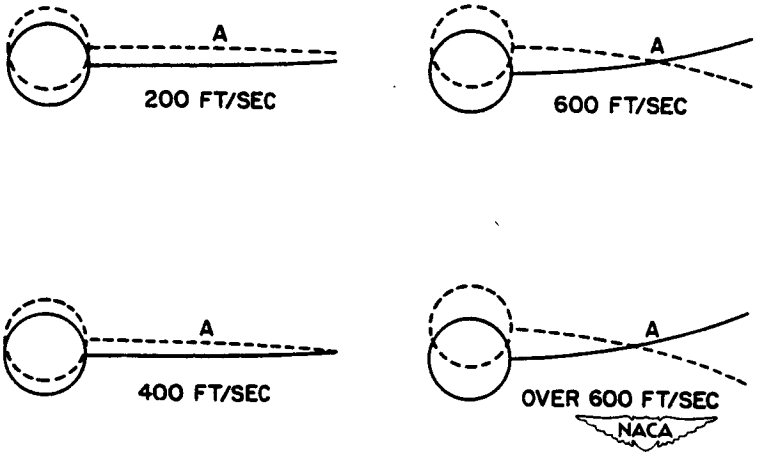


Figure 3.- Motion of wing due to pitch of model.

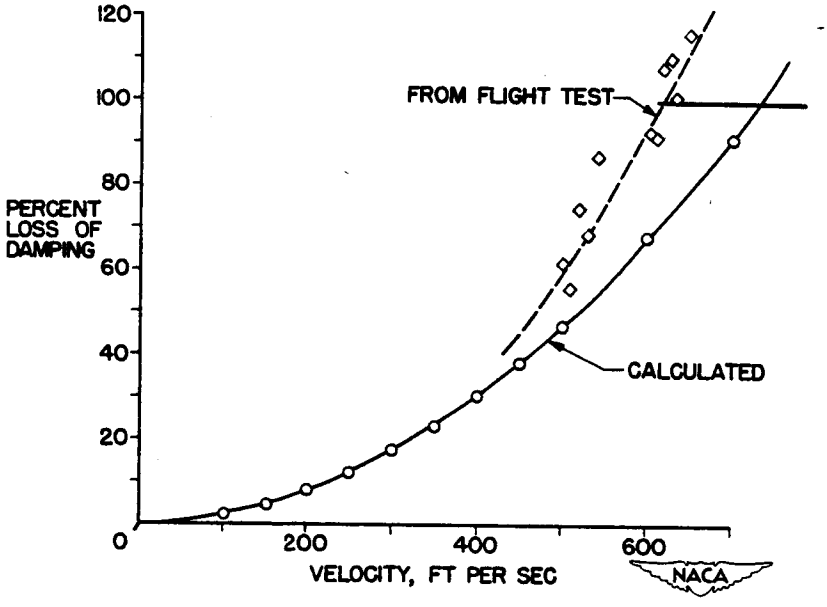


Figure 4.- Percentage loss of damping due to wing flexure.

Preceding page blank

BODIES AND WING-BODY INTERFERENCE

Preceding page blank

N65-86461

DRAG CHARACTERISTICS AT ZERO LIFT OF BODIES AT TRANSONIC SPEEDS

By Ellis R. Katz and Clarence W. Matthews

Langley Aeronautical Laboratory

The attainment of very high speeds for aircraft is largely a problem of thrust and drag. It is the intent of this paper to deal with the problems associated with the drag of bodies of revolution which for present and proposed high-speed aircraft is of the order of from 30 to 40 percent of the total configuration drag. For missiles, this value may be considerably greater.

This paper will present drag results for bodies over a wide range of Mach number and will attempt to shed some light on the flow phenomena associated with the drag rise and the validity of the linear theory in estimating flow characteristics at subsonic and supersonic speeds.

A series of body configurations, for which body shape was varied by systematic changes in fineness ratio and location of maximum diameter, are shown in figure 1. These configurations were tested at the Langley Pilotless Aircraft Research Station, Wallops Island, Va., by means of rocket-propelled models in free flight. All configurations were stabilized by three thin sweptback fins having equal exposed area for all bodies. Maximum and base diameters for all bodies were held constant. The lengths were varied to give fineness ratios of 12.5, 8.9, and 6, and the location of maximum diameter was varied from 20 to 40 to 60 to 80 percent of body length. The profiles of the bodies were determined from parabolic arcs generated from the location of maximum diameter.

The results obtained from this series of body configurations have been reported in reference 1 and are shown in figure 2. The drag coefficient for the configuration including fins has been plotted against Mach number M for the four locations of maximum diameter at each fineness ratio L/D. The three families of curves show the same general relationship. At subsonic speeds the effect of changing the location of maximum diameter is in general small. At supersonic speeds, the effect is very large and indicates that the most forward and rearward locations are the least favorable as regards drag, whereas the 60-percent location was consistently the best location tested. The force-break Mach number was highest for the midbody locations.

A representative cross-plot of these data for the family of 8.9 fineness ratio is shown in figure 3. This figure shows the experimental and calculated variation of drag coefficient with location of maximum

diameter at M = 1.4. The calculated variation represents the summation of the calculated component drags due to pressure, friction, base, and fin. The pressure drag has been calculated by means of the linear theory; the friction drag is based on a friction coefficient of 0.0020 and is assumed to vary directly as the wetted area; the base drag has been computed from base-pressure measurements on a typical body and is assumed independent of the location of the maximum diameter; and the fin drag is the result of calculated and experimental data, assuming a constant interference drag. The experimental and calculated variations indicate that the maximum diameter should be located near the midbody station for minimum drag. This plot is typical for the supersonic speed range. The divergence of the calculated values from the experimental results will be briefly discussed later in the paper.

In figure 4(a) is shown the variation of C_D with M for three of the body-fin configurations which were shown in figure 1. All had nearly identical noses of 5 diameters length. The lengths of the sterns varied, however, from 1.2 diameters to 7.5 diameters. The most apparent conclusion is that the length of the stern appears to be critical below a value of about $3\frac{1}{2}$ diameters and that above this value changing the length of the stern has very little effect. Another interesting point for consideration is that the Mach number at which maximum C_D occurs is approximately the same for all three bodies and is equal to that Mach number for shock attachment to a cone of finite length having approximately the same vertex angle as that of the test body. Figure 4(b) shows C_D plotted against the length of the stern in diameters at M = 1.4. Also shown is the calculated C_D variation. The significance of this comparison is that the calculated values are too large and that the poorest agreement is noted where the stern drag is highest.

Figure 5 shows what happens when the stern length is held constant at 5 diameters and the nose length varied. Indications are that the length of the nose is important and critical below a value of about $3\frac{1}{2}$ diameters. Although the data are complete over the Mach number range for only two of the configurations, it is apparent that the Mach number at maximum C_D varies with the nose shape (fig. 5(a)). Figure 5(b) shows C_D plotted against nose length in diameters at M = 1.4. The agreement between the experimental and calculated variations is good. The theory indicates that, at supersonic speeds, the drag contribution of the stern is almost independent of nose shape and this indication has been borne out by some experimental evidence. It may be supposed, therefore, that the variation shown in figure 5(b) is due to changes in nose drag alone.

From the preceding figures and in additional comparisons omitted for reasons of brevity, it is interesting to note that for forward positions of maximum diameter, the calculations agreed well with experiment. For rearward locations of maximum diameter, however, poor agreement was noted. It was also shown that for large changes in nose shape the calculations closely checked the experiment, whereas such was not true for changes in stern shape. This seems to indicate that the error in the calculations is largely confined to the stern section of the configuration. This error may possibly be accounted for by considering the following reasons:

(1) The high peak suctions over the shorter stern lengths as predicted by the theory may possibly not be attained because of the exceeding of the limits of the small-perturbation assumption

(2) The probable modification of the stern shape due to the boundary layer

(3) Unaccounted for variations of base pressure with body shape

(4) Body-fin interference which possibly may be most favorable for the shorter stern lengths

It appears that an experimental check on the validity of the linear theory for the shorter stern lengths may explain some of the noted discrepancies.

Figure 6 summarizes the drag results for the 60-percent location of maximum diameter which was consistently the most favorable location tested and which appears to be nearly optimum. Drag coefficient is plotted against configuration fineness ratio for supersonic, transonic, and high subsonic speeds. The optimum fineness ratio is indicated to increase through the speed range from a value of less than 9 at subsonic speeds to greater than 9 at supersonic speeds.

It is surprising to note that in going from fineness ratio 8.9 to 12.5 at supersonic speeds, the drag coefficient was almost constant, at a value of approximately 0.19 based on frontal area. This corresponds to a drag coefficient of approximately 0.13 without fins. The calculated total and viscous drag is also shown to indicate that at subsonic speeds the variation is dependent principally on viscous drag and at supersonic speeds is dependent upon both viscous and pressure-drag variations.

The Flight Research Division has recently made a free-fall flight test on a body of fineness ratio 12 on which pressure measurements were taken at 19 flush orifices on the body surface. Part of the results, which have been taken from reference 2, are shown in figure 7.

Figure 7(a) shows the measured and calculated pressure distribution over the body at M = 1.27, the highest Mach number reached. The distribution, which is rather typical for this body shape at supersonic speeds, indicates a suction peak on the stern followed by a rapid pressure recovery at the tail. Although there is almost a constant negative displacement of the theory, the agreement in variation may be considered quite remarkable. Figure 7(b) shows drag coefficient plotted against Mach number for the body drag of the subject test configuration and also the integrated pressure drag as determined from the experimental and calculated pressure distributions. The body exhibited a high force-break Mach number of approximately 0.99. The calculated pressure drag closely checked the experimental results at supersonic speeds. The difference in total drag and pressure drag represents the friction drag. This difference remains nearly constant over the Mach number range and is roughly equal to an average friction coefficient of 0.0028 (based on wetted area), a value which indicates boundary-layer transition near the nose.

The pressures on the bases of flat-ended bodies is a subject of considerable interest where power-off drag is important. Some unpublished results are available from flight tests of rocket-propelled configurations and are shown in figure 8. The bodies shown in the right-hand side of the figure had open rocket motor nozzles and thin stabilizing fins located near the tail.

Negative pressure coefficients which correspond to positive drag results are shown above the zero ordinate. It is apparent that the coefficient can vary widely at a given Mach number depending on body shape. At Mach numbers greater than approximately 1.3 the bodies having the smallest ratio of base to maximum diameter had the least suction. This characteristic is even more exaggerated when converted to base-drag coefficient referred to frontal area, for as the base diameter becomes smaller relative to the maximum diameter the reduced suction acts on a correspondingly reduced area. The variations of coefficient with Mach number below M = 1.3 are surprising for some of the configurations but a preliminary investigation of a qualitative nature has indicated that these variations may possibly be dependent to a large extent on the transonic behavior of the side pressure at the 100-percent station.

ANALYSIS OF DRAG PHENOMENA

The drag phenomena, which occur once the supercritical Mach number has been exceeded, are a result of the changes which occur in the shape of the pressure distribution over the body.

Figure 9 shows the experimentally determined pressure distributions over the free-fall body, previously introduced, at Mach numbers of 0.9, 1.01, and 1.20. The distribution at M = 0.9, which is typical for the subsonic speed range, results in very little drag because of the effective balancing out of the pressure forces on the forward and rearward sections of the body. As the free-stream Mach number increases, the local velocities over the midsection of the body also increase until at a critical value of free-stream Mach number the maximum local velocity on the surface is equal to the speed of sound. At a Mach number greater than critical, in this case 1.01, a region of local supersonic flow appears on the body near the midsection. The flow through this localized region behaves according to supersonic laws and causes large expansions which act predominantly on the convergent section of the body. Thus, large unbalanced pressure forces are created on the stern which resolve themselves into drag.

As the Mach number is increased still more, the region of supersonic flow grows until it covers almost all of the body. A typical distribution for this type of flow is shown at a Mach number of 1.20. A comparison with the distribution at a Mach number of 1.01 indicates that there has been a positive shift of the pressures over most of the body. This positive shift results in the distribution of drag moving from the stern toward the nose.

TRANSONIC PRESSURE PHENOMENA

As the pressures which occur at a Mach number of 1.0 cannot be predicted by the linearized theory, it is necessary to resort to experimental results to obtain a knowledge of the transition of pressures from the subsonic values to the supersonic values. The pressures about the free-fall body previously discussed are presented in figure 10 as functions of Mach number through the range 0.75 to 1.22 for the 5-, 50-, 76- and 90-percent stations on the body.

Figure 10 shows that the pressures tend to follow the variation predicted by the linearized theory so long as the Mach number is not too near 1.0. Over the central portion of the body the pressures form a peak at the Mach number of 1.0. Near the nose and stern a peak is also formed but is more gradual and occurs at a Mach number greater than 1.0 at the nose and less than 1.0 at the tail.

The discontinuity shown in the 75-percent-station curve is the result of the shock passing over that station. Examination of similar curves for adjacent orifices shows that a definite shock exists for only a small Mach number range. It appears at the 65-percent station

at a Mach number slightly greater than 1.02. No evidence of the shock is seen at the 90-percent station and the stations downstream of that point, indicating that the shock has left the body. This phenomenon is predicted by the linearized theory, which shows that the fluid is compressed over a finite portion of the stern of the body and hence cannot form a shock on the body. The Mach lines due to the compression converge at a finite distance away from the body so that a shock may be expected in that region. Thus, although a downstream shock exists for a body of revolution, it does not appear on the body except for a very small Mach number range near 1.0, but rather will appear at a finite distance from the body.

COMPRESSIBILITY EFFECTS AT SUBSONIC SPEEDS

The effects of compressibility at high subsonic speeds have been considered by means of the linearized theory and by pressure measurements for a prolate spheroid of fineness ratio 6. The results, reported in reference 3, are shown in figure 11 as pressure distributions at several subsonic Mach numbers. A comparison between the theory and experiment shows that the theoretical effect of compressibility is to reduce the pressures over the entire surface, whereas the experimental effect is to cause positive pressures to become more positive and negative pressures to become more negative. In consideration of the labor and inaccuracies in the theoretical prediction of subsonic compressibility effects on bodies, an analytical investigation was undertaken to reduce the complex linearized solution into more simplified forms. Two equations were obtained which give the compressibility effects near the maximum ordinate of a body as functions of fineness ratio and Mach number. One of the equations expresses the correction in the form of a pressure ratio and the other expresses the correction in the form of a pressure difference. The validity of the equations has been tested by wind-tunnel tests on three different bodies and the results, reported in reference 3, are shown in figure 12. Both formulas have been used to correct the experimental pressures at $M = 0$ to corresponding values at $M = 0.9$ for two different body shapes of fineness ratio 6 and for a third body of fineness ratio 10. Also shown are the experimental pressures at $M = 0.9$. The indications are that the ratio correction more satisfactorily predicts the compressibility effect and thus should be used rather than the increment formula.

It may also be observed by comparing the agreement of the corrected and experimental pressures on the prolate spheroid of fineness ratio 6 and the ogival body of fineness ratio 6 that the pressure increments due to compressibility are approximately the same for both bodies, thus indicating that the effects of compressibility are more or less independent of the body shape so long as the body conforms to the restrictions imposed by the assumptions of the linearized theory.

REFERENCES

1. Hart, Roger G., and Katz, Ellis R.: Flight Investigation at High-Subsonic, Transonic, and Supersonic Speeds to Determine Zero-Lift Drag of Fin-Stabilized Bodies of Revolution Having Fineness Ratios of 12.5, 8.91, and 6.04 and Varying Positions of Maximum Diameter. NACA RM L9I30, 1949. (Prospective NACA paper)

2. Thompson, J. R.: Continuous Measurements from Subcritical to Moderate Supersonic Speeds of the Drag and Pressure Distribution on a Body of Revolution. (Prospective NACA paper)

3. Matthews, Clarence W.: A Comparison of the Experimental Subsonic Pressure Distributions about Several Bodies of Revolution with Pressure Distributions Computed by Means of the Linearized Theory. NACA RM L9F28, 1949.

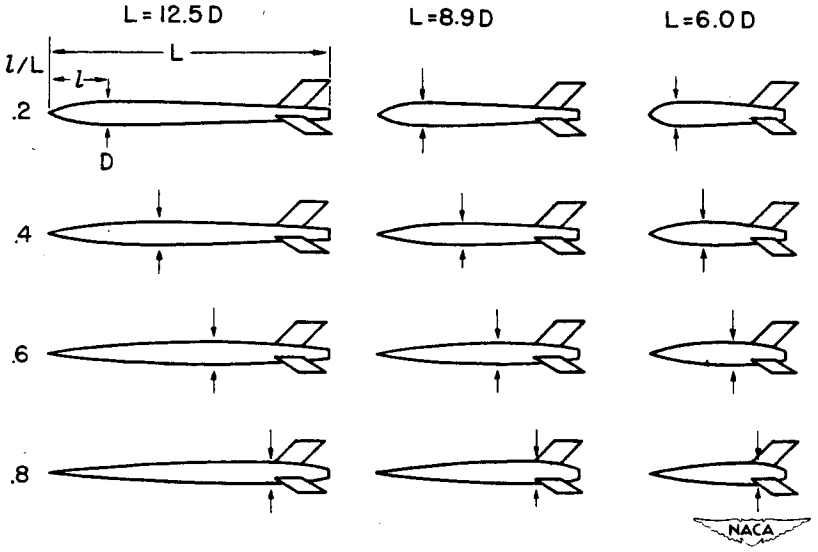


Figure 1.- General arrangements of test configurations used in body-shape investigation.

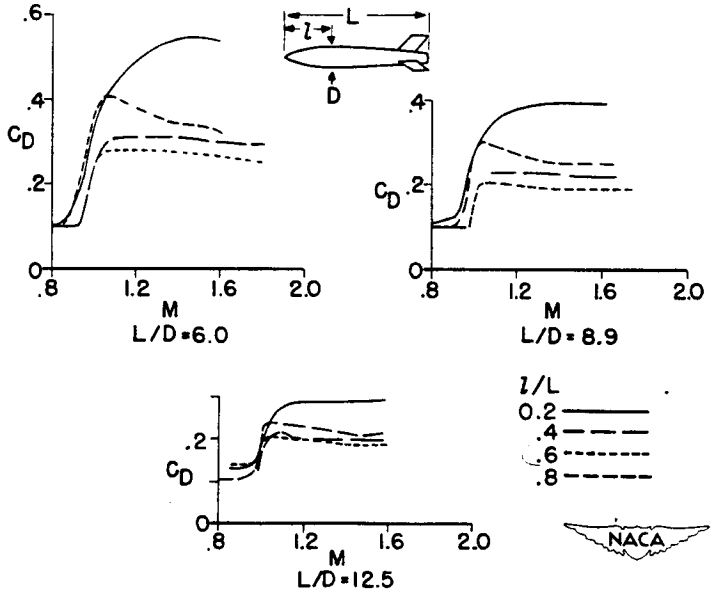


Figure 2.- Drag results from body-shape investigation.

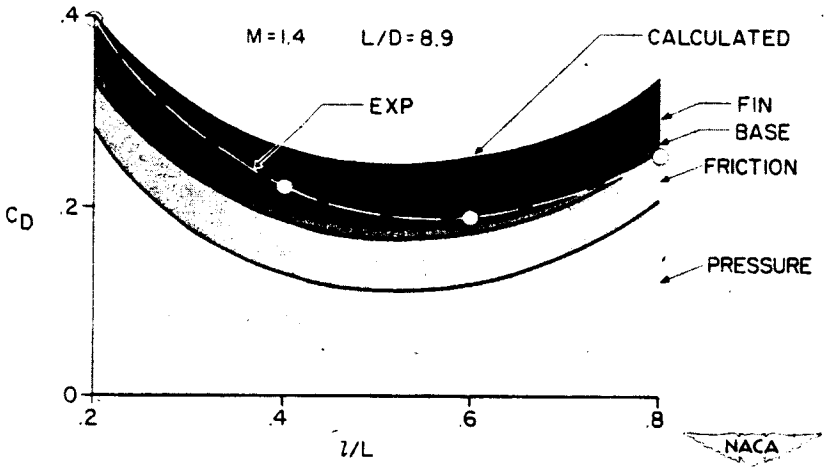
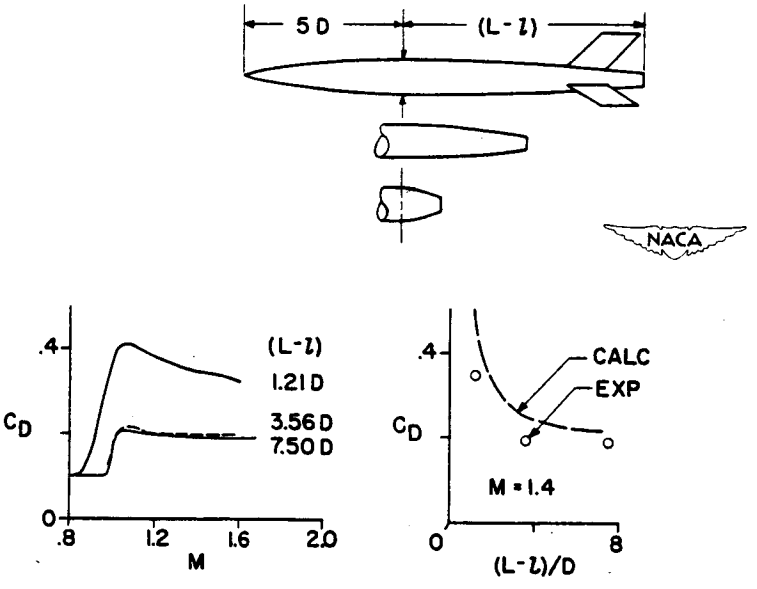


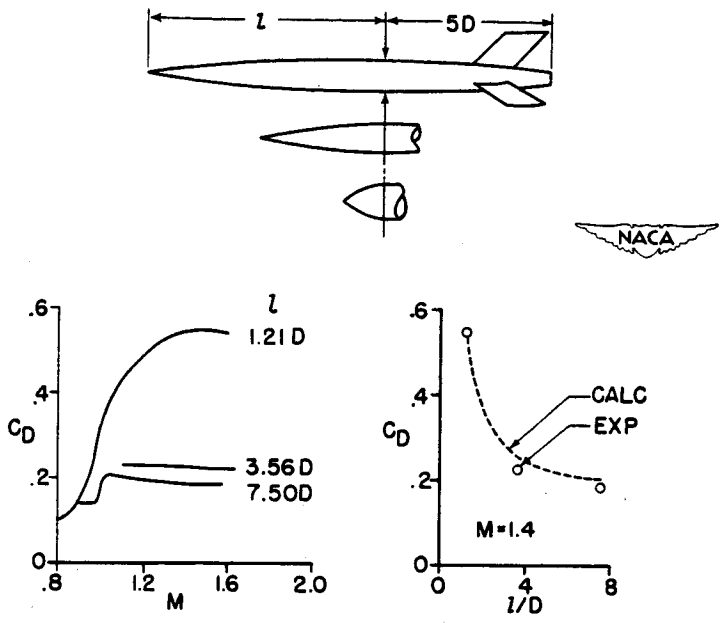
Figure 3.- Effect of location of maximum diameter l/L on drag coefficient C_D for 8.9 fineness ratio.



(a) Drag coefficient C_D for three bodies having similar noses and varying lengths of stern $(L - l)$.

(b) Calculated and experimental variations of drag coefficient C_D with stern length $(L - l)$.

Figure 4.- Effect of varying stern length.



(a) Drag coefficient C_D for three bodies having similar sterns and varying lengths of nose l.

(b) Calculated and experimental variations of drag coefficient C_D with nose length l.

Figure 5.- Effect of varying nose length.

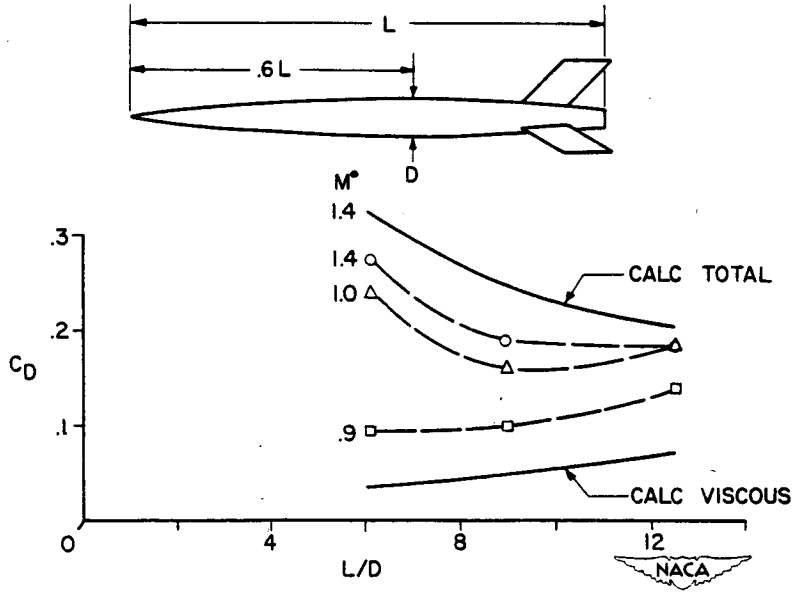
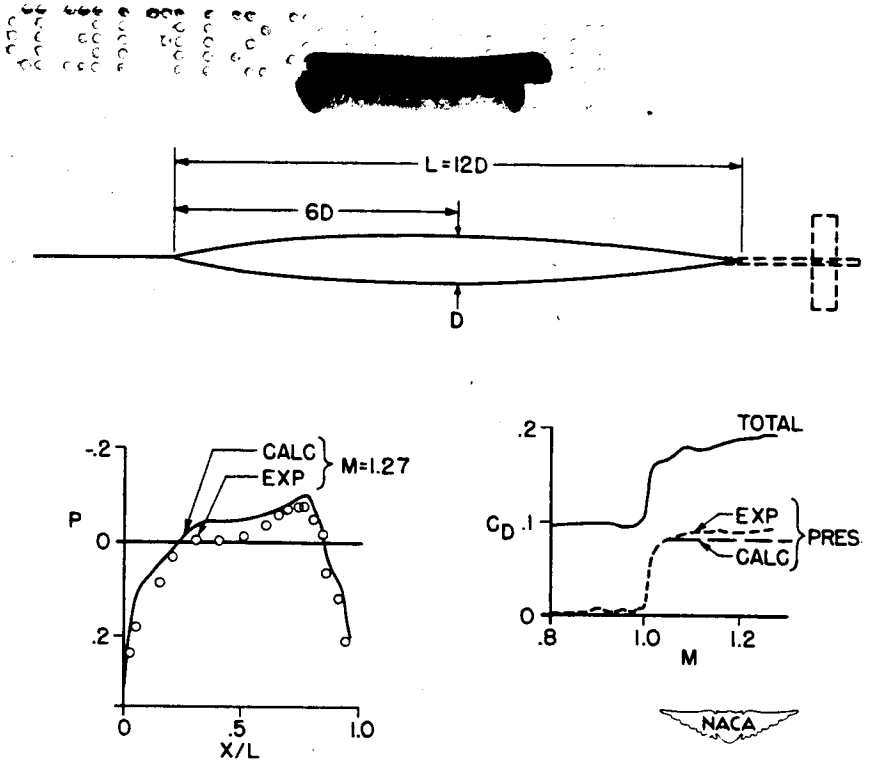


Figure 6.- Variation of drag coefficient C_D with fineness ratio L/D for bodies having maximum diameter D at 60-percent station and for three Mach numbers.



(a) Measured and calculated pressure distributions at a Mach number of 1.27.

(b) Drag-coefficient results over Mach number range of flight test.

Figure 7.- Flight-test results from free-fall model.

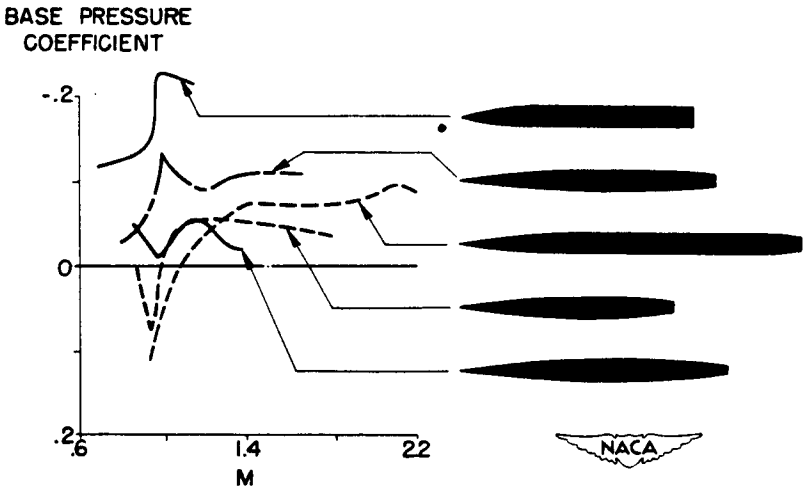


Figure 8.- Flight-test results for base-pressure coefficients against Mach number for several body configurations. All bodies had thin tail fins which are not shown.



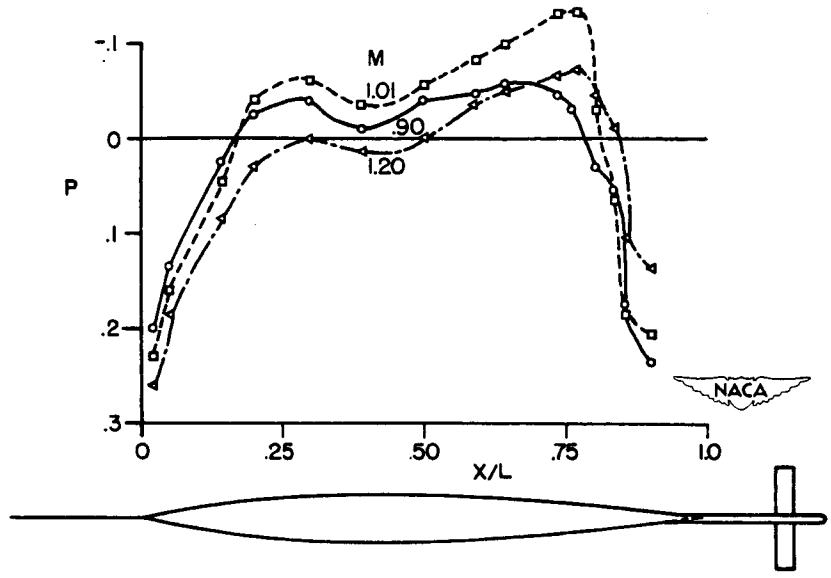


Figure 9.- Pressure distributions for free-fall body at subsonic, transonic, and supersonic speeds.

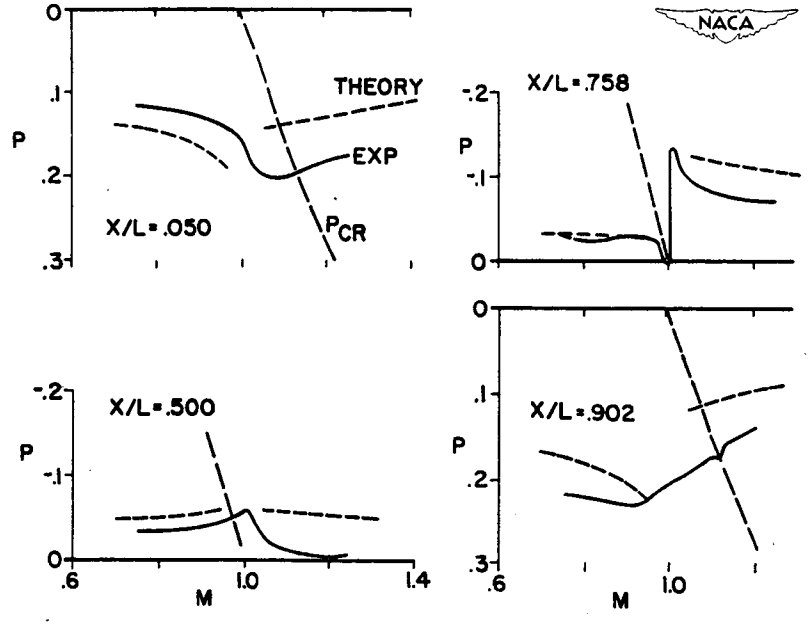


Figure 10.- Pressure-coefficient variations with Mach number at four body locations [illegible] free-fall body.

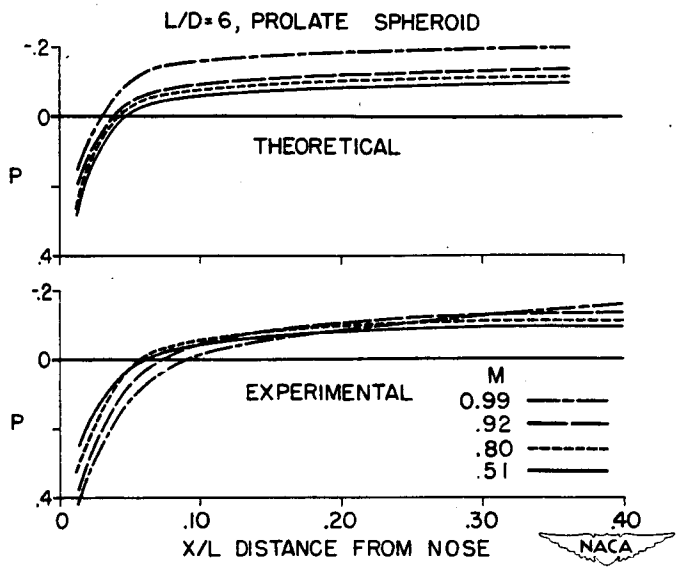


Figure 11.- A comparison of experimental and theoretical pressures on a prolate spheroid of fineness ratio 6.

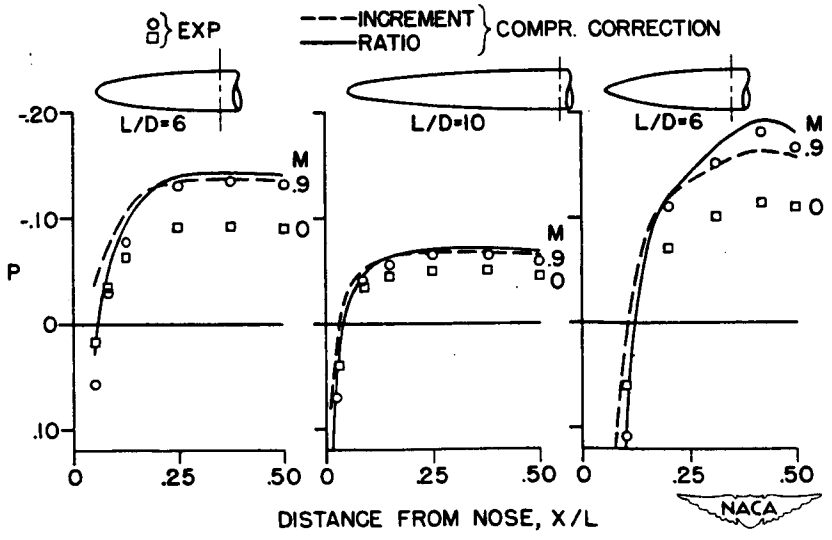


Figure 12.- Comparison of theoretically corrected incompressible pressure distributions with the corresponding experimental pressure distributions.

N65-86462

THE FLOW OVER MODERATELY SWEPT WINGS AT HIGH-SUBSONIC SPEEDS INCLUDING THE EFFECTS OF NACELLE INTERFERENCE

By George G. Edwards and Lee E. Boddy

Ames Aeronautical Laboratory

The purpose of this paper is to present the results of some recent wind-tunnel investigations of the effects of compressibility on the flow over moderately swept wings, alone and in combination with a nacelle or a fuselage. The measurements have included surface pressures and forces and moments. The discussion of the force changes will be confined to the drag and it will be shown how the effects of compressibility on the surface pressures can be correlated with the measured drags.

GENERAL CONSIDERATIONS

The analysis of the pressure data required considerations of methods by which the local critical pressure coefficient on a swept wing could be recognized from the measured pressures. The method adopted was based on the ideas illustrated in figure 1. The components of velocity on a yawed airfoil of infinite span are illustrated on the right of the figure. As pointed out by Jones in reference 1, the pressure distribution over such a wing is determined solely by the component of velocity normal to the leading edge. The local velocity vector V is then the vector sum of the free-stream velocity V_o and the additional velocity ΔV induced by the airfoil thickness. Since the incremental velocity ΔV is perpendicular to the leading edge, the resultant velocity V will be inclined at an angle θ to the free-stream direction.

In contrast to the case of an unyawed airfoil, the attainment of sonic velocity on a yawed airfoil does not necessarily signify any immediate change in the flow characteristics. Critical flow conditions analogous to those on an unyawed airfoil will not exist until the component of local velocity in a direction normal to the leading edge attains the local speed of sound. These critical flow conditions will occur along a line of constant pressure parallel to the leading edge and the shock wave, when it forms, will be inclined at the sweep

angle ϕ. The critical pressure coefficient P_ϕ is then given by the following expression:

$$P_\phi = \frac{2}{\gamma M_o^2}\left\{\left[\frac{2}{\gamma+1}\left(1 + \frac{\gamma-1}{2} M_o^2 \cos^2\phi\right)\right]^{\frac{\gamma}{\gamma-1}} - 1\right\}$$

where M_o is the free-stream Mach number and ϕ is the angle of sweep of the lines of constant pressure which will be called isobars.

The application of this equation for critical pressure coefficient to the analysis of pressures on a swept wing of finite span required additional considerations. In particular, if the intersection of the wing panels is a plane, such as for the wing shown at the left of figure 1, the isobars near the wing root will be curved so as to approach the plane of symmetry in a direction normal to the direction of flight. This phenomenon has been treated theoretically by Jones in reference 1 and also by Küchemann in reference 2. For the system of curved isobars shown in the figure, the local critical pressure coefficient P_ϕ was computed from the equation, the reference sweep angle ϕ having been evaluated by measuring the local sweep of the isobars. The heavy line in the figure indicates the points on the wing at which the component of local velocity in a direction normal to the isobars $V_\perp$ equals the local speed of sound. Since this heavy line crosses the curved isobars, it is obvious that the component of local velocity normal to this line cannot be sonic. On the evidence available at present, it is difficult to say how well this line defines the locus of critical flow conditions in a region of curved isobars. However, immediately adjacent to the plane of symmetry and at some distance from the plane of symmetry where the isobars have attained the full sweep of the wing, the use of the equation as outlined should provide a good representation of the attainment of critical flow conditions.

Also useful in the analysis of the data of the present investigation is the crest-line concept developed by Nitzberg and Crandall in reference 3. This concept is based primarily on experimental observations reported in reference 3 in which it was shown from an analysis of experimental pressure distributions on a large number of airfoil sections that the abrupt supercritical drag rise did not begin until the region of supersonic flow had enveloped the airfoil crest, the crest being defined as the chordwise point on the airfoil surface at which the surface is tangent to the undisturbed air stream.

This crest-line concept will be used in the following analysis along with the previously described equation for critical pressure coefficient to define the flow conditions at which the drag may be expected to increase rapidly with further increase in Mach number.

PRESSURES AND DRAG ON A SWEPT WING

The data to be discussed in the first part of this paper were obtained from tests in the Ames 12-foot pressure tunnel of a semispan model of a wing having an aspect ratio of 6 and a taper ratio of 0.5. The leading edge of the wing was swept back 37° and the section normal to the quarter-chord line was the NACA 64_1-212. The chordwise distribution of static pressures was measured at five spanwise stations at Mach numbers from 0.18 to 0.94 at a constant Reynolds number of 2×10^6.

In an effort to determine what portion of the wing span was contributing the most to the wing drag, the surface pressures were integrated to determine the chordwise pressure-force coefficients. Figure 2 illustrates the results of this integration at 0° angle of attack, for which angle the chordwise pressure force is the pressure drag. In the upper portion of the figure, the section pressure-drag parameter $c_c\left(\frac{c}{c_{av}}\right)$ is shown as a function of spanwise position for Mach numbers 0.18, 0.85, and 0.90. In this relation c_c is the section chord-force coefficient, c is the local chord of the wing, and c_{av} is the average chord of the wing. As predicted by Jones in reference 4, the root sections of the wing had positive pressure drag while the tip sections had negative pressure drag. Increasing the Mach number is seen to have increased both the magnitude and the spanwise extent of the region of positive pressure drag.

The reason for this distribution of pressure drag is evident from the pressure data shown in the lower portion of figure 2. Here are presented the chordwise distributions of pressure coefficient over the upper surface of the wing at three spanwise stations for Mach numbers of 0.18 and 0.85. The crest line on the upper surface at 0° angle of attack is at 40 percent of the chord. With the crest line as a reference it can be seen that positive pressure drag on the root sections was a result of the rearward displacement of the point of minimum pressure to a position behind the crest, while the negative pressure drag at the tip sections was a result of forward displacement of the point of



minimum pressure. Increasing the Mach number tended to increase this distortion of the surface pressure distribution.

In figure 3, the section pressure-drag parameter $c_c\left(\frac{c}{c_{av}}\right)$ is shown as a function of Mach number at three spanwise stations, a station near the root, one near the midsemispan, and one near the wing tip. At the station near the root, the pressure-drag parameter increased gradually with increasing Mach number up to a Mach number of approximately 0.75 and then began to rise rapidly with further increase in the Mach number. At the midsemispan station, the pressure-drag parameter decreased with increasing Mach number up to a Mach number of 0.80 and increased with further increase in Mach number. At the station near the tip, the pressure-drag parameter decreased with increasing Mach number up to the highest Mach number, 0.90. In the lower portion of figure 3, chordwise distributions of upper-surface pressure coefficient for sections near the root and near the tip are compared for several Mach numbers. The rearward movement with increasing Mach number of the point of minimum pressure near the wing root is evident from the figure on the left, while the increase in magnitude with increasing Mach number of the minimum pressure near the tip is evident from the figure at the right. Since the minimum pressure near the tip was ahead of the wing crest, this decreasing pressure resulted in a decrease in the pressure drag.

It should be emphasized that the drag so far discussed is only the drag due to surface pressures and does not include viscous effects except insofar as viscous effects influenced the surface pressures.

In the right-hand portion of figure 4, the isobars are shown for the upper surface of the 37° sweptback wing at 0° angle of attack for Mach numbers of 0.83, 0.85, and 0.88. The heavy line indicates the locus of points at which the Mach number of the component of the local flow normal to the isobar equals unity. As discussed with reference to figure 1, this line will be referred to as the line of critical flow conditions. It is noted that critical flow conditions first occurred near the root of the wing at a free-stream Mach number of 0.83 and that, with further increase of Mach number, the line of critical flow conditions moved rearward and extended outward toward the tip.

In the left-hand portion of figure 4 is a graphical illustration of the relation of the Mach numbers for the occurrence of critical flow conditions at the crest line for several stations along the wing semispan to the total drag variation with increasing Mach number. The experimental curves showing the variation with Mach number of pressure coefficient at the crest line are intersected by theoretical curves representing the variation with Mach number of local critical pressure



coefficient P_{ϕ}. The critical pressure coefficient P_{ϕ} was calculated from the expression derived previously, using the appropriate isobar sweep angle ϕ measured from the isobar diagrams. The intersection of the curves delineates the Mach number M_{ϕ} at which the critical flow condition was attained at the crest of each section. These intersections projected vertically to the drag curve below show that the drag was just beginning to rise in the range of Mach numbers thus defined. The drag-divergence Mach number, arbitrarily defined as the Mach number for which $\frac{\partial C_D}{\partial M} = 0.1$, was slightly above that at which the critical flow condition was attained at the crest of the entire wing.

In figure 5, similar data are presented for the wing at an angle of attack of 4°. In the isobar diagrams, the existence of a sharp peak in the negative pressure coefficients is indicated near the leading edge on the outer portions of the wing span. In drawing the heavy line showing the locus of critical flow conditions, this local peak near the leading edge was ignored and the critical flow conditions were defined by the rearward region of high negative pressure coefficients. As was the case at 0° angle of attack, the drag-divergence Mach number was slightly greater than the Mach number at which critical flow conditions were attained at the crest of the entire wing. Contrary to the case at 0° angle of attack, critical flow conditions were not attained at 15 percent of the semispan until a Mach number slightly greater than that Mach number at which the critical flow condition was attained near the midsemispan. It is interesting to note that, had the minimum pressure point been used as a reference instead of the crest, the critical flow condition at an angle of attack of 4° would be indicated to occur near the leading edge of the outer portion of the wing at a Mach number of 0.70, which is far below the drag-divergence Mach number of 0.81.

Since the rate of drag increase is dependent upon the rate of development of the supercritical flow region, it is important to note that this wing had the special property of attaining the critical flow condition at the crest of the various spanwise stations within a narrow range of Mach numbers. This range of Mach numbers is probably larger for more highly swept wings.

In figure 6 these results are summarized for a range of angles of attack to show a comparison of M_{ϕ} representing the Mach number at which the critical flow condition was attained at the crest, and M_D, representing the drag-divergence Mach number as previously defined. The M_{ϕ} curves, determined from the experimental data, are shown for a

station near the root and one near the midsemispan. Also shown is a curve of estimated values of M_ϕ for the station near the midsemispan of the wing. These values of M_ϕ were calculated from crest pressures measured at a Mach number of 0.18, using the Kármán–Tsien expression, modified for sweep effect, to correct for the effects of compressibility. The use of this expression, which is based on considerations of two-dimensional flow, can be justified only on the basis that near the mid-semispan of the wing the flow is least influenced by the effects of the root and the tip sections. In this calculation the sweep angle was taken as that of the crest line. The values of M_ϕ calculated from the low-speed pressure data are substantially in agreement with those based on the high-speed data.

From the results of this investigation, it is indicated that the crest-line concept as applied is a useful guide in determining the range of Mach numbers in which the abrupt drag increase can be expected to begin for a moderately swept wing. It is further indicated that the drag-divergence Mach number can be estimated from low-speed pressure-distribution measurements on the swept wing.

IMPROVEMENT OF THE FLOW AT THE WING ROOT

The interference effects at the root of a swept wing have been further investigated in a series of tests conducted in the Ames 16-foot high-speed tunnel. It was the purpose of that investigation to study means of eliminating premature compressibility effects by altering the flow at the wing root.

The geometry of the wind-tunnel model is shown in figure 7. The model was constructed so that the wing could be tested with the 50-percent-chord line either unswept or swept back 35°, and had removable panels on both the wing and the fuselage near the wing-fuselage juncture. Unswept, the wing had an aspect ratio of 9.0, a taper ratio of 0.5, and NACA 64_2A015 sections normal to the 50-percent-chord line. Sweptback 35°, the wing had an aspect ratio of 6.0. The fuselage had a cylindrical midsection and an ellipsoidal nose of sufficient length to keep the fuselage-induced velocities well ahead of the wing. It was reasoned that this arrangement would minimize the unknown and variable effects of the fuselage-induced velocities and thus provide a more reliable basis for assessing the merits of changes in design at the wing root and for comparing the characteristics of the sweptback wing with those of the unswept wing.

The two methods provided for altering the flow near the wing-fuselage juncture were: (1) Contouring the fuselage to conform to the

estimated shape of the streamlines over a yawed wing having the same section, and (2) changing the section at the root of the wing. The shape of the streamlines was estimated from the simple cosine concepts shown in figure 1.

In figure 1 it was shown that the local resultant velocity vector at any point in the field of the swept wing will be at an angle θ with respect to the free-stream velocity vector if it is assumed that only the normal component of the free-stream velocity is affected by the presence of the wing. The lateral displacement of a streamline over a yawed wing is then easily calculated by integration of the tangent of the angle θ with respect to longitudinal distance. The computed values for the lateral displacement were applied to the basic fuselage lines, resulting in a fuselage shape at the wing-fuselage juncture as shown in the upper right corner of figure 7.

No simple method was available for computing the change of section required at the wing root to counteract the interference pressures. However, it was known qualitatively that the lateral confinement of the streamlines near the root caused higher pressures over the forward portion of the chord and lower pressures over the rear portion of the chord. The modified airfoil section at the root, then, should have lower pressures forward and higher pressures rearward than the basic airfoil. The NACA 0015 section satisfied this requirement, especially over the forward half of the chord. Hence, at the juncture of the straight-sided fuselage, the modified wing section was the NACA 0015 reduced in thickness to that of the basic airfoil. The modification of the section is illustrated in figure 7. The wing section was faired linearly to the basic airfoil about half a root-chord length outboard of the juncture.

Figure 8 shows the chordwise distribution of pressure coefficient at three different spanwise stations on the swept wing at a Mach number near that for drag divergence. Note the characteristic rearward displacement of the minimum pressures near the root and the forward displacement near the tip. Also shown in figure 8 is the pressure distribution predicted for the midsemispan station of the swept wing from results of tests of the unswept wing using the simple cosine concept. The data from the unswept wing were converted to those for a swept wing by dividing the Mach number by the cosine of the sweep angle, multiplying the pressure coefficient by the square of the cosine of the sweep angle, and multiplying the angle of attack by the cosine of the sweep angle. Very good agreement was obtained at all Mach numbers below that for drag divergence, while at higher Mach numbers the agreement was only fair.

The foregoing is fairly strong evidence that the portions of the swept wing near the midsemispan behaved much as would be predicted by the simple cosine concept except, of course, for the different

boundary-layer effects. It is logical to expect, then, that altering the pressure distribution at the wing root to conform with that at the midsemispan might be beneficial.

Figure 9 shows the effect of the contoured fuselage and of the modified wing root on the wing pressures. In the upper left corner of the figure are shown the chordwise pressure distributions near the root for the three configurations. Also, shown by the dotted line is the pressure distribution for the midsemispan station. It was intended that this distribution be maintained over the inner portion of the wing. The effect of the contoured fuselage was about as had been calculated, except that the magnitude of the effect was only about half as great as desired; that is, the pressures with the contoured fuselage were about midway between those for the basic fuselage and those at the midsemispan. This deficiency may be due to the fact that the vertical extent of the modification was limited by the depth of the fuselage and, therefore, could not be made to influence the entire flow field of the wing root. The effect of the modified wing root on the pressure distribution consisted largely of a reduction of the velocities over the middle portion of the root chord. Both of these effects are reflected in the isobar diagrams shown on the right of figure 9. Note that the isobars with the modified fuselage were generally straighter and were not displaced rearward near the root as much as with the basic fuselage. Also, the modified wing root substantially reduced the peak pressures in the region of the wing root.

In the lower left corner of figure 9 is shown the effect of the two modifications on the section pressure-drag coefficient near the wing-fuselage juncture. It should be noted that these data do not provide any indication of changes in the pressure drag of the fuselage. When the fuselage shape was altered, there was no doubt a change in its pressure drag so that a comparison of the upper and lower curves of this figure is not a complete indication of the effect of this modification on the total drag. However, modification of the root section of the wing involved no change in the fuselage shape, which was straight-sided in the region of the wing. Hence, no change in the fuselage pressure drag would be expected. From a comparison of the two upper curves, it is indicated that the section pressure-drag coefficient was reduced considerably by modification of the root section, particularly at the higher Mach numbers. This effect should be reflected in an increase of drag-divergence Mach number of the entire wing.

The data presented in figure 10 serve to indicate the effect of the modifications of the wing-fuselage juncture on the total drag and also the benefits derived from sweeping the wing. Either of the modifications to the swept wing increased the Mach number for drag divergence about 0.01. It is interesting to note that application of the

simple cosine concept to the data for the unswept wing at zero lift resulted in a predicted drag-divergence Mach number of about 0.90 for the swept wing, a value only slightly in excess of that measured for the wing with the modifications.

EFFECTS OF NACELLES

An important problem in connection with the application of swept wings is the possible detrimental effect caused by nacelles or external stores. An investigation of this problem was conducted in the Ames 12-foot pressure tunnel utilizing the 37° sweptback wing described in the first portion of this paper. As shown in figure 11, a body of revolution having a fineness ratio of 6.5 was installed on the model wing with the center line of the body at 31 percent of the semispan from the plane of symmetry. The forward 40 percent of the body was one-half of a prolate spheroid and the rear portion had a slightly modified NACA 111 fuselage profile. The body was attached on the underside of the wing in such a way that the contour of the upper surface of the wing was not changed except near the leading edge.

From the data presented in figure 11, the isobars on the upper and lower surfaces of the wing-nacelle combination may be compared with the isobars on the upper surface of the wing without the nacelle. These data were obtained for the wing at 0° angle of attack at a Mach number of 0.85. As was expected, a region of high negative pressure coefficients developed near the leading edge at the inner juncture of the wing and the nacelle. On the upper surface the extent of this region was small, but on the lower surface it was of such magnitude that the isobars were warped more or less normal to the air-stream direction over most of the surface between the nacelle and the root of the wing. Outboard of the nacelle the isobars on the lower surface were approximately normal to the air stream at the juncture, but the pressures were of about the same magnitude as those on the upper surface of the wing without the nacelle.

In the upper-right part of figure 11 the chordwise distribution of pressure coefficient over the upper surface of the wing-nacelle combination at a station half-way between the nacelle and the wing root is compared with that for the wing without the nacelle. It is noted that addition of the nacelle resulted in a forward movement of the point of minimum pressure, which effect is also reflected as a small increase in the sweep of the isobars on the upper surface. Important from the standpoint of pressure drag is the fact that the pressures ahead of the crest were generally reduced by addition of the nacelle, which should tend to reduce the pressure drag at these sections.

[redacted]

In figure 12 data similar to those shown in figure 11 are presented for an angle of attack of 4° and a Mach number of 0.80. At this angle of attack the distortion of the isobars on the lower surface was not so serious with respect to critical flow conditions because the local velocities were much lower than on the upper surface. On the upper surface the intense pressure peak at the inner juncture was still confined to a small region. The favorable interference effect of the nacelle was greater than it was at zero angle of attack, resulting in greater sweep of the isobars on the upper surface between the nacelle and the wing root. The more forward position of minimum pressure and lower pressures ahead of the crest between the nacelle and the wing root should decrease the pressure drag at these sections.

In figure 13 the variation with Mach number of the total drag of the wing–nacelle combination is compared with that of the wing without the nacelle for lift coefficients of 0, 0.2, and 0.4. At zero lift the incremental drag due to the nacelle began to increase with increasing Mach number at Mach numbers well below that for drag divergence; whereas at a lift coefficient of 0.4, the incremental drag due to the nacelle remained nearly constant up to a Mach number of 0.92, the highest that was attained during the tests. It is also evident from these data that the addition of the nacelle caused only a small reduction in the drag-divergence Mach number. Thus, it appears that serious effects on the drag-divergence Mach number which were expected to occur as a result of the very high negative pressure peaks at the leading-edge juncture were partly offset by favorable interference effects. These favorable interference effects were the increased sweep of the isobars and the reduced section pressure drag near the wing root.

In figure 14 the drag-divergence Mach numbers for a range of angle of attack are summarized for the wing, the wing with the solid nacelle, and for the wing with a nacelle through which air flowed from a nose inlet. The design of the air inlet and the forebody for this air-flow nacelle was based on parameters introduced in the development of the NACA 1-series nose inlets by Baals, Smith, and Wright (reference 5). As shown in the figure, the nacelle was mounted on the lower side of the wing with the air inlet slightly behind the leading edge and with the face of the inlet normal to the air-stream direction. These data were obtained from tests conducted at an inlet velocity ratio of approximately 0.80. Additional tests at zero inlet velocity ratio showed only a slight reduction in the drag-divergence Mach number although, of course, the nacelle drag was higher.

Inspection of the data shown in figure 14 reveals that addition of either of the nacelles to the swept wing caused only small reductions in the Mach number for drag divergence. It will be recalled that at zero angle of attack there was marked distortion of the isobars on the lower surface of the wing near the nacelle; also that the drag due to

[redacted]

the nacelle increased at Mach numbers somewhat below the drag-divergence Mach number. The possibility should therefore be considered that these disturbances might cause buffeting difficulties even though they do not seriously reduce the drag-divergence Mach number.

SUMMARY OF RESULTS

In summary, the results of an investigation of the pressures and the drag on a moderately swept wing indicate that the crest-line concept is a useful guide in determining the range of Mach numbers in which the abrupt drag increase can be expected to begin. It is further indicated that the drag-divergence Mach number can be estimated from low-speed pressure-distribution measurements on the swept wing. Modifications of the wing-fuselage juncture, although not necessarily the optimums, did increase the drag-divergence Mach number. Single nacelles mounted on the lower surface of a moderately swept wing caused only small reductions in the Mach number for drag divergence.

REFERENCES

1. Jones, Robert T.: Wing Plan Forms for High-Speed Flight. NACA Rep. 863, 1947.

2. Küchemann, D.: Design of Wing Junction, Fuselage and Nacelles to Obtain the Full Benefit of Sweptback Wings at High Mach Number. Rep. No. Aero. 2219, British R.A.E., Aug. 1947.

3. Nitzberg, Gerald E., and Crandall, Stewart: A Study of Flow Changes Associated with Airfoil Section Drag Rise at Supercritical Speeds. NACA TN 1813, 1949.

4. Jones, Robert T.: Subsonic Flow Over Thin Oblique Airfoils at Zero Lift. NACA Rep. 902, 1948.

5. Baals, Donald D., Smith, Norman F., and Wright, John B.: The Development and Application of High-Critical-Speed Nose Inlets. NACA Rep. 920, 1948.

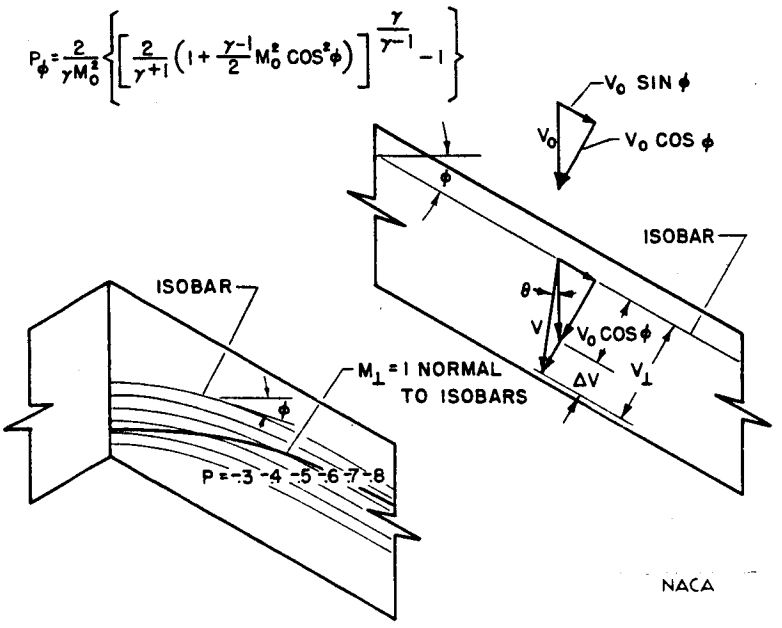


Figure 1.- Concepts used in considering the flow over swept wings.

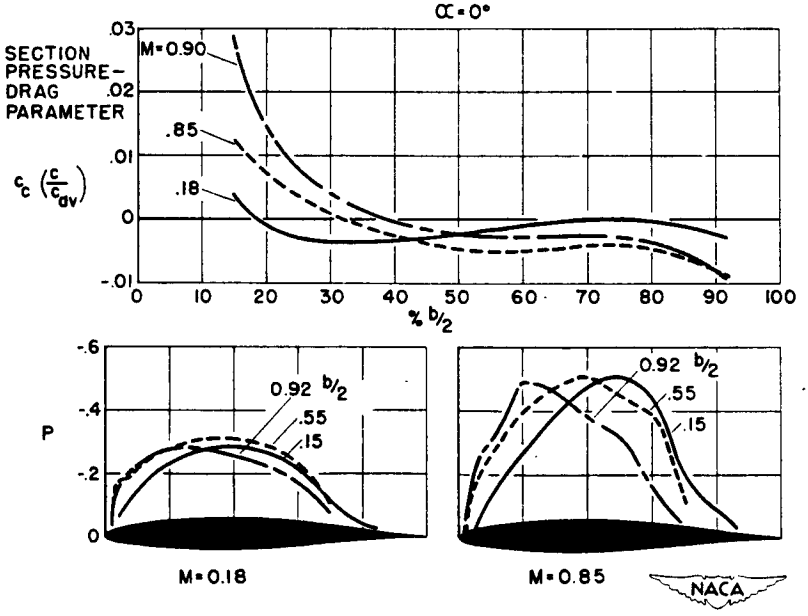


Figure 2.- The pressure drag of a 37° swept wing.

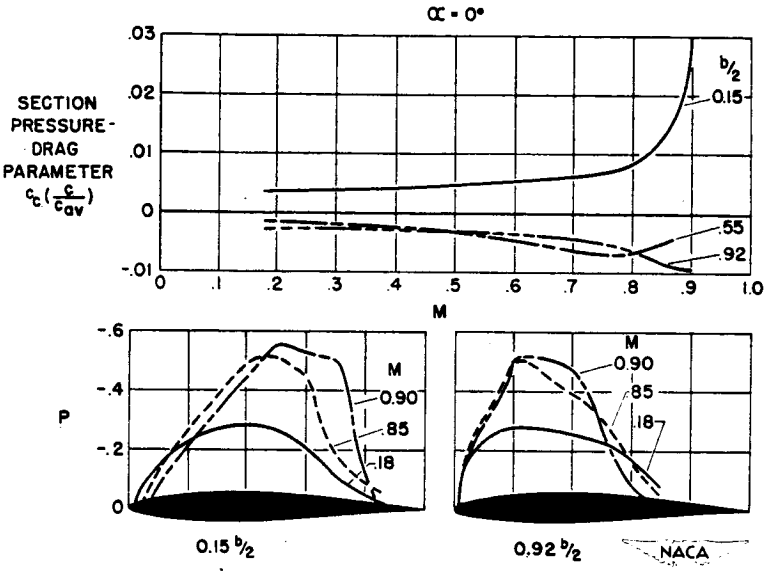


Figure 3.- Effect of Mach number on section pressure drag of a 37° swept wing.

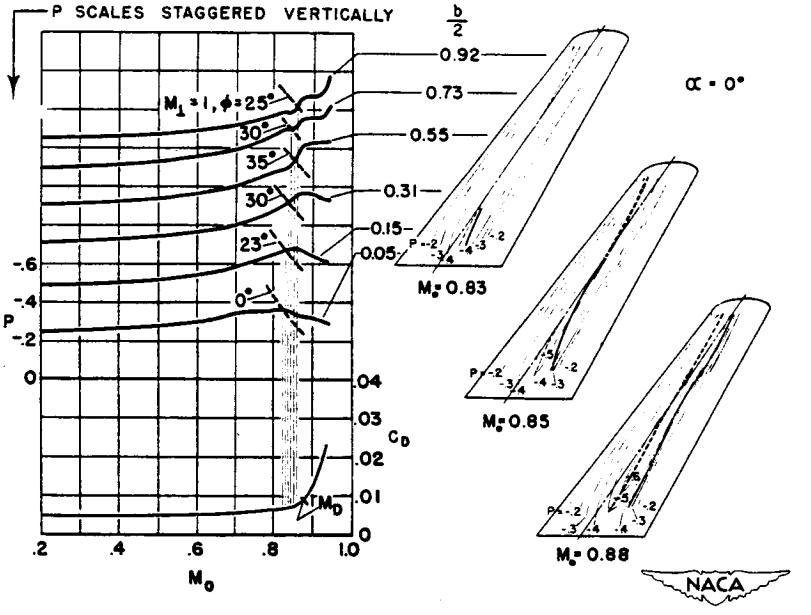


Figure 4.- Relation of critical flow conditions at the wing crest to the variation of drag coefficient with Mach number at 0° angle of attack.

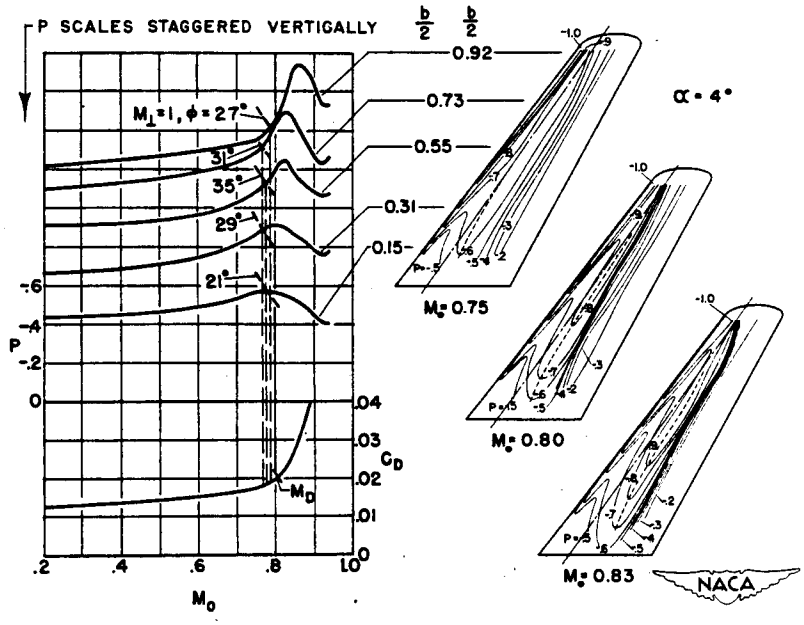


Figure 5.- Relation of critical flow conditions at the wing crest to the variation of drag coefficient with Mach number at 4° angle of attack.

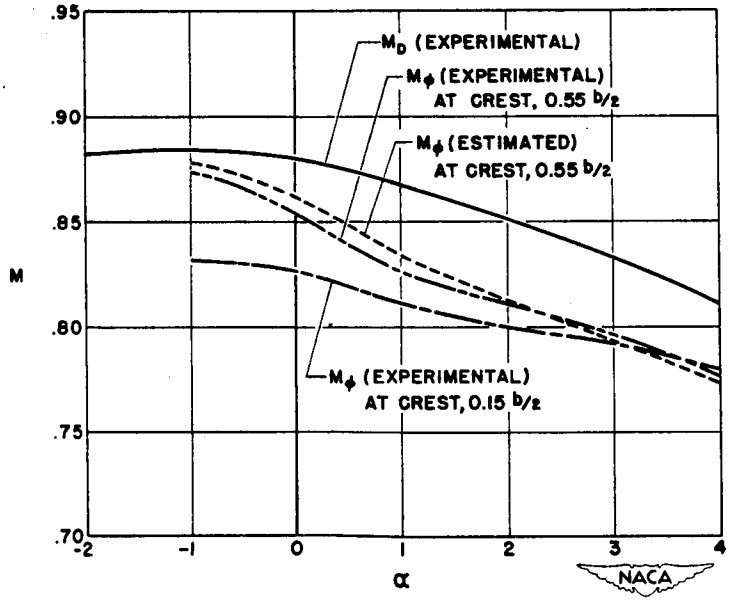


Figure 6.- Comparison of the Mach number for the attainment of the critical flow condition at the crest with the drag-divergence Mach number.

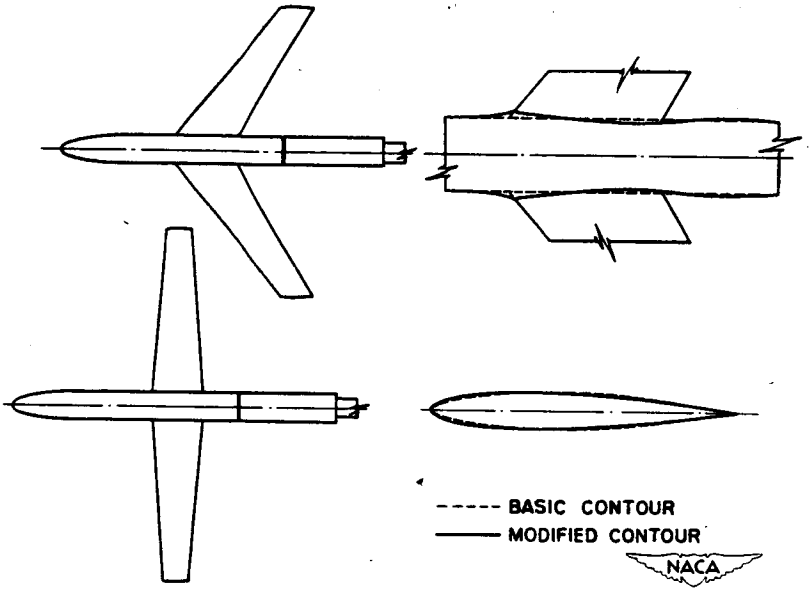


Figure 7.- The model tested in the Ames 16-foot high-speed tunnel.

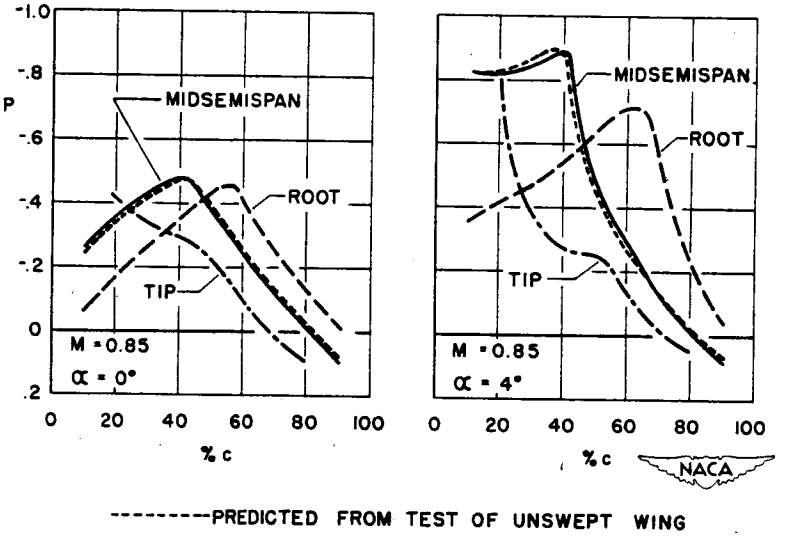


Figure 8.- Pressure distribution on the upper surface of the swept wing.

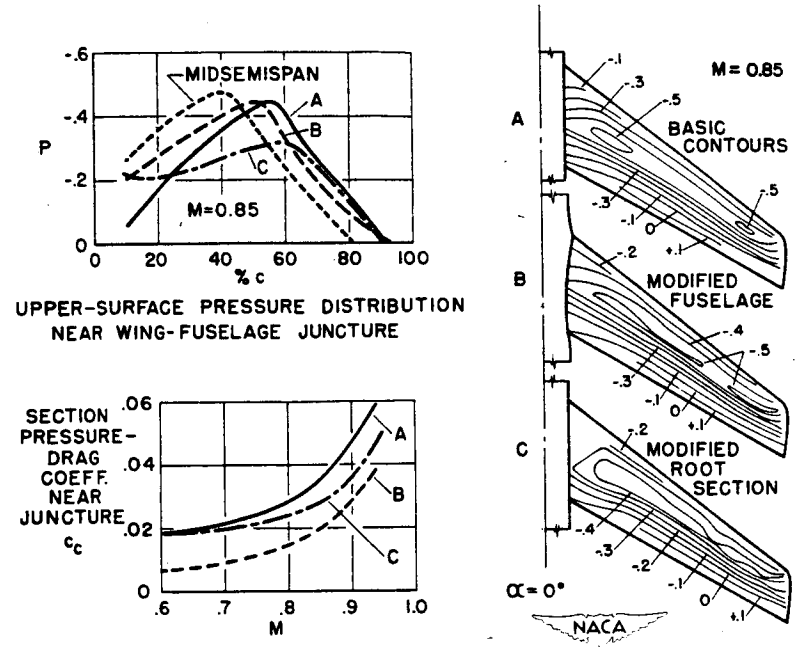


Figure 9.- Effect of modifying the wing-fuselage juncture on the wing pressures and on the pressure drag at the wing root.

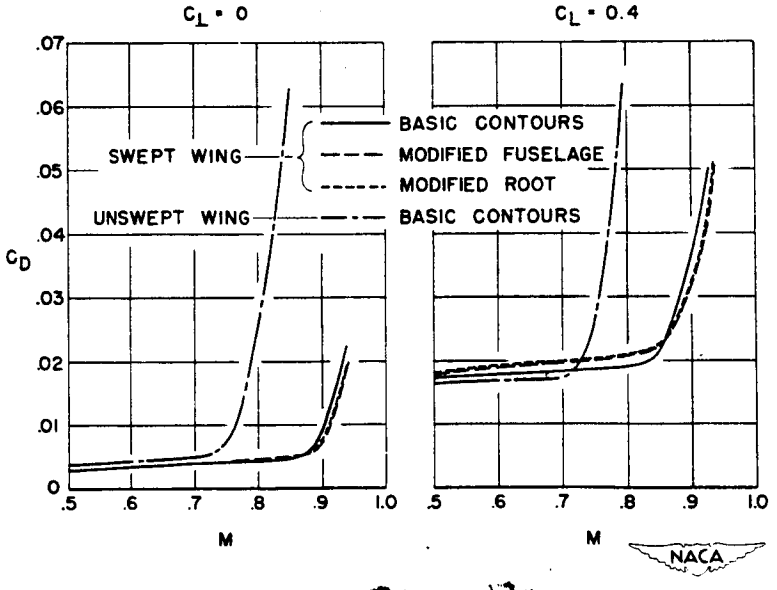


Figure 10.- Effect of modifying the wing-fuselage juncture on the variation of drag coefficient with Mach number.

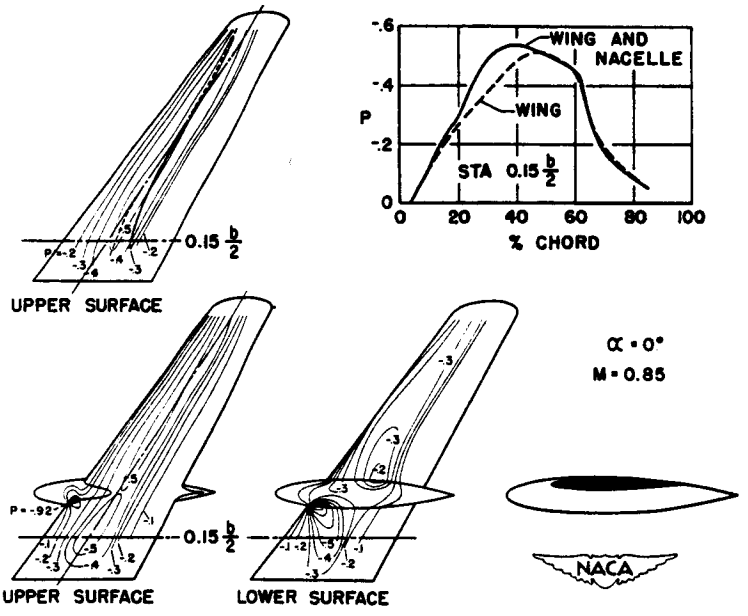


Figure 11.- Effect of a nacelle on the pressures on the 37° swept wing at 0° angle of attack and 0.85 Mach number.

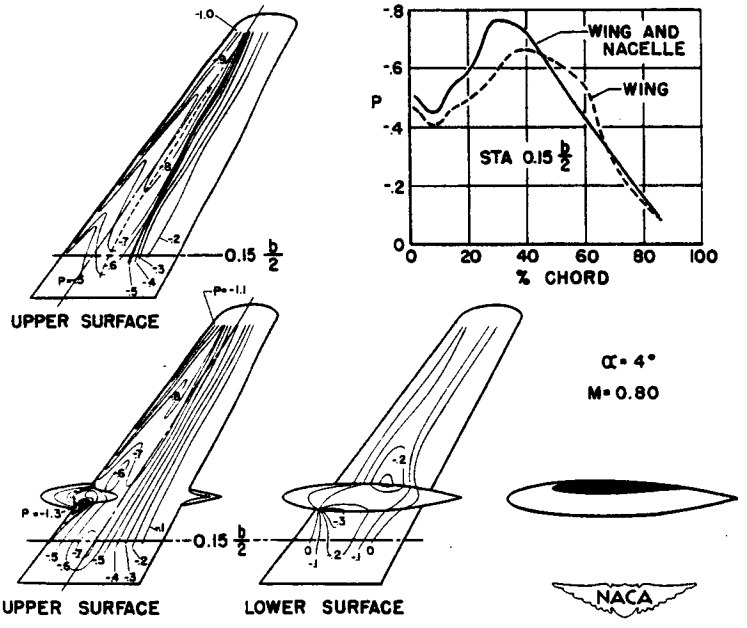


Figure 12.- Effect of a nacelle on the pressures on the 37° swept wing at 4° angle of attack and 0.80 Mach number.

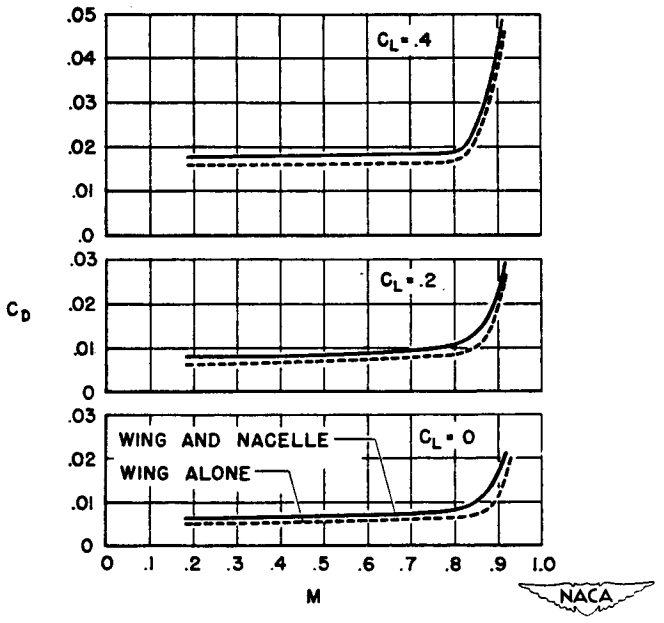


Figure 13.- Effect of a nacelle on the variation of drag coefficient with Mach number.

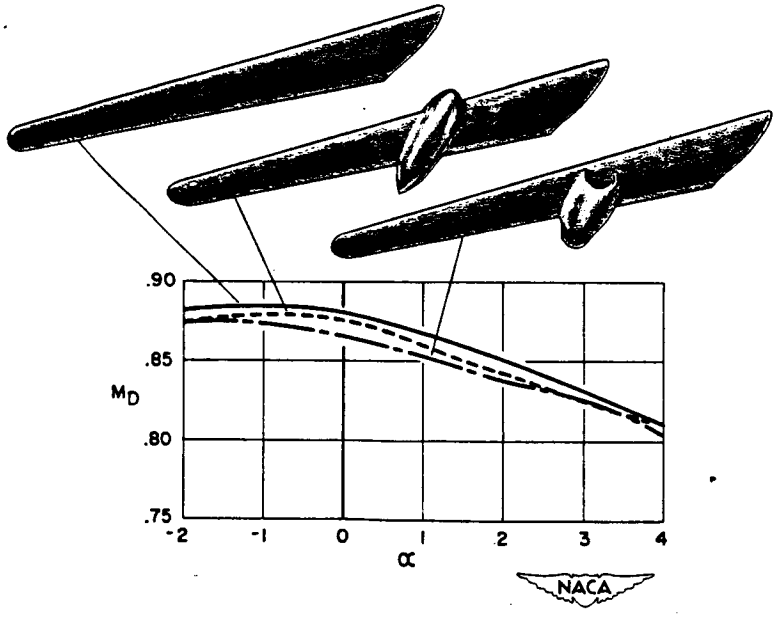


Figure 14.- Effect of nacelles on the drag-divergence Mach number of the wing.

N65-86463

EFFECT ON FORCE COEFFICIENTS OF BODIES OF REVOLUTION ATTACHED TO STRAIGHT AND SWEPT WINGS

By H. Norman Silvers

Langley Aeronautical Laboratory

Several experimental investigations have been made at the Langley and Ames Aeronautical Laboratories of the effect on force coefficients of external stores and nacelles on straight and swept wings at transonic speeds (references 1 to 7). Two general locations of such installations are dealt with in this paper. They are the inboard installation where the body is located inboard of the wing tip and the tip-mounted installation where the body is located at the wing tip.

The purpose of this paper is to indicate effects that are characteristic of each location of the body of revolution and to show briefly the steps that are being taken to eliminate certain undesirable characteristics of these installations.

Presented in figure 1 is a comparison of an inboard installation with a tip-mounted installation on models with straight wings. The solid curves represent the model in the clean condition, and the dashed curves represent the model with the body of revolution located below the wing by a pylon fairing member. Figure 1 shows that drag due to the inboard installation is considerably higher throughout the Mach number range than that of the tip-mounted installation, and that the drag-break Mach number is considerably lower than that of the clean model. This is due primarily to the high local velocities induced by the inboard installation over the lower surface of the wing.

The Mach number where the drag coefficient has risen 0.002 over the subsonic value M_B increases for the inboard installation relative to that of the clean model and decreases for the tip-mounted installation as the lift coefficient increases. This illustrates the possible performance advantages that may be obtained by an airplane with the inboard installation at the higher lift coefficients.

The lift-curve slope C_{L_α} is seen to be decreased throughout the Mach number range by the inboard installation. The tip-mounted installation, however, produces a notable increase in C_{L_α} because of the end-plate effect of this configuration.

The effects of an inboard, pylon-suspended installation on a model with a sweptback wing are shown in figure 2. It is seen that sweeping the wing has no noticable effect on the general characteristics of the

inboard installation. The drag due to the installation is high throughout the Mach number range at zero lift, the Mach number for drag break approaches that of the clean model as the lift coefficient increases, and the lift-curve slope of the clean model is reduced.

Also shown in figure 2 is the effect of a body of revolution attached directly to the sweptback wing of a model in flight. It is evident that the drag of this installation is large throughout the transonic speed range. The large absolute values of flight drag are due to the large wetted area of the model and the thick sections employed on the stabilizing fins.

The results presented in figure 3 show the effects of tip-mounted bodies of revolution on the aerodynamic characteristics of models with sweptback wings. As in the case of the inboard installation, it is apparent that sweeping the wing does not alter the variations characteristic of this installation. It is important to note, however, that unfavorable interference effects beginning at the drag-break Mach number result in large additional drag for this installation at supersonic Mach numbers. In an effort to minimize interference effects the body of revolution was moved forward on the wing tip. The results indicate that the change in position of the body did not result in any appreciable change in either the drag at supersonic Mach numbers or the drag-break Mach number at the higher lift coefficients.

The effect of changes in the chordwise position of an inboard mounted installation is shown in figure 4. On the wind-tunnel model the body was suspended below the wing by streamlined fairings. The changes in chordwise position of the body were accomplished by sweeping the fairing member either forward or back while maintaining the same vertical location of the body. The results show that either change in the body location is effective in reducing the drag at the higher Mach numbers and delaying the drag break. The lowest drag as well as the highest drag-break Mach numbers were produced by the aft-located body.

Flight tests of a body located in a middle, chordwise position and a forward position show similar results. It is also evident that a forward movement of the body materially reduces the drag at supersonic speeds. It should be noted that the change in the chordwise position of the body was accompanied by a change in vertical location.

Several investigations currently being conducted both in the wind tunnel and in flight are aimed at providing more quantitative information on the effects of changes in the chordwise position of an inboard mounted body of revolution. Recent results of a flight investigation of a high-speed body representing a solid, unfilleted nacelle on a bomber-type model are shown in figure 5. It can be seen that the nacelle reduced the drag-break Mach number and resulted in large drag at

supersonic speeds. The subsonic nacelle drag was about equal to the drag estimated for the body alone. At supersonic speeds it was about twice that estimated for the body. It is evident that changes in the nacelle position did not produce any appreciable change in the drag in contrast to favorable effects shown earlier for the lower-aspect-ratio, fighter-type models. It thus appears that, in conjunction with fore and aft location of a body on a wing, filleting adjacent fuselage shape and vertical and spanwise location of the body must also be studied.

The end-plate effect of a tip-mounted body of revolution suggests that this type installation will increase the lateral control effectiveness. To evaluate this possibility, rolling tests were made of two arrangements of tip-mounted bodies of revolution on a model with a sweptback wing. The results are presented in figure 6. The arrangements tested consisted of a body attached directly to the wing tip and toed out with a fairing between the wing and the body and a body suspended below the tip by a sweptforward pylon fairing. It is seen that the direct-mounted body increased the control effectiveness considerably, whereas the pylon-suspended installation resulted in no appreciable change. The damping parameter, however, is shown to be increased by both installations with the direct-mounted body producing the largest increases. The net result is that the rate of roll per degree control deflection was decreased for both installations.

It is felt that it will be of interest to point out several other general findings that are a result of the experimental investigation of a number of body-wing installations. The results have indicated that the largest change in the aerodynamic-center location produced by a body of revolution is less than 2.5 percent mean aerodynamic chord below the force-break Mach number on rigid wings. It has been found that the moments of the body of revolution accompanying changes in the aerodynamic center of this order of magnitude may be eliminated by small stabilizing fins attached to the body (reference 8).

It has further been found (reference 4) that the favorable maximum lift-drag ratios produced by a tip-mounted body of revolution at low speed are decreased considerably by interference effects at the higher Mach numbers. In fact, fuselage-mounted bodies of revolution have been shown to produce higher lift-drag ratios at Mach numbers greater than about 0.6 than do tip installations on a model with a sweptback wing.

It has also been shown (reference 4) by tests of a number of tip-mounted bodies that the effects of tip-mounted installations on the lateral and directional stability of a model with a sweptback wing are small.

[redacted]

[redacted]

REFERENCES

1. Silvers, H. Norman, and Spreemann, Kenneth P.: Correlation of Wind-Tunnel and Flight Determinations of the Buffet Speed of an Airplane Equipped with External Stores. NACA RM L7E20, 1948.

2. Polhamus, Edward C., and King, Thomas J., Jr.: High-Speed Wind-Tunnel Investigation of the Longitudinal Stability and Control Characteristics of a 0.10-Scale Model of the Grumman XF9F-2 Airplane - TED No. NACA DE301. NACA RM SL8K16, Bur. Aero., 1948.

3. Boddy, Lee E., and Morrill, Charles P., Jr.: The Aerodynamic Effects of Rockets and Fuel Tanks Mounted under the Swept-Back Wing of an Airplane Model. NACA RM No. A7J03, 1948.

4. Silvers, H. Norman, and Spreemann, Kenneth P.: Experimental Investigation of Various External Store Configurations on a Model of a Tailless Airplane with a Sweptback Wing. (Prospective NACA paper)

5. Welsh, Clement J., and Morrow, John D.: Effect of Wing-Tank Location on the Drag and Trim of a Swept-Wing Model as Measured in Flight at Transonic Speeds. (Prospective NACA paper)

6. Silvers, H. Norman, and Spreemann, Kenneth P.: Effects of Systematic Changes in Geometry and Position of an Underwing External Store Installation on the Aerodynamic Characteristics of a Wing with Quarter-Chord Line Swept Back 45°. (Prospective NACA paper)

7. Kuhn, Richard E., and Myers, Boyd C., II: The Effect of Tip Tanks on the Rolling Characteristics at High Subsonic Mach Numbers of a Wing Having an Aspect Ratio of 3 with Quarter-Chord Line Swept Back 35°. (Prospective NACA paper)

8. Silvers, H. Norman, and Spreemann, Kenneth P.: Experimental Investigation of the Effect of Two Wing Sections and a Tip Tank on the Aerodynamic Characteristics of an Unswept Wing of Aspect Ratio 5.16 and Taper Ratio 0.61 at High Subsonic Speeds. NACA RM L9J04, 1949. (Prospective NACA paper)

[redacted]

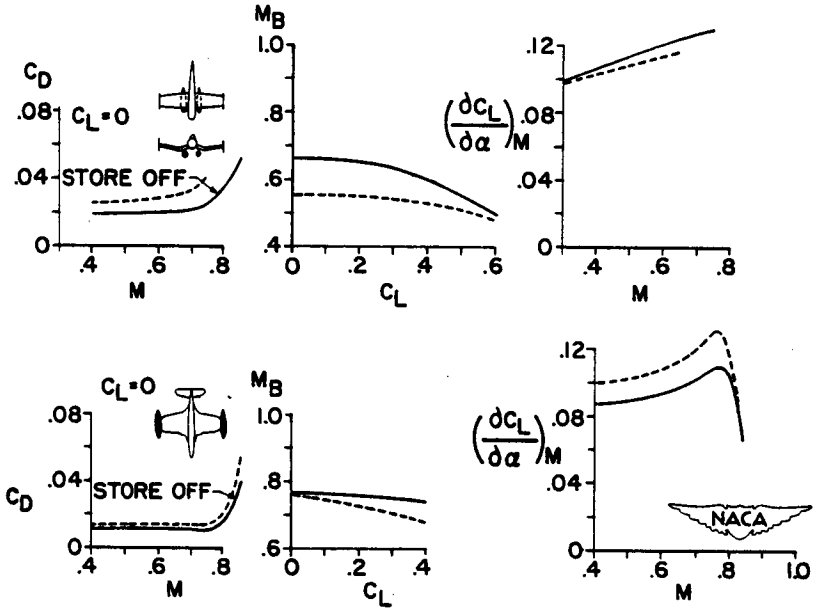


Figure 1.- Inboard installation and a wing-tip installation on models with straight wings.

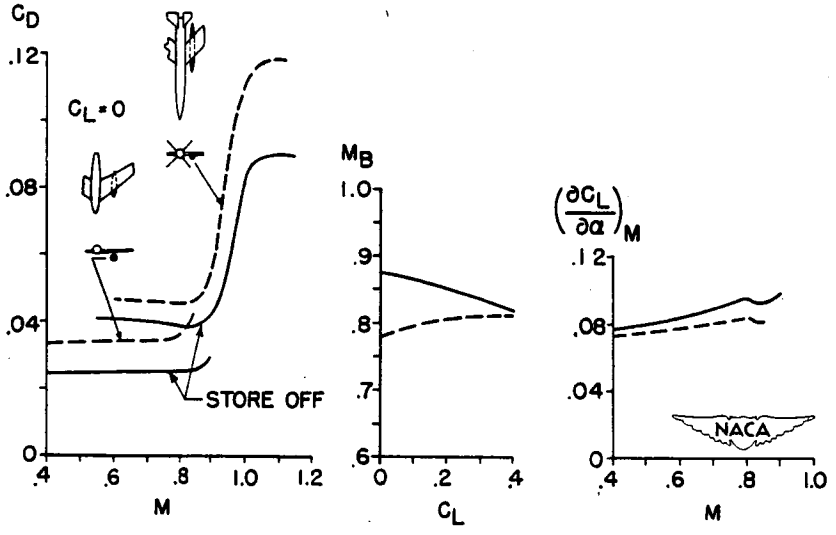


Figure 2.- Inboard installation on a model with a swept wing.

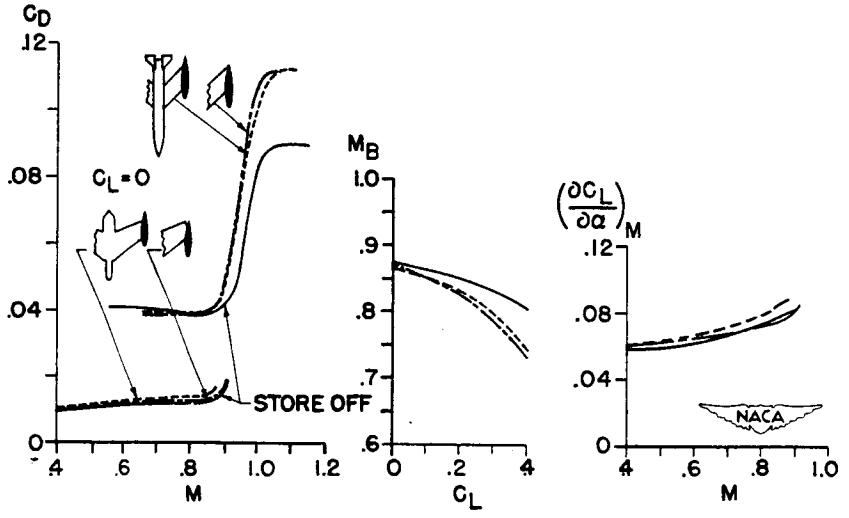


Figure 3.- Wing-tip installation on a model with a swept wing.

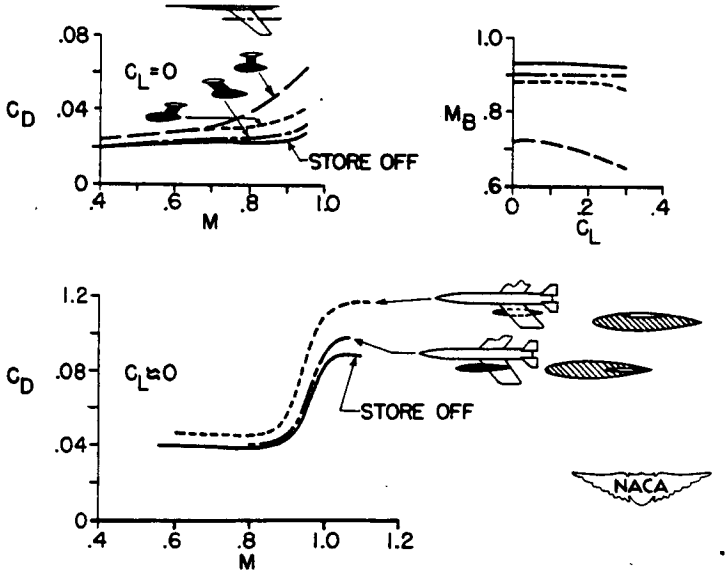


Figure 4.- Effect of chordwise position of an inboard installation on models with swept wings.

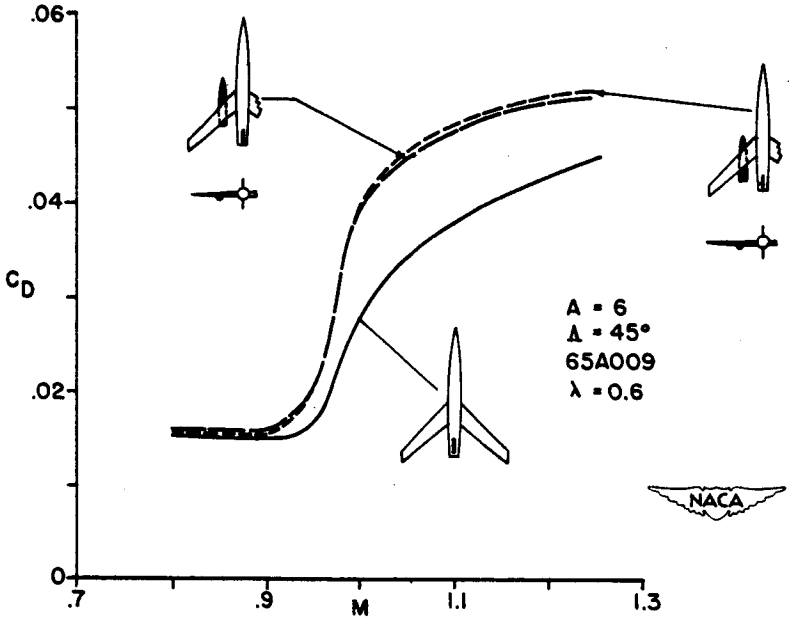


Figure 5.- Effect of chordwise position of a nacelle-like body on a swept wing, bomber-type model.

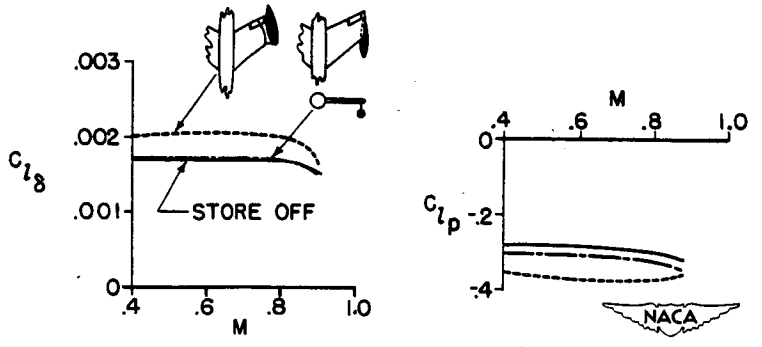


Figure 6.- Rolling characteristics of two wing-tip installations on a model with a swept wing.

Preceding page blank

N65-86464

ASSESSMENT OF THE DRAG PROBLEM

By Richard I. Sears

Langley Aeronautical Laboratory

Other papers of this conference have shown the effects on the drag coefficient of varying the geometry of wings and bodies. They have shown that the zero-lift drag coefficient of wings and bodies at supersonic speeds can be reduced to about twice that of the best wings and bodies at subsonic speeds. The drag due to lift at supersonic speeds, however, is many times that at subsonic speeds.

Some of these data and other data will be examined to assess the importance of drag reduction for flight at supersonic speeds and to point out the present status of research on the drag problem.

Figures 1 and 2 help to establish a quantitative basis for some of the numbers used in the subsequent analysis.

Figure 1 shows the wing plus wing-body interference drag at zero lift of three low-drag wings of different plan form. These data were obtained at large Reynolds numbers by the rocket technique. The wings were mounted on cylindrical bodies, and the wing plus interference drag was obtained by subtracting from the total drag the drag of the body measured on other flights. The straight wing has a double-wedge airfoil section 4.5 percent thick (DW-04.5), the delta wing has a double-wedge section 3 percent thick (DW-03), and the highly sweptback wing has an NACA 65A005 section parallel to the air stream. The straight wing shows a relatively large drag rise near Mach number $M = 1$. The drag coefficient then decreases with increasing Mach number so that at $M = 1.4$ it is of the same order as that of the swept wings shown. This variation is typical of a sharp-nose straight wing, and if the bump near $M = 1$ can be passed, the wing becomes of real interest for flight at $M \gtrapprox 1.4$.

The two wings with highly swept leading edges show not much change in the drag coefficient at zero lift C_{D_0} with M in the supersonic range. Although the delta wing has a sharp leading edge, the same level of C_{D_0} would be expected with a round-nose wing of the same thickness. Other data show that for wings with subsonic leading edges, whether the nose is sharp or round makes little difference on the zero-lift drag. The highly swept wing shown is one of the lowest-drag wings for which data have been obtained. Actually these three wings are all quite low drag wings. The value of C_{D_0} at supersonic speeds would be, for comparison, of the order of 0.06 for the X-1 wing, about 0.03 for the X-2 wing, and about 0.04 for the D-558-II wing.

Figure 2 shows values of drag-due-to-lift factor $\frac{\Delta C_D}{\Delta C_L^2}$ as a function of Mach number for wings of these same three plan forms. The data are from wind-tunnel tests at low Reynolds numbers, and are for low lift coefficients. (See references 1, 2, and 3.) The solid portions of the curves represent the regions of test data. The square symbol at $M = 1.5$ is a test point for the straight wing (reference 4). The straight wing has a sharp leading edge and the swept and delta wings, round leading edges. The airfoil sections are indicated under the pictures. The circular symbols at $M = 0.75$ and 1.5 represent the theoretical values for the correspondingly numbered wings.

The data are from small-scale tests and, therefore, do not necessarily represent the true values at large values of Reynolds number. Few data are available at large values of Reynolds number. For the straight wing, however, large-scale tests by rocket technique are in substantial agreement with the small-scale results shown here and also with theory, $\frac{\Delta C_D}{\Delta C_L^2}$ being inversely proportional to the slope of the lift curve. The degree to which the values for the swept and delta wings can be made to approach the theoretical values by cambering and twisting the wing at large values of Reynolds number is not known. The delta wing has a high value of drag due to lift because of its small aspect ratio and slope of the lift curve. It should be noted that, from $M = 1.1$ to $M = 1.3$ for example, the values of $\frac{\Delta C_D}{\Delta C_L^2}$ for all three types of low-drag wings lie between 0.2 and 0.3. This is about 5 or 6 times that of a good subsonic fighter wing. The straight wing shown here is of small aspect ratio and has a sharp leading edge which, of course, accounts for the high value at subsonic speeds. Test data have indicated that significant reductions in the drag due to lift are obtained by favorable wing-body interference. Further research is needed to find the best way to capitalize on this favorable interference and hence reduce the drag due to lift.

Figure 3 shows thrust and drag curves at 40,000 feet for a somewhat idealized transonic airplane consisting of a swept wing, a body of revolution, and a vertical tail. This particular configuration is shown, not because it has particularly low drag, but because we have large Reynolds number measurements from the rocket technique of the zero-lift drag of this wing-body-tail arrangement (reference 5). The body has a fineness ratio of 10. The wing is of NACA 65-006 section streamwise, of aspect ratio 4, taper ratio 0.6, and is swept back 45°. Its area is 16.5 times the body frontal area. The thrust coefficient C_{T_W} is based on wing area and is of a level comparable to that which has been obtained from tests simulating supersonic speeds with turbojet engines having afterburning. The maximum cross-sectional area of the

fuselage S_F has been assumed to be 1.8 times that of the engine S_N, which is not an unreasonable value. Drag-coefficient curves are shown for zero lift and for level flight at 40,000 feet with wing loadings W/S of 50 and 100 pounds per square foot. Drag due to lift has been estimated from wind-tunnel data.

Although for a wing loading of 50 pounds per square foot the curves show that for the assumed thrust the maximum Mach number is 1.2, the important thing to note is the small difference between the thrust and drag coefficients at all supersonic Mach numbers shown. For only a very slight change in thrust or drag level, large changes in maximum speed are indicated.

The rise in drag near $M = 1$ is largely attributable to unfavorable wing-body interference. Free-fall tests of similar wings bear this out. For this particular configuration the zero-lift drag of the wing and body are nearly equal at supersonic speeds. The drag due to lift, indicated by the difference between these two curves, therefore, is much less than the zero-lift wing drag.

Analysis indicates that optimum performance is attained when the drag due to lift is equal to the zero-lift wing drag so that the wing flies at its maximum lift-drag ratio L/D at the design speed. In the present case, higher altitudes could be obtained at $M = 1.2$ and also greater speed could be obtained with the same engine, fuselage, and weight, if the wing were smaller.

Figure 4 shows the effects of thrust, fuselage drag, and wing drag on the optimum wing size and the maximum altitude attainable at $M = 1.2$ for an airplane of given weight W. As the abscissa we have the difference between the thrust coefficient C_{T_F} and the fuselage drag coefficient C_{D_F} both based on fuselage cross-sectional area. This difference might be called the excess thrust coefficient and represents the thrust available to push the wing through the air. The ordinates are altitude in feet and S_W/S_F, the wing area expressed as multiples of the fuselage cross-sectional area. The upper $\frac{S_W}{S_F}$ curve shows the optimum wing size and is drawn for a low-drag wing with $(C_{D_0})_W = 0.01$. The lower curve is for a wing with 50 percent greater zero-lift drag. These curves show that as the excess thrust available to push the wing along is decreased, or as the zero-lift drag coefficient of the wing increases, the size of the wing should decrease. This is simply because the wing is there to provide lift and the most efficient way to provide this lift is to have the wing operate at its maximum ratio of lift-to-drag coefficient. For a wing of given geometric design, the wing-drag coefficient for maximum wing L/D is fixed and equal to twice the zero-lift wing-drag coefficient. This is the wing-drag coefficient

for most efficient flight at the design speed, and to attain maximum altitude the wing should be made to operate at this wing-drag coefficient. It then follows that in order to make the wing drag equal to the excess thrust available to fly the wing, the size of the most efficient wing must vary directly with the excess thrust and inversely with the zero-lift wing-drag coefficient.

The drag-due-to-lift factor $\frac{\Delta C_D}{\Delta C_L^2}$ and the zero-lift drag coefficient of the wing combine to fix the lift coefficient for maximum wing L/D. When the lift coefficient is fixed by these factors for a wing of given design, and when the wing size is determined from the considerations just mentioned, the altitude at which the lift equals the weight is determined. This altitude is shown as a function of excess thrust coefficient by the upper two curves of figure 4. It is the maximum altitude attainable at the given speed, $M = 1.2$ in this case, and corresponds to that for the optimum wing size shown below. For any other size wing the maximum altitude is less. The topmost curve is drawn for the wing with $C_{D_0} = 0.01$ and $\frac{\Delta C_D}{\Delta C_L^2} = 0.23$. These values are representative of the drag level at $M = 1.2$ of the best wings attainable in the light of present data. The increase of altitude with increasing thrust margin is readily apparent. The loss in altitude resulting from either a 50-percent increase in zero-lift wing drag or a 50-percent increase in drag due to lift is indicated by this curve. The loss, of the order of 4000 feet, indicates the importance of keeping the wing-drag coefficient small.

Point A on the curve of figure 4 for this very low drag wing represents the case of the wing plus a very low drag fuselage with the same thrust as shown in figure 3. Point B represents a fuselage of 50 percent greater drag than the low-drag fuselage of point A. The associated loss in altitude is 6000 feet. Going from point A to point C represents a 50-percent increase in engine thrust coefficient. The gain in altitude is substantial (12,000 feet).

The general over-all picture is essentially similar at higher Mach numbers. With a wing and fuselage whose zero-lift drag coefficient do not increase with Mach number, as is the case for good wings and bodies at least to $M \approx 2.0$, the maximum altitude attainable with the same engine increases slightly with increasing Mach number.

Unfortunately there is more to a practical airplane than a wing and a body of revolution. Figure 5 shows the effect on the maximum altitude at $M = 1.2$ of adding various drag items. It is assumed that the weight and thrust coefficient are held constant and that, as drag items are added, decreasing the margin of thrust available to overcome the

wing drag, the wing size is reduced, but that it always operates at its maximum L/D. The curve, therefore, represents the highest altitude that can be obtained. Other wing sizes than those given by the lower curve would result in lower altitudes.

Let us assume a basically good wing and body with enough thrust margin to permit flight at 60,000 feet; this configuration corresponds to point C in figure 4. The addition of a reasonably sized tail of as good design as the wing reduces the maximum altitude about 2500 feet. Addition of an external canopy of a size and shape typical of subsonic fighter reduces the altitude 4000 feet more. The drag increment for the canopy was obtained from one series of tests using the rocket technique (reference 6). If it is necessary to carry four missiles externally in order to make the airplane tactically useful, the maximum altitude is reduced another 4000 feet. The drag increment for the missiles was obtained from large-scale tests of a typical air-to-air missile, and no allowance has been made for possible interference drag. If for electronic or other reasons it is deemed necessary to have a hemispherical nose, the diameter of which is one-half the maximum fuselage diameter, rather than a long pointed nose, another 7000 feet of maximum altitude is lost. Although drop tanks would probably not be carried at this speed unless means of carrying them with less drag penalty is found, they are shown here for illustrative purposes. The drag increment represents that of tanks in the most favorable location found from an investigation of tanks in many different locations (reference 7). The loss in altitude is of the order of 12,000 feet. Two potentially big but as yet largely unknown drag increments are not shown. They are the drag increment due to the duct inlets and that due to interference.

The drag of the items enumerated can readily be seen to substantially lower the maximum altitude attainable even with a basically good wing-fuselage-engine combination. To date, the main emphasis of the NACA on drag research at supersonic speeds has been on wings and bodies. This is rightly so because they are really the two major drag items of an airplane. Now that considerable data have been accumulated on ways of reducing wing and body drag to a very low level, additional gains will be hard to attain. It is obvious that we must continue to be concerned with the drag of wings and bodies and particularly with ways of reducing to a minimum the drag of canopies, tails, external stores, inlets, and the like.

[redacted]

REFERENCES

1. Mas, Newton A.: Aerodynamic Study of a Wing–Fuselage Combination Employing a Wing Swept Back 63°.– Characteristics for Symmetrical Wing Sections at High Subsonic and Moderate Supersonic Mach Numbers. NACA RM A9E09, 1949.

2. Lawrence, Leslie F., and Summers, James L.: Wind–Tunnel Investigation of a Tailless Triangular–Wing Fighter Aircraft at Mach Numbers from 0.5 to 1.5. NACA RM A9B16, 1949.

3. Turner, Thomas R., and Fikes, Joseph E.: Lateral Control Investigation at Transonic Speeds of a 35–Percent–Chord Flap on a Tapered Wedge–Type Wing of Aspect Ratio 2.5. (Prospective NACA paper)

4. Vincenti, Walter G., Van Dyke, Fulton D., and Matteson, Frederick H.: Investigation of Wing Characteristics at a Mach Number of 1.53. II – Swept Wings of Taper Ratio 0.5. NACA RM A8E05, 1948.

5. Katz, Ellis: Flight Investigations from High Subsonic to Supersonic Speeds to Determine the Zero–Lift Drag of a Transonic Research Vehicle Having Wings of 45° Sweepback, Aspect Ratio 4, Taper Ratio 0.6, and NACA 65A006 Airfoil Sections. NACA RM L9H30, 1949.

6. Alexander, Sidney R.: Effect of Windshield Shape of a Pilot's Canopy on the Drag of an NACA RM–2 Drag Research Model in Flight at Transonic Speeds. NACA RM L8E04, 1948.

7. Welsh, Clement J., and Morrow, John D.: Effect of Wing–Tank Location on the Drag and Trim of a Swept–Wing Model as Measured in Flight at Transonic Speeds. (Prospective NACA paper)

[redacted]

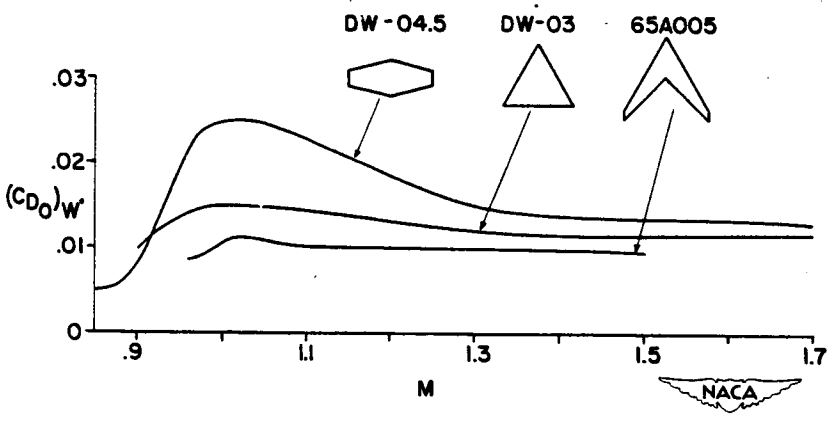


Figure 1.– Wing drag, including wing–body interference drag, for various airfoils. Reynolds number range from 3×10^6 to 10×10^6.

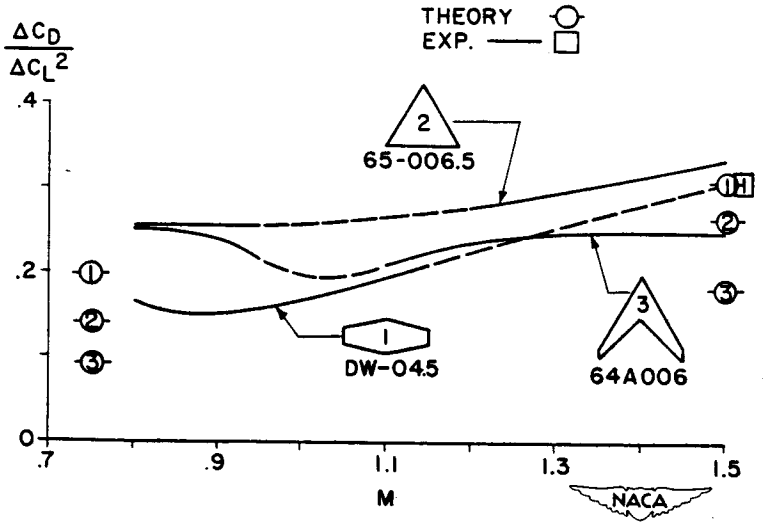


Figure 2.– Drag due to lift as a function of Mach number. Reynolds number less than 10^6.

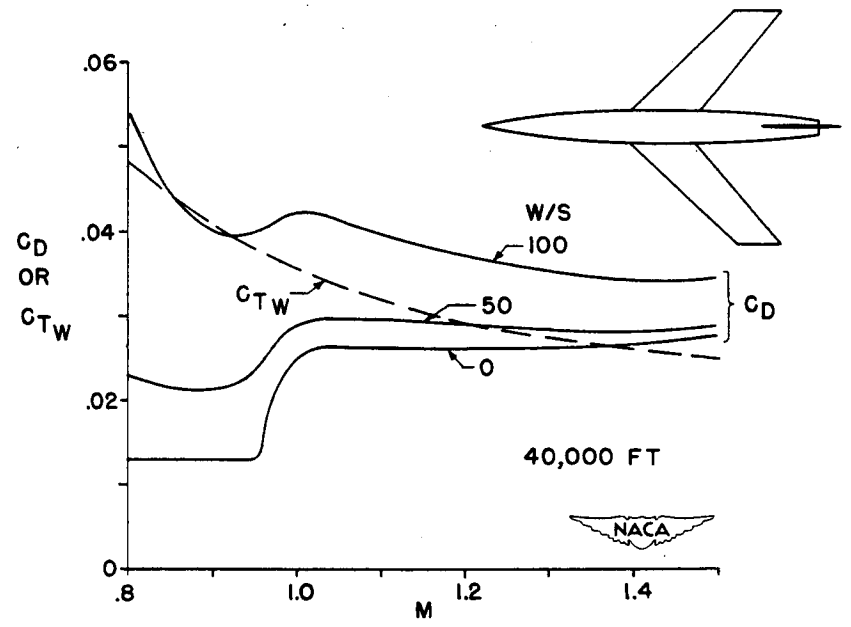


Figure 3.– Thrust and drag curves for transonic airplane at 40,000 feet. $\frac{S_F}{S_N} = 1.8$; $\frac{S_W}{S_F} = 16.5$; wing $\frac{t}{c} = 0.06$; $A = 4$; $\lambda = 0.6$; $\Lambda = 45°$.

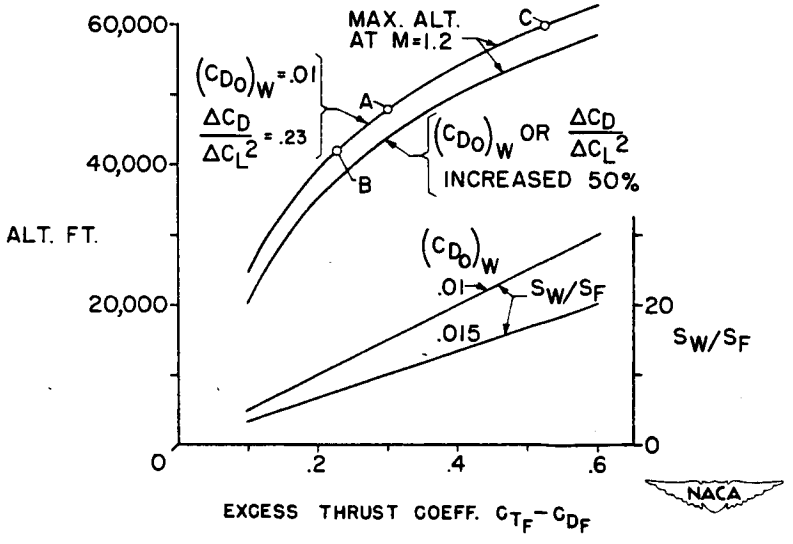


Figure 4.– Effect of thrust, fuselage drag, and wing drag on maximum altitude and wing size at $M = 1.2$. $\frac{W}{S_F} = 833$ pounds per square foot.

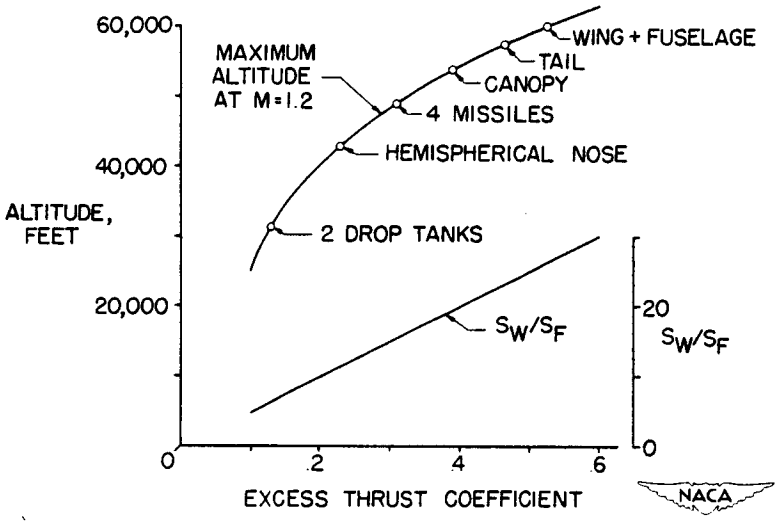


Figure 5.– Effect of additional drag items on maximum altitude attainable at $M = 1.2$. $(C_{D_0})_W = 0.01$; $C_{D_F} = 0.14$; $\frac{\Delta C_D}{\Delta C_L{}^2} = 0.23$. Optimum wing–fuselage size.

Preceding page blank

AIRSPEED MEASUREMENT

Preceding page blank

N65-86465

DESIGN AND CALIBRATION OF AIRSPEED INSTALLATIONS

By William Gracey

Langley Aeronautical Laboratory

During the past year some new information has been acquired on the measurement of static pressure in the transonic speed range. This information is presented from the standpoint of the problem of locating the static source on the airplane.

First, the problem of locating static vents on the fuselage is considered. Shown on figure 1 is a free-fall body of revolution with static pressure orifices located at various points along the body (reference 1). The extent to which the local pressures at each of these points deviates from free-stream pressure is defined by ΔP and is given as a fraction of the stream dynamic pressure q. Positive values of $\Delta P/q$ indicate that the local pressures are above stream pressure. The Mach number scale is based on stream Mach number. In the subsonic range up to $M = 0.9$ the static-pressure error for each of the orifices is roughly a constant percentage of the dynamic pressure. In the transonic range, however, the errors vary in an erratic manner and over a wide range. It is apparent from these results that even on a simple body at zero angle of attack and yaw it will be difficult to find a location which would be suitable as a static pressure source. In the case of an actual airplane, strong bow waves from the wing and tail surfaces would further complicate the picture.

Figure 2 shows the type of calibration which might be expected at specified vent locations on one particular airplane configuration. These results were obtained from wing-flow tests of a half-span model of an airplane having 35° swept wings (reference 2). In this case, the static-pressure errors are given as a fraction of the recorded impact pressure q_c' and are plotted in terms of recorded Mach number M'. In this form the results correspond to the flight calibration of an actual airspeed system. The results of these tests are similar to those shown on the previous figure in that the static-pressure errors are reasonably constant in the subsonic range but vary extensively in the transonic range. On the basis of the results of these two investigations it would appear that the problem of finding a suitable location for a static vent will be much more difficult for the transonic speed range than it has been for the subsonic speed range.

Second, the problem of locating static tubes in the vicinity of the airplane is considered. Shown on figure 3 is a static tube located 1.2 chord lengths ahead of the vertical tail of a free-fall model of

a canard airplane (reference 3). The calibration of this installation (fig. 3) and that for the rearmost vent on the wing-flow model shown on figure 2 show a marked similarity. It should be noted here that from a knowledge of the characteristics of static tubes no appreciable part of these deviations can be attributed to the static tube. From these results it is apparent that the vertical-tail installation offers no advantage over static vents located on the rear body of the fuselage.

The characteristics of static tubes located on the wing tip have been determined from wing-flow tests of a one-chord installation on a half-span model of a swept-wing airplane. (See fig. 4.) In the subsonic range, the static-pressure error is 1/2 percent below stream pressure, but in the transonic range it rises abruptly to 5 percent above stream pressure and increases thereafter to about 8 percent. This calibration is of particular interest because, as shown on the upper chart, there is a region in which the indicated Mach number does not vary with true Mach number. In other words, the installation is completely insensitive to changes in stream Mach number in this range and as such would be entirely unsatisfactory. It may be noted here that, for those installations which show a drop in the position-error curve, the curve of true against indicated Mach number would rise in a vertical direction and the installation would be very sensitive to true Mach number. Although the characteristics of one-chord installations on other wings might not be the same as regards the abrupt rise in the curve and although the Mach number at which the rise occurs might not be the same, the use of any wing-tip installation in the transonic speed range would be considered undesirable because of the effects of the wing and fuselage bow shocks at Mach numbers above 1.0.

The characteristics of static tubes on the fuselage nose have been determined from wing-flow tests of tubes at various distances ahead of simple bodies of revolution (reference 4). Figure 5 shows a typical example of the sort of calibration to be expected for these installations. For the particular case of this type of body with a tube located at 1.5 body diameters ahead of the nose, the position error in the subsonic range is $1\frac{1}{2}$ percent above stream pressure. In the transonic range the error rises to 5 percent and then falls abruptly as the fuselage bow wave moves across the tube. With the passage of shock the tube becomes isolated from the pressure field of the body, and the measured pressure for all higher Mach numbers will be very nearly equal to stream pressure. As shown on the upper chart, the rise in the position-error curve corresponds to a slight reduction in sensitivity, but it can be seen that this variation is relatively minor.

Figure 6 shows the results of an attempt to correlate the test data of the two wing-flow bodies. The first body is the same as that shown on figure 5. The shape of this body is defined by a circular arc

and the fineness ratio is 6.0. The shape of the second body is based on the shape of the fuselage of the X-1 airplane. Although this body appears more slender than the first, the fineness ratio is smaller because the distance from the nose to the point of maximum thickness is smaller. As shown on this figure, the effects of fineness ratio have been taken into account by combining the square of the fineness ratio with both the position error and Mach number terms. The result is a family of curves which depend only on the position of the tube expressed as a fraction of the body length. The points on the right represent the values of the peak position errors which occur just prior to the passage of shock, while the points on the left represent the values of the subsonic errors. This figure shows that for a body of given fineness ratio the magnitude of the position errors throughout the transonic range will decrease as the tube is moved away from the body. It also shows that for a given position of the tube, the magnitude of the position error decreases as the fineness ratio is increased. The importance of this correlation is the fact that these curves can be used for predicting the magnitude of the position errors for other fuselage-nose installations, provided the shape of the nose section is similar to that of two test bodies. By calculating the Mach numbers at which these errors occur, a calibration curve can be constructed for the entire Mach number range. For all Mach numbers below the range shown, the error will equal the subsonic value; and for all Mach numbers above that for shock passage, the error will be zero.

On the basis of the data which have been presented on the characteristics of various installations, it appears that the use of a static tube located well ahead of the fuselage nose provides the surest means of obtaining an installation with small and predictable position errors throughout the entire Mach number range.

[redacted]

REFERENCES

1. Thompson, Jim Rogers: Continuous Measurements from Subcritical to Moderate Supersonic Speeds of the Drag and Pressure Distribution on a Body of Revolution. (Prospective NACA paper)

2. Johnston, J. Ford, and O'Bryan, Thomas C.: General Characteristics of Airspeed System Using Fuselage Static Vents on a Swept-Wing Airplane. (Prospective NACA paper)

3. Kraft, Christopher C., Jr., and Mathews, Charles W.: Determination by the Free-Fall Method of the Longitudinal Stability and Control Characteristics of a Canard Model at Transonic Speeds. (Prospective NACA paper)

4. Danforth, Edward C. B., and Johnston, J. Ford: Error in Airspeed Measurement Due to Static-Pressure Field ahead of Sharp-Nose Bodies of Revolution at Transonic Speeds. NACA RM L9C25, 1949.

[redacted]

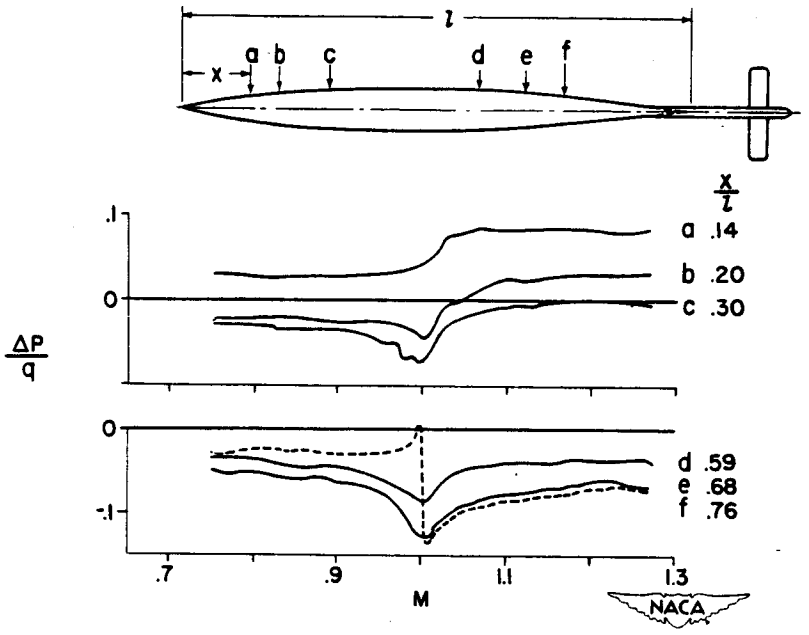


Figure 1.- Some results of pressure-distribution tests on a free-fall body of revolution ($\alpha = 0^{\circ}$).

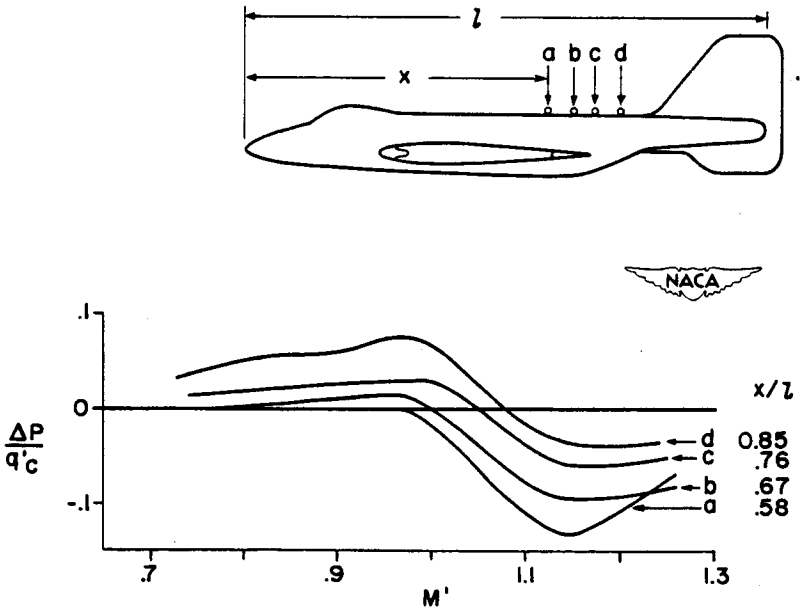


Figure 2.- Calibrations of static vents at four stations along the top of the fuselage of a $\frac{1}{2}$-span wing-flow model of a swept-wing airplane ($\alpha = 0^{\circ}$).

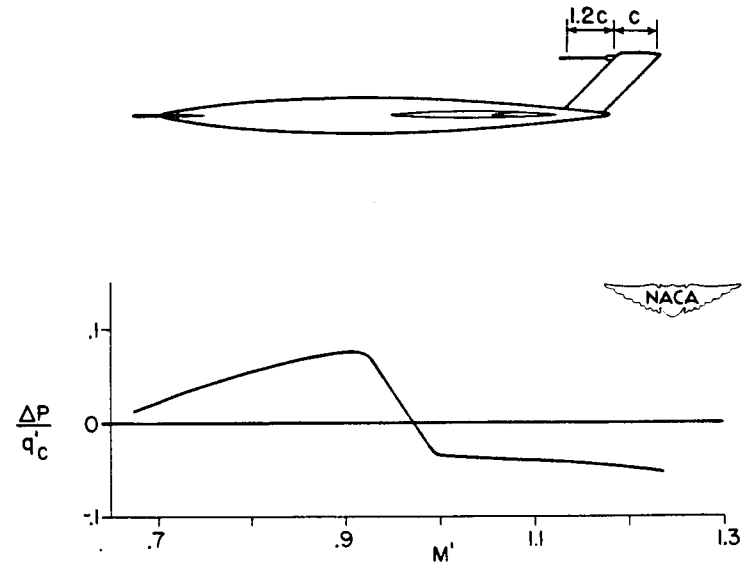


Figure 3.- Calibration of a static tube ahead of the vertical tail of a free-fall model of a canard airplane at low lift coefficients.

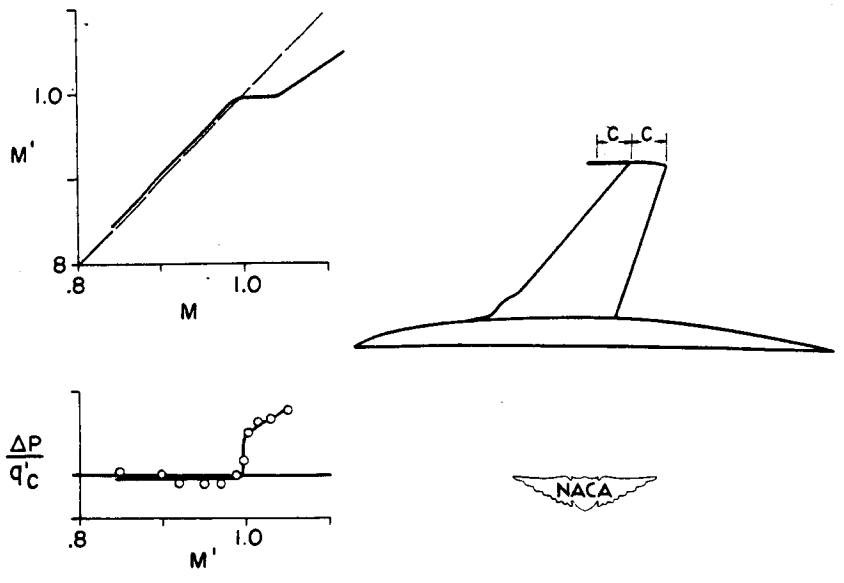


Figure 4.- Calibration of a static tube ahead of the wing tip of a $\frac{1}{2}$-span wing-flow model of a swept-wing airplane ($\alpha = 0^{\circ}$).

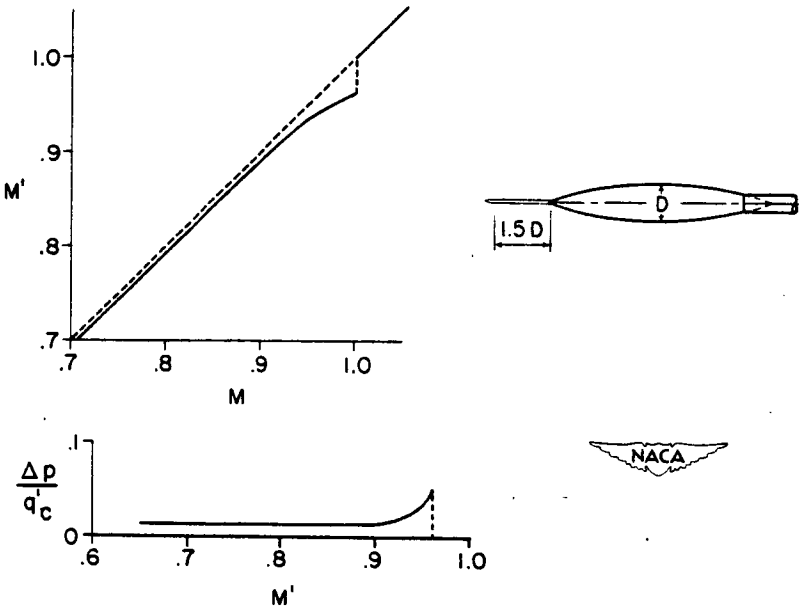


Figure 5.- Calibration of a static tube ahead of the nose of a wing-flow body of revolution ($\alpha = 0^{\circ}$).

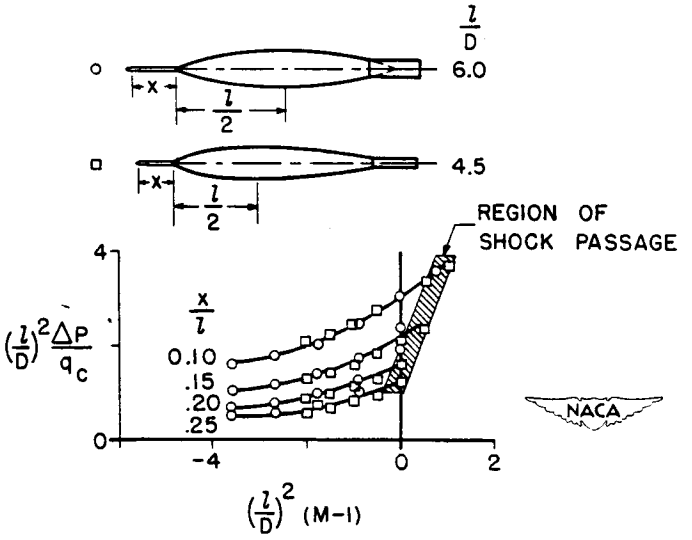


Figure 6.- Correlation of the experimental data obtained by wing-flow tests of static tubes at various distances ahead of two bodies of revolution.

Preceding page blank

STABILITY AND CONTROL

Preceding page blank

65-86466

STABILITY, CONTROL, AND DRAG CHARACTERISTICS OF A CANARD AIRPLANE CONFIGURATION AT TRANSONIC SPEEDS

By Christopher C. Kraft, Jr., and Harold L. Crane

Langley Aeronautical Laboratory

The results of many investigations have indicated that a change from the conventional airplane configuration might be desirable in order to obtain lower drag characteristics through the transonic speed range. In order to investigate interference effects between airplane components at transonic speeds a test program has been conducted by the free-fall method. One phase of the program was concerned with the effect of wing location along the body on the drag of the wing-body combination. Figure 1 shows the variation of the drag coefficient of two wing-body combinations with Mach number. These data have been presented at previous conferences and have been published. (See reference 1.) Both of these configurations had a 45° sweptback wing of aspect ratio 4.1, and a fineness-ratio-12.0 body. In one case the wing was located forward of, and in the other case behind, the maximum body diameter.

Throughout the test Mach number range, the wing-aft configuration had considerably lower drag. Consequently, it appeared desirable to investigate an airplane configuration which incorporated such a wing-body combination. A configuration with the wing located behind the maximum body diameter was more adaptable to the canard or tail-first arrangement. Theoretical analysis indicated that the stability and control characteristics of a canard with a triangular all-movable horizontal tail would be satisfactory. The delta tail was selected because previous investigations had indicated that such a plan form had low drag and good control effectiveness through the transonic speed range. An investigation was made of a canard configuration by the free-fall and wing-flow methods to measure the transonic drag and longitudinal stability and control characteristics.

Figure 2 is a photograph of the free-fall model. The configuration tested had a wing similar to but slightly larger than that used on the wing-body models. The wing was located behind the maximum body diameter on a fuselage having a slightly higher fineness ratio, 13.5. The model had a triangular all-movable horizontal tail of aspect ratio 2.0 and a 45° sweptback vertical tail of aspect ratio 1.5. An automatic control sensitive to normal acceleration operated the horizontal tail in such a manner as to control the model at 1/2g. The drag results, shown in figure 3, indicate that the drag of the canard at zero lift fell in the same range as that of the two wing-body combinations. At subsonic Mach numbers the canard drag was somewhat higher, because of the increased surface area of the configuration, and at Mach numbers above 1.0 the drag became approximately equal to that of the wing-aft combination.

The canard would be expected to have higher drag than the wing–aft configuration because of the addition of the tail surfaces. However, because of the decreases in drag due to the higher fineness ratio of the canard fuselage and the higher Reynolds number of the canard test, the resulting drag of the canard at Mach numbers near 1.2 was approximately the same as that of the wing–aft configuration. The important point is that the favorable wing–body interference characteristics were not affected by addition of the tail surfaces. It should be noted that the drag of the canard configuration is very low compared to the drag of other airplane configurations.

Several papers have been published in recent years that predicted the drag of various airplane configurations at supersonic speeds. In order to show the capability of the theory in predicting the drag of the canard, a comparison has been made of the measured drag and the drag calculated by the methods of Jones, and Squire and Young. (See references 2 to 6.)

Figure 4 shows that in this case the theory checked the experimental results closely up to a Mach number of 1.15. However, the theory takes no account of wing-fuselage-interference effects or the variation of wing-fuselage-interference effects with wing position which was shown to be quite large by the data presented in figure 1. In addition, above a Mach number of 1.15, and as has been shown by other experimental comparisons, the theoretical drag increases at a much greater rate than the experimentally determined drag. It appears that the increase in drag predicted by the theory as the Mach lines approach the leading edge either does not occur or is of a much smaller magnitude than predicted.

The maximum lift–drag ratio of this configuration was estimated by an approximate method which made use of the minimum-drag data from the free–fall tests and wind tunnel data for a somewhat similar wing–fuselage combination. The maximum lift–drag ratio at subsonic Mach numbers was found to be approximately 12; it decreased to about 7.5 at a Mach number of 1.25, and occurred in both cases at a lift coefficient of 0.45.

Figure 5 is a photograph of the 0.075–scale semispan wing–flow model of the free–fall canard which was used to measure longitudinal stability characteristics of the configuration. Figure 6 presents the measured variation of normal–force coefficient and pitching–moment coefficient with angle of attack for several Mach numbers in the transonic range.

The angle-of-attack range covered (up to 28°) was unusually large at transonic Mach numbers. These data show that the effect of Mach number on the lift and moment characteristics was slight. The variation of normal-force coefficient with angle of attack tended to become more

linear at the higher Mach numbers. The moment curves indicate that the canard configuration was stable up to approximately 10° and unstable above that angle of attack throughout the test Mach number range.

Additional wing-flow data indicated that the effectiveness of the tail as a control surface as measured by the variation of pitching-moment coefficient with stabilizer incidence increased with increasing Mach number.

Figure 7 presents plots of variation of tail incidence required for trim with Mach number measured during the free-fall tests and calculated from the wing-flow data. The lift coefficients at which the free-fall model was trimmed and which were used in calculating the trim curve from the wing-flow data are also presented. It should be noted that this trim curve is valid only for the flight conditions of the free-fall model which was in a dive from 30,000 feet to 14,000 feet. Both sets of data indicate that the variation of tail incidence required for trim was gradual over the test Mach number range. Agreement between the data from the two sources was rather good.

From these tests it appears that the canard configuration may be desirable for aircraft designed to fly at transonic speeds. Some of the advantages of such a configuration are:

1. Low drag at transonic and low-supersonic Mach numbers compared to other configurations.

2. Favorable control-effectiveness characteristics as a result of the increase in control effectiveness with increasing Mach number.

3. An aerodynamic-center shift due to Mach number as small as that of any configuration previously tested.

The difficulty of designing a canard airplane with satisfactory stalling qualities is the principle disadvantage. However, it appears that application of leading-edge stall control devices to improve the stalling characteristics of the wing would considerably reduce the difficulty of obtaining satisfactory stalling characteristics for a canard airplane without undue sacrifice of maximum lift.

[redacted]

REFERENCES

1. Mathews, Charles W., and Thompson, Jim Rogers: Comparison of the Transonic Drag Characteristics of Two Wing–Body Combinations Differing Only in the Location of the 45° Sweptback Wing. NACA RM L7I01, 1947.

2. Jones, R. T.: Estimated Lift–Drag Ratios at Supersonic Speed. NACA TN 1350, 1947.

3. Squire, H. B., and Young, A. A.: The Calculation of a Profile Drag of Aerofoils. R. & M. No. 1838, British A.R.C., 1938.

4. Squire, H. B., and Winterbottom, N. E.: Note on further Wing Profile Drag Calculations (Addendum to R. & M. 1838). Rep. No. B.A. 1634, British R.A.E., Oct. 1940.

5. Harmon, Sidney M., and Swanson, Margaret D.: Calculations of the Supersonic Wave Drag of Nonlifting Wings with Arbitrary Sweepback and Aspect Ratio. Wings Swept behind the Mach Lines. NACA TN 1319, 1947.

6. Puckett, Allen E.: Supersonic Wave Drag of Thin Airfoils. Jour. Aero. Sci., vol. 13, no. 9, Sept. 1946, pp. 475–484.

[redacted]

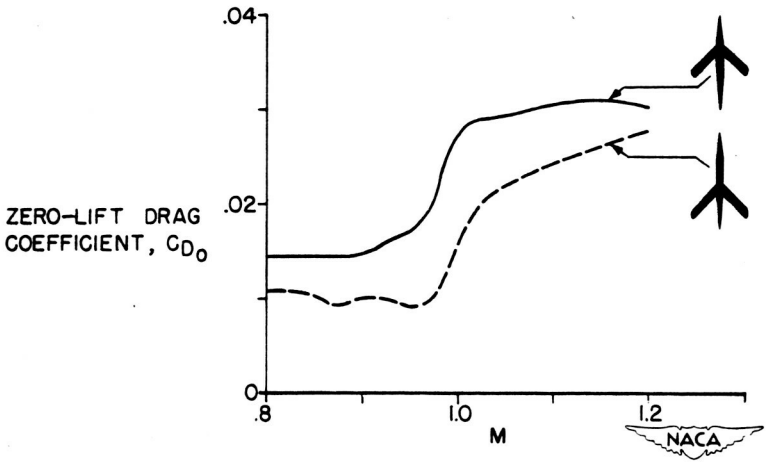


Figure 1.– Variation of drag coefficient with Mach number for two wing–body combinations.

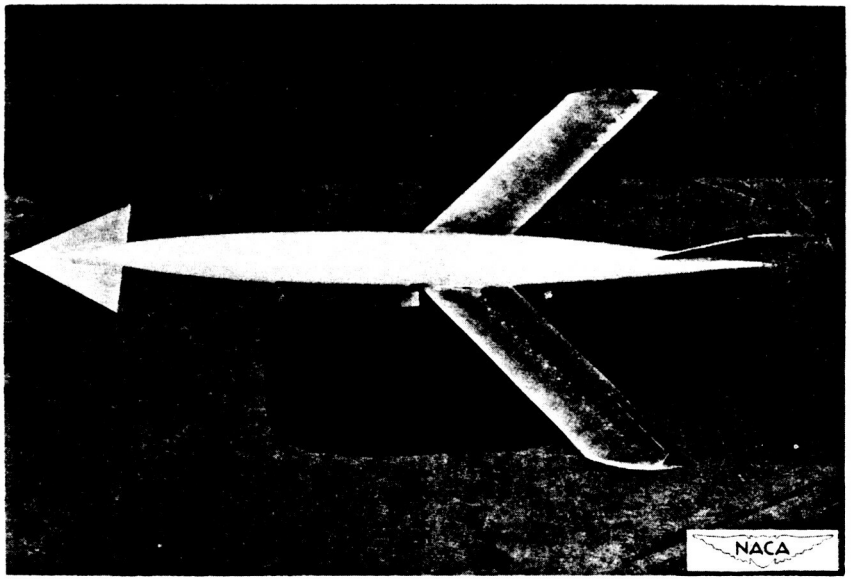


Figure 2.– Photograph of free–fall canard model.

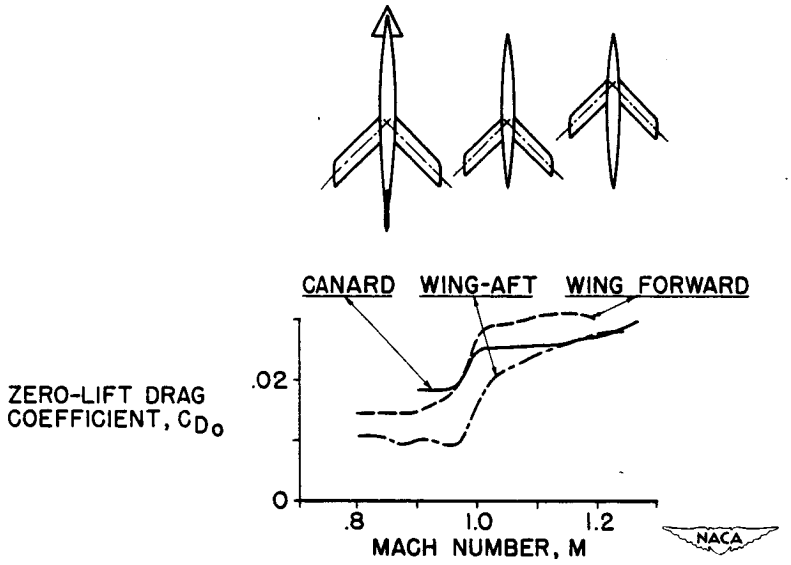


Figure 3.— Comparison of zero-lift drag of canard with the drag of two wing-body combinations.

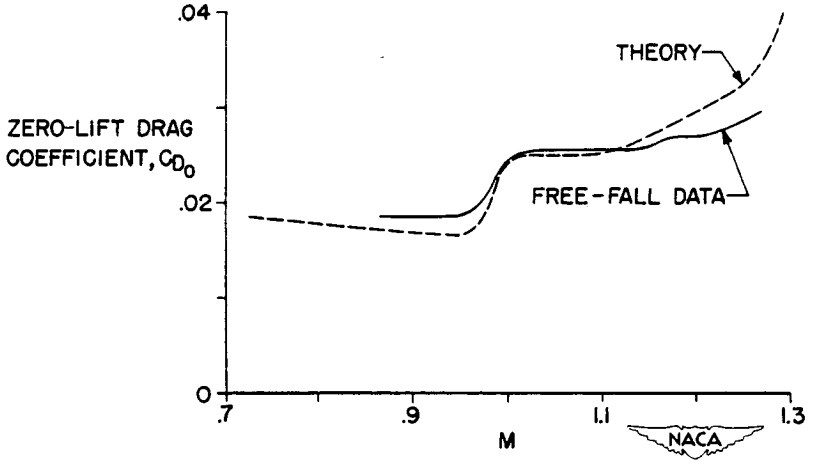


Figure 4.— Comparison of theoretical and measured drag of the canard at zero lift.

Preceding page blank

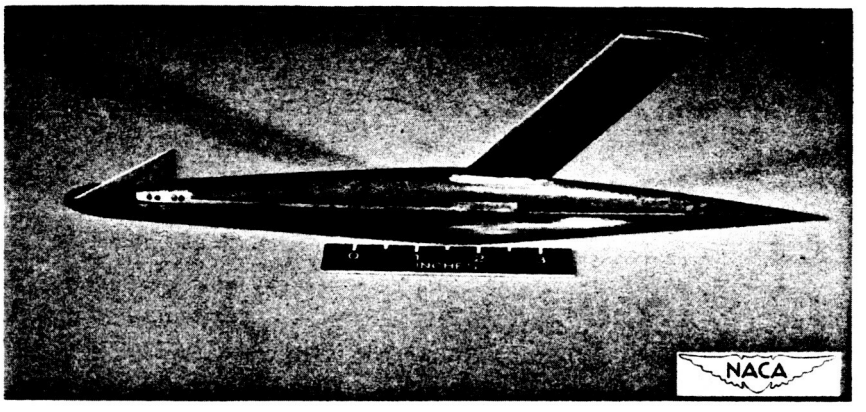


Figure 5.– Photograph of semispan wing–flow model of the canard configuration.

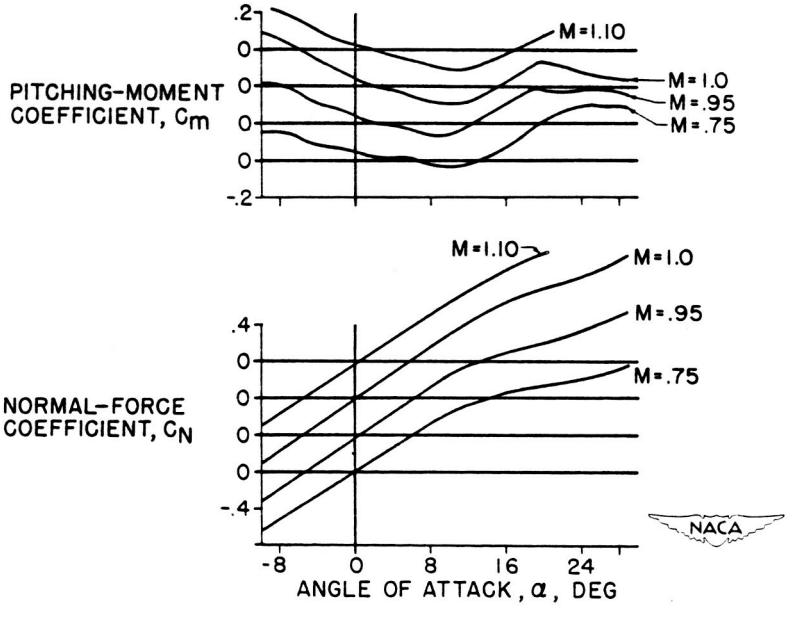


Figure 6.– Variation of normal–force and pitching–moment coefficients with angle of attack at several Mach numbers.

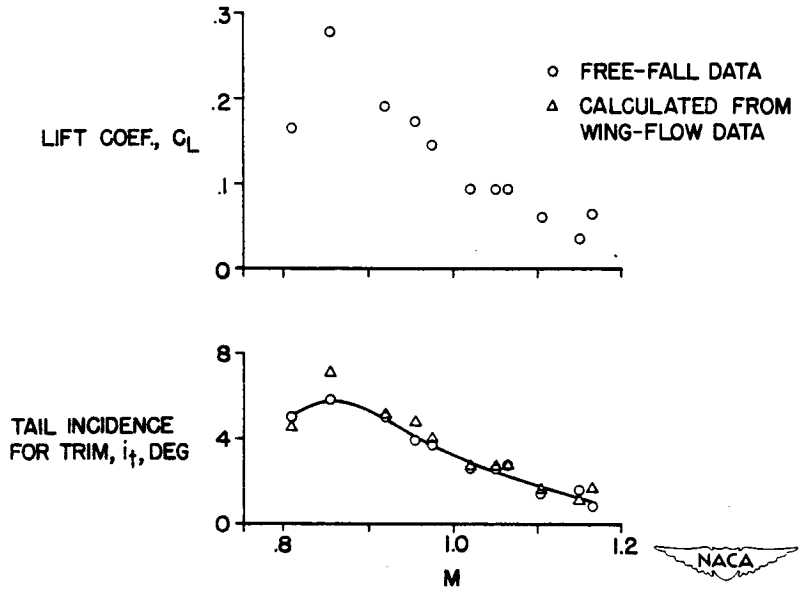


Figure 7.– Variation of tail incidence for trim and of trimmed lift coefficient with Mach number for the flight conditions of the free-fall canard.

Preceding page blank

SOME EFFECTS OF SWEEPBACK AND AIRFOIL THICKNESS ON LONGITUDINAL STABILITY AND CONTROL CHARACTERISTICS AT TRANSONIC SPEEDS

By Charles J. Donlan and Arvo A. Luoma

Langley Aeronautical Laboratory

N65-86467

INTRODUCTION

The accumulation of information on the longitudinal stability and control characteristics of complete transonic airplane configurations has proceeded less rapidly than other phases of aerodynamic research because of the difficulties involved in obtaining such data in the transonic speed range. Current information is largely based on the results of a few specific rocket model configurations (also the following paper by Clarence L. Gillis) and a few wind-tunnel investigations of complete models (references 1 to 3), plus whatever qualitative guidance can be provided from a number of wing-flow and transonic-bump investigations (references 4 to 10). In the present paper an attempt has been made to piece together some of this information in a form that might indicate whether or not a consistent pattern of behavior exists in regard to effects of airfoil thickness and sweepback on over-all stability and control characteristics at transonic speeds.

It is generally expected that airplane designs employing wings of low aspect ratio should encounter less severe stability and control difficulties in the transonic speed range and, consequently, most of the investigations that are useful for studying the effects of sweep and airfoil section on stability and control characteristics have been conducted on configurations employing wings of low aspect ratio.

STRAIGHT-WING CONFIGURATIONS

Scope.- The three straight-wing models shown in figure 1 represent similar but not identical configurations. All three models possessed somewhat different fuselage shapes but the plan forms of the wings and tail as well as the tail location were about the same. Model A was a complete configuration that was investigated at high subsonic Mach numbers in the Langley 8-foot high-speed tunnel and model B was a complete configuration investigated through the transonic range as a rocket model. The major difference between the models is found in the thickness ratios of airfoil sections employed. Model C was not actually a complete model at all but rather a synthetic configuration produced by combining wing-fuselage aerodynamic characteristics obtained from bump tests with the

measured downwash and wake characteristics appropriate to the particular tail arrangement. Models C and B had the same airfoil sections for the wing and tail.

Stability characteristics.- The variation of the stabilizer required for trim with Mach number for the three configurations is shown for an altitude flight condition in the upper part of figure 2. Although the wind-tunnel data are limited to $M = 0.95$ it is evident that the configuration A, with the thicker airfoil section, experienced earlier, more rapid, and larger trim changes than the rocket model (model B), which behaved quite satisfactorily throughout the Mach range investigated. It is also interesting to find that the synthetic bump configuration (model C) employing essentially the same wing and tail as the rocket model also indicated small and gradual trim changes throughout the Mach number range.

The lower part of figure 2 illustrates one manner in which maneuvering stability may influence the amount of trim change that can be safely tolerated. The variation in control required for 1g and 2g flight for model A is almost identical. Only the curves for 1g and 2g are shown here but actually similar variations were found for higher accelerated flight conditions also. With a control characteristic of this kind - particularly if the stick-force variation follows a similar pattern - the pilot may easily experience abrupt accelerations as a result of slight inadvertent Mach number changes. The behavior exhibited by model C, on the other hand, is much more desirable inasmuch as accelerations must be produced by control movement and cannot arise from slight inadvertent changes in Mach number.

The reasons for the superior characteristics exhibited by the models with the thinner wings and tail surfaces are found in the behavior of the various stability components. Unfortunately, breakdown information of this kind is lacking for model B, but such a breakdown study has been made for models A and C and is presented in figure 3.

Stability analysis.- Figure 3 summarizes all the information essential to the analysis of configurations having nonlinear stability characteristics. It illustrates how the basic stability components vary with Mach number for the particular flight plan selected and the manner in which these components combine to produce the final result. The three factors on the left - $C_{m_{WF}}$, α_{WF}, and ϵ - may be thought of as the primary components and the three factors on the right - α_T, $(\alpha - \epsilon)$, and i_t - as the derived components. The factor α_T is the angle of attack of the tail (relative, of course, to the local flow direction) required to balance the wing-fuselage pitching-moment coefficient $C_{m_{WF}}$ at each value of Mach number. Nonlinearities in the lift characteristics of the tail itself are manifested directly in this quantity also. The

factor $(\alpha - \epsilon)$ is the local flow angularity existing at the tail and i_t, of course, is merely $\left[\alpha_T - (\alpha - \epsilon)\right]$ and represents the amount the stabilizer must be adjusted to produce the angle of attack α_T relative to the local flow direction $(\alpha - \epsilon)$. If the models possessed linear variations of $C_{m_{WF}}$, α, and ϵ with C_L all the factors shown should vary in a gradual hyperbolic manner with M in the absence of compressibility effects. It is evident that model A exhibited more marked irregularities in all components than model C. Model A is a particularly useful one for illustrating the complexity of the problem. Inasmuch as $C_{m_{WF}}$, α_{WF}, ϵ, and α_T all exhibit specific irregularities of their own, the values of i_t at each Mach number represent only one of several values that might have resulted from combinations of these variables. For example, the rapid rise in the effective downwash angle ϵ at $M = 0.90$ has been traced to local interference effects between the vertical fin, the horizontal tail, and the fuselage rather than to the wing itself (reference 2). Yet, because of compensating effects in other components, the over-all variation of i_t in the Mach number range considered is less with this interference effect than it would have been without it. Thus, a configuration can be conceived of that has excellent stability and trim characteristics as a whole despite the fact that individual components may indicate rather erratic behavior. Such fortunate compensating circumstances are obviously difficult to anticipate, however, and satisfactory characteristics are more likely to be obtained if the basic stability components vary less violently with Mach number as, for example, occurred for the model with the thinner wing and tail.

SWEPT-WING CONFIGURATIONS

A similar study of the effect of wing thickness on the stability characteristics of a swept-wing configuration for which Langley 8-foot high-speed-tunnel results and rocket-model results are available is shown in figure 4.

Models.- The wind-tunnel and rocket models are designated as models A and B. These models were of identical geometry except for the sweepback of the horizontal tail. For the sake of comparison a bump model has been added. The bump model had a somewhat different fuselage but had essentially the same plan form of the wing and tail and approximately the same tail height and tail length as models A and B. The main difference between the models is again in the thickness of the airfoils employed. The airfoil for models A and B is designated as normal to the 0.30-chord line. The tip section, however, corresponds to a streamwise thickness ratio of about 10 percent as compared with the 6-percent wing of model C.

[redacted]

Stability characteristics.- The results for level flight for the assumed flight plan indicated that the rocket model (model B) underwent rapid, irregular, and large trim changes in the transonic range. The wind-tunnel model (model A) indicated an initial trim change similar to model B but occurring at a slightly higher Mach number. Unfortunately, no data were available in the critical transonic range but the point at $M = 1.2$ is consistent with the trends indicated by the rocket model. The absolute differences in trim between models A and B may be partially due to the difference in tail plan form and Reynolds numbers although much of it is believed to be caused by the greater flexibility of the rocket model. This may account also for the earlier Mach number at which trim changes occurred on the rocket model. Model C, with the thinner profile, appeared, on the other hand, to be free of rapid and large trim changes in the transonic range. An analysis of the component data available for models A and C indicated that for this case the superior behavior of model C was associated with less irregular downwash changes at the tail and less irregular lift characteristics of the thinner horizontal tail.

EFFECT OF SWEEP

A comparison of the wind-tunnel results for model A with those for the straight-wing model of similar thickness as shown in figure 2 would have indicated some improvement due to sweep, particularly in regard to the delay in initial trim changes. On the basis of the limited results given in figure 4, however, it appears that airfoil thickness is so important that it may completely mask any effects of sweep. It is important, therefore, in evaluating the effects of sweep to compare configurations having airfoil sections of comparable thickness. At the present time the only extensive systematic information of this kind that is available was obtained from bump tests of the configurations shown in figure 5.

Methods.- The models were tested as wings alone and as wing-fuselage combinations and some of the basic force and moment characteristics, as well as the downwash and wake characteristics existing at the tail, are discussed in the paper entitled "The Lift, Drag, and Pitching-Moment Characteristics of Wings and Wing-Body Combinations in the Transonic Speed Range" by Edward C. Polhamus and in a subsequent paper entitled "Downwash and Wake Characteristics at Transonic Speeds" by Joseph Weil and Ralph P. Bielat. As for the present analysis, an attempt has been made to synthesize the stability and control characteristics of the four configurations shown by combining the basic wing-fuselage data with the isolated force characteristics of a horizontal tail operating in the particular flow field existing at the tail. Inasmuch as wake and downwash data were available for a number of vertical positions the study

[redacted]

was also extended to include the effect of tail height. It is realized that this procedure of adding together component data does not take account of any interference effects at the tail but may serve, nevertheless, to indicate qualitative trends, particularly for thin wings where these interference effects are not so pronounced. The calculations, which are summarized in figure 6, were made for level flight for one flight condition and, except for the 60° case, the center of gravity was selected to provide a static margin of about 0.10 at zero lift. For the 60° configuration it was necessary to adopt a larger static margin - about 0.30 - because the unstable break in the wing pitching-moment data occurred at a smaller lift coefficient.

Stability characteristics.- The most interesting result of these calculations is that for this series of wings of aspect ratio 4 and 6-percent thickness ratio there was no particular sweep angle or tail height that was outstandingly superior to the others. The least trim changes encountered did seem to occur for the 35° configuration, particularly for the highest tail position, but all the configurations appear to be quite satisfactory. It will be necessary, of course, to extend such studies to include accelerated flight conditions to establish definitely the superiority of any one configuration. Such studies, however, must await the acquisition of data at higher lifts, and particularly at higher Reynolds numbers and these investigations are now underway.

The discussions of stability and control thus far have considered the use of an all-moving tail as the longitudinal control. If an elevator control is used the accompanying trim changes will, in general, depend on the particular stabilizer setting employed. This effect is illustrated in figure 7.

EFFECT OF ELEVATOR CONTROL

The example selected to illustrate the effect of elevator control is the zero-sweep configuration of figure 6, although the i_t variation for the configuration shown in figure 7 is for a tail height of $0.20\frac{b}{2}$. The elevator angle required for trim for two stabilizer settings also has been computed by using flap-effectiveness data obtained by the transonic-bump method on a 0.30c full-span flap (reference 11). The reason for the different trim characteristics exhibited by the elevator control is traceable to the effectiveness characteristics shown on the right side of the figure. This figure shows the manner in which the tail lift due to angle of attack C_{L_α} and the tail lift due to flap deflection C_{L_δ} vary with Mach number, expressed as a fraction of their values at $M = 0.80$.

If the C_{L_δ} variation with M were identical to the C_{L_α} variation - that is, if the ratio $C_{L_\delta}/C_{L_\alpha}$ were constant - the elevator trim curves would be found to have identical variations with Mach number and would be merely displaced from one another by an amount dependent on the value of α/δ. Inasmuch as the ratio α/δ is unlikely to be a constant with Mach number it appears that the trim changes obtained with elevator control can always be expected to depend on the particular value of stabilizer used and, hence, also on the particular flight plan employed, and, perhaps, on the piloting technique itself.

SUMMARY

In recapitulation, the limited results obtained thus far suggest that a thin wing is of paramount importance in securing minimum stability and control changes at transonic speeds and that if the wing and horizontal tail are thin enough the effects of sweep on the over-all stability and control characteristics at transonic speeds may be of secondary importance. The beneficial effects of sweep do increase, however, as the wing thickness increases. It appears also from aerodynamic considerations alone that an all-moving tail is to be preferred as the longitudinal control instead of an elevator control if stability and control characteristics are to be less dependent on particular flight conditions and piloting techniques.

REFERENCES

1. Wright, John B.: High-Speed Wind-Tunnel Tests of a $\frac{1}{16}$-Scale Model of the D-558 Research Airplane. Longitudinal Stability and Control of the D-558-1. NACA RM L8C23, 1948.

2. Robinson, Harold L.: High-Speed Wind-Tunnel Tests of a $\frac{1}{16}$-Scale Model of the D-558 Research Airplane - Dynamic Pressure and Comparison of Point and Effective Downwash at the Tail of the D-558-1. NACA RM L8H05, 1948.

3. Osborne, Robert S.: High-Speed Wind-Tunnel Investigation of the Longitudinal Stability and Control Characteristics of a $\frac{1}{16}$-Scale Model of the D-558-2 Research Airplane at High Subsonic Mach Numbers and at a Mach Number of 1.2. NACA RM L9C04, 1949.

4. Silsby, Norman S., and Kennedy, Robert M.: Longitudinal Characteristics of a Semispan Model of the Grumman Airplane Design 83 Having a Sweptback Wing and of the Model with a Straight Wing, as Determined from Wing-Flow Tests at Transonic Speeds - TED No. NACA DE337. NACA RM SL9A19, Bur. Aero., 1949.

5. Weil, Joseph, and Goodson, Kenneth W.: Aerodynamic Characteristics of a Wing with Quarter-Chord Line Swept Back 45°, Aspect Ratio 4, Taper Ratio 0.6, and NACA 65A006 Airfoil Section. Transonic-Bump Method. NACA RM L9A21, 1949.

6. Sleeman, William C., Jr., and Becht, Robert E.: Aerodynamic Characteristics of a Wing with Quarter-Chord Line Swept Back 35°, Aspect Ratio 4, Taper Ratio 0.6, and NACA 65A006 Airfoil Section. Transonic-Bump Method. NACA RM L9B25, 1949.

7. King, Thomas J., Jr., and Myers, Boyd C., II: Aerodynamic Characteristics of a Wing with Quarter-Chord Line Swept Back 60°, Aspect Ratio 4, Taper Ratio 0.6, and NACA 65A006 Airfoil Section. Transonic-Bump Method. NACA RM L9G27, 1949.

8. Myers, Boyd C., II, and King, Thomas J., Jr.: Aerodynamic Characteristics of a Wing with Quarter-Chord Line Swept Back 45°, Aspect Ratio 4, Taper Ratio 0.3, and NACA 65A006 Airfoil Section. Transonic-Bump Method. NACA RM L9E25, 1949.

9. Goodson, Kenneth W., and Morrison, William D., Jr.: Aerodynamic Characteristics of a Wing with Unswept Quarter-Chord Line, Aspect Ratio 4, Taper Ratio 0.6, and NACA 65A006 Airfoil Section. Transonic-Bump Method. NACA RM L9H22, 1949.

10. Myers, Boyd C., II, and Wiggins, James W.: Aerodynamic Characteristics of a Wing with Unswept Quarter-Chord Line, Aspect Ratio 4, Taper Ratio 0.6, and NACA 65A004 Airfoil Section. Transonic-Bump Method. (Prospective NACA paper.)

11. Vogler, Raymond D.: Lateral-Control Investigation of Flap-Type Controls on a Wing with Quarter-Chord Line Swept Back 45°, Aspect Ratio 4, Taper Ratio 0.6, and NACA 65A006 Airfoil Section. Transonic-Bump Method. NACA RM L9F29a, 1949.

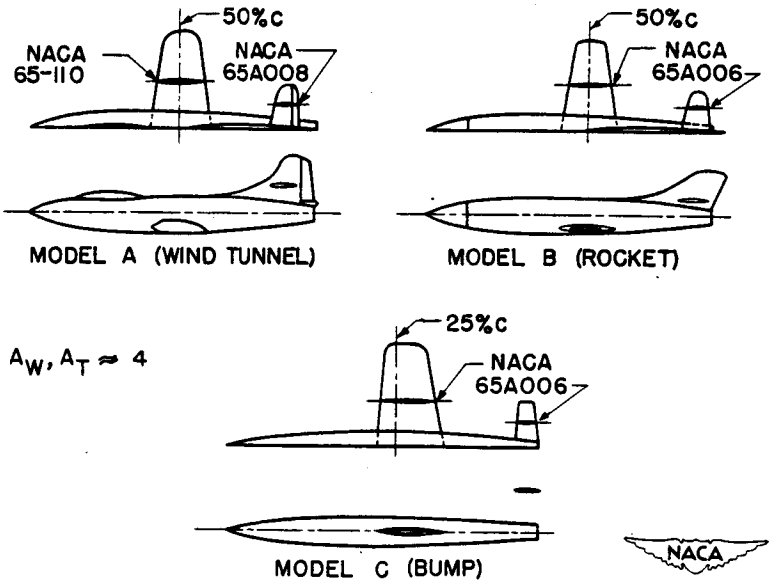


Figure 1.- Straight-wing models.

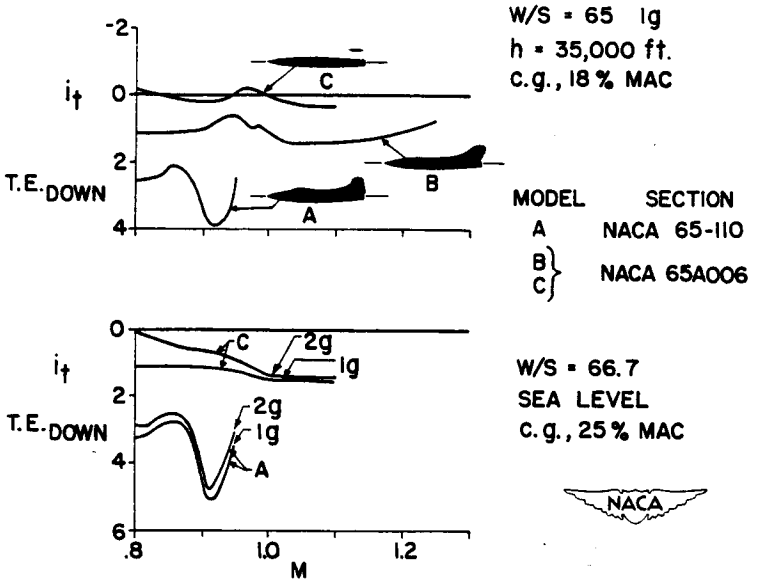


Figure 2.- Longitudinal stability characteristics of straight-wing configurations.

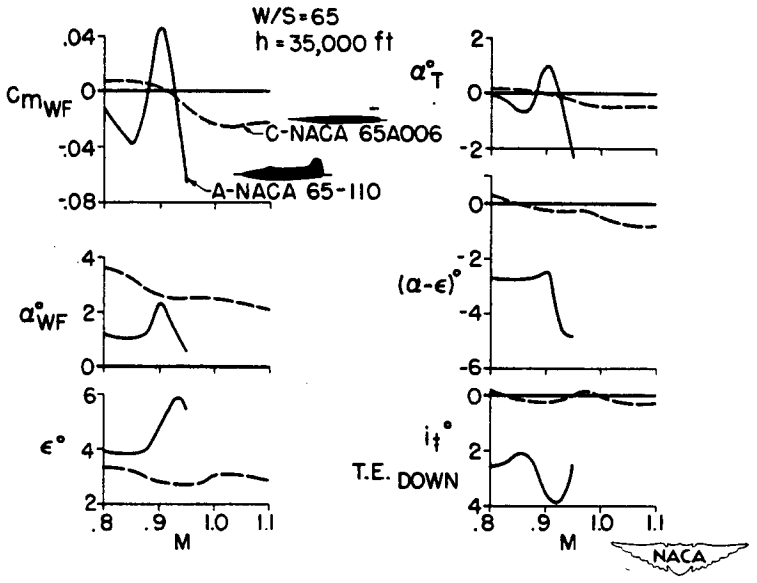


Figure 3.- Stability analysis of straight-wing models A and C.

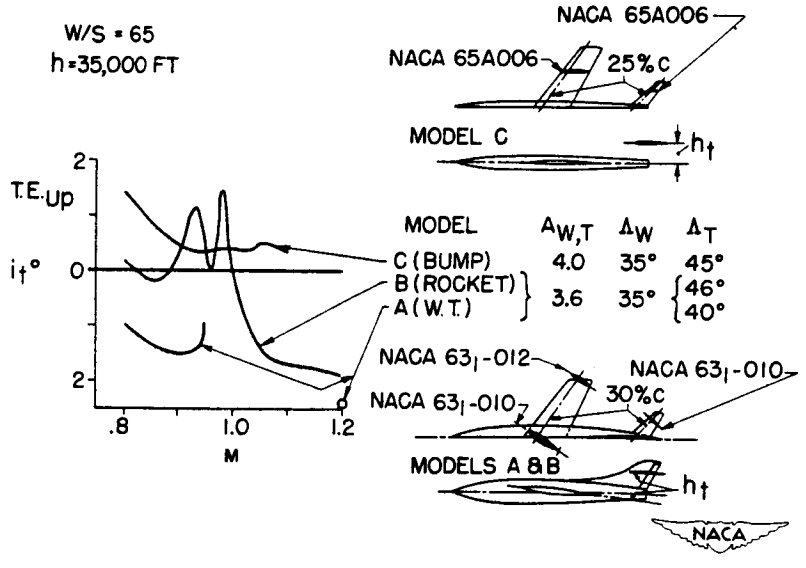


Figure 4.- Longitudinal stability characteristics of swept-wing configurations.

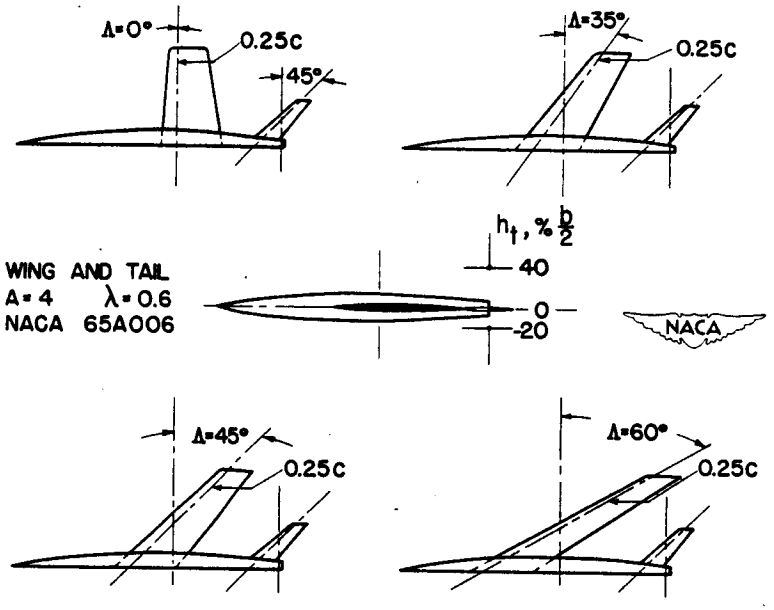


Figure 5.- Systematic-sweep series.

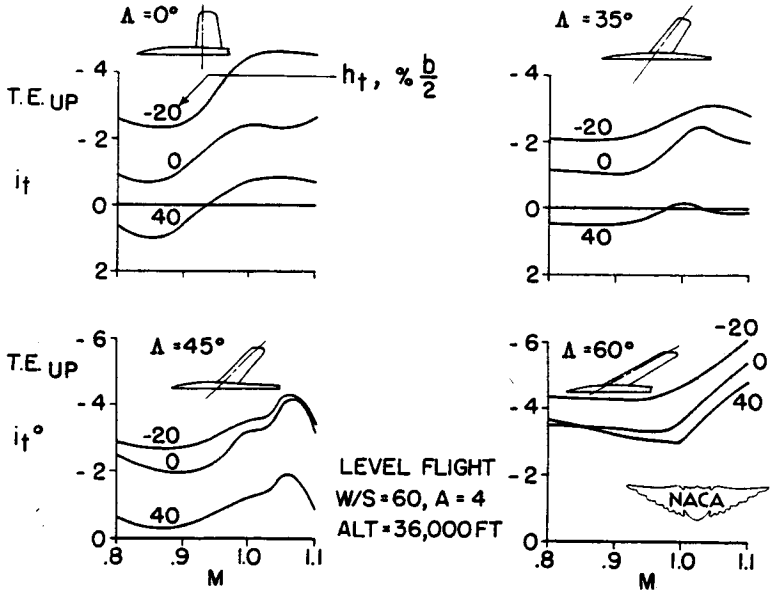


Figure 6.- Stability characteristics of systematic-sweep series.

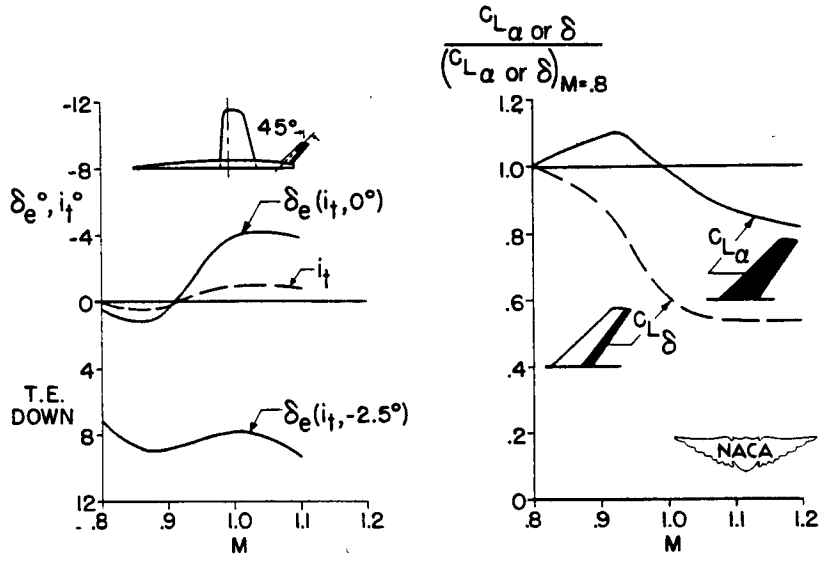


Figure 7.- Effect of elevator control on stability characteristics.

CONFIDENTIAL

N65-86468

A COMPARISON OF THE LONGITUDINAL STABILITY AND CONTROL CHARACTERISTICS OF THREE AIRPLANE CONFIGURATIONS

By Clarence L. Gillis

Langley Aeronautical Laboratory

One of the interesting types of wings proposed for flight in the transonic and supersonic regions is the triangular wing. Investigations of the longitudinal stability and control characteristics of several triangular wing configurations have been conducted by the NACA in various research facilities. In this paper a comparison will be shown of data obtained from several research facilities on one tailless triangular-wing configuration which has been rather extensively investigated. A comparison will also be made of some of the flying qualities of this triangular-wing configuration with those of two other more conventional configurations designed for flight at transonic and supersonic speeds.

The triangular-wing configuration used in the comparison is shown in figure 1. It is a tailless design having 60° sweepback of the leading edge which results in an aspect ratio A of 2.31. The airfoil section is an NACA 65-series with a thickness ratio of 6.5 percent. Longitudinal control is obtained by a constant-chord elevator having an area of about 30 percent of the exposed wing area (S_e/S) or 20 percent of the area including that within the fuselage. A model having a fuselage as shown by the dashed lines, which included an annular air inlet at the nose, has been investigated in the Ames 1- by $3\frac{1}{2}$-foot tunnel and the Ames 1- by 3-foot supersonic tunnel (references 1 and 2). A similar model has also been tested on the transonic bump in the Southern California Cooperative Wind Tunnel. A model with the fuselage shown by solid lines was studied by means of rocket-propelled models in free flight (references 3 and 4). The device on the nose of the model is an angle-of-attack vane and the projection on the bottom of the fuselage is a streamlined fairing for a total-head tube mounted along the lower edge.

The procedure for obtaining data from wind-tunnel tests is fairly familiar. The method of obtaining the data described herein from free-flight rocket models may require some explanation. The models are accelerated to supersonic speeds by a booster rocket and the data are obtained by telemeter and radar instrumentation during the decelerating flight following booster rejection. During the flight the elevator is periodically given rapid positive and negative deflections by means of a power unit within the model. The aerodynamic characteristics are obtained by analysis of the model angle of attack and accelerations following the rapid control deflections.

A comparison of some of the data obtained on the triangular-wing configuration at transonic speeds is shown in figure 2. The wind-tunnel data shown are from the Ames 1- by $3\frac{1}{2}$-foot tunnel, indicated by the short dashed lines, the Ames 1- by 3-foot supersonic tunnel, indicated by the small circles, and the Southern California Cooperative Wind Tunnel, indicated by the long dashed lines. The rocket-model data are shown by the solid curves. The Reynolds numbers for the tunnel tests were about 1×10^6, or a little greater, and those for the rocket models were about 11×10^6.

The data show fairly gradual changes in the various stability parameters with Mach number. In general, the agreement of the data from the three wind tunnels and the rocket models is good, considering the different fuselage shapes used, the differences in Reynolds number, and differences in test conditions. Data not shown from the Ames wind-tunnel tests show some nonlinearity of the various quantities with lift coefficient and elevator deflection. The values of the aerodynamic parameters plotted are those occurring near zero lift and in general are applicable up to lift coefficients of about 0.4 or higher. At a lift coefficient of about 0.5 the aerodynamic center moves forward to about 25 percent of the mean aerodynamic chord, as indicated by the Ames tests. In the transonic region, the total rearward shift of the aerodynamic center at low lift coefficients is about 15 percent of the mean aerodynamic chord.

The elevator lift effectiveness decreases by about half through the transonic region. The decrease in the rate of change of pitching-moment coefficient with elevator deflection C_{m_δ} in the transonic region is less than that for the rate of change of lift coefficient with elevator deflection C_{L_δ}, indicating the rearward shift in the center of pressure of the lift due to elevator deflection.

Another interesting comparison is afforded by low-speed tests made in the Ames 40- by 80-foot tunnel of a configuration having the same wing and vertical-tail geometry as the models shown here but with a fuselage of higher fineness ratio. These tests, at a Reynolds number of 16.4×10^6 and a low Mach number, gave values of 0.043 for the rate of change of lift coefficient with angle of attack C_{L_α}, 0.022 for C_{L_δ}, 0.011 for C_{m_δ}, and 37 percent for the aerodynamic-center location, which are in close agreement with the trends shown in figure 2.

Flight tests that have been made with two other transonic-airplane configurations by means of rocket-propelled models furnish data for a comparison with the tailless triangular-wing configuration. These two are: A very thin straight wing and tail configuration and a sweptback wing and tail configuration.

The straight-wing configuration is shown in figure 3. The wing was of aspect ratio 3 and had modified double-wedge airfoil sections with a thickness ratio t/c of 4.5 percent. The wing actually had 16° sweepback of the quarter-chord line, but this was selected from aeroelastic considerations. Since the aerodynamic benefits of this amount of sweepback would be very small, the wing is considered as straight for purposes of discussion and comparison. The horizontal tail was identical to the wing in plan form and section. During the flight this tail was operated as an all-movable tail for elevator control. The horizontal-tail volume coefficient V_t was 0.71, a value somewhat higher than usual.

The data obtained on the straight-wing configuration are shown in figure 4. Two models were flown. They were identical except that one had a solid steel wing (reference 5) while the other had a solid duralumin wing. If no errors in model construction or test and analysis procedures were incurred, then the differences between the results for the two models show the effects of the torsional flexibility of the wing. The results from both models indicate some nonlinearity of the lift and pitching-moment curves at subsonic speeds, although the results were not conclusive for the pitching-moment curves as indicated by the short dashed line for the steel-wing model. The increase in lift-curve slope and decrease in stability at subsonic speeds and the reverse effects at supersonic speeds are consistent and are what might be expected considering the wing geometry. In the region near Mach numbers of 1.00 to 1.05 where increases in both lift-curve slope and stability occur, such generalizations are useless in view of the probable changes in flow conditions taking place. These results re-emphasize the point mentioned in the previous paper by Charles J. Donlan and Arvo A. Luoma that, when comparing results of model tests at high Mach numbers from different test facilities, or with full-scale flight tests, the flexibility of the test models or airplanes must be taken into account.

The movement of the aerodynamic center with Mach number is more erratic than for the triangular-wing model. Other rocket-model (reference 6), transonic-bump, and wing-flow tests (reference 7) indicate that this may be characteristic of straight-wing configurations. The total shift in aerodynamic center from subsonic to supersonic speeds is about twice as great as that for the triangular-wing airplane when compared on the basis of a percentage of the mean aerodynamic chord, but the shift measured in inches on a full-scale airplane would be approximately the same in both cases.

The values of C_{L_δ} and C_{m_δ} do not vary much with Mach number, which can be attributed to the all-movable tail. Since the tail surfaces were made of duralumin on both models there should be no difference due to flexibility between the C_{L_δ} and C_{m_δ} values for the two models. Both C_{L_δ} and C_{m_δ} are probably also nonlinear with lift coefficient in the subsonic region but this could not be determined from the data. The values plotted represent average values over the lift-coefficient range covered.

The third configuration tested as a rocket model is shown in figure 5. The inversely tapered wing had 37.2° sweepback of the quarter-chord line, or 40° of the half-chord line. The airfoil sections in the stream direction had a thickness ratio of 7.6 percent and had a small amount of camber. The tail was also swept back 40° and had an elevator area of 30 percent of the tail area. The tail volume coefficient was 0.32 which is less than half of that for the straight-wing model discussed previously.

The aerodynamic data obtained from one model of this configuration are shown in figure 6. Although the model attained a Mach number of 1.2 the telemeter record was unreadable above a Mach number of 1.02, except for one value of stability obtained at 1.2. The rearward movement of the aerodynamic center from subsonic to supersonic speeds is greater than that for the triangular-wing configuration but a little less than that for the straight-wing configuration when based on percent of the mean aerodynamic chord. If this is again converted to inches of movement on a full-scale airplane the aerodynamic-center shift is about the same as for the other two configurations. The elevator effectiveness decreases by about 45 percent between Mach numbers of 0.7 and 1.0.

A second model of this configuration has been flown but the data have not yet been reduced to final form. A preliminary calculation for the second model indicates that above a Mach number of 1.0 the aerodynamic center moves rearward only slightly farther than shown by the end of the curve plotted and then remains constant or perhaps moves forward a little as the Mach number is increased.

Another item obtained from the rocket-model tests is the total longitudinal damping factor, shown in figure 7. This factor is the sum of the pitching moment due to rotational velocity in pitch C_{m_q} and the pitching moment due to rate of change of angle of attack $C_{m_{\dot{\alpha}}}$. It is not possible to separate these two factors when only angle of attack and normal acceleration are measured during the flight. The numerical values shown here are for rates of motion in radians per second. The

damping coefficients are considerably larger for the straight-wing model than for either the swept-wing or triangular-wing models. This can be largely accounted for by the large tail-volume coefficient on the straight-wing configuration. The rather extreme variations in damping factor in the transonic region for the straight-wing model were confirmed by the similar results that were obtained on both models of this configuration that were flown. Some additional confirmation of the trends shown for the straight-wing configuration is indicated by the circled points which were obtained from a somewhat different straight-wing rocket model (reference 6). This is the model described by Charles J. Donlan and Arvo A. Luoma in a previous paper. These points were obtained by disturbing the model in pitch by means of small rockets fired from the bottom of the model near the tail.

A comparison of the flying qualities of these three configurations requires the assumption of certain flight conditions for the full-scale airplanes. The effect of altitude on the flight characteristics is known to be very great, but since airplanes designed for attaining supersonic speeds will probably do so at very high altitudes, at least initially, an altitude of 40,000 feet has been chosen for the calculations. The mass characteristics of such widely different airplane configurations would, of course, also be considerably different. The wing loadings used for the calculations were 27 for the triangular-wing airplane, 58 for the swept-wing airplane, and 118 for the straight-wing airplane.

A comparison of the trim characteristics of the three configurations as obtained from the rocket-model data is shown in figure 8. The plot on the left is the elevator deflection δ_e required for level flight. These values are dependent on the airplane stability, the control effectiveness, and the zero-lift pitching moment which in the case of the swept-wing airplane is affected by stabilizer setting. Because of the influence of all these factors, the curves shown should be viewed qualitatively rather than for the purpose of quantitative comparison of the three configurations. In all the following figures a dashed line is used to indicate data obtained with the more flexible of the straight-wing models.

It is interesting to note that the three airplanes all have the same type of trim change with Mach number as indicated by the elevator deflection required to counteract these changes. That is, the airplanes all have a nose-up pitching tendency starting somewhere below a Mach number of 0.8. At a Mach number somewhere between 0.85 and 0.90 the pitching tendency changes to nose-down, and then at Mach numbers from 0.95 to 1.00 the pitching tendency again changes to nose-up.

On the right in figure 8 is a plot of the normal acceleration in g's that would be encountered by the airplanes if they were trimmed

[redacted]

for level flight at a Mach number of 0.8 and the controls were then locked and the airplanes accelerated through the transonic region. Apparently all the airplanes could perform this sequence with no more than 0.6g change in normal acceleration at an altitude of 40,000 feet.

Figure 9 shows the maneuvering effectiveness of the elevator in terms of normal acceleration developed per degree of elevator deflection. The loss in elevator effectiveness for the swept-wing airplane is clearly shown here. The triangular-wing and straight-wing configurations maintain approximately constant maneuvering effectiveness. Although the stability increases with Mach number for these two configurations and the elevator effectiveness decreases for the triangular-wing configuration these effects are just about balanced by the increase in dynamic pressure with Mach number. As noted previously the more flexible straight-wing model had greater stability at a Mach number of 1.05 than the more rigid model which results in the difference in maneuvering effectiveness at that Mach number. The data shown are for center-of-gravity locations such that the straight-wing configuration has about twice the static stability margin at subsonic speeds as the other two configurations. For equal static stability margins the straight-wing configuration would have considerably more elevator power than the values shown.

Although the ability of the elevator to produce normal acceleration of the airplane is about the same for the straight-wing and triangular-wing configurations, its ability to change the lift coefficient is about four times greater for the straight-wing airplane. The reason for this is that the acceleration depends on the wing loading, and the wing loading assumed for the straight-wing airplane is four times that for the triangular-wing airplane. The rocket-model tests on the straight-wing configuration indicated that at high subsonic speeds the airplane could be trimmed from zero lift to the maximum lift coefficient with a range of elevator deflections from 2° to -5° (reference 5).

Figure 10 shows the period p, in seconds, of the short-period longitudinal oscillation and the number of cycles required to damp to one-tenth amplitude $c_{1/10}$. For these figures the centers of gravity have been adjusted to give the same static stability margin at a Mach number of 0.8. All the airplanes show decreasing periods of oscillation at higher Mach numbers because of the increased stability and dynamic pressure.

The number of cycles required to damp to one-tenth amplitude is of the same order of magnitude for all three airplanes. The time in seconds required to damp to one-tenth amplitude would be about twice as long for the straight-wing configuration as for the other two configurations. Although the damping coefficients shown previously were largest for the straight-wing configuration and smallest for the triangular-wing

configuration, the actual damping for the airplanes, as indicated here, is in the reverse order. This is because of the much lower values of wing loading and moment of inertia for the triangular-wing airplane. It appears that none of the three airplanes, at an altitude of 40,000 feet, satisfy the usual criterion of damping to one-tenth amplitude in one cycle. The damping would be better at lower altitudes, however.

It appears, then, that all three of these configurations, designed for transonic and supersonic flight, could be safely flown and controlled through the transonic region at an altitude of 40,000 feet.. All three apparently maintained sufficient elevator control and could be flown through a Mach number of 1.0 with controls locked if necessary. The longitudinal oscillations would be rather lightly damped and of short period.

[redacted]

REFERENCES

1. Lawrence, Leslie F., and Summers, James L.: Wind-Tunnel Investigation of a Tailless Triangular-Wing Fighter Aircraft at Mach Numbers from 0.5 to 1.5. NACA RM A9B16, 1949.

2. Scherrer, Richard, and Wimbrow, William R.: Wind-Tunnel Investigation at a Mach Number of 1.53 of an Airplane with a Triangular Wing. NACA RM A7J05, 1948.

3. Mitcham, Grady L., Stevens, Joseph E., and Norris, Harry P.: Aerodynamic Characteristics and Flying Qualities of a Triangular-Wing Airplane Configuration as Obtained from Flights of Rocket-Propelled Models at Transonic and Low Supersonic Speeds. (Prospective NACA paper)

4. Mitcham, Grady L.: A Preliminary Analysis of the Flying Qualities of the Consolidated Vultee MX-813 Delta-Wing Airplane Configuration at Transonic and Low Supersonic Speeds as Determined from Flights of Rocket-Powered Models. NACA RM SL9E13, U. S. Air Force, 1949.

5. Gillis, Clarence L., Peck, Robert F., and Vitale, A. James: Preliminary Results from a Free-Flight Investigation at Transonic and Supersonic Speeds of the Longitudinal Stability and Control Characteristics of an Airplane Configuration with Thin Straight Wings of Aspect Ratio 3. (Prospective NACA paper)

6. Parks, James H., and Mitchell, Jesse L.: Longitudinal Trim and Drag Characteristics of Two Airplane Configurations of a Rocket-Propelled Transonic Research Model. (Prospective NACA paper)

7. Silsby, Norman S., and Kennedy, Robert M.: Longitudinal Characteristics of a Semispan Model of the Grumman Airplane Design 83 Having a Sweptback Wing and of the Model with a Straight Wing, as Determined from Wing-Flow Tests at Transonic Speeds - TED No. NACA DE 377. NACA RM SL9A19, Bur. Aero., 1949.

[redacted]

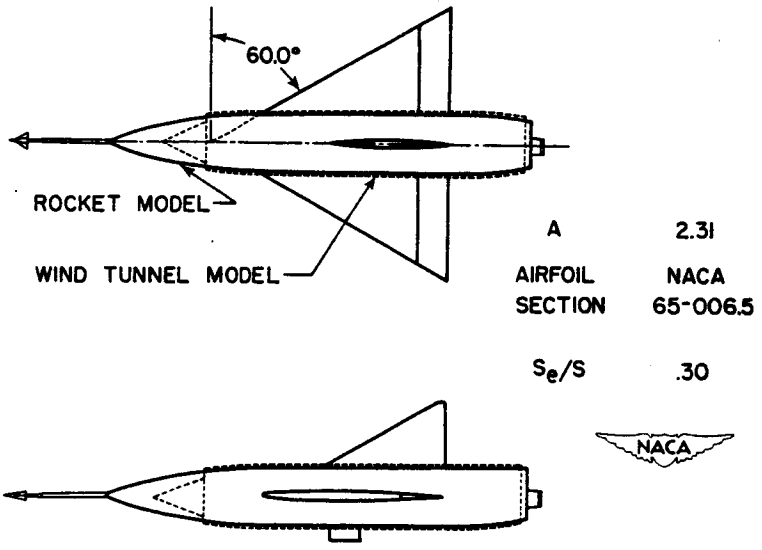


Figure 1.– Triangular–wing configurations.

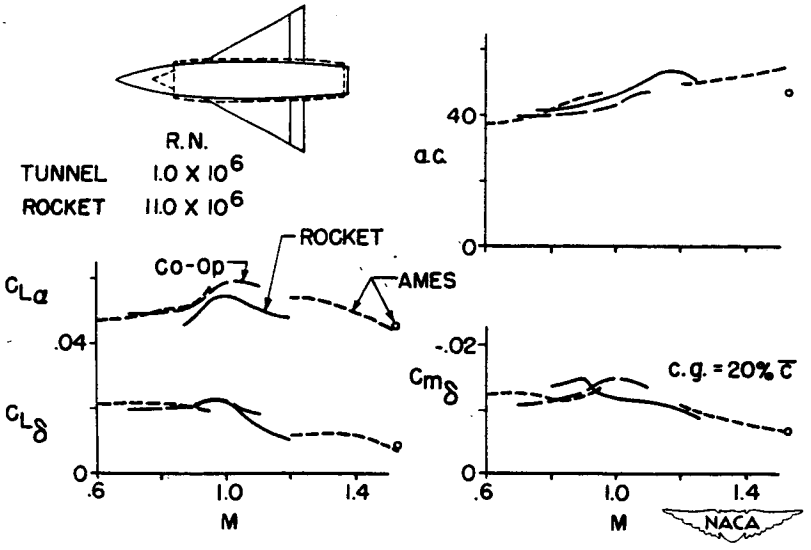


Figure 2.– Aerodynamic characteristics of the triangular–wing configurations from wind–tunnel and rocket–model tests.

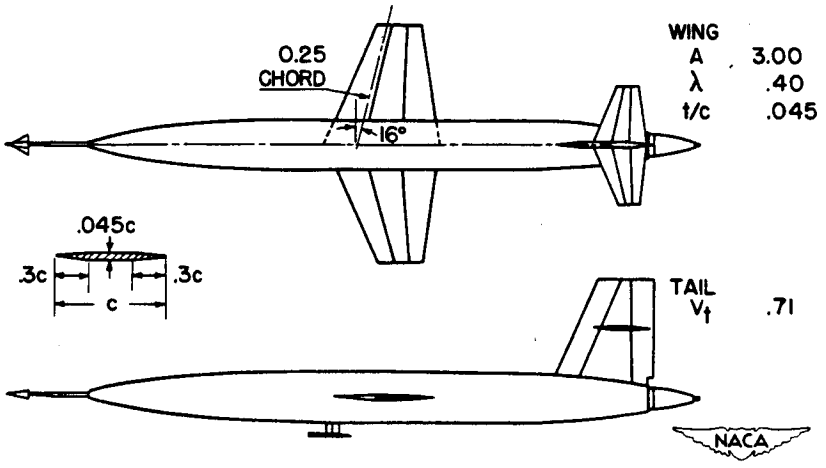


Figure 3.- Straight-wing configuration.

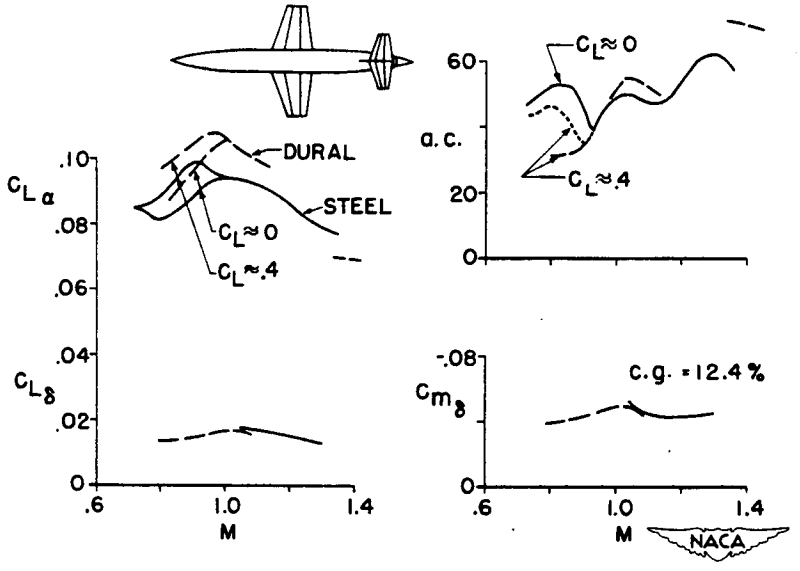


Figure 4.- Aerodynamic characteristics of the straight-wing configuration from rocket-model tests.

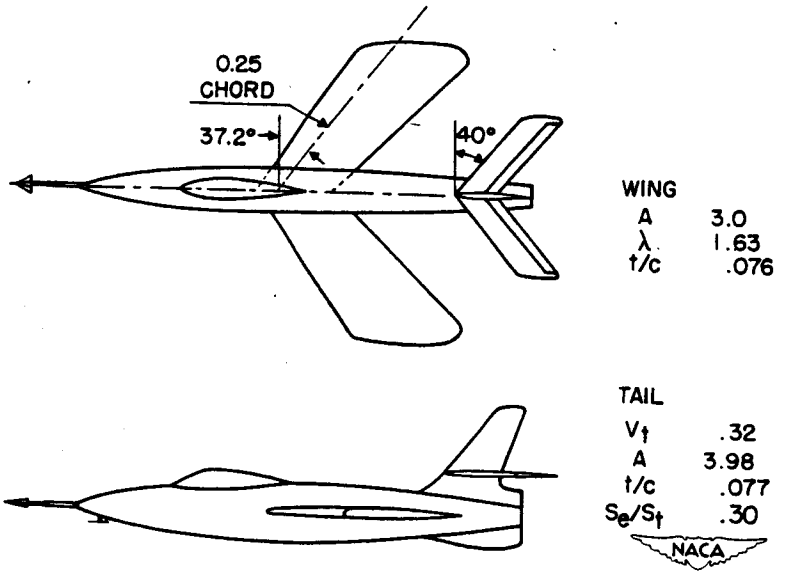


Figure 5.- Sweptback-wing configuration.

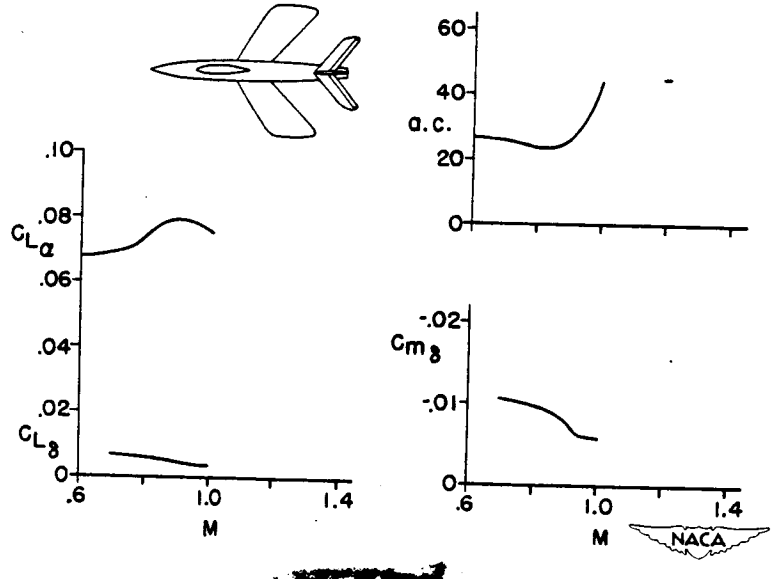


Figure 6.- Aerodynamic characteristics of the sweptback-wing configuration from rocket-model tests.

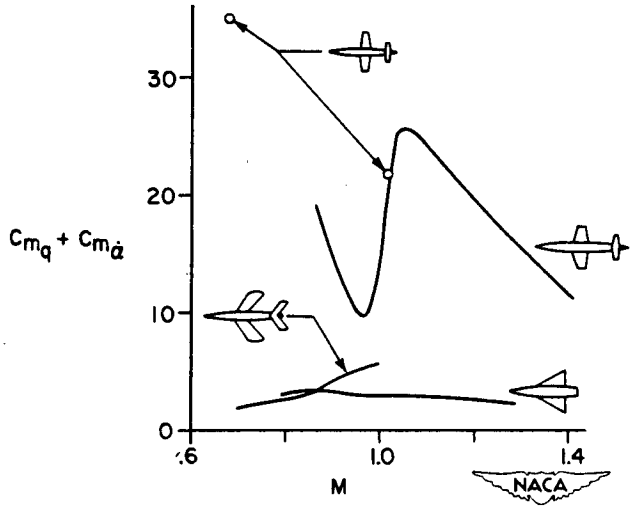


Figure 7.– Longitudinal damping coefficients.

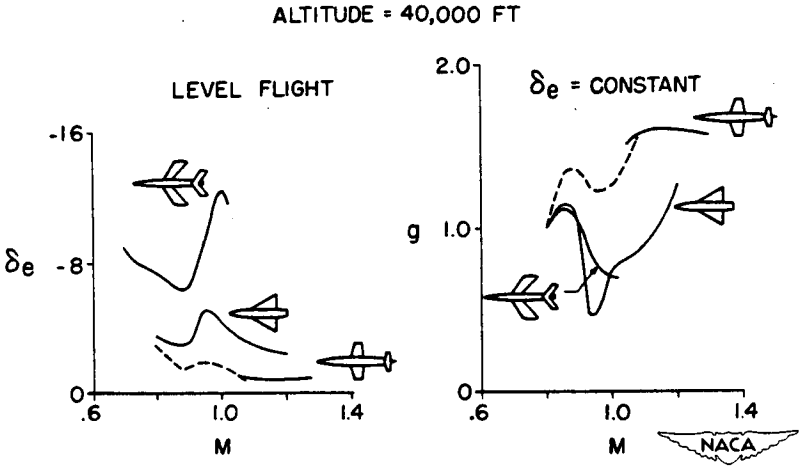


Figure 8.– Trim characteristics.

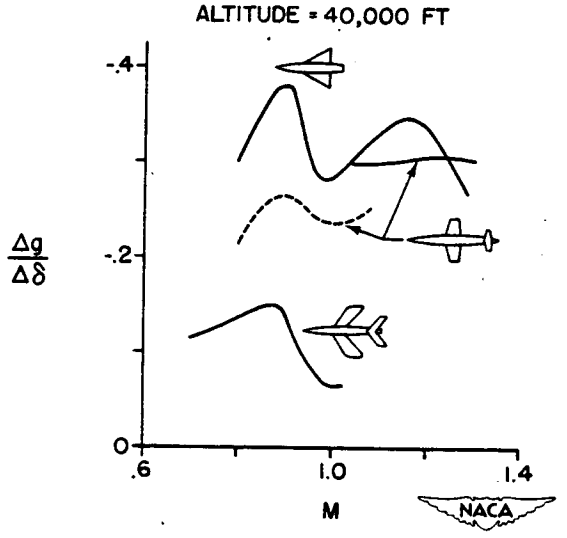


Figure 9.– Maneuvering effectiveness of elevator.

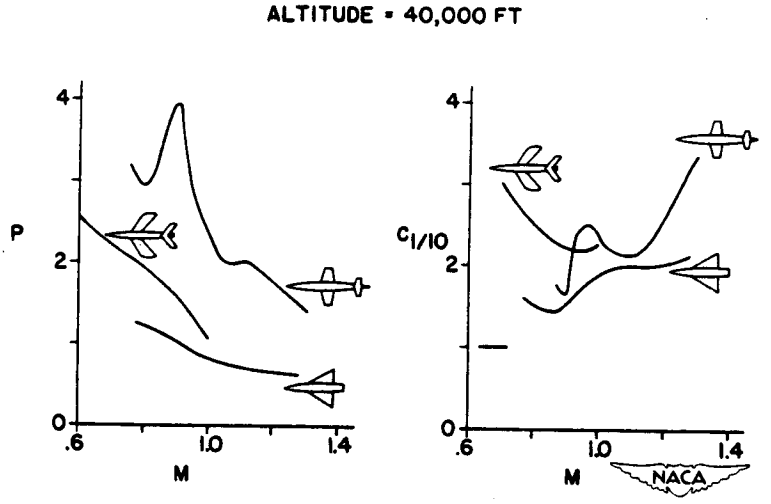


Figure 10.– Characteristics of short-period longitudinal oscillation.

Preceding page blank

DOWNWASH AND WAKE CHARACTERISTICS AT TRANSONIC SPEEDS

By Joseph Weil and Ralph P. Bielat

Langley Aeronautical Laboratory

N65-86469

INTRODUCTION

A knowledge of the transonic downwash and dynamic pressure characteristics at the tail plane is required by the aircraft designer to effect a rational design of transonic airplanes equipped with horizontal tail surfaces. During the past year a fairly systematic experimental study of the effect of design variations on the flow in the region of the tail plane has been made using the transonic-bump technique. Some of the results of this investigation together with pertinent data from other sources are summarized briefly.

DOWNWASH CHARACTERISTICS

Effective downwash angles were determined in the investigations made on the bump by measuring the floating angles of a series of swept-back free-floating tails located behind the various models. A typical test set-up is shown in figure 1. A tail spacing was used that enabled design information to be rapidly obtained, for a reasonable range of tail heights, with negligible interference between floating tails at transonic speeds. For studies of the downwash characteristics of wing-fuselage configurations the centrally located tail was replaced by a geometrically similar tail mounted on the fuselage, and, therefore, a slightly more outboard spanwise region was surveyed by this tail.

The semispan wing configurations for which downwash characteristics were investigated on the bump were part of a transonic research program and plan-form silhouettes are shown summarized in figure 2. A basic sweep study was made for a series of models with the wing quarter-chord line sweep being varied from 0° to 60°, aspect ratio 4, and taper ratio 0.6. Wings of 35° and 45° sweepback of aspect ratio 6 and a wing with 60° sweepback and aspect ratio 2 were also tested. A wing of 45° sweep and 0.3 taper ratio and a delta wing of aspect ratio 4 rounded out the bump plan-form series. The basic airfoil section in a streamwise direction was the NACA 65A006. In addition, an unswept plan form of aspect ratio 4 was investigated with an NACA 65A004 section and a 45° swept wing of aspect ratio 6 was studied with an NACA 65A009 section. As means of expediency, the same series of 45° swept tails of aspect ratio 4 were used to measure the effective downwash behind all plan forms. Therefore, inasmuch as the wing area was identical

for all models, the simulated tail volume was constant only for those configurations in which the wing aspect ratio and taper ratio were the same. The results of the investigations on these configurations that were tested on the transonic bump are presented in references 1 to 11. Other high-speed downwash data considered in this paper were obtained from investigations made in the Langley 8-foot high-speed tunnel, the Ames 12-foot pressure tunnel, and by the wing-flow method. (See references 12 to 17.)

As has been pointed out in previous papers, the maneuvering and control position stability of airplanes depend on many factors which are affected by both wing and tail geometry. It is obviously impossible to divorce all other factors and arrive at an optimum configuration from the isolated consideration of downwash. In some instances large changes in the downwash characteristics at the tail plane will compensate for changes in other parameters and the net change in stability and trim will be small. In other instances the reverse might well be true. However, in our discussion it will be assumed desirable to avoid large or sudden changes in the rate of change of downwash angle with lift coefficient $\partial\epsilon/\partial C_L$.

The effect of wing sweepback on the variation of the parameter $\partial\epsilon/\partial C_L$ with Mach number with the tail located on chord line extended and 30-percent of the wing semispan above the chord line extended is shown in figure 3. The data are presented for wing-fuselage combinations incorporating 6-percent-thick wings of aspect ratio 4 and taper ratio 0.6, and the slopes presented were measured at low angles of attack. A study of the curves reveals the absence of any large and sudden changes in $\partial\epsilon/\partial C_L$. The small vertical ticks placed on the curves indicate the Mach numbers for peak lift-curve slope or lift force break. An upper limit above which flow changes might be expected to occur that would invalidate subsonic theory is thus provided. It is seen that $\partial\epsilon/\partial C_L$ is essentially constant at subsonic speeds to within at least 0.05 of the force break Mach number. At Mach numbers of or slightly above force break, a decrease in downwash slope with increasing Mach number is evident for all swept-wing configurations with the tail located on the wing chord plane extended. This trend is delayed to a Mach number close to unity for the unswept wing. For a tail height of 30 percent of the wing semispan above the wing chord line extended the changes in $\partial\epsilon/\partial C_L$ with M are generally somewhat reduced. There is evident a very large change in downwash slope with tail height for the 60° sweptback wing configuration from about 8.8 at the chord-line extended tail to about 4.0 for the high tail position. Theoretical calculations showed an extremely large spanwise gradient in $\partial\epsilon/\partial C_L$, and it is estimated that fully half of

the apparent change in slope with tail height for the 60° swept wing can actually be attributed to the slightly more outboard spanwise location occupied by the floating tail mounted in the fuselage.

The downwash characteristics obtained from several specific complete model studies conducted in the Langley 8-foot high-speed tunnel are summarized in figure 4. The airfoil sections were about 10 percent thick measured in a streamwise direction. All configurations were representative of airplanes with fairly high tail locations. A study of the curves associated with the upper two silhouettes indicates that changing from a basically unswept to a 35° sweptback plan form delays the occurrence of large changes in $\partial\epsilon/\partial C_L$ at transonic speeds. The suddenness and magnitude of the changes, however, appear to be only slightly affected by the increased sweepback. Reducing the aspect ratio of the basically unswept 10-percent-thick wing from about 4 to 2 caused earlier and even more drastic changes in $\partial\epsilon/\partial C_L$.

The effect of aspect-ratio changes for the 6-percent-thick bump series is shown in figure 5 for wing-fuselage arrangements utilizing wings of 35°, 45°, and 60° of sweepback. Decreasing the aspect ratio appears to increase the changes in $\partial\epsilon/\partial C_L$ with M in all instances. The effect of aspect ratio on downwash slope at $M = 1.1$ is decidely less than at subcritical speeds for the more highly sweptback configurations.

The effect of wing thickness is illustrated in figure 6 for both unswept and sweptback designs. For the 45° sweptback wing of aspect ratio 6 there is very little effect of thickness at Mach numbers below 0.875. Above $M = 0.9$, however, $\partial\epsilon/\partial C_L$ for the 9-percent-thick wing increases rapidly and reaches a value about twice as large as for the thinner wing at $M = 1.0$. This large increase in $\partial\epsilon/\partial C_L$ for the thicker swept wing is attributable to flow separation at the wing tip which moves the center of loading inboard. The curves in the lower part of figure 6 are for an unswept model of aspect ratio 4 with a tail height 40-percent semispan above the chord line extended. The data for the 4-percent- and 6-percent-thick wings which were obtained on the bump show practically no change in downwash slope with Mach number. The curve for the 10-percent-thick wing, which was obtained from a complete-model investigation of a very similar configuration studied in the Langley 8-foot high-speed tunnel, indicates a large decrease in $\partial\epsilon/\partial C_L$ slightly above lift force break probably caused by a loss of loading over the root sections.

Some of the effects of model geometry on the experimental variations of $\partial\epsilon/\partial C_L$ with Mach number have been described. The question that naturally arises is: How well can these trends be

estimated for at least preliminary design work? First of all, can $\partial\epsilon/\partial C_L$ near zero lift be predicted at subcritical speeds? Inasmuch as the results of the theoretical analysis of reference 18 and our experimental data indicated little affect of compressibility on $\partial\epsilon/\partial C_L$ up to force break, it was decided to calculate the theoretical downwash at $M = 0.7$ by use of incompressible theory.

The span-load distributions determined by the Weissinger modified lifting-line method were obtained from the convenient charts of reference 19 for the range of plan forms for which high-speed experimental effective downwash data were available. The downwash parameter $\partial\epsilon/\partial C_L$ was then calculated across the span of the tail and weighted by the local chord. Most of the theoretical checks on the experimental data obtained on the transonic bump were made in the plane of the wake center line. For these calculations the wing was replaced by a series of stepped horseshoe vortices distributed along the swept lifting line with a strength proportional to the loading. It was then possible to calculate the downwash very rapidly by use of the tables given in reference 20. The downwash for tail heights other than at the wake center line were computed by the superposition of horseshoe vortices as utilized in reference 21. A comparison of the experimental and calculated downwash at $M = 0.7$ for different model configurations and data sources is shown in figure 7.

The agreement between theory and experiment is only fair as can be seen from the orientation of the points relative to the line of perfect agreement. No account was taken of the fuselage effect on the span-load distribution. The bump data shown, however, which represent both wing-alone and wing-fuselage configurations indicated that the degree of correlation was not materially affected by the presence of the fuselage. In the several instances investigated, the bump data showed less change in $\partial\epsilon/\partial C_L$ with tail height than was calculated, with better agreement being shown for the higher tail positions. Inasmuch as the majority of the calculated downwash slopes were within 20 percent of the experimental values, the methods used might be expected to give an acceptable first approximation for preliminary design.

In the speed range between lift-force break and low supersonic Mach numbers no theory is available with which to estimate $\partial\epsilon/\partial C_L$. From the experimental results shown, it would appear that no large changes in $\partial\epsilon/\partial C_L$ in this region are likely if the wing is thin enough to avoid large and sudden changes in the lift characteristics. An idea of the thickness required to minimize the change in lift slope at speeds above force break for unswept wings was given in the paper "The Lift, Drag, and Pitching-Moment Characteristics of Wings and Wing-Body Combinations in the Transonic Speed Range" by Edward C. Polhamus.

The supersonic downwash characteristics behind a delta wing of aspect ratio 4 have been calculated in references 22 and 23 by use of a supersonic doublet method. The downwash for this wing at $M = 0.7$ is represented by the point A in figure 7, and it is seen to be one of the farthest from agreement with subsonic theory. A comparison of the theoretical and experimental variation of $\partial\epsilon/\partial C_L$ with Mach number for the delta-wing configuration with tail on wing chord line extended is presented in figure 8. As just shown, the theoretical estimate at subsonic speeds is considerably above the experimental; however, the supersonic experimental downwash is in very good agreement with the theoretical values. On the upper part of the figure a comparison of the theoretical and experimental effect of tail height on $\partial\epsilon/\partial C_L$ is shown for $M = 1.08$. The experimental points fall on the theoretical curve and the agreement is once again very good.

The supersonic line-vortex method outlined in reference 24 appears promising from the standpoint of speed and accuracy and is currently being used in conjunction with load distributions obtained by available theoretical methods (for example, references 25 to 27) in order to compute the downwash of plan forms for which experimental data are available at low supersonic speeds.

The results of one such calculation are shown in figure 9. In the lower part of the figure the experimental variation of $\partial\epsilon/\partial C_L$ with Mach number is presented for the 4-percent- and 6-percent-thick unswept wing configurations for the chord-line-extended tail position. In the same figure the low-speed theoretical value of $\partial\epsilon/\partial C_L$ has been extended to peak lift-slope Mach number. The theoretical supersonic values of $\partial\epsilon/\partial C_L$ between $M = 1.1$ and 1.3 estimated by use of the equations of reference 24 has been plotted and a smooth curve drawn connecting the two theoretical curves. Once again the experimental and estimated curves show good agreement above $M = 1.0$. The variation of $\partial\epsilon/\partial C_L$ with tail height at $M = 1.10$ is shown in the upper part of the figure. A comparison of the experimental points and theory indicates very good agreement at low tail heights, but the experimental data are considerably above theory for the more extreme tail positions.

DYNAMIC PRESSURE RATIOS AT TAIL

It is also necessary to have knowledge of the magnitude of the wake losses and the extent of the wake in the region of the tail at transonic speeds in order to avoid locating the tail in a position where large stability changes and unsteady flow might be encountered. As part of the transonic research program on the bump, wake surveys



were made for a range of tail heights at the same tail length as was used in the downwash studies. The effect of sweepback on the ratio of wake dynamic pressure to free-stream dynamic pressure is presented in figure 10 for 6-percent-thick wing-fuselage combinations of aspect ratio 4, at a lift coefficient of approximately 0.3. The variation of this dynamic-pressure ratio with tail height indicates a substantially larger wake at $M = 1.10$ than at subsonic speeds for the unswept wing. As the sweep angle is increased, the magnitude of the wake losses at $M = 1.10$ becomes progressively less.

Analysis of data obtained on the 9-percent-thick 45° swept wing of aspect ratio 6 (reference 9) indicated the wake losses in the region of the horizontal tail to be as small as for the geometrically similar wing 6-percent thick (reference 7). From these data it may be concluded that the horizontal-tail location on thin swept-wing airplanes is less apt to be determined from considerations of static wake losses at transonic speeds than on thin unswept airplanes.

CONCLUSIONS

In conclusion, it has been shown that a smooth variation of $\partial\epsilon/\partial C_L$ with Mach number at transonic speeds can be expected regardless of sweep angle if thin wings are utilized. The agreement between calculated and experimental $\partial\epsilon/\partial C_L$ at subcritical speeds is only fair, but the results of preliminary correlations between theory and experiment at low supersonic speeds appear promising.



REFERENCES

1. Weil, Joseph, and Goodson, Kenneth W.: Aerodynamic Characteristics of a Wing with Quarter-Chord Line Swept Back 45°, Aspect Ratio 4, Taper Ratio 0.6, and NACA 65A006 Airfoil Section. Transonic-Bump Method. NACA RM L9A21, 1949.

2. Sleeman, William C., Jr., and Becht, Robert E.: Aerodynamic Characteristics of a Wing with Quarter-Chord Line Swept Back 35°, Aspect Ratio 4, Taper Ratio 0.6, and NACA 65A006 Airfoil Section. Transonic-Bump Method. NACA RM L9B25, 1949.

3. Myers, Boyd C., II, and King, Thomas J., Jr.: Aerodynamic Characteristics of a Wing with Quarter-Chord Line Swept Back 45°, Aspect Ratio 4, Taper Ratio 0.3, and NACA 65A006 Airfoil Section. Transonic-Bump Method. NACA RM L9E25, 1949.

4. Sleeman, William C., Jr., and Becht, Robert E.: Aerodynamic Characteristics of a Delta Wing with Leading Edge Swept Back 45°, Aspect Ratio 4, and NACA 65A006 Airfoil Section. Transonic-Bump Method. NACA RM L9G22a, 1949.

5. King, Thomas J., Jr., and Myers, Boyd C., II: Aerodynamic Characteristics of a Wing with Quarter-Chord Line Swept Back 60°, Aspect Ratio 4, Taper Ratio 0.6, and NACA 65A006 Airfoil Section. Transonic-Bump Method. NACA RM L9G27, 1949.

6. Goodson, Kenneth W., and Morrison, William D., Jr.: Aerodynamic Characteristics of a Wing with Unswept Quarter-Chord Line, Aspect Ratio 4, Taper Ratio 0.6, and NACA 65A006 Airfoil Section. Transonic-Bump Method. NACA RM L9H22, 1949.

7. Goodson, Kenneth W., and Few, Albert G., Jr.: Aerodynamic Characteristics of a Wing with Quarter-Chord Line Swept Back 45°, Aspect Ratio 6, Taper Ratio 0.6, and NACA 65A006 Airfoil Section. Transonic-Bump Method. NACA RM L9I08, 1949.

8. Sleeman, William C., Jr., and Morrison, William D., Jr.: Aerodynamic Characteristics of a 35° Sweptback Wing of Aspect Ratio 6, Taper Ratio 0.6, and NACA 65A006 Airfoil Section. Transonic-Bump Method. (Prospective NACA paper)

9. Spreemann, Kenneth P., Morrison, William D., Jr., and Pasteur, Thomas B., Jr.: Aerodynamic Characteristics of a Wing with Quarter-Chord Line Swept Back 45°, Aspect Ratio 6, Taper Ratio 0.6, and NACA 65A009 Airfoil Section. Transonic-Bump Method. (Prospective NACA paper)

10. Myers, Boyd C., II, and King, Thomas J., Jr.: Aerodynamic Characteristics of a Wing with Quarter-Chord Line Sweptback 60°, Aspect Ratio 2, Taper Ratio 0.6, and NACA 65A006 Airfoil Section. Transonic-Bump Method. (Prospective NACA paper)

11. Myers, Boyd C., II, and Wiggins, James W.: Aerodynamic Characteristics of a Wing with Unswept Quarter-Chord Line, Aspect Ratio 4, Taper Ratio 0.6, and NACA 65A004 Airfoil Section. Transonic-Bump Method. (Prospective NACA paper)

12. Wright, John B.: High-Speed Wind-Tunnel Tests of a $\frac{1}{16}$-Scale Model of the D-558 Research Airplane. Longitudinal Stability and Control of the D-558-I. NACA RM L8C23, 1948.

13. Osborne, Robert S.: High-Speed Wind-Tunnel Investigation of the Longitudinal Stability and Control Characteristics of a $\frac{1}{16}$-Scale Model of the D-558-2 Research Airplane at High Subsonic Mach Numbers and at a Mach Number of 1.2. NACA RM L9C04, 1949.

14. Wright, John B., and Luoma, Arvo A.: Longitudinal Stability and Control Characteristics at High Subsonic Speeds of Two Models of a Transonic Research Airplane with Wings and Horizontal Tails of Aspect Ratio 4.2 and 2.0. (Prospective NACA paper)

15. Johnson, Ben H., Jr., and Rollins, Francis W.: Investigation of a Thin Wing of Aspect Ratio 4 in the Ames 12-Foot Pressure Wind Tunnel. V - Static Longitudinal Stability and Control Characteristics Throughout the Subsonic Speed Range of a Semispan Model of a Supersonic Airplane. (Prospective NACA paper)

16. Crane, Harold L.; Preliminary Results of an Investigation by the Wing-Flow Method of the Longitudinal Stability Characteristics of a $\frac{1}{50}$-Scale Semispan Model of the McDonnell XP-88 Airplane. NACA RM SL8E28a, U. S. Air Force, 1948.

17. Silsby, Norman S., and McKay, James M.: Effect of Airplane Components on the Longitudinal Characteristics of a Semispan Model of a Supersonic Airplane Configuration at Transonic Speeds from Tests by the NACA Wing-Flow Method. (Prospective NACA paper)

18. Goldstein, S., and Young, A. D.: The Linear Perturbation Theory of Compressible Flow, with Applications to Wind-Tunnel Interference. R. & M. No. 1909, British A.R.C., 1943.

19. DeYoung, John: Theoretical Additional Span Loading Characteristics of Wings with Arbitrary Sweep, Aspect Ratio, and Taper Ratio. NACA TN 1491, 1947.

20. Staff of Mathematics Divison: Tables of Complete Downwash Due to a Rectangular Vortex. Rep. No. 10754, British A.R.C., July 21, 1947.

21. Polhamus, Edward C.: Jet-Boundary-Induced-Upwash Velocities for Swept Reflection-Plane Models Mounted Vertically in 7- by 10-Foot, Closed, Rectangular Wind Tunnels. NACA TN 1752, 1948.

22. Heaslet, Max. A., and Lomax, Harvard: The Calculation of Downwash behind Supersonic Wings with an Application to Triangular Plan Forms. NACA TN 1620, 1948.

23. Lomax, Harvard, and Sluder, Loma: Downwash in the Vertical and Horizontal Planes of Symmetry behind a Triangular Wing in Supersonic Flow. NACA TN 1803, 1949.

24. Mirels, Harold, and Haefeli, Rudolph C.: Line-Vortex Theory for Calculation of Supersonic Downwash. NACA TN 1925, 1949.

25. Busemann, A.: Infinitesimal Conical Supersonic Flow. NACA TM 1100, 1947.

26. Stewart, H. J.: The Lift of a Delta Wing at Supersonic Speeds. Quarterly Appl. Math., vol. IV, no. 3, Oct. 1946, pp. 246-254.

27. Cohen, Doris: The Theoretical Lift of Flat Swept-Back Wings at Supersonic Speeds. NACA TN 1555, 1948.

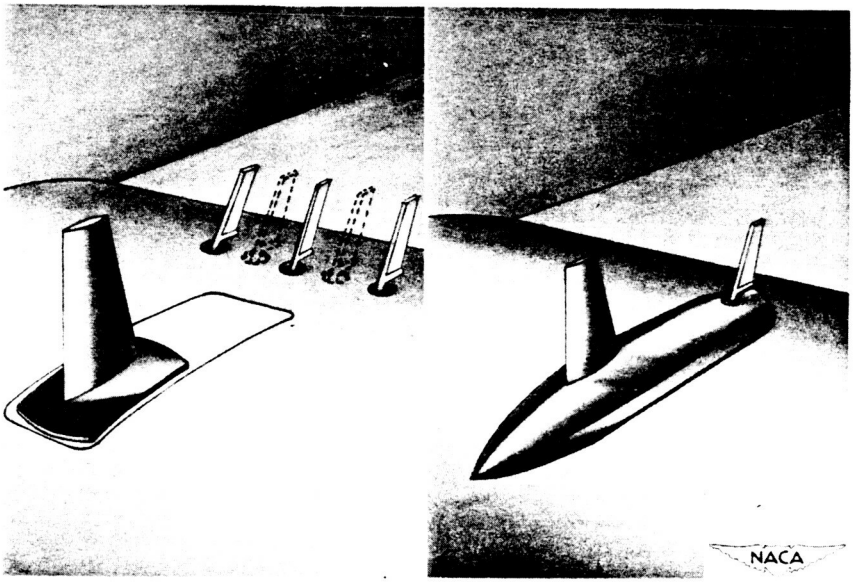


Figure 1.– Arrangement of free–floating vanes used for downwash measurements on transonic bump.

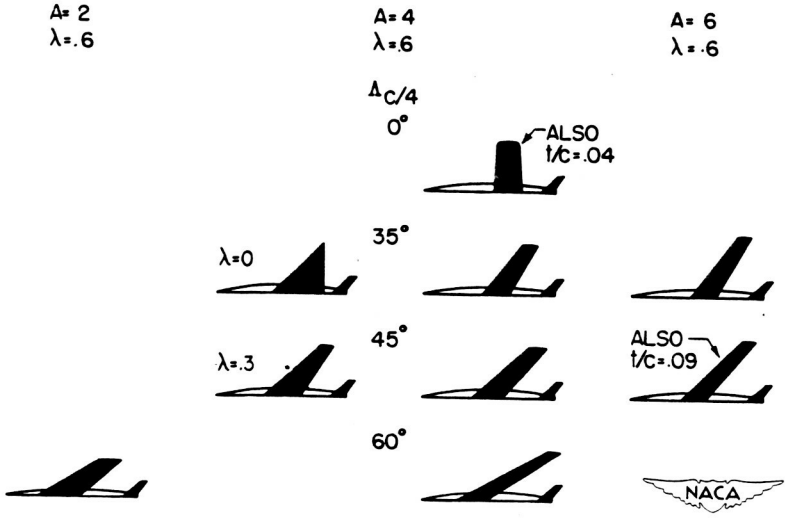
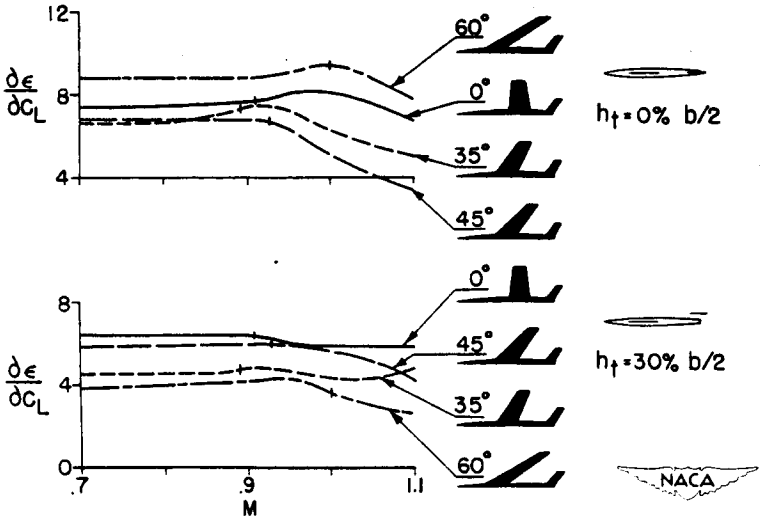


Figure 2.– Summary of configurations investigated on transonic bump.

Preceding page blank



WING FUSELAGE A=4 λ=.6 t/c=.06

Figure 3.– Effect of sweepback on downwash characteristics. Transonic bump.

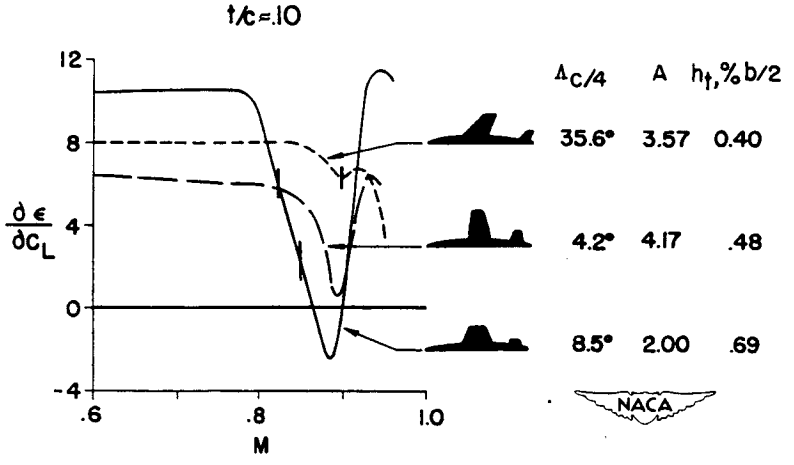


Figure 4.– Effect of sweepback and aspect ratio on downwash characteristics. Langley 8-foot high-speed tunnel.

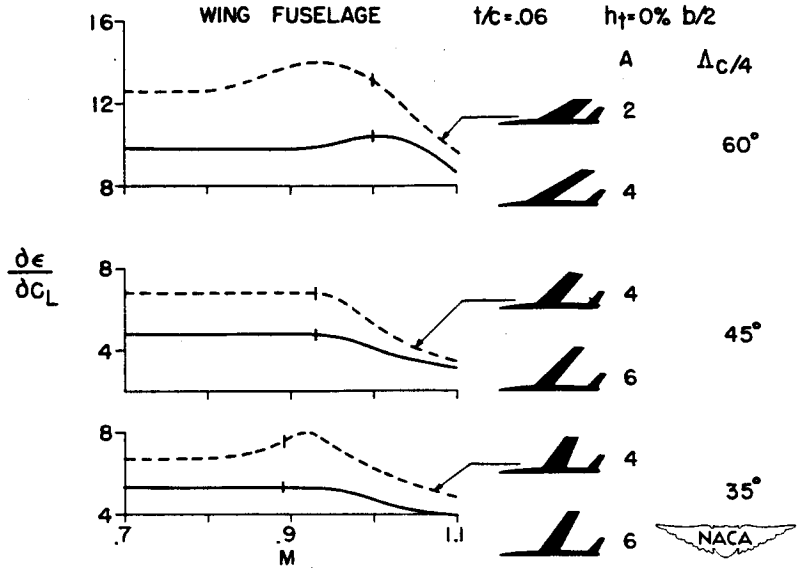


Figure 5.– Effect of aspect ratio on downwash characteristics. Transonic bump.

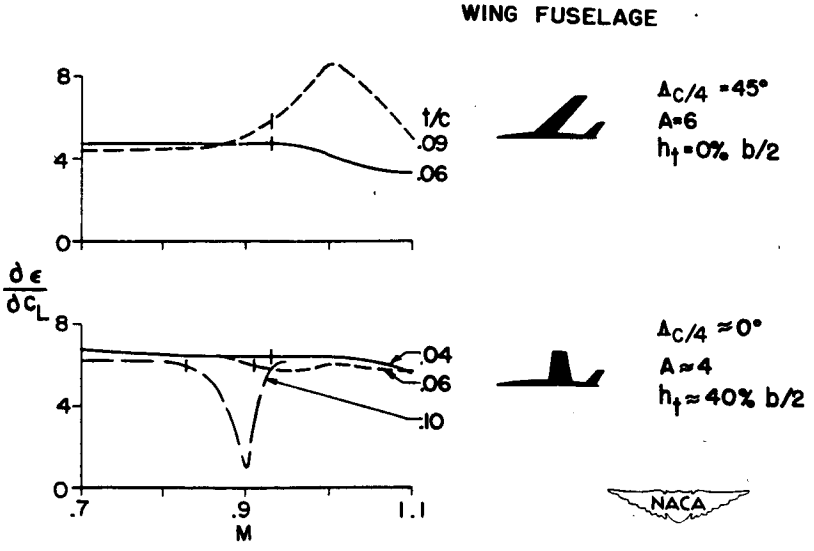


Figure 6.– Effect of wing thickness on downwash characteristics.

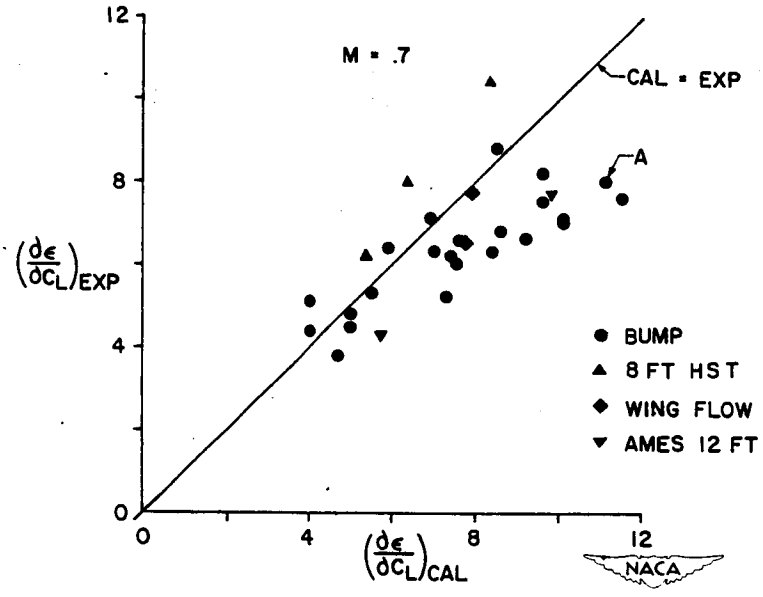


Figure 7.– Comparison of calculated and experimental $\partial\epsilon/\partial C_L$. M = 0.7.

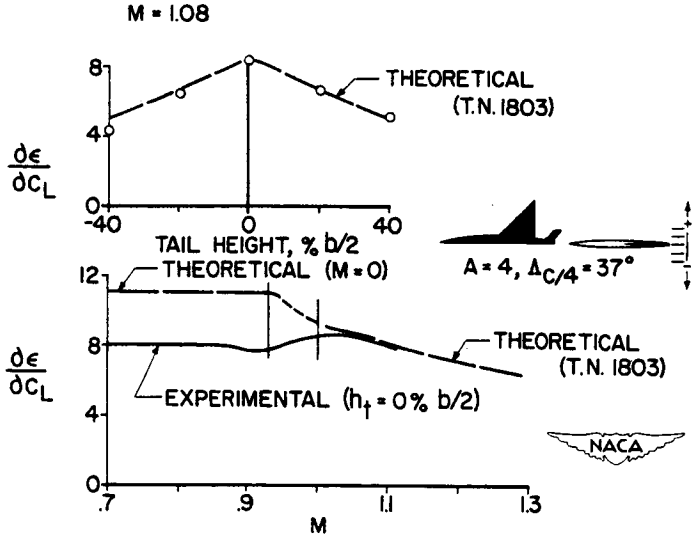


Figure 8.– Comparison of calculated and experimental $\partial\epsilon/\partial C_L$. Triangular-wing configuration.

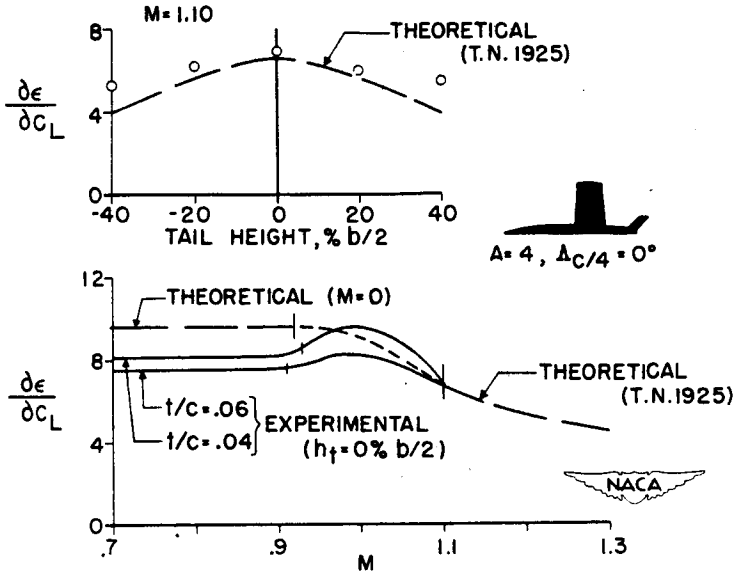


Figure 9.– Comparison of calculated and experimental $\partial\epsilon/\partial C_L$. Unswept wing configurations.

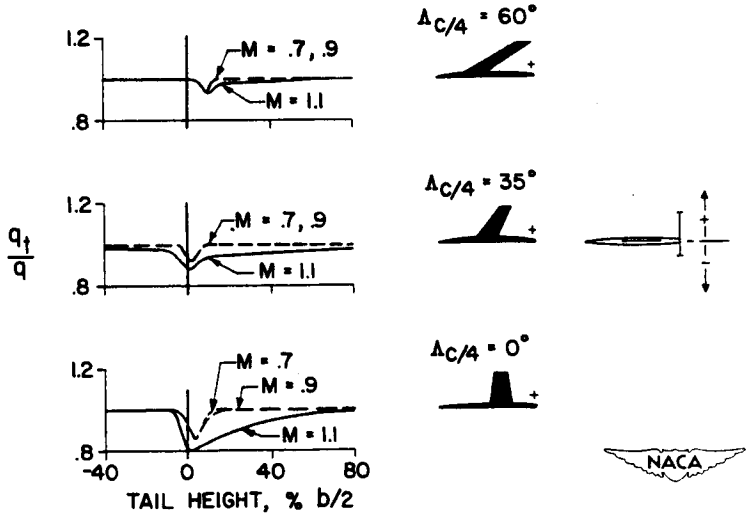


Figure 10.– Effect of sweepback on dynamic-pressure ratio.

EFFECT OF STALL-CONTROL DEVICES ON THE LOW-SPEED CHARACTERISTICS OF SWEPT WINGS

By G. Chester Furlong and William B. Kemp, Jr.
Langley Aeronautical Laboratory

N65-86470

PART I - FIXED SWEEP

By G. Chester Furlong

INTRODUCTION

Present-day transonic airplanes utilize swept wings having either round or sharp-nose airfoil sections and straight low-aspect-ratio wings employing sharp-nose airfoil sections. Although straight low-aspect-ratio wings are more truly a supersonic plan form, they necessarily provide an entrance to the transonic range as well.

The purpose of this paper is to consider some of the low-speed problems associated with these wings, such as longitudinal stability and maximum lift. Because of the limited time available, it has been necessary to impose certain limitations in the scope of this paper. Low-speed data for straight low-aspect-ratio wings (references 1 to 4) have not pointed out any significant differences since Herbert A. Wilson, Jr., and Laurence K. Loftin, Jr., presented their paper entitled "Landing Characteristics of High-Speed Wings" at the NACA Conference on Aerodynamic Problems of Transonic Airplane Design in 1947. With regard to swept wings, both theory and experiment indicate that sweepback and sweepforward increase the force divergence Mach number; however, the structural divergence inherent in sweptforward wings has seriously limited their application to present-day designs.

For these reasons, the emphasis is on recent low-speed work of sweptback wings although several interesting low-speed investigations on sweptforward wings are available (references 5 to 7).

SCALE EFFECT

An important consideration in the application of wind-tunnel data is an understanding of the scale effect that can be encountered with swept wings.

Figure 1 indicates the type and magnitude of scale effect on several of the aerodynamic parameters (references 8 and 9) of a 52° sweptback wing. It can be seen that the effects of Reynolds number on the maximum lift are small, but that rather large effects occur in the

pitching moment, drag, effective dihedral C_{l_ψ}, and directional (weathercock) stability C_{n_ψ}. With the exception of the directional-stability parameter C_{n_ψ} the low Reynolds number data give conservative results which can be very misleading. This wing has a streamwise thickness of 8 percent; however, reducing the wing thickness will minimize the favorable scale effect shown in figure 1. It should be pointed out that severe roughness on the leading edge can practically eliminate the desirable scale effect and is therefore a condition to be avoided, not only from the drag standpoint but also the longitudinal- and lateral-stability standpoint as well.

In view of rather large scale effects shown herein, the current work of facilities capable of providing low-speed large-scale data constitute, insofar as possible, the basis for the present paper.

FLOW CHARACTERISTICS

The type of flow separation over the tip sections which produces the unstable pitching-moment break at maximum lift on sweptback wings is fairly well understood. It has been found, however, that as the sweep angle of a wing is increased, a vortex type of flow can be encountered which will cause large undesirable variations in longitudinal stability prior to maximum lift. The sweep angle at which the vortex flow occurs appears to be related to the leading-edge radius. Hence, as the wing thickness defines the leading-edge radius on subsonic airfoils, the thinner the airoil section, the lower the sweep angle at which the vortex flow is observed. Sufficient experimental studies of the flow on swept wings are now available to form the nucleus for some generalization (references 6, 8, and 10 to 12).

The sharp-leading-edge wing is an extreme case, and is used to illustrate the mechanics of the vortex type of flow. Figure 2 contains the results of an investigation on a wing of circular-arc airfoil section having approximately 48° sweepback and an aspect ratio of 3.5 (reference 11). The leading-edge separation bubble common to such airfoil sections forms a real vortex lying on the wing surface, as indicated by the schematic ribbon. The vortex flow is perceptible at an angle of attack dependent on both the sweep angle and Reynolds number involved. The presence of this vortex flow reduces the leading-edge pressures but at the same time broadens the regions of high chordwise loading and causes rearward shifts in center of pressure. These effects have a pronounced influence on the section-lift characteristics and, in turn, on the over-all wing pitching-moment characteristics. The section-lift coefficients have been plotted against wing-lift coefficient for several spanwise stations. At the outermost station (0.80b/2),

the concentration of boundary layer is probably sufficient to counteract the effects of the vortex flow and the resulting lift curve is low but fairly linear below the stall. With an increase in angle of attack, the vortex becomes stronger and moves inboard into regions of less boundary-layer concentration; hence these stations experience an increase in lift-curve slope as indicated by the data for the 0.60b/2 station. The increases in lift-curve slope at the outboard stations produce the initial dip in the pitching-moment curve. With further increases in angle of attack, the vortex moves inboard along the trailing edge, leaving more of the tip sections in a stalled flow, while the inboard sections are experiencing an increase in lift-curve slope due to the increased strength of the vortex flow. Both of these effects produce the destabilizing moment variation in the moderately high lift range. At maximum lift the vortex flow has moved inboard sufficiently to cause a rearward shift in the centers of pressure of the inboard sections, thus producing the stable pitching-moment break at the stall.

With moderately swept wings employing round leading-edge airfoils approximately 10 to 12 percent thick, the vortex flow is nonexistent. The pitching-moment variation for such a wing is indicated in figure 3 for a wing of 42° sweepback and round leading-edge airfoils. The stability is relatively uniform through the lift range. At maximum lift the center sections are still highly loaded, the inboard centers of pressure are still forward, and loss in lift at the tip sections due to the large induced upwash produces the destabilizing pitching-moment variation through maximum lift. The results for a wing of similar plan form, but incorporating circular-arc airfoil sections, indicate the presence of the vortex type of flow. In the case of a 52° sweptback wing employing the same round-nose airfoil sections as the 42° wing, a vortex flow similar to that described for the sharp-leading-edge wing was observed. It is apparent from a comparison of the pitching-moment characteristics for this 52° sweptback wing with one of similar plan form, but incorporating circular-arc airfoil sections, that the stability changes are similar but delayed to a higher value of lift coefficient.

In order to indicate the importance of aspect ratio on the stability changes associated with this vortex type of flow, the results obtained on two 63° wings are shown in figure 3. (See reference 13.) Both wings were relatively thin with round leading-edge airfoils, and the pitching-moment variations would indicate the presence of the vortex type of flow. As the aspect ratio is increased from 1.9 to 3.5, the break in pitching moment is hastened and the unstable rise is more pronounced. Inasmuch as the moment arms of the tip sections of the higher-aspect-ratio wing are much larger than those on the lower-aspect-ratio wing, small changes in loading and center of pressure are magnified in terms of over-all wing pitching-moment characteristics.

Thus it can be seen that, except for the small aspect-ratio range indicated by Shortal and Maggin in reference 14, sweptback wings will possess longitudinal instability at maximum lift or well below maximum lift if the vortex flow is present. The problem is therefore one of controlling the tip stall or the vortex flow in the case of sharp-leading-edge or thin highly swept wings.

STALL-CONTROL DEVICES

The low-speed work then has been directed toward improving the longitudinal stability in the high-lift range and through maximum lift by the use of stall-control devices. The devices to be considered in the present paper consist of extensible leading-edge flaps, extended leading-edge slats, droop-nose flaps, fences, and boundary-layer control by suction.

The extensible leading-edge flap and extended leading-edge slat may be considered to provide essentially similar relief to tip stalling; however, for expediency, wind-tunnel work has favored the leading-edge flap, thus avoiding the detailed positioning studies required for slat installation. In the case of each device, the extension in chord reduces the spanwise-flow tendency, camber is introduced in the leading edge of the tip section, and a plan-form discontinuity exists at the inboard end of the leading-edge device. It should be pointed out that the plan-form discontinuity is important in providing the location for initial separation.

The results obtained with extensible leading-edge flaps on three sweptback wings are shown in figure 4. (See references 15 to 17.) The extensible leading-edge flaps were effective in providing acceptable longitudinal stability through the lift range, and in the case of the 52° sweptback wing, were effective in controlling the stability changes which resulted from the formation of the vortex type of flow.

For each wing the optimum extensible leading-edge flap span has been used and is defined as the leading-edge flap span which will produce the greatest increment in maximum lift and yet provide acceptable pitching-moment variations through the lift range. Although it is shown in figure 4 that the optimum leading-edge flap span decreases with increasing sweep, the effects of other wing parameters, such as aspect ratio, are at present unknown. Hence, design criteria cannot be formulated to aid in the determination of the optimum span for any particular wing.

It has been found that both the type and span of trailing-edge high-lift devices (fig. 5) can affect the successful application of extensible leading-edge flaps. Some results are shown of an investigation to determine the effects of trailing-edge flaps on the optimum extensible leading-edge flap span. (See reference 16.) The wing has 48° sweepback, an aspect ratio of 6.0, and round-nose airfoil sections. A very small range of leading-edge flap spans will provide stable moment variations of the type shown here. The addition of the double slotted flaps slightly increased the usable range of leading-edge flap spans, but more important is the fact that a trailing-edge flap span was reached, which made all spans of leading-edge flap ineffective in providing longitudinal stability through the lift range.

It has been reported previously that on a wing of lower sweep and lower aspect ratio, full-span split flaps did not cause the optimum leading-edge flap to become ineffective.

Tests of a 42° sweptback wing have also shown that the optimum leading-edge flap span may be reduced by the addition of standard roughness (reference 18) and also by the addition of a fuselage (reference 15).

As previously stated, the action of the extended leading-edge slat should be comparable to that of the extensible leading-edge flap. The droop nose, on the other hand, with a sharper break in the airfoil section, a smaller leading-edge radius than the extensible flap, and with no extension of the chord, would probably not be as positive a stall-control device. A comparison of the three types of devices has been made on a tapered wing of 37° sweepback, aspect ratio of 6, and NACA 64_1-212 airfoil sections (reference 19). In each case the initial separation occurs at the spanwise station at which the discontinuity in plan form occurs. Although it is important that the initial separation occurs at the inboard end of these leading-edge devices, the effectiveness of the device is measured by its ability to restrain the outward spread of the separated region so that the loss in lift over the inboard sections will produce the stable moment variation through maximum lift. Both the leading-edge flap and slat are capable of restraining this outward spread of the separated area. The droop nose, however, is not effective in this respect, and the accompanying pitching-moment variation through maximum lift is unstable.

Attempts have been made to control mechanically the spanwise flow on sweptback wings by means of fences or vanes. Other than being useful in combination with additional stall-control devices, however, the fence or vane has not proved too effective. The full-chord fence, for example, has been used successfully in several cases to increase the

optimum extensible leading-edge flap span. Inasmuch as such a device would probably not be retractable, it is interesting to note that its drag has in one case been shown to amount to as much as 7 percent of the total drag at zero angle of attack through the transonic-speed range (reference 20).

The problem of obtaining satisfactory stability when the vortex flow is present may not necessarily require an improvement of the flow over the tip sections but may rather be a matter of reorientating the vortex flow. In this regard, the results recently obtained in the Langley 19-foot pressure tunnel by a mere extension of the local chord over the outer portion of a highly sweptback wing are very promising. In figure 6 are presented the pitching-moment variations with lift for a 52° wing of circular-arc airfoil sections and that wing equipped with an extensible leading-edge flap over the outer. 25 percent of the wing span and a 20-percent-chord extension located over the inboard $12\frac{1}{2}$ percent of the span previously occupied by the leading-edge flap. The basic moment curve indicates the presence of the vortex flow. With the extensible leading-edge flap, the stability changes were very small up to a lift coefficient of approximately 0.8. This lift coefficient is well below the maximum lift of the plain wing, which in this case is 1.0. The chord extension produced only small stability changes through the entire lift range. They amounted to only an 8-percent shift in aerodynamic center between zero and maximum lift. The low-speed drag of this local chord extension has been found to be negligible. The ability of this chord extension to provide acceptable stability variations through the lift range lies in the fact that the plan-form discontinuity determines the location of the initial separation in the same manner as the extensible leading-edge flap and prevents the increase in lift-curve slope over the tip sections. Such results as these indicate the need for further research in the control of the vortex flow common to thin highly swept wings.

The application of boundary-layer control (fig. 7) at the leading-edge as a means of providing longitudinal stability through the maximum lift has recently been investigated on the wing having 48° sweepback and aspect ratio of 3.4 and round-nose airfoil sections (reference 21). It can be seen that with the 50-percent-span slot, satisfactory longitudinal stability characteristics through the entire lift range were obtained. Similar to the extensible leading-edge flap, a comparison of the results obtained with the 50-percent-span and 74-percent-span slots indicates that there is an optimum slot span.

[redacted]

HORIZONTAL-TAIL EFFECTIVENESS

The effectiveness of a horizontal tail in contributing stability to a swept-wing airplane has been rather thoroughly investigated at low speeds (references 7, 17, and 22 to 24). The results indicate that the vertical position of the horizontal tail is the most important parameter to be considered. Figure 8 is a summary of a portion of these data. The values of Γ basically represent the stabilizing effectiveness of the horizontal tail in terms of the flow parameters downwash ϵ and dynamic-pressure ratio $\frac{q_t}{q}$.

$$\Gamma = \frac{1}{V\left(C_{L_{\alpha_t}}\right)_{\text{isolated}}} \frac{dC_{m_t}}{d\alpha_w} = -\left[\left(1 - \frac{d\epsilon}{d\alpha_w}\right)\left(\frac{q_t}{q} + \alpha_w \frac{d\frac{q_t}{q}}{d\alpha_w}\right) + i_t \frac{d\frac{q_t}{q}}{d\alpha_w}\right]$$

A minus value of Γ signifies the tail is contributing stability, and a positive value of Γ necessarily means the tail is contributing instability. In both the low and high position the horizontal tail is stabilizing to moderately high values of lift coefficient. It can be seen, however, that in the high-lift range the tail in the high positions will contribute instability; whereas the tail in the low positions, which are slightly below the chord plane extended, will contribute stability. The stability contributed by the tail in the low position arises mainly from the fact that the tail lies below the wake and, hence, experiences the very stabilizing effect of the rate of change of dynamic-pressure ratio with angle of attack as the tail emerges from the influence of the wake in the high angle-of-attack range. Of course, the tail located above the wake experiences just the opposite effects.

These results are not to be interpreted as defining the optimum horizontal-tail location. For example, if the wing-fuselage combination is extremely stabilizing, it might be found that the low tail may provide an uncontrollable amount of stability, which would necessitate the use of a higher tail location. Further, the effect of vertical location on the horizontal-tail effectiveness in the transonic range, as discussed in a preceding paper, must be considered.

The ability to calculate the downwash variation behind sweptback wings for preliminary design work has been briefly investigated (reference 25). It has been possible to obtain relatively good agreement between calculated and experimental downwash up to a rather high value of lift coefficient on a 42° sweptback wing of aspect ratio 4.0.

The method of calculation is that of NACA Rep. 651, modified for the sweep of bound vortices. The value of this method lies in the fact that the calculations of downwash above and below the vortex plane can be readily made. The success of these calculations is due to the fact that potential-flow concepts hold for this wing up to relatively high values of lift coefficient. Spanwise loadings for sharp-leading-edge swept wings (reference 11) show radical departures from those calculated by potential-flow concepts. Hence, preliminary downwash calculations behind such wings or wings which exhibit the vortex-flow phenomena are not feasible because methods are not available to calculate the loading on such wings.

MAXIMUM LIFT

The other problem to be considered is that of maximum lift. To review briefly, simple sweep theory would indicate that maximum lift will vary as the $\cos^2\Lambda$; however, as shown in the 1947 NACA Conference on Aerodynamic Problems of Transonic Airplane Design, this value of lift coefficient generally underestimates the value of maximum lift obtained. In addition, recent systematic tests (reference 26) of a family of thin swept wings incorporating NACA 65A006 airfoil sections parallel to the plane of symmetry, as shown in figure 9, indicate that maximum lifts much in excess of the zero-sweep value are obtained when the vortex flow is present. It can be seen that the maximum lift of the plain wing actually exceeds the two-dimensional value for the airfoil section at a sweep angle slightly in excess of 30°, and that aspect ratio has little effect. These gains in maximum lift with an increase in sweep angle are of limited value, however, because they are obtained at very large angles of attack, and abrupt pitching-moment breaks occur with the formation of the vortex flow. In order to define the lift at which these pitching-moment breaks occur, the terms "inflection" lift, denoted by the dash line, or "usable" maximum lift have been used. The adverse effects of vortex flow appear at approximately 30° of sweep and rapidly reduce the inflection lift as the sweep angle is increased. An increase in aspect ratio greatly decreases the lift coefficient at which the breaks in pitching-moment curve occur. Taper ratio has little effect on the maximum lift and inflection lift.

The application of trailing-edge high-lift devices of normal design, such as the split flap shown here, have revealed that the lift effectiveness is greatly reduced as the sweep angle is increased. Again, as in the case of the plain wing, the vortex flow defines the inflection lift, and the effects of aspect ratio are similar.

[redacted]

Figure 10 summarizes the maximum-lift data from several investigations (references 15, 16, 17, 19, and 27). The longitudinal stability for each plain wing was undesirable either at maximum lift or prior to maximum lift. For the configurations with leading-edge flaps, alone and in combination with the trailing-edge flaps, acceptable pitching-moment variations through the lift range were obtained. It can be seen that the effectiveness of the trailing-edge high-lift devices is relatively small; although, as indicated for the 42° wing shown here, the extended split flaps would provide an increase over the normal split flap.

In the case of the 52° wing, the advantage of the extended split flap over the normal split flap is even more pronounced. For the case of the double-slotted flap, only a very slight gain in maximum lift was obtained over that for the normal split flap, although the beneficial shift in angle of zero lift is obtained with the double-slotted flaps.

N65-86471

PART II - VARIABLE SWEEP

By William B. Kemp, Jr.

The information so far presented emphasizes the problems encountered on an airplane using highly swept wings. A possible method of avoiding these problems is to provide an airplane with wings the sweep angle of which can be changed in flight so that a low sweep angle can be used when it is desired to fly at high lift coefficients. Some points of interest in connection with the design of such an airplane are illustrated by the results of a recent investigation at low Mach number of a variable-sweep airplane model (reference 28). Figure 11 illustrates schematically the model used and the longitudinal stability characteristics. As the sweep angle is increased by rotating the wing panels about a pivot point in the fuselage, the wing center of pressure moves rearward causing a large increase in longitudinal stability. In order to overcome this, the wing panel pivot point must be allowed to translate forward as the wings are rotated rearward. For illustrative purposes the wing pivot was allowed to translate in such a manner that the tail-off aerodynamic center remained at a fixed location over the range of sweep angles from 23° to 63°. This required a movement of the wing pivot point of about 25 percent of the reference length, which in this example represents the mean aerodynamic chord at 53° sweep, or about 2 feet on the airplane considered. It is of interest to note that at the higher sweep angles the reduced loading over the inboard portions of the wing required the quarter mean aerodynamic chord to move forward about 15 percent of the reference length to obtain constant tail-off stability. Addition of the horizontal tail provided an increasing stability increment with increasing sweep.

Although for sweep angles greater than 23° instability is indicated near maximum lift, a variable-sweep airplane would be expected to use the high sweep angles primarily for low-lift-coefficient phases of flight. The trim changes associated with changing sweep angle, as shown here, are small enough to be controlled by the horizontal tail but could be further reduced by a modification of the relationship between wing pivot movement and sweep angle.

The directional and lateral stability characteristics of a variable-swept-wing airplane are indicated in figure 12 by variations of directional-stability parameter C_{n_ψ} and the effective-dihedral parameter C_{l_ψ} for the model at two extremes of sweep (reference 29). It can be seen that the same vertical tail is capable of providing directional stability over the entire lift range for the 23° swept wing and to moderately high values of lift coefficient for the 63° swept wing. The loss in directional stability occurring at high lift coefficients

with 63° sweep is not related to the principle of variable sweep, but rather is a problem which can be encountered on any highly swept wing. The loss in directional stability is related to the very high angles of attack required for high lift coefficients when large sweep angles are used.

CONCLUDING REMARKS

To reiterate some of the high points of the material presented:

1. On moderately swept wings the instability at maximum lift results from a loss of lift over the outboard sections and has been eliminated by use of extensible leading-edge flaps or extended leading-edge slats.

2. The successful application of boundary-layer control to provide longitudinal stability through the lift range was shown for one case.

3. An increase in sweep angle, or a reduction in wing thickness, may produce a vortex type of flow which will cause severe stability variations prior to maximum lift. It has been indicated that where the vortex flow is present the problem of obtaining satisfactory longitudinal stability is not necessarily a matter of improving the flow over the tip sections, but rather a matter of reorientating the vortex flow.

4. Trailing-edge high-lift devices are not effective in the high-sweep range with regard to maximum lift, although extended split flaps have shown some advantage.

5. The possibility of using variable sweep has been indicated.

REFERENCES

1. Johnson, Ben H., Jr.: Investigation of a Thin Wing of Aspect Ratio 4 in the Ames 12-Foot Pressure Wind Tunnel. I - Characteristics of a Plain Wing. NACA RM A8D07, 1948.

2. Johnson, Ben H., Jr., and Bandettini, Angelo: Investigation of a Thin Wing of Aspect Ratio 4 in the Ames 12-Foot Pressure Wind Tunnel. II - The Effect of Constant-Chord Leading- and Trailing-Edge Flaps on the Low-Speed Characteristics of the Wing. NACA RM A8F15, 1948.

3. Johnson, Ben H., Jr., and Demele, Fred A.: Investigation of a Thin Wing of Aspect Ratio 4 in the Ames 12-Foot Pressure Wind Tunnel. III - The Effectiveness of a Constant-Chord Aileron. NACA RM A8I17, 1948.

4. Johnson, Ben H., Jr., and Reed, Verlin D.: Investigation of a Thin Wing of Aspect Ratio 4 in the Ames 12-Foot Pressure Wind Tunnel. IV - The Effect of a Constant-Chord Leading-Edge Flap at High Subsonic Speeds. NACA RM A8K19, 1949.

5. McCormack, Gerald M., and Cook, Woodrow L.: A Study of Stall Phenomena on a 45° Swept-Forward Wing. NACA TN 1797, 1949.

6. McCormack, Gerald M., and Cook, Woodrow L.: Effects of Several Leading-Edge Modifications on the Stalling Characteristics of a 45° Swept-Forward Wing. NACA RM A9D29, 1949.

7. Martina, Albert P., and Deters, Owen J.: Maximum Lift and Longitudinal Stability Characteristics at Reynolds Numbers up to 7.8×10^6 of a 32° Sweptforward Wing Equipped with High-Lift and Stall-Control Devices, Fuselage, and Horizontal Tail. NACA RM L9H18a, 1949. (Prospective NACA paper)

8. Fitzpatrick, James E., and Foster, Gerald V.: Static Longitudinal Aerodynamic Characteristics of a 52° Sweptback Wing of Aspect Ratio 2.88 at Reynolds Numbers from 2,000,000 to 11,000,000. NACA RM L8H25, 1948.

9. Salmi, Reino J.: Yaw Characteristics of a 52° Sweptback Wing of NACA 64_1-112 Section with a Fuselage and with Leading-Edge and Split Flaps at Reynolds Numbers from 1.93×10^6 to 6.00×10^6. NACA RM L8H12, 1948.

10. Wilson, Herbert A., Jr., and Lovell, J. Calvin: Full-Scale Investigation of the Maximum Lift and Flow Characteristics of an Airplane Having Approximately Triangular Plan Form. NACA RM L6K20, 1947.

11. Whittle, Edward F., Jr., and Fink, Marvin P.: Full-Scale Investigation of the Aerodynamic Loads on a Drooped-Nose Flap on a 47.5° Sweptback Wing Having Symmetrical Circular-Arc Airfoil Sections at a Reynolds Number of 4.3×10^6. (Prospective NACA paper)

12. May, Ralph W., Jr., and Hawes, John G.: Low-Speed Pressure-Distribution and Flow Investigation for a Large Pitch and Yaw Range of Three Zero-Taper-Ratio Wings Having Leading Edge Swept Back 60° and Biconvex Sections. NACA RM L9J07, 1949. (Prospective NACA paper)

13. McCormack, Gerald M., and Walling, Walter C.: Aerodynamic Study of a Wing-Fuselage Combination Employing a Wing Swept Back 63°. - Investigation of a Large-Scale Model at Low Speed. NACA RM A8D02, 1949.

14. Shortal, Joseph A., and Maggin, Bernard: Effect of Sweepback and Aspect Ratio on Longitudinal Stability Characteristics of Wings at Low Speeds. NACA TN 1093, 1946.

15. Graham, Robert R., and Connor, D. William: Investigation of High-Lift and Stall-Control Devices on an NACA 64-Series 42° Sweptback Wing with and without Fuselage. NACA RM L7G09, 1947.

16. Salmi, Reino J.: Effect of Leading-Edge and Trailing-Edge Flap Span on the Longitudinal Aerodynamic Characteristics of two 47.7° Sweptback Wings of Aspect Ratios 5.1 and 6.0 and NACA 64-210 Airfoil Sections. (Prospective NACA paper)

17. Foster, Gerald V., and Fitzpatrick, James E.: Longitudinal-Stability Investigation of High-Lift and Stall-Control Devices on a 52° Sweptback Wing with and without Fuselage and Horizontal Tail at a Reynolds Number of 6.8×10^6. NACA RM L8I08, 1948.

18. Pratt, George L., and Bollech, Thomas V.: The Effect of Span and Deflection of Split Flaps and Leading-Edge Roughness on the Longitudinal Stability and Gliding Characteristics of a 42° Sweptback Wing Equipped with Leading-Edge Flaps. NACA RM L9E02, 1949.

[redacted]

19. Koven, William, and Graham, Robert R.: Wind-Tunnel Investigation of High-Lift and Stall-Control Devices on a 37° Sweptback Wing of Aspect Ratio 6 at High Reynolds Numbers. NACA RM L8D29, 1948.

20. Osborne, Robert S.: High-Speed Wind-Tunnel Investigation of the Longitudinal Stability and Control Characteristics of a $\frac{1}{16}$-Scale Model of the D-558-2 Research Airplane at High Subsonic Mach Numbers and at a Mach Number of 1.2. NACA RM L9C04, 1949.

21. Pasamanick, Jerome, and Sellers, Thomas B.: Full-Scale Investigation of Leading-Edge Suction in Combination with High-Lift Devices on a Wing-Fuselage Configuration Having 47.5° Leading-Edge Sweep. (Prospective NACA paper)

22. Spooner, Stanley H., and Martina, Albert P.: Longitudinal Stability Characteristics of a 42° Sweptback Wing and Tail Combination at a Reynolds Number of 6.8×10^6. NACA RM L8E12, 1948.

23. Woods, Robert L., and Spooner, Stanley H.: Effects of High-Lift and Stall-Control Devices, Fuselage, and Horizontal Tail on a Wing Swept Back 42° at the Leading Edge and Having Symmetrical Circular-Arc Airfoil Sections at a Reynolds Number of 6.9×10^6. NACA RM L9B11, 1949.

24. Foster, Gerald V., and Griner, Roland F.: A Study of Several Factors Affecting the Stability Contributed by a Horizontal Tail at Various Vertical Positions on a Sweptback-Wing Airplane Model. NACA RM L9H19, 1949.

25. Furlong, G. Chester, and Bollech, Thomas V.: Downwash, Sidewash, and Wake Surveys behind a 42° Sweptback Wing at a Reynolds Number of 6.8×10^6 with and without a Simulated Ground. NACA RM L8G22, 1948.

26. Cahill, Jones F., and Gottlieb, Stanley M.: Low-Speed Aerodynamic Characteristics of a Series of Swept Wings Having NACA 65A006 Air-Foil Sections. NACA RM L9J20, 1949. (Prospective NACA paper)

27. Neely, Robert H., and Koven, William: Low-Speed Characteristics in Pitch of a 42° Sweptback Wing with Aspect Ratio 3.9 and Circular-Arc Airfoil Sections. NACA RM L7E23, 1947.

28. Kemp, William B., Jr., and Becht, Robert E., and Few, Albert G., Jr.: Stability and Control Characteristics at Low Speed of a $\frac{1}{4}$- Scale X-5 Airplane Model. Longitudinal Stability and Control. (Prospective NACA paper)

29. Kemp, William B., Jr., and Becht, Robert E.: Stability and Control Characteristics at Low Speed of a $\frac{1}{4}$- Scale X-5 Airplane Model. Lateral and Directional Stability and Control. (Prospective NACA paper)

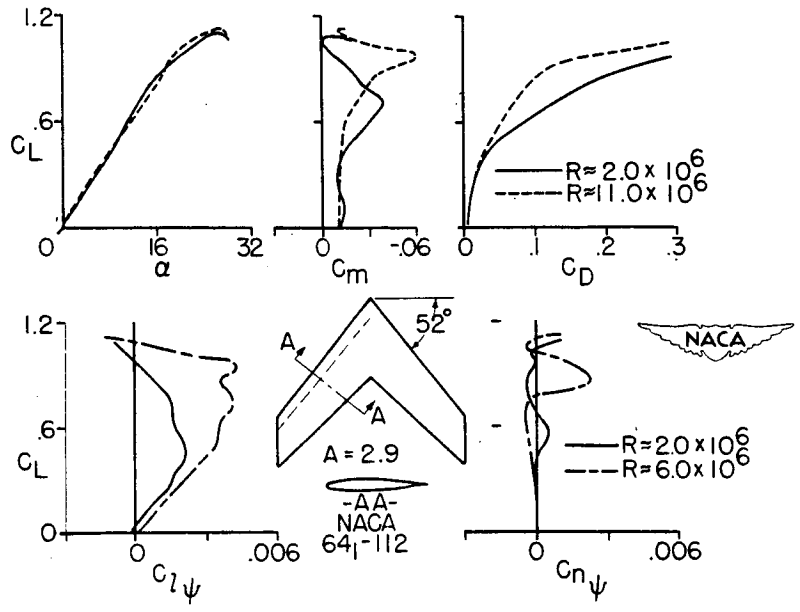


Figure 1.- Scale effect on 52° sweptback wing.

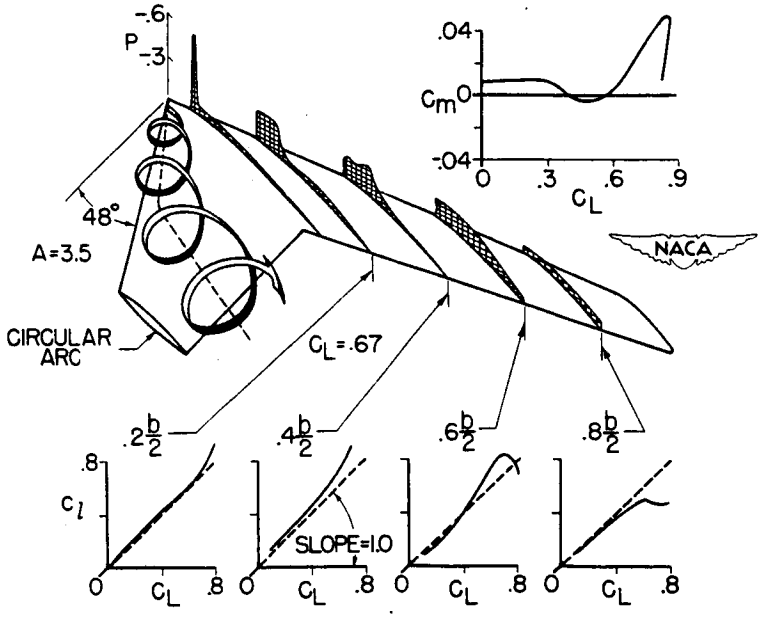


Figure 2.- Effects of vortex flow on the aerodynamic characteristics of a 48° sweptback wing employing circular-arc airfoil sections.

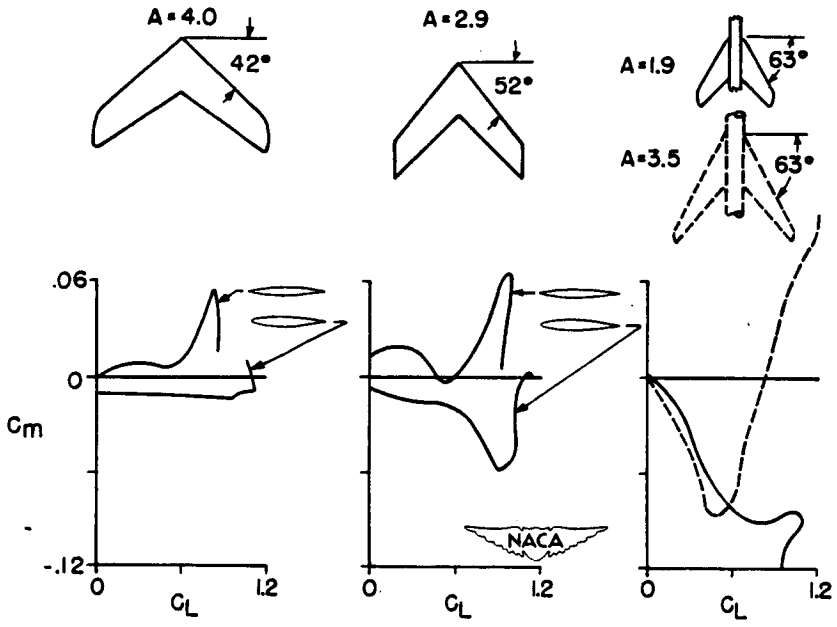


Figure 3.- Effects of airfoil section and aspect ratio on the pitching-moment characteristics of several sweptback wings.

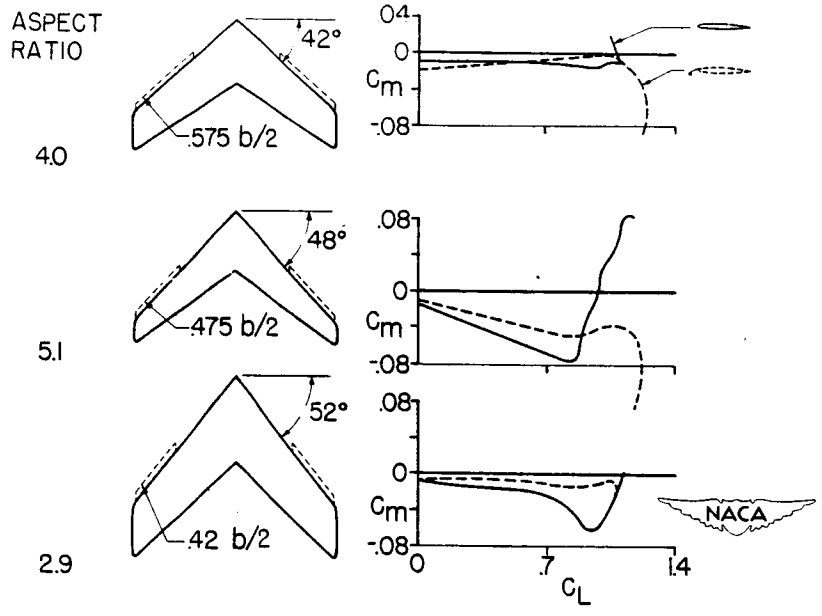


Figure 4.- Effect of extensible leading-edge flaps on the pitching-moment characteristics of three sweptback wings.

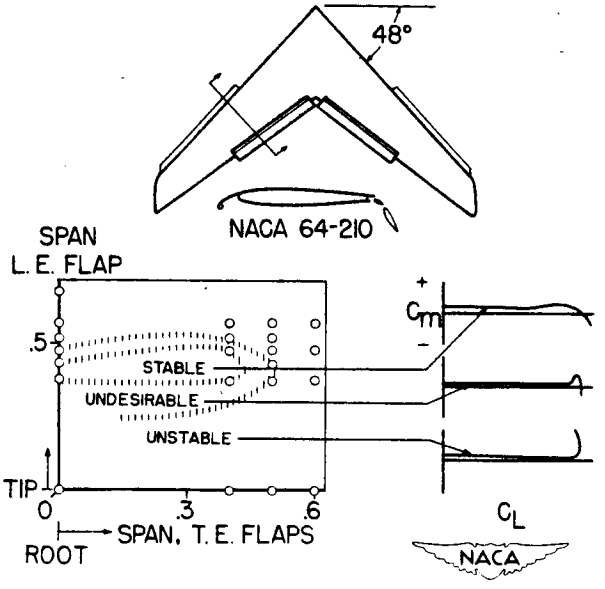


Figure 5.- Effect of leading-edge and trailing-edge flaps on the longitudinal stability of a 48° sweptback wing.

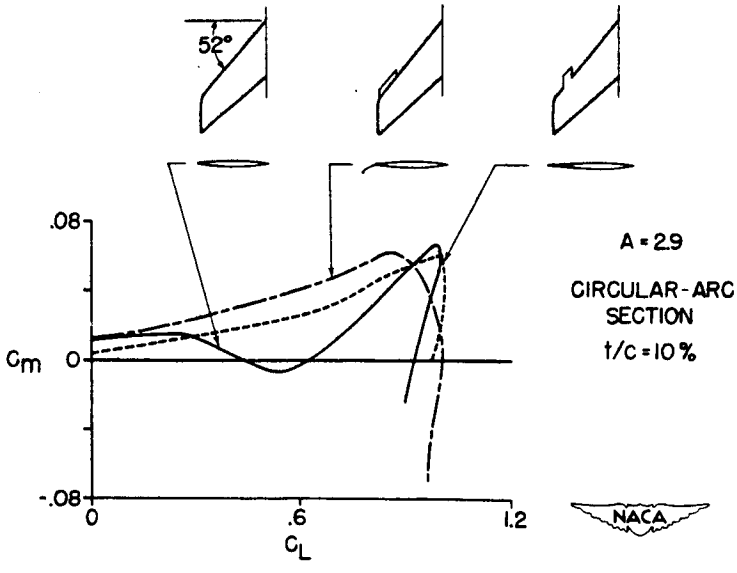


Figure 6.- Effect of a chord extension on the pitching-moment characteristics of a 52° sweptback wing.

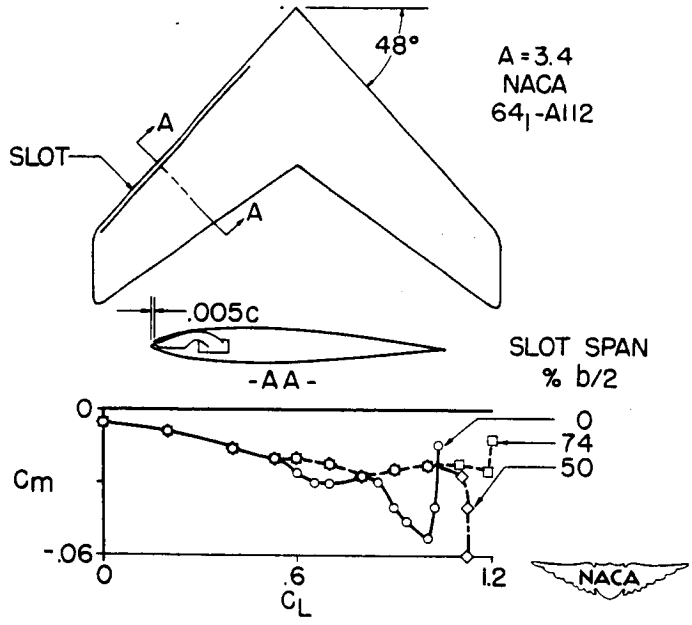


Figure 7.- Effect of boundary-layer control on the pitching-moment characteristics of a 48° sweptback wing.

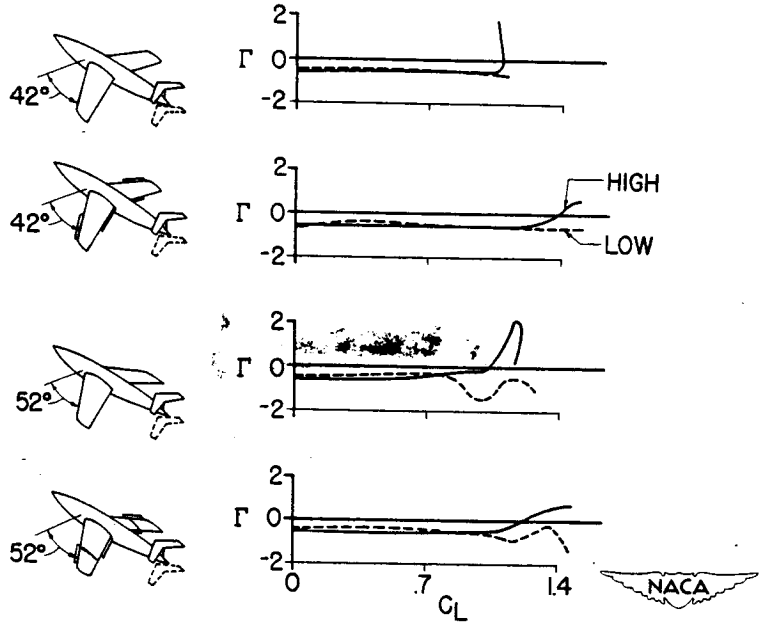


Figure 8.- Stabilizing effectiveness of a horizontal tail at two vertical postions behind two sweptback wings.

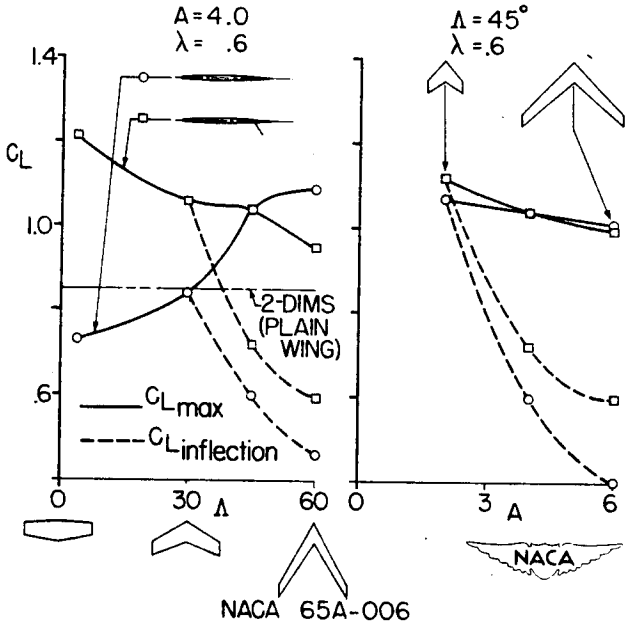


Figure 9.- Effects of sweep angle and aspect ratio on the maximum and inflection lift of a family of wings.

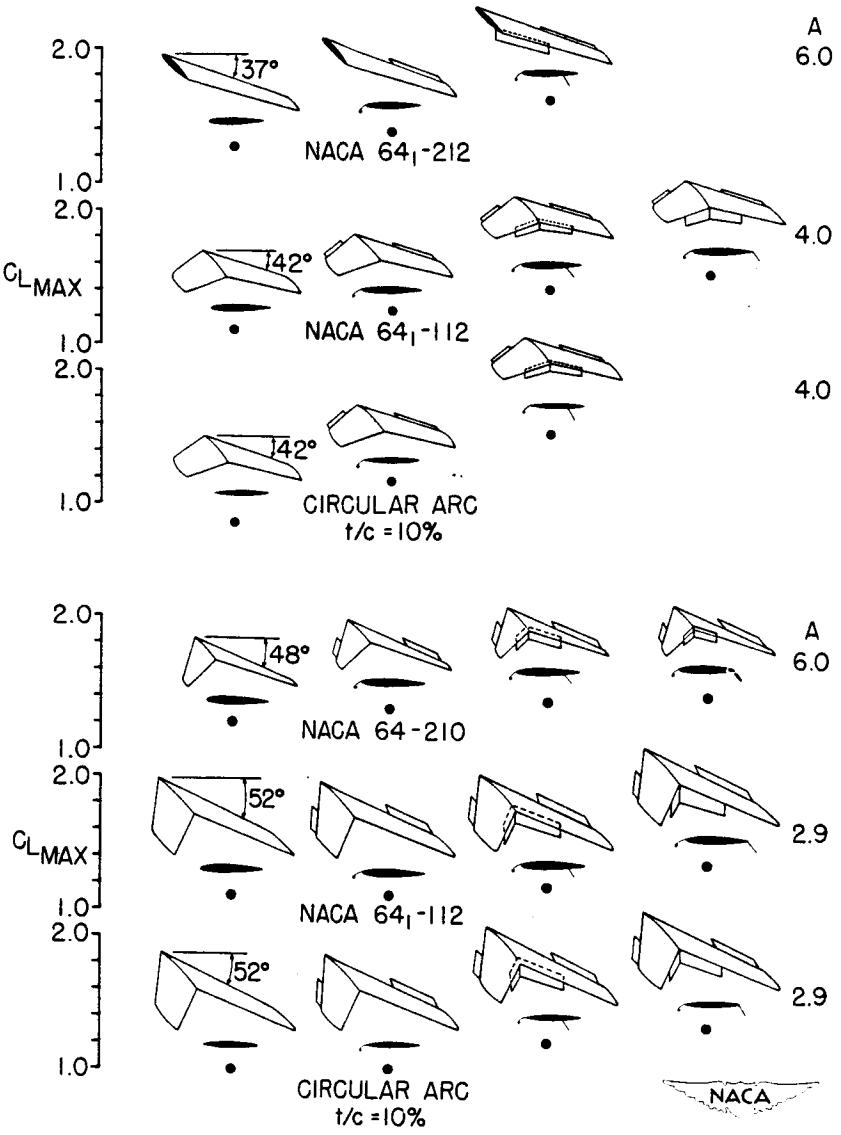


Figure 10.- Summary of maximum lift.

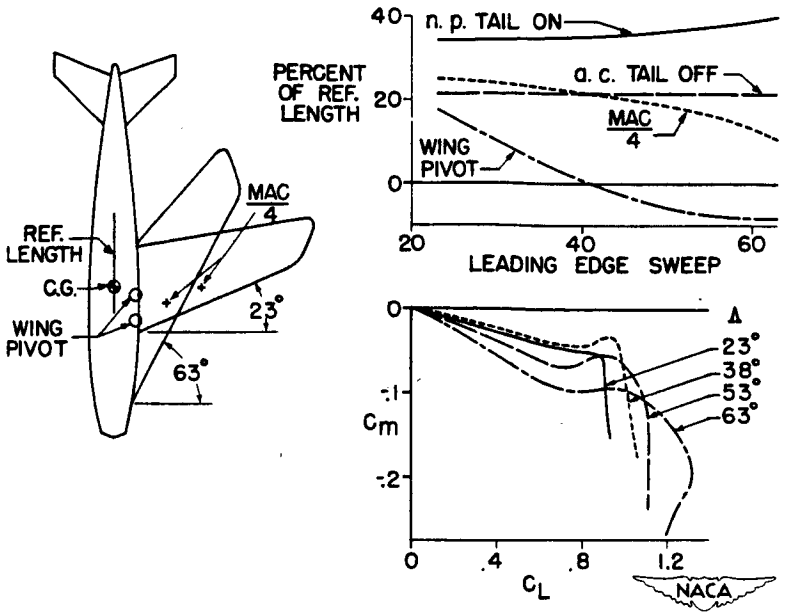


Figure 11.- Pivot point movement and longitudinal stability of a variable sweep airplane model.

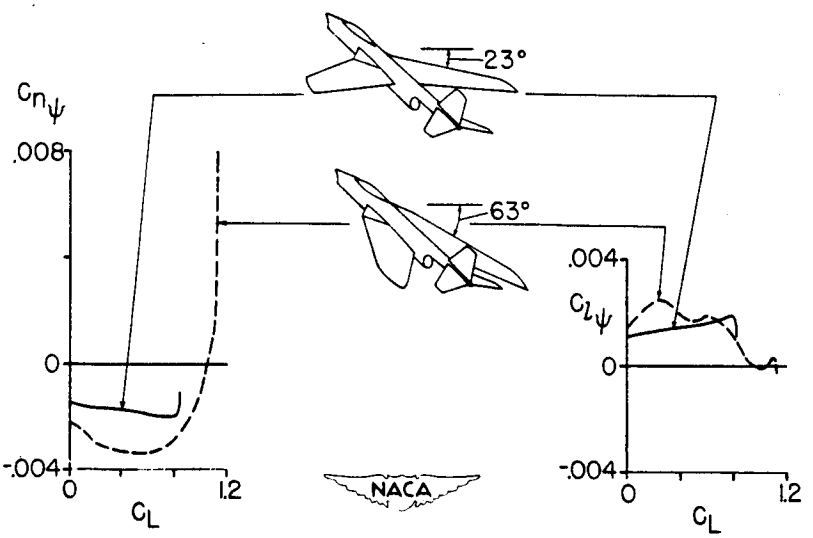


Figure 12.- Directional and lateral stability of a variable sweep airplane model.

N65-86472

EFFECT OF TWIST AND CAMBER ON THE LOW-SPEED CHARACTERISTICS OF A SWEPT WING

By Lynn W. Hunton

Ames Aeronautical Laboratory

The study of the subcritical aerodynamics of swept wings from both a theoretical and experimental standpoint is now sufficiently advanced to provide a good understanding of a majority of the factors controlling their characteristics. From these studies it is becoming increasingly clear that, in order to effect an improvement in the over-all performance of highly swept thin wings, contrary to the procedures of the past, the characteristically poor low-speed qualities of these wings can no longer be accepted as inevitable, and that the design must be based along lines dictated by the requirements of low speed as well as those of high speed. In this discussion an attempt will be made to present the basic concepts and show the results of an application of these concepts to the design of a swept wing using twist and camber.

The deficiencies in the characteristics of swept wings in the moderate-to-high lift range, as compared with straight wings, is traceable to four prime factors. The first of these factors is basic to the very concept of swept wings; that is, the stream velocity can be divided into two components, one chordwise and one spanwise relative to the swept-wing panel; the magnitude of the pressures and their distribution on each chordwise section depends primarily on the chordwise component of the velocity. This concept represents exactly conditions on an infinitely long wing and, within practical limits, represents conditions on a finite wing except for the immediate vicinity of the root and tip. Hence, to a first approximation it means that, if we expect a lift coefficient of 1 from a 45° swept wing, the sections will have to support a load of $\frac{1}{\cos^2 45^\circ}$, or a value of 2, with respect to the effective chordwise component of the velocity. Thus, we start out by demanding more, sectionwise, of a swept wing than has been customary to attain on a straight wing. Furthermore, even at wing lift coefficients for high-speed flight, the sections are operating at far higher lift coefficients than have been encountered on the straight wing.

The second factor to which the high-lift deficiencies of swept-back wings are traceable is the commonly recognized induction effect which tends to load up the tips. This is illustrated in figure 1 in which is shown the variation of the section loading per unit chord

with the fraction of the semispan for a straight wing and a 45° sweptback wing both with aspect ratio 6 and 2:1 taper. This loading on the sweptback wing at a lift coefficient of 1 resembles that of a straight wing of equal aspect ratio and taper but with 13° of washin; or, considered another way, it has the same high tip loading as that supported by an aspect-ratio-6 wing with a 12:1 taper. On either of these straight wings, tip-stalling troubles would be expected, and so it is clear why on the swept wing we experience erratic pitching-moment variations at moderate lift coefficients and limitations of $C_{L_{max}}$ due to early tip stall.

The third factor tending to reduce the lift capabilities of normal swept-wing designs is the necessary use of thin sections imposed by the requirement of high critical speed. Section data amply demonstrates that on sections of 10-percent thickness or less, particularly those with location of maximum thickness back at the 40- or 50-percent-chord station, the maximum lift coefficients obtainable are of the order of only 1.1 to 1.2. This reduced $c_{l_{max}}$ is traceable to the fact that these thin high-speed symmetrical sections have relatively small nose radii and the $c_{l_{max}}$ is therefore established by early leading-edge separation. This reduced maximum lift attainable is doubly serious when considered in the light of the previously discussed increased section-lift requirements imposed by the swept-wing design.

The fourth factor influencing the lift capabilities of swept wings is the spanwise drainage of the boundary-layer air. This is a mixed factor as will be demonstrated later in this paper since, although the accumulated boundary layer at the outboard sections promotes premature stall and a reduced lift-curve slope at these tip sections, the drainage or removal of the boundary-layer air from the inboard sections increases the lift capabilities of these sections. However, for reasons pointed out previously, the tip sections are the more critical so that on normal swept-wing designs the net effect of spanwise boundary-layer drain is a reduction in the attainable or usable $C_{L_{max}}$.

The foregoing four factors combine not only to limit the attainable $C_{L_{max}}$ on swept wings but contribute to the appearance of premature separation far below $C_{L_{max}}$. The occurrence and subsequent spread of this early separation causes erratic pitching-moment variations in the moderate lift-coefficient range and seriously reduces the L/D's in the landing and climb range compared with those that would be obtainable on straight wings of equal aspect ratio. The effects, of course, become more unfavorable as the sweep is increased and, to some

extent, as aspect ratio is increased. For example, fairly satisfactory characteristics can be obtained on wings with sweep of the order of 35°, but the deficiencies assume considerably less tolerable proportions on wings of 45° sweep and above. In fact, the magnitude of sweep which it is practical to incorporate in a design is probably less a function of the high-speed characteristics than it is of the limitations imposed by the low-speed deficiencies under discussion.

It can be shown that most of the current devices used to improve the high-lift characteristics of swept wings are directed at one or more of the four factors just discussed. For instance, inboard flaps derive some of their effectiveness from the change in span loading and tip relief associated with them; leading-edge devices are normally directed at postponing leading-edge separation and increase the available $C_{L_{max}}$ thereby; boundary-layer fences represent an attempt to minimize the effect of boundary-layer drain; and the use of a variable-sweep wing has been considered in order to minimize the $\cos^2$ effect. A more detailed discussion of the quantitative effects of many such devices is discussed in the paper by G. Chester Furlong and William B. Kemp, Jr. "Effect of Stall-Control Devices on the Low-Speed Characteristics of Swept Wings."

A recent study of this problem has indicated that each of the foregoing four factors are amenable to control, to some degree at least, by a logical application of existing design principles. The span loading deficiencies can be overcome by wing twist. By virtue of this twist and resultant spanwise redistribution of the loading, the boundary-layer drain to some extent should be discouraged. And lastly, the relatively high section lifts desired, even in high-speed level flight, and the necessary avoidance of leading-edge separation both can be realized through use of camber. It is the purpose of this discussion to outline the manner in which these principles were applied in one case and to discuss the results obtained.

Tests recently have been run in the Ames 40- by 80-foot tunnel on two semispan 45° sweptback wing-fuselage models, one untwisted and uncambered which provides a base for comparison, the other incorporating a degree of twist and camber chosen to provide improvement in the low-speed characteristics of the wing without any undue compromise in its high-speed characteristics. The procedure used in choosing the twist and camber incorporated in the second wing will be first outlined and the resultant changes in force characteristics, stall progression, and pressure distribution then scrutinized.

The basic plan form of both wings is shown in figure 2. It had an aspect ratio of 6, a 2:1 taper, and the sweep of the quarter-chord line was 45°. The shaded area indicates the portion of the wing covered

by the fuselage. This relatively high aspect ratio was chosen because it was considered that the effects of twist and camber would be more clearly apparent on high-aspect-ratio wings. Also, in choosing the plan form, we had in mind a hypothetical, high-speed, high-altitude bomber which would, in the first place, favor use of high aspect ratio and, secondly, would have a relatively high, high-speed, operating lift coefficient, a factor which favors the use of camber and significant amounts of twist. A NACA 64A010 thickness distribution was chosen as being typical and acceptable from a high-speed standpoint.

To obtain a starting point to fix twist and camber, a design-wing lift coefficient of 0.4 was chosen. The twist and camber were then determined to give uniform spanwise and, within practical limits, chordwise loading. By virtue of the $\cos^2$ rule, the section normal to the quarter-chord line became an NACA 64A810. The variation of the theoretical wing twist, spanwise, required for uniform loading at the design C_L is shown by the solid curve in figure 2. It is evident that a rapid decrease in washout at the tip was required to carry the loading uniformly to the tip. Such a distribution not only would tend to promote a local stall at the extreme tip but, in addition, from a fabrication standpoint, would require doubly curved surfaces. Therefore, a modified twist distribution, shown by the dashed line in figure 2, which resulted in 10° of washout at the tip was chosen to give singly curved surfaces and provide tip relief which appeared advantageous.

In figure 3 are shown comparisons of the theoretical spanwise variation of the effective section lift coefficient, based on the chordwise component of the velocity for the wing with and without this modified twist distribution (computed by the method of references 1 and 2) at wing lift coefficients of 0.4 and 1.0. It is evident from the curves at a wing C_L of 1.0 that the twist reduces the peak c_l, but, more importantly, moves the peak inboard from the critical tip sections and thus should improve $C_{L_{max}}$ and delay tip stall. At the high-speed design C_L of 0.4 it can be seen that even for this condition the modified twist reduces slightly the peak c_l and thus should not significantly alter the wing critical speed.

At the time of the design layout, the effect of camber on either the low- or high-speed characteristics could not be simply estimated. If the full benefit of 0.8 section camber were realized in terms of section $c_{l_{max}}$, then a 0.4 gain in the usable wing lift-coefficient range would result. Consideration of section pressures indicated that the use of camber would also improve the critical speed of the

section. Subsequently, the investigations reported by Donald J. Graham in the paper entitled "The Effects of Systematic Variation of Several Shape Parameters on the Characteristics of Airfoil Sections at High-Subsonic Mach Numbers," verified these conclusions to a degree. The $c_{l_{max}}$ of the section was shown to be increased from 1.1 to 1.7. The drag-divergence Mach number for the design condition was shown to be increased 0.1 from 0.57 to 0.67 or, accounting for sweep effect, an increase of 0.2 in the flight drag-divergence Mach number for this 45° swept wing. In the use of camber it is recognized that a possible source of danger exists in the supercritical speed condition where, it was shown, camber causes large changes in angle of zero lift and pitching-moment coefficient at zero lift. However, unlike the picture on the straight wing wherein changes in section characteristics dominate the wing characteristics, it is anticipated that, on highly swept wings, section changes are minimized and span loading changes emphasized in their respective effects on the over-all wing characteristics. This point, however, is one which most needs experimental investigation at the present time.

Having presented in the foregoing discussion the factors involved in the design of the wing models, attention will now be directed to the results obtained. The gross force characteristics of the two wing models are shown in figure 4. The drag coefficient, angle of attack, and pitching-moment coefficient are plotted as a function of lift coefficient. It may be noted here that the cambered, twisted wing markedly reduced the drag increase with lift in the upper lift-coefficient range. In fact, the initial occurrence of separation was delayed from a C_L value of roughly 0.7 to almost 1.1, thus indicating that the anticipated gains regarding premature separation were fully realized with this improvement of 0.4 in C_L. Cambering and twisting the wing also gave a moderate increase in $C_{L_{max}}$ from 0.94 to 1.09. The plain untwisted, uncambered wing showed a typical pitching-moment curve for a wing of this plan form. The pitching-moment curve for the twisted, cambered wing is stable in the lower C_L range followed by a less stable variation of moment as $C_{L_{max}}$ is approached and, finally, by a very unstable variation of pitching moment just prior to and following $C_{L_{max}}$. While these gross characteristics are of interest, information of considerably greater value results from consideration of the factors which produced them.

Tuft studies show qualitatively the nature of the wing stall. In figure 5 are shown sketches of the stalling patterns for the plain and the cambered, twisted wing. The plain wing shows a typical swept-wing stall pattern, with leading-edge stall appearing at a lift coefficient of 0.71, which corresponds to the point of both drag increase and pitching-moment break. The stalled region spreads slowly inboard as

the wing exhibits more and more flat-plate characteristics. In contrast to this stalling behavior, the cambered, twisted wing shows no evidence of stall until a C_L value of 1.07 is reached, when a small stalled area appears at the wing trailing edge near the midpoint of the semispan followed by a large area of separation both inboard and outboard of this point. Several conclusions can be obtained from these pictures. It is possible by means of twist and camber to move the point at which stall first appears on a swept wing away from the tip to a midsemispan station. It is possible, through use of camber to a degree acceptable for high-speed flight, to eliminate premature leading-edge separation on thin airfoil sections. It is difficult to prevent inboard stall at one point on a swept wing from stalling all sections outboard of this point. Finally, it appears that separation does not account for the unstable curvature of the pitching-moment curve prior to $C_{L_{max}}$ on the twisted and cambered wing since no significant amount of flow separation is in evidence prior to $C_{L_{max}}$. A consideration of this pitching-moment behavior will be given at a later point in this paper.

From the span loading distribution shown in figure 6, obtained from integration of experimental section-pressure-distribution data, more quantitative information can be obtained. Here the spanwise variation of the effective section lift coefficients based on the velocity normal to the quarter-chord line are shown. Thus, the area under the curves is approximately twice the wing lift coefficient based on the free-stream velocity. For purposes of orientation of the loading curves with respect to stalling on the wings, a sketch of the pitching-moment variation with wing lift coefficient is also included in the figure. The symbols shown serve to orient the loading curves with respect to the stall on each wing.

The maximum section lift coefficient of the 64A010 section is of the order of 1.1 to 1.2. It will be seen that this is realized on the outboard portion of the plain wing just before initial stall, as was indicated by the force tests and the tuft studies. It is further apparent that below the point of first stall the section load distribution tends to even itself out and not attain the high tip loading predicted by theory and that, subsequent to tip stall, the loading of the inboard section rises sharply. Presumably both of these phenomena are attributable to the natural boundary-layer drainage.

It was shown in a previous paper that the $c_{l_{max}}$ of the NACA 64A810 section is about 1.7. Examination of the span loading on the twisted and cambered wing shows this section $c_{l_{max}}$ was exceeded at the 67-percent-semispan station where the first appearance of stall occurred, while sections farther inboard reached even higher values of section lift coefficient due presumably to the beneficial influence

of natural boundary-layer drainage. The possibility is suggested that a still further improvement in $C_{L_{max}}$ and associated characteristics might be attained by a design aimed specifically at securing the optimum balance between increase of the lift of the inboard sections and decrease of lift of the outboard sections due to boundary-layer drainage. A quantitative evaluation of the favorable and detrimental effects of boundary-layer behavior appears necessary, however, before rational use can be made of this phenomenon.

The results presented so far serve to show the extent to which the theoretical gains were realized, the manner in which the compromise twist affected the results, and to point to further needs for study. They do not wholly explain the gross force-test results. It is clear why the drag break was delayed and why the maximum lift coefficient was increased. The explanation of the behavior of the pitching moments, however, is more clearly shown by examination of individual section lift curves shown in figure 7.

Here again, the effective section lift coefficients normal to the quarter-chord line of the wing are shown and are plotted as a function of the angle of attack of the wing-root section for various percent semispan stations. For purposes of orientation, the wing pitching moments are also shown as a function of angle of attack at the top of the figure.

In the case of the plain wing, it is evident that the tip sections stalled at a wing angle of attack of 11.5° or a wing-lift coefficient of about 0.67. This initial stalling results in loss of section lift and a rearward shift of the center of pressure of the tip sections, and the continued increase of lift of the inboard sections previously attributed to boundary-layer drainage. At first the rearward movement of the center of pressure of the tip sections exerts the predominating influence on the pitching-moment trend of the complete wing resulting in the small stable break. As $C_{L_{max}}$ is approached, the spanwise redistribution of lift becomes more important and the inboard movement of the center of lift accounts for the unstable trend of the pitching moment.

Examination of the section lift-curve slopes for the cambered, twisted wing shows that, considerably prior to the attainment of $c_{l_{max}}$ on any section, all but the most inboard section show decreasing slopes. This decrease may be seen to be greatest for the sections near the tip. Here again it can be reasoned that boundary-layer drain is the principal cause. The thickening of the boundary layer over the trailing edge of a section is known to have an effect similar to a deflected flap. If the boundary-layer air is collecting on the upper surface, then its effect would resemble an upward deflected flap and reduce lift. This

explanation is supported by an examination of the tip-section pressure distributions which, as angle of attack is increased, assume the characteristics to be anticipated from increasing trailing-edge reflex. Inboard sections, in contrast, showed some gain from the reverse effect of boundary-layer removal. The over-all effect on the wing results in the gradually decreasing lift-curve slope and increasing positive moment (due to inboard shift of center of lift) prior to the stall.

All the data presented so far were obtained at a Reynolds number of 8 million. Data were also obtained at lower Reynolds numbers during the tests and are of interest to aid in interpretation of data from facilities where Reynolds number of tests is necessarily low. In figure 8 are shown the drag coefficient, angle of attack, and pitching-moment coefficient as a function of lift coefficient for both wing models at test Reynolds numbers of 8 and 2.5 million. As might be expected, where boundary-layer growth and flow play such an important part in the final results, the wing characteristics were markedly affected by Reynolds number. It would be concluded from this that, where twist and camber are used to control the high-lift characteristics, considerable care should be exercised in the interpretation of low Reynolds number data.

In summarizing the results of this investigation, the conclusion should not be drawn that the results obtained from these wings in any measure represent those to be expected from an optimum design. These data should be used as a guide in judging the correctness of the theories regarding the design of swept wings and in determining the next step required to refine the theory to enable selection of a better combination of wing design parameters. It seems fairly clear that the span loading theory is adequate for predicting the loading due to angle of attack or twist. Control can thus be exercised over the location of the point at which stall first appears. The section theory appears adequate to predict the first appearance of stall where this occurs away from the wing tip or root. Camber of the degree desirable on swept wings can eliminate leading-edge separation. Thus, the preliminary findings of this investigation appear encouraging. It has been demonstrated that significant gains in the low-speed performance of highly swept thin wings can be achieved by applying design principles which theory would indicate to be desirable from both a high-speed and low-speed standpoint.

There are certain phases of this program, however, that need immediate clarification before any sound judgment regarding the merits of twist and camber can be made. Such undesirable qualities as the unstable pitching moment near $C_{L_{max}}$ points to the need for further research on more optimum types of twist distributions and better mean

camber-line loadings. The wide variations in section characteristics across the span at the higher wing lift coefficients indicate a definite need for a study of the effect of boundary-layer accumulation or drain on section characteristics. And finally, the high-speed qualities of twist and camber-design combinations must be thoroughly investigated at supercritical speeds.

REFERENCES

1. DeYoung, John: Theoretical Additional Span Loading Characteristics of Wings with Arbitrary Sweep, Aspect Ratio, and Taper Ratio. NACA TN 1491, 1947.

2. Stevens, Victor I.: Theoretical Basic Span Loading Characteristics of Wings with Arbitrary Sweep, Aspect Ratio, and Taper Ratio. NACA TN 1772, 1948.

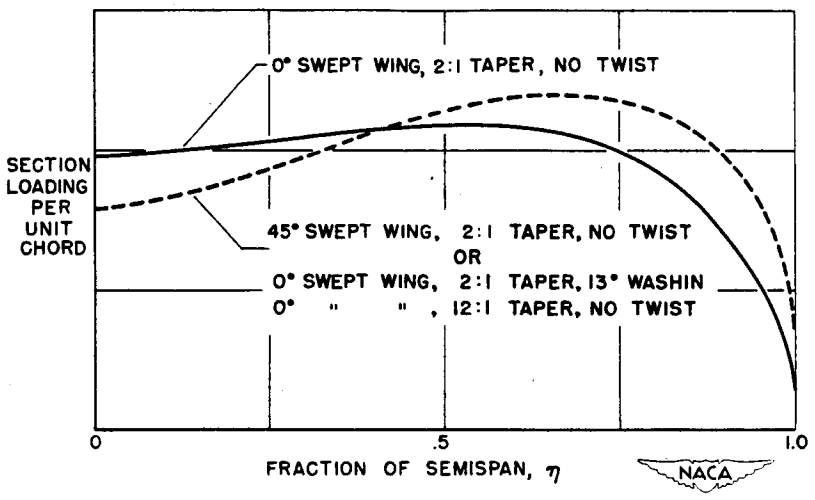


Figure 1.- The effect of wing sweep, taper, and twist on span loading.

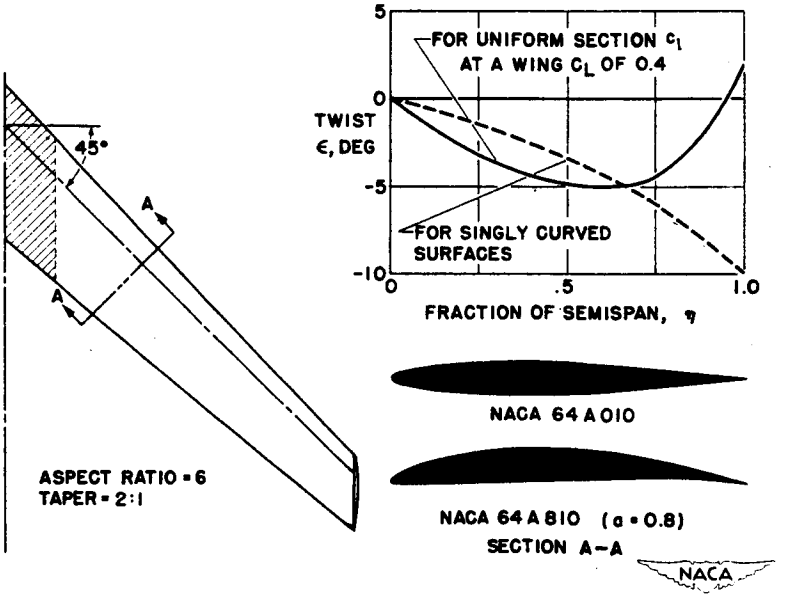


Figure 2.- Geometry of the semispan wing-fuselage models.

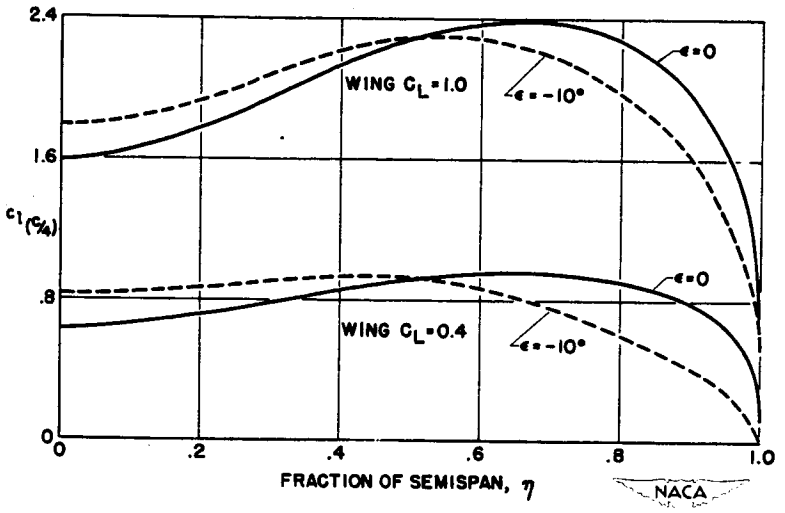


Figure 3.- The theoretical effect of modified twist on the span loading.

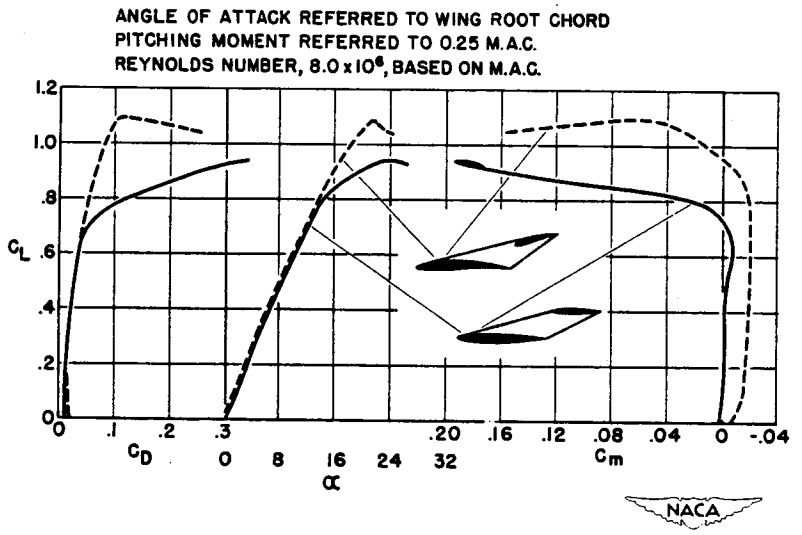


Figure 4.- The aerodynamic characteristics of the plain and the cambered, twisted wing models.

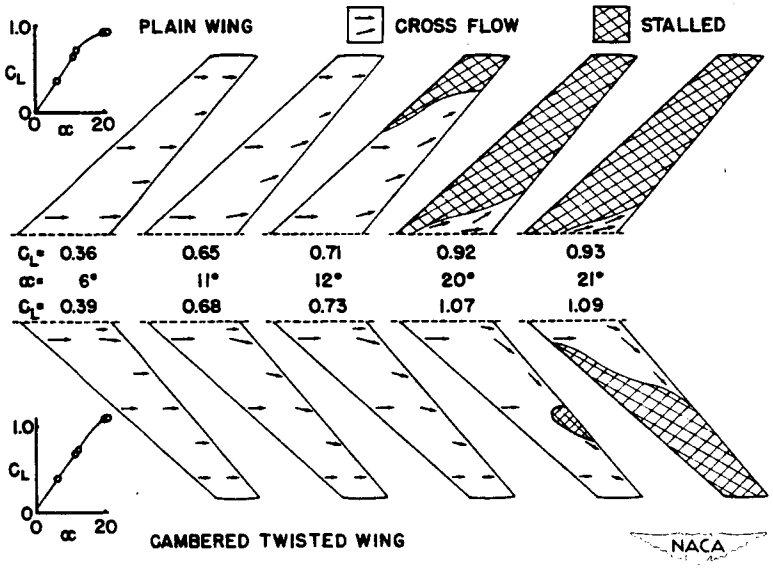


Figure 5.- Stalling pattern on the plain and on the cambered, twisted wings.

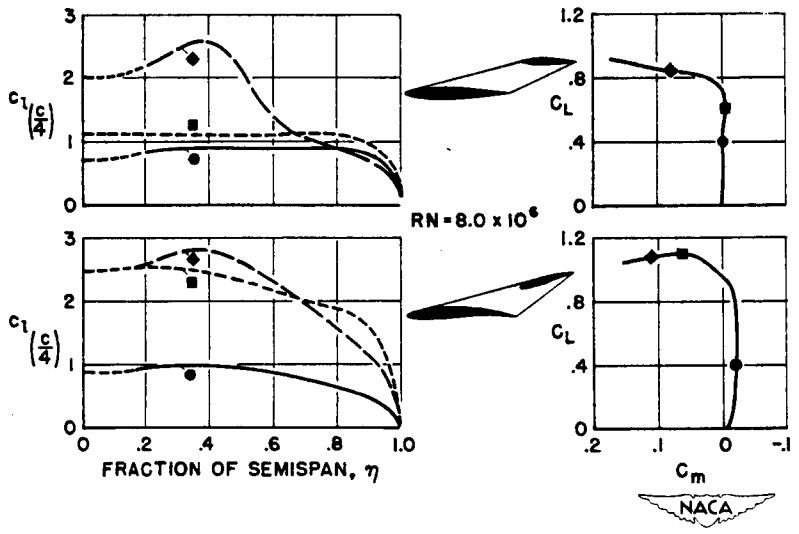


Figure 6.- Spanwise variation of the section loading for the plain and the cambered, twisted wing.

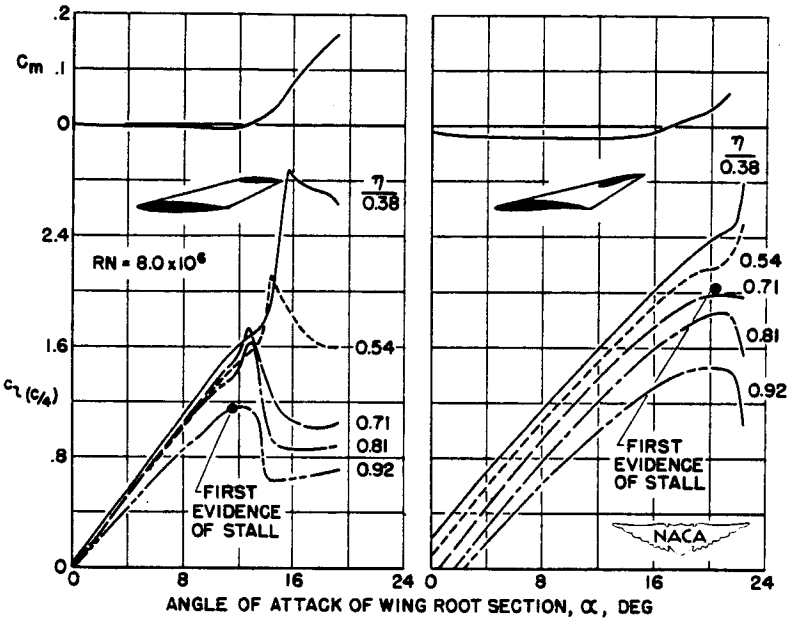


Figure 7.- Section lift characteristics for several semispan stations on the plain and the cambered, twisted wings.

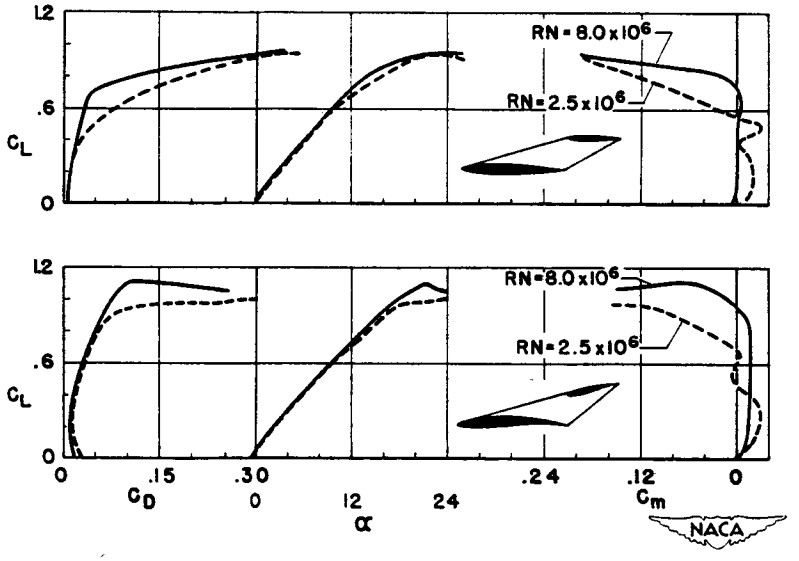


Figure 8.- Effect of Reynolds number on the aerodynamic characteristics of the plain and the cambered, twisted wings.

Preceding page blank

N65-86473

PRELIMINARY INVESTIGATIONS OF THE EFFECT OF PLAN FORM, SWEEP, AND SECTION ON THE DAMPING-IN-ROLL CHARACTERISTICS OF WINGS THROUGH THE TRANSONIC SPEED REGION

By David G. Stone and John W. McKee

Langley Aeronautical Laboratory

INTRODUCTION

For satisfactory rolling characteristics of aircraft from a Mach number less than one to a Mach number greater than one, one of the factors of importance is the dynamic stability derivative, damping in roll. In order to enable a choice of a satisfactory wing-control combination, the effects of transition from subsonic to supersonic flow on the damping in roll must be known for various wing plan forms, sweeps, and airfoil sections. Considerable progress has been achieved in the last year in determining experimentally these effects on the damping-in-roll parameter at transonic speeds. The work has been carried out through the use of different test techniques, each of which has its own limitations with regard to such items as Mach number range, Reynolds number range, and types of measurements. Some investigations have been systematic in nature and some have dealt only with isolated configurations. In such a variety of data conflicting results do occur, but definite trends are established, resulting in configurations which merit further study and those which must be avoided.

TEST METHODS

Before the experimental results are discussed, the techniques which furnished the data for the paper will be described. Figure 1 shows four of the various test arrangements with the Mach number and Reynolds number ranges listed. In the upper left-hand corner is shown the sting-mounted free-to-roll technique. The model is supported by a sting extending forward into the test section from a vertical strut which houses the balance system. Rolling-moment data with ailerons deflected are obtained from balance measurements with the sting restrained in roll. Next, the model is permitted to roll freely under the moment created by the deflected ailerons and the rate of roll recorded.

On the upper right is shown the transonic-bump twisted-semispan wing arrangement. In this technique the test wing is twisted to

provide a nearly linear variation of twist along the span corresponding to the upgoing wing panel of an airplane. A wing-tip helix angle of approximately 0.06 radian is usually simulated for a rolling wing. In some cases another identical wing which is not twisted is tested to provide a basis for determining the amount of rolling moment due to twist.

On the lower left is shown one of the rocket model techniques. The basic principle of this technique is that the model is forced to roll by a nonaerodynamic rolling moment of known magnitude which is produced by the canted-nozzle assembly, and the damping in roll is computed by balancing the moments acting on the model. Inasmuch as both the damping moment and out-of-trim moment are unknown, two conditions must be found for the same Mach number. This is accomplished by using both sustainer-on (power-on) flight and coasting flight. The measurements consist of velocity by Doppler radar and rate of roll by a spinsonde within the model.

In the lower right-hand corner is shown another rocket model technique in which the test wing is mounted on a sting in front of the vehicle proper. The entire vehicle is forced to roll by built-in incidence of the large rear stabilizing surfaces. The model is attached to a calibrated spring within the sting mount, and the deflection of this spring (the measurement of the damping moment) is telemetered to the ground. The other measurements of velocity and rate of roll are gained by the Doppler radar and spinsonde, respectively.

Other rocket-powered model techniques, not shown on the figure, gave measurements of the damping in roll. On one of these, the two wings of a cruciform arrangement were mounted on calibrated beams which gave a direct measurement of the damping moment as the vehicle was forced sinusoidally in roll by ailerons on the other two wings. Also, the damping in roll was determined for an automatically roll-stabilized, cruciform, canard configuration by the roll-response characteristics of the autopilot-airframe combination, as it was disturbed in roll by a set disturbing ailerons distinct from the control ailerons.

All the data reported in this paper are for the damping-in-roll coefficient characteristics at or near zero lift. Geometric characteristics of the various wings investigated are presented in table I.

RESULTS

Straight wings.- Figure 2 shows the results of some tests of unswept wings by the transonic-bump and the rocket torque-nozzle techniques. Note that for wing 1, aspect ratio 6, taper ratio 0.5, and

NACA 65-108 airfoil sections, an abrupt dip occurs near $M = 0.9$ and a gradual reduction of C_{l_p} through transonic speeds; whereas as for wing 2 of lower aspect ratio (4), taper ratio 0.6, and NACA 65A006 airfoil sections no dip occurs, only the gradual reduction at transonic speeds. For the rocket tests (wing 3) two thicknesses are shown, NACA 65A006 airfoil and NACA 65A009 airfoil, for aspect ratio 3.71 and no taper (reference 1). These wings show lower values of C_{l_p} at transonic speeds, and at supersonic speeds the thinner wing has a greater value of C_{l_p}. These data are compared with theory (references 2, 3, and 4) and show theoretical values of C_{l_p} to be slightly less at subsonic speeds and greater at supersonic speeds. In general, for these aspect ratios, taper ratios, and thicknesses, an average value of $C_{l_p} = -0.4$ is indicated for straight wings at transonic speeds.

Swept wings.- Figure 3 shows the results of some tests of sweptback wings by the transonic-bump, sting-mounted free-to-roll, and the rocket torque-nozzle techniques. For wing 4, aspect ratio 4, taper ratio 0.6, and NACA 65A006 airfoil sections, a gradual decrease in C_{l_p} occurs through transonic speeds from a peak value of -0.37 to -0.28. Also, a wing of 35° sweep, aspect ratio 3, and 10.5 percent thick is shown for comparison at subsonic speeds. For this wing (wing 5) the subsonic value of C_{l_p} is slightly lower than wing 4. Also shown are the results from rocket tests of a nontapered 45° sweptback wing of aspect ratio 3.71. For this wing (wing 6) the damping appears lower than might be expected; consequently, an analytical check was made of the effect of torsional stiffness. Knowing the stiffness characteristics of the test wing and assumptions for the aerodynamic-center and elastic-axis relative locations, it was found that the C_{l_p} might be 17 percent higher at $M = 1.3$ and only 9 percent greater at $M = 0.9$ for a rigid wing. In general, for these swept wings of low aspect ratios, lower values of C_{l_p} are indicated at supersonic speeds than at subsonic speeds, no abrupt changes in C_{l_p} occur through transonic speeds, and C_{l_p} values compare favorably with theoretical values (reference 2) at subsonic speeds.

Shown in figure 4 is the effect of trailing-edge contour modification on the damping-in-roll characteristics of a sweptback wing (reference 5). This wing (wing 7) of 40° sweep, aspect ratio 4, taper ratio 0.5, and of 10-percent-thick circular-arc airfoil section perpendicular to the 50-percent-chord line had the trailing edge of the half-span aileron built up to one-half the thickness of the section at the 80-percent-wing-chord line. Note that the effect of thickening

the trailing edge is to change the reduction of C_{l_p} near $M = 0.9$ to an increase in C_{l_p}, making C_{l_p} considerably greater at $M = 0.925$ for the thickened trailing edge, and also note that the modified section has greater values of C_{l_p} throughout. These effects are probably due to separation on the normal-contour wing near the 80-percent-chord line, whereas the thickened trailing edge tends to fill up the region of separation or reduced pressure gradient and thus prevent or delay separation. Also, additional tests on the bump gave a larger lift-curve slope for the thickened trailing edge than the normal-contour sections. Shown in the figure is an additional curve for a larger sting-mounted free-roll model with the thickened trailing edge which corroborates the data from the bump at subsonic speeds.

A summary of the effect of sweep on damping in roll for wings of aspect ratio 4, taper ratio 0.6, and NACA 65A006 airfoil sections is shown in figure 5. Three wings of 0°, 35°, and 45° sweep of the quarter-chord line were tested by the transonic-bump and sting-mounted techniques. From these results it may be seen that at a sweep angle of 30° a gradual but small reduction in C_{l_p} begins for subsonic and transonic speeds. At supersonic speeds the effect of sweepback is more noticeable in that the gradual reduction in C_{l_p} is evident at small sweep angles. In general, the results indicate that the damping in roll for swept wings is slightly lower than for corresponding straight wings.

Delta wings.- Figure 6 presents the damping-in-roll characteristics of two delta wings of 45° leading-edge sweepback (wing 8) by the sting-mounted, forced-roll, rocket-powered, vehicle technique. Here, the detrimental effect of thickness is shown by these tests of two identical models except in maximum thickness of wedge section at the 50-percent-chord line. Note the large reduction in C_{l_p} for the 9-percent-thick wing near $M = 0.95$ and the gain back to the subsonic C_{l_p} values at supersonic speeds as compared with the 4-percent-thick wing, which shows a gradual rise of C_{l_p} up to $M = 1.0$, the sudden drop to the subsonic values of C_{l_p} at supersonic speeds. Also, as was the case with the other wings, the thinner wing possesses higher values of C_{l_p} at supersonic speeds. The comparison with theory (references 3 and 6) is again made and shows a favorable comparison at subsonic speeds and experimental values at supersonic speeds to be less than theory, as would be expected due to thickness.

The damping-in-roll characteristics of a 60° delta wing for various wing-body arrangements and rocket test techniques are shown in figure 7. This delta wing of 60° sweepback (wing 9) has a flat-sided or hexagonal section of constant thickness which corresponded to

a thickness ratio of 3 percent at the wing-body root, varying to 9 percent at the tip end of the flat-sided portion. In all the models the relation between wing span to body diameter was constant. The solid line shows the C_{l_p} values obtained from the forced oscillation technique where the rolling moment of one set of the cruciform wings is recorded directly (reference 7). The long dashed line shows the results from the torque-nozzle technique with a 3-wing arrangement of the wings. Note the close agreement for these two tests except between $M = 0.9$ to 0.95. Adequate reasons for this discrepancy have not yet been determined as this may be a rate-of-roll effect or number-of-wing effect. Also, shown are C_{l_p} values obtained from a roll-stabilized, cruciform, canard, missile configuration which utilized these wings (reference 8). Again good agreement is shown in that the missile with the canard surfaces gave C_{l_p} values above and comparable to the other techniques. The fact that the C_{l_p} values from the autostabilized model gives this agreement confirms the damping in roll measured by the other rocket techniques to be the values actually experienced by stabilized missiles. Inasmuch as the values of the tip helix angle $\frac{pb}{2V}$ varied from less than 0.01 radian to more than 0.06 radian for the various rocket models C_{l_p} is indicated to be linear with $\frac{pb}{2V}$ at supersonic speeds. Comparison with theory (reference 3) is good at subsonic speed, but experimental values of C_{l_p} are approximately 75 percent of theoretical values (reference 6) at supersonic speeds. In comparing the 60° delta wing with the 45° delta wing, it may be noted that C_{l_p} of the 60° delta is approximately 20 percent lower at subsonic and supersonic speeds.

CONCLUDING REMARKS

In conclusion the following remarks may be made concerning the preliminary results of damping-in-roll investigations at zero angle of attack:

1. Increasing the thickness has a detrimental effect on the variation of the damping-in-roll characteristics through transonic speeds for straight, swept, and delta wings.

2. Effect of sweep on a wing of aspect ratio 4 tapered 0.6 is a small reduction in C_{l_p}.

3. Of the wings tested, none show a complete loss of C_{l_p} through transonic speeds.

REFERENCES

1. Edmondson, James L., and Sanders, E. Claude, Jr.: A Free-Flight Technique for Measuring Damping in Roll by Use of Rocket-Powered Models and Some Initial Results for Rectangular Wings. NACA RM L9I01, 1949. (Prospective NACA paper)

2. Bird, John D.: Some Theoretical Low-Speed Span Loading Characteristics of Swept Wings in Roll and Sideslip. NACA TN 1839, 1949.

3. Polhamus, Edward C.: A Simple Method of Estimating the Subsonic Lift and Damping in Roll of Sweptback Wings. NACA TN 1862, 1949.

4. Harmon, Sidney M.: Stability Derivatives of Thin Rectangular Wings at Supersonic Speeds. Wing Diagonals Ahead of Tip Mach Lines. NACA TN 1706, 1948.

5. Lockwood, Vernard E.: Damping-in-Roll Characteristics of a 42.7° Sweptback Wing as Determined from a Wind-Tunnel Investigation of a Twisted Semispan Wing. NACA RM L9F15, 1949.

6. Brown, Clinton E., and Adams, Mac C.: Damping in Pitch and Roll of Triangular Wings at Supersonic Speeds. NACA Rep. 892, 1948.

7. Martz, C. William, and Church, James D.: Flight Investigation at Subsonic, Transonic, and Supersonic Velocities of the Hinge-Moment Characteristics, Lateral Effectiveness, and Wing Damping in Roll of a 60° Sweptback Delta Wing with Half-Delta Tip Ailerons. (Prospective NACA paper)

8. Gardiner, Robert A., and Zarovsky, Jacob: Rocket-Powered Flight Test of a Roll-Stabilized Supersonic Missile Configuration. (Prospective NACA paper)

[redacted]

TABLE I.- WING DIMENSIONAL CHARACTERISTICS

Wing	Aspect ratio	Taper ratio	Sweep	Airfoil section
Straight wings:				
1	6	0.5	2° of c/4 line	NACA 65-108
2	4	.6	0° of c/4 line	NACA 65A006
3	3.71	1.0	0°	NACA 65A006 NACA 65A009
Swept wings:				
4	4.0	0.6	45° of c/4 line	NACA 65A006
5	3.0	.6	35° of c/4 line	Symmetrical $\frac{t}{c} = 0.105$
6	3.71	1.0	45°	NACA 65A009
7	4.0	.5	40° of c/4 line	Circular-arc $\frac{t}{c} = 0.105$
Delta wings:				
8	4.0	0	45° of L.E.	Wedge $\frac{t}{c} = 0.04$ $\frac{t}{c} = 0.09$
9	2.31	0	60° of L.E.	Hexagonal root $\frac{t}{c} = 0.03$ tip $\frac{t}{c} = 0.09$

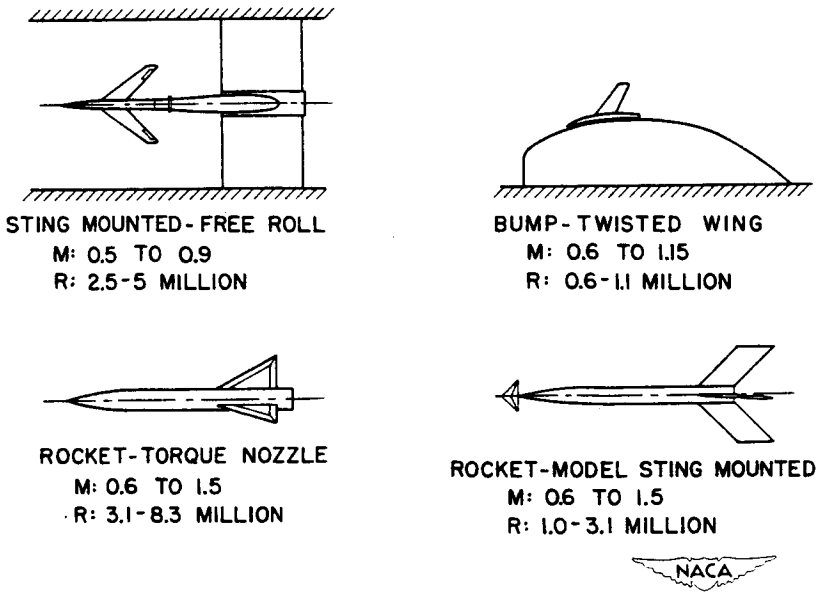


Figure 1.– Various NACA test arrangements used in determining the damping-in-roll characteristics of various wings at transonic speeds.

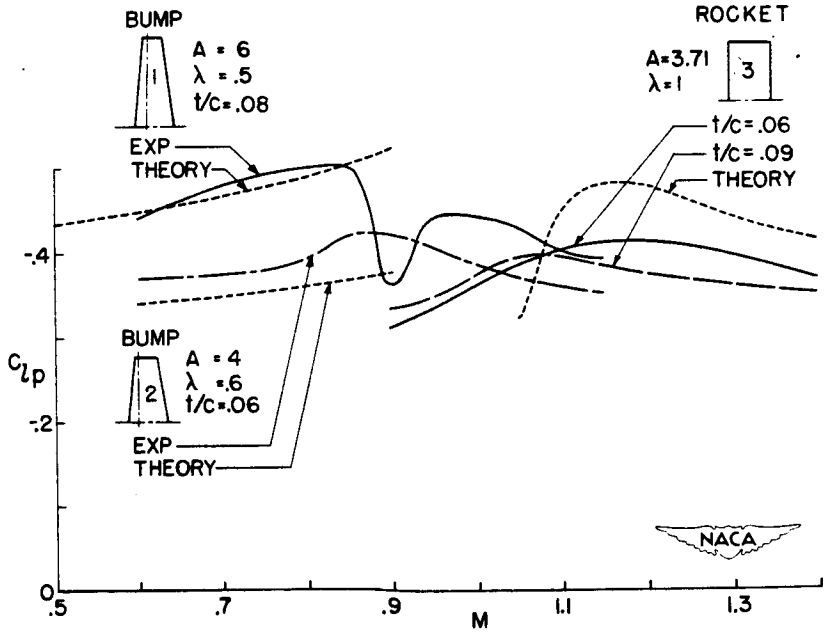


Figure 2.– Damping-in-roll characteristics of some straight wings of various aspect ratios, and thicknesses.

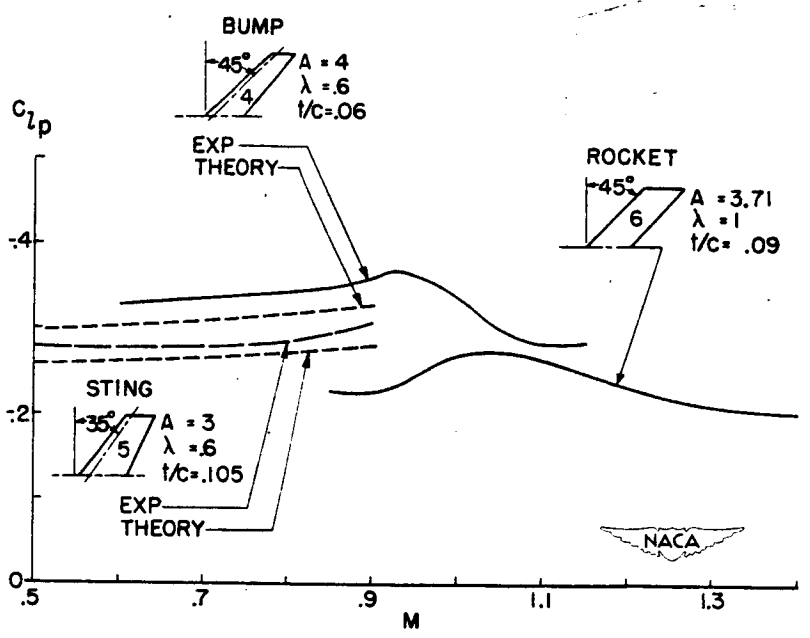


Figure 3.- Damping-in-roll characteristics of some sweptback wings of various aspect ratios, taper ratios, and thicknesses.

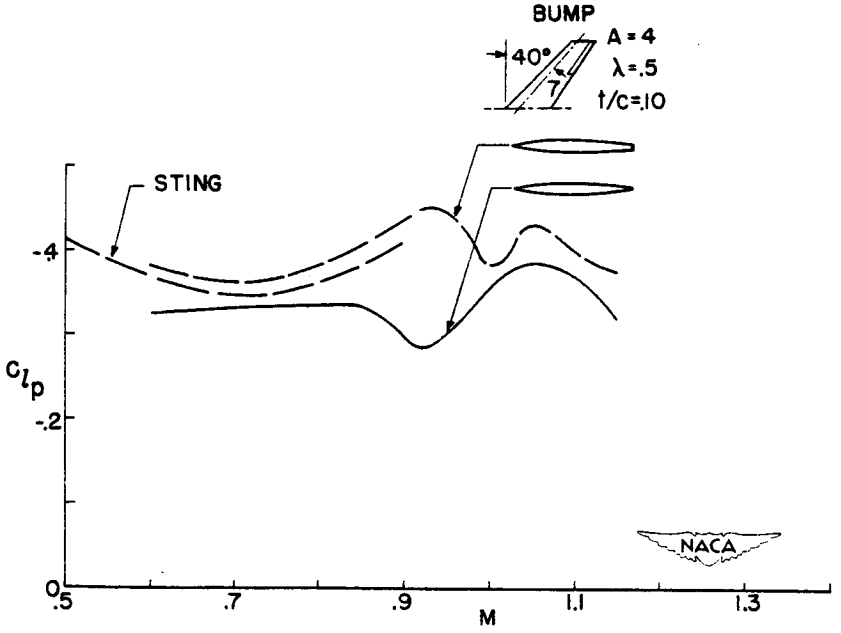


Figure 4.- Effect of thickening the aileron trailing edge on the damping-in-roll characteristics of a sweptback wing.

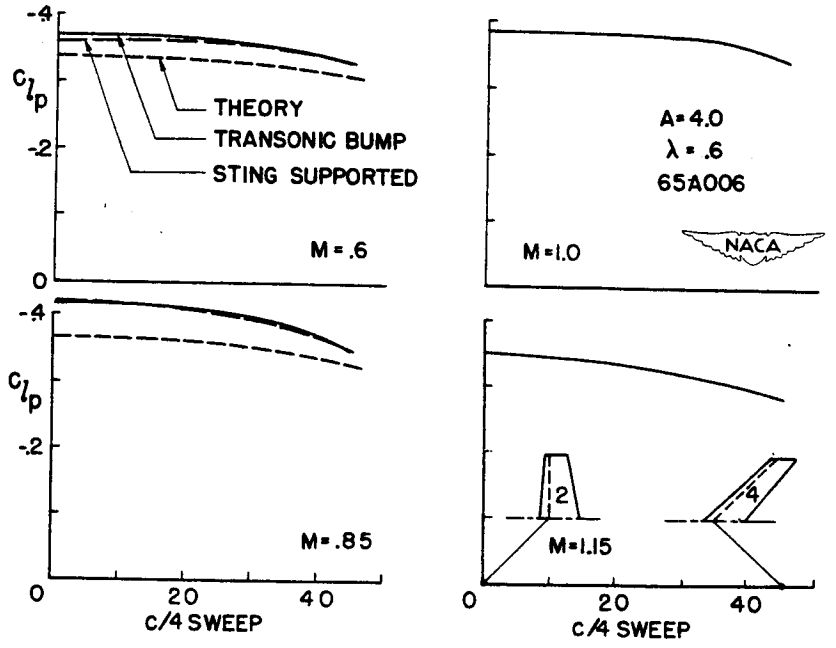


Figure 5.– Summary of the effect of sweepback on the damping–in–roll characteristics of wings of aspect ratio 4, taper ratio 0.6, and NACA 65A006 airfoil sections.

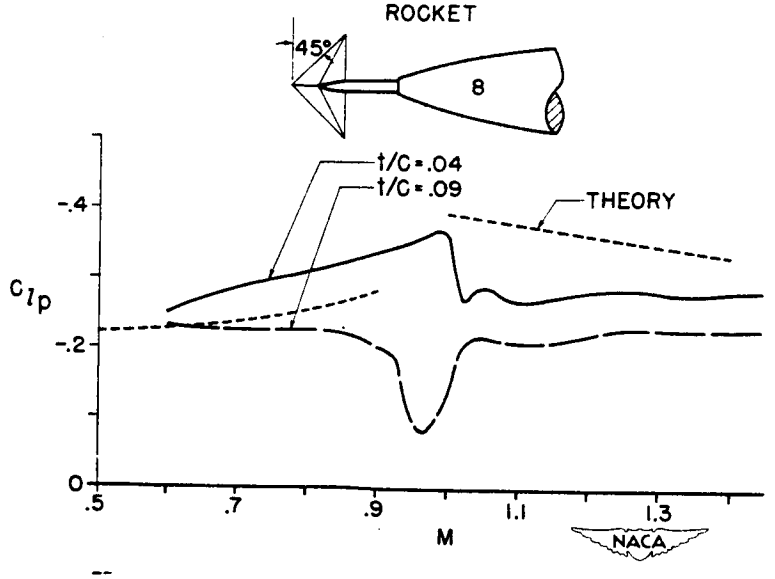


Figure 6.– Damping–in–roll characteristics of a 45° delta wing with thickness ratios of 4 percent and 9 percent.

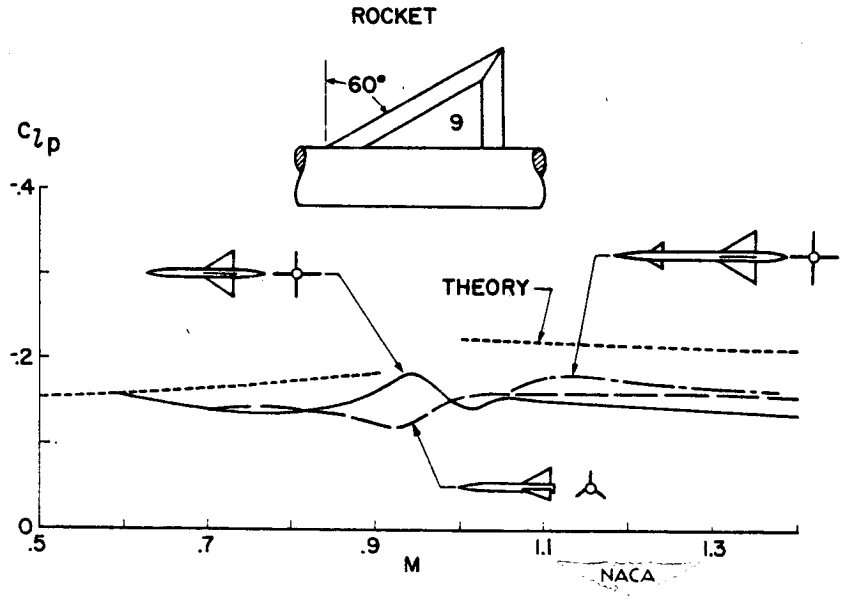


Figure 7.– Damping–in–roll characteristics of a 60° delta wing for various wing–body arrangements.

[redacted]page blank

N65-86474

CONTROL-SURFACE CHARACTERISTICS AT TRANSONIC SPEEDS

By John G. Lowry and Carl A. Sandahl

Langley Aeronautical Laboratory

INTRODUCTION

At the NACA Conference on Aerodynamic Problems of Transonic Airplane Design, November 1947, a method for predicting the effectiveness of controls on swept wings at low speeds was presented (references 1 and 2). By using this method (reference 2) it is possible to predict the effectiveness at low speeds of flap-type controls on swept wings. In addition, a theoretical method (reference 3) for prediction of control hinge moments has been made available.

The picture at transonic speeds is not so clear. Despite a concerted effort on the part of the NACA, there are still too few data available to formulate rational design procedures. It will be our purpose, therefore, to discuss the effects of certain variables pertinent to the design of controls rather than to attempt to present design procedures.

The data which will be presented have been selected because of their systematic nature and have been obtained from several sources; namely, the conventional wind tunnels, wing-flow technique, transonic-bump technique, and rocket-powered test vehicles. Since experience has shown that, for Mach numbers below 0.6, low-speed design procedures are satisfactory in most cases, in the present paper the discussion will be limited to the transonic speed range.

FLAP-TYPE CONTROLS ON SWEPT WINGS

Recently a systematic series of wings was investigated by the bump technique (references 4 to 8) and a few of the same configurations were studied using the rocket-model technique (reference 9). In figure 1 is shown the effect of sweep on the aileron effectiveness for a series of wings with a 30-percent-chord full-span aileron. The wings were all of aspect ratio 4, taper ratio 0.6, and had NACA 65A006 airfoil sections parallel to the free-stream direction. The aileron effectiveness C_{l_δ} as a function of Mach number is presented for wings having 0°, 35°, 45°, and 60° sweep of the quarter-chord line. For this plot the aileron deflection was taken normal to the hinge line. Only the results for the full-span aileron are shown; the other aileron

[redacted]

spans investigated show similar trends with sweep and Mach number. It can be seen that the effectiveness in the subsonic range decreases with sweep to a marked degree; this effect was discussed in detail at the transonic conference in 1947 (references 1 and 2). All the configurations suffered a loss in effectiveness near the speed of sound - the loss, however, decreased as the sweep was increased. In addition, the Mach number at which the effectiveness decreased was increased with increasing sweep. These results are similar to those obtained previously in rocket tests (reference 10).

There has been considerable discussion in the last year pertaining to the spanwise location of an aileron on a sweptback wing that will produce the greatest effectiveness for a given aileron span. At the last transonic conference in 1947 it was pointed out that, at subsonic speeds, the effectiveness of outboard ailerons relative to that of the inboard ailerons was decreased as the wing sweepback was increased. This effect has also been noted in rocket tests at transonic and moderate supersonic speeds (reference 11). Recently tests have been made by means of the transonic-bump technique which provide further information on this subject. Some of the bump results are shown in figure 2.

In figure 2 is shown the effect of aileron span and spanwise location for two of the wing configurations shown in figure 1. The wings have an aspect ratio of 4, a taper ratio of 0.6, and a thickness ratio of 0.06. The aileron chord is 30 percent of the wing chord. Again the aileron effectiveness C_{l_δ} is given as a function of Mach number for four aileron configurations on both the 0° and 60° swept wings. The aileron spans shown are the outboard quarter-span, the outboard half-span, the inboard half-span, and the full span. For the unswept wing, the outboard quarter-span aileron is about one-half as effective as the outboard half-span aileron. The outboard half-span aileron is about two-thirds as effective as the full-span aileron. The inboard half-span aileron is only about two-thirds as effective as the outboard half-span aileron. This is the variation that would be expected on the basis of subsonic experience (references 2 and 12). For the 60° wing the effectiveness of the outboard quarter-span aileron is very low - only about one-third of that of the outboard half-span aileron. It will also be noted that the inboard half-span aileron is more powerful than the outboard half-span. These results indicate that, to a rough approximation, the variation of the effectiveness of the partial-span ailerons with spanwise location as predicted for low speeds for sweptback wings (reference 1) holds throughout the transonic speed range. These effects must, however, be combined with the aeroelastic properties of the wing and control under consideration to determine the optimum aileron span and location. The results which have been presented are for essentially infinitely rigid wings.

The results thus far discussed were all obtained from transonic-bump tests. In order to indicate the reliability of these data, a comparison of the rolling-effectiveness parameter $\frac{pb/2V}{\delta}$ calculated from transonic-bump measurements with measurements obtained at higher Reynolds numbers by means of rocket-propelled test vehicles (reference 9) is shown in figure 3. In obtaining the bump results the appropriate values of C_{l_δ} shown in the preceding figures were combined with values of C_{l_p} obtained in bump tests utilizing the twisted-wing technique. The rocket results were obtained with free-rolling models having fixed aileron deflections. Fairly good agreement has been obtained between the bump and the rocket results for the 35° sweptback wing. The agreement for the 45° sweptback wing, however, is poor. A possible explanation for this lack of agreement has become apparent from very recent measurements of the damping in roll of wings having deflected flaps. These results show that the variation of C_{l_p} with Mach number at high subsonic and transonic speeds is affected by flap deflection, particularly as the wing sweep is increased. Inasmuch as the bump rolling-effectiveness values shown in this figure were obtained by using values of C_{l_p} measured for a wing with undeflected flaps, the differences noted for the more highly swept wing are to be expected. Work is now underway to determine the damping in roll of the 45° swept wing with flaps deflected. It is anticipated that these measurements will improve the agreement for the 45° swept wing.

At low subsonic speeds the manner in which the chord of a control changes its effectiveness is very well known (references 1 and 13). In order to study the effects of control chord at transonic speeds, an investigation was made of controls having several chord ratios on an aspect-ratio-2.5, unswept, 6-percent-thick wing by means of the transonic bump (references 14 and 15). Figure 4 shows the variation of aileron effectiveness C_{l_δ} with Mach number for controls having chords equal to 25, 35, and 45 percent of the wing chord. The aileron had a span of 50 percent of the wing semispan. The variation of C_{l_δ} at a Mach number of 0.6 is about as would be expected from low-speed calculations (references 1 and 13). The increase in control effectiveness with increased chord becomes larger as the Mach number is increased to about 0.9. Above $M = 0.9$ the effectiveness of all the flap chords investigated falls off with increasing Mach number. The 45-percent-chord flap loses only about one-fourth of its low-speed effectiveness at Mach number of about 1.15, whereas the 25-percent-chord flap loses about one-half of its low-speed effectiveness. These results indicate that increasing the chord of a control will be beneficial from the effectiveness point of view in the transonic range; however, considerations of control hinge moment and wing twist will limit the control chord for any particular configuration.

Previous investigations by both the bump and rocket techniques (references 16, 17, 18, and 19) have indicated that the shape of the rearward part of the airfoil section and particularly the trailing-edge angle has an important effect on the effectiveness of plain flap-type controls at transonic speeds. In general, previous work has shown that the effectiveness of plain flaps was seriously impaired or even reversed for certain airfoil sections which had trailing-edge angles on the order of 20°. It has also shown that the reversal could generally be eliminated by reducing the trailing-edge angle to about 12°. In an effort to investigate this behavior and in particular to establish, if possible, a maximum usable trailing-edge angle, an investigation (reference 20) was made utilizing the family of sections shown in figure 5. The various sections, all of which had a thickness ratio of 0.06, were obtained from the basic symmetrical circular-arc section by introducing parallel flat sections beginning at the 50-percent-chord point and terminating at 60, 70, and 80 percent of the chord. The remaining rearward portions of the sections were formed by circular arcs which were tangent to the end of the flat sections, this process resulting in the trailing-edge angles listed. The forward 50 percent of the sections was identical to that of the basic symmetrical circular-arc section. The results, which were obtained by means of free-roll rocket-test vehicles, are shown on the lower part of the chart as curves of $\frac{pb}{2V}$ against M for 5° aileron deflection measured in the free-stream direction.

For the unswept wing, increasing the trailing-edge angle lowers the Mach number at which loss of effectiveness occurs and up to $\phi = 23°$ reduces the minimum effectiveness at transonic speeds. Further increase in ϕ to 34° resulted in an increase of the minimum transonic effectiveness. At the higher supersonic Mach numbers investigated the effectiveness is relatively independent of ϕ for the values investigated.

The results obtained with the sweptback wing are, in general, similar to those obtained with the straight wing. At subsonic speeds the loss of effectiveness obtained with increasing values of trailing-edge angle is increased. At supersonic speeds increasing ϕ from 14° to 23° resulted in a large decrease in effectiveness. Further increase in ϕ increased the effectiveness at supersonic speeds. The results of these tests indicate that the trailing-edge angle of a plain flap should not exceed 14° and should probably be less.

Some additional results obtained by means of wing-flow tests (reference 21) relating to the effects of trailing-edge angle are shown in figure 6. The wing tested had NACA 65-009 airfoil sections normal to the leading edge and was of aspect ratio 3. Three 0.2-chord aileron configurations were tested: an unsealed true-contour aileron,

an unsealed aileron with a 23° bevel, and a sealed aileron with a 23° bevel. The Reynolds number was about 1.0×10^6 at a Mach number of 1. The results are plotted as curves of lift effectiveness C_{L_δ} and hinge-moment coefficient C_{h_δ} as functions of Mach number. Comparing the results for the first two configurations shows that the bevel produced a bucket in the effectiveness curve and substantially reduced the hinge moments up to a Mach number of about 0.96. It will be noted that the balancing effect of the bevel is lost as the effectiveness is regained at Mach numbers above 0.96. Sealing the gap of the beveled aileron increased the effectiveness and increased the Mach number range over which the bucket in the effectiveness curve occurs. The seal also preserves the balancing effect of the bevel to a higher Mach number.

A method which has been used to reduce the loss of effectiveness at transonic speeds characteristic of plain flaps having large trailing-edge angles consists of modifying the aileron contour as shown in figure 7. Previous work (see references 16, 17, and 18) has shown that these aileron modifications can eliminate the reversal of effectiveness which was obtained with the original true-contour ailerons of this configuration at transonic speeds. The effects of these modifications on the hinge-moment characteristics are shown on the lower part of the figure as curves of C_{h_δ} and C_{h_α} against Mach number. Referring to the curves of C_{h_δ} it will be noted that the true-contour ailerons, which had a trailing-edge angle of 20°, were slightly underbalanced up to a Mach number of 0.9. In the Mach number range from 0.9 to slightly over 1.0 the true-contour ailerons became strongly overbalanced. The effectiveness, not shown here, also reversed in the same Mach number range. Increasing the trailing-edge thickness eliminated the reversal of effectiveness and increased the hinge moments markedly. The same trends are shown in the C_{h_α} curves on the right-hand side of the figure. This work is reported in reference 22.

SPOILER CONTROLS ON SWEPT WINGS

The loss in effectiveness associated with some flap-type controls at transonic speeds has led to investigations of other types of controls (see, for example, reference 16). One control that has shown promise is the spoiler (references 23 to 28). In figure 8 are shown some results of tests (reference 8) of a spoiler on a 60° sweptback wing having an aspect ratio of 2, a taper ratio of 0.6, and NACA 65A006 airfoil sections. The spoilers were located along the wing 70-percent-chord line and had a projection of 5 percent of the wing chord. This

chart shows the rolling moment produced by the spoilers as a function of Mach number for four spoiler-span configurations. The span configurations are the same as those presented previously for the flap-type control; that is, full-span control, outboard half-span control, inboard half-span control, and outboard quarter-span control. In general, the same variation of effectiveness of the partial-span spoilers with spanwise location is shown as for the partial-span flap-type controls on a 60° swept wing discussed previously. That is, the outboard quarter-span control showed little or no effectiveness, whereas the inboard half-span control was more effective than the comparable outboard control. A striking difference in shape of curves from those for flap-type controls is immediately noticeable in that the spoilers are more effective near Mach number of 1 than at low subsonic Mach numbers; in fact, throughout the speed range tested, the effectiveness is never below that at $M = 0.6$. In addition to the increase in effectiveness, preliminary studies have shown that the twisting moment about the wing 35-percent-chord station is only about one-fifth as great as for a conventional aileron giving the same rolling moment.

A question is usually raised regarding the variation of effectiveness with projection for small projections. No data are available for this particular wing, but data at high subsonic and transonic speeds for an unswept wing (reference 24) and for swept wings (references 16 and 26) show a very nearly linear variation of rolling moment with projection. Based on these results, it would appear that linear effectiveness with deflection can be obtained with a spoiler without a loss in effectiveness at transonic speeds and with less adverse wing twist than given by flap-type controls. In addition, spoiler configurations can be made which will have very low hinge moments. On the basis of these considerations, it appears that spoilers warrant further investigation.

CONTROLS ON DELTA WINGS

Of the several wing configurations proposed for transonic and supersonic flight, the delta wing has certain advantages. In order to provide information relating to the effectiveness of controls on delta wings, tests have been made of the configurations shown in figure 9 by means of free-roll rocket-propelled test vehicles. The ratio of control area to exposed wing area was 0.2 for the three configurations. The control deflection was measured in the free-stream direction. The controls tested included a plain flap, a full-delta flap with the hinge line swept 60° and a half-delta flap with the hinge line passing through the centroid of the control area. The results are presented as curves of $\frac{pb/2V}{\delta}$ against Mach number. The plain flap had the

highest subsonic effectiveness and the lowest supersonic effectiveness. The experimental values are considerably lower than those calculated by means of the linearized-supersonic-flow equations. The delta ailerons have higher supersonic effectiveness and a smaller variation of effectiveness over the Mach number range investigated. The good agreement with theory which is obtained is probably fortuitous inasmuch as other work has shown that both the theoretical C_{l_δ} and C_{l_p} are higher than experimental values by roughly the same factor. This work is reported in reference 29.

The hinge-moment characteristics of configurations similar to those just discussed are presented in figure 10 as curves of C_{h_α} and C_{h_δ} as functions of Mach number. Results are presented for a plain flap, a full-delta control with and without aerodynamic balance and a half-delta control with the hinge line located at 64 percent of the aileron root chord. The parameter C_{h_δ} was obtained by considering the control deflection measured in the free-stream direction. The hinge-moment coefficient of the plain flap increased rapidly with increasing Mach number up to 1.0. The hinge moments of the unbalanced full-delta flaps are high and are relatively constant. The results for the balanced full-delta flap indicate that this arrangement was slightly overbalanced and show that this type of flap can be closely balanced. The results for the half-delta flap indicate that this configuration was slightly overbalanced up to a Mach number of about 0.9. Above a Mach number of 0.9 the hinge moment was substantially zero. By suitable location of the hinge axis, this control could be closely balanced over the entire speed range. These results are reported in references 30, 31, 32, and 33.

SUMMARY

To summarize then, we have presented recent additional experimental results showing that increasing wing sweep decreases control effectiveness and reduces the loss of effectiveness at transonic speeds. For both flap and spoiler-type controls of partial span the optimum spanwise location, neglecting wing-twist considerations, moves inboard from the wing tip as the wing sweep is increased. The control effectiveness increases with increased chord. The loss of control effectiveness at transonic speeds due to large trailing-edge angles has been discussed and the hinge-moment characteristics of several aileron modifications which eliminate the control reversal have been given. The effectiveness and hinge-moment characteristics of several controls suitable for delta wings have also been discussed.

REFERENCES

1. Lowry, John G., Axelson, John A., and Johnson, Harold I.: Effects of Sweep on Controls. NACA RM L8A28c, 1948.

2. Lowry, John G., and Schneiter, Leslie E.: Estimation of Effectiveness of Flap-Type Controls on Sweptback Wings. NACA TN 1674, 1948.

3. Toll, Thomas A., and Schneiter, Leslie E.: Approximate Relations for Hinge-Moment Parameters of Control Surfaces on Swept Wings at Low Mach Numbers. NACA TN 1711, 1948.

4. Hammond, Alexander D.: Lateral-Control Investigation of Flap-Type Controls on a Wing with Quarter-Chord Line Swept Back 0°, Aspect Ratio 4, Taper Ratio 0.6, and NACA 65A006 Airfoil Section. Transonic-Bump Method. (Prospective NACA paper)

5. Thompson, Robert F.: Lateral-Control Investigation of Flap-Type Controls on a Wing with Quarter-Chord Line Swept Back 35°, Aspect Ratio 4, Taper Ratio 0.6, and NACA 65A006 Airfoil Section. Transonic-Bump Method. (Prospective NACA paper)

6. Vogler, Raymond D.: Lateral-Control Investigation of Flap-Type Controls on a Wing with Quarter-Chord Line Swept Back 45°, Aspect Ratio 4, Taper Ratio 0.6, and NACA 65A006 Airfoil Section. Transonic-Bump Method. NACA RM L9F29a, 1949.

7. Vogler, Raymond D.: Lateral-Control Investigation of Flap-Type Controls on a Wing with Quarter-Chord Line Swept Back 60°, Aspect Ratio 4, Taper Ratio 0.6, and NACA 65A006 Airfoil Section. Transonic-Bump Method. (Prospective NACA paper)

8. Hammond, Alexander D.: Lateral-Control Investigation of Flap-Type and Spoiler-Type Controls on a Wing with Quarter-Chord Line Swept Back 60°, Aspect Ratio 2, Taper Ratio 0.6, and NACA 65A006 Airfoil Section. Transonic-Bump Method. (Prospective NACA paper)

9. Strass, H. Kurt, Fields, Edison M., and Schult, Eugene D.: Investigation of the Rolling Effectiveness of Flap-Type Controls on a Wing with Quarter-Chord Line Swept Back 45°, Aspect Ratio 4, Taper Ratio 0.6, and NACA 65A006 Airfoil Section as Obtained at Transonic and Supersonic Speeds in Free Flight. (Prospective NACA paper)

10. Sandahl, Carl A., and Strass, H. Kurt: Additional Results in a Free-Flight Investigation of Control Effectiveness of Full-Span 0.2-Chord Plain Ailerons at High-Subsonic, Transonic, and Supersonic Speeds to Determine Some Effects of Wing Sweepback, Aspect Ratio, Taper, and Section Thickness Ratio. [redacted]1, 1948.

11. Strass, H. Kurt, and Fields, Edison M.: The Variation of the Rolling Effectiveness with Aileron Span on Untapered Wings of 0° and 45° Sweepback as Determined in Free Flight at Transonic and Supersonic Speeds. (Prospective NACA paper)

12. Weick, Fred E., and Jones, Robert T.: Résumé and Analysis of NACA Lateral Control Research. NACA Rep. 605, 1937.

13. Langley Research Staff (Compiled by Thomas A. Toll): Summary of Lateral-Control Research. NACA Rep. 868, 1947.

14. Turner, Thomas R., and Fikes, Joseph E.: Lateral-Control Investigation at Transonic Speeds of a 35-Percent-Chord Flap on a Tapered Wedge-Type Wing of Aspect Ratio 2.5. (Prospective NACA paper)

15. Turner, Thomas R., and Lockwood, Vernard E.: The Effect of Flap Chord on the Control Characteristics of Several Wings at Transonic Speeds. (Prospective NACA paper)

16. Turner, Thomas R., Lockwood, Vernard E., and Vogler, Raymond D.: Preliminary Investigation of Various Ailerons on a 42° Sweptback Wing for Lateral Control at Transonic Speeds. NACA RM L8D21, 1948.

17. Turner, Thomas R., Lockwood, Vernard E., and Vogler, Raymond D.: Aerodynamic Characteristics at Supersonic and Transonic Speeds of a 42.7° Sweptback Wing Model Having an Aileron with Finite Trailing-Edge Thickness. NACA RM L8K02, 1949.

18. Sandahl, Carl A.: Free-Flight Investigation at Transonic and Supersonic Speeds of the Rolling Effectiveness of Several Aileron Configurations on a Tapered Wing having 42.7° Sweepback. NACA RM L8K23, 1949.

19. Sandahl, Carl A., Bland, William M., Jr., and Strass, H. Kurt: Effects of Some Airfoil-Section Variations on Wing-Aileron Rolling Effectiveness and Drag as Determined in Free Flight at Transonic and Supersonic Speeds. NACA RM L9D12, 1949.

20. Strass, H. Kurt, Fields, Edison M., and Schult, Eugene D.: The Variation of the Rolling Effectiveness of a Plain Unbalanced Aileron with Systematic Modifications to the After Portion of a 6-Percent Circular-Arc Airfoil as Determined in Free Flight at Transonic and Supersonic Speeds. (Prospective NACA paper)

21. Johnston, H. I., and Brown, B. P.: Measurement of Aerodynamic Characteristics of a 35° Sweptback NACA 65-009 Airfoil Model with Quarter-Chord Beveled Trailing-Edge Flap. (Prospective NACA paper)

22. Thompson, Robert F.: Investigation of Effects of Aileron Contour on Aileron Hinge-Moment Characteristics of a 42.7° Sweptback Wing at Transonic Speeds. (Prospective NACA paper)

23. Fischel, Jack, and Hammond, Alexander D.: Investigation of Effect of Span and Spanwise Location of Plain and Stepped Spoiler Ailerons on Lateral-Control Characteristics of a Wing with Leading Edge Swept Back 51.3°. (Prospective NACA paper)

24. Fischel, Jack, and Schneiter, Leslie E.: High-Speed Wind-Tunnel Investigation of an NACA 65-210 Semispan Wing Equipped with Plug and Retractable Ailerons and a Full-Span Slotted Flap. NACA TN 1663, 1948.

25. Schneiter, Leslie E., and Ziff, Howard L.: Preliminary Investigation of Spoiler Lateral Control on a 42° Sweptback Wing at Transonic Speeds. NACA RM L7F19, 1947.

26. Schneiter, Leslie E., and Hagerman, John R.: Wind-Tunnel Investigation at High Subsonic Speeds of the Lateral-Control Characteristics of an Aileron and a Stepped Spoiler on a Wing with Leading Edge Swept Back 51.3°. NACA RM L9D06, 1949.

27. Schneiter, Leslie E., and Watson, James M.: Low-Speed Wind-Tunnel Investigation of Various Plain-Spoiler Configurations for Lateral Control on a 42° Sweptback Wing. NACA TN 1646, 1948.

28. Strass, H. Kurt: Additional Free-Flight Tests of the Rolling Effectiveness of Several Wing-Spoiler Arrangements at High Subsonic, Transonic, and Supersonic Speeds. NACA RM L8I23, 1948.

29. Sandahl, Carl A., and Strass, H. Kurt: Comparative Tests of the Rolling Effectiveness of Constant-Chord, Full-Delta and Half-Delta Ailerons on Delta Wings at Transonic and Supersonic Speeds. (Prospective NACA paper)

30. Kolbe, Carl D., and Tinling, Bruce E.: Tests of a Triangular Wing of Aspect Ratio 2 in the Ames 12-Foot Pressure Wind Tunnel. III - The Effectiveness and Hinge Moments of a Skewed Wing-Tip Flap. NACA RM A8E21, 1948.

31. Wiley, Harleth G.: Aerodynamic Characteristics at Transonic Speeds of a 60° Delta Wing Equipped with a Delta-Plan-Form Flap Having Overhang Balance. (Prospective NACA paper)

32. Mitcham, G. L., Stevens, J. E., and Norris, H. P.: Aerodynamic Characteristics and Flying Qualities of a Triangular-Wing Airplane-Like Configuration as Obtained from Flights of Rocket-Propelled Models at Transonic and Low Supersonic Speeds. (Prospective NACA paper)

33. Martz, C. William, and Church, James D.: Flight Investigation at Subsonic, Transonic, and Supersonic Velocities of the Hinge-Moment Characteristics, Lateral Control Effectiveness, and Wing Damping in Roll of a 60° Sweptback Delta Wing with Half-Delta Tip Ailerons. (Prospective NACA paper)

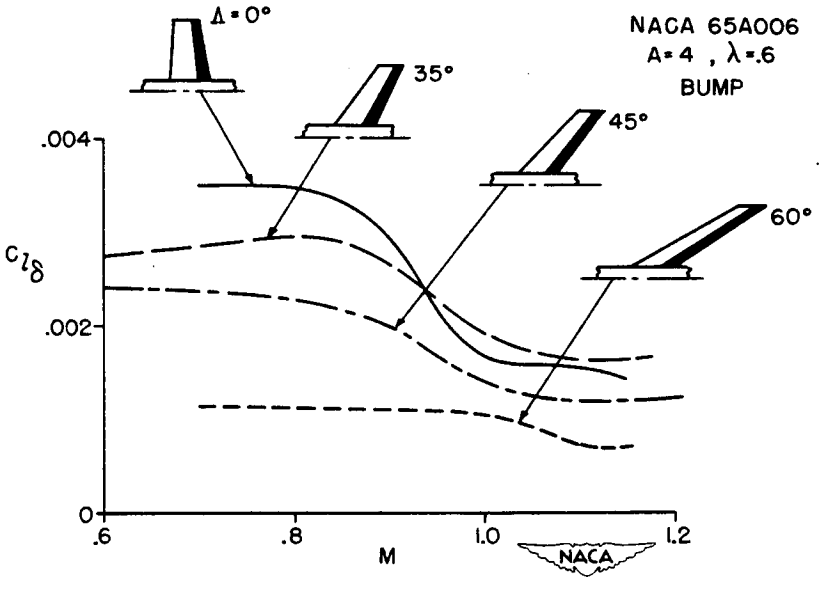


Figure 1.- Effect of wing sweep on aileron effectiveness. Aileron deflection measured normal to hinge line.

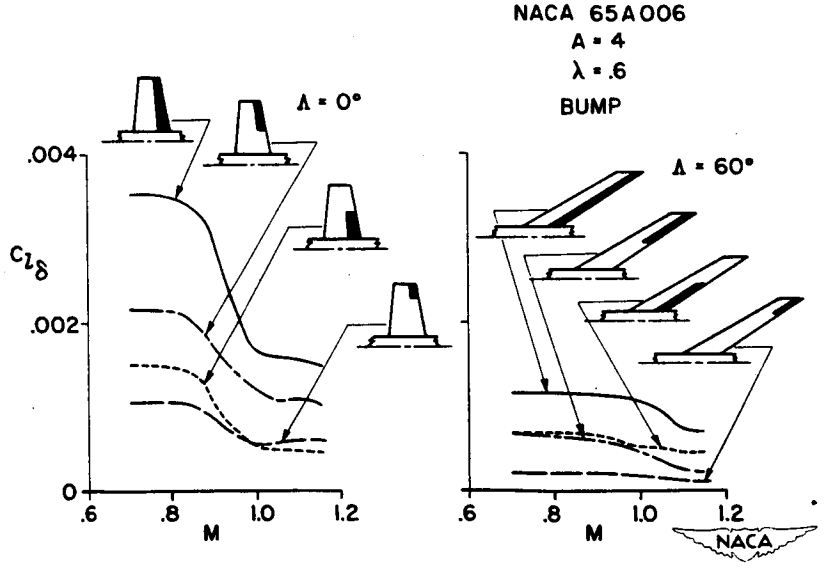


Figure 2.- Effect of spanwise location of aileron on aileron effectiveness. Aileron deflection measured normal to hinge line.

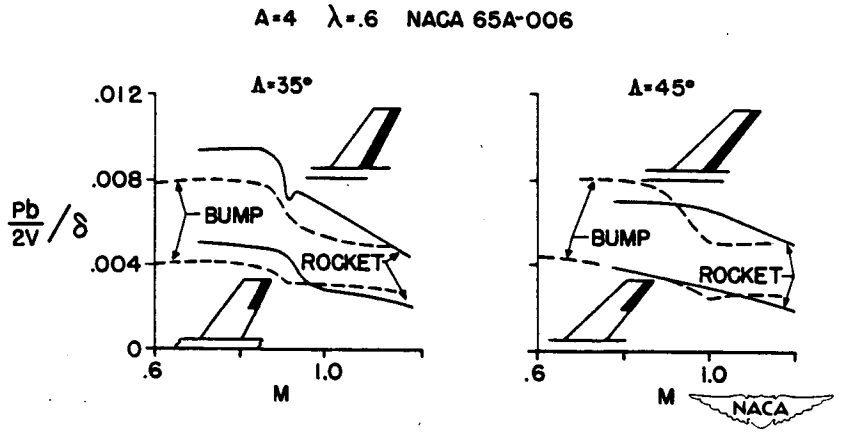


Figure 3.- Comparison of transonic-bump and rocket results. Aileron deflection measured normal to hinge line.

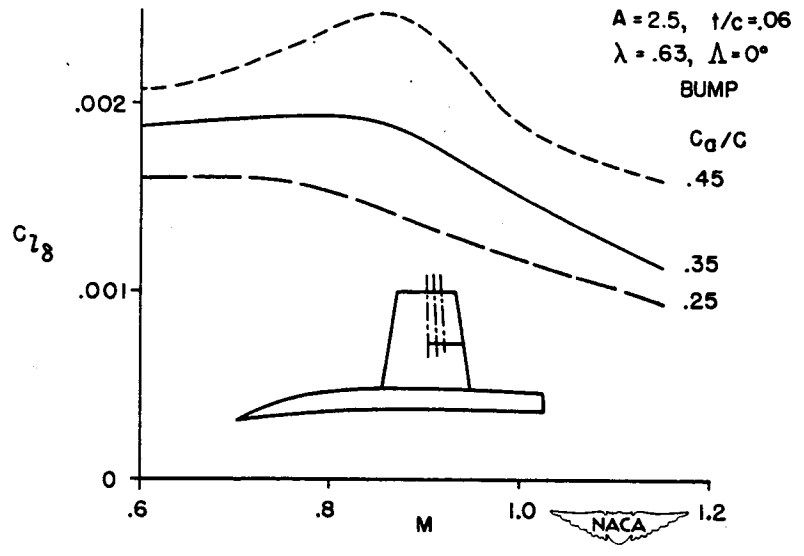


Figure 4.- Effect of aileron chord on aileron effectiveness.

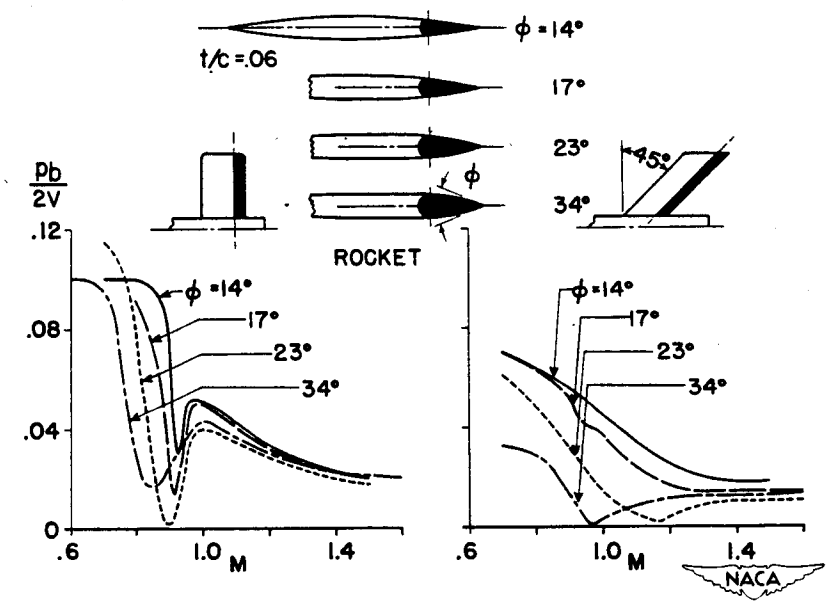


Figure 5.- Effect of trailing-edge angle on aileron effectiveness. Aileron deflected 5°, measured in free-stream direction.

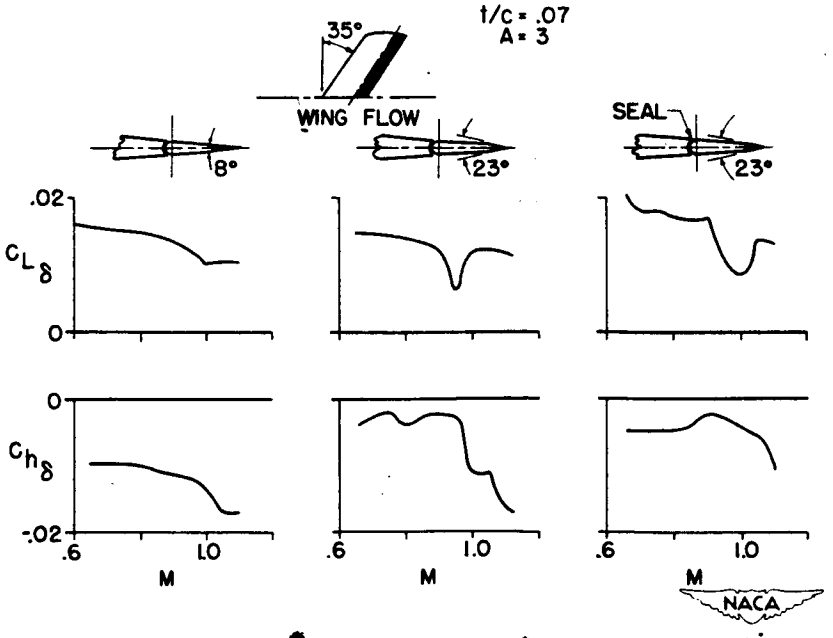


Figure 6.- Effect of trailing-edge bevel on aileron characteristics. Aileron deflection measured normal to hinge line.

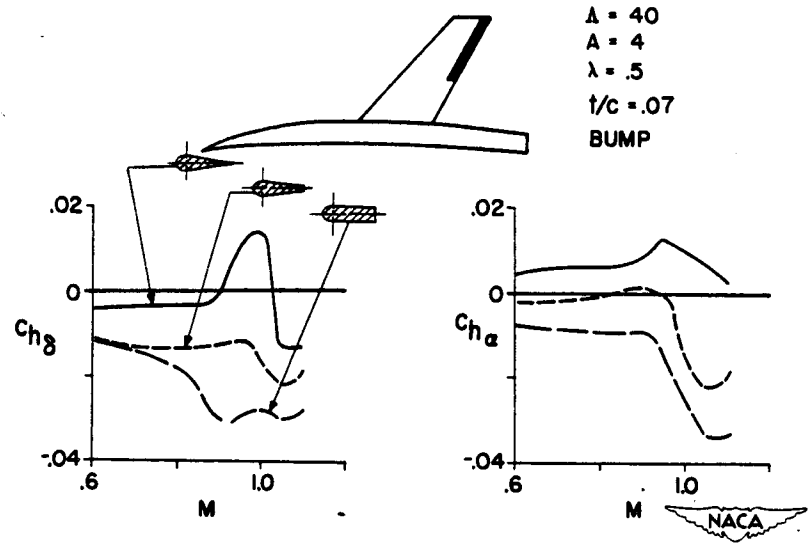


Figure 7.- Effect of trailing-edge modifications on aileron hinge-moment characteristics. Aileron deflection measured normal to hinge line.

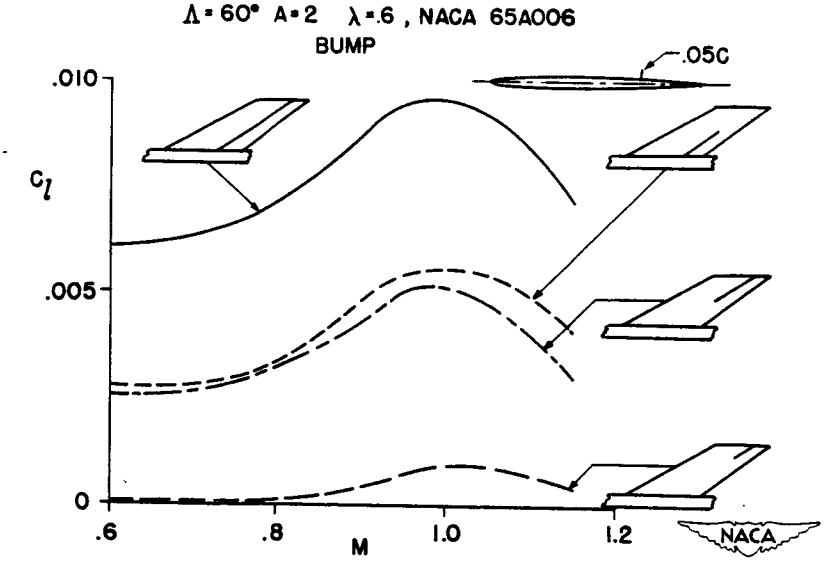


Figure 8.- Effect of spanwise location of spoilers on spoiler rolling effectiveness.

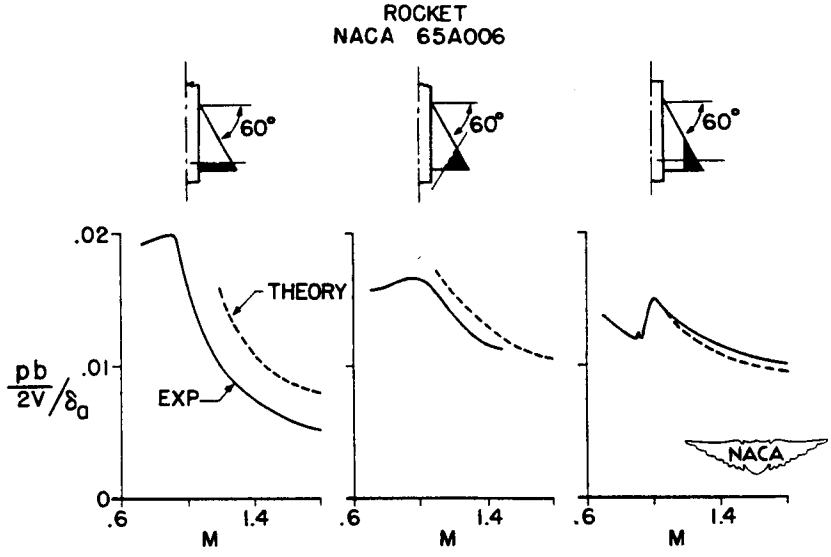


Figure 9.- Rolling effectiveness of three aileron configurations on a delta wing. Aileron deflection measured in free-stream direction.

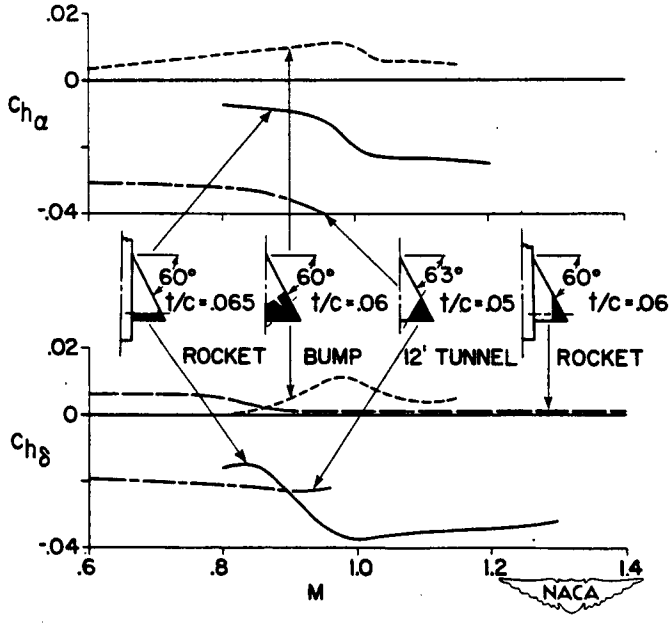


Figure 10.- Hinge-moment characteristics of four aileron configurations on delta wings. Aileron deflection measured in free-steam direction.

DYNAMIC LATERAL STABILITY OF TRANSONIC AIRPLANES

By William M. Kauffman

Ames Aeronautical Laboratory

and Charles H. Zimmerman

Langley Aeronautical Laboratory

N65-86475

INTRODUCTION

The choice of fin area and dihedral for a modern high-performance airplane is not a clear-cut process. As has been shown by theoretical predictions and verified by flight tests, the configurations and operating conditions associated with high-performance airplanes have led to difficulties in the form of poorly damped lateral oscillations of short period. Related problems of response to disturbances and control deflection have increased, and the effect of vertical-tail area on performance has become more critical.

The objective of the NACA is to present research findings which will assist the designer in providing transonic airplanes with satisfactory dynamic lateral stability characteristics at a minimum sacrifice of performance and maneuverability. The problem of providing this research information is twofold. First, it is necessary to know what flying characteristics are desirable, or at least tolerable. Second, it is necessary to have sufficient information on the aerodynamic and mass characteristics of proposed design configurations so that the dynamic lateral behavior can be estimated accurately. Active steps are being taken by the NACA to provide adequate information on both phases of the problem.

The current lateral-dynamic-stability requirement, based on the period-damping relationship, is illustrated in figure 1. The characteristics of a typical World War II fighter-type airplane and a typical transonic airplane are shown for comparison. Detailed study has shown that the general tendency toward unsatisfactory behavior can be attributed, directly or indirectly, to the trend toward clean, high-performance designs with high wing loadings, no propellers, sweptback wings, nose-wheel landing gears, and large high vertical tails. Although the records are incomplete, the authors know of no swept-wing fighter to which authentic report or rumor has not attributed a tendency to perform unpleasant lateral oscillations. Unfortunately, we have had difficulty in obtaining reliable flight records for high-speed airplanes, but the available records indicate that the lateral motions conform to the classical theory. Even in cases of "snaking," which has at times been

considered a separate phenomenon, the data indicate that the snaking motion is a Dutch roll of small amplitude, generally involving non-linearities.

CURRENT INVESTIGATIONS RELATIVE TO THE REQUIREMENTS

In view of the trend toward shorter oscillation periods, considerable interest has arisen in the ability of pilots to control the oscillations of present and future aircraft. An investigation is under way at the Langley Laboratory on this subject. A mock-up of a pilot's seat has been arranged to oscillate in yaw; wide variations in period and damping can be obtained. The pilot concentrates on rapidly damping the oscillations which follow an initial disturbance by use of rudder pedals which control the swinging motion. Although there was considerable difference between pilots and a marked learning ability, figure 2 shows the typical measured trend of damping ability with period. For periods greater than 3 seconds, damping ability was great. As the period was decreased, the damping ability rapidly became worse; and it is seen that it would have been virtually impossible for the pilot to damp an oscillation of 1-second period. The ability to damp the oscillation was not affected appreciably by the natural damping; that is, for a given period, the pilot could control an unstable oscillation nearly as well as a damped one.

The specification of what constitutes satisfactory dynamic lateral behavior is not a simple problem. It is complicated by confusion and conflict with other related handling characteristics, by differences in opinion among pilots, and by differences in the tactical missions of various types of aircraft. Recently, there have been indications that the present period-damping boundary will not adequately define desirable dynamic lateral behavior. For example, there are two swept-wing fighters with very similar period-damping characteristics. One is reported to have satisfactory dynamic lateral stability, the other is reported to be objectionable. On a delta-wing configuration the period-damping relationship is apparently satisfactory; however, maintenance of roll equilibrium is difficult due to high sensitivity to outside disturbances and to control deflections. The Ames Laboratory is presently conducting a flight investigation in which important lateral-stability derivatives and associated handling qualities of a conventional fighter airplane can be varied readily over sufficient ranges to simulate the behavior of new and unusual high-speed configurations. It is hoped that, through correlation of the recorded data and pilots' opinions, a more complete and rational basis for lateral-stability requirements may be developed. The initial phase of the Ames program consisted essentially of the determination of the tolerable range of effective dihedral of the test airplane for the cruise and simulated approach conditions. An aileron-actuating servomechanism described in reference 1 was employed

to obtain large variations in effective dihedral during flight. Figure 3 summarizes the results of this program, which has been reported in reference 2. This figure shows a consensus of five pilots on the general lateral handling characteristics for various amounts of effective dihedral. The term "intolerable" describes a condition which was considered dangerous for normal fighter operation, "tolerable" describes a condition which was not dangerous but was not pleasant, and "good" describes a desirable or pleasant condition. It is seen that the pilots would tolerate small amounts of negative dihedral in both flight conditions. For values more negative than about -5°, the adverse rolling response to rudder control became dangerously large, and spiral-divergence tendencies necessitated continual control, especially in rough air. High control friction and "slop" in the control system would accentuate the difficulties of continual control. Also, it has been found that a change in dihedral effect with airspeed from positive to negative values is very disconcerting to a pilot. In view of these factors, it appears that the negative dihedral effect which could be tolerated in transonic airplanes would be very small. Fortunately, from the standpoint of the characteristics of sweptback plan forms, large positive values of dihedral were considered desirable in the low-speed approach condition. The maximum tolerable dihedral at cruising speed was about 22°, whereas at approach speed the highest test dihedral of 28.4° was considered tolerable. It is interesting to examine these results on the basis of the current dynamic-stability requirement. The period-damping relationship for the positive test values of dihedral are shown in figure 4. Dihedral values and corresponding adjective ratings are noted for each point. For the cruise condition, the pilot rating changed from good to tolerable as the current boundary was crossed, and the point well inside the boundary was termed "intolerable". However, note that in the approach condition, a point well inside the boundary was considered good and that the point for 28.4° dihedral, characterized by a mildly unstable oscillation which doubled amplitude in 38 seconds, was considered tolerable. The marked difference in rating for these high-dihedral cruise and approach conditions could not be attributed entirely to the small difference in oscillation period. Study of pilots' comments showed that the high dihedral in the cruise condition was considered intolerable primarily because of the large and poorly damped rolling motions which followed disturbances. In the approach condition, the mildly unstable oscillation was not considered a serious deficiency, because the period was fairly long, the rolling motions generally were small, and the rudder was very effective in producing roll. The difference in rolling tendencies for the two cases, is indicated by figure 5, which presents time histories of control-fixed lateral oscillations. The magnitude of the sideslip oscillations is roughly the same for each condition. However, the larger values of rolling velocity p for the intolerable cruise condition are apparent. A convenient measure of roll tendency employed in this investigation was the dimensionless ratio of the oscillatory bank motion ϕ to the oscillatory sideslip motion β. This ratio,

written as $|\phi/\beta|$, can be evaluated simply from the double-amplitude values of the given rolling velocity and sideslip records. Comparison of the 5.4 value of $|\phi/\beta|$ for the intolerable cruise condition with the 2.3 value for the tolerable approach condition is indicative of the relatively high roll excitation considered undesirable by the pilots in the cruise condition. The results obtained to date in this investigation indicate that no single period-damping criterion will adequately specify desirable dynamic lateral stability characteristics. It appears that other factors such as the excitation and cross coupling of the rolling and yawing motions influence the pilot's impressions, and that further study of the problem is required. The Ames Laboratory is extending the investigation just discussed by flight tests of the same airplane equipped with an apparatus for varying, simultaneously with dihedral effect, the static directional-stability and rotary-damping parameters C_{n_β} and C_{n_r} over wide ranges in flight. The Langley Laboratory is conducting a similar investigation of the effects of variations in C_{n_r} on a highly loaded jet fighter airplane. These programs will permit study of widely varying combinations of oscillation period, damping, excitation, and other factors affecting lateral handling characteristics and, it is hoped, will lead to a more complete understanding of desirable and tolerable dynamic stability characteristics.

ESTIMATED DYNAMIC LATERAL STABILITY CHARACTERISTICS

In the estimation of any dynamic lateral stability or response characteristics, the major difficulty lies in the correct evaluation of the various mass parameters and aerodynamic derivatives which are substituted in the classical equations of motion. In order to illustrate current information on the evaluation of the derivatives and some dynamic-stability problems encountered on transonic designs, the period and damping of an aircraft configuration typical of the apparent trend in transonic fighters will be presented and discussed. Although not the only factors which define lateral flying characteristics, the oscillation period and damping are and no doubt will continue to be of importance.

With regard to the mass characteristics, one of the major uncertainties in some dynamic-stability calculations is the location of the principal axis of inertia; often it has been necessary to guess this location with an accuracy at best of $\pm 1^\circ$. Occasionally such an uncertainty will change the estimated damping from a point well on one side of the criterion boundary to a pcint well on the other side, and there are cases in which failure to know the principal-axis location within $\pm 1/2^\circ$ makes impossible an accurate estimate of the oscillation damping, no matter how closely the aerodynamic derivatives can be evaluated.

With regard to the aerodynamic derivatives, the static and rotary lateral stability derivatives of plain wings at low speed have been investigated extensively both by an analytical approach (references 3 to 9) and by experimental techniques (references 10 to 19). The analytical methods in use are based largely on strip theory, with only an approximate account of the effects of aerodynamic induction. The strip-theory method has been found to be reasonably accurate, and it is extremely useful in that it can be applied to design problems which are too complicated for treatment by more rigorous means. The rolling-flow and curved-flow equipment of the Langley stability tunnel has facilitated the experimental determination of the rotary stability derivatives, and systematic investigations of various configurations are now feasible. The results of such investigations have been utilized to evaluate empirical corrections to the theory for several of the rotary derivatives. As a result of this work, it is considered that the low-speed steady-flow derivatives for most plain wings can be estimated quite accurately. Figure 6 illustrates one phase of this work - a recently developed semiempirical method presented in reference 20 for estimating the rolling moment due to yawing velocity C_{l_r}. In this method the value of C_{l_r} calculated from simple theory is corrected by the addition of the difference between the rolling moment due to sideslip C_{l_β} as calculated by simple theory and the value of C_{l_β} measured by any suitable technique. This method of estimating C_{l_r} can be justified on the basis that the breakdown in flow on sideslipping wings is similar to the breakdown on a yawing wing, and the effects on C_{l_β} and C_{l_r} are therefore similar. That this is actually the case appears to be verified by the agreement between measured and estimated values of C_{l_r} for 22 wing configurations and 8 complete models considered in reference 20. One of the chief merits of this method lies in the fact that C_{l_β} can be measured at much higher speeds and Reynolds numbers than is possible at present in the case of C_{l_r}.

With the exception of the yawing moment due to rolling C_{n_p}, tail contributions to the stability derivatives can be estimated by existing analytical methods given in reference 21. Some experimental information is also available. (See references 22 to 24.) Recent tests in both the Langley stability tunnel and the Langley free-flight tunnel have shown that the value of C_{n_p} due to the tail obtained from the expressions in reference 21 is much too positive. Figure 7 shows a typical example. It is seen that the measured values approached the estimated values with the wing off but were made appreciably less positive by the addition of the wing. The investigation is not complete, but a tentative explanation of this difference is that the rotational wake behind the rotating wing gives rise to a sidewash at the vertical tail which is responsible for the observed negative increment in C_{n_p}. Unfortunately,

this effect reduces the damping on the lateral oscillation, often to a serious extent.

Analytical methods for estimating the effects of trailing-edge flaps on stability derivatives so far have not been developed to the point that reliable estimates of the flap effect can be made at high lift coefficients. However, results of experimental investigations, such as those reported in references 16 and 17, can be used to provide rough estimates. In general, it has been found that leading-edge flaps or slats merely extend the linear variations of the stability derivatives to higher lift coefficients; and thus, with these devices installed, the potential-flow theory of plain wings is applicable over almost the range of lift coefficients obtainable for the wing with leading-edge flaps or slats.

Figure 8 shows the effect of flaps on the dynamic lateral stability characteristics of the typical transonic airplane at a lift coefficient of 0.8. It should be realized that, in addition to effects on the stability derivatives, trailing-edge flaps result in a decrease in the angle of attack for a given lift coefficient, which amounts to a downward tilt of the principal axis. The large destabilizing effect of flap deflection noted for this airplane resulted primarily from this rotation of the principal axis. The effects of the flaps on the stability derivatives were of secondary importance.

Theoretical corrections for the effects of compressibility on aerodynamic characteristics generally can be derived with the aid of the Prandtl-Glauert rule, provided a satisfactory incompressible-flow theory is available. At the present time, procedures for estimating the stability derivatives of swept wings are based largely on strip theory, with the effects of aerodynamic induction accounted for in an approximate manner. More rigorous solutions have been obtained for only a few derivatives, such as the lift-curve slope and the damping in roll, and these solutions have provided only slight improvement over the strip-theory methods. The strip theory provides a basis for deriving convenient corrections for the effects of compressibility on the wing and tail contributions to the lateral stability derivatives. Such an analysis has been presented in reference 25. Although experimental verification for the corrections is almost completely lacking, it is believed that the method has a sufficiently sound basis to indicate the order of magnitude of the corrections and to indicate the trends resulting from variations in such geometric parameters as the aspect ratio and the sweep angle. One general result of the analysis has been that, for all of the lateral stability derivatives, variations with Mach number become smaller as the sweep angle is increased and the aspect ratio is reduced.

An indication of the extent to which calculated dynamic lateral stability characteristics of the representative transonic airplane are

affected by consideration of the effects of compressibility is given by figure 9. In this case, the dynamic lateral stability characteristics calculated with compressibility effects included were nearly the same as those with compressibility effects neglected. For an airplane having a higher aspect ratio or a smaller sweep angle, larger effects of the compressibility corrections might be expected.

There are at present no satisfactory methods for estimating any of the lateral stability derivatives at transonic speeds. We do not have satisfactory methods for measuring any of the derivatives except damping-in-roll and static directional stability in this same range. In order to estimate the dynamic lateral stability of the transonic fighter in the transonic range, it has been necessary to resort to estimates that are little more than guesses for the rolling moment due to sideslip C_{l_β} and the rolling moment due to yawing C_{l_r}. The situation for C_{n_r}, the yawing moment due to yawing, is somewhat better since it is believed that the major contribution is made by the tail and the problem is primarily one of estimating the slope of the force curve against angle, a characteristic which has been experimentally determined for a wide range of plan forms at transonic speeds. Yawing moment due to sideslip C_{n_β} presents a similar problem and here a slight amount of data on fuselage-tail combinations is available. Yawing moment due to rolling C_{n_p} is a very important factor which is difficult to evaluate, not only because of uncertainties as to the wing contribution but also because of the previously mentioned uncertainty as to the magnitude of the rotational wash at the tail due to the rotating wing ahead. In order to form some idea of the stability at transonic speeds, the stability of the typical transonic airplane at Mach numbers of 1.0, 1.1, and 1.2 has been estimated; the results are presented in figure 10. It should be pointed out that, within the accuracy of the estimates of the derivatives, the period and damping values might be one-half or twice those which are shown. However, unless the estimated values of several of the derivatives are unconservative, the airplane would not meet the present period-damping requirement at transonic speeds. It is also apparent that the damping will deteriorate with altitude.

Since the typical transonic fighter does not meet the criterion for satisfactory period and damping characteristics, the effect of several possible changes, which were studied in an attempt to improve those characteristics, has been considered. Figure 11 shows these results, which are not very encouraging. Changes in vertical tail area move the period-damping point nearly parallel to the criterion boundary and an extremely large tail is required to meet the criterion at the short-period end. The addition of fin area near the center of gravity has a favorable effect but is not sufficient for the case investigated. Fin area under the nose of the fuselage will bring about sufficient damping but this is considered an undesirable configuration from other

standpoints. Reduction of the dihedral or reduction of the incidence is beneficial in this instance, but impractically large reductions are required to cross the boundary.

AUTOMATIC STABILIZATION

In the present example, it appears that no reasonable change in airplane configuration would result in compliance with the current period-damping requirements. At the present time, artificial stabilization appears to be the only solution in such cases. During the recent war, the Germans and British studied and applied in a few cases various means of artificial stabilization. In this country, the Boeing Airplane Company (reference 26) has employed such a method on the B-47, a bomber similar in many ways to the typical transonic fighter, and other experimental applications have been reported. The NACA has made theoretical studies of the problem, reported in references 27, 28, and 29, in order to supply information which will aid in the design of satisfactory stabilization systems. The obvious and possibly best method for increasing the damping of the lateral oscillation is by the addition of a damping yawing moment obtained by movement of the rudder in proportion to a yawing-velocity signal. However, care must be exercised that time lag and lost motion in the system do not defeat the purpose of the installation. A rate-gyro installation with time lag will increase appreciably the damping of the original oscillation but will tend to introduce a new oscillatory mode. With high gearing ratios, a surprisingly small amount of lag may result in a hunting oscillation of considerably shorter period than the natural oscillation.

In an attempt to avoid this condition a study has been made of the use of rudder response in proportion to the signal of an angular accelerometer responding to acceleration in yaw. Such a device will also result in a hunting oscillation if the gearing and lag are sufficiently great, but much larger amounts of lag can be tolerated than in the rate system. The possibilities of automatic stabilization using response to other components of the motion, such as a rudder movement proportional to acceleration in rolling, are now being studied.

The Langley free-flight tunnel is proving a very useful aid in these studies. Models have been flown with widely varied values of C_{l_p}, C_{n_p}, C_{l_r}, and C_{n_r} obtained artificially from a rate-gyro installation in the model. The work done to date has been of a qualitative and exploratory nature but certain important points have been brought out. Decreases in lateral oscillatory stability were obtained by making C_{l_p} and C_{n_r} less negative and C_{n_p} and C_{l_r} less positive, as would be expected from theoretical considerations. Changes in these derivatives in the opposite direction made the oscillatory stability better, but in the cases of C_{n_p} and C_{l_r} these more

positive values lead to very undesirable tendencies to diverge and it becomes very difficult to avoid crashes.

In one interesting case, the gyro was first used to increase C_{n_r}, the damping of yawing, but, although this change improved the stability considerably, the model was still hard to fly because of fast rolling motions in response to gusts and control movements. The gyro was then used to increase C_{l_p}, and this arrangement proved very satisfactory. In addition to being stable the model was very easy to fly because of the much smaller rolling motions. Subsequent theoretical studies of a configuration similar in both mass and aerodynamic characteristics showed that this particular configuration was very susceptible to improvement of the stability by increase in C_{l_p}, for which moderate changes normally have little effect on dynamic stability. This study emphasized the danger of generalizations in the consideration of dynamic lateral stability. Each configuration must be considered individually in order to obtain correct conclusions.

The inclination, on the part of most designers at least, has been to avoid artificial stabilization because of the desire to avoid additional weight and complication of an already complicated machine. However, if autopilot or control boost systems are already installed in the airplane, these disadvantages can be reduced by multiple use of existing components. There has been a feeling that airplanes should have, as nearly as possible, completely satisfactory stability without artificial stabilizing means, and that artificial stabilization should only make up the relatively small difference. Actually, experience may prove that substantial weight saving and performance improvement will be possible in certain cases by providing only the minimum natural stability necessary for tolerable behavior in the event of failure of the artificial stabilizing system, and by providing the remainder artificially. The use of artificial stabilization also offers the possibility that the stability may be adjusted in flight, either automatically or by the pilot, to suit the particular circumstances of the moment.

ESTIMATED RESPONSE CHARACTERISTICS

In addition to lateral-oscillation period and damping difficulties just indicated for a typical transonic design, the physical features and operating conditions of current and planned high-performance airplanes often lead to related unusual lateral response and control problems. A theoretical study, employing an analogue computer, of the lateral motions of typical transonic airplanes following various gust disturbances and control motions is being conducted at the Ames Laboratory. One notable feature of the work to date is the tendency shown by

several transonic configurations toward high roll excitation in response to side gusts. Time histories of the response to a small impulse-type yawing-moment disturbance of a highly swept, a delta-wing, and a straight low-aspect-ratio-wing configuration are shown in figure 12. Large ratios of roll to sideslip are apparent in all cases. The value of $|\phi/\beta|$ for the oscillatory mode is in all cases greater than 3, whereas for lower-speed designs it is generally less than 3. This trend is attributable in part to increases in wing loading and altitude. Dihedral effect has, of course, an important influence on this type of roll excitation. For this airplane a change in geometric dihedral from 0° to -5°, corresponding to about a 50-percent reduction in C_{l_β}, results in sizeable reductions in the amount of roll and, since the sideslip motions remain essentially the same, in $|\phi/\beta|$. However, even though C_{l_β} is still negative with -5° wing dihedral, left stick deflection would be required for balance in a steady right sideslip. This reversed lateral-control-position gradient, unsatisfactory on the basis of present requirements, arises from the large rolling moment produced by the rudder and tends to limit the amount of negative geometric dihedral which can be used on an airplane with a high vertical tail. Unusual response to control deflections may occur on high-speed designs, such as a large reduction or eventual reversal due to high effective dihedral, of the rolling velocity in low-speed aileron rolls. Another example is indicated in figure 13, which shows the response to an abrupt rudder deflection. The large rolling moment due to rudder, arising from the high vertical tail, causes an initial adverse rolling motion and a resultant delay in the development of the normal rolling motion. Detrimental effects on lateral handling qualities of such unusual response characteristics may be aggravated if, as indicated previously may be the case, the oscillation period-damping relation is deficient in the approach condition. Flight data obtained with current and future high-speed designs and in investigations such as the Ames variable-stability flight program should show the nature and seriousness of these problems.

SNAKING

So far only lateral oscillations of the type that have been recognized as the Dutch roll and were considered predictable by the classical equations of motion have been discussed. Several modern fighter airplanes show, under one flight condition or another, a tendency to perform a neutrally damped oscillation of small amplitude, generally referred to as "snaking."

The most common cause of snaking is rudder motion. Fuel sloshing has also caused or augmented snaking in some cases. These types of snaking and the remedies have been well covered in the literature.

However, there are apparently some true cases of snaking which are caused neither by rudder motion nor fuel sloshing. In such records as we have seen, the motion was a combined rolling and yawing motion indistinguishable from a Dutch roll except that the damping was a function of amplitude and fell to zero at small amplitudes. It seems obvious that in such cases certain of the important stability derivatives are nonlinear near zero amplitude because of flow separations or boundary-layer effects, possibly combined with phase-angle shifts in the flow about the fuselage. Theoretical studies assuming nonlinear derivatives confirm this conclusion.

It is very difficult to measure the extremely small changes in pressure coefficients on the tail or fuselage, which are sufficient to cause snaking. The normal fluctuations in stream direction in an ordinary wind tunnel produce pressure fluctuations in excess of those which cause snaking. However, the NACA wing-flow method provides a means of model testing at high speeds in smooth flow. It was thought that, although the true snaking motion is a three-degree-of-freedom motion involving rolling, yawing, and lateral displacement, the deficiency in damping was almost certainly in the yawing motion and that, if no damping existed for small amplitudes, it would cause snaking oscillations of a model mounted to have freedom in yawing only. Figure 14 is a perspective view of a wing-flow model which was attached to a friction-free device with freedom to oscillate in yaw. The results obtained by this method are presented in figure 15 in the form of records of the yawing motion of the model for various conditions. For the original configuration, a snaking motion is apparent in the transonic speed range. Addition of a tail cone to the jet-exhaust opening increased the amplitude of the oscillations. Removal of the horizontal tail had no effect. Use of a slab-sided vertical surface caused a slight improvement. A wire placed around the fuselage near the aft end or near the front end made no difference. Not until the fuselage lines were carried straight aft from the maximum thickness points, giving a cylindrical aft portion of the fuselage, was it possible to eliminate the oscillation. It is not recommended that fuselages be made cylindrical to avoid snaking; however, this experiment does show that snaking can be caused by a flow condition about the aft end of a fuselage. That such is the case is also indicated by certain cases of full-scale snaking, which have been reported to be critically affected by small changes in jet engine rpm and by changes in center-of-gravity location. The effect of changes in center-of-gravity location can be explained as resulting from changes in horizontal-tail loading and, hence, in horizontal-tail interference effects.

A scientific study of this phenomenon will be very difficult because of the small quantities to be measured and the probably critical nature of the flow involved. A complete study will require work with oscillating models in a wind tunnel having a very smooth and

steady flow. It is possible that Reynolds number effects will be large, and these will have to be carefully accounted for and correlated with full-scale conditions. It appears that such an experimental program is necessary if it is to be possible to design with assurance that no snaking will be encountered, and preliminary work is now under way at the Langley Laboratory.

CONCLUDING REMARKS

It is apparent that the provision of adequate dynamic lateral stability characteristics is a problem that cannot be neglected in the design of a transonic airplane. Both theory and experience indicate that undesirable period, damping, and response characteristics are likely to occur even when considerable design effort is expended in their avoidance. In some cases it may be necessary or desirable to provide artificial stabilizing devices.

The need for additional research information to aid the designer in solving this problem is twofold. First, in order to furnish design goals, more complete information is required on the dynamic lateral stability characteristics which are associated with satisfactory and with tolerable flying qualities. Modifications and additions to the present requirements, which concern primarily the period-damping relationship, may be necessary. Data and pilots' opinions from flight tests of high-speed and special variable-stability airplanes will furnish the primary source of information. Second, in order to attain the design goals, more comprehensive data are needed to permit accurate estimation of those aerodynamic derivatives which govern lateral motion. Extensive research on airplane components and combinations in both steady and unsteady rectilinear and rotational flows will be necessary.

At present, it is possible to predict with reasonable accuracy the subsonic-speed values of the steady-flow static and rotary stability derivatives.

As yet, no method is known for measuring or predicting nonlinearities which apparently exist in certain cases of snaking. Tests of oscillating models in tunnels having very smooth and steady flow may be necessary. Initial studies are under way, and a preliminary study is being made of correlative flight tests of full-scale airplanes.

In the transonic range no method is available for predicting or measuring the lateral stability derivatives, with the exception of the rolling moment due to rolling. Studies of techniques for making such measurements are in progress.

REFERENCES

1. Kauffman, William M., Smith, Allan, Liddell, Charles J., Jr., and Cooper, George E.: Flight Tests of an Apparatus for Varying Dihedral Effect in Flight. NACA TN 1788, 1948.

2. Liddell, Charles J., Jr., Van Dyke, Rudolph D., Jr., and Heinle, Donovan R.: A Flight Determination of the Tolerable Range of Effective Dihedral on a Conventional Fighter Airplane. NACA TN 1936, 1949.

3. Toll, Thomas A., and Queijo, M. J.: Approximate Relations and Charts for Low-Speed Stability Derivatives of Swept Wings. NACA TN 1581, 1948.

4. Fischel, Jack, and Tamburello, Vito: Investigation of Effect of Span, Spanwise Location, and Chordwise Location of Spoilers on Lateral Control Characteristics of a Tapered Wing. NACA TN 1294, 1947.

5. Goodman, Alex, and Fisher, Lewis R.: Investigation at Low Speeds of the Effect of Aspect Ratio and Sweep on Rolling Stability Derivatives of Untapered Wings. NACA TN 1835, 1949.

6. Bird, John D.: Some Theoretical Low-Speed Span Loading Characteristics of Swept Wings in Roll and Sideslip. NACA TN 1839, 1949.

7. Queijo, M. J., and Jaquet, Byron M.: Calculated Effects of Geometric Dihedral on the Low-Speed Rolling Derivatives of Swept Wings. NACA TN 1732, 1948.

8. Queijo, M. J., and Jaquet, Byron M.: Investigation of Effects of Geometric Dihedral on Low-Speed Static Stability and Yawing Characteristics of an Untapered 45° Sweptback-Wing Model of Aspect Ratio 2.61. NACA TN 1668, 1948.

9. Goodman, Alex, and Adair, Glenn H.: Estimation of the Damping in Roll of the Wings through the Normal Flight Range of Lift Coefficient. NACA TN 1924, 1949.

10. Brewer, Jack D., and Fisher, Lewis R.: Effect of Taper Ratio on the Low-Speed Rolling Stability Derivatives of Swept and Unswept Wings of Aspect Ratio 2.61. NACA RM L8H18, 1948.

11. Goodman, Alex, and Brewer, Jack D.: Investigation at Low Speeds of the Effect of Aspect Ratio and Sweep on Static and Yawing Stability Derivatives of Untapered Wings. NACA TN 1669, 1948.

12. Letko, William, and Brewer, Jack D.: Effect of Airfoil Profile of Symmetrical Sections on the Low-Speed Rolling Derivatives of 45° Sweptback-Wing Models of Aspect Ratio 2.61. NACA RM L8L31a, 1949.

13. Jaquet, Byron M., and Brewer, Jack D.: Low-Speed Static-Stability and Rolling Characteristics of Low-Aspect-Ratio Wings of Triangular and Modified Triangular Plan Forms. NACA RM L8L29, 1949.

14. Letko, William, and Jaquet, Byron M.: Effect of Airfoil Profile of Symmetrical Sections on the Low-Speed Static-Stability and Yawing Derivatives of 45° Sweptback Wing Models of Aspect Ratio 2.61. NACA RM L8H10, 1948.

15. Letko, William, and Cowan, John W.: Effect of Taper Ratio on Low-Speed Static and Yawing Stability Derivatives of 45° Sweptback Wings with Aspect Ratio of 2.61. NACA TN 1671, 1948.

16. Lichtenstein, Jacob H.: Effect of High-Lift Devices on the Low-Speed Static Lateral and Yawing Stability Characteristics of an Untapered 45° Sweptback Wing. NACA RM L8G20, 1948.

17. Queijo, M. J., and Lichtenstein, Jacob H.: The Effects of High-Lift Devices on the Low-Speed Stability Characteristics of a Tapered 37.5° Sweptback Wing of Aspect Ratio 3 in Straight and Rolling Flow. NACA RM L8I03, 1948.

18. Letko, William, and Wolhart, Walter D.: Effect of Sweepback on the Low-Speed Static and Rolling Stability Derivatives of Thin Tapered Wings of Aspect Ratio 4. NACA RM L9F14, 1949.

19. Hunton, Lynn W., and Dew, Joseph K.: Measurements of the Damping in Roll of Large-Scale Swept-Forward and Swept-Back Wings. NACA RM A7D11, 1947.

20. Campbell, John P., and Goodman, Alex: A Semiempirical Method for Estimating the Rolling Moment due to Yawing of Airplanes. (Prospective NACA paper)

21. Bamber, Millard J.: Effect of Some Present-Day Airplane Design Trends on Requirements for Lateral Stability. NACA TN 814, 1941.

22. Bird, John D., Lichtenstein, Jacob H., and Jaquet, Byron M.: Investigation of the Influence of Fuselage and Tail Surfaces on Low-Speed Static Stability and Rolling Characteristics of a Swept-Wing Model. NACA RM L7H15, 1947.

23. Bird, John D., Jaquet, Byron M., and Cowan, John W.: Effect of Fuselage and Tail Surfaces on Low-Speed Yawing Characteristics of a Swept-Wing Model as Determined in Curved-Flow Test Section of the Langley Stability Tunnel. NACA RM L8G13, 1948.

24. Jaquet, Byron M., and Brewer, Jack D.: Effects of Various Outboard and Central Fins on Low-Speed Static-Stability and Rolling Characteristics of a Triangular-Wing Model. NACA RM L9E18, 1949.

25. Fisher, Lewis R.: Approximate Corrections for the Effects of Compressibility on the Subsonic Stability Derivatives of Swept Wings. NACA TN 1854, 1949.

26. White, Roland J.: Interim Report on Directional Control Damper Development for XB-47 Airplane. Boeing Airplane Co., Rep. No. D-9469, Nov. 1948.

27. Sternfield, Leonard: Effect of Automatic Stabilization on the Lateral Oscillatory Stability of a Hypothetical Airplane at Supersonic Speeds. NACA TN 1818, 1949.

28. Beckhardt, Arnold R.: A Theoretical Investigation of the Effect on the Lateral Oscillation of an Airplane of an Automatic Control Sensitive to Yawing Accelerations. (Prospective NACA paper)

29. Sternfield, Leonard, and Gates, Ordway B., Jr.: Method for Determining the Effect of Time Lag in an Automatic Stabilization System on the Lateral Oscillatory Stability. (Prospective NACA paper)

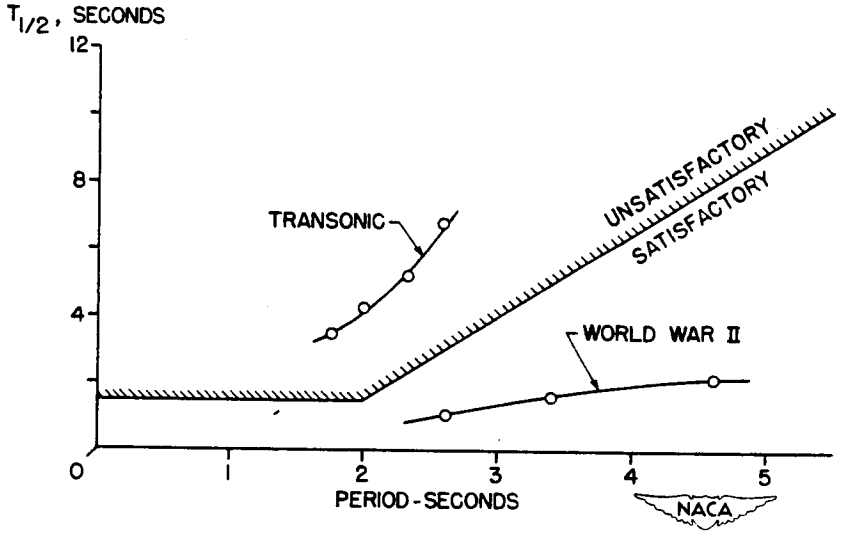


Figure 1.– Trend in lateral–oscillation period–damping characteristics.

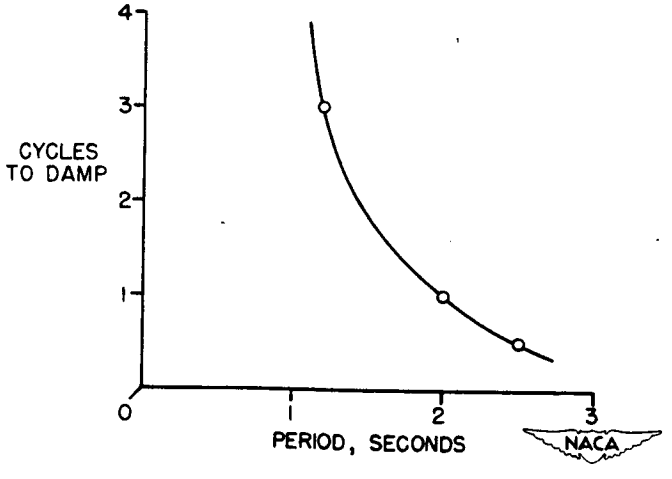


Figure 2.– Variation with period of the cycles required to damp yawing oscillations of a swinging seat.

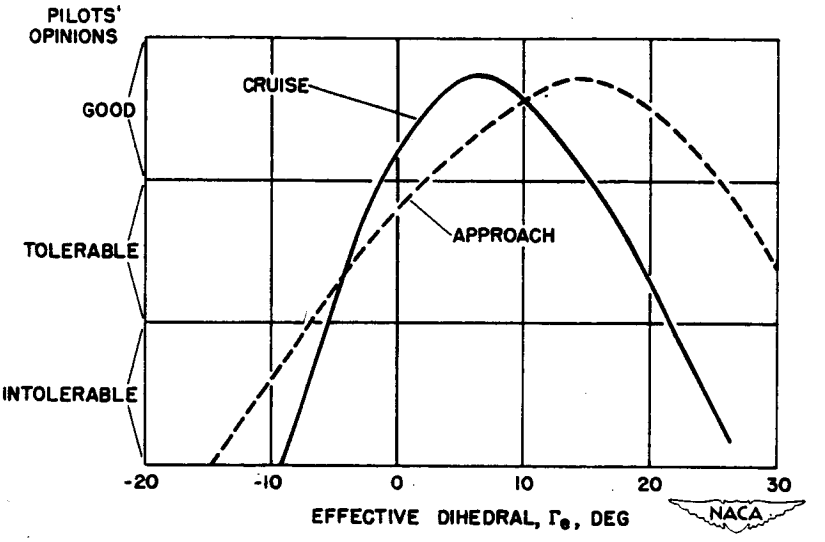


Figure 3.– Summary of pilots' opinions of the general lateral handling characteristics as a function of effective dihedral.

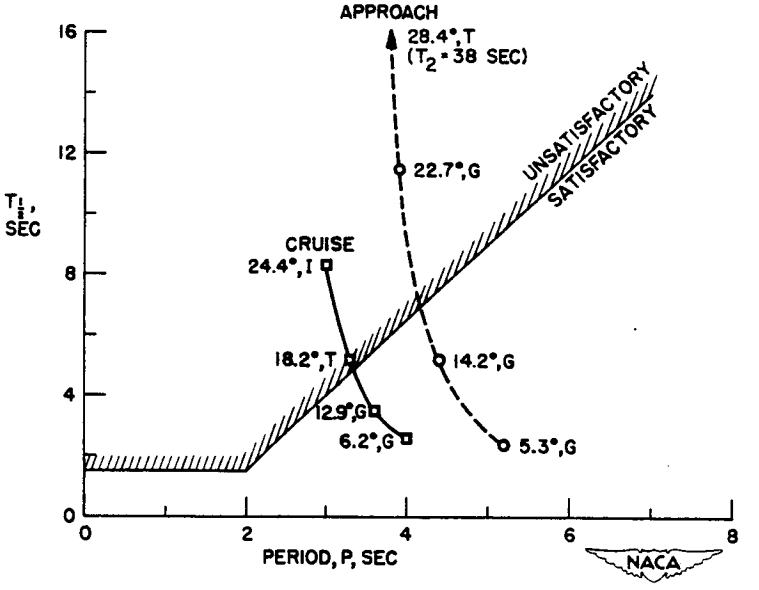


Figure 4.– Lateral-oscillation period-damping characteristics for the positive test values of dihedral.

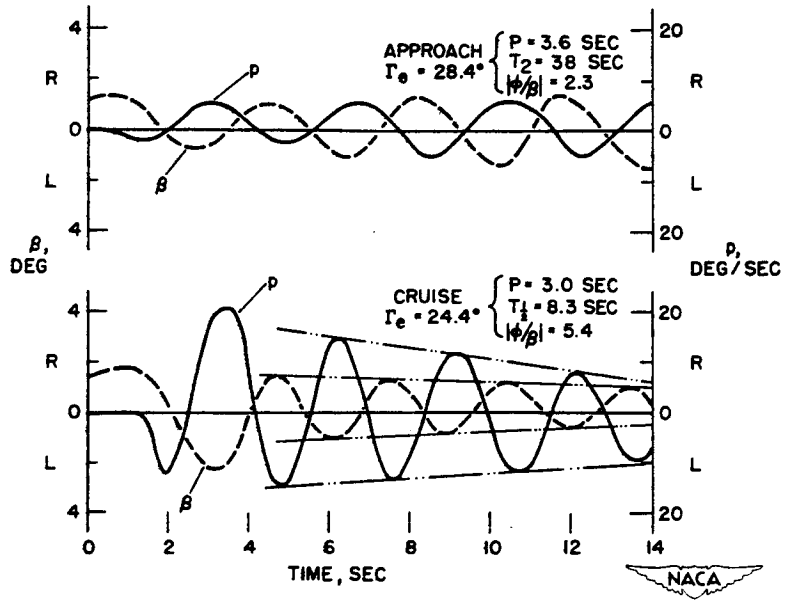


Figure 5.- Time histories of control-fixed lateral oscillations.

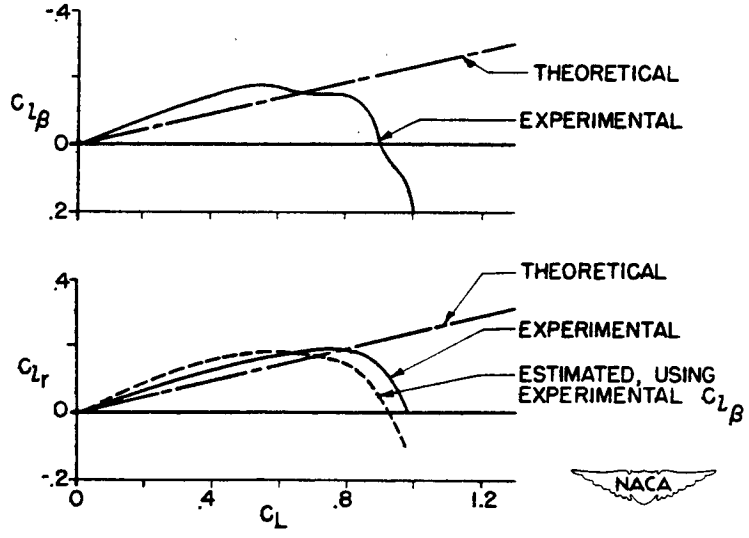


Figure 6.- Sample application of a semiempirical method for estimating C_{l_r}.

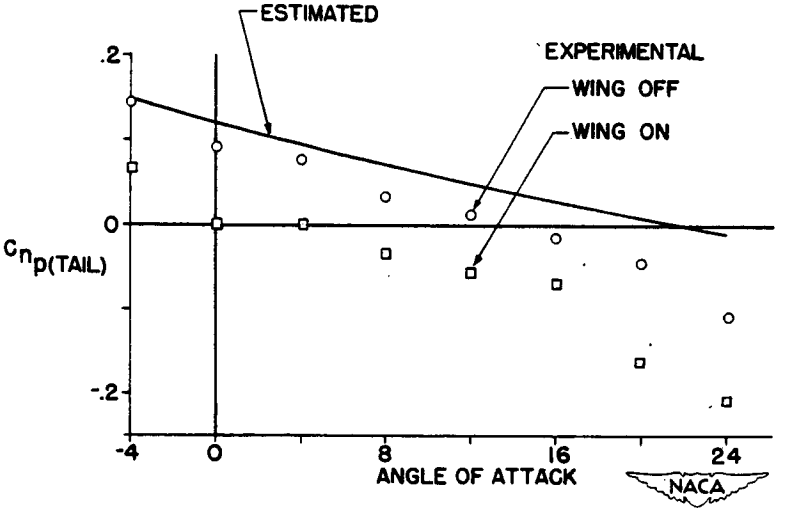


Figure 7.– Comparison of measured and estimated values of C_{n_p}.

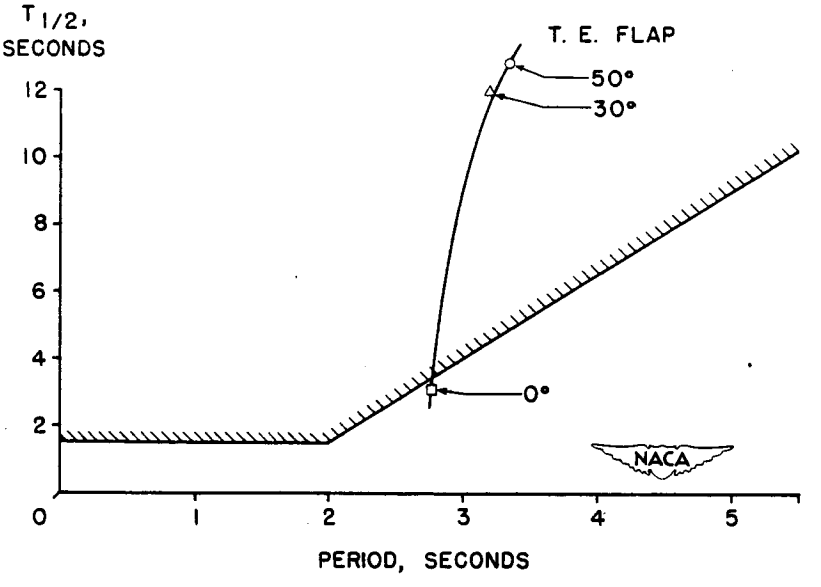


Figure 8.– Lateral–oscillation period–damping characteristics of the typical transonic airplane for various flap deflections. $C_L = 0.8$.

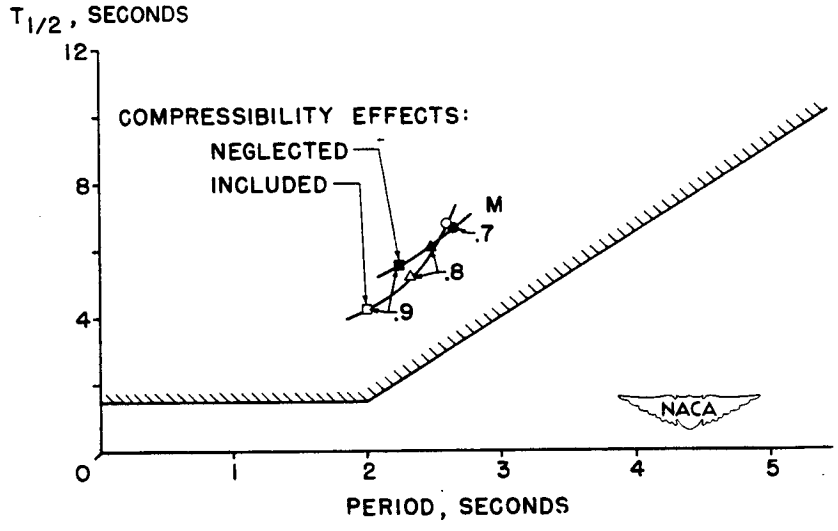


Figure 9.– Lateral–oscillation period–damping characteristics of the typical transonic airplane at high subsonic speeds.

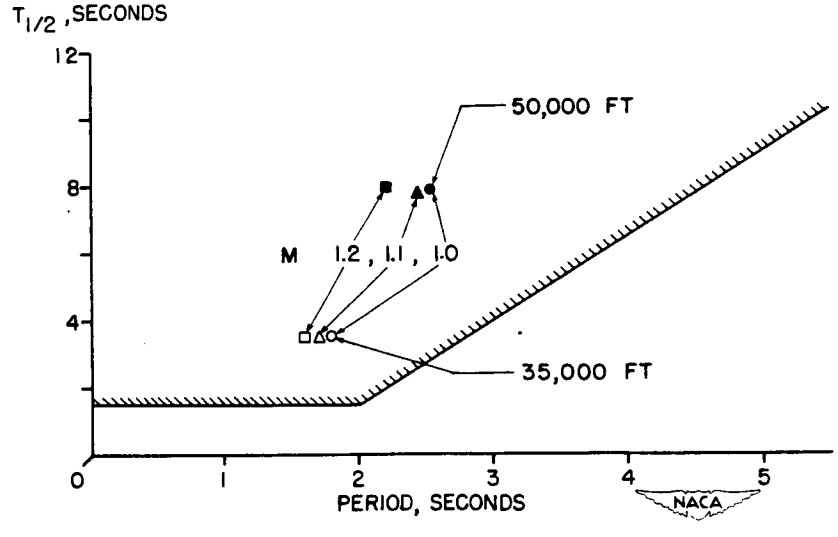


Figure 10.– Lateral–oscillation period–damping characteristics of the typical transonic airplane at transonic speeds.

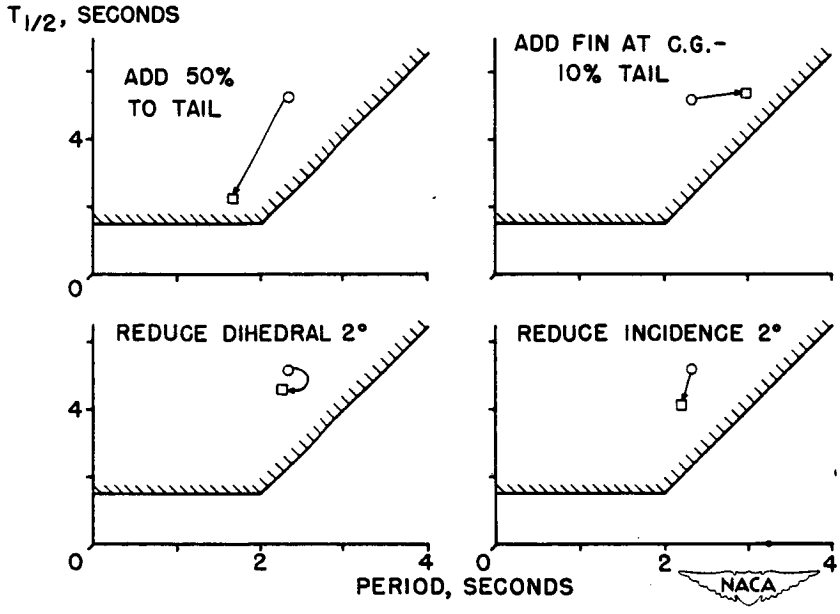


Figure 11.- Effect of changes in configuration on the lateral-oscillation period-damping characteristics of the typical transonic fighter.

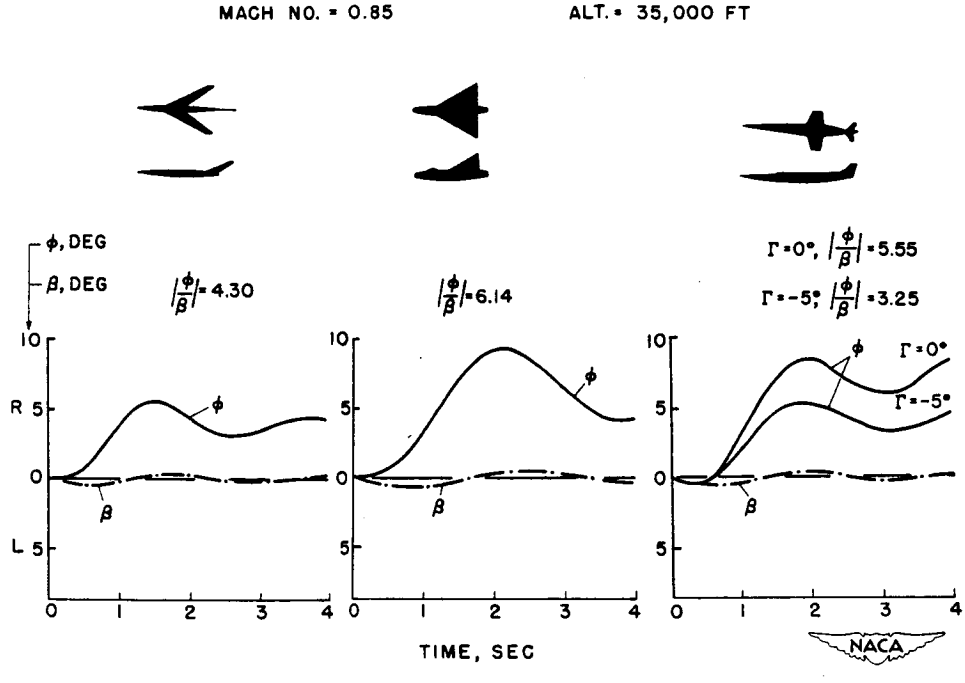


Figure 12.- Calculated time histories of the response of three high-speed airplanes to an impulse-type yawing-moment disturbance.

Preceding page blank

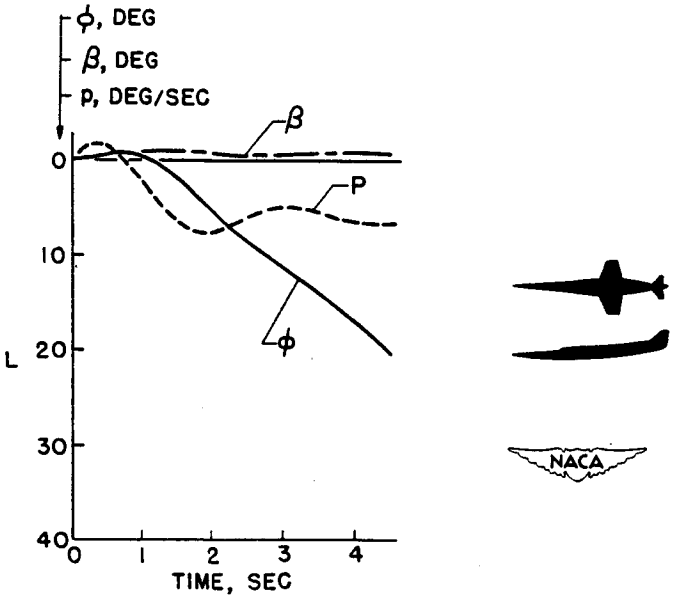
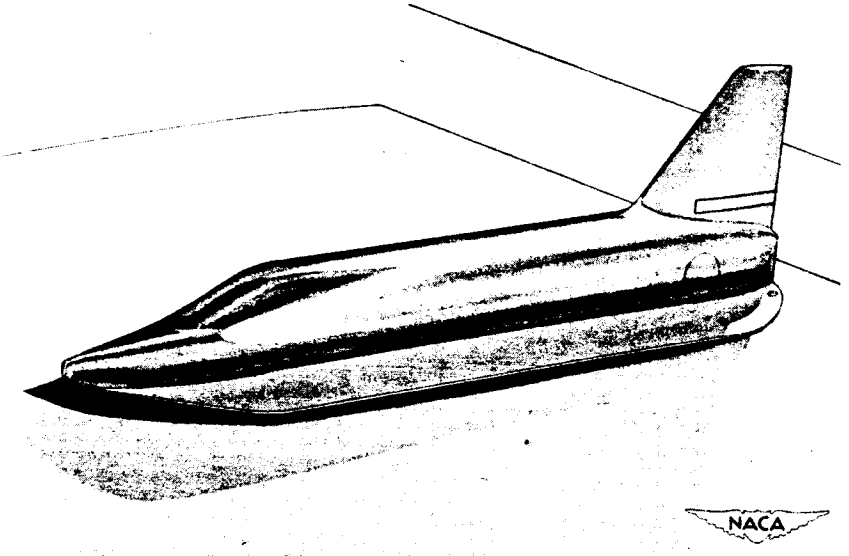


Figure 13.– Calculated time history of the response of a high-speed airplane to an abrupt rudder deflection.



WING-FLOW MODEL MOUNTED ON OSCILLATION APPARATUS

Figure 14.– Wing-flow model used in the snaking investigation.

Preceding page blank

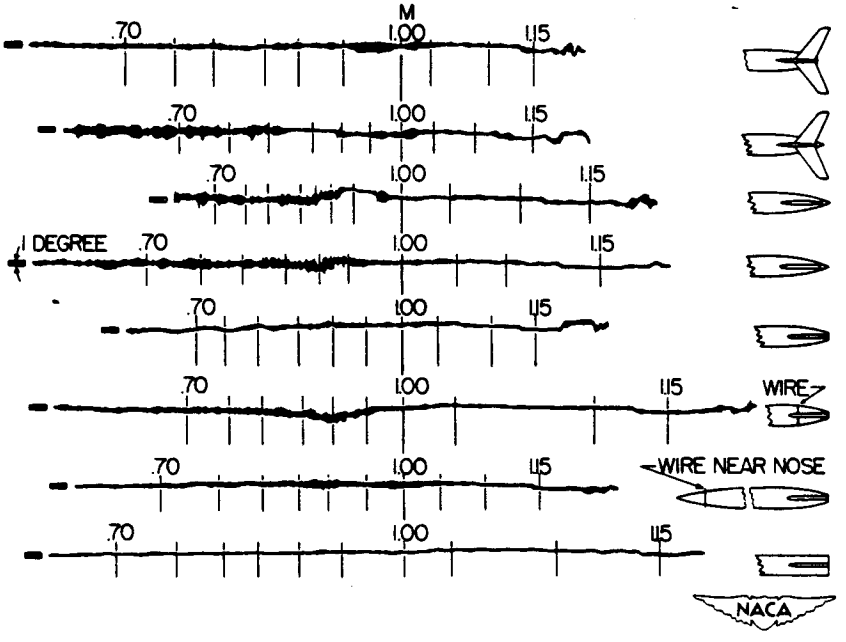


Figure 15.- Records of the yawing motion of various configurations of the wing-flow model in the transonic speed range.

Preceding page blank

INLETS, DIFFUSERS AND JETS

Preceding page blank

N65-86476

SUMMARY OF INFORMATION ON AIR INLETS

NOSE AND WING-ROOT INLETS

By Mark R. Nichols

Langley Aeronautical Laboratory

From the viewpoint of obtaining maximum pressure recovery, the most desirable place to locate the air inlet of an airplane is at a stagnation point, either at the nose of the fuselage or nacelle or along the leading edge of the wing. This location is desirable because the absence of initial boundary layer in these regions permits most of the required diffusion to be accomplished externally with negligible losses. The F-86 and B-47 airplanes are examples of the application of the nose inlet to high-speed aircraft. Because of the trend toward thin wings, no corresponding example can be cited of the application of the wing-leading-edge inlet, as such; however, the wing-root inlet, a compromise between the wing-leading-edge inlet and the fuselage scoop, is being used extensively both here and abroad. The F9F and F-88 are examples of high-speed airplanes equipped with this special type of wing inlet.

An important contribution in the field of nose-inlet research was the development of the NACA 1-series nose inlets. The initial research on these inlets resulted in subsonic design charts both for the basic inlets (reference 1) and for the basic inlets in combination with protruded central bodies suitable for accessory housings or propeller spinners (reference 2). These design charts were constructed to permit the direct selection of nose inlets of high internal-flow pressure recovery for desired critical Mach numbers up to about 0.89.

In order to study the NACA 1-series nose inlets at transonic speeds, three of the inlets have been further investigated in the Langley 8-foot high-speed tunnel at subsonic Mach numbers up to 0.92 and at a supersonic Mach number of 1.2 (references 3 and 4). The three inlets investigated were the 1-65-050 (M_{cr} = 0.72), the 1-50-100 (M_{cr} = 0.81), and the 1-40-200 (M_{cr} = 0.89). (Symbols are defined in an appendix.) In each inlet designation, the 1 identifies the NACA 1-series family, the second group of numbers specifies the inlet diameter in percent of the maximum body diameter, and the third group of numbers specifies the nose-inlet length in percent of the maximum body diameter. The 1-65-050 and 1-50-100 inlets were tested both alone and with various central bodies. The test body was 3 inches in diameter. As shown at the top of figure 1, this body was composed of the nose inlet (in this case, the 1-40-200 inlet), a cylindrical center section which was varied in length to maintain the same over-all body length for the three inlets and, for the tests at subsonic Mach numbers, a faired tail section

between the cylindrical center section and the sting. A three-inch-diameter sting was used for the tests at M = 1.2, so that there was no contraction at the tail of the body for this test condition.

Pressure distributions over the body with the 1-40-200 nose inlet operating at its design flow rate are shown at the bottom of figure 1. At the Mach number of 0.40, the pressure distribution over the inlet is typical of the external pressure distributions for the 1-series inlets at subcritical speeds. Beyond the maximum diameter station, the surface pressure dropped to near stream values along the cylindrical center section and finally became positive at the tail.

The pressures over the nose inlet became progressively more negative as the Mach number was increased, but a pressure distribution of essentially the same shape was maintained up to the critical Mach number of 0.89. As shown by the data for a Mach number of 0.92, a negative pressure peak was formed just ahead of the maximum-diameter station as the Mach number was further increased. This pressure peak was followed by a shock. The pressure recovery at the tail of the body indicates that this shock did not cause flow separation. The absence of flow separation was definitely confirmed by wake surveys.

For the Mach number of 1.20, a detached bow shock occurred ahead of the model; however, all the pressure coefficients shown correspond to supersonic flow. The pressure distribution over the inlet for this Mach number was similar in shape to that for the supercritical Mach number of 0.92, except that the negative pressure peak was broader and located farther back. Downstream of the pressure peak the flow was compressed gradually to the stream value along the cylindrical portion of the body without a discrete shock. An examination of this pressure distribution indicates that the pressure drag of a body using this nose inlet would not be significantly greater than that for a well-shaped solid-nose body of the same fineness ratio at this Mach number.

Surface pressures over the three inlets at their design flow rates are shown in the left part of figure 2 for a supercritical Mach number of 0.92. In the case of the 1-65-050 inlet for which the critical Mach number was only 0.72, the pressures reached large negative values over a broad region. The peak local Mach number was about 1.5. A strong shock occurred just rearward of maximum diameter; however, as in the previous case, the pressure recovery at the tail of the body and wake-surveys at the body-sting juncture show that this strong shock did not cause flow separation. The strength of the shock decreased rapidly as the nose-inlet critical Mach number was increased to 0.81 for the 1-50-100 inlet and to 0.89 for the 1-40-200 inlet. The minimum pressure coefficient for the 1-40-200 inlet corresponds to a peak local Mach number of only 1.06.

The external drag coefficients for the body with the three inlets operating at their design flow rates are shown in the right part of figure 2 as a function of the free-stream Mach number. These drag coefficients were determined from the previously mentioned surveys of the wake at the body-sting juncture. At the lower Mach numbers, the drag was essentially friction drag, with the differences shown being caused mainly by large differences in the extent of laminar flow. These differences, of course, might disappear at the higher Reynolds numbers of flight installations.

Critical Mach numbers predicted from the pressure distributions measured at the Mach number of 0.40 are indicated by the ticks on the curves. The actual critical Mach numbers determined from the high-speed pressure measurements are marked by the arrows. In each case, the measured critical Mach number exceeded the predicted critical Mach number by a small amount. A further appreciable margin always existed between the measured critical Mach number and the Mach number for which the drag increased rapidly due to compressibility effects. The design Mach numbers specified in the NACA 1-series nose-inlet design charts correspond to the ticks on the curves. Hence, the present results show that the specified design Mach numbers are conservative by margins of 0.05 or greater with respect to the force-break Mach numbers.

At the highest subsonic Mach number of 0.92, the external drag coefficient for the body with the 1-65-050 inlet installed was about 3 times that for the body with the 1-40-200 inlet. The difference was caused almost entirely by the difference in the direct shock losses. The magnitude of these shock losses stresses the importance of designing the inlet of a transonic airplane for a high critical Mach number.

Drag measurements were not obtained at the Mach number of 1.20 because the shock extended well beyond the end of the wake-survey rake. However, there is some evidence to indicate that the 1-40-200 nose inlet does not contribute an important increment to the drag of the body in the transonic range. First, the force-break Mach number for the body with this inlet is about the same as that for a well-shaped solid-nose body of the same fineness ratio. Second, as mentioned previously, an examination of the surface pressure measurements indicates that the pressure drag of a body in which this inlet is used would not be significantly greater than that for a well-shaped solid-nose body of the same fineness ratio at the supersonic Mach number of 1.20.

The effects of inlet-velocity ratio on the surface pressures and external drag coefficients of the 1-65-050 and 1-40-200 inlets are shown in figure 3. For both inlets, reducing the inlet-velocity ratio from the design value to zero caused the formation of a negative pressure peak on the inlet lip at subcritical speeds (M = 0.60 and 0.84). The negative pressure peak on the 1-65-050 inlet decreased in magnitude as

[redacted]

the Mach number was increased and was completely eliminated at the highest subsonic test Mach number of 0.92. In contrast, the negative pressure peak on the 1-40-200 inlet persisted to the higher Mach number. The Mach number for supercritical drag rise was not affected by flow rate in either case. Hence, it may be concluded that the NACA 1-series inlets may be used at much lower inlet-velocity ratios than those specified in the NACA 1-series nose inlet design charts without reducing the force-break Mach number. Any such reduction in inlet-velocity ratio, however, may result in an increase in the friction drag by moving the point of transition forward.

At the design inlet-velocity ratio, increasing the angle of attack from 0° to 3.7° had an effect on the pressure distributions over the top sections of the inlets similar to that obtained by decreasing the inlet-velocity ratio to zero. Inasmuch as the decreases in surface pressure were small and were localized at the top sections, the force-break Mach numbers for the NACA 1-series inlets appear to be insensitive also to small variations in angle of attack or yaw.

The effects of a protruded elliptical central body on the surface pressures and external drag of the 1-50-100 inlet operating at its design inlet-velocity ratio are shown in figure 4. As shown by the differences between the solid lines which are for the basic inlet and the dotted lines which are for the combination of the inlet and central body, installation of the central body had only a very small effect on the surface pressures both at a subsonic Mach number of 0.80 and at the supersonic Mach number of 1.20. The force-break Mach number consequently was not reduced by the presence of the central body.

Total pressure surveys were made inside the inlets after a small area expansion. The measurements at the design inlet-velocity ratios show ram recoveries exceeding 97 percent of the free-stream impact pressure for all configurations throughout the subsonic test range and also at the supersonic Mach number of 1.20.

In summary, the results of this investigation of NACA 1-series nose inlets and 1-series nose inlets combined with various central bodies indicate that: (1) The existing NACA 1-series nose-inlet design charts (references 1 and 2) are unduly conservative with respect to the Mach number to which these inlets may operate without large drag increases due to compressibility effects; (2) An NACA 1-series nose inlet designed for a critical Mach number of 0.89 or greater probably will not contribute a substantial increment to the external drag of the body in the transonic range; (3) In contrast to the view held previously, a pressure peak on the lip of this type of inlet, brought about by operation below the design flow rate or by operation at small angles of attack or yaw, has a negligible effect on the force-break Mach number; and (4) An inlet of this type can be designed to provide a ram recovery exceeding 97 percent of the free-stream impact pressure up to a Mach number of 1.2.

The wing-leading-edge inlet would be expected to have characteristics roughly similar to those for the nose inlet. Because of the presence of an initial boundary layer, it is not obvious that similar desirable characteristics would be obtained in the case of the wing-root inlet. Therefore, an investigation of the inlet in the root of a swept wing, an arrangement of great interest currently for the transonic airplane, has been started at the Langley Laboratory. The ultimate objective of this research is the determination of the configurations suitable for the transonic airplane and the procurement of comprehensive design information for these configurations. The results which will be discussed were obtained in the exploratory low-speed phase of the investigation currently under way in the Langley two-dimensional low-turbulence tunnel.

A bottom view and sketches of the semispan model used in the initial low-speed tests are shown in figure 5. The basic wing was composed of NACA 64-008 airfoil sections, had a leading-edge sweep of 47° and a taper ratio of 0.6, and was located in the midwing position on the half section fuselage. In order to permit installation of the inlet, the wing was flared from the original 8-percent-thick section at the outboard end of the inlet to a 13-percent-thick section of twice the original chord at the fuselage. The inlet lips were then faired in as shown in section AA by use of existing wing-inlet section data (references 5, 6, and 7) as a guide.

Figure 6 presents a comparison of the lift and external drag characteristics of the basic model and the model with the inlet operating at an inlet-velocity ratio of 0.6. The coefficients given are based on the projected area of the basic wing. Installation of the inlet is shown to have increased both the maximum lift coefficient and the lift-curve slope. An analysis of the results indicates that the increased lift may be accounted for by the triangular area added at the wing root. The external drag was essentially unaffected by installation of the inlet.

Total-pressure measurements in the flow entering the inlet along the side of the fuselage are presented in figure 7 for angles of attack of 0° to 10° at inlet-velocity ratios of both 0.4 and 1.0. The entering boundary layer remained thin and did not separate over this broad range of operating conditions. Pressure gradients in the vicinity of the entrance apparently caused some of the boundary layer approaching the entrance to turn and pass above and below the wing rather than to enter the inlet. Thus, control of the boundary layer along the side of the fuselage does not appear necessary for inlets of this type when, as in the present case, the inlet height at the fuselage is small relative to the inlet span.

Total-pressure recoveries measured by two vertical rakes well inside the inlet are presented in figure 8. The test conditions are the

same as those for figure 7 except that data for angle of attack of 6° have been added. At the inboard station, the ram recovery remained near 100 percent for the entire range of test conditions. The ram recovery at the outboard station also was high up to the angle of attack of 6°, but dropped off for the 10° angle of attack because of flow separation from the lower lip. It is probable that the onset of this separation can be retarded to satisfactorily large angles of attack and inlet-velocity ratios by small modifications that are being made to the lower lip.

The minimum pressures on the external surfaces of the inlet were only slightly more negative than the corresponding minimum pressures on the wing of the basic model, except at the outboard inlet section where sharp local pressure peaks existed. Again it is probable that these localized pressure peaks also can be eliminated by small modifications to the lip shape.

In summary, the results obtained so far in this initial low-speed phase of this investigation of a swept-wing-root inlet are promising. No phenomena have been encountered which would appear to preclude the attainment of a high level of ram recovery and low drag in high-speed flight. The high-speed phase of the investigation must be conducted to evaluate the performance of the inlet at transonic speeds before it can be recommended for transonic applications.

[redacted]

APPENDIX

SYMBOLS

M	Mach number
M_{cr}	critical Mach number
P	pressure coefficient $\left(\frac{p - p_o}{q_o}\right)$
P_{cr}	pressure coefficient corresponding to critical Mach number
V_i	average velocity in entrance
V_o	free-stream velocity
C_L	lift coefficient
C_D	drag coefficient
D	maximum diameter of body
x	distance from nose of body
H_i	total pressure just inside entrance
p	local static pressure
p_o	free-stream static pressure
q_o	free-stream dynamic pressure
α	angle of attack

[redacted]

REFERENCES

1. Baals, Donald D., Smith, Norman F., and Wright, John B.: The Development and Application of High-Critical-Speed Nose Inlets. NACA ACR L5F30a, 1945.

2. Nichols, Mark R., and Keith, Arvid L., Jr.: Investigation of a Systematic Group of NACA 1-Series Cowlings with and without Spinners. NACA RM L8A15, 1948.

3. Pendley, Robert E., and Smith, Norman F.: An Investigation of the Characteristics of Three NACA 1-Series Nose Inlets at Subcritical and Supercritical Mach Numbers. NACA RM L8L06, 1949.

4. Pendley, Robert E., and Robinson, Harold L.: An Investigation of Several NACA 1-Series Nose Inlets with and without Protruding Central Bodies at High Subsonic Mach Numbers and at a Mach Number of 1.2. (Prospective NACA paper)

5. Racisz, Stanley F.: Development of Wing Inlets. NACA ACR L6B18, 1946.

6. Bartlett, Walter A., Jr., and Goral, Edwin B.: Wind-Tunnel Investigation of Wing Inlets for a Four-Engine Airplane. NACA RM L6L11, 1947.

7. Dannenberg, Robert E.: A Design Study of Leading-Edge Inlets on Straight Wings. (Prospective NACA paper)

[redacted]

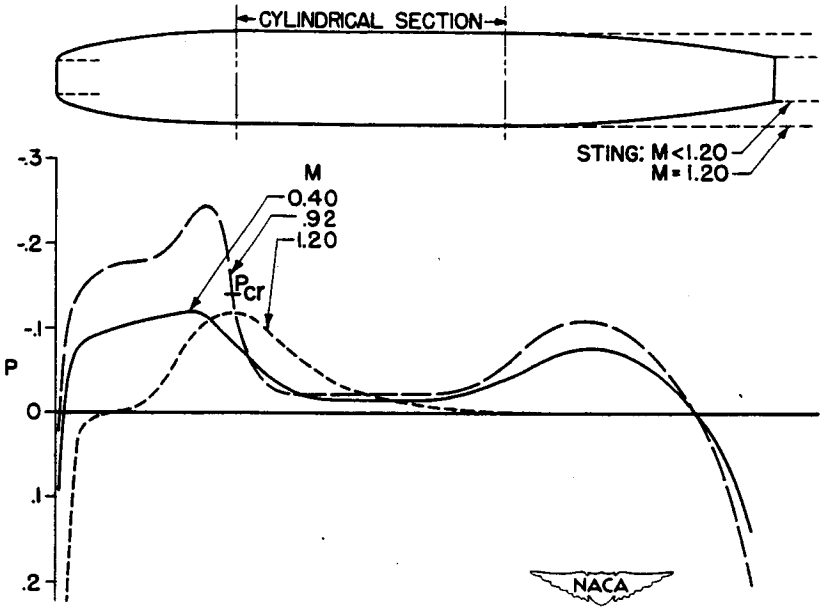


Figure 1.- Pressure distributions over body with NACA 1-40-200 nose inlet. $\alpha = 0^{o}$; $\frac{V_i}{V_o} = 0.4$.

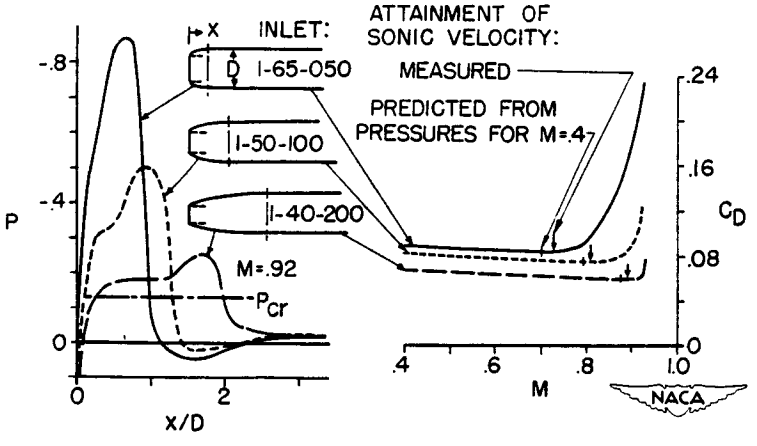


Figure 2.- Effects of inlet proportions on surface pressures and external drag.. $\alpha = 0^{o}$, design $\frac{V_i}{V_o}$.

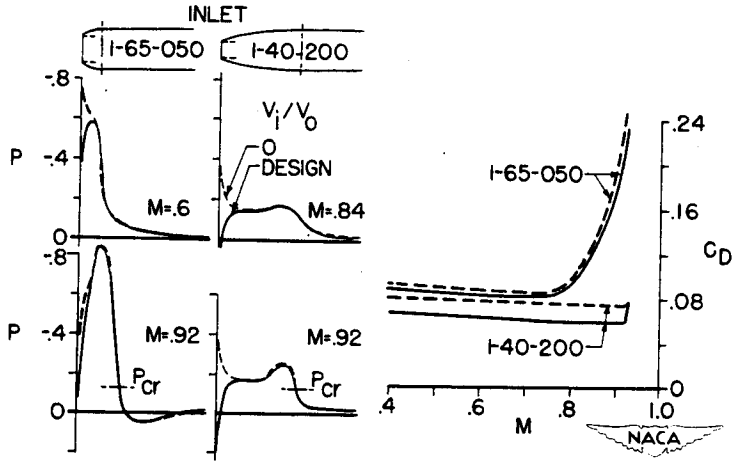


Figure 3.- Effects of inlet-velocity ratio on surface pressures and external drag. $\alpha = 0^{\circ}$.

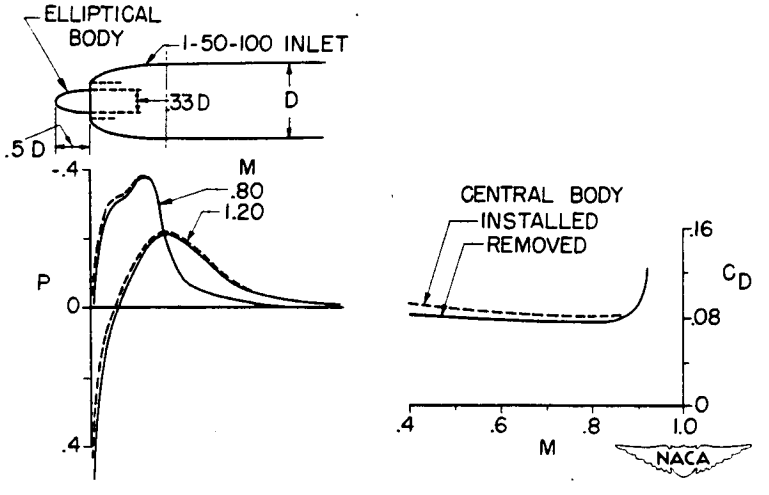


Figure 4.- Effects of central body on surface pressures and external drag. $\alpha = 0^{\circ}$; design $\frac{V_i}{V_o}$.

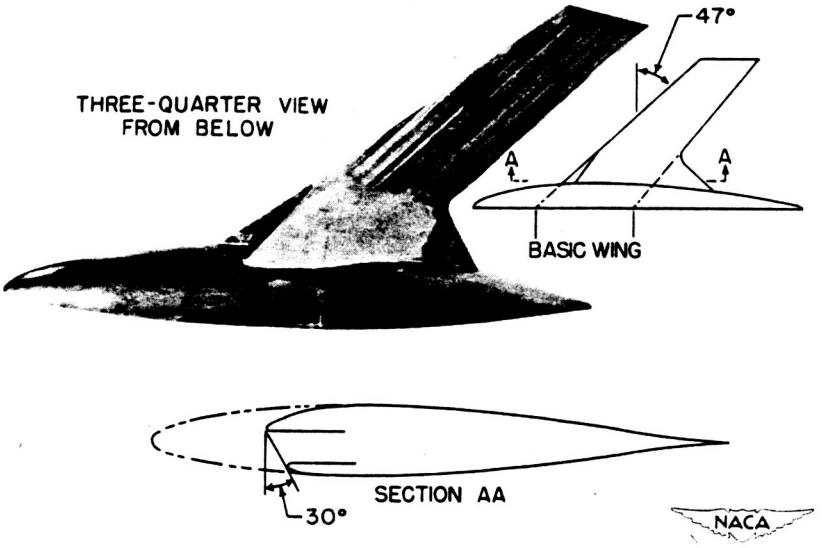


Figure 5.- Semispan wing-root inlet model.

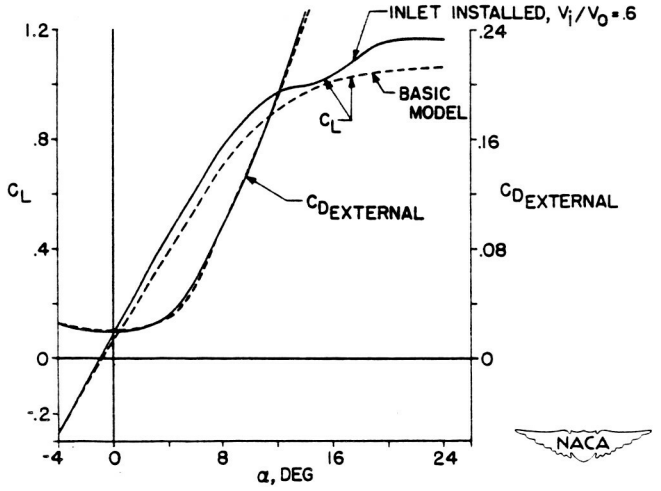


Figure 6.- Effects of inlet installation on lift and drag characteristics. (Coefficients are based on projected area of wing of basic model.)

Preceding page blank

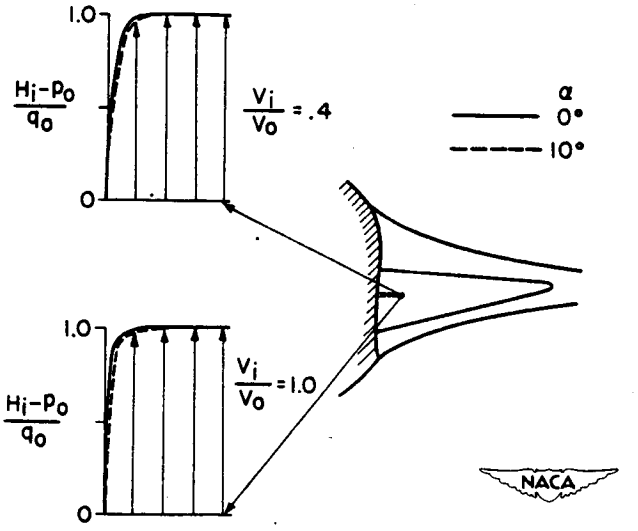


Figure 7.- Total-pressure recoveries in flow entering inlet along side of fuselage.

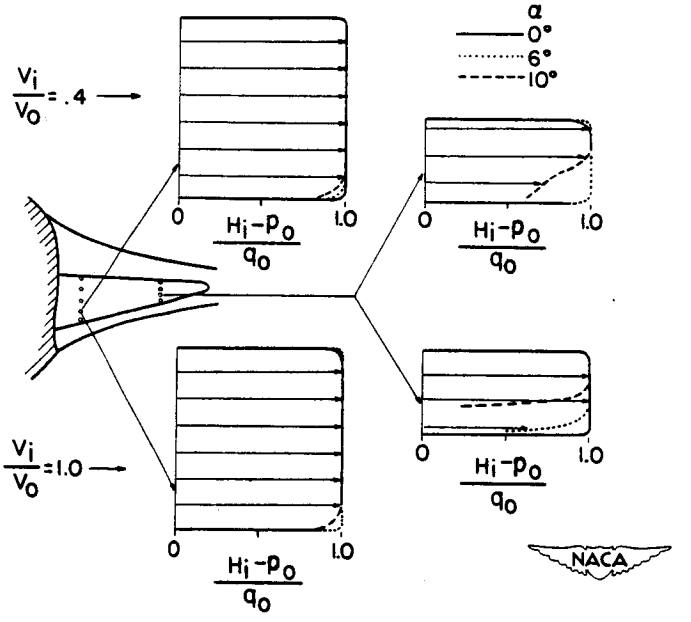


Figure 8.- Total-pressure recoveries at two vertical stations inside inlet.

Preceding page blank

N65-86477

SUMMARY OF INFORMATION ON AIR INLETS

NACA SUBMERGED INLETS

By Emmet A. Mossman

Ames Aeronautical Laboratory

Selecting a type of air inlet suitable for a high-speed airplane is no longer a question merely of obtaining optimum pressure recovery, or of structural or arrangement desirability. Air inlets are becoming a principal factor in determining the fuselage size and shape, which in turn directly affect the airplane drag. The increased importance of fuselage drag in the transonic speed range has been pointed out by Schamberg in reference 1.

Submerged inlets have been shown to be practicable at high subsonic speeds for certain engine installations. (See references 2, 3, and 4.) An example of this is the Republic Aviation Corporation's modification of an F-84 Thunderjet airplane in which the installation of a radar nose was made possible by substitution of submerged inlets for the conventional nose inlet. The installation is shown in figure 1. This change was reportedly accomplished with no loss in airplane performance. However, knowledge of the characteristics of these and other inlets at transonic speeds is rather meager. This lack of information has been the result of the limitations of testing facilities in this speed range, and of the higher priority of other research. Investigations are now under way of the inlet types thought to be most promising. The data presented in this paper summarize the recent results of research at transonic speeds on NACA submerged inlets. Three transonic testing techniques were used: the wind-tunnel transonic bump, the flight wing-flow method, and a small high-speed wind tunnel.

The NACA divergent-wall submerged inlet has been investigated on a transonic bump in the Ames 16-foot high-speed tunnel. A schematic view of the bump mounted in the wind tunnel, with the submerged inlet installed, is shown in figure 2. Angle of attack for side-inlet installations was simulated by angular changes of the model in the plane of the bump surface. The pressure-recovery measurements were taken by 30 total-pressure tubes in six rows just behind the duct lip, and the pressure recoveries shown are the weighted averages of these measurements.

Some results of the transonic-bump investigation are shown in figure 3 for a duct having a width-depth ratio of 4.0 ($W/d = 4$). The ordinate for these curves is ram-recovery ratio, which is the ratio of the ram pressure recovered to the ram pressure available. It may be

seen that there was a gradual but slight decrease in pressure recovery in the Mach number range from 0.9 to 1.1 for mass-flow ratios of 0.35, 0.45, and 0.55, where mass-flow ratio is defined as the ratio of the mass of air flowing into the inlet M_1 to the mass of air flowing through an equal area in the free stream M_0. The pressure recovery was increasing again at the highest free-stream Mach number of 1.15. The effect on the pressure recovery of changes in angle of attack for angles up to 8° was found to be slight within the range of these tests. In some cases, increasing the angle of attack was beneficial to the pressure recovery. These data are believed to indicate the trend that may be expected in the transonic speed range with this type of inlet. However, the ram-recovery ratios obtained with this arrangement, while useful qualitatively, should not be construed as a precise indication of the true entrance pressure loss to be expected on a full-scale airplane. The severe flow angularity in the corner regions of the duct entrance, the low mass-flow ratios, and the thickness of the transonic-bump boundary layer make precise measurement difficult. The effect on the pressure recovery of the boundary layer into which the inlet was placed is shown in figure 4. The abscissa is a boundary-layer parameter h/d representing the ram defect of the boundary layer at the inlet position $\left[\frac{h}{d} = \frac{1}{d}\int_0^{\delta} \frac{\Delta H}{H_0 - p_0}\, dy, \text{ (reference 5)}\right]$ where

ΔH loss in total pressure in the boundary layer

$H_0 - p_0$ free-stream ram pressure

d depth of the duct

δ boundary-layer thickness

Larger boundary-layer losses are represented by larger values of h/d. The pressure loss in the boundary layer, as indicated by h/d, can be seen to be greater for the transonic bump than was observed in a previously reported test of a $\frac{1}{4}$-scale model of a fighter airplane.

The effect of this thicker boundary layer on the pressure recovery in the inlet is seen to be of large magnitude. For comparable Mach numbers and mass-flow ratios the values of ram-recovery ratios are approximately 0.84 for the transonic-bump investigation and 0.92 for the $\frac{1}{4}$-scale airplane model installation. Mach number distributions along the ramp center line corresponding to free-stream Mach numbers of 0.74, 1.02, and 1.15 are shown in figure 5. A shock formation was

evidenced at about 60 percent of the ramp length at a Mach number of 1.02. As the free-stream Mach number was increased, the shock became stronger and moved downstream slightly. These tests will be extended, and data for higher mass-flow ratios will be obtained.

Although test data from the transonic bump indicate no adverse effects on the pressure recovery at transonic speeds, exploratory tests in flight utilizing the wing-flow technique showed that the operation of the inlet at transonic speeds is critical to changes in inlet geometry. In this investigation the pressure gradient down the ramp was more unfavorable than in the bump tests because of an increase in the width to depth ratio of the entrance. Separation due to boundary-layer shock-wave interaction did occur at transonic speeds for mass-flow ratios below 0.4.

The ability of the divergent-wall inlet to operate with satisfactory pressure recovery at free-stream Mach numbers somewhat greater than 1.0 has been attributed to the thinness of the boundary layer along the inlet ramp. A comparison of the boundary-layer growth on parallel-wall and divergent-wall ramps is shown in figure 6 for a mass-flow ratio of 0.6. Here the momentum thickness down the center line of the ramp is given from measurements and from theoretical calculations by use of the known pressure distributions. It may be seen from this figure that the growth of the boundary layer in the divergent-wall inlet, as experimentally measured at low speeds, is approximated theoretically by assuming a three-dimensional growth (reference 6) which allows for thinning of the boundary layer due to lateral motion. The agreement between the measured boundary-layer growth and the growth calculated by theory for the parallel-wall inlet is shown by the two upper plots. The boundary-layer momentum thickness for the divergent-wall inlet can be seen to have been much thinner than for the parallel-wall inlet. Research on the interaction of boundary layers with shock waves has shown that a thin boundary layer does not separate as readily in the presence of a shock wave as does a thicker boundary layer. In the transonic-bump investigation, the interaction of the ramp shock wave with the ramp boundary layer did not become severe enough to cause separation along the ramp of the divergent-wall inlet. Thus, the relatively thin ramp boundary layer of the NACA submerged inlet enhances both the subsonic and the transonic operation of the inlet.

Of course, during subsonic operation at mass-flow ratios above 0.4, the pressure losses due to the boundary layer in the divergent-wall inlet are not the principal pressure losses. In the absence of boundary-layer separation, the main part of the pressure losses of an NACA submerged inlet is in the turbulent mixing regions which originate along the side walls of the ramp (reference 7). It has been shown that these loss regions are actually rolled-up vortex sheets generated along the outside edges of the divergent walls. Flow pictures were obtained by

[redacted]

plunging a small model of the submerged inlet into a tank of water which had aluminum powder sprinkled on the surface. (See fig. 7.) The model was mounted on a rack and lowered into the water. The resulting vortex formation from the oblique side walls (fig. 8) is shown in the two regions indicated by the broad arrows. The effect of the passing of these vortex regions through the oblique shock wave on the ramp is not known, but the results of the transonic-bump tests in the Ames 16-foot high-speed tunnel indicate that it was not adverse. Successful transonic operation of the submerged inlet is believed to be a function of the intensity of the interaction between the ramp boundary layer and the shock wave.

It has been suggested that boundary-layer control be utilized to delay the onset of shock-wave induced separation. Tests were made at low speeds of a large-scale model of an NACA submerged inlet in which the rearward 45 percent of the inlet ramp was constructed of porous bronze material. The model of the air-induction system was mounted on a dummy wall of an Ames 7- by 10-foot tunnel. The tunnel boundary layer passed beneath the dummy wall. Measurements were made in the duct by a rake of 90 total-pressure tubes. Some preliminary results of these tests are shown in figure 9. Removal of the ramp boundary layer had the greatest effect at the low mass-flow ratios. According to an analysis which is to be presented by Norman J. Martin in a subsequent paper, instability of twin-inlet operation should be almost eliminated with a suction mass-flow ratio of 0.06. The ramp boundary layer at the end of the porous plate was almost completely eliminated for the conditions shown in figure 9. It should be noted that the quantity of air removed through the porous plate and the estimated power required for removal of this air is small. These results are from low-speed tests, however, and the efficacy of removing the ramp boundary layer through a porous surface at transonic speeds and thus extending satisfactory inlet operation has not yet been proven. Preliminary tests at transonic speeds of a simulated NACA submerged inlet in a small wind tunnel have shown no separation of the ramp boundary layer at free-stream Mach numbers of approximately 1.15. These results are similar to those obtained in the Ames 16-foot high-speed tunnel. Thus, since boundary-layer separation induced by shock formation was not encountered, porous suction had no noticeable effect when applied in the small-wind-tunnel test.

The results presented in this paper indicate that the pressure recovery characteristics of NACA submerged inlets at transonic speeds are promising; however, the data are as yet incomplete, and further research is needed.

REFERENCES

1. Schamberg, R.: Effects of Flight Speed and Propulsive System on Aircraft Range. Rep. R-114, Rand Corp., Aug. 13, 1948.

2. Hall, Charles F., and Barclay, F. Dorn: An Experimental Investigation of NACA Submerged Inlets at High Subsonic Speeds. I - Inlets Forward of the Wing Leading Edge. NACA RM A8B16, 1948.

3. Hall, Charles F., and Frank, Joseph L.: Ram-Recovery Characteristics of NACA Submerged Inlets at High Subsonic Speeds. NACA RM A8I29, 1948.

4. Anon.: All-Weather Thunderjet. Aviation Week, vol. 51, no. 2, July 11, 1949, p. 14.

5. Mossman, Emmet A., and Randall, Lauros M.: An Experimental Investigation of the Design Variables for NACA Submerged Duct Entrances. NACA RM A7I30, 1947.

6. Kehl, A.: Investigations on Convergent and Divergent Turbulent Boundary Layers. R.T.P. Translation No. 2035, British Ministry of Aircraft Production. (From Ingenieur Archiv. Vol. XIII, No. 5, 1943, pp. 293-329.)

7. Delany, Noel K.: An Investigation of Submerged Air Inlets on a 1/4-Scale Model of a Typical Fighter-Type Airplane. NACA RM A8A20, 1948.

Preceding page blank

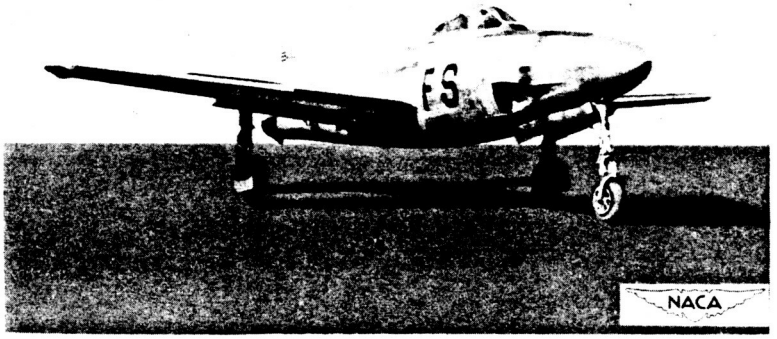


Figure 1.- The Republic F-84 with NACA submerged inlets.

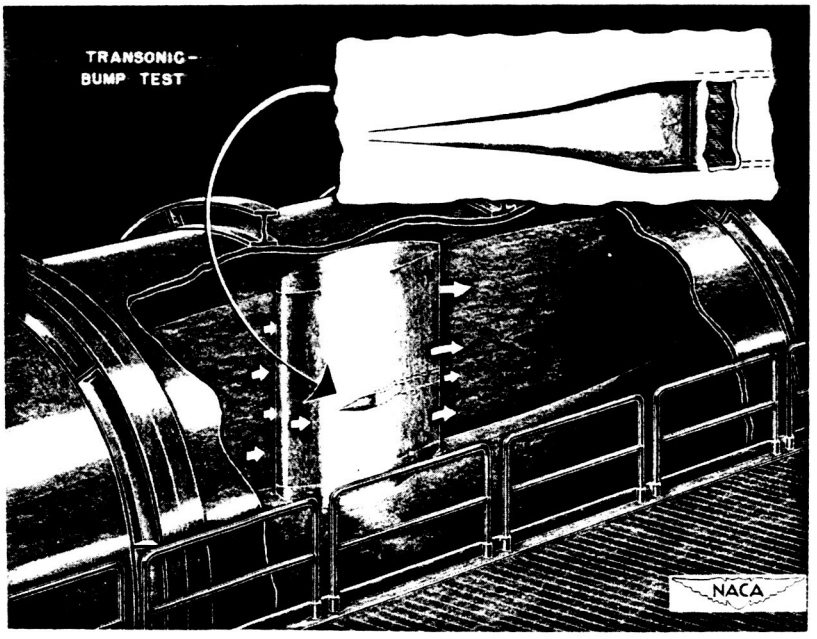


Figure 2.- The transonic-bump installation in the Ames 16-foot high-speed tunnel.

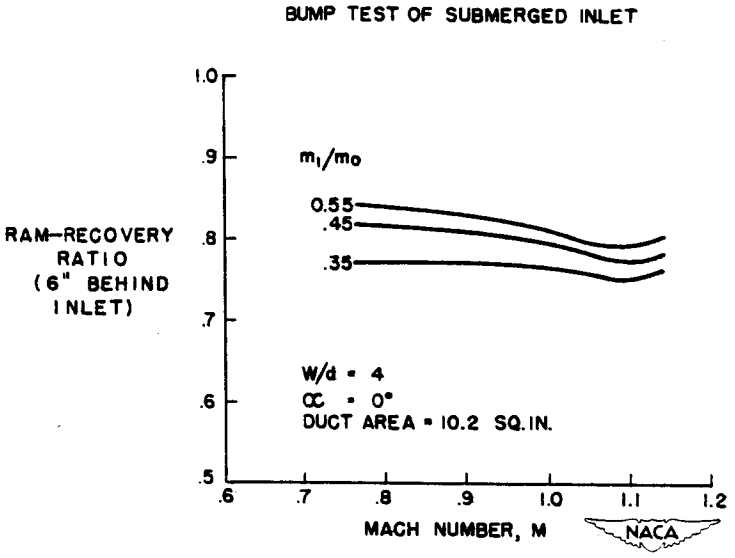


Figure 3.- Effect of Mach number on the ram-recovery ratio from the transonic-bump tests of an NACA submerged inlet.

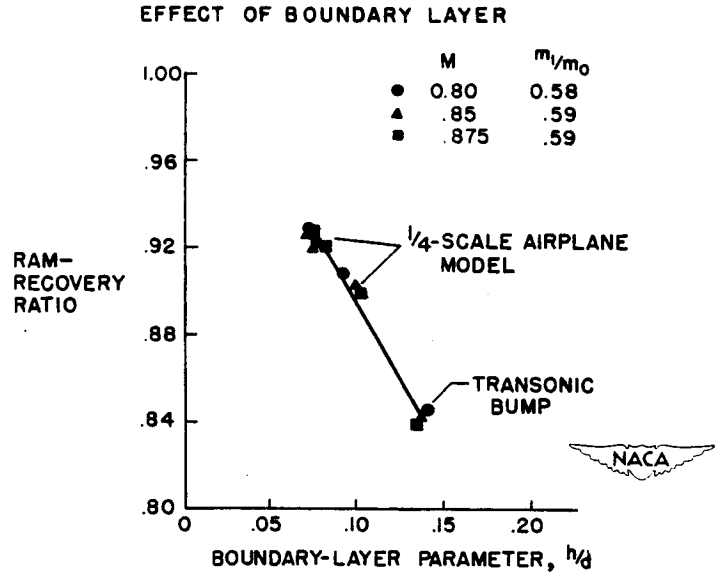


Figure 4.- Effect of boundary layer on the pressure recovery of NACA submerged inlets.

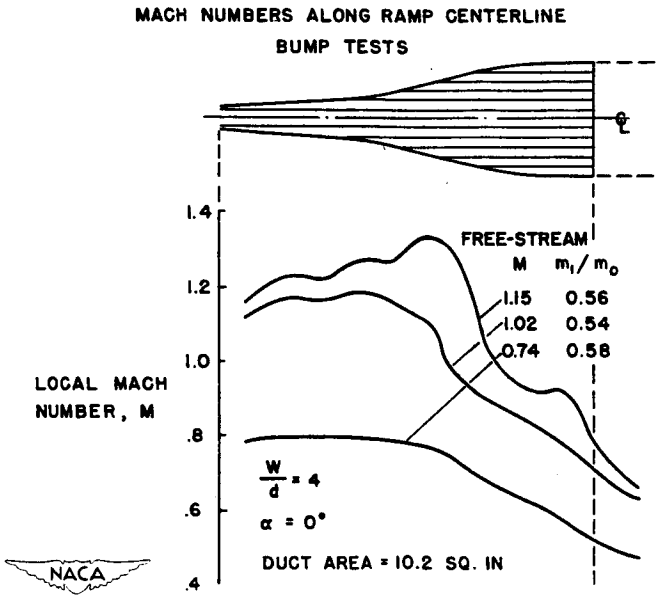


Figure 5.- Mach number distribution along the ramp center line from the transonic-bump tests of an NACA submerged inlet.

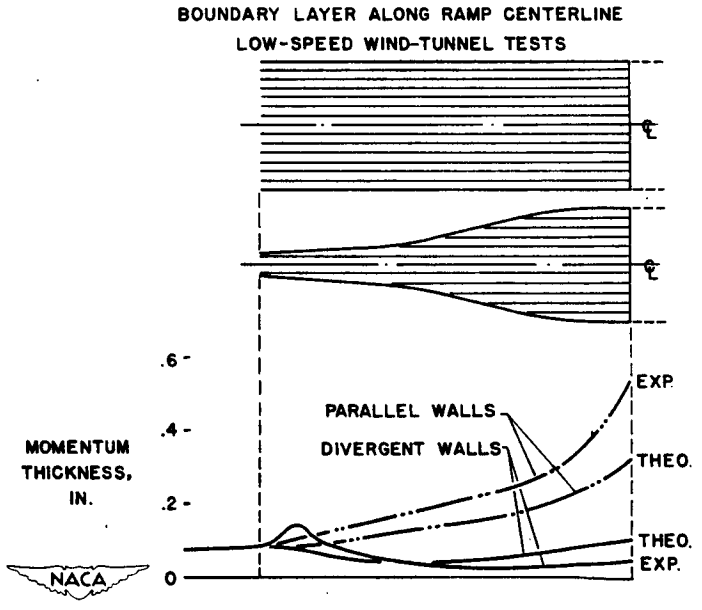


Figure 6.- Comparison of the experimental and theoretical boundary-layer growth along the ramps of submerged inlets.

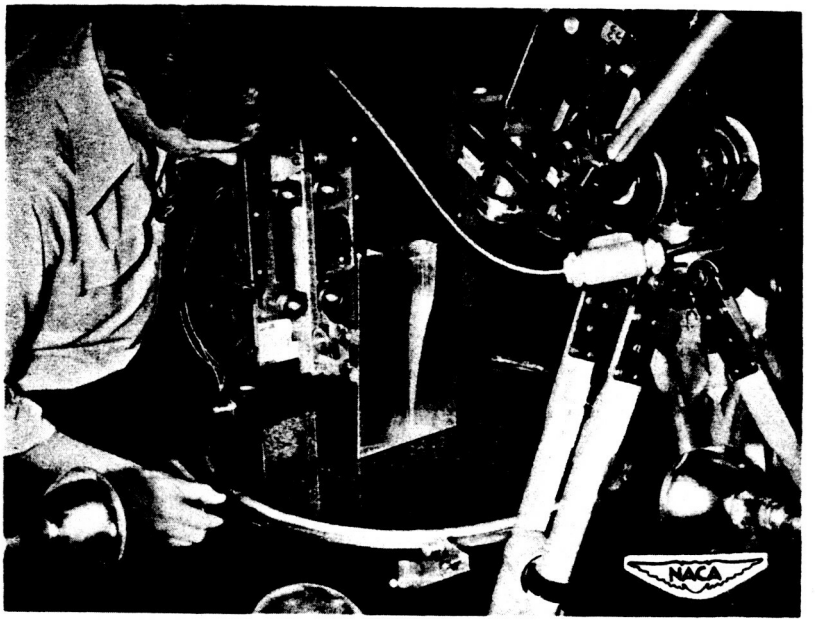


Figure 7.- Water-flow study apparatus.

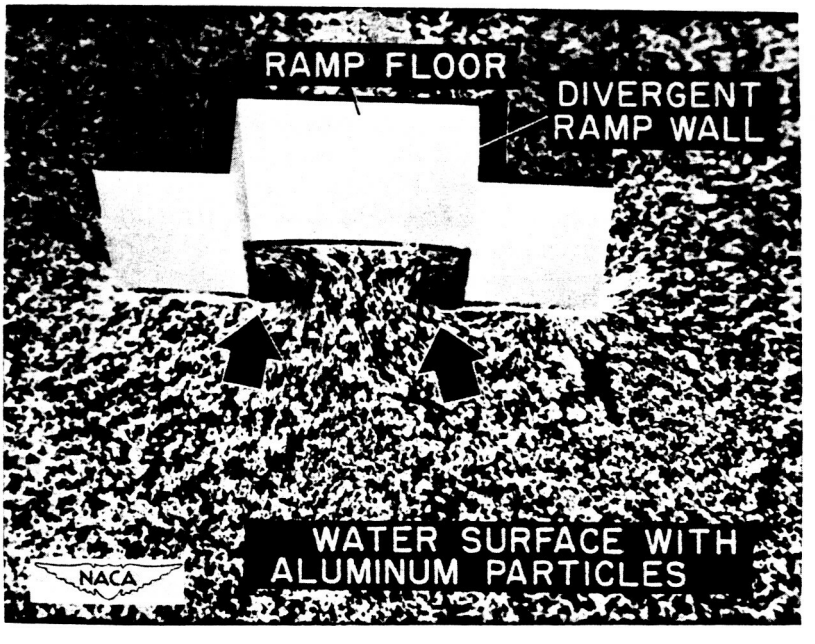


Figure 8.- Vortex formed in an NACA submerged inlet.

Preceding page blank

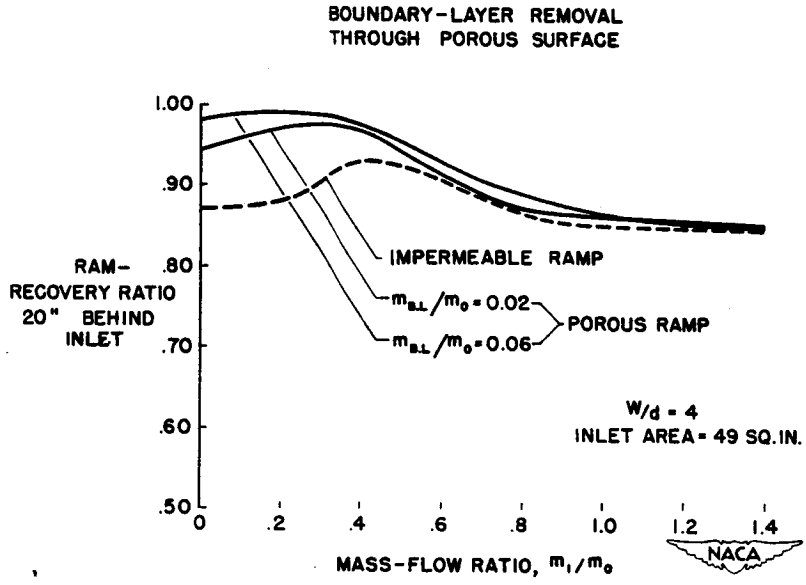


Figure 9.- Effect of boundary-layer removal through a porous ramp on the pressure recovery of an NACA submerged inlet.

Preceding page blank

N65-86478

DIFFUSERS FOR HIGH-SPEED AIRCRAFT

By Kennedy F. Rubert

Langley Aeronautical Laboratory

Intake diffusers for transonic and supersonic aircraft assume a variety of configurations, some of which are shown in figure 1. The inlet may be a simple divergent passage, convergent-divergent, or either of these in conjunction with an inner body. Depending upon operating conditions, subsonic flow makes its first appearance ahead of the inlet or only in the aft portion. Whatever the configuration and operating condition, there is one problem common to all: diffusion from a maximum subsonic speed, usually close to sonic, to the low-speed condition ultimately desired. The success with which the desired diffusion can be accomplished depends in large measure upon the initial boundary-layer conditions and the geometrical detail in the high-speed region. It is the purpose of this paper to discuss the performance of subsonic diffusers with high-speed inlet flows in relation to these factors.

In an actual duct, Mach number and pressures vary across any cross section because of boundary layers and local wall curvatures. In describing performance, mean values of these varying quantities are used for simplicity. Performance so described is rated in comparison with that of a hypothetical diffuser having isentropic flow throughout and constant velocity across any cross section.

Most of the available diffuser data are for Mach numbers less than 0.4 and Reynolds number less than 120,000, with fully developed turbulent pipe flow at the inlet (reference 1). In aircraft application the speeds approach sonic, Reynolds number is in the millions, and the boundary layer, although turbulent, does not reach the center of the stream. Performance (from reference 2) of a representative high-speed, large Reynolds number conical diffuser is given in figure 2. The diffuser has a 21-inch diameter cylindrical inlet, faired by a 5-inch radius into a 12° total-angle cone having an over-all area ratio of 2 to 1. Dotted lines indicate the converging inlet bell and exit tailpipe used in blower-testing the diffuser. The initial boundary layer is very thin with a displacement thickness nearly constant at 0.035 inch over the speed range. Performance coefficients are plotted against inlet Mach number, a mean value which is the Mach number which an identical mass flow would have exhibited if constant in velocity over the cross section.

The first performance coefficient is that of total pressure loss, which is the ratio of loss in mean total pressure between inlet and outlet to the mean dynamic pressure at the inlet. The loss coefficient changes little with increasing Mach number up to the onset of inlet

choking, which because of boundary layer and local wall curvature effects occurs at a mean Mach number less than unity. When fully choked no further increase in inlet Mach number is possible, and the loss-coefficient curve becomes vertical.

The loss coefficient of itself is not a complete index of diffuser performance, because it fails to indicate how much of the available dynamic pressure is converted to static pressure. Because the boundary layer has less dynamic pressure than the main flow, it must increase in area proportionately more than the main flow in order to develop the same pressure rise. This excess thickening of the boundary layer reduces the enlargement of the center stream so that the conversion of dynamic pressure is less than that ideally possible. This effect, which is quite distinct from any losses incurred, is often important. In figure 2 the diffusion factor, or ratio of actual to ideal dynamic pressure conversion, is, however, practically unity throughout the speed range. The effectiveness, or ratio of actual to ideal static pressure rise, is an over-all performance curve which shows the resultant performance after paying for the total pressure losses from that dynamic pressure which has been converted to static pressure. In this case the effectiveness has a nearly constant value of about 0.95.

Thickening the initial boundary layer has a profound influence upon the performance of the diffuser. Results obtained when the inlet boundary layer was thickened about five times by inserting a length of straight tube between the bell and diffuser inlet are given in figure 3 (from reference 2). The loss coefficient is almost doubled at low speed and exhibits a sharp rise with increasing speed which is attributed to upstream movement in the diffuser of flow separation. The diffusion factor is much less than unity and exhibits a downward trend with increasing Mach number. The over-all performance reflects these changes and the effectiveness, which is less than 0.8 at low speed, drops steadily with increasing Mach number. In this case, inability to convert dynamic pressure to static pressure is a greater element in lowering the effectiveness than is the total pressure loss.

It appears at least for thin boundary layers that the loss coefficient is closely related to the absolute thickness of the boundary layer, whereas the diffusion factor is more closely related to the proportionate thickness of the boundary layer in relation to the diffuser inlet diameter. This is shown by figure 4 in which results from the preceding discussion are compared at an inlet Mach number of 0.7 with the results from a geometrically similar diffuser 10 inches in diameter (from reference 3). At nearly equal boundary-layer thickness the loss coefficients are about equal, but the diffusion factor of the smaller diffuser is 0.81 as contrasted with 0.98 for the larger diffuser, with consequent impaired effectiveness. It should be noted

that, as a fraction of the inlet diameter, the boundary layer for the small diffuser is twice that for the larger. Somewhat similar results are obtained when the initial boundary layers are thicker, but here there is some evidence in the data that relative as well as absolute thickness may influence the total pressure loss.

Annular diffusers are of importance because of the application to turbojet engines. Figure 5 shows as dashed lines loss coefficients and effectiveness for two annular diffusers (from reference 4). Also shown, as solid lines, are these same coefficients obtained at equal initial boundary-layer thickness for the previously discussed 21-inch 12° conical diffuser. The annular diffusers had a cylindrical outer shell 31 inches in diameter, an annular exit to match a full-scale turbojet engine, and an inner body such that the area ratio was 1.75. The length was such as to give an increase in area with length equivalent to that of a simple 12° cone in one case and a 6° cone for the other.

The 12° annular diffuser exhibits a loss coefficient about twice that of the simple cone, as might be anticipated from the excess wetted area. Because the relative boundary-layer thickness is greater than for the cone, the diffusion factor is reduced and the diffuser effectiveness is thereby impaired. With the 6° annular diffuser the loss coefficient is again greater as the result of the greater wetted surface. Despite this, the effectiveness is slightly higher than that of the 12° annular diffuser because the greater opportunity for momentum exchange and flattening of the exit velocity profiles increases the diffusion factor. It may be noted that the mean Mach number at which choking occurs is substantially higher for the annular diffusers than for the cone. This is because the radii used to fair the transitions in the annular diffusers were much larger than that used for the cone.

Because skin friction increases with wetted area, it appears reasonable to suppose that the equivalent conical angle for minimum loss should increase with the ratio of actual wetted area in the annular form to wetted area of an equivalent cone. The results of calculations along this line are shown in figure 6. The anticipated increase with wetted-area ratio of the angle for minimum loss is almost linear. The loss-coefficient factor associated with the optimum angle does likewise. It should be noted that the annular form is inherently a high-loss configuration, even at the optimum angle. These curves are presented as indicative of trends only. Where, because of excessive boundary-layer thickness, strength of pressure gradient, or similar reasons, skin friction ceases to be a dominant factor in annular diffuser loss, these curves should not be considered as applicable.

From the foregoing discussion, it can be seen that thick initial boundary layers are productive of serious performance impairment,

increasingly so with speed. It appears therefore that where such are unavoidable, boundary-layer control by suction, vortex generators, or similar devices should be employed. When the initial boundary layer is thin, it remains so to design the inlet as to avoid unwanted increases in Mach number due to local wall curvature or friction-induced density change.

The upper sketch in figure 7 shows the Mach number variation at the edge of high-speed flow in the vicinity of the transition from a straight duct to a cone. As the flow goes over the fairing, it first speeds up; then it slows down very sharply. The boundary layer changes thickness so that the point of maximum velocity is downstream of the point of greatest curvature. The smaller the radius of curvature and the larger the diffuser divergence angle, the greater is this local acceleration and the lower is the mean Mach number at which sonic velocity first occurs. It is estimated from the limited amount of available data and some rough analyses that in ducts of the size under discussion, fairing radii twice that of the duct should be sufficient to avoid important local curvature effects.

At high speed the Mach number in a constant-area straight tube increases rapidly in the direction of flow because of friction-induced density changes. This may be prevented by a small amount of conical divergence, as shown in figure 7 by curves of the minimum conical angle for nonincreasing Mach number plotted against flow Mach number, for three values of (tube-diameter-based) Reynolds number. These curves are derived from calculations based on the analysis of reference 5. Although a divergence of 1° should suffice to insure diffusion in most cases, a larger angle is, of course, advantageous in order to reduce the length of run at high velocity.

Figure 8 (from data in reference 3) has been included to show some of the mechanism of the loss development at the onset of choking. The wall segment between cylinder and cone is shown to scale with associated graphs of pertinent data. The diagrams at the left show the condition as losses begin to rise with the onset of choking. Peak velocity occurs just downstream of the fairing section, a small region of supersonic flow followed by compression shock appears, and the losses so incurred are barely visible in the downstream total pressure profile. A slight separation of the downstream flow is seen, which, however, was observed at less than choking speeds. The diagrams at the right show the same duct when supersonic flow is fully developed and losses are high. The line of unit Mach number has moved upstream of the fairing section and extends to the center of the duct. A line of shock has moved downstream and also extends to the center of the duct. A large loss associated with shocks from high Mach numbers in the main body of the stream is evident in the downstream pressure profile. The point of separation of the flow from the duct wall has been displaced downstream and occurs at the location of the shock.

Shock losses in the stream rather than shock-induced separation appear to be the principal source of total pressure loss for this diffuser. Similar flows are obtained with thicker initial boundary layers with the principal difference that the upstream displacement of the line of sonic velocity is greater.

The question naturally arises as to the applicability of blower-test duct data to flight conditions where the subsonic diffuser may be preceded by supersonic compression and followed by a power plant such as a ram jet. The answer to this question appears in figure 9 which shows flight-measured performance of an annular diffuser under just such conditions obtained by the Lewis Flight Propulsion Laboratory (reference 6). A spike-type supersonic inlet was used, with the minimum area point at the start of the internal passage. The diffuser discharged into the combustion chamber of an operating ram jet.

By cross-plotting the results of numerous flights with varying operating conditions, a curve of over-all loss coefficient from free stream to diffuser exit has been obtained for the condition of inlet Mach number close to unity over a range of flight Mach number including the design value of 1.6. Increasing Reynolds number associated with the flight plan accounts for the decreasing loss up to $M = 1.2$, and increasing external shock losses causes the curve to rise again. At the design Mach number of 1.6, a data point has been added which is taken from cold tests in a wind tunnel of a comparable model (see reference 7). It is apparent that the flight performance has not been impaired by the burner operation. By deducting the external shock losses, the dashed line of figure 9 for subsonic diffuser performance has been derived. An identical result is obtained by making a wetted-area adjustment of subsonic conical-diffuser data; this result indicates the applicability of blower-test results.

It can be concluded therefore that, where the inlet boundary layer is thin and proper care has been exercised to avoid friction-induced or curvature-induced velocity increases in the inlet, satisfactory performance of the subsonic diffuser in transonic flight can be predicted and realized, either cold or in conjunction with the operating power plant.

REFERENCES

1. Henry, John R.: Design of Power-Plant Installations. Pressure-Loss Characteristics of Duct Components. NACA ARR L4F26, 1944.

2. Copp, Martin R., and Klevatt, Paul L.: Investigation of High-Subsonic Performance Characteristics of a 12° 21-Inch Conical Diffuser, Including the Effects of Change in Inlet Boundary-Layer Thickness. NACA RM L9H10, 1949. (Prospective NACA paper)

3. Little, B. H., Jr., and Wilbur, Stafford W.: High-Speed Performance Characteristics and Boundary-Layer Investigations of a 12° 10-Inch Conical Diffuser. (Prospective NACA paper)

4. Nelson, William J., and Popp, Eileen G.: Performance Characteristics of Two 6° and Two 12° Diffusers at High Flow Rates. NACA RM L9H09, 1949.

5. Young, A. D., and Winterbottom, N. E.: High Speed Flow in Smooth Cylindrical Pipes of Circular Section. Rep. No. Aero. 1785, R.A.E., (British), Nov. 1942.

6. Carlton, William W., and Messing, Wesley E.: Free-Flight Performance of 16-Inch-Diameter Supersonic Ram-Jet Units. I - Four Units Designed for Combustion-Chamber Inlet, Mach Number of 0.12 at Free-Stream Mach Number of 1.6 (Units A-2, A-3, A-4, and A-5). NACA RM E9F22, 1949. (Prospective NACA paper)

7. Ferri, Antonio, and Nucci, Louis M.: Preliminary Investigation of a New Type of Supersonic Inlet. NACA RM L6J31, 1946.

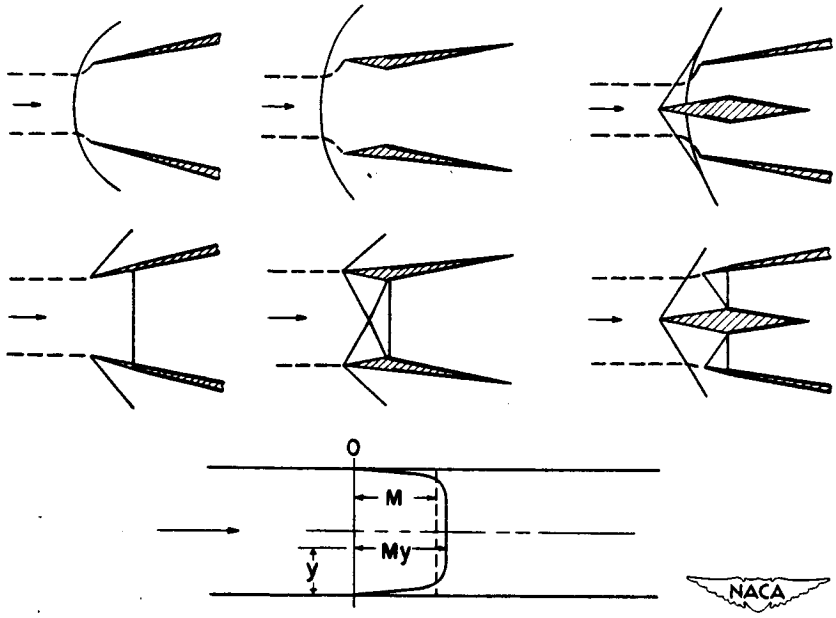


Figure 1.- Configurations of intake diffusers.

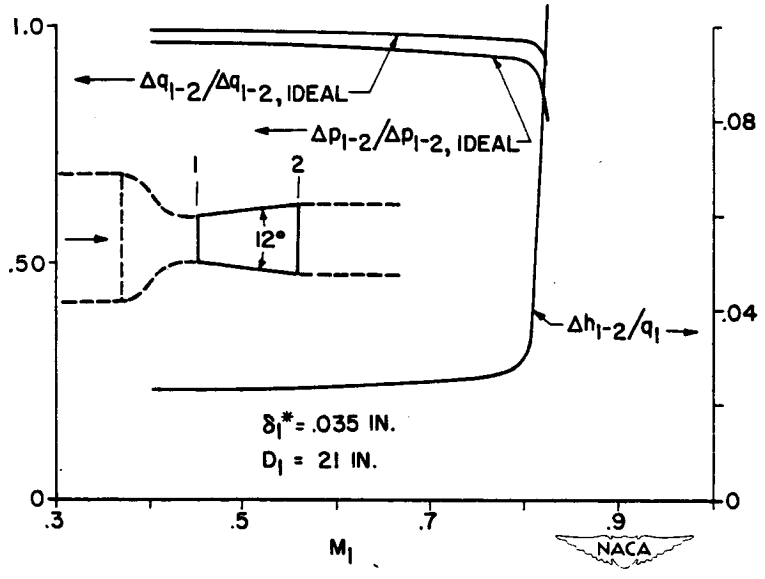


Figure 2.- Performance coefficients of a representative high-speed, large Reynolds number conical diffuser. Initial displacement thickness, 0.035 inch. (From reference 2.)

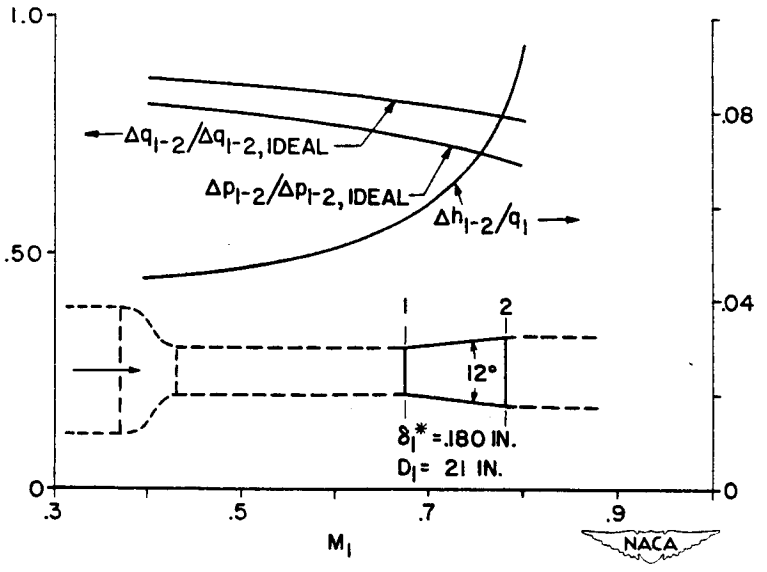


Figure 3.- Performance coefficients of a representative high-speed, large Reynolds number conical diffuser. Initial displacement thickness, 0.180 inch. (From reference 2.)

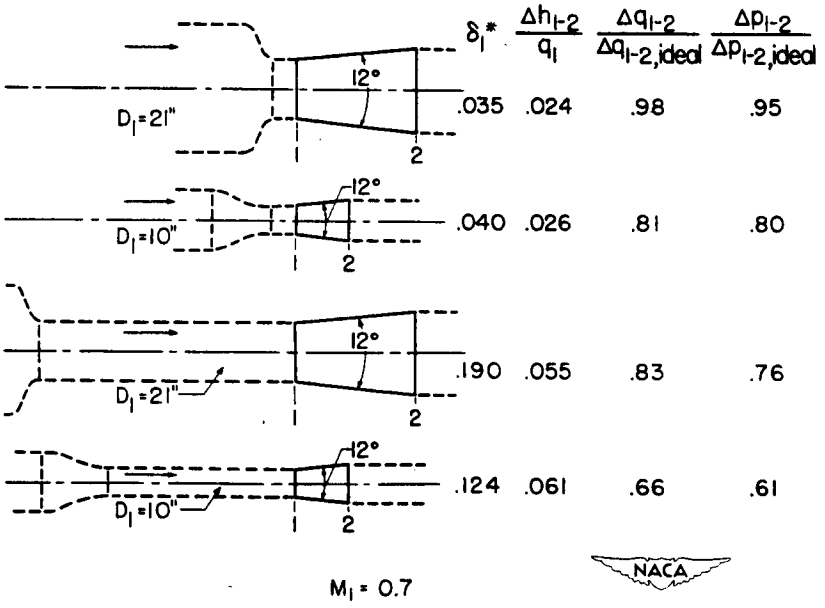


Figure 4.- Comparison of loss coefficients, total pressure loss, and diffusion factor for geometrically similar diffusers. Inlet Mach number, 0.7. (From references 2 and 3.)

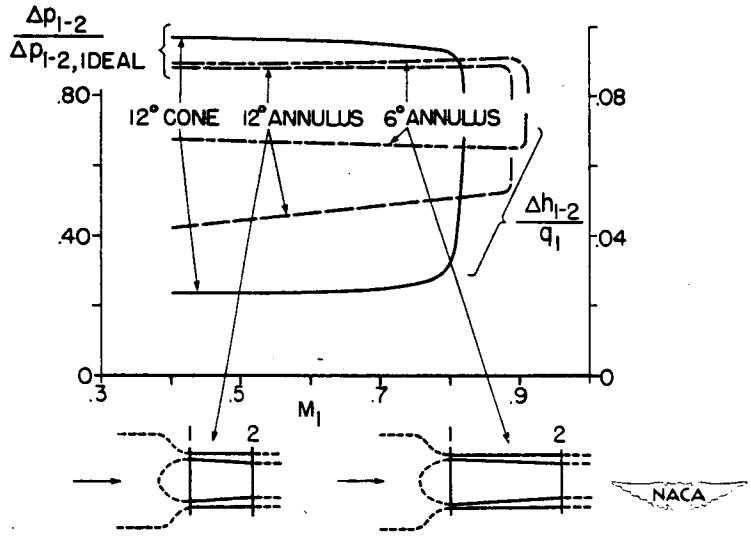


Figure 5.- Loss coefficients and effectiveness for two annular diffusers. (From reference 4.)

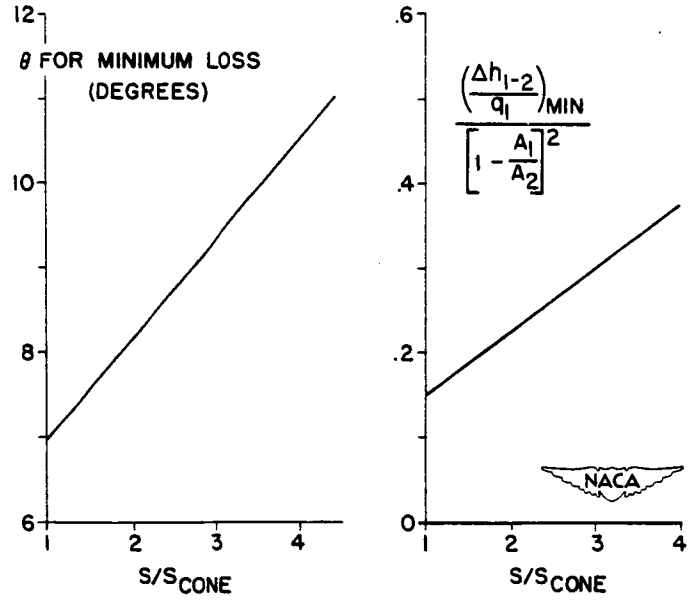


Figure 6.- Variation of conical angle for minimum loss and corresponding minimum loss-coefficient factor with wetted-area ratio.

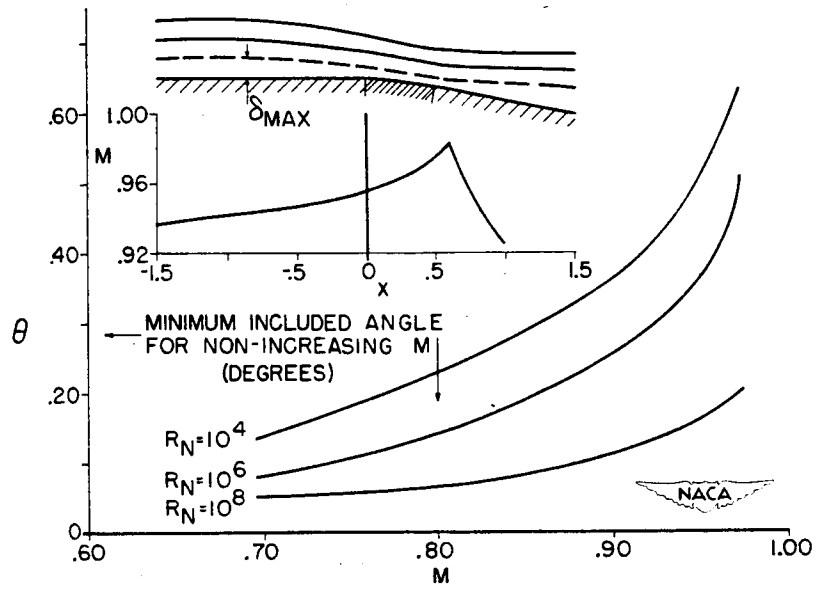
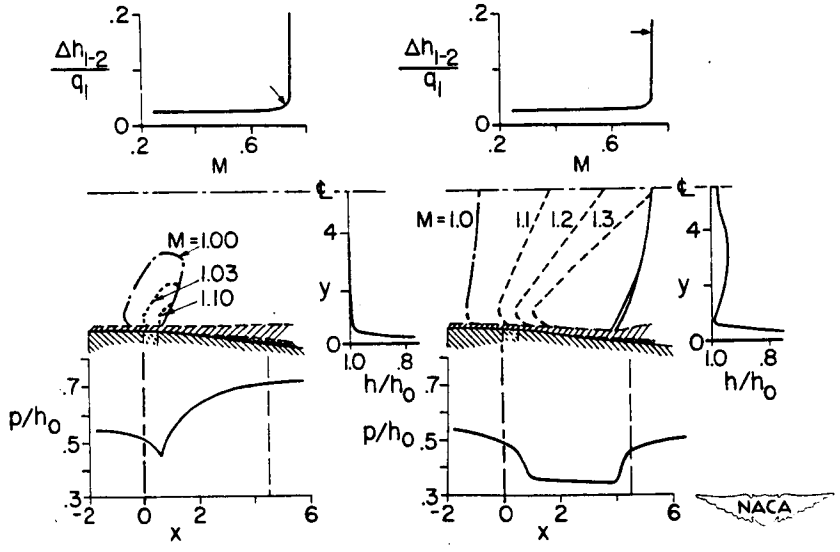


Figure 7.- Variation of minimum conical angle for nonincreasing Mach number with flow Mach number. Upper sketch: typical variation of Mach number in the vicinity of the transition from a straight duct to a cone.



(a) Onset of choking. (b) Fully developed choking.

Figure 8.- Loss development at the inlet of a high-speed diffuser. (From reference 3.)

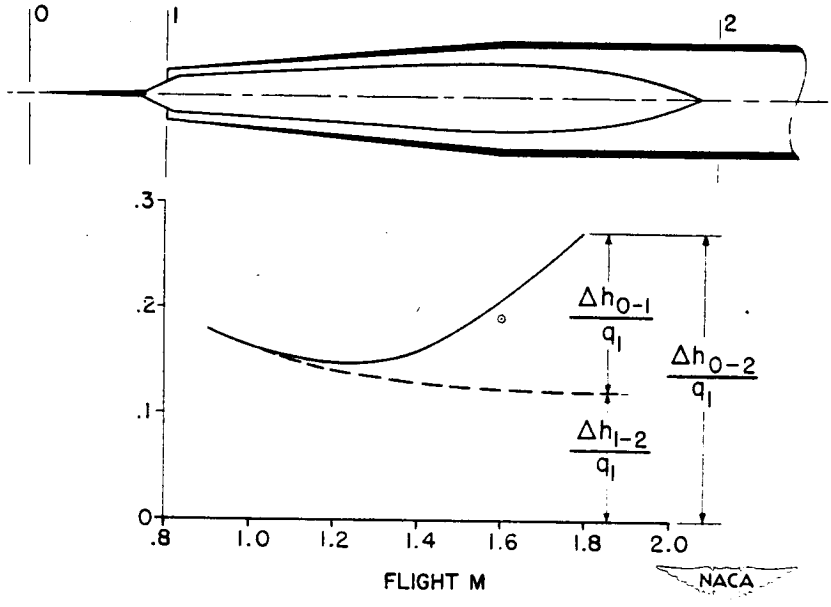


Figure 9.- Flight measured performance characteristics of an annular diffuser with an operating ram jet. (From reference 6.)

Preceding page blank

N65-86479

ANALYSIS OF THE STABILITY CHARACTERISTICS OF TWIN-INTAKE AIR-INDUCTION SYSTEMS

By Norman J. Martin

Ames Aeronautical Laboratory

Experimental investigations of air-induction systems in which the air flow of two intakes join in a common duct have indicated that many of these systems are subject to an air-flow instability at low inlet-velocity ratios. This instability is characterized by fluctuations of the quantity of flow in each duct and usually results in reversal of flow in one of the ducts as the system inlet-velocity ratio is further reduced. It has been observed that flow instability has occurred when the intake pressure-recovery characteristics are similar to those shown in figure 1. Here is shown the ram-pressure recovery $1 - \frac{\Delta H}{q_o}$ as a function of inlet-velocity ratio V_1/V_o. It can be noted that over a portion of the inlet-velocity-ratio range the ram-pressure recovery increases with an increase of inlet-velocity ratio.

The generally accepted qualitative explanation for the air-flow instability is as follows:

1. Consider that the intakes are symmetrical, geometrically and aerodynamically, and are operating at a system mass flow where the ram-pressure recovery is increasing with an increase of inlet-velocity ratio. A disturbance, such as a boundary-layer fluctuation, which would change the aerodynamic symmetry, would result in a decrease of inlet-velocity ratio for one intake and an increase for the other. The intake having the initial decrease of inlet-velocity ratio would have a decreased pressure recovery which in turn would tend to further decrease the mass flow of that intake. The intake having the initial increase of inlet-velocity ratio would have an increased pressure recovery which would tend to further increase the mass flow of that duct. As a result, the intakes would continue to operate at increasingly different inlet-velocity ratios and the possibility of flow reversal in one of the intakes would exist. Thus, the pressure recovery has a destabilizing effect on the air flow through the ducts.

2. By similar reasoning it can be shown that the pressure recovery would have a stabilizing effect on the air flow with the system operating at inlet-velocity ratios at which the ram-pressure recovery decreased with an increase of inlet-velocity ratio.

The foregoing explanation is not entirely satisfactory because it gives no quantitative indication of the inlet-velocity ratio for flow instability. Although this explanation indicates that the division between stable and unstable flow is at the inlet-velocity ratio for maximum ram-pressure recovery, the duct station at which ram-pressure recovery should be considered is not defined. Furthermore, no indication is given of the system inlet-velocity ratio at which flow reversal will occur in one duct. Therefore, an analysis has been made in order to provide a more quantitative explanation of the flow instability and reversal. This paper presents the results of this analysis.

In principle, the method of analysis is relatively simple. The twin-intake air-induction system and its flow characteristics have been treated in a manner similar to that used for analysis of divided flow in pipes. In the case of the twin-intake system (fig. 2), the point of division is in the undisturbed stream ahead of the model (station 0). The point of rejoining, obviously, is at the juncture of the two ducts (station 2). We may relate the flow between station 0 and station 2 of each duct by means of Bernoulli's theorem. If incompressible flow is assumed, this relation is shown by

$$p_{2_A} + \frac{\rho V_{2_A}^2}{2} + \left(\Delta H_{o-2}\right)_A = p_o + \frac{\rho V_o^2}{2} \tag{1}$$

and

$$p_{2_B} + \frac{\rho V_{2_B}^2}{2} + \left(\Delta H_{o-2}\right)_B = p_o + \frac{\rho V_o^2}{2} \tag{2}$$

Equations (1) and (2) may be transformed into more convenient form by rearranging the terms, dividing by the free-stream dynamic pressure, and expressing the velocity at station 2 in terms of the inlet velocity V_1 as

$$\frac{p_{2_A} - p_o}{q_o} = \left[1 - \frac{\left(\Delta H_{o-2}\right)_A}{q_o}\right] - \left(\frac{A_1 V_1}{A_2 V_o}\right)_A^2 \tag{3}$$

$$\frac{p_{2_B} - p_o}{q_o} = \left[1 - \frac{\left(\Delta H_{o-2}\right)_B}{q_o}\right] - \left(\frac{A_1 V_1}{A_2 V_o}\right)_B^2 \tag{4}$$

The next step is to determine the relation between the flows of the two ducts. The quantity which the two flows have in common is the static pressure immediately after joining (station 3). For the type of ducting system shown in figure 2, the common static pressure can be taken as the static pressure at station 2. With the static pressures p_{2_A} and p_{2_B} equal to each other, equation (3) can be set equal to equation (4). From this equality, it may be seen that the quantity of flow in duct A can be different from that in duct B provided the resulting difference in dynamic pressure is equal to the difference in ram-pressure recovery of the two ducts. The assumption that the static pressure is equal at station 3 to that at station 2 and is constant across station 3 can be justified by considering the possible flow conditions, shown in figure 3, as follows:

1. With equal mass flow through each duct of a twin-intake system, such as indicated in part (A), the static-pressure assumptions would obviously be valid.

2. For the same type of system but with zero flow in one of the ducts, as indicated in part (B), the flow pattern becomes similar to that with sudden expansion. The determination of losses encountered with sudden expansion is made theoretically by the assumption that the static pressure just after discharge is equal to the static pressure just before discharge and is constant across the discharge section. Since the calculated and measured losses due to sudden expansion are in good agreement, the validity of the static-pressure assumptions appear reasonable for this case.

3. The intermediate case with such a system, where there is unequal flow through each duct, is shown in part (C). This case is similar to that of a jet discharging into a stream. It has been observed that the measured static pressure across the discharge section of a jet is close to that of the stream. Thus, it appears that the static-pressure assumptions are also reasonable for the case with unequal flow in the two ducts.

4. The foregoing statements would seem to apply also to air-induction systems in which the ducts empty into a plenum chamber, as shown in part (D). The validity of the static-pressure assumptions with this type of system would depend somewhat upon the distance between the two ducts.

In both types of systems the validity of the static-pressure assumptions would appear to depend in some degree upon the angle φ at which the ducts join. For most systems this angle is small and, therefore, need not be considered.

A graphical application of equations (3) and (4) to determine the flow instability and reversal characteristics for an assumed twin-intake air-induction system is shown in figure 4(a). In this figure the total and the static pressure-recovery characteristics at station 2 are shown for each duct operating independently. The assumed variation of the total or ram-pressure recovery with inlet-velocity ratio is shown by the upper curve; whereas the lower curve shows the static-pressure recovery at station 2 as a function of inlet-velocity ratio. By following lines of constant static-pressure recovery, the inlet-velocity ratios at which each duct will operate in combination with the other can be determined. For example, with one duct operating at location 1, an inlet-velocity ratio of 0.2, the other duct could be operating at location 2, an inlet-velocity ratio of 0.7. The system inlet-velocity ratio is the average of the two individual inlet-velocity ratios or 0.45, as indicated by location 3. At this system inlet-velocity ratio, both of the ducts could, of course, be operating at this third location; that is, at an inlet-velocity ratio which is the same as that of the system. However, this balanced flow condition is unstable for, as shown previously in the qualitative analysis, increasing pressure recovery with increasing flow tends to produce more flow in one duct than in the other once the symmetry is disturbed. Thus, an unbalanced flow condition would exist: one duct would operate at location 1 and the other, at location 2. This unbalanced flow condition is not entirely stable, however, for another sufficiently large disturbance could conceivably result in an interchange of the quantity of flow in each duct. As the system mass flow is reduced so that each duct will be operating farther from the maximum point of the curve, the disturbance will need to be greater to make the relative flow quantities in each duct interchange.

It can be seen from figure 4(a) that, with a uniform static pressure at station 2, the minimum inlet-velocity ratio for stable flow would be at the maximum point of the static-pressure-recovery curve, an inlet-velocity ratio of 0.55, instead of at the maximum point of the ram-pressure-recovery curve as was suggested in the qualitative analysis. It can also be observed that, if the ram-pressure recovery decreased constantly with increase of inlet-velocity ratio, the static-pressure recovery would also decrease constantly with increase of inlet-velocity ratio and there would be no flow instability.

The predicted values of inlet-velocity ratio of each duct at given system inlet-velocity ratios for the assumed system is shown in figure 4(b). In this figure individual inlet-velocity ratio is shown as a function of system inlet-velocity ratio. The portion of the curve above a system inlet-velocity ratio of 0.55 is in the stable flow region in which the predicted inlet-velocity ratio of each duct is the same as the system inlet-velocity ratio (that is, there is balanced flow). Below a system inlet-velocity ratio of 0.55 the two diverging curves

represent the predicted values of individual inlet-velocity ratio for ducts A or B. The straight line running to zero would represent the individual inlet-velocity ratios of ducts A and B if the flow symmetry were not disturbed. The indicated individual inlet-velocity ratios at locations 1, 2, and 3 are the same as those shown in figure 4(a). In decreasing the system inlet-velocity ratio to 0.4 the flow through one duct becomes zero and reversal of flow is imminent.

Again, looking at the static-pressure-recovery equation, we may note that the system inlet-velocity ratio for instability and the ratio for flow reversal are dependent upon the ratio of the areas at stations 1 and 2 (that is, the amount of diffusion) and upon the total pressure loss from station 0 to station 2. The total pressure loss from station 0 to station 2 is composed of a duct loss as well as an inlet loss. Although the duct loss is somewhat dependent upon the amount of diffusion, it can be stated that, in general, the inlet-velocity ratio for flow instability and the ratio for flow reversal decrease both with an increase of duct losses and with a decrease of diffusion before joining of the two air flows.

Verification of this quantitative analysis by comparison with experiment is obviously desirable. The data necessary to make the comparisons are meager. It has been possible, however, to apply this analysis to two dissimilar air-induction systems for which some data are available. A comparison of the predicted and measured inlet-velocity ratios of each intake for one system is shown in figure 5(a). The ducting arrangement of this system is shown schematically on the upper left, and the pressure-recovery characteristics are shown on the lower left. On the right, the individual inlet-velocity ratio is shown as a function of the system inlet-velocity ratio. The solid lines indicate the predicted values of inlet-velocity ratio for each intake. The experimental points are indicated by symbols, the open symbols being for one intake and the filled-in symbols being for the other intake. The data were obtained from several runs. The predicted results were in good agreement with the experimental results. It is interesting to note that reversal of flow did not always occur in the same duct.

Less complete data are available for the other system. Figure 5(b) shows a comparison of these data with the predicted results. The ducting arrangement and pressure-recovery characteristics are again shown on the upper left and lower left, respectively, and the individual inlet-velocity ratio is shown as a function of system inlet-velocity ratio on the right. Although the data for this model are not as complete as desired, the experimentally determined points showing stable flow were in the predicted stable region, and the experimental points showing flow reversal were in the region in which reversal of flow was predicted.

[redacted]

[redacted]

In summary, it can be stated that the method of analysis provides a means of predicting the inlet-velocity ratio for flow instability and flow reversal. The method gave results which were in good agreement with the available experimental data.

[redacted]

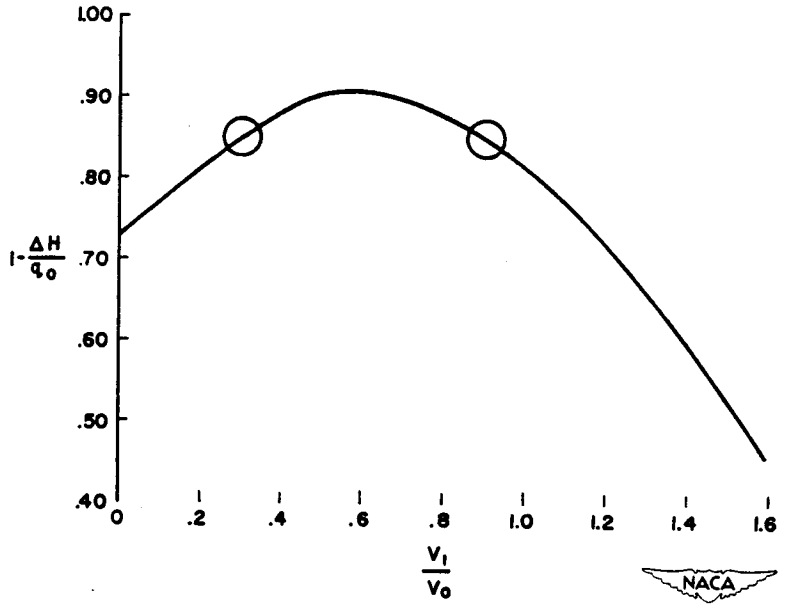
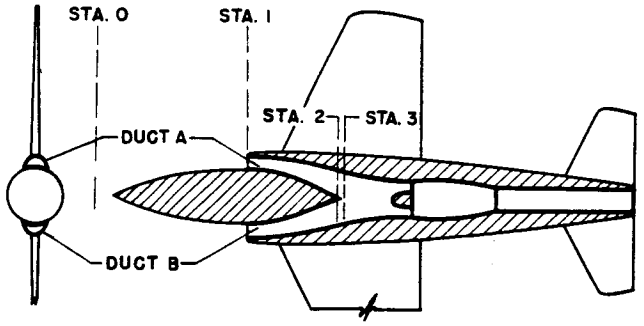


Figure 1.- Typical pressure-recovery characteristics of a twin-intake air-induction system exhibiting air-flow instability.



(1) $$p_{2_A} + \frac{\rho V_{2_A}^2}{2} + (\Delta H_{0-2})_A = p_0 + \frac{\rho V_0^2}{2}$$

(2) $$p_{2_B} + \frac{\rho V_{2_B}^2}{2} + (\Delta H_{0-2})_B = p_0 + \frac{\rho V_0^2}{2}$$

(3) $$\frac{p_{2_A} - p_0}{q_0} = \left[1 - \frac{(\Delta H_{0-2})_A}{q_0}\right] - \left(\frac{A_1 V_1}{A_2 V_0}\right)_A^2$$

(4) $$\frac{p_{2_B} - p_0}{q_0} = \left[1 - \frac{(\Delta H_{0-2})_B}{q_0}\right] - \left(\frac{A_1 V_1}{A_2 V_0}\right)_B^2$$

NACA

Figure 2.- Typical twin-intake air-induction system.

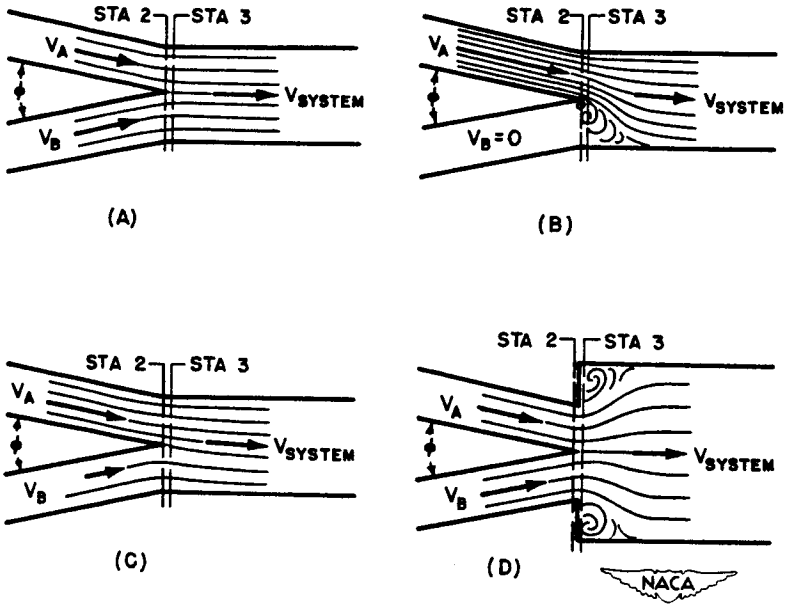
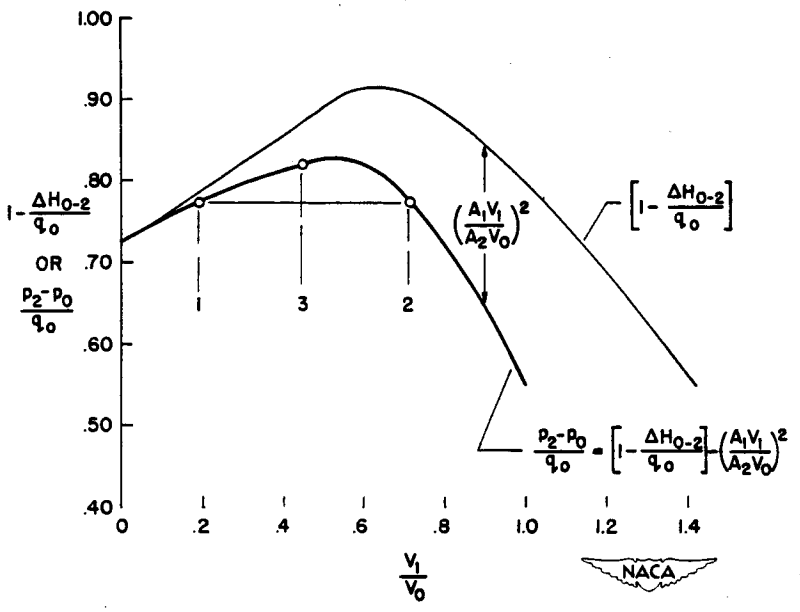
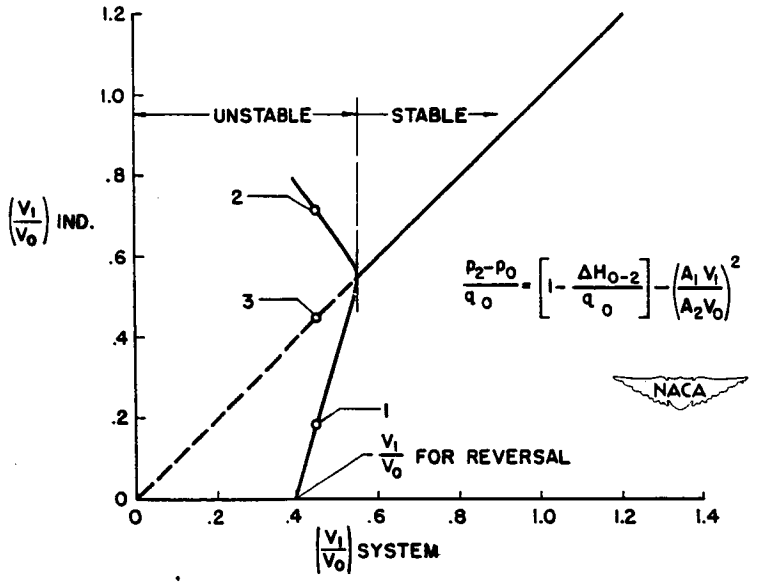


Figure 3.- Possible air-flow conditions in twin-intake air-induction systems.

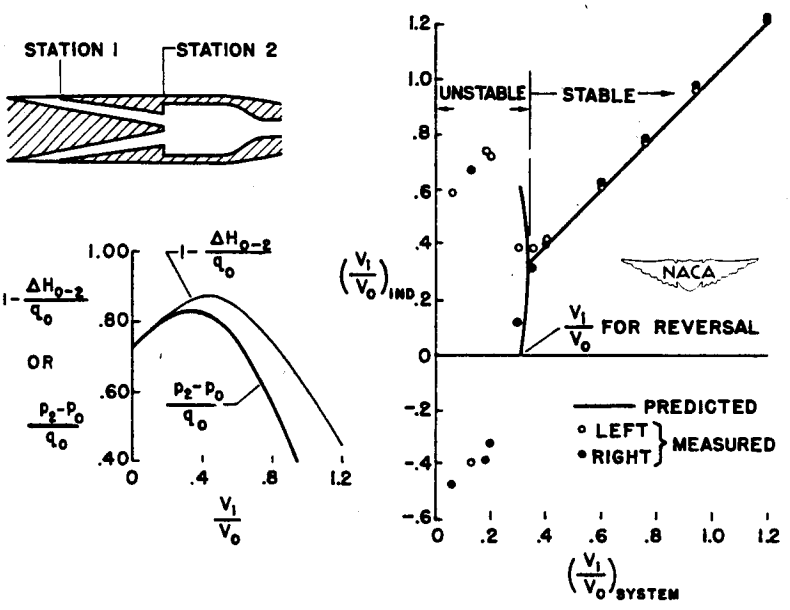


(a) Assumed pressure-recovery characteristics.

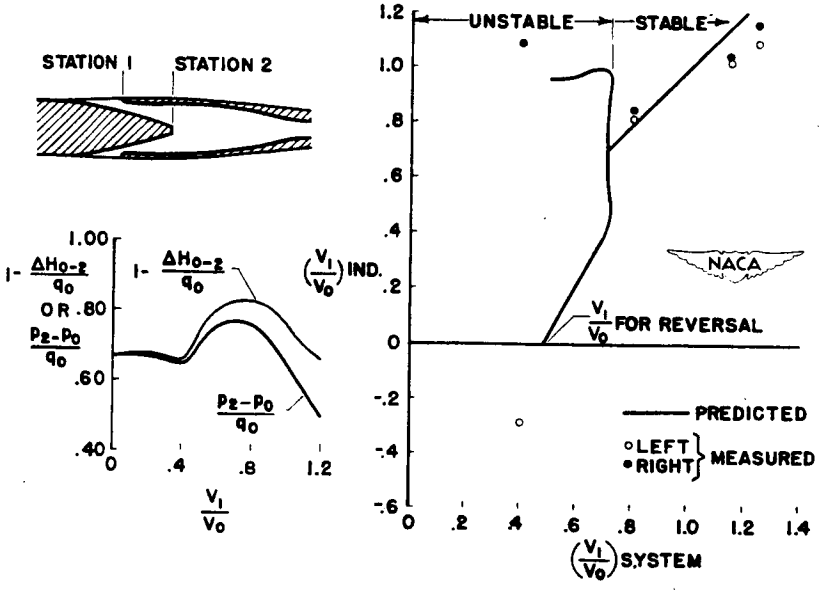


(b) Predicted air-flow characteristics.

Figure 4.- Application of the analysis to an assumed twin-intake air-induction system.



(a) Model 1.



(b) Model 2.

Figure 5.- Comparison of predicted and measured air-flow characteristics of experimental twin-intake air-induction systems.

N65-86480

JET EXHAUST CHARACTERISTICS

By Morris D. Rousso

Lewis Flight Propulsion Laboratory

Aircraft designed for transonic and supersonic speeds require extremely high-powered jet-propulsion engines and, depending on the particular requirements of a given design, single or multiple jets may be used. From a drag standpoint, it is desirable that the engine-body combination be as compact as possible. This consideration frequently leads to single- and twin-jet installations wherein the jets must discharge in close proximity to the aircraft. A large amount of spreading will occur in the immediate vicinity of the discharging jets, particularly at high engine compression ratios. If any aircraft surfaces are located in this zone, serious structural problems may arise as a result of heating of these surfaces by the hot jets. In addition, the control surfaces may be affected by the aerodynamic disturbances in the jet wake. When more than one engine is used, another complication arises from the interaction between the jets. In order to locate such jets properly, the wake characteristics over a wide range of operating conditions must be known.

Investigations are being conducted at the Lewis Laboratory of the NACA to study the characteristics of spreading jets. The initial phase of the program, consisting of pressure and temperature surveys of single and twin jets discharging into quiescent air, is discussed herein.

APPARATUS AND PROCEDURE

The apparatus for the first phase of the program is shown schematically in figure 1. Essentially it consisted of a primary chamber with two convergent nozzles that discharged into a low-pressure receiver. Single-jet studies were made by plugging one of the nozzles. Variation of the spacing parameter, or the ratio of distance between nozzles to the nozzle diameter, was accomplished by varying the nozzle diameter. The pressure ratio across the nozzle was varied by changing the pressure in the receiver. Hot tests were made by heating the atmospheric air in the primary chamber. A total-head pressure rake was used to survey the wake. A complete survey was made in one quadrant of the wake and, in addition, points on the boundary in an adjacent quadrant were determined to ascertain symmetry.

A curve that illustrates the technique used in defining the jet boundary is shown in figure 2. The ratio of receiver static pressure p_0 to rake total pressure P_R at any point in the jet wake is plotted as a function of distance above the jet center line. Because the velocity in the jet mixing region approaches zero asymptotically, the jet boundary is defined as the locus of points for which the Mach number ratio $M_x/M_j = 0.11$, where M_x is the Mach number at any point in the jet fringe and M_j is the Mach number of the jet expanded isentropically to receiver ambient pressure. Although arbitrary, the Mach number ratio of 0.11 was selected because of convenience in measuring technique. The static pressure in the jet mixing zone was assumed constant at ambient pressure. For this investigation the values of the pressure ratio p_0/P_R varied from 0.950 to 0.987 for the boundaries defined in this manner.

DISCUSSION OF RESULTS

Jet boundaries showing the spreading of a single jet are presented in figure 3 for pressure ratios P_P/p_0 of 2.5, 4.5, 9.5, and 15.0, where P_P is the atmospheric total pressure entering the primary chamber. Distance from the jet center line in nozzle diameters is plotted as a function of distance downstream of the nozzle exit in nozzle diameters. The boundaries of the spreading jets, presented relative to the nozzle exit, show the effect of pressure ratio on the rate of jet expansion. Increasing the pressure ratio resulted, as expected, in increased expansion of the jet immediately downstream of the nozzle. Following the initial rapid expansion, the rate of growth of the jet diameter decreased and appeared to vary only slightly with distance downstream.

In order to show the correspondence between the jet boundary arbitrarily defined by the Mach number ratio 0.11 and the jet visible in a schlieren photograph, points on the boundary of a single jet at a pressure ratio of 2.5 have been superimposed on the photograph of the same jet. The photograph in figure 4, showing the points determined by a pressure survey, would provide a fair prediction of the boundary in this case; although, as the mixing region grows in thickness, the boundary becomes less clearly defined in the schlieren photograph.

When twin jets are employed, interaction between the jets is an additional factor influencing jet spreading. This point is illustrated in figure 5, where boundaries are shown for twin jets

spaced 1.738 nozzle diameters apart. These boundaries were obtained for pressure ratios of 2.5, 9.5, and 15.0 at axial stations 1 and 6 diameters from the nozzle exits. Distance from the jet center line in nozzle diameters is plotted as a function of distance from the center line A–A between the jets in nozzle diameters. At the 1-diameter station, the interaction or pile-up between the jets is noticeable at a pressure ratio of 9.5 and becomes more pronounced at a pressure ratio of 15.0. As shown by the jet boundaries in a plane 6 diameters downstream of the nozzles, this pile-up between the jets has increased considerably. Despite this jet interaction and resultant pile-up of the jet wake in the center plane region between the jets, it was observed that the boundaries clear of the zone of interaction were relatively unaffected; that is, if a single jet were superimposed on one of the twin jets, their boundaries would coincide except in the zone of interaction.

The pile-up between twin jets on the plane A–A as a function of distance downstream of the nozzle exits is further illustrated in figure 6. The boundaries of the mixing jets are plotted to scale for pressure ratios of 2.5, 4.5, 9.5, and 15.0 The delay of the initial points of jet interaction with decreasing pressure ratio is clearly shown. These points correspond closely to the points of interaction as predicted by spacing two single jet boundaries the same distance apart.

An additional factor influencing the boundary of twin interacting jets is the distance between the nozzle axes. Boundaries for twin jets having spacings of 1.42 and 2.5 diameters are shown in figure 7. These boundaries, plotted to scale, were obtained at an axial station of 2 diameters at pressure ratios of 2.5, 9.5, and 15.0 Increasing the spacing delayed the point of jet interaction and thus decreased the jet pile-up at the expense of widening the over-all jet boundary. Further illustrating this point, figure 8 shows the jet pile-up in the plane of symmetry between the jets for nozzle spacings of 1.42, 1.738, and 2.5 diameters at a pressure ratio of 9.5. In this figure the delay in jet interaction with increased spacing and the resultant decrease in pile-up are again apparent.

The effect of nozzle spacing on jet interaction is also illustrated by the schlieren photograph in figure 9. Nozzle spacings of 2.5 and 1.42 diameters are pictured at a pressure ratio of 15.0. With the closer spacing the shock wave interaction was more pronounced. Although the increase in the amount of interaction between the jets is accomplished by decreasing the spacing as shown, approximately the same effect would be brought about by maintaining a constant spacing and increasing the pressure ratio across the nozzles.

The results presented thus far concern only cold jets at approximately 80° F. It is now of interest to know to what extent the cold-jet boundaries approximate those of hot jets. A partial answer to this question has been obtained from pressure surveys of twin hot jets at a temperature of 950° F. A comparison of the hot- and cold-jet boundaries is presented in figure 10. The boundaries were obtained at axial stations of 2 and 6 diameters. The nozzles were spaced at 1.738 diameters and operated at pressure ratio of 9.5. This scale plot of the boundaries is typical of the data obtained and shows that the hot-jet boundary falls within that of the cold jets near the nozzle exits, as shown at the 2-diameter station. Farther downstream the difference is less pronounced, however, and at a station of 6 diameters the hot- and cold-jet boundaries are identical. The greatest difference between the boundaries occurred at the point midway between the jets. On the basis of preliminary investigations, the cold-jet studies thus appear to be conservative in predicting the jet boundaries.

OTHER TESTS

Another technique has been employed at the Lewis Laboratory in which studies of the spreading of twin hot jets were made by means of temperature surveys. The apparatus used for these investigations is pictured in figure 11. A rocket utilizing hydrogen peroxide as a fuel furnished the hot gas for the jets. The convergent nozzles spaced at 1.42 diameters were machined into a flat plate attached to the combustion chamber and operated at a pressure ratio of 9.5. A chromel-alumel thermocouple rake was used to survey the expanding jets. Because of the extremely short duration of burning, quick-reading, automatic recording instruments were used.

The boundary in the plane of symmetry between the jets is shown in figure 12. In these studies the jet boundary was arbitrarily defined by the dimensionless ratio $\frac{T_x - T_0}{T_j - T_0} = 0.10$, where T_x is the temperature measured at any point in the jet wake, T_j is the jet temperature at the nozzle exits, and T_0 is the ambient temperature. In addition to the jet boundary, lines of constant temperature ratio of 0.30 and 0.50 are shown in figure 12. For a jet-exhaust temperature of 3600° R, selected as a representative value for a jet engine with afterburning, these lines represent jet-wake temperatures of 810° R, 1430° R, and 2050° R. Also shown is the boundary determined by means of a pressure survey of twin cold jets at the same nozzle spacing and pressure ratio. The distance from the jet center line to the line of constant temperature ratio of 0.10 is slightly

larger than that to the Mach number ratio line of 0.11. The temperature line corresponding to a given pressure line is yet to be determined.

A serious problem resulting from the interaction between twin jets arises at take-off, where the jets may be reflected from the ground onto the tail surfaces of the aircraft. Accordingly, investigations were made to determine the jet boundary for a case in which these conditions were simulated. The apparatus used is pictured in figure 13. The flow of hot gases from a full-scale turbojet engine was divided into parallel straight-pipe nozzles spaced at 1.42 diameters and operated at a pressure ratio of 1.5. The jets were directed at an angle of 20° onto a flat plate. A chromel-alumel thermocouple was used to survey the jets.

The boundary in the plane of symmetry between the jets is shown in figure 14, where distance above the ground is plotted as a function of distance downstream of the nozzle exits in nozzle diameters. The jet boundary is again defined by the ratio $\frac{T_x - T_0}{T_j - T_0} = 0.10$. Lines of constant temperature ratio of 0.30 and 0.50 are also shown in the figure. Again, when a jet-exhaust temperature of 3600° R is assumed, these lines represent jet-wake temperatures of 810° R, 1430° R, and 2050° R. The boundary shown is the height of the mixing jets in the plane of symmetry between the jets for specified conditions of spacing, pressure ratio, and angle of deflection. Changing any of these conditions would undoubtedly result in a different jet boundary.

CONCLUDING REMARKS

The results that have been presented represent the first phase of a study of the spreading characteristics of jets. These results include the boundaries of single and twin jets discharging into quiescent air. These boundaries were determined by total-pressure surveys for a range of pressure ratios and for different nozzle spacings in the case of the twin jets. The most significant fact brought out by the investigations is that the spreading of twin jets is principally influenced by the pressure ratio across the nozzle exits, and nozzle spacing.

It has also been shown that the boundaries of hot jets, as determined by pressure surveys, appear to be smaller than those of cold jets, except at large distances downstream of the nozzles for the cases studied.

Correspondence between the pressure and temperature lines has not yet been established. In addition, the effects of cooling shrouds, varying Reynolds number, and external flow at angles of attack on jet spreading have yet to be determined.

A systematic research program on this problem is under way and is designed to provide sufficient information to make possible the prediction of jet growth over a wide range of design and operating conditions.

[redacted]

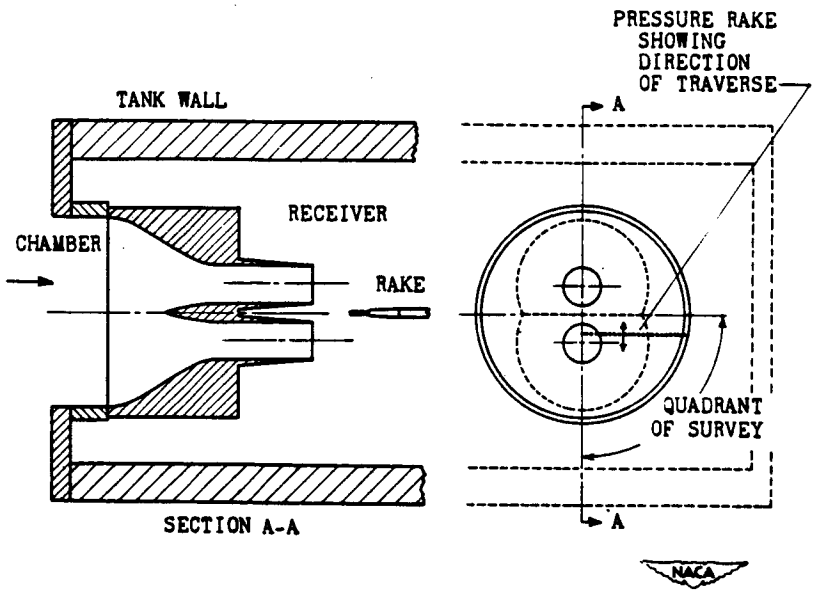


Figure 1.- Schematic diagram of test apparatus.

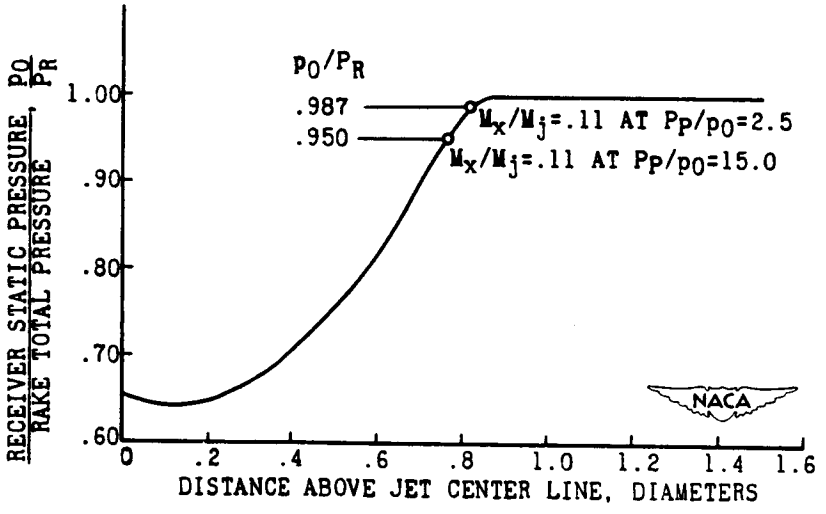


Figure 2.- Pressure distribution in jet wake.

Preceding page blank

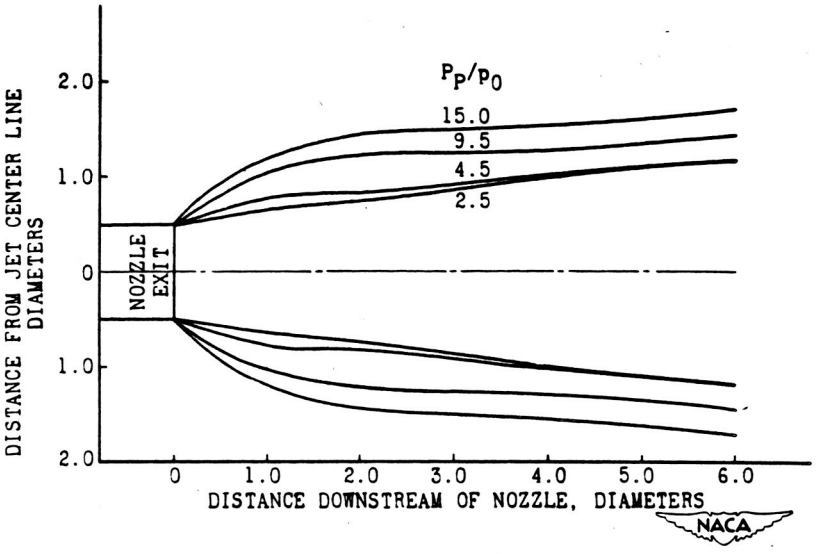


Figure 3.- Spreading of a single jet. $\frac{M_x}{M_j} = 0.11$.

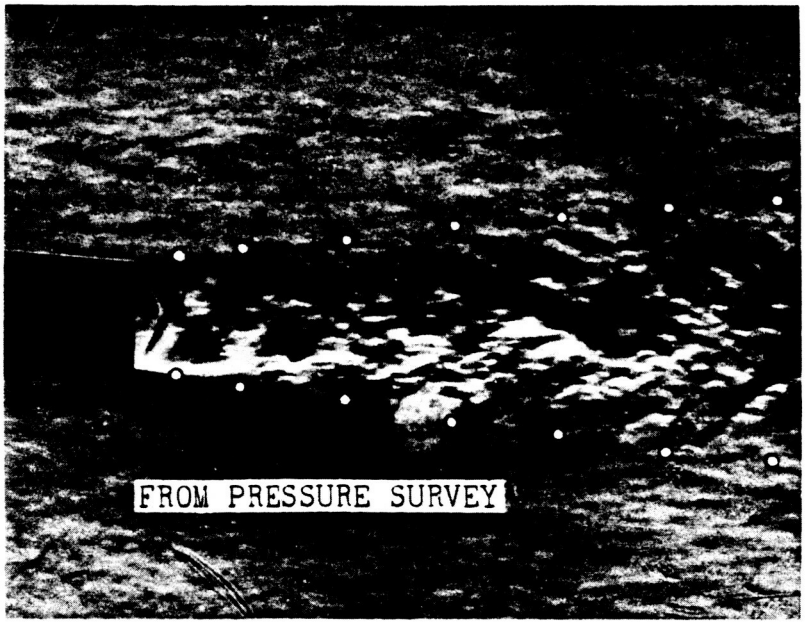


Figure 4.- Schlieren photograph of single jet at $\frac{P_P}{P_0} = 2.5$.

NACA

Preceding page blank

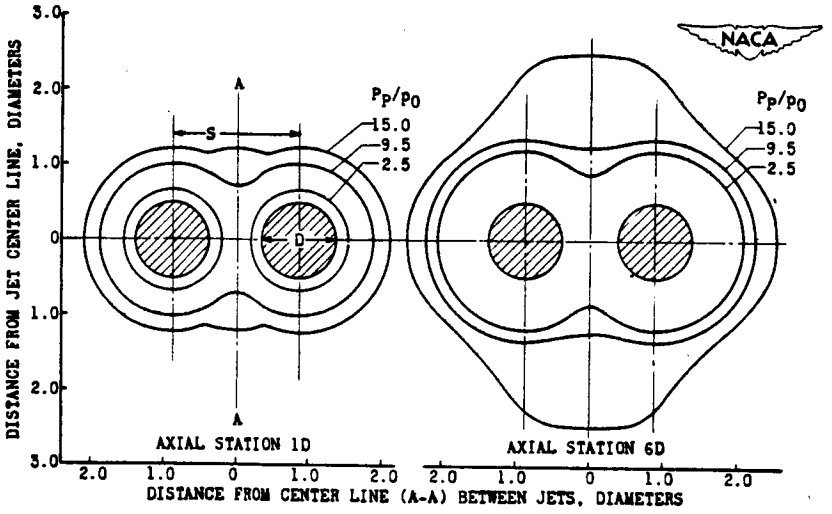


Figure 5.- Jet boundary as function of axial position. Twin jets; nozzle spacing, 1.738D; $\frac{M_x}{M_j} = 0.11$.

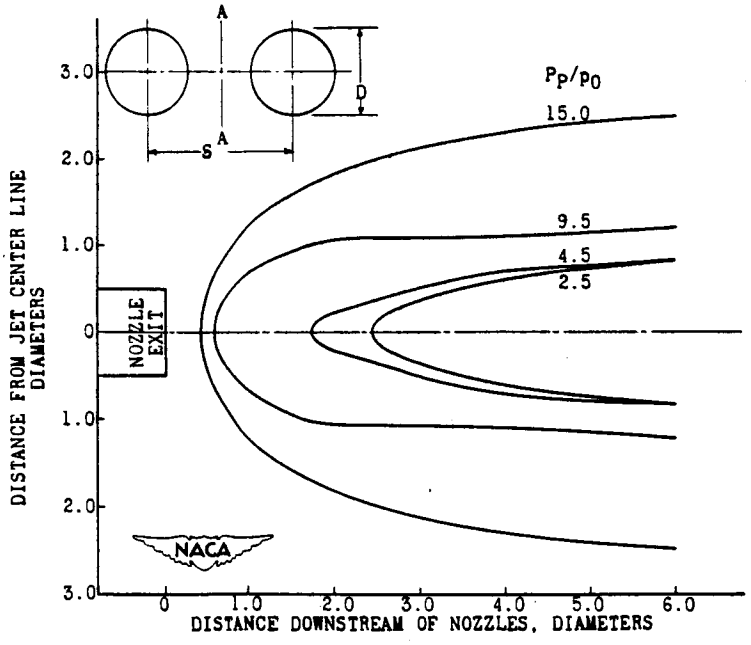


Figure 6.- Jet boundary in vertical plane through A-A. Twin jets; nozzle spacing, 1.738D; $\frac{M_x}{M_j} = 0.11$.

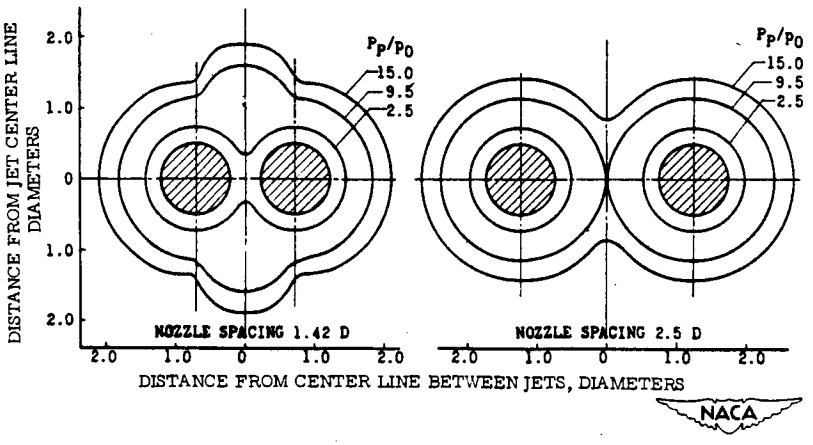


Figure 7.- Jet boundary as function of nozzle spacing. Twin jets; axial station, 2D; $\frac{M_x}{M_j} = 0.11$.

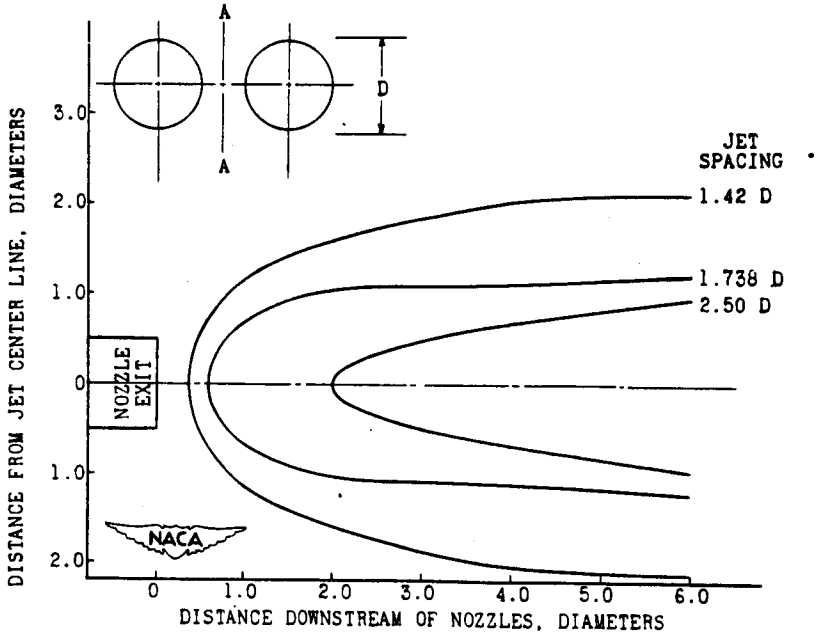


Figure 8.- Jet boundary in vertical plane through A-A. Twin jets; $\frac{M_x}{M_j} = 0.11$; $\frac{P_P}{P_0} = 9.5$.

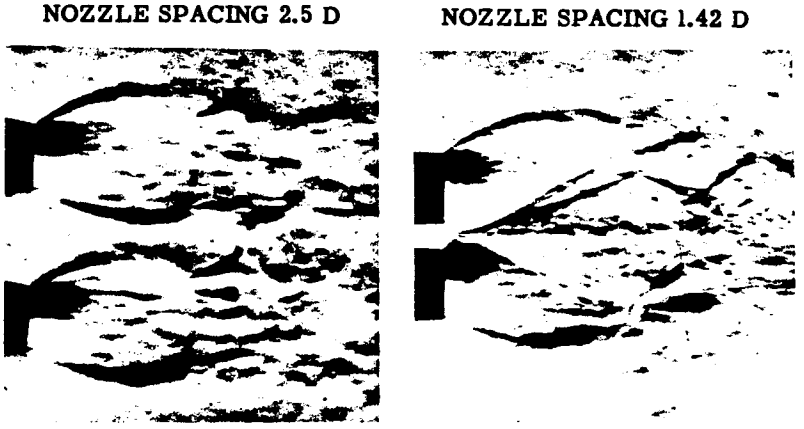


Figure 9.- Schlieren photographs of twin jets at $\frac{P_P}{P_0} = 15.0$.

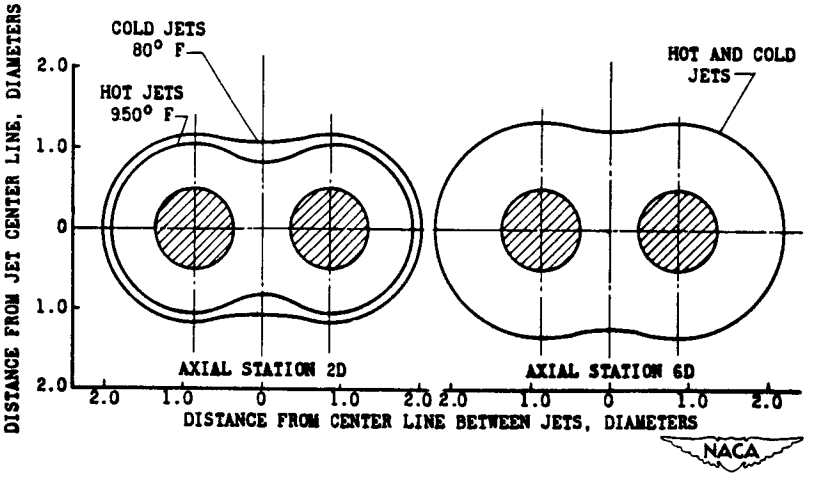


Figure 10.- Jet boundary as function of jet temperature. Twin jets; nozzle spacing, 1.738D; $\frac{M_x}{M_j} = 0.11$; $\frac{P_P}{P_0} = 9.5$.

Preceding page blank

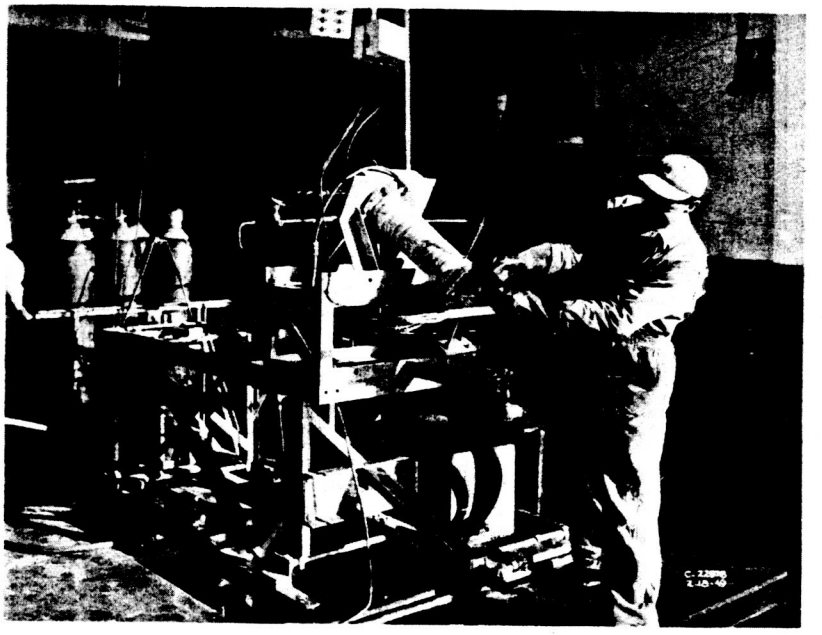


Figure 11.- Rocket combustion chamber, twin nozzle plate, and temperature survey rake.

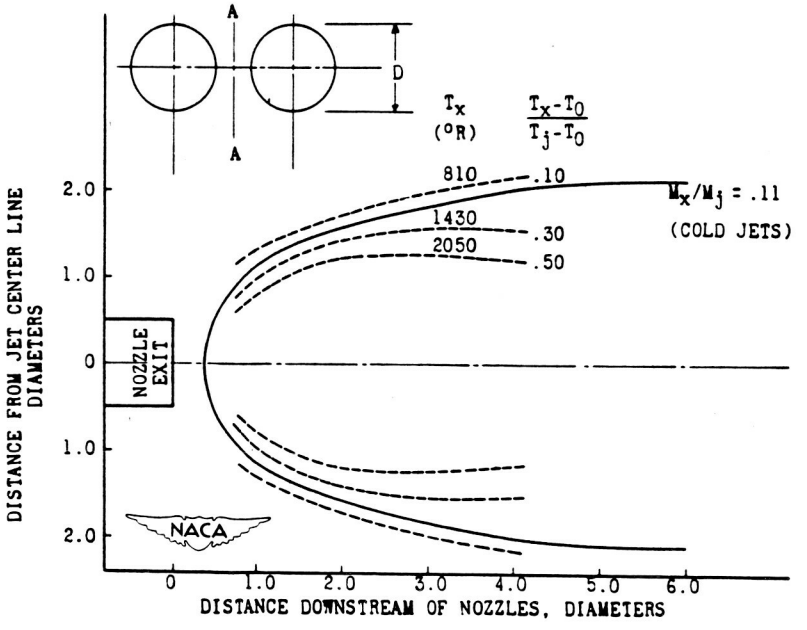


Figure 12.- Jet boundary in vertical plane through A-A. Twin jets; nozzle spacing, 1.42D; $\frac{P_P}{P_0} = 9.5$.

Preceding page blank

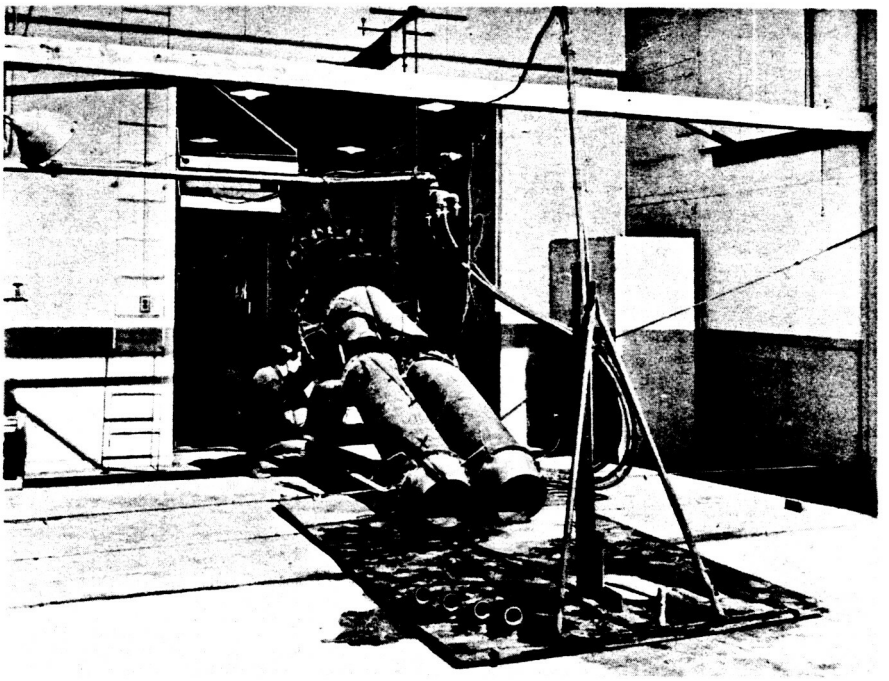


Figure 13.- Inclined jet nozzles and temperature survey rake.

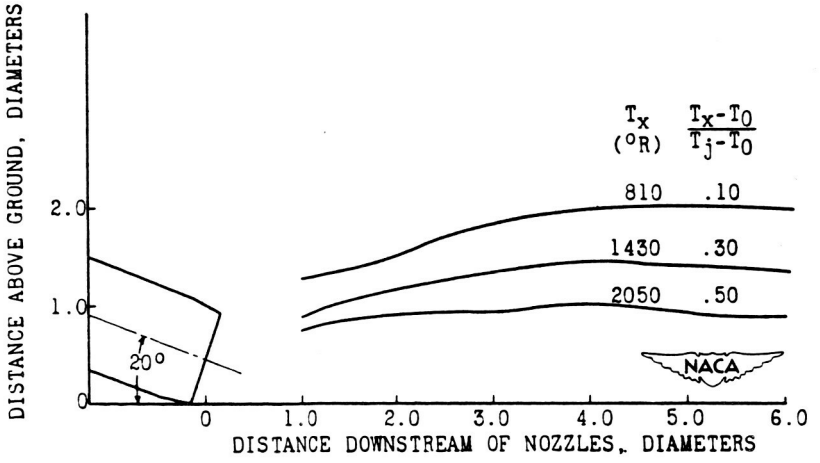


Figure 14.- Boundary on center line between twin jets deflected at 20° angle.

Preceding page blank

PROPELLERS FOR AIRCRAFT

Preceding page blank

N65-86481

BLADE-SECTION CHARACTERISTICS FROM PRESSURE DISTRIBUTIONS ON THE SECTIONS OF OPERATING PROPELLERS

By Julian D. Maynard

Langley Aeronautical Laboratory

INTRODUCTION

A need for two-dimensional propeller blade-section characteristics in the transonic speed range has long been recognized, but because of wind-tunnel choking effects progress in obtaining such data has been slow. In the low-subsonic speed range propeller characteristics may be predicted from a knowledge of the two-dimensional airfoil characteristics. In the important transonic speed range, however, it is not known whether the two-dimensional airfoil characteristics, even if they were available, could be used for the accurate prediction of propeller performance. A knowledge of the effects of velocity gradient along the blade, the three-dimensional tip effects, and the action of centrifugal force on the boundary layer along the blade would also be desirable.

To fill this urgent need for detailed information a preliminary investigation was made in the Langley 16-foot high-speed tunnel to determine the propeller section characteristics by measuring the pressure distribution on the airfoil sections of an operating propeller. The results of this investigation have been published in reference 1 and, since these results were very promising, more comprehensive tests were made.

APPARATUS

A sketch of the apparatus used in the tests is shown in figure 1. A 2000-horsepower propeller dynamometer located in the 16-foot tunnel test section was used to drive 10-foot-diameter propellers. Although the forward Mach number did not exceed 0.65 in these tests, the resultant of the rotational and forward speeds produced blade-section Mach numbers up to about 1.2. The test propellers had a rectangular plan form with a blade width of 8 inches. Twelve pressure tubes were imbedded in the upper surface and twelve in the lower surface of one of the blades of the propeller. After installation of the pressure tubes, the blade surfaces were carefully refinished to their original contours. Orifices could then be drilled in the tubes at any desired radial station. A resistance thermometer was installed in the thrust face of the blade in order to correct the pressures read on a manometer for the pressure due

to the centrifugal force of the air column in a pressure tube. The pressure tubes were brought out of the blade surface inside the rotating spinner. The shape of this spinner was calculated from a distribution of sources and sinks to produce a body of revolution which would give a uniform velocity field in the plane of the propeller. After leaving the blade the pressure tubes were run through the hollow dynamometer shaft to a pressure transfer device mounted in the rear. Details of the transfer device, which transmitted the 24 pressures from rotating tubes to stationary ones, are shown in figure 2.

The pressure tubes from the propeller blade were connected to the tubes marked B (fig. 2) which were soldered in the hollow shaft A. Each pressure transfer chamber is formed by one rotating spacer C, four "O" ring gaskets D, two Synthe-seal ball bearings E, and one stationary spacer F. The smaller "O" ring gaskets form a static airtight seal between each bearing inner race, shaft, and rotating spacer. The bearings are restrained at the outer race by the stationary spacers which are sealed by the larger "O" ring gaskets. The rotating seal is formed by a pliable synthetic rubber wiping lip always in contact with a ground concentric sealing surface on the inner race of the bearing. To prolong the lift of the synthetic rubber wiping lip, a water jacket is used to carry away the heat generated by the bearings. The pressure tubes shown in the stationary spacers were brought out at the rear end plate and connected to a multiple-tube manometer located outside the tunnel test section.

SCOPE OF TESTS

All of the blade sections were of the NACA 16-series. The lower plot in figure 3 shows the variation of the thickness ratio h/b along the blade radius. There were 5 different blade designs. Three of the blades had the same camber (or design lift coefficient, 0.3) at all radii, but had different thickness ratios. By comparing the section characteristics of these three blade designs the effect of thickness ratio can be determined for sections having the same camber. The circles on the curves in figure 3 indicate the radii along each blade for which the section pressure distributions were obtained. Note that the range of thickness ratios is from about 3 to 30 percent. Also note that a few radial stations were chosen so that the characteristics of sections having the same thickness ratio and the same camber could be compared, the only difference being in the radial location of the section. The other two blade designs had section design lift coefficients of 0 and 0.5 at all radii, and had a thickness distribution the same as for the medium-thick blade. The crosses on the curve in figure 3 indicate the radii along each of these two blades for which the section pressure distributions were obtained. By comparing the section characteristics of the three blades having the medium thickness distribution the effect of camber can be determined for sections having the same thicknesses.

The upper plot in figure 3 shows the variation of section Mach number along the blade radius, and indicates the range of Mach numbers covered for each of the radial stations. For example, the range of Mach numbers covered for the sections located at the 0.3 tip radius was from 0.3 to 0.7; and for the sections located at the 0.975 tip radius the range of Mach numbers was from 0.6 to 1.15. Also shown on the upper plot of figure 3 are the highest lift coefficients attained for several radial stations for both the upper and lower limits of the Mach number range. These figures indicate the approximate range of lift coefficients attained for the various radial stations, since the lowest lift coefficient in each case was approximately zero. It should be pointed out that some of the higher lift coefficients for the upper Mach number limits were attained by operating the blade as a one-blade propeller instead of a two-blade propeller. This was necessary because of the power limitations of the dynamometer.

Some idea of the magnitude of this investigation may be had by considering that a total of 47 blade sections were tested over a range of Mach number and angle of attack by measuring 6554 pressure distributions. This mass of data was further supplemented by results of force tests, wake-survey measurements, and measurements of the blade deflections. Consequently, the data have not yet been reduced to a form suitable for a thorough analysis. At the present time only about 4000 of the pressure distributions have been plotted and integrated. However, some typical results will be presented at this time.

PRESSURE DISTRIBUTIONS

Figure 4 shows some typical variations of the pressure coefficient along the section chord. These diagrams were obtained with an NACA 16-series section located at the 0.9 radius, having a design lift coefficient of 0.3, thickness ratio of 4 percent, and operating at an angle of attack of 0.6°, for several values of Mach number. At the subcritical speed, Mach number number 0.64, a typical subsonic pressure distribution was obtained which is relatively flat and in close agreement with the theoretical two-dimensional pressure distribution calculated for this section. At this Mach number, the section had a normal-force coefficient of 0.2. With no change in angle of attack and going to a Mach number of 0.9, which is just at the critical speed of this section, no great change in the shape of the pressure diagram was found except an increase in the magnitude of the pressures and slight irregularities near the leading edge. With this increase in Mach number the normal-force coefficient increased to a value of 0.34, which is almost exactly the increase predicted by the Prandtl-Glauert rule. When the Mach number is increased beyond the critical to a low-supersonic speed the pressure diagram undergoes considerable change.

The pressures near the leading edge of the airfoil become more positive and over most of the upper surface supersonic flow is established which terminates in a shock close to the trailing edge of the airfoil. In this transition the normal-force coefficient has dropped back to a value appreciably lower than was obtained at the critical speed. Note that at subcritical speeds the pressure distribution is more or less uniform about the midchord point. Low pressures on the rear half of the airfoil are counterbalanced by low pressures over the forward part with the result that pressure drag is negligible. At the supersonic speed, however, pressures over the rear half of the airfoil are much more negative than those over the front half with the result that there exists a large chordwise pressure force or drag and also a sharp change in the pitching moment about the quarter-chord point. Pressure diagrams such as these have been integrated to obtain values of the section normal-force, chordwise-force, and moment coefficients.

BLADE LOADING

In figure 5 values of the normal-force coefficient have been plotted for the various radial blade sections of the propeller having the thickness variation shown, which is the thinnest propeller tested. It should be emphasized that the loading curves thus obtained show the actual loading at the propeller blade, as distinguished from the usual loading downstream as obtained from wake-survey measurements. The loading curves shown were all obtained at an advance ratio of 2.2 and for the five values of stream Mach number shown in figure 5. The upper curves in the figure show the variation of blade-section Mach number along the blade radius, and the line legends correspond to the lines of the loading curves below. Note that as the stream Mach number increases from 0.38 to 0.56 the loading over the outer portion of the blade increases progressively. This increase corresponds to the increase shown by the second diagram in figure 4. As the stream Mach number is further increased to 0.60, the outboard sections lose some of their lift because of compressibility effects. At a stream Mach number of 0.65 the blade sections outboard of the 0.6 radius are operating at Mach numbers above the critical, and at the 0.7 radius the section normal force has dropped to a comparatively low value. However, at the 0.8-radius station where the section is operating at a Mach number of about 1.0, there is a considerable recovery of the lift.

In addition to providing a picture of the lift along a propeller blade, such loading curves are important in the reduction of the data for two reasons:

(1) The radial loading affects the blade deflections which must be taken into account in the determination of the true section angle of attack, and

(2) The radial loading affects the induced angle of a section which must also be taken into account in the determination of the true angle of attack.

BLADE DEFLECTIONS

In figure 6 are shown the changes in the blade angle along the blade radius for the loading curves shown in figure 5. These deflections were accurately measured under operating conditions by means of an optical deflectometer and mirrors fastened to the surfaces of the propeller blade. Furthermore, the deflections have been checked by calculations from a knowledge of the loading along the blade radius. It should be pointed out that since the advance ratio is the same for all the data shown in figure 5, the angle of attack of a blade section at a particular radius would be the same for all of the stream Mach numbers if the deflections and induced effects are disregarded. The curves in figure 6 show that the deflections cannot be disregarded since there is a change in deflection angle from 1.8° to about −0.7° at the propeller tip when the stream Mach number is increased from 0.56 to 0.65. It is interesting to note the radical changes in the shapes of the deflection curves corresponding to the radical changes in the loading curves shown in figure 5.

INDUCED-ANGLE CORRECTION

Figure 7 shows the necessity of applying a correction for the induced angle. On the left is shown the variation of the normal-force coefficient with angle of attack for several outboard radial stations operating at a constant section Mach number of 0.65. No correction for the induced angle has been applied to the values of angle of attack ($\alpha_x' = \beta_x - \phi_0 + \Delta\beta$). Since the outer sections of the blade are slightly thinner than the inboard ones the slopes of the curves for the outer sections would be expected to be slightly greater than for the inboard ones. It appears from the curves on the left (fig. 7) that a correction for the induced angle must be applied, and the induced angle

of the sections nearest the tip is evidently quite large. On the right (fig. 7) are shown the same curves with a correction applied for the induced angle, assuming an optimum (or Goldstein) loading along the blade radius. Although the correction increases the slopes of the curves, the magnitude of the correction is insufficient. If the actual loading along the blade radius is considerably different from a Goldstein loading, then the actual loading must be used for calculating the induced angle of a blade section. In figure 8 the usual loading parameter, bC_L, for a Goldstein loading is compared with the loading obtained experimentally for the same operating condition. Since the curves are quite different, the induced angles calculated for the blade sections using Goldstein factors do not give the correct values of the induced angle. At the present time attempts are being made to develop a method for calculating the induced angle for an arbitrary loading. One method being tried utilizes the equation derived by Hans Reissner (reference 2), but the calculations are quite tedious, and no completed results may be shown as yet.

In figure 7 it may be noted that the error introduced in assuming an optimum loading for calculation of the induced angle is probably small for some of the inboard blade sections. For this reason some of the data for the 0.78-radius station have been reduced to the usual lift and drag coefficients to show the trends typical of the blade-section characteristics. There is, of course, some error in the values of the angle of attack because of the assumption of an optimum loading.

TYPICAL DATA

Figure 9 shows some typical data from a single test plotted to show the variation of section Mach number, normal-force coefficient, chordwise-force coefficient, moment coefficient, and section angle of attack with the advance ratio V/nD. From several plots such as this, cross plots may be made to show the variation of lift and drag coefficients with Mach number, using angle of attack as a parameter.

Lift coefficient.- The data shown in figure 10 are for a 16-series blade section having a design lift coefficient of 0.3 and a thickness of 5.8 percent. The section was located at the 0.78-radial station. Note the rise in the lift coefficient with increase in Mach number until the critical speed is reached. In this case the critical Mach number is approximately 0.8. At Mach numbers above the critical the lift drops rapidly, and for the range of Mach numbers shown in figure 10 there is no recovery at the supercritical speeds. For the sections nearer the tip, operating at higher Mach numbers, the data will undoubtedly show some recovery of lift.

Drag coefficient.- Figure 11 shows the variation of drag coefficient with Mach number, using angle of attack as a parameter, for the same blade section as in figure 10. The curves (fig. 11) show the usual trends with a rapid rise in the drag coefficient after the critical speed is reached. It should be pointed out that an error in the angle of attack will have a greater effect on the values of the drag than on the lift because of the trigonometric relations used in calculating the drag from the normal and chordwise forces. At Mach numbers below the critical most of the pressure drag is caused by the pressures over the leading edge of the blade section. It was not possible to install pressure tubes in the blades at the leading edge, and consequently the values of drag at the lower Mach numbers are greatly affected by the fairing of the pressure-distribution curves in the region of the leading edge. The values of the drag coefficient shown in figure 11 have been increased by 0.004 to allow for the friction drag. In general, the values of the drag coefficient shown are believed to be too high, particularly at Mach numbers below the critical.

Moment coefficient.- In figure 12 is shown the variation of the moment coefficient (about the quarter-chord point) with Mach number, using lift coefficient as a parameter. The blade section is the same as in figures 10 and 11. Note that the pitching moments are negative, that is, they tend to reduce the blade angle. In general, the moment coefficients become slightly more negative as the Mach number increases, and at the lower lift coefficients this trend is reversed when the critical Mach number is reached.

In conclusion it may be said that data such as these presented in figures 9 to 12 may be used to calculate propeller efficiency with fair accuracy, since the efficiency will not be greatly affected by small errors in the angle of attack.

REFERENCES

1. Evans, Albert J., and Liner, George: Preliminary Investigation to Determine Propeller Section Characteristics by Measuring the Pressure Distribution on an NACA 10-(3)(08)-03 Propeller under Operating Conditions. NACA RM L8E11, 1948.

2. Reissner, Hans: A Generalized Vortex Theory of the Screw Propeller and Its Application. NACA TN 750, 1940.

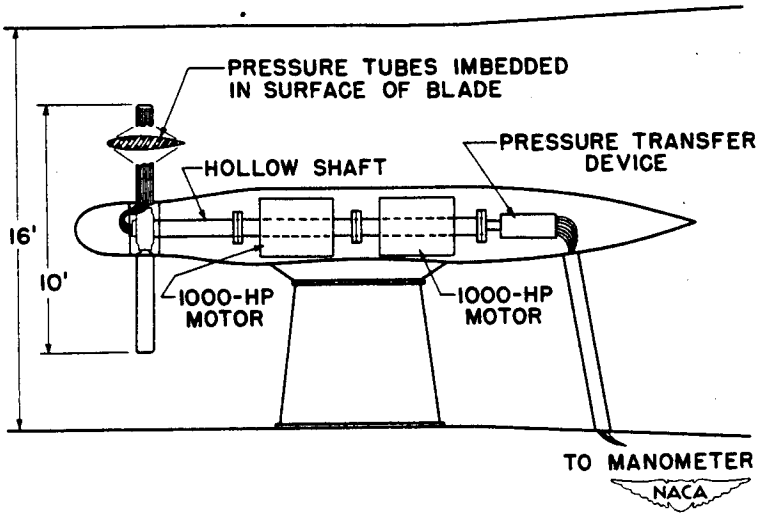


Figure 1.- Sketch of the apparatus used in the investigation of pressure distributions on the sections of operating propellers.

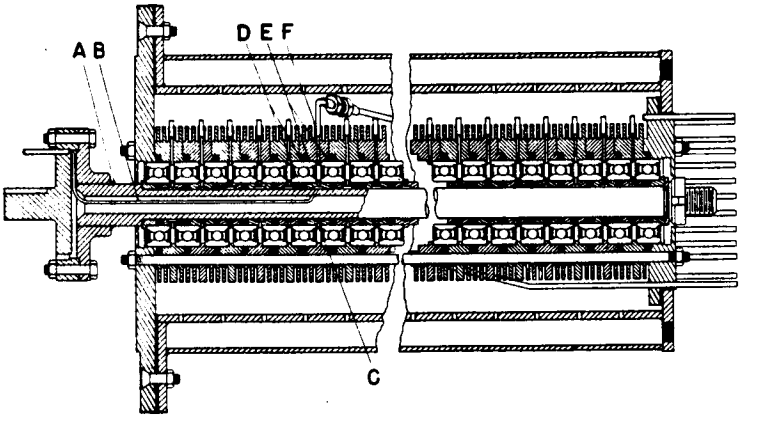


Figure 2.- Details of the pressure transfer device.

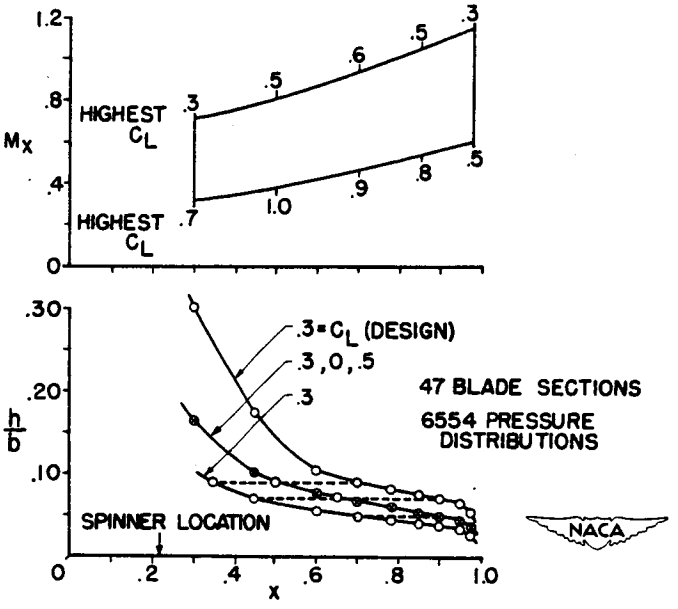


Figure 3.- Chart showing the scope of the investigation.

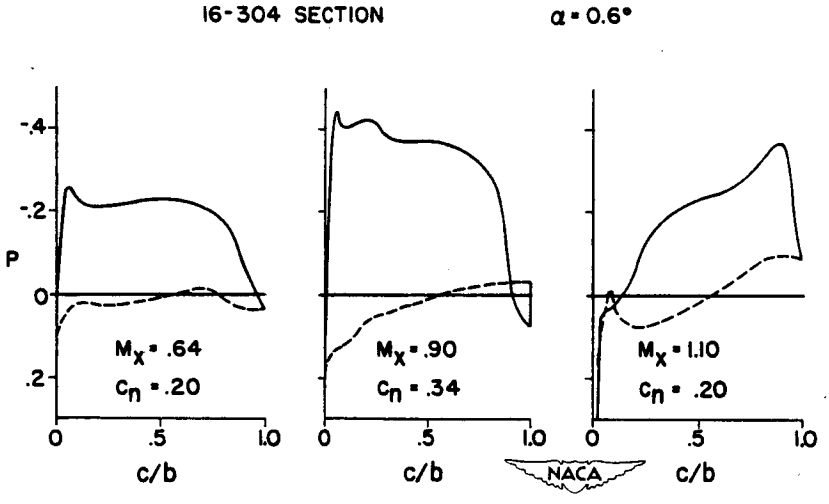


Figure 4.- Typical pressure distributions obtained on a blade section at the 0.9 radius.

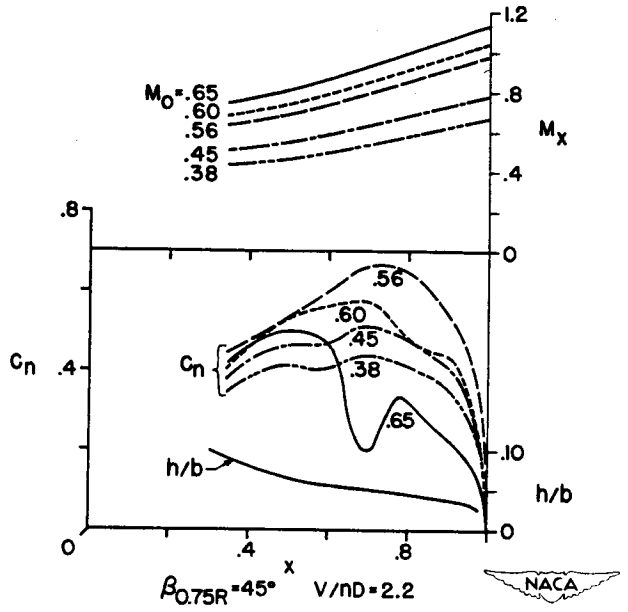


Figure 5.- Variation of the normal-force coefficient and section Mach number along the blade radius for the thinnest propeller tested.

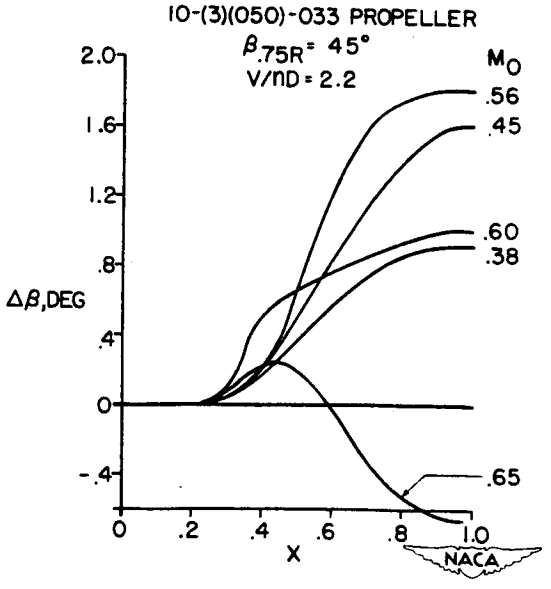


Figure 6.- Variation of the blade deflection angle along the blade radius for each of the loading curves in figure 5.

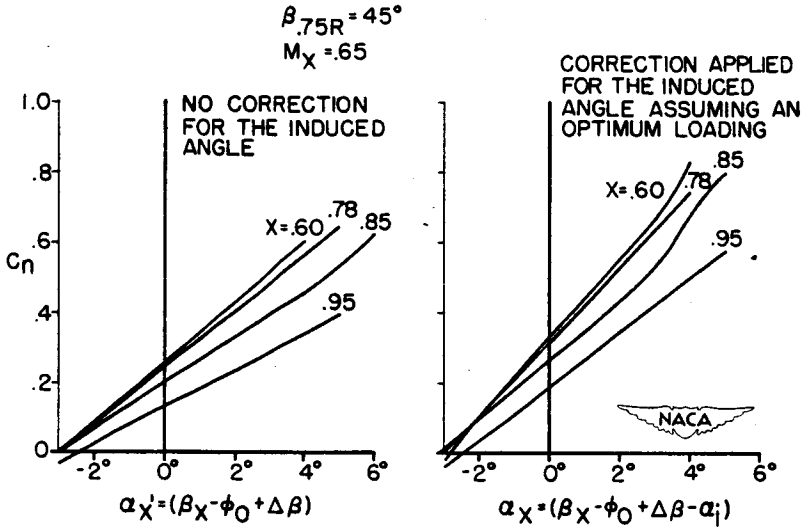


Figure 7.- The effect of the induced-angle correction on the slopes of the normal-force-coefficient curves.

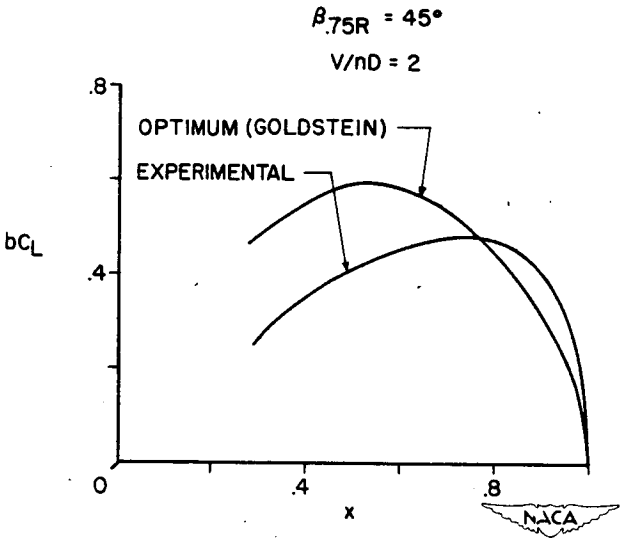


Figure 8.- Comparison of the measured loading curve with the optimum loading for the same condition of operation.

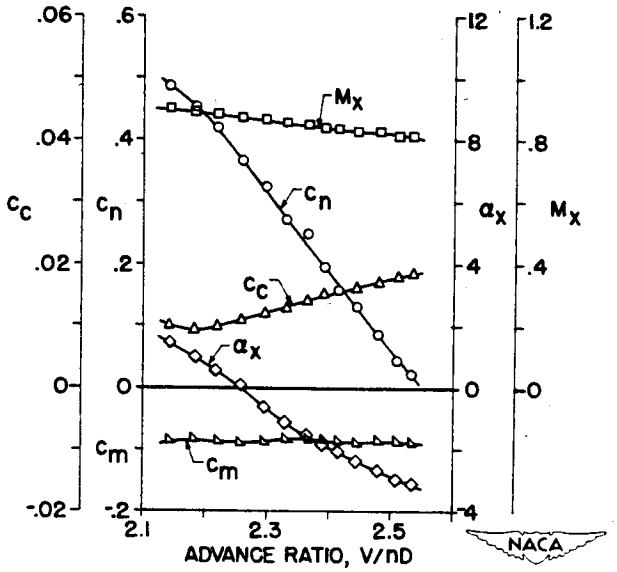


Figure 9.- Typical data obtained during a single test at a forward Mach number of 0.56.

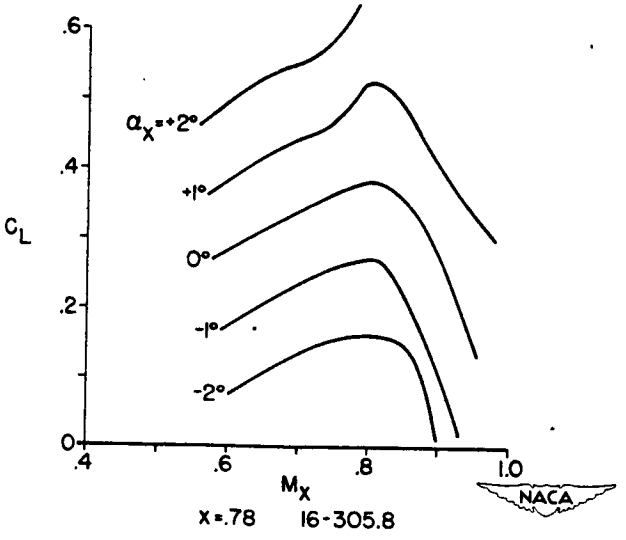


Figure 10.- Variation of blade-section lift coefficient with Mach number for several values of angle of attack.

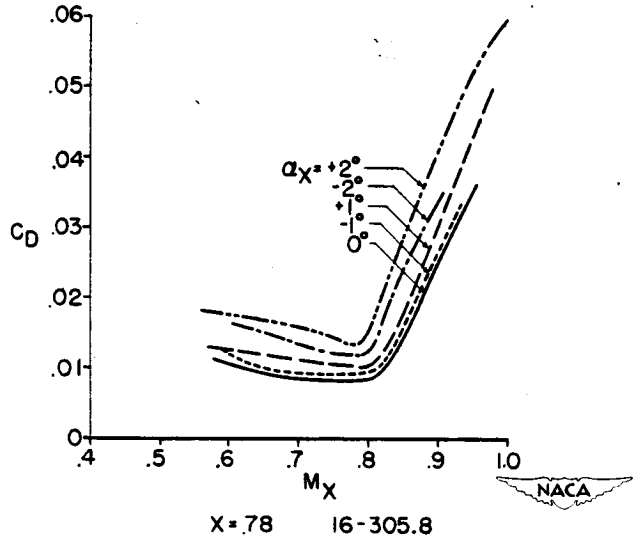


Figure 11.- Variation of the blade-section drag coefficient with Mach number for several values of angle of attack.

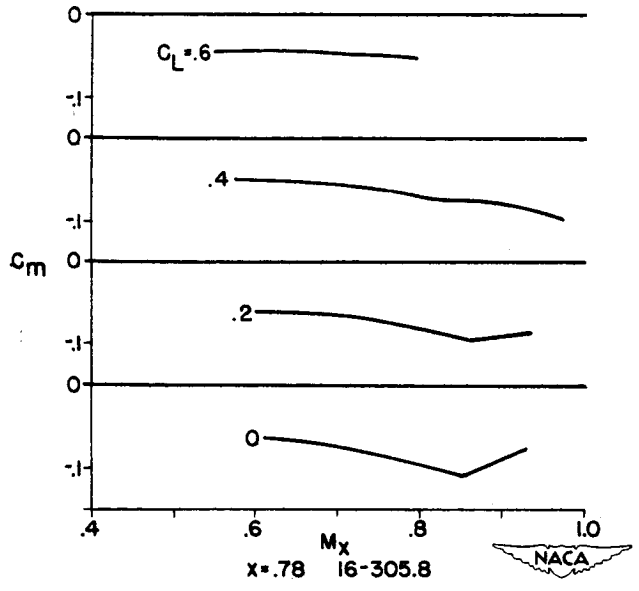


Figure 12.- Variation of the blade-section moment coefficient (about the quarter-chord point) with Mach number for several values of lift coefficient.

Preceding page blank

N65-86482

AN EXPERIMENTAL INVESTIGATION OF SINGLE-ROTATION PROPELLER CHARACTERISTICS AT HIGH-SUBSONIC MACH NUMBERS

By Richard T. Whitcomb, James B. Delano, and Melvin M. Carmel

Langley Aeronautical Laboratory

INTRODUCTION

An extensive investigation of propellers has been made in the Langley 8-foot high-speed tunnel to determine the characteristics of propellers at high-subsonic speeds and to establish the effects of various changes in design on these characteristics. In the first phase of this investigation, seven single-rotation, two-blade propellers have been tested at Mach numbers up to 0.925 over a range of blade angles and rotational speeds. The results of these investigations establish the effects of changes in blade-section camber and thickness ratio and sweep.. The complete data obtained are available in references 1 to 5. A brief summary of the conclusions drawn from these data is presented herein.

APPARATUS

Dynamometer

The propellers were investigated on the dynamometer shown in figure 1. The dynamometer consists of two similar units placed on either side of the propeller plane, which is located at the minimum section of the tunnel. These units are supported in the tunnel by 6-percent-thick struts shown in section in figure 1. Each unit includes two electric drive motors. The four motors together provide 900 horsepower for limited periods. This power is equivalent to approximately 14,000 horsepower for a 4-blade, 16-foot-diameter propeller operating at 35,000 feet altitude. Continuous rotational-speed control is provided by the use of a variable-frequency power supply. Torque and thrust are measured by hydraulic means. The design of the dynamometer is such that the errors in the various measured quantities are less than 0.25 percent. The dynamometer is described completely in reference 1. The change in the total pressure produced by the propeller has been measured by rakes of total pressure placed behind the propeller disk as shown in figure 1.

The entire test configuration is such that the flow at the propeller plane is uniform except in the boundary layer and the maximum Mach number

obtained at the propeller plane is not limited by choking at the dynamometer support struts. The maximum tunnel Mach number is limited to 0.94 by choking at the survey-rake support. In order to avoid any effects of choking on the results obtained, the maximum test Mach numbers have been limited to a value of 0.925.

Propellers

The NACA designations and dimensions of six of the propeller blades investigated are listed in figure 2. The first number in the designations indicates the propeller diameter, which was 4 feet for all propellers of the present investigation. The numbers within the first set of parentheses indicate the design lift coefficients for the design sections at the 0.7-radius stations of the blades, while those within the second parentheses show the thickness ratios for those sections. The numbers after the second dashes indicate the solidities of the blades at the 0.7-radius stations. The solidity is the ratio of the blade width to the circumference. For the swept blades, an additional group of numbers has been added to indicate the sweep of the blade at the 0.7-radius station in degrees. The plan forms, the design lift coefficients and the thickness ratios for several sections, and the design blade angle at the 0.7-radius station for the various blades investigated are listed under the designation.

The first blade for which dimensions are presented is uncambered. At the design station, the thickness ratio is 0.08, the blade angle is 61.44°, and the solidity is 0.045. The blade is essentially untapered. The second and third blades are cambered and are identical except for camber, one having a design lift coefficient of 0.3 at the 0.7-radius station, the other, 0.5 at that station. The results obtained with these two blades of different cambers indicate that the effect of camber is small at the high subsonic Mach numbers. Therefore, these results will not be discussed further.

The fourth and fifth blades shown were investigated to determine the effects of the largest amount of sweep that can reasonably be applied to a blade within the structural limitations (reference 6). Both have the same blade-angle distributions and sections parallel with the air stream. One is unswept, the other is sweptback and forward as shown in figure 2. The sweep at the design station is 45°. The solidities of the various sections of the swept blades are increased by the cosines of the local sweep angles over those for the same sections of the comparable unswept blade, in an attempt to obtain the same thrust coefficients for the swept as for the unswept blades. Another swept blade that differed only in the distribution of blade angle from the first was also investigated. The results obtained with the two swept blades are essentially the same and therefore only the results obtained

for the first version will be presented and discussed. The methods used to design these propellers are described in reference 7.

The last blade listed has been investigated to determine the effect of a pronounced reduction in the thickness ratios of the blade sections. In order to provide this indication exactly, this blade was made to differ from the first solely in the thickness ratios of the sections. At the 0.7-radius station of this blade, the thickness ratio is 0.03 instead of 0.08 as for the first blade.

RESULTS AND DISCUSSION

The efficiencies for the numerous operating conditions of the propellers have been determined by use of the measured torques, thrusts, and rotational speeds. The total errors in the efficiencies are probably less than 1 percent.

Effects of Advance Ratio

Data for the NACA 4-(0)(08)-045 propeller are presented in figure 3 to show the important effect of advance ratio on propeller efficiency at high subsonic Mach numbers. Variations of maximum efficiency with Mach number for advance ratios of 3 and 4 are presented in this figure. The data indicate that the use of a higher advance ratio results in a delay in the reduction of efficiency associated with the onset of shock and separation. The use of a higher advance ratio is the usual method for delaying this effect. However, when the Mach number is increased to higher values, the efficiency for the higher advance ratio drops abruptly. For these particular conditions of this one blade, the efficiency for the higher advance ratio falls below that for the lower advance ratio at a Mach number of approximately 0.85. At a Mach number of 0.9 the efficiency for the lower advance ratio is about 12 percent greater than that for the higher advance ratio. The increase in efficiency with reduction in advance ratio is associated primarily with the geometry of force vectors acting on the various blade elements.

The Mach number at which the efficiency for the higher advance ratios drops below that for the lower advance ratios depends upon the design of the propeller. For example, calculations indicate that reducing the thickness ratios of the sections moves the cross-over point to a higher Mach number. These calculations also indicate that reducing the thickness ratios also reduces the difference between the efficiencies at the higher Mach numbers. The effect of advance ratio on the characteristics of propellers with thinner blades is discussed in a subsequent paper by Eugene C. Draley, Blake W. Corson, Jr., and John L. Crigler.

[redacted]

It might be pointed out here that the propeller operating at the lower advance ratios at the higher subsonic Mach numbers is essentially a supersonic propeller since the resultant velocities over most of the elements of the blade are fully supersonic.

It may be concluded that one must use a low advance ratio to obtain the best possible efficiencies at high subsonic Mach numbers. It should be added that the use of a lower advance ratio will also result in higher thrusts for a given propeller or, conversely, will allow the use of a propeller of a smaller diameter to obtain a given thrust.

Effects of a Large Amount of Sweep

The variations with Mach number of the maximum envelope efficiencies and the maximum efficiencies for advance ratios of 3.0 and 4.0 for the unswept NACA 4-(4)(06)-04 and the highly swept NACA 4-(4)(06)-057-45 propellers are presented in figure 4. The data presented indicates that the use of a large amount of sweep delays and reduces the losses in the maximum efficiencies associated with the effects of compressibility. The effects are such that at a Mach number of 0.80 the maximum efficiencies are increased by approximately 10 percent. For an advance ratio of 3.0, at which conditions the effect of sweep is the greatest, the delays and reductions are approximately one-quarter of those predicted by use of the simple infinite-span sweep theory and the sweep of the design section. The effects are about one-half of those expected on the basis of a study of the flow over swept wings at high speeds (reference 7). The variation of the advance ratio from 4.0 to 3.0 results in the same general changes in the efficiency characteristics for the NACA 4-(4)(06)-04 propeller as for the NACA 4-(0)(08)-045 propeller. However, for the highly swept propeller the change in advance ratio from 4.0 to 3.0 has little effect on the maximum efficiency, up to the highest test Mach number.

The probable reasons for the large discrepancies between the measured and expected effects of the large amount of sweep are indicated by a study of the total-head measurements made behind the swept and comparable unswept propellers. In figure 5 radial distributions of the incremental thrust coefficients, $dC_T/d(r/R)_W$, are presented for the unswept and swept propellers. For the unswept propeller, data are presented for a blade angle of 60° and an advance ratio of 3.5; whereas for the swept propeller they are given for a blade angle of 60° and an advance ratio of 3.0. The advance ratios were selected such that the data presented for subcritical speeds correspond approximately to peak efficiency conditions and the thrust coefficients for the two propellers are approximately the same. Data are presented for various Mach numbers. Since the data for a given propeller are for a given geometric condition, any variations shown indicate the effect of compressibility.

When the Mach number is increased from 0.65 to 0.70, the incremental thrust coefficient for the outboard section of the unswept blade decreases because of the onset of shock and separation. At higher Mach numbers, the thrust coefficients for sections farther inboard are also reduced.

For the swept propeller, no loss in the incremental thrust coefficients occurs between forward Mach numbers of 0.65 and 0.70 as it does for the comparable unswept blade so that a definite delay in the effects of compressibility due to sweep are indicated. For the swept propeller, the initial loss in incremental thrust occurs at about the 0.65-radius station instead of farther outboard as for the comparable unswept propeller. This difference is probably due to the lack of sweep at the knee of the swept blade, which is centered at the 0.5-radius station. When the Mach number is increased from 0.80 to 0.85, the incremental thrust coefficients produced by the outboard sections decrease abruptly. This reduction is probably due to separation of the boundary layer on these outboard sections. Most of the difference between the measured and expected effect of sweep is probably due to this severe separation on the outboard sections. This separation is associated with an outflow of this boundary-layer air. The outflow is due to the spanwise pressure gradients and the centrifugal forces acting on the air particles in the boundary layer.

In an attempt to retard the outflow of the boundary layer and thus reduce the separation on the outboard sections, various fence configurations were attached to the rearward parts of the upper surfaces of the swept propeller blades in the region from about the 0.6-radius station to 0.7-radius station. None of these fences resulted in changes in the propeller characteristics at supercritical speeds. No other device or change in design has yet been proposed which might logically lead to significant improvement in the characteristics of the highly swept propeller.

The moderate gains in propeller efficiency that can or might be obtained through the use of sweep, with the attendant severe structural and mechanical problems can be obtained simply by reducing the thickness ratios of the blade sections by relatively small amounts.

Effects of Blade-Section Thickness Ratio

A comparison of maximum efficiencies obtained for the NACA 4-(0)(03)-045 and 4-(0)(08)-045 propellers are presented in figure 6. The NACA 4-(0)(03)-045 propeller has been investigated only at a blade angle of 60°. The blade failed before data could be obtained at other conditions. Therefore, the comparison has been made for this one condition only. Reducing the thickness ratios of the blade sections

greatly increases the maximum efficiencies at high speeds. This effect is strongest at speeds just above critical for the thin blade. For example, at a Mach number of 0.85, the maximum efficiency for the NACA 4-(0)(03)-045 propeller is approximately 80 percent compared with 60 percent for the NACA 4-(0)(08)-045 propeller. At a Mach number of 0.90 the efficiency for the NACA 4-(0)(03)-045 propeller drops to approximately 75 percent while that for the NACA 4-(0)(08)-045 remains at approximately 60 percent.

Also shown in figure 6 are several values of efficiency calculated for the NACA 4-(0)(03)-045 propeller by use of section data obtained from pressure-distribution measurements on propellers, wind-tunnel force measurements and calculations for the supersonic conditions. The calculations were made by use of the ideal load distribution and the maximum lift-drag ratios for the sections even though these conditions were not obtained for the actual propeller. The calculated values agree quite well with the measured quantities. As might be expected, the agreement is least satisfactory at a Mach number of 0.90.

Greatly reducing the thickness ratios of the propeller blade sections will allow the attainment of relatively high efficiencies at the highest subsonic Mach numbers. However, severe increases in the vibrational problems are associated with such reductions.

CONCLUDING REMARKS

An analysis of the results of investigations of seven propellers at Mach numbers to 0.925 in the Langley 8-foot high-speed tunnel leads to the following conclusions: Reductions of the advance ratio result in increases in the efficiencies of unswept propellers at high subsonic speeds; the use of large amounts of sweep leads to only moderate reductions in the losses of propeller efficiency at high subsonic speeds; reductions of the thickness ratios of the sections of a propeller have a pronounced favorable effect on the high-speed efficiency of the propeller.

REFERENCES

1. Delano, James B., and Carmel, Melvin M.: Investigation of the NACA 4-(5)(08)-03 Two-Blade Propeller at Forward Mach Numbers to 0.925. NACA RM L9G06a, 1949.

2. Delano, James B., and Morgan, Francis G., Jr.: Investigation of the NACA 4-(3)(08)-03 Two-Blade Propeller at Forward Mach Numbers to 0.925. NACA RM L9I06, 1949.

3. Delano, James B., and Harrison, Daniel E.: Investigation of the NACA 4-(4)(06)-04 Two-Blade Propeller at Forward Mach Numbers to 0.925. NACA RM L9I07, 1949.

4. Delano, James B., and Harrison, Daniel E.: Investigation of the NACA 4-(4)(06)-057-45A and 4-(4)(06)-057-45B Two-Blade Swept Propellers at Forward Mach Numbers to 0.925. (Prospective NACA paper)

5. Delano, James B., and Carmel, Melvin M.: Investigation of the NACA 4-(0)(03)-045 and 4-(0)(08)-045 Two-Blade Propellers at Forward Mach Numbers to 0.925. (Prospective NACA paper)

6. Whitcomb, Richard T.: Method for Stress Analysis of a Swept Propeller. NACA RM L8F11, 1948.

7. Whitcomb, Richard T.: A Discussion of the Design of a Highly Swept Propeller Blade. (Prospective NACA paper)

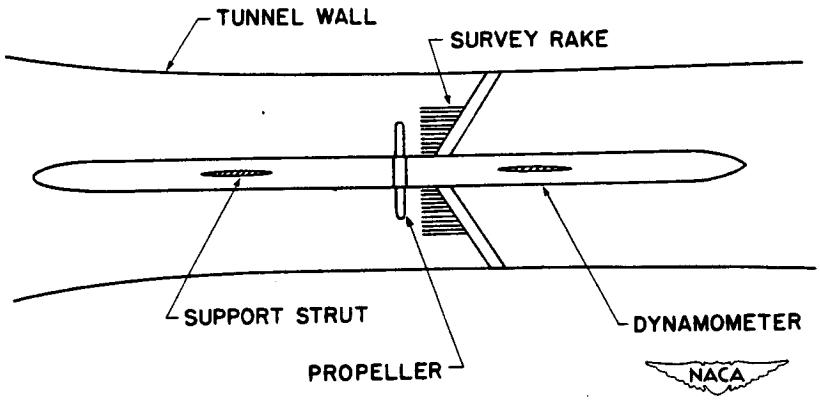
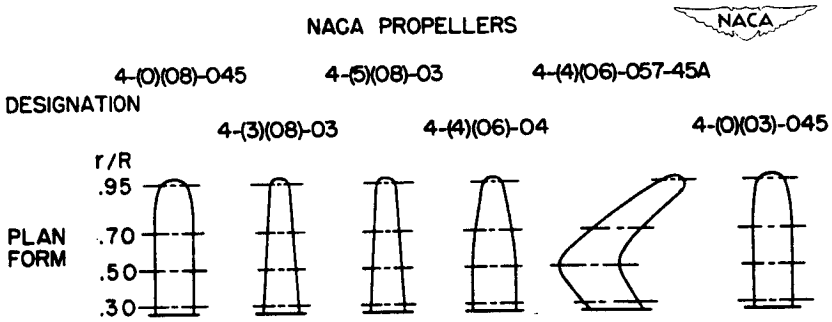


Figure 1.– Test apparatus.

NACA PROPELLERS



16-SERIES SECTIONS

r/R	c_l t/c					
.95	0-.048	.20-.048	.34-.048	.32-.025	.32-.025	0-.019
.70	0-.080	.30-.080	.50-.080	.40-.060	.40-.060	0-.030
.50	0-.102	.25-.102	.42-.102	.30-.100	.30-.100	0-.052
.30	0-.130	.14-.130	.24-.130	.21-.100	.21-.100	0-.126
$\beta_{0.7R}$	61.44°	44.75°	44.75°	60.00°	60.00°	60.32°

Figure 2.– Dimensions of blades investigated.

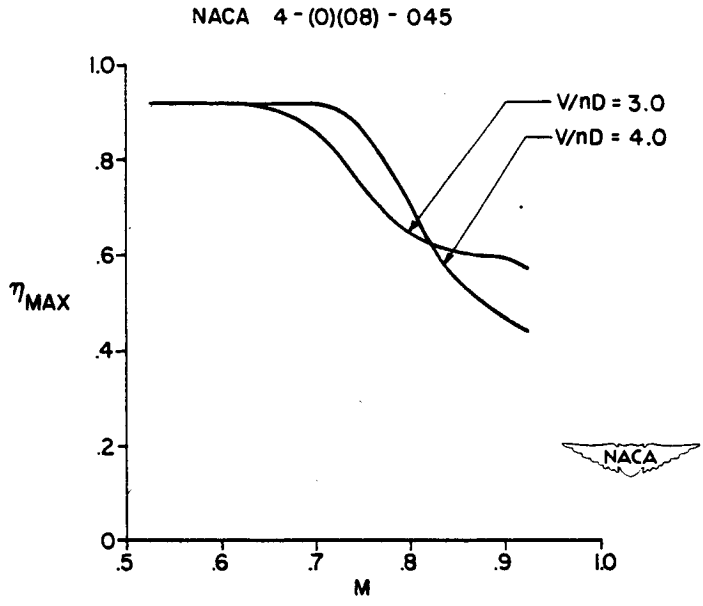


Figure 3.– Variations of maximum efficiency with Mach number for advance ratios of 3.0 and 4.0 for NACA 4–(0)(08)–045 propeller.

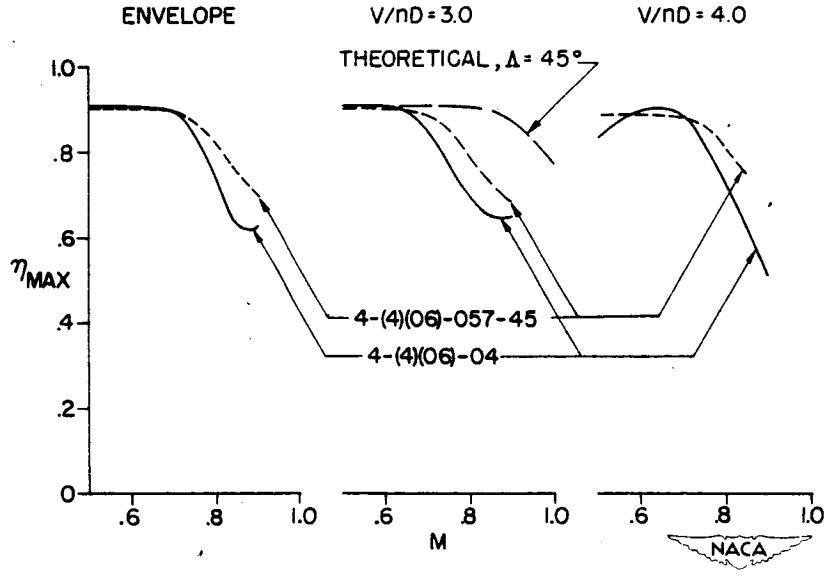


Figure 4.– Variations of maximum efficiency with Mach number for NACA 4–(4)(06)–04 and NACA 4–(4)(06)–057–45 propellers.

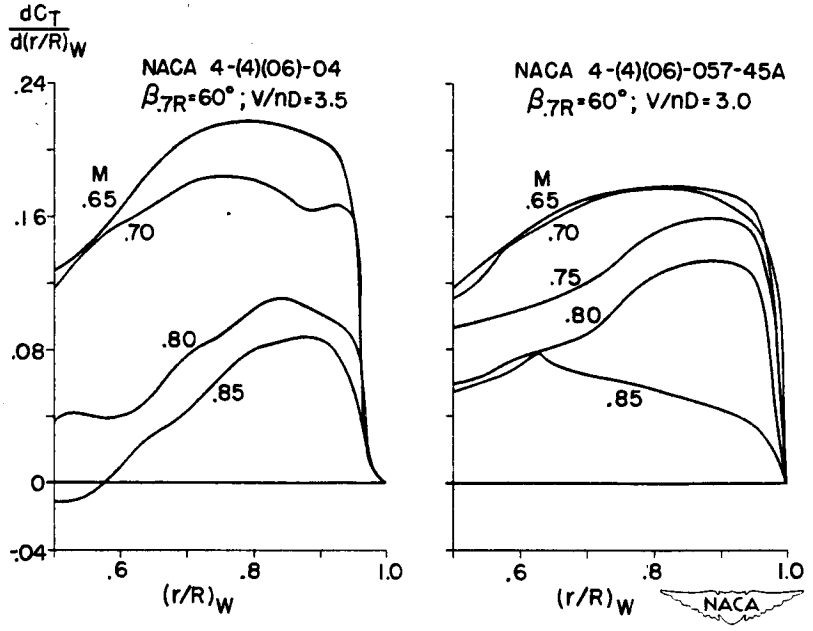


Figure 5.- Radial variations of incremental thrust coefficient obtained from wake measurements for NACA 4-(4)(06)-04 and NACA 4-(4)(06)-057-45 propellers.

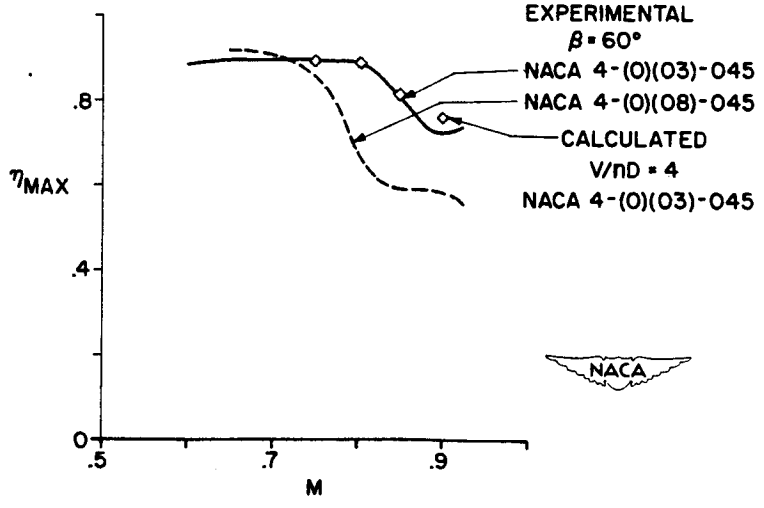


Figure 6.- Variations of efficiency with Mach number for blade angle of 60° for NACA 4-(0)(08)-045 and NACA 4-(0)(03)-045 propellers.

N65-86483

SUMMARY OF RESULTS OF UNITED AIRCRAFT WIND-TUNNEL TESTS OF A SUPERSONIC PROPELLER[1]

By Thomas B. Rhines

Hamilton Standard Division,
United Aircraft Corporation

Under Air Force Contract No. AF33(038)-2209 the Research Department of United Aircraft Corporation has conducted for Hamilton Standard Division wind-tunnel tests of a two-blade model of a supersonic propeller. (See fig. 1.) The model propeller was of 4-foot diameter with rectangular steel blades of 6-inch chord. The blade thickness varied linearly from 5 percent at the 1/4 radius to 2 percent at the tip. The propeller hub and fairing covered the inner 25 percent of the blade radius. Standard propeller force measurements were made at four or more blade angles for stream Mach numbers from 0.5 to 0.92 and one run was made at Mach number 0.975. See two examples, figures 2 and 3.

The envelope propeller efficiencies as a function of stream Mach number from these tests show values of about 91 percent at 0.5, 87 percent at 0.7, 80 percent at 0.9, and 78 percent at 0.975. (See fig. 4.) For the last of these points, operation at only a single blade angle of 50° was involved, allowing the suggestion that slightly higher values might be available elsewhere on an envelope curve. Performance at low speeds is also acceptable even though the blade design emphasized high-speed efficiency. The power absorbed at good efficiency is such as to allow diameters about two-thirds those of normal subsonic design.

It is particularly interesting to note that the efficiencies achieved by test exceed those found by calculation in a preliminary phase of the United Aircraft supersonic propeller program. The calculations at the time were believed to be conservative and the test results were therefore not unexpected. A specific comparison at the 0.9 Mach number shows 74-percent efficiency by calculation and 80 percent in the wind tunnel.

It appears that for propellers operating in the supersonic region, important performance gains are available through proper aerodynamic design of the blades, as compared with the performance levels that can be achieved in operation of even the best subsonic propellers at the high Mach numbers. A previous wind-tunnel survey with a relatively conventional blade of good aerodynamic proportions showed important

[1]This paper was offered by Mr. Rhines in the form of comments in regard to the preceding paper by Richard T. Whitcomb, James B. Delano, and Melvin M. Carmel.

losses in performance between Mach number 0.7 and 0.8 such that only 70-percent efficiency was available at the latter condition. There thus remains a major problem of propeller development to reduce to practice the design of supersonic propellers incorporating thin airfoils.

The continuing program with its important structural phases and propeller control phases will be expensive. This appears to be an appropriate time to inquire regarding the over-all desirability of such a program, now that there is ample evidence that propeller aerodynamic performance as such can be expected to be thoroughly satisfactory.

The inherent effects on airplane design of using a propeller, given good propeller performance, are complex. These effects generally react to the disadvantage of the propeller as compared with jet-engine installations. This fact has lead various representatives of the aircraft industry to imply that even if the propeller is good, it is not wanted. As long as it remained impossible to offer assurance that propeller performance could be good, such an attitude did not particularly require careful evaluation. At this time, however, this question assumes primary importance.

United Aircraft is interested in continuing with the development of the supersonic propeller to follow up from the point now attained by the government-sponsored aerodynamic tests, provided industry and government support of the required program will be available. The guidance of the entire industry is, however, necessary at this time to be sure that time and money invested in such a continuation will benefit government and industry as a whole.

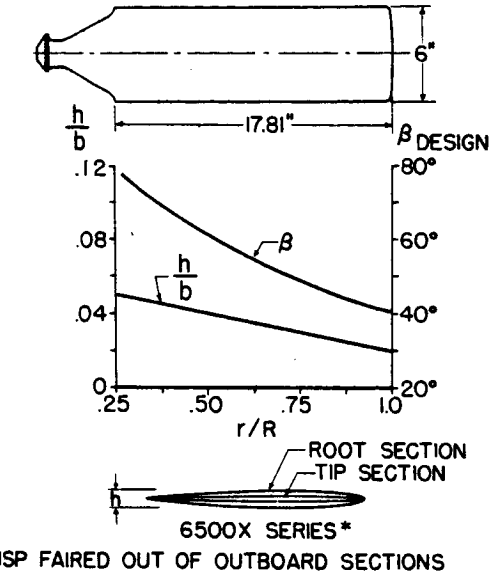


Figure 1.– Blade characteristics for supersonic propeller number 1.

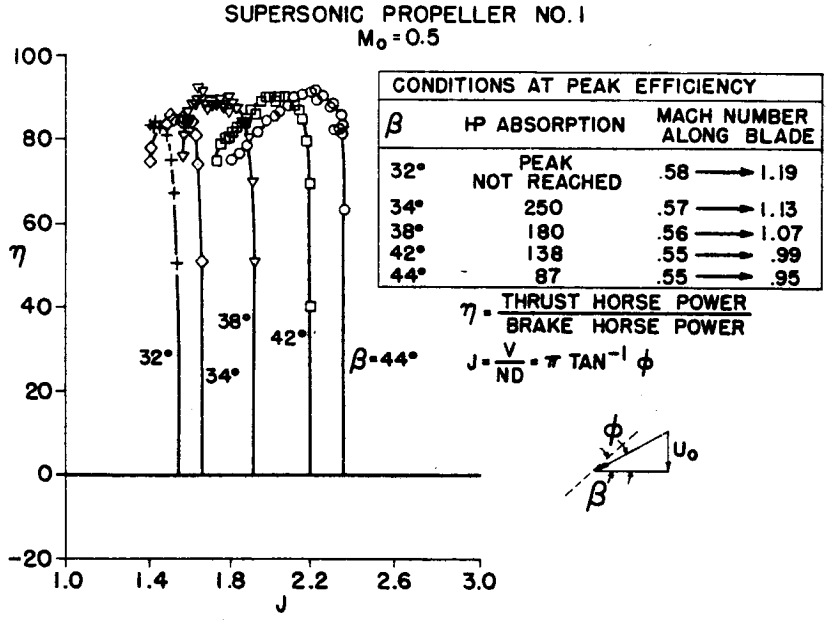


Figure 2.– Low-speed basic characteristics.

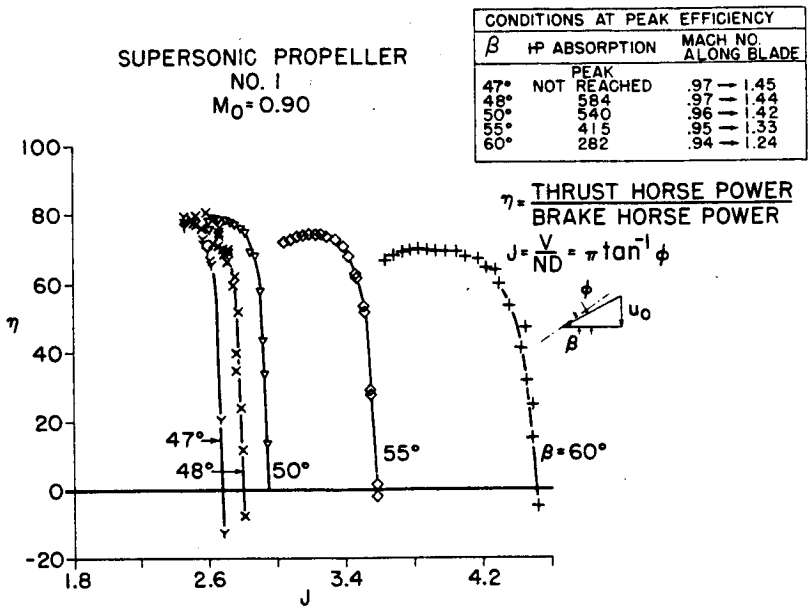


Figure 3.- High-speed basic characteristics.

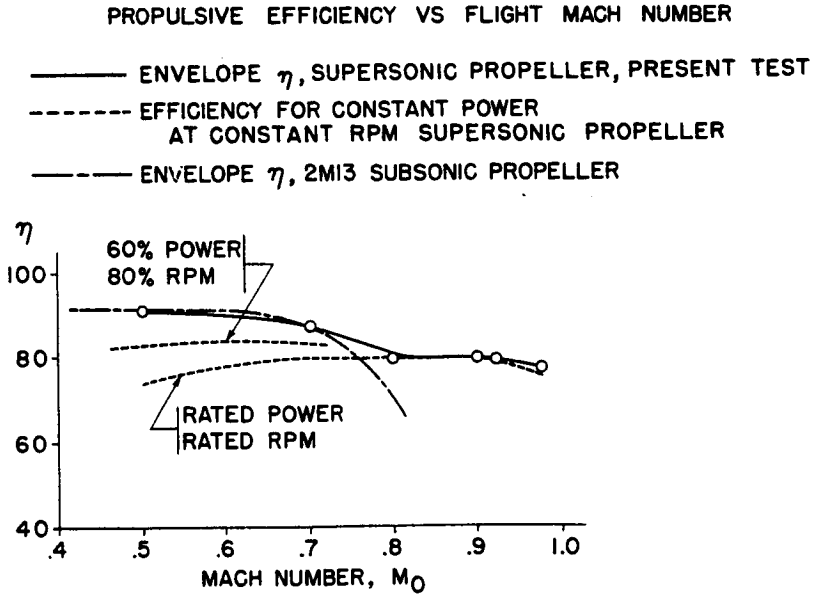


Figure 4.- Envelope propeller efficiencies as a function of stream Mach number.

N65-86484

INVESTIGATION OF A DUAL PROPELLER AT HIGH-SUBSONIC MACH NUMBERS

By Robert J. Platt, Jr., and Jean Gilman, Jr.

Langley Aeronautical Laboratory

At the present time the Langley 8-foot high-speed tunnel is testing a dual-rotating propeller having a total of eight blades. The front and rear propellers, each made up of four blades, turn in opposite directions. This propeller is designed for a very high blade angle, about 75°, the object being to achieve good efficiency at high forward Mach numbers by means of a low rotational speed so that the resultant Mach numbers along the blade are only slightly greater than the forward Mach number. The design value of advance ratio V/nD is high, about 7.1, so that the tip Mach number is only 10 percent higher than the forward Mach number.

Figure 1 shows a side-view diagram of the propeller dynamometer. This dynamometer is the same one used for the single-rotating-propeller tests that were discussed in the paper "An Experimental Investigation of Single-Rotation Propeller Characteristics at High-Subsonic Mach Numbers" by Richard T. Whitcomb, James B. Delano, and Melvin M. Carmel. However, the two units are not connected for a dual-propeller test. The two motors in the front unit drive the front propeller and the two motors in the rear unit drive the rear propeller. Each unit is suspended from the tunnel wall by a thin strut. The propeller diameter is 3 feet, so the spinner diameter is comparatively large, about 36 percent of the propeller diameter. In the tests the forces on the spinners are subtracted from the measurements so that the final results represent the forces acting on the propeller blades only.

Figure 2 shows the blade-form curves of the propeller and the plan form. The quantity r/R is the station along the blade, 1.0 representing the tip. The quantity b/D is the ratio of blade chord to propeller diameter; β_F is the blade angle of the front propeller at the design condition and β_R is the blade angle of the rear propeller; h/b is the maximum thickness of the sections. Notice that thin sections are used, 5 percent thick from the tip to the 0.7 radius and about 10 percent at the root. The design lift coefficient C_{l_d} is 0.3 for all sections. NACA 16-series airfoil sections are used.

Presented in figure 3 is a comparison of the design load distribution on the dual propeller with the Goldstein loading for a single-rotating propeller at the same value of V/nD. The loading is expressed as the ratio of the chord b multiplied by the operating lift coefficient C_l to the quantity bC_l at the 0.7-radius station. In the case of single rotation the loading near the root is kept small because rotational losses tend to become large near the root. Most of the load is therefore carried near the tip. However, in the case of a dual propeller, these rotational losses will be much smaller because the rotation imparted to the air by the front propeller tends to be removed by the rear propeller since it is rotating in the opposite direction. Therefore, the dual propeller can be loaded more highly inboard and less load is required near the tip. Compressibility losses on the outboard sections will then be delayed to a higher Mach number for the dual propeller, because the dual propeller will be operating at a lower lift coefficient.

In figure 4 is shown the variation of the measured maximum efficiency of the dual propeller with forward Mach number for the several blade angles that were tested. The front blade angle was set at the values shown and the rear propeller was set at a slightly lower blade angle. This was done in order to have the front and rear propellers absorb equal power at maximum efficiency.

The maximum efficiency at low-speeds is about 90 percent. With increasing blade angle (and therefore increasing V/nD) the point at which severe compressibility losses are encountered is shifted to higher Mach numbers. However, it appears that a blade angle of 80° is excessive since its efficiency is lower than the 75° case over the entire test Mach number range.

The maximum efficiencies at the high blade angles are good. For instance, at a Mach number of 0.85 it is possible to reach 80-percent efficiency at the design blade angle of 75°. At a Mach number of 0.90, this propeller can operate with an efficiency of 66 percent.

Figure 5 shows a comparison of the experimental maximum efficiency of the dual propeller with the calculated maximum efficiency. In this case the variation of efficiency with forward Mach number is shown for a constant value of the advance ratio rather than for a constant blade angle. In order to obtain the calculated values it was assumed that all sections operated at their maximum lift-to-drag ratios and that rotational losses were zero. The ratios of lift to drag were obtained from pressure-distribution measurements on rotating propellers. These calculated values, then, are really for an ideal dual propeller. The fact that the experimental values are only a few percent less than the calculated indicates that most of the rotational losses of the front propeller have been recovered by the rear propeller.

The data indicate, then, that a dual propeller such as the one tested can operate at high forward Mach numbers and high advance ratios with good efficiency. This is made possible by the use of thin airfoil sections, a large diameter spinner, and dual rotation, which serves to recover a large part of the rotational losses.

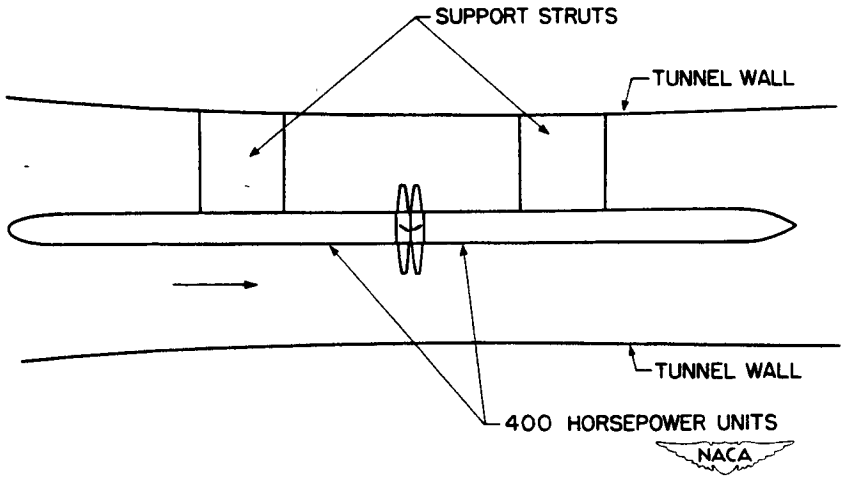


Figure 1.- Side-view diagram of propeller dynamometer.

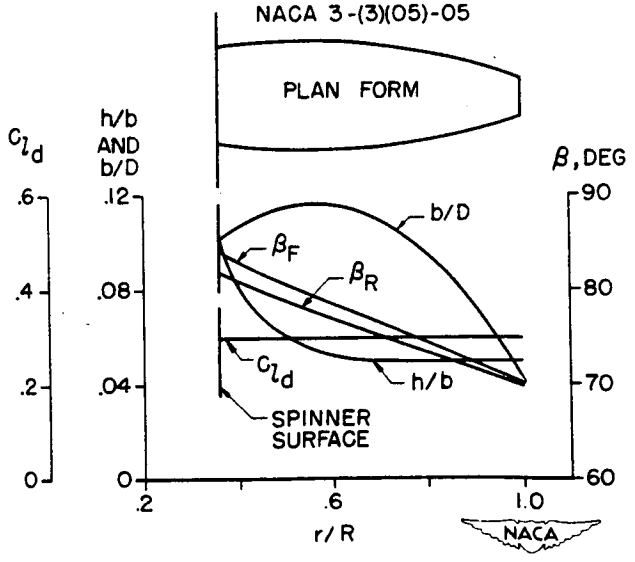


Figure 2.- Blade-form curves and plan form of propeller.

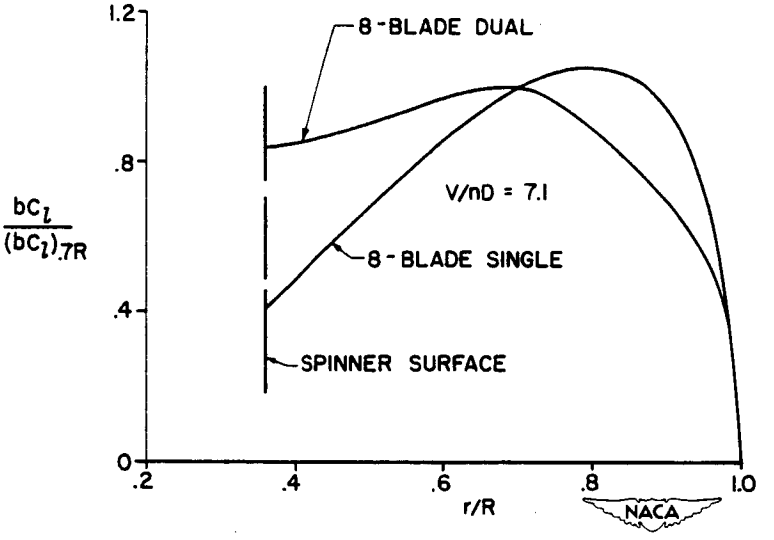


Figure 3.- Comparison of design blade loading of test propeller with blade loading of optimum single-rotating propeller.

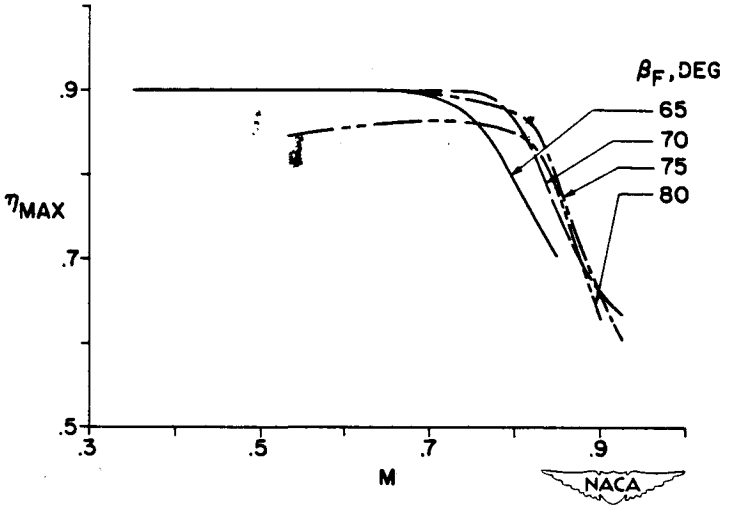


Figure 4.- Variation of maximum efficiency with forward Mach number.

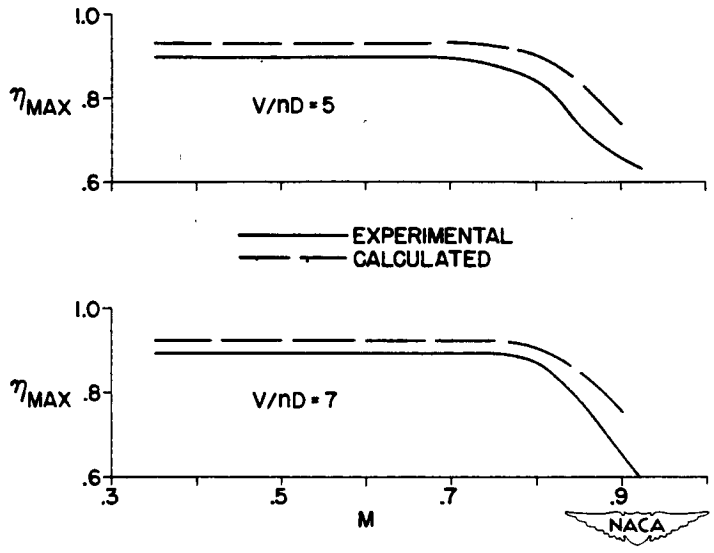


Figure 5.- Comparison of experimental and calculated maximum efficiency.

N65-86485

VIBRATION OF AIRCRAFT PROPELLERS

By Mason F. Miller and W. H. Gray

Langley Aeronautical Laboratory

Vibrations of aircraft propellers may arise from two sources, namely (1) the fluctuating aerodynamic forces acting on a propeller blade, and (2) the fluctuating forces of the aircraft engine driving the propellers. With the turbine-propeller driven aircraft currently being designed, little difficulty is anticipated from vibrations caused by the fluctuating forces of the engine, as these fluctuating forces are expected to be small. Vibrations produced by fluctuating aerodynamic forces, however, are of great concern in the design of these high-speed aircraft. This concern arises from the fact that, in addition to the increase in fluctuating aerodynamic forces with airspeed, the propellers must have thin sections to obtain high aerodynamic efficiency for high-speed flight. Consequently, it is very desirable that designers of high-speed airplanes work in close collaboration with propeller designers from the first conception of the airplane.

The structural aspects of propeller vibrations can be adequately treated by methods of calculation developed by the propeller industry. Question has arisen, however, concerning the ability to predict the fluctuating aerodynamic loads, and therefore the NACA has conducted research on two types of aerodynamically excited vibrations. The first type of vibration investigated is that which is caused by operation of a propeller in the wake of a wing on pusher-propeller aircraft such as the B-36. The second type is that which is caused by operation of a propeller with its thrust axis inclined in the air stream. In both cases the aerodynamic excitation is produced by fluctuations of the angle of attack and velocity of the blade sections. Each project will be considered separately in the following discussion.

Tests of pusher propeller.- The pusher-propeller investigation (reference 1) was conducted in the Langley 16-foot high-speed tunnel with the NACA 2000-horsepower propeller dynamometer. The configuration for this investigation is shown in figure 1. The tests were conducted with a three-blade 10-foot-diameter propeller operating at distances of 9, 18, and 30 inches behind the trailing edge of a low-drag airfoil which spanned the tunnel at propeller-thrust-axis level. This airfoil had a chord of 5 feet and a thickness-chord ratio of 12 percent. Although the ratio of the wing chord to the propeller diameter was representative of a propeller operating behind the tail surface of an airplane, the wake-velocity profile of large wings could be simulated very well by moderate deflections of a balanced flap. The drag of the wings was varied over a wide range with the use of balanced and split flaps

and was measured by wake surveys at the 9-, 18-, and 30-inch stations behind the trailing edge. Wing drag measurements were also made with the tunnel scale system. Vibratory stresses of the blades were measured with the conventional wire-strain-gage setup.

The vibration of the propeller was caused by the changes in angle of attack and velocity of the blade sections associated with the passage of each propeller blade through the wake region. In such a case the aerodynamic excitation forces of the blades have many frequency components of integral multiples of propeller speed frequency. These tests concern the response of a propeller to the excitation component having a frequency of twice the propeller rotational speed, the tests being conducted in the propeller speed range at which resonance at this frequency occurred. The investigation is therefore referred to as the 2-P vibration investigation in figure 1.

Some results of this investigation are shown by figure 2. It may be noted that the resonant-peak vibratory stress varies linearly with the wing drag coefficient and the free-stream velocity. This linearity was predicted from the treatment based on simple blade-element theory given in reference 2. These tests were conducted at blade-section speeds for which the effects of compressibility are small. As the vibratory stress is known to vary directly with blade-section lift-curve slope, increase of the free-stream velocity beyond that shown by the upper plot would be expected to produce stresses increasingly higher than the extended linear stress-velocity curve until the force-break Mach number of the blade sections occurs. Further increase in free-stream velocity would be expected to result in blade stresses below that predicted by the low-speed linear curve. The magnitude of the vibratory stresses can be predicted with reasonable accuracy from the second-order component of the aerodynamic excitation due to the wing wake.

Zero stress occurs at zero drag for the 30-inch spacing, as required by theory. At the 9-inch spacing, however, a finite value of vibratory stress was obtained at zero drag. This increment of stress is believed to be caused by mutual interference of the propeller and the wing, because the increment of stress became successively greater as the spacing between the propeller and the wing was decreased and harmonic analysis of the wake excitation showed that the 2-P excitation due to the wake does not change with spacing. This interference is believed to be the presence of the wing and blades in the field of flow of each other as the blades pass the wing during rotation. A spacing of 9 inches (about one-blade chord) is smaller than is usually employed. For a more common spacing of 18 inches (two-blade chords) the increment of stress due to interference was slightly less than for 9 inches. An

indication of the increment of stress due to interference on any particular airplane could be obtained from this investigation for the same effective spacing, because the increment obtained in this investigation can be converted into an equivalent aerodynamic excitation.

Tests of propellers inclined in air stream.- Propeller vibrations caused by inclination of the propeller in the air stream are of particular importance in the design of long-range bomber airplanes which operate over a wide range of angle of attack. Because the vibratory stresses which occur may be very high and numerous instances arose in which the measured vibratory stresses of propellers in flight could not be predicted with sufficient accuracy, a broad research program was initiated to study the problem. One part of the experimental phase of the program was to conduct tests of a propeller inclined in a uniform air stream (reference 3). The other part of the experimental program was to test a propeller inclined in the nonuniform flow field of a wing-fuselage nacelle combination of an airplane in the Ames 40- by 80-foot wind tunnel.

The configuration for the tests in a uniform air stream is shown in figure 3. These tests were conducted with the NACA 2000-horsepower propeller dynamometer in the Langley 16-foot high-speed tunnel at inclinations of 4.5° and 9.8°. This figure shows the 10-foot-diameter propeller inclined at an angle of 9.8° in this tunnel. A survey rake alined with the air stream was mounted at six angular positions behind the propeller to determine the variation of aerodynamic load per revolution of the propeller. Vibratory stress measurements on the propeller were also made with strain-gage equipment. The investigation is designated as the 1-P investigation in figure 3 because the vibrations caused by the fluctuating angle of attack and velocity due to propeller inclination have one cycle per revolution of the propeller.

The top part of figure 4 shows a comparison of the measured and calculated variations of blade-section thrust coefficient per revolution at four section radii (x) for a moderate tip Mach number M_t of 0.82 and an inclination of 4.55°. ($\Delta C_T'$ is defined as the difference between blade section thrust coefficients for the tilted and untilted propeller.) The bottom part of this figure shows a similar comparison for the thrust-coefficient variation of the entire blade. The peak positive change in thrust is about 40 percent of the steady-state thrust of the propeller operating near peak efficiency. The magnitude of the measured thrust-coefficient variations is in good agreement with the calculated thrust coefficient variations over the entire blade. The calculated variations were based on the steady-state theory of Crigler and Gilman (reference 4), which was extended to include the effect of Mach number variation per revolution for the blade sections. The calculations were made with the use of section

thrust coefficients measured with the survey rake with the propeller not inclined. The lag of the measured thrust-coefficient variations behind the calculated thrust-coefficient variations based on steady-state theory is to be expected from consideration of unsteady-lift theory. The indication based on unpublished calculations by John C. Houbolt and Lyle Sanders of the Langley Laboratory is that an accurate description of the blade dynamics including damping is needed to predict this phase lag. The moderate phase lag indicated is of relatively little importance, however, compared with the magnitude of the thrust-coefficient variations which apparently can be predicted from the steady-state theory in this range of frequency.

Figure 5 shows similar comparisons at a tip Mach number of 1.04. In calculating the thrust-coefficient variations for this case in which a portion of the blade operates in the transonic speed range, consideration of Mach number variation per revolution for the blade sections is especially important. The magnitude of the calculated and measured variations of thrust coefficient are in agreement over the inboard portion of the blade but are not in agreement at the 0.9 radius station where the section is operating in the transonic speed range. As the disagreement between measurements and calculations occur only in the region of the blade tips, the calculated and measured thrust coefficient values for the blade are in agreement.

Figure 6 shows another comparison between calculated and measured thrust coefficients for a tip Mach number of 1.12. The long-dash lines in the calculated curves represent extrapolations. At this Mach number, it may be noted that the poorest agreement occurs at the 0.75-radius station. Again the calculated and measured blade thrust coefficients are in good agreement.

A plot of the difference between the peak-positive and peak-negative values of the thrust-coefficient variations along the blade span is shown in figure 7 for the three tip Mach numbers. It may be noted that the dips in the curves for tip Mach numbers of 1.04 and 1.12 occur at the 0.9- and near the 0.75-radius stations, respectively. These are the regions of poorest agreement between the measurements and calculations shown by the previous figures.

A plot of the vibratory stress at the 0.45-radius station against the parameter $\alpha_T q$ is shown in figure 8. The symbol α_T designates the angle of inclination of the propeller and q designates the free-stream dynamic pressure. The only points plotted are those approximating peak-efficiency operation of the propeller. The vibratory stress varies linearly with $\alpha_T q$ at low speeds for both inclination angles of 4.55° and 9.8° as predicted by theory. At the higher tip

Mach numbers, however, it may be noted that the measured stress is less than that predicted by the low-speed linear curve for both angles of inclination of the propeller. This result is to be expected because of the reduction in tip loading occurring at the transonic speeds.

Figure 9 shows a similar plot of vibratory stress at the 0.45-radius station. In this figure, however, the abscissa is modified by the term $(a + 2c_l \cot \phi)b$, the elements of which are evaluated for an assumed effective radial station of 0.7R (R, tip radius). The elements of the term are identified as follows: a, blade-section lift-coefficient slope; c_l, blade-section lift coefficient; $\cot \phi$, function of advance ratio; b, blade-section chord. Points representing operation of the propeller at efficiencies other than peak efficiency are included in this plot and form a straight line for low speeds. The points representing operation at the high tip Mach numbers, however, are below the low-speed linear curve as in the previous chart. This plot shows that the effective radial station for application of the vibration load which may be used at low speeds cannot be applied throughout the speed range because of the large changes in blade loading which occur at high speeds.

It may be concluded from both research investigations which have been discussed that the fluctuating aerodynamic loads of a propeller may be calculated with satisfactory accuracy if the blade-section characteristics and field of flow at the propeller are known.

REFERENCES

1. Gray, W. H., and Solomon, William: An Investigation of Wake-Excited Propeller Vibrations. (Prospective NACA paper)

2. Corson, Blake W., Jr., and Miller, Mason F.: Considerations of Wake-Excited Vibratory Stress in a Pusher Propeller. NACA ACR No. L4B28, 1944.

3. Gray, W. H., Hallissy, J. M., Jr., and Heath, A. R., Jr.: A Wind-Tunnel Investigation of the Effects of Thrust Axis Inclination on a Propeller. (Prospective NACA paper)

4. Crigler, John L., and Gilman, Jean, Jr.: Calculation of Aerodynamic Forces on a Propeller in Pitch or Yaw. NACA RM L8K26, 1949.

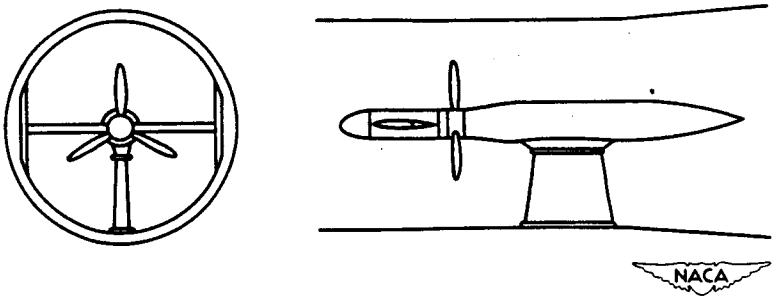


Figure 1.- Configuration of 2P vibration investigation.

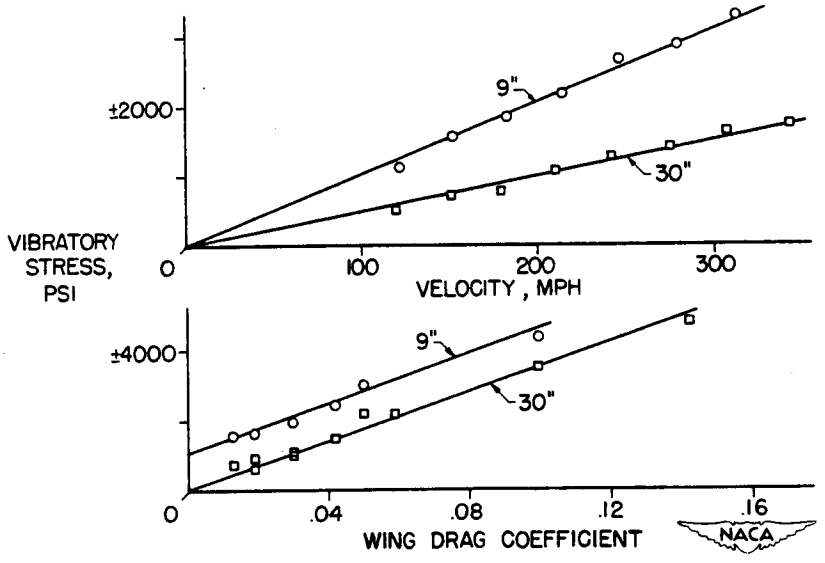


Figure 2.- Variation of vibratory stress with free-stream velocity and wing drag for two spacings.

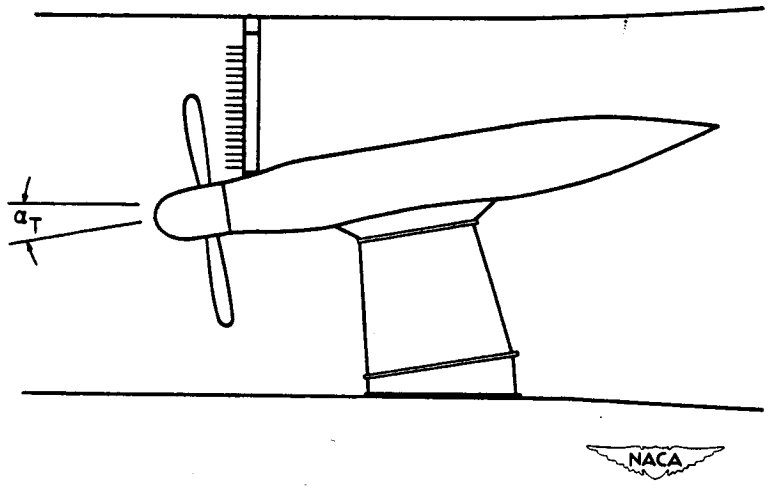


Figure 3.- Configuration for 1P vibration investigation.

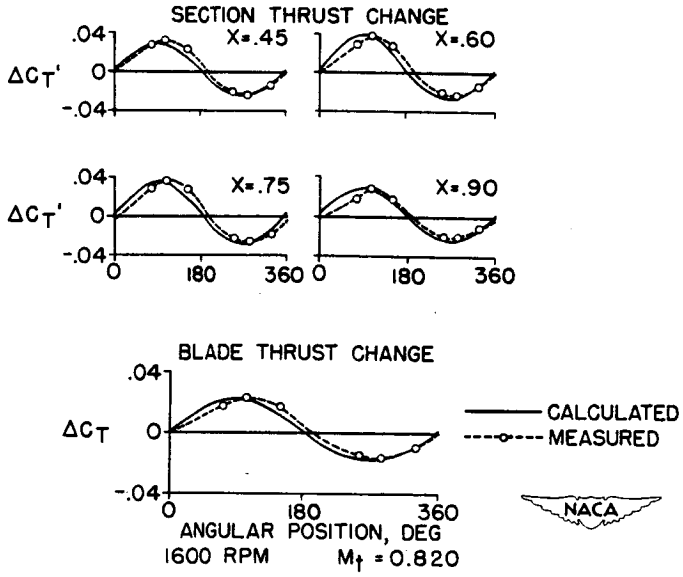


Figure 4.- Change in thrust coefficient with rake angular position. M_t = 0.820.

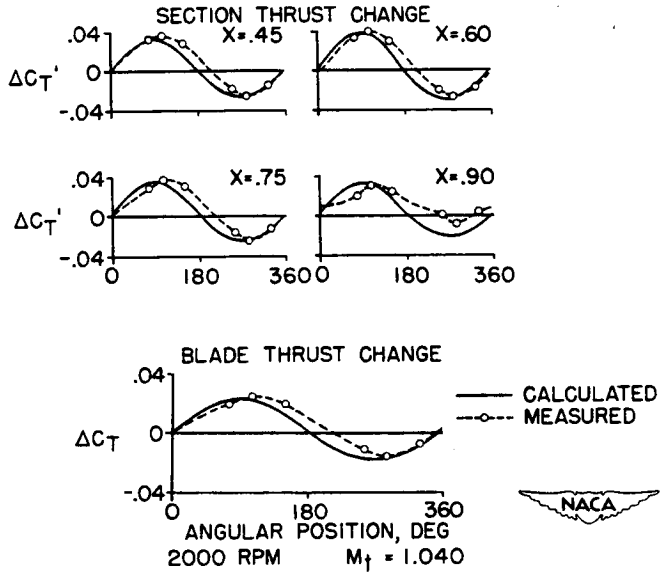


Figure 5.- Change in thrust coefficient with rake angular position. $M_t = 1.040$.

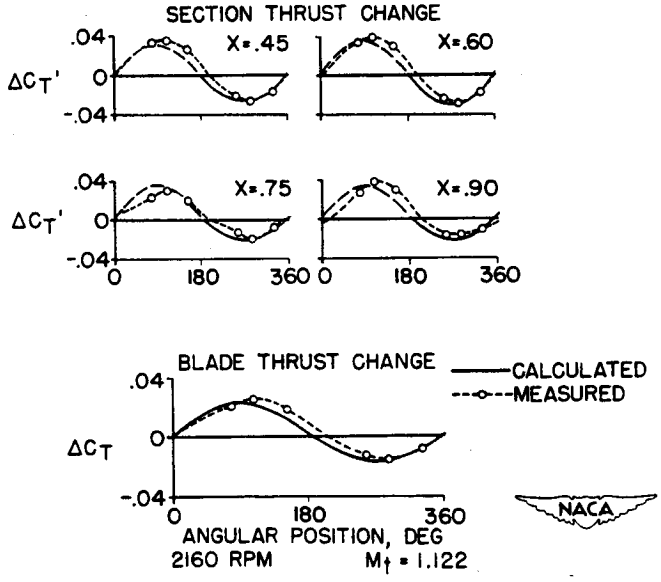


Figure 6.- Change in thrust coefficient with rake angular position. $M_t = 1.122$.

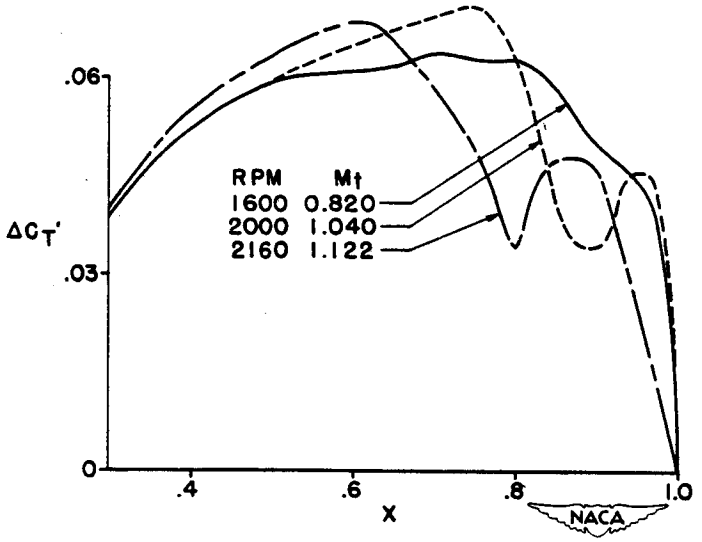


Figure 7.- Effect of tip Mach number on radial distribution of change in section thrust coefficient.

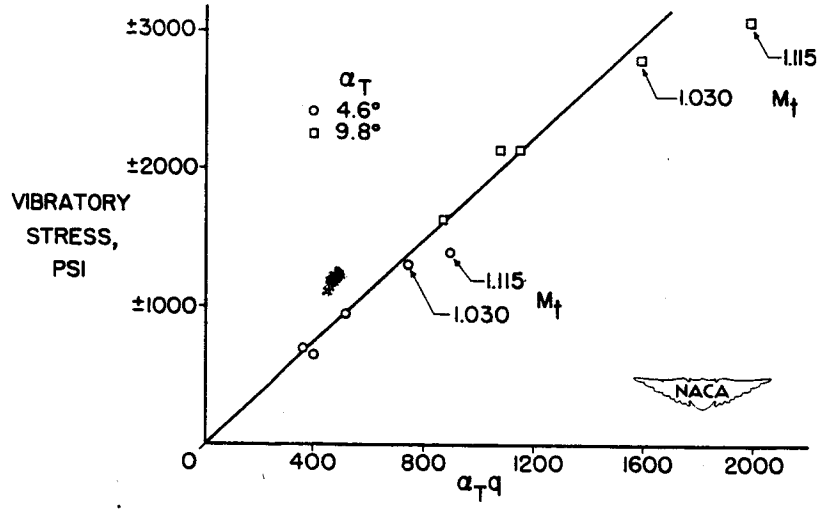


Figure 8.- Vibratory stress as function of $\alpha_T q$ for operating conditions near maximum efficiency.

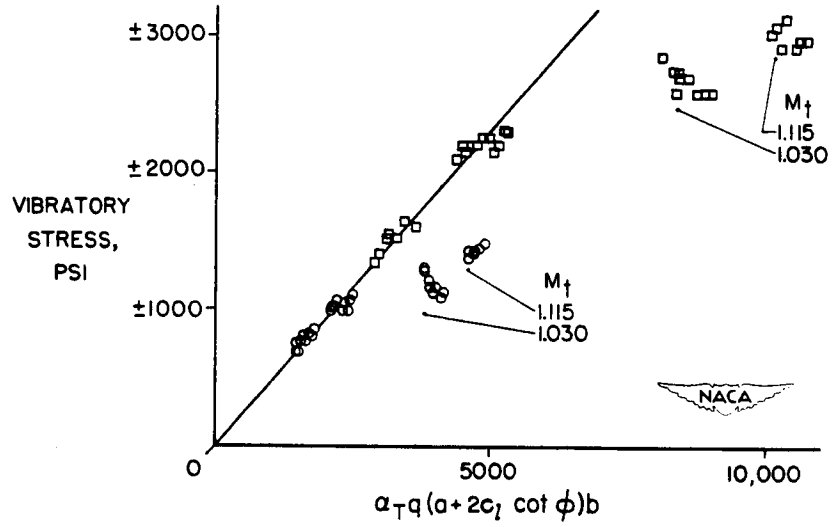


Figure 9.- Vibratory stress as a function of $\alpha_T q$ as modified for aerodynamic changes at $x = 0.7$.

[redacted]

N65-86486

PREDICTION OF FIRST-ORDER VIBRATORY STRESSES FOR A PROPELLER OPERATING IN THE FLOW FIELD OF A WING-NACELLE-FUSELAGE COMBINATION

By Vernon L. Rogallo

Ames Aeronautical Laboratory

An investigation is being conducted in the Ames 40- by 80-foot tunnel to determine the first-order vibratory stresses in a propeller operating in the unsymmetrical flow field of a wing-nacelle-fuselage combination. The purpose of the investigation is to determine the reasons why existing methods of predicting the vibratory stresses have not always given satisfactory results and to establish what refinements, if any, are necessary to improve the accuracy of the methods. Tests of one particular propeller have been completed. This paper presents the significant test results and compares them with predicted results.

The wing-nacelle-fuselage combination used for the investigation was a twin-engine fighter-type airplane (fig. 1). The measurements were confined to the left side of the airplane. The size and location of the propeller disk relative to the components of the airplane are indicated. In order to provide precise control of operating conditions during the test and also to avoid engine-excited propeller vibrations, the conventional reciprocating engine was replaced by a 1500-horsepower electric motor.

A Curtiss four-blade hollow steel propeller having a diameter of 13 feet and 2 inches was used for the investigation. The type, plan form, and typical cross sections of the blade are shown in figure 2. The propeller was quite flexible; it had a static natural frequency of approximately 12.5 cycles per second for both the first reactionless and the first antisymmetric flatwise bending modes.

The prediction of the first-order stresses for a propeller operating in the presence of a wing-nacelle-fuselage combination involves the following three steps:

(1) A determination of the characteristics of the flow field

(2) Calculation of the air-load variation on the propeller operating in this flow field

(3) Computation of the stresses in the propeller due to this air-load variation.

[redacted]

Since each of these steps involves certain simplifying assumptions, any one or all of the steps may be responsible for inaccuracies. Therefore, in conducting the investigation, data were obtained to evaluate each step of the method of prediction. Thus, in order to obtain the necessary information for step (1), stream-angle and velocity surveys were made at the propeller plane before installing the propeller. With the propeller installed, thrust and stress measurements were made to provide the necessary information for steps (2) and (3).

The survey of the flow field at the propeller plane consisted of the measurement of upflow and sidewash angles, and the ratio of the local velocity to the free-stream velocity for various angles of attack of the airplane. Typical results are presented in figure 3. These data are for the 0.7 radius of the propeller disk when the airplane was at an angle of attack α_G of 8° (referred to thrust axis). Shown in the figure are the variations with angular position around the disk of the sidewash angle σ, the ratio of local to free-stream velocities V_l/V_o, and the upflow angle, $\alpha_G + \epsilon$ (the geometric plus induced angles).

In order to illustrate the effect of flow-field distortion on the varying air load of an inclined propeller, figure 4 has been prepared from the previously shown results. Steady-state propeller theory (references 1 to 3) was used in calculating the values of incremental section-thrust coefficients which are plotted against angular position around the disk. These calculations are for the 0.7-radius station of the propeller. Two propeller-operating conditions were considered:

(1) The isolated propeller at an angle of attack

(2) The propeller in the measured flow field

At this 8° geometric angle of attack, the distorted flow field nearly doubles the magnitude of the air-load variation and greatly changes the shape of the variation. The greater portion of the change in magnitude was due to the induced upwash, the sidewash and velocity distribution contributing significantly only to the change in shape. Since the induced upflow angles so greatly affected the air loads, an attempt was made to compute them from lifting-line theory. Such a procedure failed to predict more than one-third of the measured upwash, even though the experimental span-loading distribution was used. It is apparent that step (1) - the determination of the characteristics of the flow field - is a likely source of error in existing procedures for predicting first-order vibratory stresses.

With the flow field known the next step is to determine whether the steady-state propeller theory is adequate for predicting the oscillating air load. The adequacy of the theory is indicated by figure 5. The upper part of the figure shows a comparison between the calculated

and experimentally determined air-load variation. The calculated variation is that shown in the previous figure for the case where the flow-field data were used. The experimental data were obtained by propeller-wake surveys. Excellent agreement in magnitude and wave form may be noted. A phase difference between the curves is quite apparent. No attempt has been made to account for this difference since stress predictions are only dependent upon the magnitude of the oscillating air load and are independent of the angular position of the blade. The component parts of the measured and the calculated total air loads are shown in the lower half of the figure. The main component is 1-P, the remainder is 2-P. Again, excellent agreement in magnitude between the measurement and computation may be noted. The comparisons shown are typical of those for other blade stations and other propeller-operating conditions. It can be concluded, therefore, that steady-state propeller theory is adequate for the second step - the prediction of the oscillating air load from the flow-field data.

The third and final step remains - the prediction of the vibratory stresses in the propeller due to the oscillating air loads. Before this step was taken, the test results were analyzed to determine whether there was any evidence of an approach to resonance. The phase relation between the air load and the stress was used as an indication. Although the peak stress lagged the peak air load, there was no appreciable change in the amount of lag with increasing propeller speed. The absence of any appreciable change in the phase angle between the stress and thrust was taken to be indicative of the absence of a close approach to resonance. No explanation is offered for the fact that the stress and thrust were not in phase. A similar result was noted from the Langley Laboratory tests of an isolated propeller.

With the lack of resonance indicated, a method of prediction based on a consideration of forced vibrations could thus be used. The calculated stresses to be presented in this paper were obtained by the integration method developed by the Propeller Division of the Curtiss-Wright Corporation. The significant assumptions of the method are that the vibration is nonresonant, the oscillating air load is sinusoidal, and the blade, in effect, is untwisted and has a blade angle equal to that of the blade section about which the majority of the blade tends to deflect. A comparison of calculated and measured stress distributions is shown in figure 6. The comparison at the top of the figure is for the set of test conditions at which the highest 1-P stresses were encountered. The lower half of figure 6 presents a comparison for another set of conditions for which the measured stress distribution is more complete. Very good agreement is noted in both cases except in the region of highest stress. The slight disagreement found here is believed due to local deformation, or "oil canning," characteristic of hollow steel propellers without internal stiffeners. Such a disagreement was noted between computed and measured stresses for a static loading condition of the propeller.

From the foregoing considerations, then, it can be concluded that an accurate prediction of nonresonant first-order vibratory stresses can be obtained for similar propellers and propeller-operating conditions if the characteristics of the flow field are accurately known or can be accurately estimated. In the present case it was found that the values of upwash angle – the largest factor in the flow-field distortion – could not be predicted with sufficient accuracy by lifting-line theory where account is taken of the effect of the nacelle on wing span-load distribution. It appears that, until more refined theories are developed, flow-field data of sufficient accuracy for the purpose of predicting nonresonant propeller stresses can be obtained only by experiment.

REFERENCES

1. Crigler, John L., and Gilman, Jean, Jr.: Calculation of Aerodynamic Forces on a Propeller in Pitch or Yaw. NACA RM L8K26, 1949.

2. Lindsey, W. F., Stevenson, D. B., and Daley, Bernard N.: Aerodynamic Characteristics of 24 NACA 16-Series Airfoils at Mach Numbers between 0.3 and 0.8. NACA TN 1546, 1948.

3. Theodorsen, Theodore, and Stickle, George W.: Effect of a Trailing-Edge Extension on the Characteristics of a Propeller Section. NACA ACR L4I21, 1944.

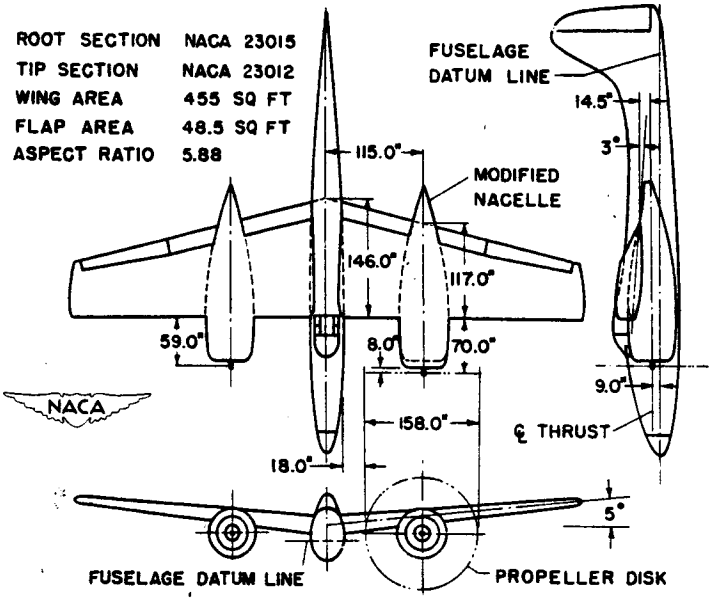


Figure 1.- Airplane used for the propeller tests.

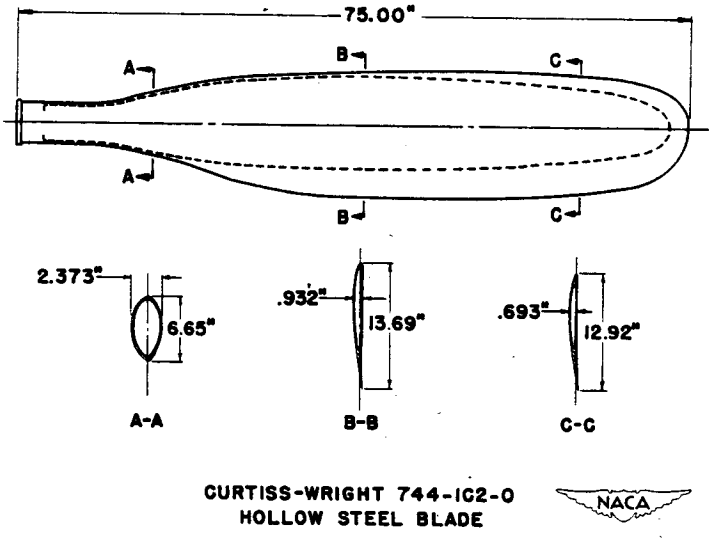


Figure 2.- Blade of the test propeller.

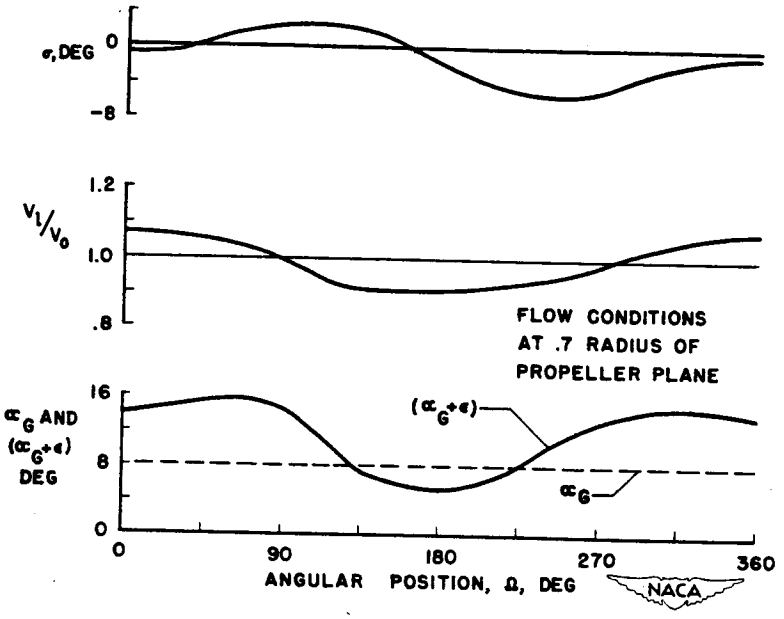


Figure 3.- Typical measured characteristics of the flow field.

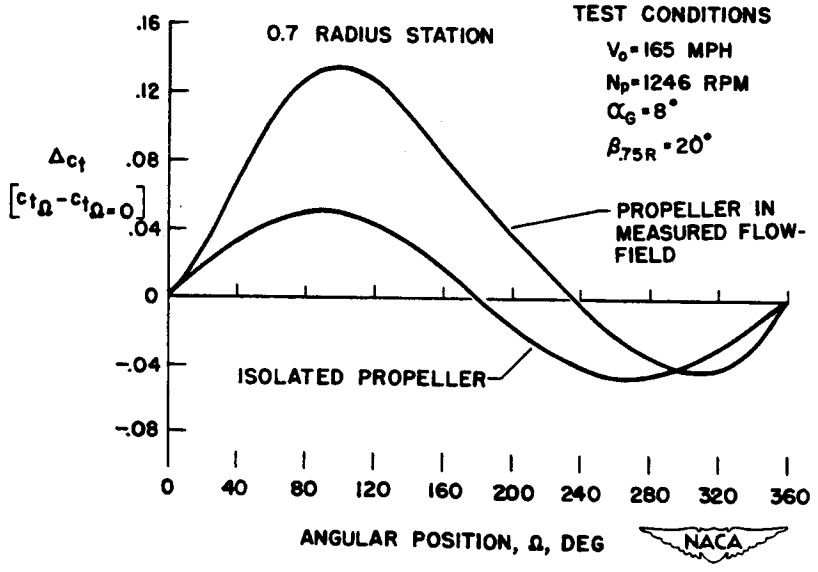


Figure 4.- Effect of the flow-field characteristics on the air-load variation.

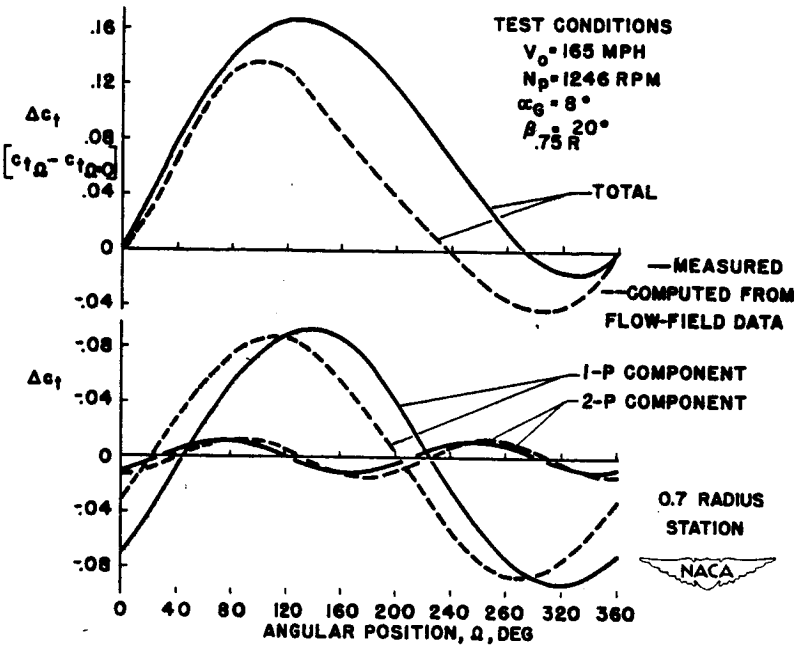


Figure 5.- Comparison of the measured and computed air-load variations.

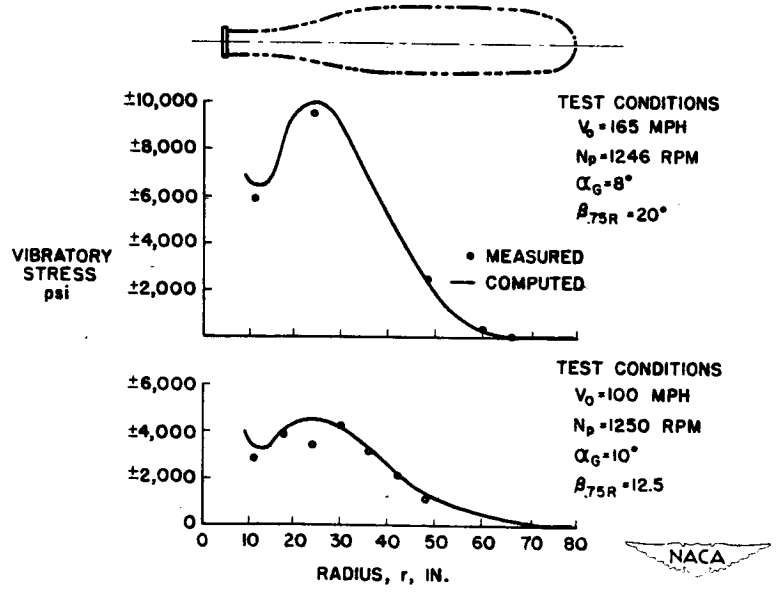


Figure 6.- Comparison of the computed and measured stress distributions.

Preceding page blank

N65-86487

THE PROPELLER FLUTTER PROBLEM FOR HIGH-SPEED AIRPLANES

By John E. Baker and Arthur A. Regier

Langley Aeronautical Laboratory

INTRODUCTION

The status of propeller flutter is becoming more important with the existance of high-speed propeller-driven aircraft. In the past, propellers have been made excessively strong to keep the blades from fluttering without paying an appreciable aerodynamic penalty. Papers that have been presented earlier in this conference have shown large increases in efficiency by making the airfoil sections of propellers operating in the transonic speed range as thin as possible. One of the limitations of this change in design would be the possibility of flutter. The NACA has undertaken a test program to determine the critical variables and to attempt to devise a solution for predicting the minimum flutter speed for propellers. Since the program is still in its early stages, the present paper must therefore be limited to a discussion of the problem and the presentation of test results to date.

SYMBOLS

$V_{0.8R}$	velocity at flutter at 0.8 radius
V_{SF}	minimum stall flutter velocity at 0.8 radius
b	semichord of airfoil section at 0.8 radius
ω_α	uncoupled angular torsional frequency of the blade
$\beta_{0.8R}$	blade angle setting at 0.8 radius
σ_B	blade solidity at 0.8 radius
t	thickness to chord ratio at 0.8 radius
G	shear modulus
ρ	mass density of blade material

RESULTS AND DISCUSSION

Figure 1 shows the apparatus used for the present test program. (See reference 1.) The propeller assembly is mounted in a steel tank in which the pressure can be varied. The propeller models are whirled by means of the motor shown and operate at zero forward velocity except for the induced flow. Flutter is recorded with the aid of strain gages on the blades by a recording oscillograph.

Figure 2 demonstrates the propeller flutter problem (reference 1). The nondimensional flutter coefficients are plotted as a function of the blade-angle setting at 0.8 radius. The curves represent the lowest speeds at which flutter was encountered on a Clark Y section propeller for the various blade-angle settings at pressures of 0.32, 0.47, 0.69, and 1.0 atmospheres. The open parts of the curves indicate no flutter up to the top speed of the tests. The flow is potential at low blade-angle settings, and flutter obtained under these conditions is believed to be similar to the classical flutter of wings. A method of calculating the classical flutter speed of propellers has been derived in reference 2 based on the assumption that two-dimensional oscillating air forces are applicable to propellers.

At large positive and negative pitch settings, the flutter speeds are much lower than the classical flutter speeds. This flutter is associated with stall and is commonly called stall flutter. Its character is different from the classical case in that the flutter is almost entirely torsional. It is similar to the stall flutter of wings as reported in reference 3. The stall flutter speeds obtained from reference 3 were successfully calculated in reference 4 by use of experimentally determined oscillating air forces of stalled airfoils. More recently, the classical flutter theory was modified in reference 5 by shifting the phase angle of the potential oscillating air forces by an angle which is a function of the nonlinearity of the steady-state lift curve. It is not known how much of this technique can be applied to propellers.

The Langley 8-foot high-speed and the Langley 16-foot high-speed tunnels have observed flutter during some of their propeller tests, and, when it occurred, it was generally experienced near the peak of the thrust-coefficient curve. This condition corresponds to the lowest points on these curves. These data indicate that the propeller flutter problem is not a classical but a stall flutter problem. Therefore, the object of the present experiments is to determine a method for predicting the minimum stall flutter speeds for propellers.

Experiments reported in reference 6 showed that, at the peak of the flutter-speed curves, the aerodynamic center of pressure coincides with the blade-section center of gravity. Since the center of pressure is dependent on lift and moment coefficients, propeller blades can be designed to have the maximum flutter speed occur at any lift coefficient within the unstalled range. The tests of reference 7 proved this to be the case. These tests also indicated that stall flutter is predominate at subsonic speeds, and that, at supercritical speeds, stall flutter is difficult to obtain.

Figure 3 shows some of the results of the current propeller flutter test program. Flutter-speed curves for tests made at atmospheric pressure are shown for three models having the following airfoil sections: NACA 16-006 made of wood, NACA 16-003 made of steel, and NACA 16-003 made of duralumin. These models are identical in plan form and are untwisted and untapered. The natural torsional frequency for the two NACA 16-003 models is the same, but the wooden model has a 10-percent lower torsional frequency. Since the semichord is the same and the torsional frequencies are nearly the same, these curves represent the relative flutter speeds of the three models. The torsional stiffness for the steel model is about ten times that for the wooden model, so, for the classical flutter case, the dynamic pressure at flutter should vary approximately with torsional stiffness, and the flutter speeds should be approximately proportional to the square root of the torsional stiffness. The curves at low blade-angle settings show this to be the case. However, the flutter-speed curves tend to converge at stall at a constant value of $V_{0.8R}/b\omega_\alpha$ of 1.0. Therefore, torsional stiffness appears to have no significance in connection with stall flutter.

In order to check the generality of these tests, data obtained by the U. S. Air Forces at Wright Field during some propeller whirl tests (reference 8) are shown by the x symbols. These propellers were twisted and had chord and torsional frequencies about twice those of the models of the current NACA tests. The flutter speeds were about four times and the Reynolds numbers were 8 times those obtained in the present tests. In spite of these added variables, the flutter coefficients are very close to the minimum values encountered during the present tests.

It is interesting to note the position of the reduced frequency of the Kármán street vortices in relation to the experimental flutter data. At stall the Kármán wake frequency approaches the experimental data which indicate that a condition of resonance may be induced. Further indication of the possibility of resonance is the fact that some propellers set at large blade angles could operate above the stall flutter speed without flutter. Results similar to these have been observed in experiments on wings oscillating in torsion. (See reference 9.)

[redacted]

If the minimum stall flutter speed for propellers occurs at a fixed value of $V_{0.8R}/b\omega_\alpha$, the flutter speed will be directly proportional to $b\omega_\alpha$, the product of the semichord and torsional frequency. If the propeller blade is treated as a thin elliptic cylinder, this relationship for the minimum stall flutter speed can be written as $V_{SF} \approx C\sigma_B\omega_\alpha\sqrt{\frac{G}{\rho}}$ where C is a constant depending on blade taper and the type of blade construction.

Further inspection of the equation shows that the product $\sigma_B t$ offers a means of changing the minimum stall flutter speed. For example, reducing the thickness ratio of an airfoil by a factor of two will also halve the stall flutter speed. However, if the chord is doubled at the same time, the flutter speed will be restored to its original value. The constant C can also be used as a means of varying the minimum stall flutter speed. For example, increasing taper or using hollow blade sections raises the value of C which, in turn, raises the minimum stall flutter speed.

It must be kept in mind that the present test program is still in its early stages and that future research may change the present conceptions somewhat. Mach number, especially at supercritical speeds, is expected to be very important. The effect of changes in the section center of gravity and Reynolds number will also be studied.

[redacted]

REFERENCES

1. Baker, John E., and Paulnock, Russell S.: Experimental Investigation of Flutter of a Propeller with Clark Y Section Operating at Zero Forward Velocity at Positive and Negative Blade-Angle Settings. NACA TN 1966, 1949.

2. Turner, M. J., and Duke, James B.: Propeller Flutter. Jour. Aero. Sci., vol. 16, no. 6, June 1949, pp. 323-336.

3. Studer, Hans-Luzi: Experimentelle Untersuchungen über Flügelschwingungen. Mitt. no. 4, Inst. für Aerod. Tech. H. S. Zürich, Gebr. Leemann & Co. (Zürich), 1936.

4. Victory, Mary: Flutter at High Incidence. R. & M. no. 2048, 1943.

5. Mendelson, Alexander: Effect of Aerodynamic Hysteresis on Critical Flutter Speed at Stall. NACA RM E8B04, 1948.

6. Theodorsen, Theodore, and Regier, Arthur A.: Effect of the Lift Coefficient on Propeller Flutter. NACA ACR L5F30, 1945.

7. Regier, Arthur A., Barmby, John G., and Hubbard, Harvey H.: Effect of Critical Mach Number and Flutter on Maximum Power Loading of Ducted Fans. NACA TN 1330, 1947.

8. Shaw, Alex E.: Whirl Test of Hartman Design Propeller Blades for Use in Aerodynamic Testing in Wind Tunnel at Langley Field, Virginia. ACTR No. 5007, Materiel Command, Army Air Forces, Sept. 2, 1943.

9. Chuan, Raymond L., and Magnus, Richard J.: A Study of Vortex Shedding As Related to the Self-Excited Torsional Oscillations of an Airfoil. GALCIT, May 1948.

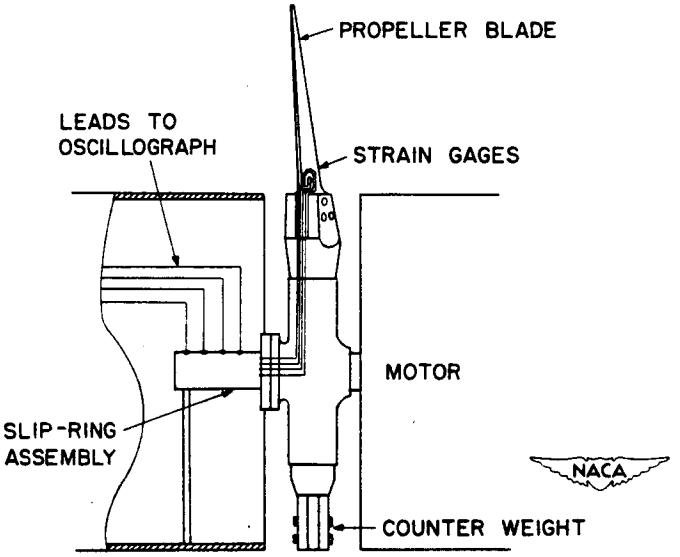


Figure 1.- Apparatus used for the propeller flutter investigation.

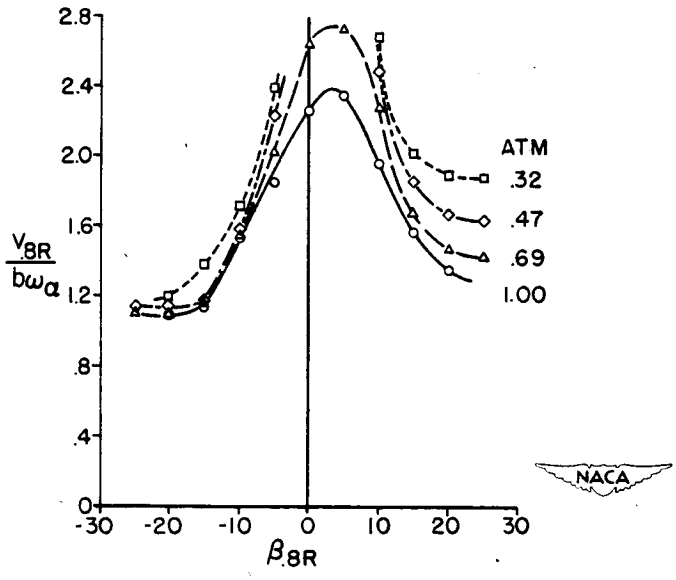


Figure 2.- Flutter-speed variations on a Clark Y section propeller with blade-angle settings.

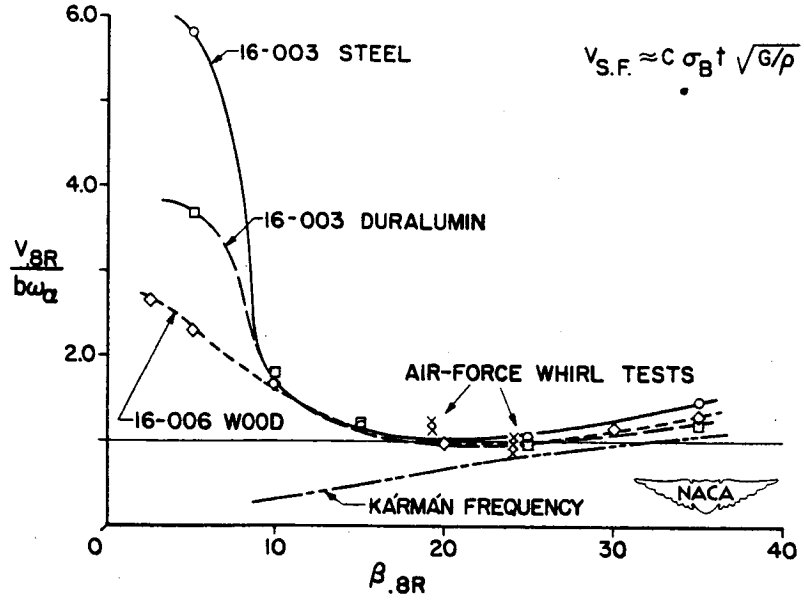


Figure 3.- Flutter-speed variations with blade-angle settings for propeller flutter models used in the current test program.

Preceding page blank

N65-86488

TRENDS IN THE DESIGN AND PERFORMANCE OF HIGH-SPEED PROPELLERS

By Eugene C. Draley, Blake W. Corson, Jr., and John L. Crigler

Langley Aeronautical Laboratory

INTRODUCTION

Recent propeller research conducted by the National Advisory Committee for Aeronautics has been of sufficient scope to indicate clearly the most promising trends to be followed for the development of efficient propellers for operation at transonic speeds. The papers in the section, Propellers for Aircraft, have presented a few of the more significant results of investigations dealing with blade-section thickness, advance ratio, sweep, dual rotation, vibration, and flutter. The purpose of this paper is to consolidate the conclusions indicated by this work to give direction to the development of high-speed propellers and to consider the physical characteristics and performance of the resulting type of propeller.

SYMBOLS

a	speed of sound in air, feet per second
b	blade chord, feet
D	diameter, feet
h	blade-section maximum thickness, feet
L/D	lift-drag ratio
M	Mach number
n	rotational speed, revolutions per second
R	radius to propeller tip
r	radius to blade section
T	thrust, pounds

β blade angle, degrees

η propeller efficiency

BLADE-SECTION THICKNESS RATIO

The factor shown to have the strongest effect in reducing compressibility losses on propellers is the use of thin blade sections. Figure 1 provides a summary of the information concerning the effects of blade thickness ratio on propeller performance. In the lower part of this figure is shown the variation of the maximum value of section lift-drag ratio with section Mach number for three 16-series airfoil sections having thickness ratios of 8, 5, and 3 percent. In the lower speed range, represented by the solid parts of the lines, the data were obtained from the integration of propeller blade-section pressure distributions measured in the Langley 16-foot high-speed tunnel. For the higher speeds, indicated by the dash lines, the values were calculated by use of two-dimensional supersonic airfoil theory. The results clearly indicate the large improvements in lift-drag ratios at transonic and supersonic speeds associated with reductions in thickness ratio. While the differences in lift-drag ratio at supersonic speeds do not appear to be large, the percentage differences are very large, being of the same order of magnitude as shown at the lower speeds. In the upper part of the figure is plotted some of the experimental results obtained from the Langley 8-foot high-speed tunnel tests (as presented by Richard T. Whitcomb, James B. Delano, and Melvin M. Carmel) showing the variation of maximum efficiency with forward Mach number. For a blade angle of 60° at the 0.75 radius and advance ratio of approximately 3.8, results are presented for three propellers. Two of the propellers differed only in thickness ratio. The thicker propeller was 8 percent thick and the thinner, 3 percent at the design station, $\frac{r}{R} = 0.7$ (NACA 4-(0)(03)-045 and NACA 4-(0)(08)-045 propellers). This figure indicates the improvement in propeller performance corresponding to the increase in lift-drag ratio indicated in the lower part of the figure as obtainable by the use of thinner sections. Not only has a large delay in the onset of compressibility effects been obtained, but the magnitude of the adverse effects are considerably diminished by the use of the thinner blade sections. As a result, the 3-percent-thick propeller is 15 percent more efficient than the 8-percent-thick propeller at a forward Mach number of 0.9. Thus, with blade-section thickness ratios of the order of 3 percent, propeller efficiencies of 70 percent or more can be obtained at forward Mach numbers near 0.9.

For purposes of comparison, there is also included in the upper figure a curve representing the experimental results for the

6-percent-thick swept propeller tested in the Langley 8-foot high-speed tunnel. The efficiency for this propeller, swept 45°, falls only slightly above values which would be expected of an unswept 6-percent-thick propeller. When it is considered that the practical stress and hub problems for a swept propeller are actually more severe than those for a 3-percent-thick straight propeller, it is concluded that the use of sweep in propellers is less effective than the use of very thin blade sections for maintaining good efficiency at transonic speeds and therefore does not warrant consideration in the design of high-speed propellers.

ADVANCE RATIO

The values of blade-section lift-drag ratio presented in the lower part of figure 1 have been used in calculating the performance of a family of propellers in which the diameter has been varied so that each of these propellers would absorb 5200 horsepower at a forward Mach number of 0.90 and at an altitude of 40,000 feet. The results are presented in figure 2. For these calculations, it is assumed that the propeller blade sections operate at maximum values of lift-drag ratio and that an ideal type of blade loading is obtained under all operating conditions. Such calculations, however, have been shown to be reliable by the comparison made in a previous paper by Whitcomb, Delano, and Carmel, between calculated and experimental results. In the lower left-hand corner the assumed variation in the thickness ratio of the blade sections is indicated. Calculations have been made for values of the advance ratio of 2, 4, and 6. Attention is called to the fact that these calculated results differ from both the calculated and the experimental results for the 3-percent-thick propeller presented in the paper by Whitcomb, Delano, and Carmel, in that each of these propellers has been designed to operate at a fixed value of power, and the disk loading is considerably higher than for the cases considered by Whitcomb, Delano, and Carmel. Hence, the level of the low-speed efficiencies is lower because of greater induced losses. In addition, the inboard sections for these propellers are somewhat thinner than those previously discussed and, consequently, the adverse effects of compressibility are less.

At low speeds the calculated values of efficiency range from 83 to 87 percent. Note that the inversion point, the value of Mach number above which best efficiency is obtained with the low-advance-ratio propeller, occurs at a much higher value of Mach number than was obtained with the thicker propeller considered in the paper by Whitcomb, Delano, and Carmel. For these thin propellers, the point of intersection for the three values of advance ratio considered occurs at a forward Mach number of 0.925, and only at higher speeds does there appear to be

an efficiency advantage obtainable by the use of low advance ratio. Of interest also is the fact that at speeds above forward Mach numbers of about 0.9 and below 0.6, the efficiency of the low-advance-ratio propeller is equal to or better than the efficiencies for the other advance ratios; however, in the speed range between these two Mach numbers, the propeller having an advance ratio of 4 has as much as 5 percent greater efficiency. If for a design speed of about 0.9 or greater the cruising speed were selected to fall in the intermediate range where best efficiency is obtained at other advance ratios, some sacrifice in cruising performance would result. With the relatively high levels of propeller efficiency indicated, it might be expected that the selection of the cruising speed would be determined by the characteristics of the airplane rather than by those of the propeller, particularly if the airplane drag force-break Mach number should lie in the cruising speed range. In that case, the selection of a cruising speed above the Mach number for drag force break would be impractical because relatively low values of airplane lift-drag ratio would be encountered.

While only small efficiency advantages accrue from the use of a thin low-advance-ratio propeller in the Mach number range around 0.9, consideration of propeller diameter is an important factor which would further tend to favor the use of low advance ratio. As shown in the sketches, for the design conditions assumed, a relatively small propeller (diameter of 12 ft) is required for an advance ratio of 2.0; whereas an unusually large propeller (diameter of 26 ft) would be required for an advance ratio of 6.0. The differences in the propeller diameter required are associated with the fact that at a given forward speed, as the advance-diameter ratio is reduced, the rotational speed is proportionately increased so that higher resultant velocities at the blade sections are produced. With increased section dynamic pressure a greater absolute load can be carried by each section or, conversely, a given required total load can be carried by a propeller of smaller diameter. For a forward Mach number of 0.9 all the blade sections of the low-advance-ratio propeller operate at supersonic speeds. The saving in weight occurring because of the smaller diameter of the low-advance-ratio propeller would probably offset any small gains in efficiency associated with the use of the higher-advance-ratio propellers. The low-advance-ratio propeller therefore is recommended principally by its relatively small size.

DESIGN FEATURES OF SUPERSONIC-TYPE PROPELLER

Advance ratio and thickness ratio.- The material thus far presented indicates two important features of a propeller designed for operation

at supercritical speed, namely thin blades and operation at a low value of advance ratio. A tabulation of these and other physical characteristics regarded as desirable for such a propeller is presented in chart I.

Blade width.- With regard to blade width the design trend for the supersonic-type propeller requiring a specified solidity would be toward the use of a few relatively wide blades rather than many blades of narrow width. Recent investigations made by John E. Baker and Arthur A. Regier, indicate that increasing blade width alleviates the flutter problem. The increased stiffness of a relatively wide blade tends to reduce vibratory stresses. For solid metal blades there is no first-order effect upon centrifugal stress of changes in blade width. Increased centrifugal force resulting from an increase in blade width is accompanied by a proportionate increase in blade cross-sectional area carrying the force. For hollow metal blades the same is true in general, but because the forces and stresses are determined by skin thickness as well as by blade width the designer may have better control over the centrifugal stresses in a relatively wide blade than in one of narrow chord.

Two aerodynamic effects influenced by blade width are tip relief and induced loss. Increasing the relative width of a blade in effect reduces its aspect ratio. Investigations at high subsonic speeds of wings differing only in aspect ratio (reference 1) indicate that the adverse effects of compressibility are less pronounced for wings of low aspect ratio than for those of high aspect ratio. Tests of propellers having the same number of blades but differing in solidity (reference 2) have also indicated the beneficial effect of using wide blades when the blade tip sections operate at supercritical speed. Hence, the results of both wing and propeller investigations indicate that some aerodynamic benefit will be realized from the use of a few relatively wide blades rather than a greater number of narrow blades of equal total solidity. Propeller theory indicates that this trend will result in a slightly greater induced loss, but this effect is of second order when the propeller has at least four blades (reference 3).

Practical considerations involved in choosing the blade width are fabrication, weight, and the blade-spinner juncture. The adaptability of relatively wide blades in combination with extremely thin sections further increases the attractiveness of the high-solidity blade. This trend, however, may involve a weight penalty, because for a fixed value of thickness ratio, diameter, and total propeller solidity, blade weight increases directly with blade width. Compensating the increased blade weight, however, is reduction of hub complexity and weight resulting from the use of fewer blades. A definite disadvantage associated with wide blades is the increased difficulty of providing a

juncture between the blade root and spinner which is both aerodynamically clean and mechanically feasible.

Plan form.- Consideration of only the structural aspects of plan form leads to the use of a large amount of taper. By decreasing the mass of the blade tip region and increasing the blade cross-sectional area near the root the maximum centrifugal stress is greatly reduced. The tapered plan form also results in a blade with root sections having relatively large moments of inertia and the blade is therefore less susceptible to vibration and flutter.

Spinner.- Although spinner size is frequently controlled by the design of the aircraft rather than of the propeller, a relatively large spinner is believed to be desirable for use with the propeller type here proposed. A large spinner minimizes the mutual interference of adjacent blade roots and more easily accomodates the mechanism associated with an aerodynamically clean blade-spinner juncture. By reducing the blade length a large spinner of necessity reduces the blade root stresses, but in so doing aggravates hub and spinner stresses. Moreover, all problems encountered in hub and spinner design, fabrication, balance, icing, and maintenance become more severe with increased size.

Blade loading.- A comprehensive discussion of the aerodynamics of a supersonic-type propeller is beyond the scope of this paper. While a radial distribution of load on the blade which results in minimum induced energy loss is believed to be as desirable for this type of propeller as for the subsonic type, this factor is regarded as of secondary importance in comparison with the effects of section lift-drag ratio and blade stresses. Experience with subsonic propellers has shown that operation over a wide range of advance ratio and blade angle, in which distribution of blade load underwent drastic changes, resulted in negligible effect on propeller efficiency. Associated with blade loading, however, is the estimation of stream angle with reference to the blade sections which is an important factor in obtaining best values of section lift-drag ratio. Adequate theory exists for the design of subsonic and completely supersonic propellers. For the transonic speed range, theory is incomplete.

Blade section.- When blade sections are made extremely thin the basic shape of the sections becomes of secondary importance. Recent work has indicated that thin subsonic sections with rounded leading edges perform as well at transonic and low-supersonic speeds as do double-wedge and biconvex sections and are naturally superior at subcritical speeds. Because the operation of a high-solidity propeller is similar to that of a cascade in that considerable curvature of the flow takes place in the propeller disk, more camber may be required for

a propeller section than for an airfoil section exerting the same lift. The mutual effects of blade-section camber and propeller solidity requires investigation at transonic speeds.

BLADE-FORM CURVES

Figure 3 presents an illustrative sketch and blade-form characteristics of the proposed supersonic-type propeller. The design value of advance ratio, thickness ratio, solidity, and taper conform to the recommendations listed in chart I. The values shown are those assumed in calculating the performance of the 12-foot-diameter single-rotation propeller discussed in figure 2. The rectangular appearance of the blades in the front view is merely the projected view; the blades are actually tapered. Note that in this propeller the portion of the blade extending out of the spinner is only 4 feet long. The calculated maximum centrifugal stress for the propeller is approximately 16,500 pounds per square inch at 2200 rpm for solid duralumin blades.

DUAL ROTATION

Consideration of single-rotation-propeller theory has indicated that best efficiency at flight Mach numbers near 0.9 and above can be obtained by operation at an advance ratio of approximately 2.0.

Two factors which influence the operation of the dual-rotation propeller make it inherently well adapted to operation at high values of advance ratio. These factors are recovery of most of the induced rotational loss and the shift toward the inboard radii of the blade load. At high values of advance ratio, most of the induced loss for a single-rotation propeller appears as rotation of the slipstream; in a dual propeller a large part of the slipstream rotational energy is recovered; hence at subcritical speeds the dual propeller can operate efficiently at high values of advance ratio at which the single propeller would be hopelessly inefficient. At a given forward speed, high advance ratio is synonymous with low rotational speed and low section speed; hence the dual-rotation propeller can maintain subcritical section operation at high forward speeds by operation at high advance ratio. An attempt to follow this process with a single-rotation propeller results in large rotational loss and unacceptably low efficiency.

In comparison with a single-rotation propeller the blades of a dual-rotation propeller inherently carry a greater portion of their load on the inboard stations and less outboard near the blade tips

(reference 4). This fact is equivalent to saying that the blade-tip region of the dual-rotation propeller operates at lower values of lift coefficient or has relatively less solidity than a comparable single-rotation propeller. Consequently, the adverse effects of compressibility, which in subcritical operation become manifest first near the blade tip sections, are less severe for the dual-rotation than for the single-rotation propeller and, therefore, permit the dual-rotation propeller to maintain subcritical operation at higher forward speed than can the single-rotation propeller.

Experimental results showing the variation of efficiency with flight Mach number at values of Mach number up to 0.925, for a two-blade single-rotation propeller and an eight-blade dual-rotation propeller (given in papers by Richard T. Whitcomb, James B. Delano, and Melvin M. Carmel and Robert J. Platt, Jr., and Jean Gilman), are presented in figure 4. Although the data for each propeller were taken at an approximately constant value of advance ratio, 3.8 for the single rotation and 7.0 for the dual rotation, the values in each case are close to those for envelope efficiency in the critical range. While the disk power loading for the dual-rotation propeller was much higher than that of the single-rotation propeller, the efficiency of the dual-rotation propeller was equal to that of the single-rotation propeller up to a forward Mach number of 0.85, indicating that the dual-rotation propeller was operating effectively in recovering the slipstream rotational energy. The design values of thickness ratio for these propellers were 0.03 for the single and 0.05 for the dual. It is safe to assume that the comparison would have been more favorable for the dual-rotation propeller, if the design thickness ratio had been the same for both. From this comparison based on efficiency alone it is concluded that dual-rotation propellers should be given due consideration for application at flight Mach numbers up to 0.85.

An important point brought out in this comparison (fig. 4) is that at forward Mach numbers above 0.85 the single-rotation propeller operating at a relatively low value of advance ratio and with high rotational speed is superior to the dual-rotation propeller operating at high advance ratio. At a forward Mach number of 0.9, the most effective sections of the single-rotation propeller have passed through their critical speed range into supersonic operation and the propeller efficiency has begun to level off at a relatively high value, about 0.73. At the same value of flight Mach number, the sections of the dual-rotation propeller, because of the high value of advance ratio, are still operating in the midrange of critical speed, and further increase in Mach number can result only in a continued decrease in efficiency.

At this point the question arises as to the desirability of designing a dual-rotation propeller for operation at a relatively low value of advance ratio. This design change is aerodynamically feasible.

Presumably the efficiency of the dual-rotation propeller at supercritical speeds could be made to level off at as high a value as attained by the single propeller, but in so doing the advantages of the high-advance-ratio dual-rotation propeller would be sacrificed. Further, because operation at low advance ratio is accompanied by an increase in rotational speed, the mechanical design problems for the dual-rotation propeller would be much more severe than for the single-rotation propeller.

THRUST CHARACTERISTICS

In order to provide a more realistic indication of the performance of both a typical low-advance-ratio single-rotation propeller and a high-advance-ratio dual-rotation propeller of the types already indicated to give good performance, figure 5 has been prepared in which calculations of the thrust and efficiency characteristics for a wide forward speed range are presented. The calculations have been made to represent the thrust produced by the two propellers of different type when absorbing 7500 horsepower at sea level, and for powers varying from 4150 horsepower at 400 miles per hour to 5200 horsepower at 600 miles per hour at an altitude of 40,000 feet. These powers have been selected as typical shaft powers obtained for gas-turbine power plants. It has been assumed that the design point of the two propellers was 5200 horsepower at the 600 miles per hour at 40,000 feet altitude, which corresponds to a forward Mach number of 0.9. The calculations of efficiency and thrust have been determined by estimating the variations in advance ratio and other propeller-operating conditions occurring when changes in forward speed and power were made. Thus, the thrust curves represent typical thrust-available characteristics for a turbopropeller combination.

It should be emphasized that the thrust levels in the high-speed altitude conditions are of the order of 2500 pounds of thrust in both cases. Such thrust values are thus representative of very large jet engines. Of particular interst is the fact that these values can be obtained with a 12-foot-diameter propeller. Note that both the efficiency and the thrust of a dual-rotation propeller are somewhat greater than for the single-rotation propeller in the speed range of from 400 to 550 miles per hour, owing to the smaller induced losses of the larger diameter dual propeller. At the maximum-speed case, however, there is a reversal of this trend because of the somewhat greater thickness ratios used in the dual calculations and because of the advantage of low advance ratio in this speed range. These calculations are based on the same type of approach that was used in the papers by Whitcomb, Delano, and Carmel and Platt and Gilman. It was assumed that best lift-drag ratios were obtained all along the blade and that the ideal type of loading was obtained.

For the sea-level case, the relative thrust characteristics of the two propellers are diametrically opposed to what would at first be expected. The dual-rotation propeller produces considerably less thrust than the single-rotation propeller, in spite of its larger diameter. This relatively lower thrust in the lower-speed range, below approximately 250 miles per hour, occurs because the blades of the dual-rotation propeller absorbing high power at low rotational speed become stalled. For high advance-diameter ratios, the resultant velocities all along the blade radius for a propeller are largely made up from the forward-speed component, and thus when the forward speed is greatly reduced the resultant velocities become so low that the blade sections exceed their maximum lift in absorbing the specified power. An indication of the relative section speeds for the two propellers is shown by the values of the rotational tip Mach number given in the upper right-hand part of the figure. The single-rotation propeller has a rotational tip Mach number of 1.195 as compared to 0.412 for the dual-rotation propeller. The corresponding values of rotational speed are 2200 rpm and 650 rpm, respectively. If the design speed for the dual-rotation propeller were somewhat reduced, the blade stalling problem would be correspondingly reduced and it appears that in certain specific applications the problem of blade stall might be avoided. This result illustrates that a design compromise problem can be expected in the case of the dual-rotation propeller. It also illustrates the usefulness of a two-speed gear to permit increases in the rotational speed at the low forward speeds. In such a case, both the thrust and the efficiency characteristics of the dual-rotation propeller would be greatly improved and would exceed the values shown for the single-rotation propeller by a considerable margin.

RANGE

The propulsive efficiency levels shown for propellers are considerably in excess of the corresponding efficiency values for jet engines, even at the maximum speeds shown in figure 5. On the other hand, it is known that the turbopropeller-engine combinations would be considerably heavier than turbojet engines, and thus it becomes of interest to establish the relative performance of an aircraft when the advantages in efficiency and disadvantages in weight of turbopropeller engines as compared to turbojet engines are considered. Figure 6 has been prepared to illustrate these effects. In this figure, the range characteristics of a given airplane have been calculated for two cases. The airplane assumed had a gross weight of 200,000 pounds, a wing loading of 70 pounds per square foot, and the power-plant weight plus the fuel weight was taken as 52 percent of the gross weight. The calculations were based on cruise at constant speed at 40,000 feet altitude.

The first case involves the use of a turbopropeller installation in which typical fuel-consumption figures for gas-turbine engines have been used (approx. 0.45 lb/shaft hp-hr). The propeller performance figures used are the same as those previously presented for the 12-foot-diameter single-rotation propeller having an advance-diameter ratio of 2. It should be noted that the calculations are presented to include a range of power-plant weights, because an analysis of typical airplanes using such power plants has indicated that a relatively wide range of weights might occur in specific cases. Moreover, the use of a dual-rotation propeller instead of a low-advance-diameter-ratio single-rotation propeller would increase the power-plant weight. The band shown is considered to represent the typical ranges through which the power-plant weights might vary.

The second case has been calculated for the same airplane and the same conditions of flight for the airplane, but with the use of turbojet engines. These characteristics have been based upon the use of typical efficiency and specific fuel-consumption figures (approx. 1.3 lb/thp-hr) for jet engines and, as a matter of fact, when compared on the same basis the specific fuel consumptions for the two engines are almost the same. The resulting comparison, therefore, between the airplane with the turbopropeller combination and the airplane with the turbojet engine results primarily from the differences in propulsive efficiency and the weight differences between the installations. The drag and lift-drag ratios for the two cases were almost the same, the lower drag and higher lift-drag ratios were used with the jet-engine installation. It should be noted that these calculations are made for a specific airplane, and while the comparisons shown are considered to be typical, there would be expected in some individual cases rather marked deviations from the absolute values and shapes of individual curves shown, depending upon the specific parameters involved in any case.

The example taken clearly indicates that despite the greater weights assumed for the turbopropeller engines, greater range characteristics were obtained with that type of engine than for the turbojet engines even for the highest speeds at which these calculations were made. It is interesting to note that at a Mach number of 0.9 the gain in efficiency associated with going from turbojets to propellers is sufficiently great so that the turbopropeller system would still show a gain in range in the case where the power plants were more than twice as heavy for the turbopropeller as for the turbojet. (Compare the power-plant gross-weight ratio of 0.12 for the turbojet with the curve for power-plant weight to gross-weight ratio of 0.25 for the turbopropeller.) Thus, it appears that through the use of the types of propellers herein discussed, having very thin sections and utilizing in general small-diameter, low-advance-diameter-ratio propellers that the

gain in propulsive efficiencies associated with these propellers as compared to jet-engine efficiencies can be sufficiently great to offer increases in the range of an airplane of specified gross weight and wing loading despite the greater weights inherent in the turbo-propeller engines.

CONCLUDING REMARKS

In summary, it appears that through the use of a low-advance-diameter-ratio supersonic type of propeller having relatively small diameter and having very thin sections, propeller efficiencies of the order of 75 percent or greater are possible at high subsonic Mach numbers. Dual-rotation propellers operating at high advance-diameter ratios also appear to give efficiencies comparable to the single-rotation propeller of the type just mentioned up to speeds just below Mach numbers of 0.9. The difference in the propulsive efficiency of these types of propellers as compared to typical efficiencies for jet engines are indicated to lead to an improvement in the range characteristics of a long-range airplane despite the greater weights associated with the turbopropeller combinations. Thus, the use of a propeller should be given consideration in the design of long-range aircraft for forward Mach numbers up to 0.9.

REFERENCES

1. Stack, John, and Lindsey, W. F.: Characteristics of Low-Aspect-Ratio Wings at Supercritical Mach Numbers. NACA Rep. 922, 1949.

2. Delano, James B.: The Effect of High Solidity on Propeller Characteristics at High Forward Speeds from Wind-Tunnel Tests of the NACA 4-(3)(06.3)-06 and NACA 4-(3)(06.4)-09 Two-Blade Propellers. NACA RM L6L19, 1946.

3. Crigler, John L., and Talkin, Herbert W.: Charts for Determining Propeller Efficiency. ACR L4I29, 1944.

4. Crigler, John L.: Application of Theodorsen's Theory to Propeller Design. NACA RM L8F30, 1948.

CHART-I
DESIRABLE CHARACTERISTICS – SUPERSONIC-TYPE PROPELLER

A. DESIGN $\frac{V}{nD} \approx 2.0$

B. THINNEST PRACTICAL BLADE SECTION

C. WIDE BLADE
- REDUCES VIBRATION AND FLUTTER PROBLEM
- CENTRIFUGAL STRESS PROBLEM NOT AGGRAVATED
- GREATER EFFECT OF TIP RELIEF
- NEGLIGIBLE INCREASE IN INDUCED LOSS
- POSSIBLE ADVANTAGES IN FABRICATION
- POSSIBLE WEIGHT PENALTY
- GREATER BLADE-SPINNER JUNCTURE PROBLEM

D. TAPERED-BLADE PLAN FORM
- REDUCES CENTRIFUGAL STRESS PROBLEM
- REDUCES VIBRATION AND FLUTTER PROBLEM

E. LARGE SPINNER DIAMETER
- REDUCES BLADE-ROOT INTERFERENCE
- REDUCES BLADE STRESS PROBLEMS
- REDUCED BLADE-SPINNER JUNCTURE PROBLEM
- HUB AND SPINNER PROBLEMS INCREASED

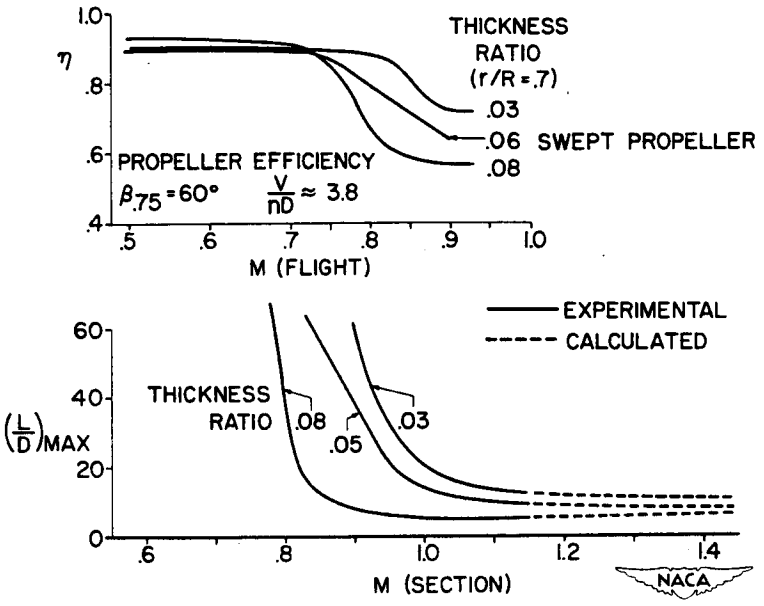


Figure 1.– Effect of Mach number and thickness ratio on blade–section characteristics and propeller efficiency.

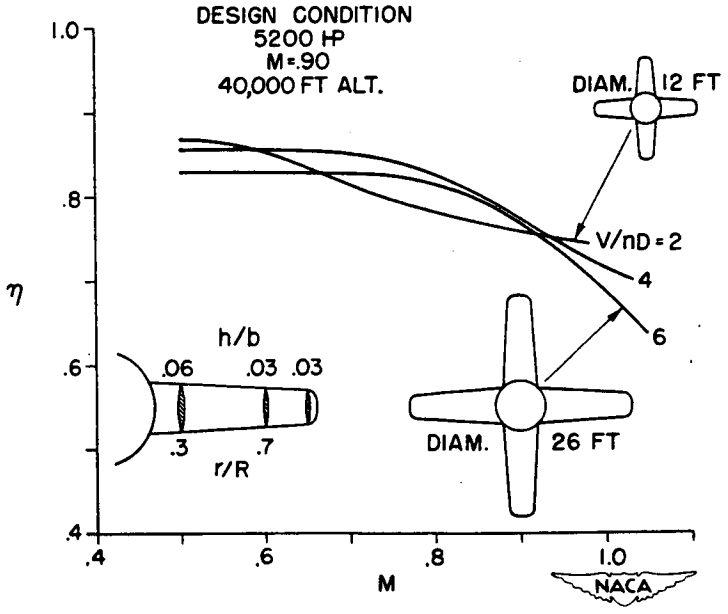


Figure 2.– Calculated effect of Mach number and adverse ratio on propeller size and efficiency.

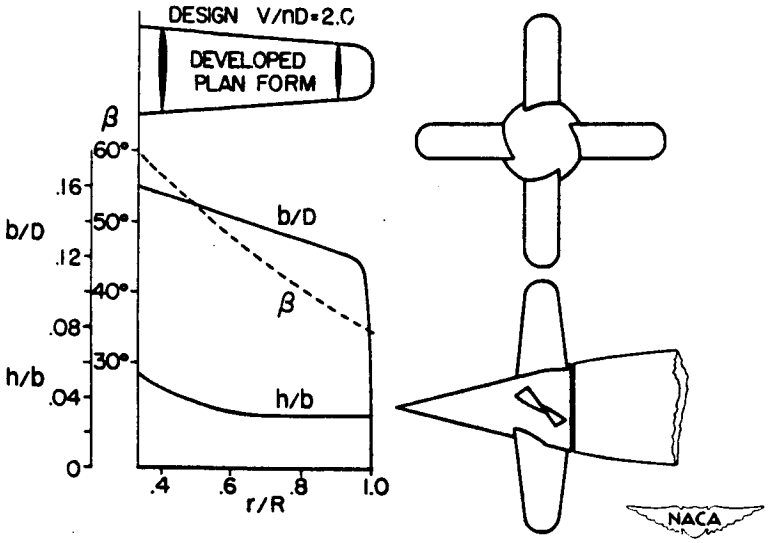


Figure 3.- Physical characteristics of supersonic-type propeller.

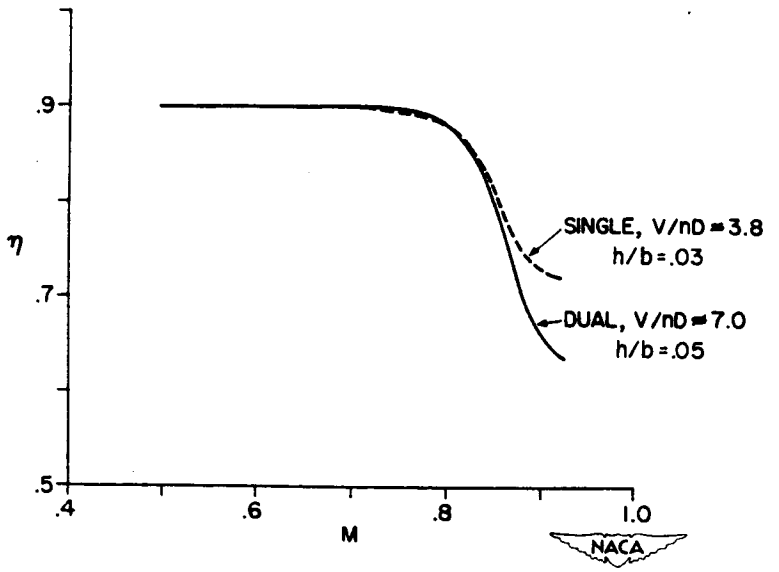


Figure 4.- Comparison of experimental efficiencies for a single-rotation and a dual-rotation propeller.

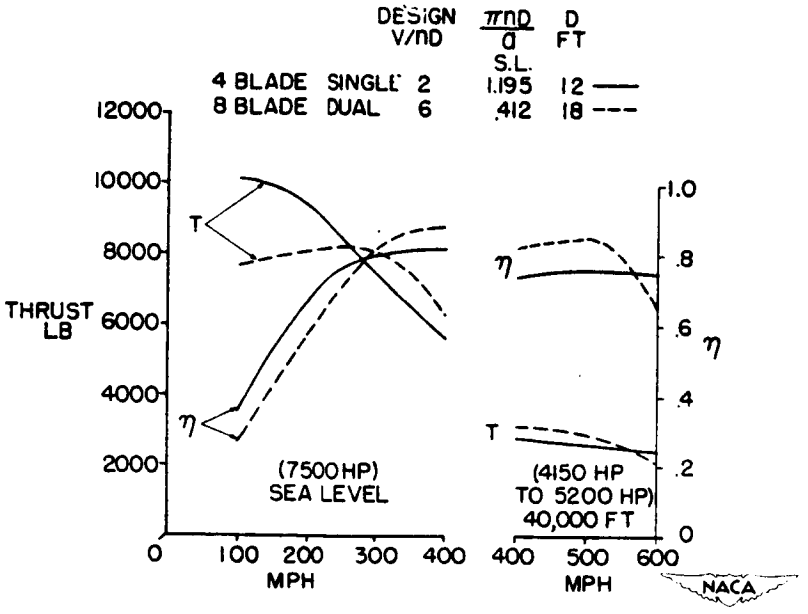


Figure 5.- Calculated thrust and efficiency characteristics for a single-rotation and a dual-rotation propeller.

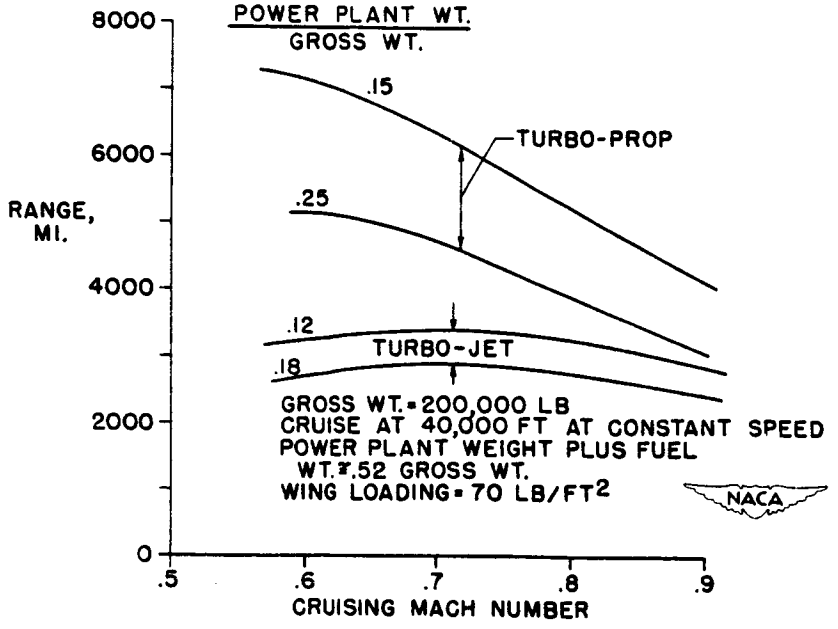


Figure 6.- Calculated range characteristics of an airplane power a turbojet or turbopropeller.